BEILSTEIN JOURNAL OF ORGANIC CHEMISTRY

Green chemistry III: Technologies shaping future directions in synthesis

Edited by Anna G. Slater, Luigi Vaccaro and Yanlong Gu

Generated on 02 November 2026, 02:51

Imprint

Beilstein Journal of Organic Chemistry
www.bjoc.org
ISSN 1860-5397
Email: journals-support@beilstein-institut.de

The *Beilstein Journal of Organic Chemistry* is published by the Beilstein-Institut zur Förderung der Chemischen Wissenschaften.

Beilstein-Institut zur Förderung der Chemischen Wissenschaften
Trakehner Straße 7–9
60487 Frankfurt am Main
Germany
www.beilstein-institut.de

The copyright to this document as a whole, which is published in the *Beilstein Journal of Organic Chemistry*, is held by the Beilstein-Institut zur Förderung der Chemischen Wissenschaften. The copyright to the individual articles in this document is held by the respective authors, subject to a Creative Commons Attribution license.

BEILSTEIN JOURNAL OF ORGANIC CHEMISTRY

Recent advances in the electrochemical synthesis of organophosphorus compounds

Babak Kaboudin*, Milad Behroozi, Sepideh Sadighi and Fatemeh Asgharzadeh

Review

Open Access

Address:
Department of Chemistry, Institute for Advanced Studies in Basic Sciences (IASBS), Gava Zang, Zanjan 45137-66731, Iran

Email:
Babak Kaboudin* - kaboudin@iasbs.ac.ir

* Corresponding author

Keywords:
electrosynthesis; green synthesis; organophosphorus compounds; P–C bond formation; P–heteroatom bond formation

Beilstein J. Org. Chem. **2025,** *21,* 770–797.
https://doi.org/10.3762/bjoc.21.61

Received: 26 November 2024
Accepted: 04 April 2025
Published: 16 April 2025

This article is part of the thematic issue "Green chemistry III".

Associate Editor: L. Vaccaro

© 2025 Kaboudin et al.; licensee Beilstein-Institut.
License and terms: see end of document.

Abstract

In this review, we describe recent advances in electrochemical green methods for the synthesis of various organophosphorus compounds through the formation of phosphorus–carbon, phosphorus–nitrogen, phosphorus–oxygen, phosphorus–sulfur, and phosphorus–selenium bonds. The impact of different electrodes is also discussed in this matter. Graphite, platinum, RVC, and nickel electrodes have been used extensively for the electrochemical synthesis of organophosphorus compounds. The recent advances in the electrochemical synthesis of organophosphorus compounds have made this method a promising method for preparing various structures. This review is an introduction to encourage scientists to use electrosynthesis as a green, precise, and low-cost method to prepare phosphorous structures.

Introduction

The electrochemical synthesis is a valuable and beneficial method for the preparation of organic compounds. In recent years, many advances have been made in this field of research, and researchers have been able to synthesize many compounds and confirm various uses for chemical compounds in this field. The significant progress in this field of research led to the name of this field as “greener chemistry”. Today, electrochemical synthesis has many applications in industry, and thousands of tons of chemicals are produced by this method every year [1-11].

In electrochemical synthesis, only electricity is used instead of oxidizing or reducing substances. Electricity can perform the oxidation and reduction process by exchanging electrons on the electrode surface in a region called the double layer (DL) [12]. Unlike traditional methods that require high temperature, pressure, and external oxidants, electrochemistry is an efficient and energy-saving approach that controls reaction selectivity by adjusting voltage or current [13]. Simple synthetic systems in electrochemical methods are limited to electrodes, cells, electrolytes, and power supplies. Today, in addition to the above, light, metallic, and organic catalysts are also used to increase the efficiency of reactions [14-21].

Organophosphorous compounds are essential materials with broad applications in medicinal chemistry, synthesis, agricul-

ture, as ligands, and intermediates to prepare complex compounds. Due to their importance, scientists have introduced many studies in recent years on developing new methods for synthesizing organophosphorus compounds [22-35].

Developing sustainable and green methods for synthesizing organophosphorus materials is a growing field. Methods based on photocatalysis [36], flow-based technologies [37,38], and microwave irradiation [39-42] have been developed. The electrochemical synthetic method is a creative, simple, and new process for preparing organophosphorus compounds [43].

In recent years, various articles have been reported on the electrochemical synthesis of organophosphorus compounds, in which phosphorus is attached to carbon or heteroatom centers. In this article, we describe recent advances in electrochemical green methods for the synthesis of various organophosphorus compounds through the formation of phosphorus–carbon, phosphorus–nitrogen, phosphorus–oxygen, phosphorus–sulfur, and phosphorus–selenium bonds. The impact of different electrodes is also discussed in this matter. Graphite, platinum, reticulated vitreous carbon (RVC), and nickel electrodes have been used extensively for the electrochemical synthesis of organophosphorus compounds.

Review

Electrochemical reaction cells

When a redox reaction occurs indirectly, chemical energy is transformed into electrical energy. A device that facilitates this conversion is known as an electrochemical cell. Electrochemical reaction cells are divided into two primary categories: galvanic (voltaic) and electrolytic. They consist of two electrodes – anode (where oxidation occurs) and cathode (where reduction occurs) – immersed in an electrolyte.

Galvanic cell

The redox reaction occurs spontaneously in these cells, converting chemical energy into electrical energy. The potential difference between the two electrodes generates an electric current. Some of its applications include batteries (e.g., lithium-ion batteries) and fuel cells. These cells are usually in a divided state.

Electrolytic cell

These cells require an external voltage to drive chemical reactions. They use electrical energy to carry out a non-spontaneous reaction. Some of their applications include hydrogen and oxygen production, metal electroplating, and organic compound synthesis using electrochemical methods. Depending on the reaction conditions, these cells can be divided or undivided.

Divided vs undivided cells

In divided cells, oxidation and reduction occur in separate compartments, separated by a diaphragm or salt bridge, to prevent reactant mixing and improve efficiency (e.g., Daniel cell). However, in undivided cells, both reactions occur in a single compartment without separation, resulting in a more straightforward design but potentially lower efficiency (e.g., some electrolytic cells).

Role of electrolytes in organic electrochemical reactions

Electrolytes are crucial for conductivity and reaction stability in organic electrochemical reactions. They are categorized as supporting electrolytes, which enhance conductivity, reduce resistance, and maintain ion balance (e.g., $LiClO_4$, n-Bu_4NBF_4), and active electrolytes, which participate directly in redox reactions, acting as oxidizing or reducing agents (e.g., H_2SO_4, Et_4NOH). Choosing the proper electrolyte affects reaction efficiency, selectivity, and overall performance.

Electrodes in the synthesis of organophosphorus compounds

Electrodes (any conductive materials) are one of the vital components in electrochemical cells (divided or undivided cells) for synthesizing organic compounds. The results of any electrosynthesis process depend entirely on the contact surface of the electrode with the reaction solution. The oxidation–reduction process complements each other, and the surface of the electrode in the reaction is critical. The material of the electrode is essential [44]. Various electrodes, including carbon (C), platinum (Pt), nickel (Ni), and reticulated vitreous carbon (RVC), are extensively used in the electrosynthesis of organophosphorus compounds (Table 1).

Table 1: Electrodes used in the electrosynthesis of organo-phosphorus compounds.

Material	Anode	Cathode
C	62%	12%
Pt	31%	74%
Ni	–	14%
RVC	5%	–

Carbon (C) electrode: The carbon electrode is one of the most widely used electrodes in electrochemical synthesis. This electrode is a porous material that allows chemicals to penetrate it. On the other hand, this electrode is one of the inexpensive electrodes. Usually, the carbon electrode needs to modify the surface, which allows for more straightforward chemical modification by installing it on other electrodes. The high fragility of the

carbon electrodes and the difficulty of their cleaning are disadvantages of these electrodes. A wide range of electrodes, such as graphite, glassy carbon, and pyrolytic carbon, are based on carbon. In synthesizing organophosphorus compounds by electrochemical methods, more than 60% of the anodes were made of carbon. The carbon electrode did not respond well as a cathode and was used only in ≈10% of the synthesis of organophosphorus compounds by electrochemical methods.

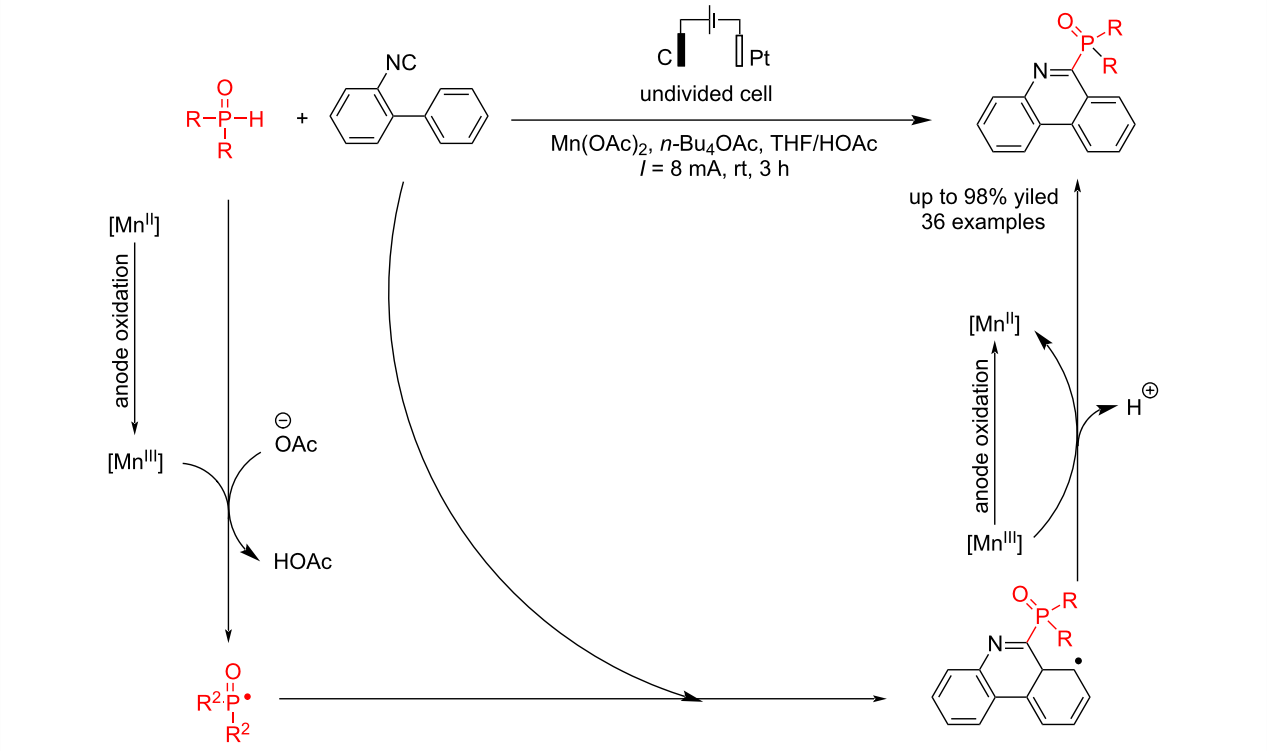
Platinum (Pt) electrode: The platinum electrode has an extensive oxidation range, is difficult to enter into the reaction, and can be very inert. This electrode is beneficial in electrosynthesis processes and can work well as the anode and cathode. This electrode has high stability in the electrochemical environment and is easy to clean, but caution should be taken when using it as a cathode because of low H_2 overpotential. Platinum electrodes are very popular and valuable as cathodes in the electrochemical synthesis of organophosphorus compounds. They are used as the cathode in more than 70% and as the anode in ≈30% of electrosynthesis processes.

Nickel (Ni) electrode: Nickel is not usually used as the anode but as a sacrificial anode in electrosynthesis. Using nickel as the cathode has a better performance, and it has not been used as the anode in the electrosynthesis processes of organophosphorus compounds.

Electrochemical synthesis of organophosphorus compounds

Electrochemical C–P bond formation

Various articles on the electrochemical synthesis of organophosphorus compounds have been reported in recent years. Recently, an electrochemical reaction of 2-isocyanobiaryls with diphenylphosphine oxides has been reported by Li et al. [45] using a Mn catalytic system with C(anode)/Pt(cathode) in an undivided cell. Different products were obtained with up to 85% yield in a constant flow for three hours. Studies showed that a Mn catalyst is critical for synthesizing derivatives of phenanthridine-based diarylphosphine oxides. The reaction yield decreased in the absence of the ligand, and eliminating both the ligand and manganese salt suppressed the reaction. Moreover, a slight decrease in the reaction yield was observed with increased reaction temperature. 2-Isocyanobiaryl compounds showed better reactivity when they contained electron-withdrawing groups. Diarylphosphine oxides containing a methyl group reacted well under standard conditions, regardless of their position. Mechanistic studies showed that when the reaction was carried out in the presence of TEMPO as a radical scavenger, a side product, TEMPO-P(O)R_2, was formed (it was confirmed using high-resolution mass spectrometry). The results revealed that the reaction proceeded in a radical pathway (Scheme 1). Based on the cyclic voltammetry experiments, the oxidation current increased further with the addition of

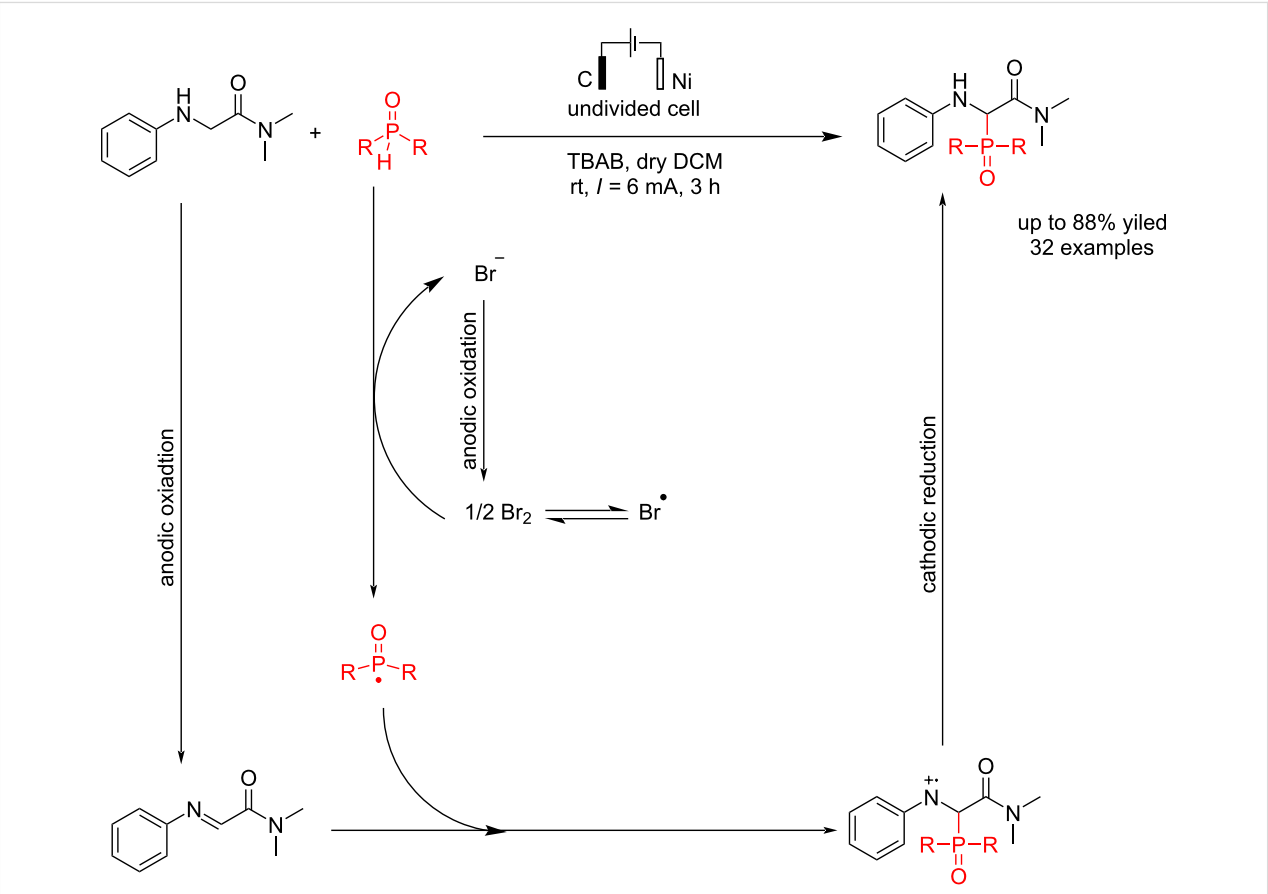


Scheme 1: Electrosynthesis of phenanthridine phosphine oxides.

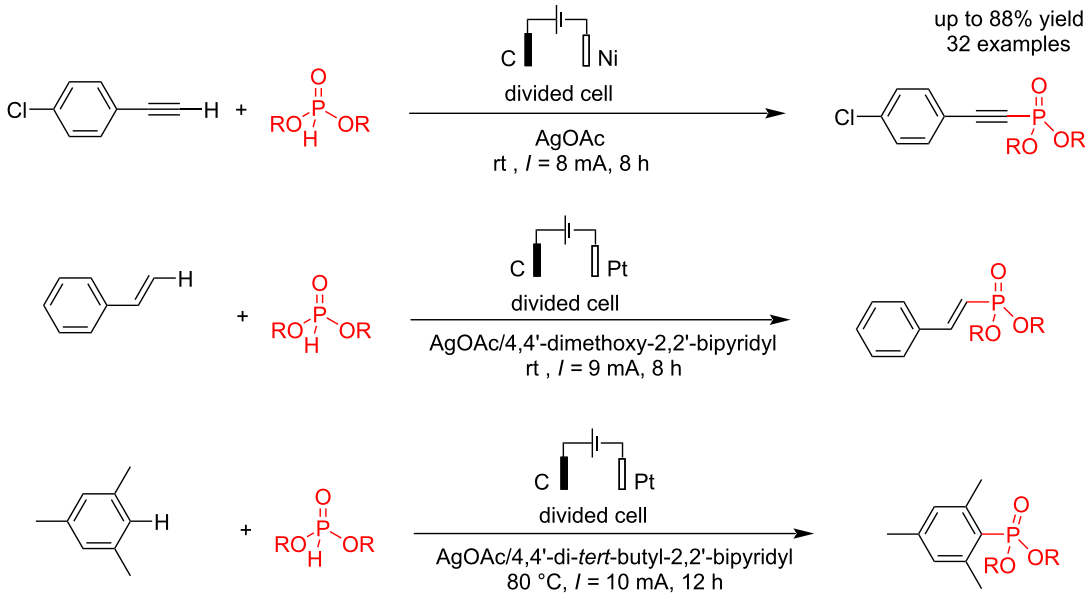
diphenylphosphine oxide to the mixture of $Mn(OAc)_2$ and 2,2-bipyridine. This suggests that 2,2-bipyridine likely influenced the oxidation of Mn(II) and reacted with diphenylphosphine oxide. Further studies have also shown that the platinum electrode as a cathode is very suitable for the process. Increasing the contact surface of the anode using a graphite felt electrode instead of a graphite rod in the reaction medium was one of the ways to improve the result.

In 2023, Wang et al. [46] reported an electrochemical reaction of amide derivatives of glycine with diarylphosphine oxide ($R_2P(O)–H$) for the synthesis of 1-aminoalkylphosphine oxides without the use of any transition metal catalyst or external oxidant. In this conversion, 1-aminoalkylphosphine oxides were formed in an undivided cell using a carbon electrode as the anode and nickel as the cathode in the presence of tetrabutylammonium bromide (TBAB) at the constant current of 6 mA. The electrodes used in the reaction are all in plate form. The presence of TBAB causes the resulting bromide anion to oxidize to bromine radical and react with $R_2P(O)–H$ to produce a radical phosphorus center. The reaction yield was higher when nickel was used as the cathode and graphite as the anode compared to the setup where nickel was replaced with graphite for the cathode and/or graphite was replaced with nickel for the anode (Scheme 2). This method is suitable for phosphorylating glycine amides with electron-withdrawing or electron-donating groups on their aromatic ring, producing products with yields ranging from 51% to 82%.

In 2023, Lei and co-workers [47] reported an electrochemical C–P bond formation via a coupling reaction of C–H bonds of alkynes, alkenes, and aryl compounds with dialkyl phosphonates at carbon and platinum electrodes as the anode and cathode in the presence of a silver catalyst in a divided cell (Scheme 3). According to the report, the silver catalyst is central to the coupling reaction. The study of the effect of alternating current (a.c.) electrolysis parameters on silver-catalyzed C–H phosphorylation revealed that variations in current intensity, frequency, and duty ratio influence product yield. To achieve optimal reactivity, the duty ratio must exceed 50%. Additionally, an analysis of silver deposition on carbon and platinum electrodes indicated that silver accumulation is minimal in alkynylation and arylation processes. In contrast, silver deposition was observed on the platinum electrode surface in alkenylation reac-



Scheme 2: Electrosynthesis of 1-aminoalkylphosphine oxides.



Scheme 3: Various electrochemical C–P coupling reactions.

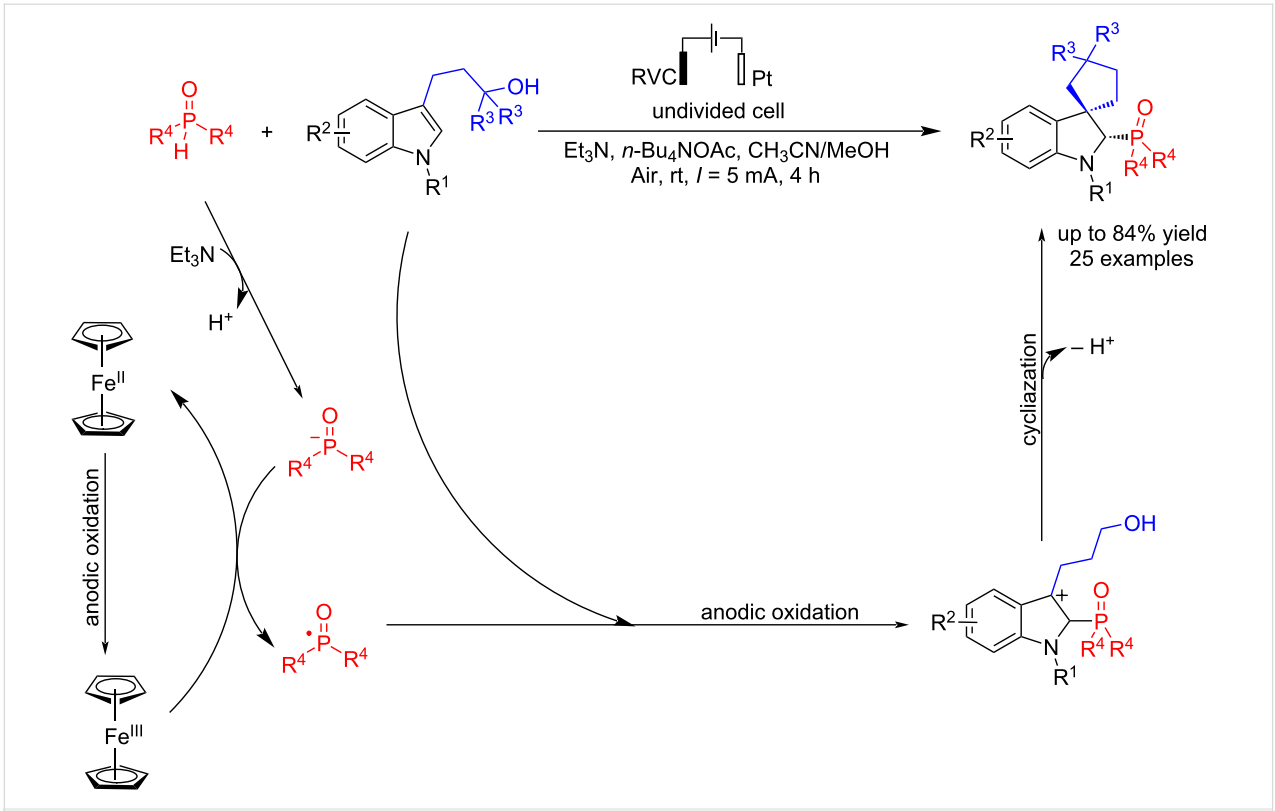
tions. The article does not provide a mechanistic description of the reaction. Further investigations suggested that modifying the shape and contact area of the electrodes led to different reaction outcomes.

Spirocyclic indolines have broad applications in medicine. The phosphorylated structures of indolines have also played a significant role in synthesis and industry. In 2023, Mo et al. [48] reported the electrochemical synthesis of a wide range of these compounds (25 compounds of phosphonylated 3,3-spiroindolines) in a convenient process. The C–P bond formation reaction of phosphine oxides with *N*-Boc-indolines was carried out in the presence of Cp_2Fe, but the reaction did not occur in its absence. When the reaction was performed in the presence of TEMPO, the product of TEMPO-P(O)R_2 was formed, which showed that the process proceeded through a radical path. In addition, the reaction was carried out in an electrochemical environment with an undivided cell, using graphite and platinum plate electrodes as the anode and cathode at constant current for 1 hour (Scheme 4). Platinum is usually used as the cathode for its ease of use, and a carbon plate electrode as the anode because of its cheapness and stability at high voltages. Further studies showed that using a reticulated vitreous carbon (RVC) electrode as the anode gave much better results than a graphite plate. The desired product was likely not formed due to the higher oxidation potential of diethyl phosphonate. Cyclic voltammetry experiments confirmed that Cp_2Fe is oxidized first due to its lower oxidation potential than other compounds. Moreover, the reaction proceeded smoothly without Et_3N or acetate, indicating that these compounds do not play a role in the reaction process (Table 2).

Table 2: Optimization studies.

Variation from the standard conditions	Yield (%)
none	62
without Cp_2Fe	n.r.
without Et_3N	31
CH_3CN/HOAc instead of CH_3CN/MeOH	22
CH_3CN/H_2O instead of CH_3CN/MeOH	22
RVC(+)|Pt(−) instead of C(+)|Pt(−)	74
without electricity	n.r.

To study ferrocene's electrochemical direct phosphorylation reaction with diphenylphosphine oxide, Chen et al. [49] examined and reported electrochemical C–P bond formation of ferrocene and ruthenocene via coupling reaction. This method provides an efficient and versatile synthetic approach for producing phosphorylated metallocenes but also aids in interpreting the regioselectivity and reactivity of C−H functionalization in unsymmetric metallocenes. They used a platinum electrode as the cathode and changed the anode electrode to find the best efficiency. The platinum plate electrode is more suitable than felt due to its larger contact surface, and using graphite electrodes in the form of a rod had good efficiency. The best results were obtained using a RVC electrode as the anode at a constant current at 50 °C in methanol for 6 h. This method also

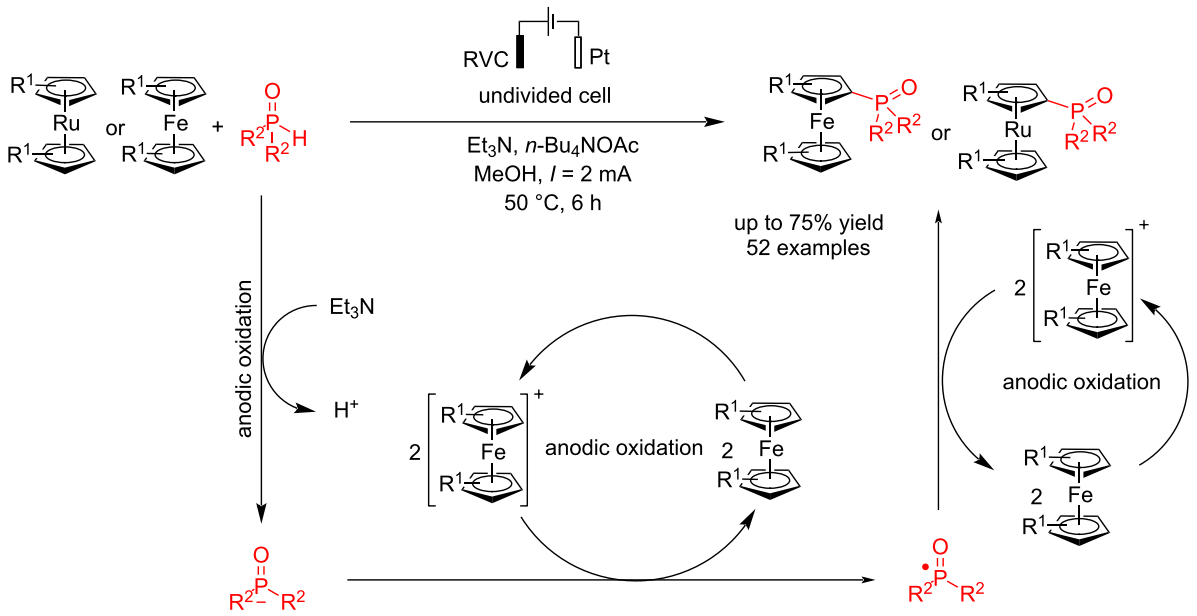


Scheme 4: Electrochemical C–P coupling reaction of indolines.

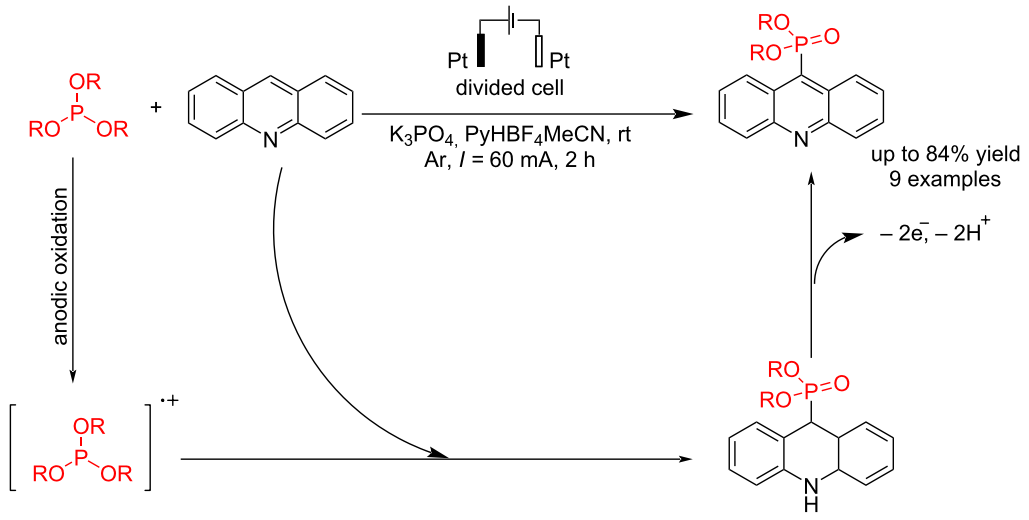
obtained a small amount of over-phosphorylated products. Phosphorylation occurred even when no functional group was present at the α-position of the aryl ring. Products with good yields were synthesized despite methyl, bromine, or phenyl groups at the α-position. The researchers noted that the lower yields were due to substrate decomposition or poor conversion rather than regioselectivity issues. Additionally, this method was also suitable for the phosphorylation of ferrocenes. For mechanistic studies, the reaction was examined in the presence of TEMPO as a radical scavenger, and the results revealed that the reaction proceeded through a radical pathway. The results of control experiments suggested that the phosphorylation might proceed through ferrocenium. It should also be noted that ferrocene and ruthenocene compounds have a low oxidation potential and can be oxidized quickly to act as a catalyst (Scheme 5).

Acridines are important nitrogen-containing heterocyclic compounds used as the building block for preparing medicinally active compounds. The conjunction of phosphorus with acridine increases its biological activities. Budnikova et al. [50] reported a C–P bond formation via the reaction of acridine compounds with trialkyl phosphites in electrochemical conditions without metal catalysts and strong oxidizing reagents, conducting selective C9 phosphorylation with high yield. The reaction was carried out in an undivided cell at room temperature, and three different electrodes, graphite, platinum, and glassy carbon (GC), were examined during the reaction. The best result was obtained when platinum electrodes were used as the anode and cathode. Although the reaction was less efficient in undivided cells, increasing the electricity passed improved the reaction yield. The use of commercial acetonitrile without additional drying reduced the yield of the target product due to the formation of byproducts $(RO)_3PO$ and $(RO)_2P(O)H$. It suggested that the reaction proceeded via anodic oxidation of trialkyl phosphite followed by treatment with acridine to give the corresponding coupling product (Scheme 6).

Vinylphosphonates have many applications in pharmaceutical, agricultural, and industrial processes. Zhang et al. [51] reported a novel electrochemical C–P coupling of specific alkenes with different types of phosphonates and phosphine oxides using a nickel catalyst. The use of nickel complex is an important and primary factor in the C–P coupling process. Notably, the inexpensive and environmentally readily available nickel catalysis was more effective for phosphorylation than other 3D metals. Moreover, it exhibited higher stability compared to 4d and 5d transition metals. Through the study of a series of previous experiments, it was shown that the electron density of the nitrogen atom in the quinoline structure significantly affects the efficiency of nickel-electrocatalysis; however, other *N*,*N*- or *N*,*O*-



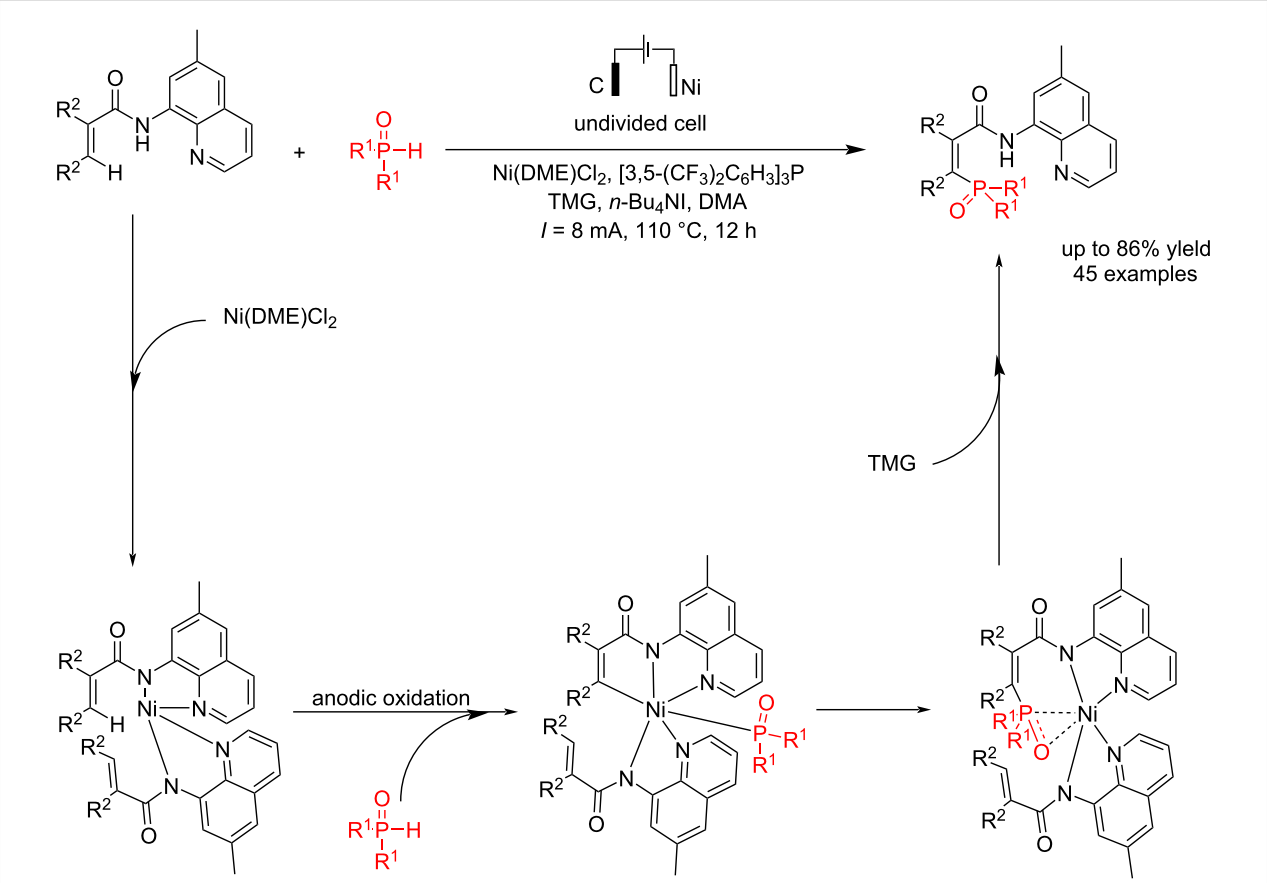
Scheme 5: Electrochemical C–P coupling reaction of ferrocene.



Scheme 6: Electrochemical C–P coupling reaction of acridines with phosphites.

bidentate groups were unable to accelerate this reaction. To perform the reaction in an electrochemical environment, they used graphite (felt form) and nickel (nickel foam) electrodes as the anode and cathode, respectively, under a constant current of 8 mA at 110 °C. A non-radical reaction mechanism process was proposed by conducting the reaction in the presence of TEMPO (Scheme 7). The electron-deficient and sterically encumbered diaminophosphine oxide could also produce the corresponding products in this method. Gas chromatography analysis confirmed that molecular hydrogen was the only byproduct of this process.

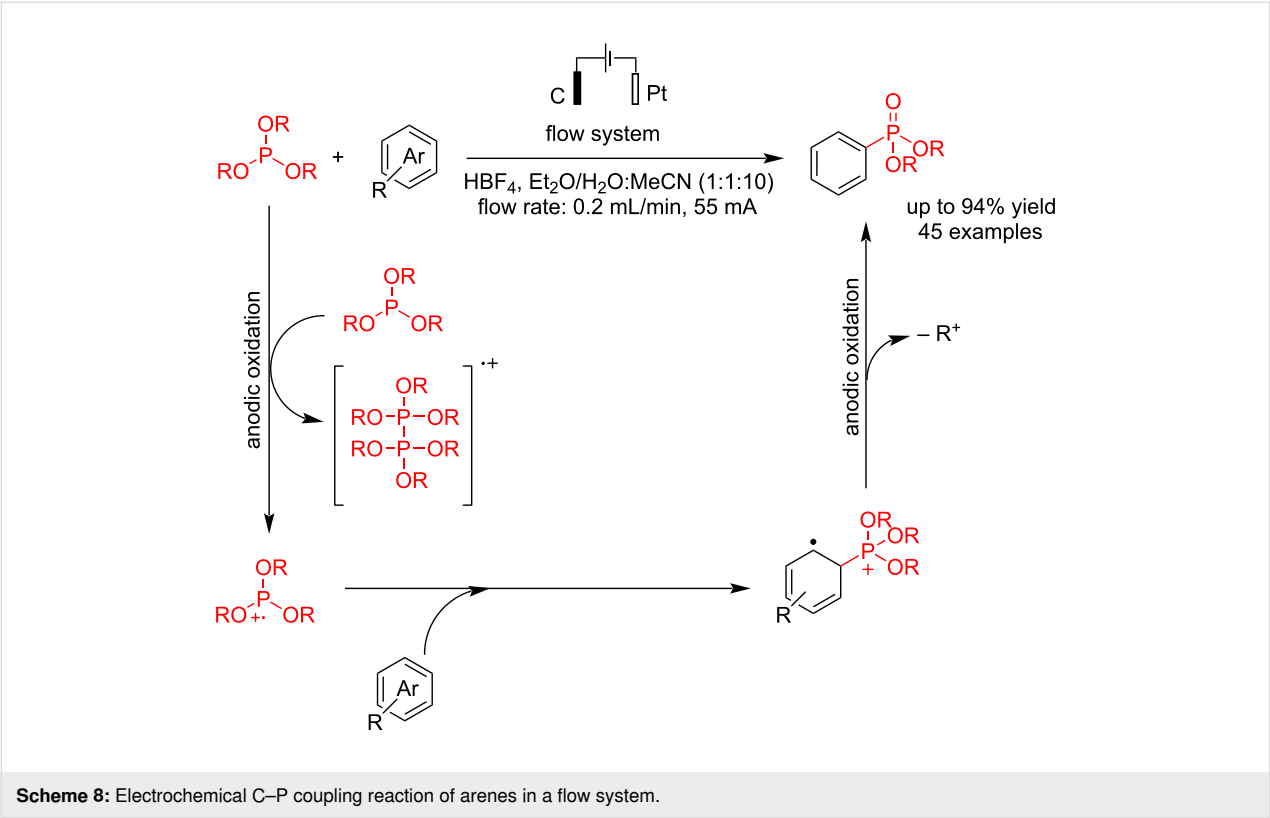
Arylphosphonates are essential compounds with a wide range of applications in pharmaceutical, biological, and agricultural materials. Therefore, finding new methods for preparing arylphosphonates is a significant challenge for scientists. Usually, metal catalysts are used to synthesize arylphosphonates via carbon–phosphorus bond formation. In 2021, Xu et al. [52] reported an electrochemical process for synthesizing arylphosphonates through the hetero-coupling reaction of CH of arenes with a trialkyl phosphite. They have prepared 45 arene phosphonates with good to excellent yields and reported the gram-scale preparation of some samples. An electrochemical flow system was



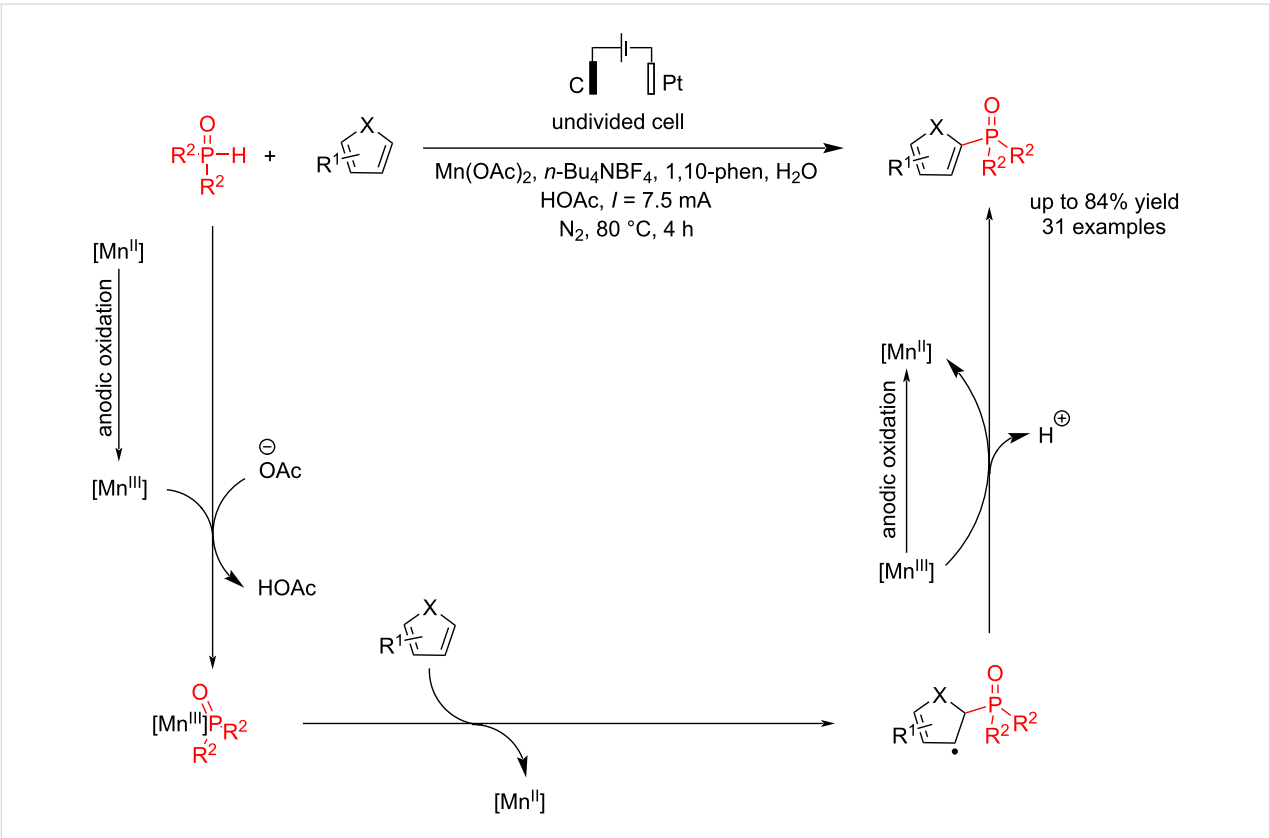
Scheme 7: Electrochemical C–P coupling reaction of alkenes.

used in this method, in which carbon and platinum electrodes were used as the anode and cathode, respectively, at a constant current of 55 mA (Scheme 8). Due to the steric hindrance caused by the *tert*-butyl group, the reaction occurred at the *ortho* position relative to the ester group. Also, after a few hours, the reaction yield decreased when the reactants were premixed with HBF_4. A series of analyses revealed that $P(OEt)_3$ decomposes into various phosphorus species without H_2O. Additionally, the studies showed that $P(O)(OR)_2$ is derived from the compound $P(OR)_3$, not from $HP(O)(OR)_2$. Although the exact role of $HP(O)(OR)_2$ remains unclear, it has been established that its presence is essential for the C–H phosphorylation. In this case, a radical cation intermediate was suggested for this conversion.

Heteroaromatic compounds such as furan and thiophene can be critical materials if attached to the phosphorus group. Wang et al. [53] reported an electrochemical process for the coupling of five-membered heteroaromatic rings with the P–H bond of diarylphosphine oxide in the presence of $Mn(OAc)_2$. This report found that using manganese acetate as a catalyst is essential, and the reaction failed to produce any product without the catalyst. Other catalysts besides Mn were tested, but they showed poor reactivity. Other strong polar solvents were also used in this method, but they resulted in lower yields of the products. The reaction was carried out in an undivided cell with a graphite rod electrode as the anode and platinum as the cathode at a constant current of 7.5 mA under N_2 for 4 h. Thiophenes with strong electron-withdrawing groups, and halogens produced moderate yields. However, a good yield was achieved when more thiophene and catalyst were added. On the other hand, heteroaromatics could not generate the corresponding products, likely due to their electron-rich nature and the presence of the active N–H group. The researchers noted that just one methyl group did not affect the reactivity. However, good-yield products were obtained when two methyl groups were positioned at the *para* or *meta* positions. The evaluation of the synthetic potential of the C−P bond formation revealed that the cleavage of the C−H bond in thiophene likely does not participate in the rate-determining step. Based on the experiments, a radical process was proposed for this coupling reaction via an Mn(III)–P intermediate (Scheme 9). The method was also applied to scale up to gram-scale synthesis.



Scheme 8: Electrochemical C–P coupling reaction of arenes in a flow system.



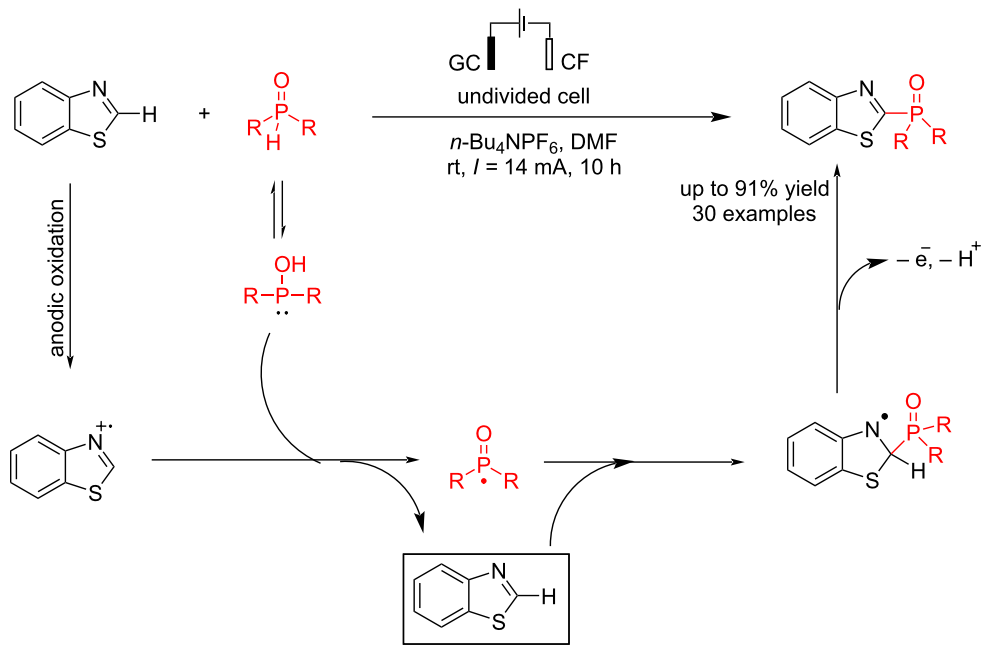
Scheme 9: Electrochemical C–P coupling reaction of heteroarenes.

In 2023, Wu et al. [54] also reported another heteroaromatic C–P coupling of benzothiazole with diarylphosphine oxides by an electrochemical method. They have synthesized 30 different thiazole phosphine oxides with up to 91% yield at room temperature without using an external metal or oxidant. The reaction was carried out in an undivided cell using glassy carbon as the anode and foamed copper as the cathode electrodes at a constant current of 14 mA for 10 h (Scheme 10). Other electrodes, including platinum, nickel foam, and graphite, were also examined for this reaction. The reaction failed to give the corresponding product using graphite as the anode and platinum as the cathode. The reaction showed lower efficiency under a nitrogen atmosphere, indicating that anodic oxidation is the main pathway of the reaction, and oxygen may have a positive effect. (Table 3). Functional groups at the 4-position moderately reduced the reaction yield. The nitro group was incompatible in this system, likely due to its preferential reduction ability. Some other heteroarenes were also tested, but only quinoxaline was compatible with this system under the standard conditions. A radical pathway was proposed in this reaction. At first, a thiazole radical cation was formed via anodic oxidation, followed by a reaction with phosphine oxides to give a phosphine oxide radical. The coupling product was obtained via the reaction of a phosphine oxide radical with thiazole compound.

Table 3: Optimization studies.

Variation from the standard conditions	Yield (%)
none	91
C (+), Pt (–)	16
Pt (+), Pt (–)	22
CH_3OH instead of DMF	n.r.
CH_3CN instead of DMF	10
under N_2	84
without electricity	n.r.

In another study on heteroaromatic compounds' electrochemical C–P coupling reactions, Gao et al. [55] reported an electrochemical reaction of indole derivatives with trialkyl phosphite in an undivided cell. The C–P product was selectively produced using *n*-Bu_4NClO_4 as electrolyte and carbon and platinum electrodes as the anode and cathode at a constant current for 4 h. Using *n*-Bu_4NI instead of KI resulted in a similar outcome, but KBr was less effective (Table 4). The desired C2-phosphorylated indole was obtained with high selectivity when *n*-Bu_4NClO_4 was used as the electrolyte. Additionally, under certain conditions that reduced the reaction yield, the C3-phosphorylated product was also observed. Similar to previous heteroaromatic coupling reactions with phosphine oxides [53,54], this reaction proceeded via anodic indole oxidation, followed by a reaction with trialkyl phosphite to give the corresponding indole phosphonate (Scheme 11). Cyclic voltammetry experiments confirmed that free indole can oxidize at the anode and generate a radical-cation intermediate. Also, no product was detected when $HP(O)(OEt)_2$ was used as the starting material.



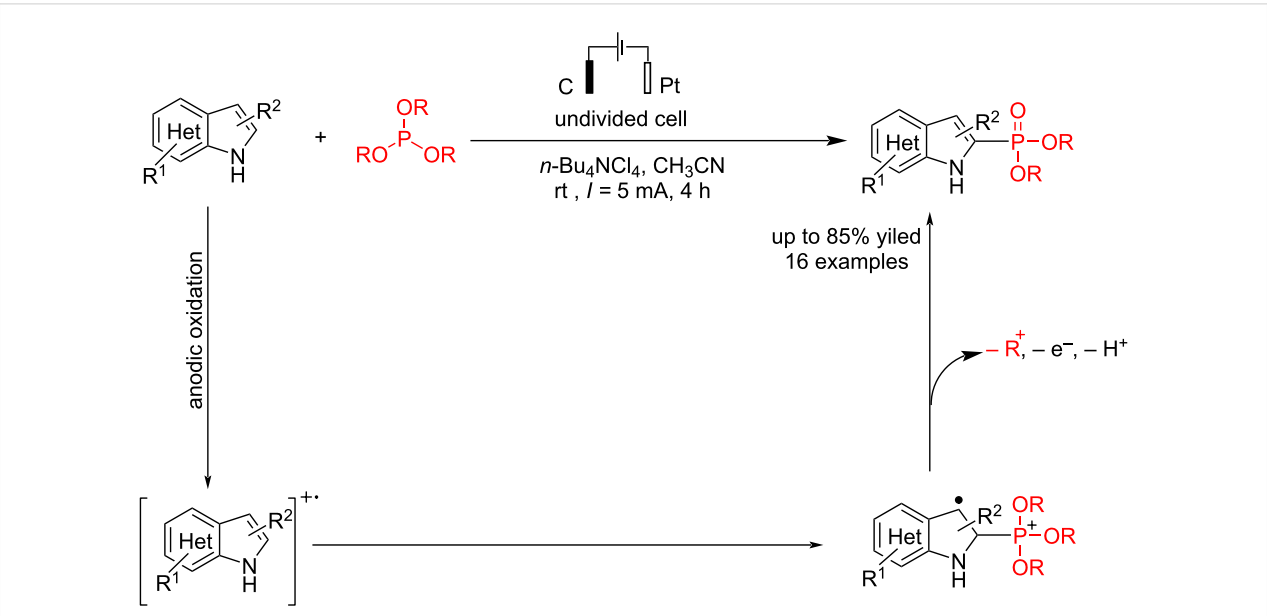
Scheme 10: Electrochemical C–P coupling reaction of thiazoles.

Table 4: Reaction parameters.

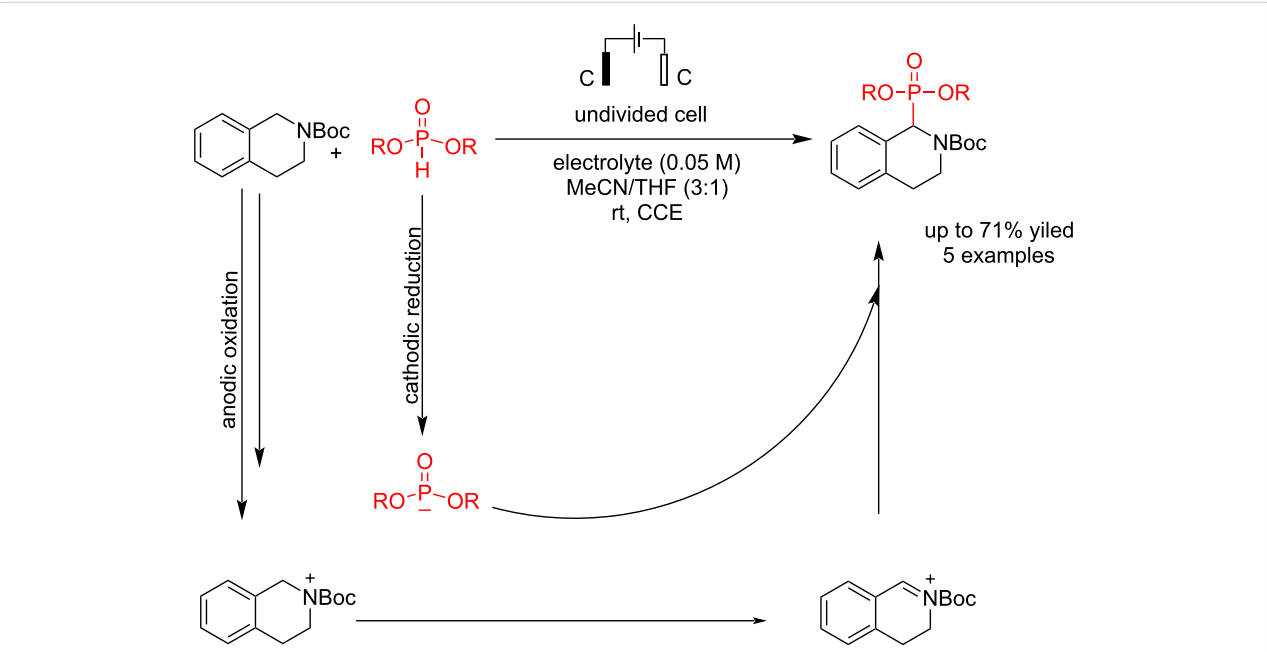
Electrolyte	$P(OE)_3$	Yield (%)
KI	3 equiv	n.d.
n-Bu_4NI	3 equiv	n.d.
KBr	3 equiv	n.d.
n-Bu_4NClO_4	4 equiv	75
n-Bu_4NBF_4	4 equiv	30
$NaBF_4$	4 equiv	58
KI	3 equiv	n.d.

Electrosynthesis processes of tetrahydroisoquinoline usually have a lower yield in the final product due to two electroactive positions in the molecule. Sengmany et al. [56] reported an electrochemical C–P bond formation of *N*-Boc-tetrahydroisoquinoline with dialkyl phosphites for synthesizing 1-amino phosphonates. The reaction was carried out at a constant current using graphite electrodes in both the anode and cathode. The optimal current intensity was observed when a 10 mA current was applied to the system. At higher current intensities, the reaction yield slightly decreased, and the formation of the Boc-deprotected product increased. When the reaction was performed in acetonitrile without THF, a greater quantity of the Boc-deprotected product was produced, which led to its degradation. This can be attributed to the Boc-deprotected compound being more easily oxidizable than the initial THIQ-N-Boc. Conversely, increasing the amount of THF relative to acetonitrile had the opposite effect on the yield. The use of diisopropyl phosphite decreased the reaction yield, which is presumed to be due to its steric effects. Moreover, phosphorylation did not occur with diphenyl phosphite, which can be attributed to its oxidizability. Unlike other phosphites, diphenyl phosphite is more easily oxidized than THIQ-*N*-Boc, preventing the coupling reaction. The reaction proceeded by coupling a cation intermediate of *N*-Boc-tetrahydroisoquinoline at the anode and phosphonate anion at the cathode (Scheme 12).

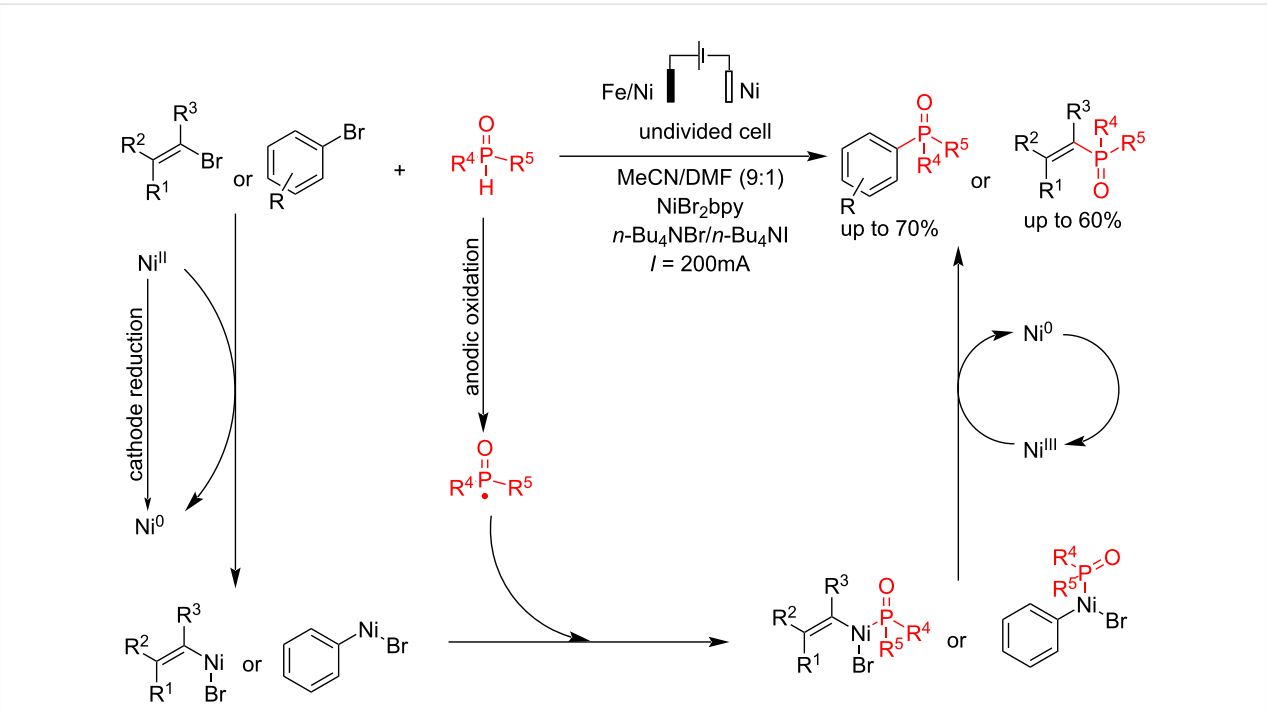
The C(sp^2)–X in aryl and vinyl halides is suitable in organic coupling reactions that are usually active in electrochemical environments. The use of combined electrodes is one of the creative methods in electrosynthesis processes. Léonel et al. [57] reported an electrochemical coupling reaction of aryl and vinyl bromides with different types of alkyl H-phenylphosphinates in the presence of $NiBr_2$ as a catalyst. The reaction was carried out with an alloy of Ni-Fe as the anode and nickel as the cathode in an undivided cell at a constant current for 0.5–2 h (Scheme 13). It should be noted that the reaction failed to give good results using Ni or Fe as the anode (<10%). However, using an iron/nickel alloy electrode with 64% iron and 36% nickel gave good results. This method can also be applied to heteroaromatic bromides, although it shows an increased tendency for hydro-dehalogenation. Tetrabutylammonium halide was chosen as the electrolyte due to its lower hygroscopicity and reduced tendency for reductive homocoupling of 4-bromobenzotrifluoride. In the presence of chlorinated substituents, neither the double coupling product nor the hydrodechlorination product was observed. This notable result suggests performing a second coupling using conventional chemical methods, such as the Suzuki–Miyaura reaction. Further-



Scheme 11: Electrochemical C–P coupling reaction of indole derivatives.



Scheme 12: Electrosynthesis of 1-amino phosphonates.



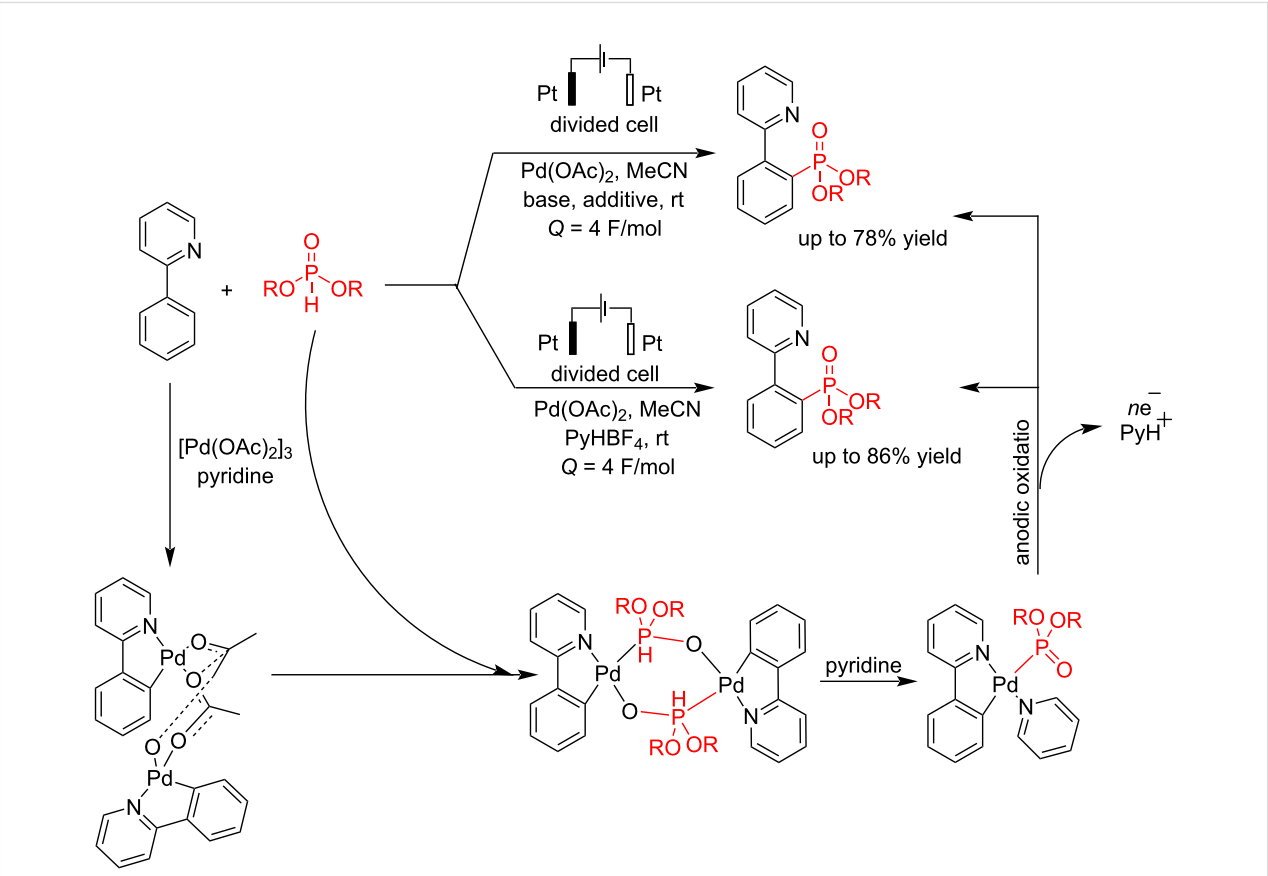
Scheme 13: Electrochemical C–P coupling reaction of aryl and vinyl bromides.

more, the coupling yield decreased for phenyl bromides bearing bulky *ortho*-substituents while hydrodehalogenation byproducts formed. The reaction proceeded via an oxidative addition and reductive elimination processed in the presence of Ni(0), which was produced in situ from $NiBr_2$ in the cathode.

Palladium is one of the most important metals used as a catalyst in non-electrochemical reactions. In 2020, Budnikova et al. [58] reported a coupling reaction of phenylpyridine with dialkylphosphonate in the presence of palladium. It should be noted that the presence of palladium is an essential factor, and

the results showed that the coupling reaction failed in the absence of palladium. Under pyridine-mediated conditions, the reaction follows a mononuclear palladacycle pathway, where a high electrolysis potential facilitates the formation of the *ortho*-phosphonate product with a favorable yield. On the other hand, when acid was used, forming a tetranuclear palladium intermediate led to the creation of a C–O–P bond. This reaction was carried out in a divided cell using platinum electrodes as the anode and cathode in the presence of pyridine as a base and ligand (Scheme 14). The catalyst behavior of palladium is attributed to its ability to form palladium clusters of specific sizes that exhibit high catalytic activity. However, this can lead to lower reaction yields because various reaction pathways, including those involving unstable metal-organic intermediates, may become involved. Cyclic voltammetry analysis in both solution and solid phases, using a carbon paste electrode (CPE), revealed that the nature of the bridging ligand and the overall structure of the complex highly influence the oxidation potential of Pd(II). At first, a complex of phenylpyridine with palladium (including insertion of Pd to C–H bond) and dialkyl phosphonate was formed, followed by anodic oxidation to give the final coupling product.

In 2023, Zhou et al. [59] reported an electrochemical method for the synthesis of phosphorylation of oxindoles and indolo[2,1-*a*]isoquinoline-6(5*H*)-ones using Cp_2Fe through a radical addition/cyclization reaction at room temperature under argon gas. This research shows that this method is effective with various functional groups and can help to find new drug candidates. The reaction was carried out in an undivided cell where the anode was platinum, and the cathode was graphite at a constant current of 5 mA. The mechanistic study showed that a radical process might be involved in the reaction, and the role of phosphorus-centered radical intermediates was confirmed. The importance of Cp_2Fe and the amount of diphenylphosphine oxide became evident when a significant decrease in reaction yield was observed both in the absence of Cp_2Fe (Table 5) and when a lower amount of diphenylphosphine oxide was used. Both electron-donating and electron-withdrawing groups produced products with yields ranging from 71% to 91%, and they were found to be effective in forming the corresponding polycyclic products (Scheme 15). Through cyclic voltammetry experiments, the researchers confirmed that since the oxidation potential of Cp_2Fe is lower than that of other substances, it is most likely oxidized first.

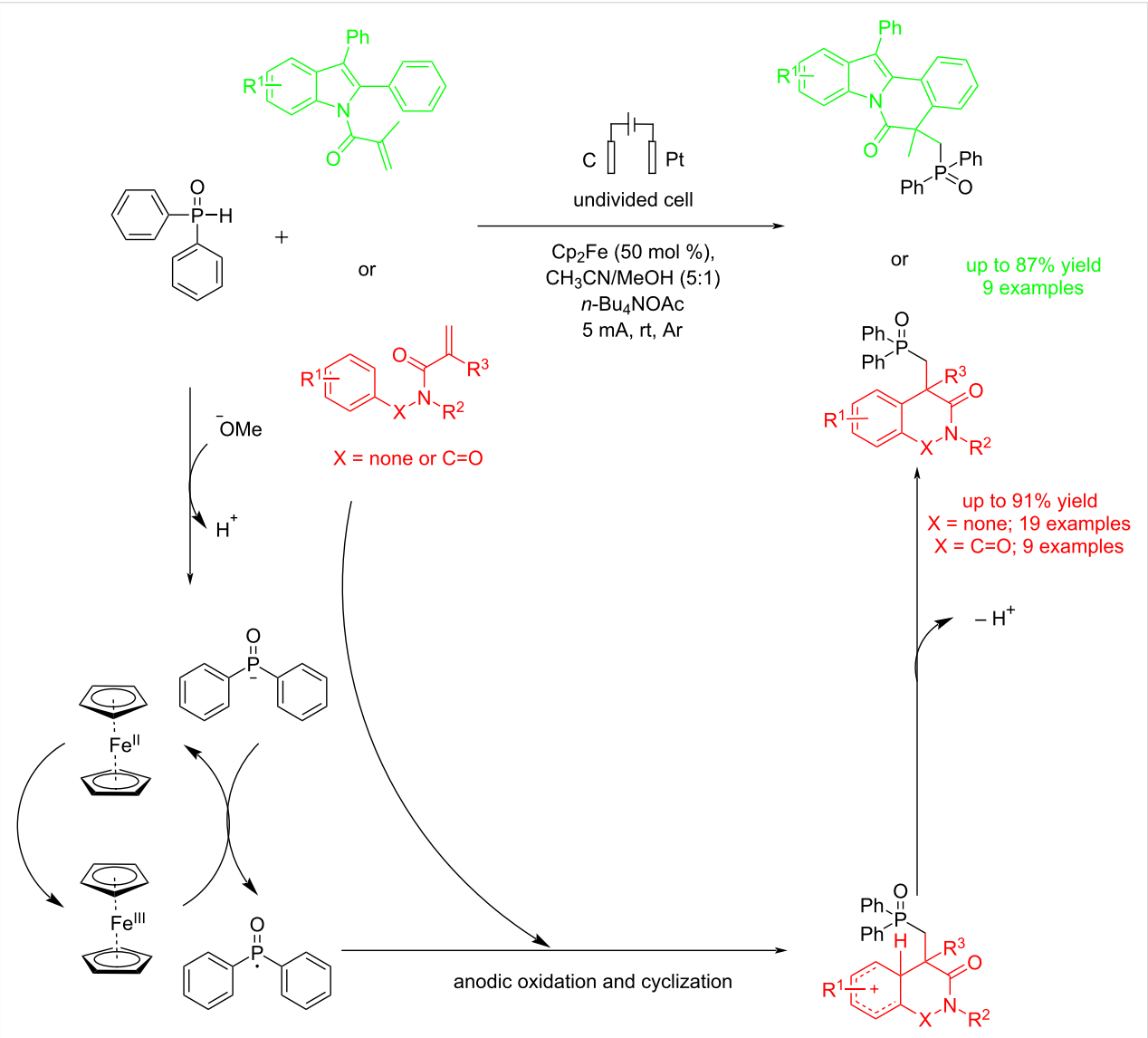


Scheme 14: Electrochemical C–P coupling reaction of phenylpyridine with dialkyl phosphonates in the presence of Pd.

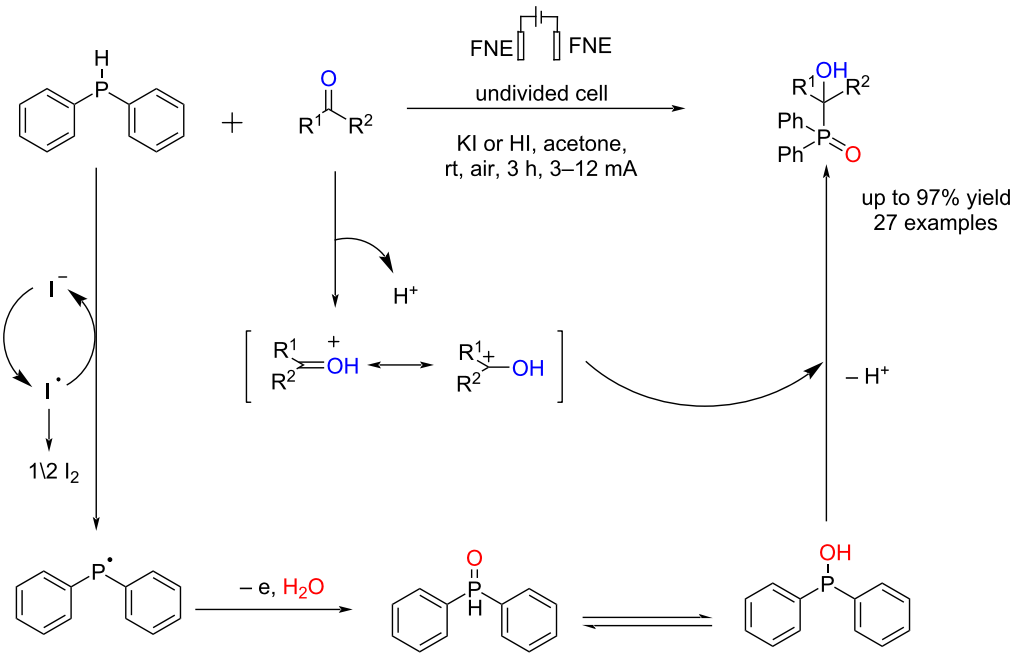
Table 5: Optimization studies.

Variation from the standard conditions	Yield (%)
without Cp_2Fe	<10
$MnCl_2$ instead of Cp_2Fe	23
CH_3CN/HOAc instead of CH_3CN/MeOH	11
without electricity	n.r.

In 2023, Ma et al. [60] reported an electrochemically oxidative/metal catalyst-free method for the synthesis of the α-hydroxyphosphine oxides through the reaction of diphenylphosphine as a phosphine source with aldehydes or ketones. They used nickel foam as both anode and cathode electrodes in an undivided cell under air at room temperature. The reaction was carried out in the presence of KI as an electrolyte, a key additive, and acetone as a solvent. HI increases the reaction yield due to the activation of the carbonyl group. The halide salts did not lead to product formation, indicating that chloride and bromide anions cannot generate the corresponding radicals to accelerate the conversion of diphenylphosphine. The reaction yield decreased when the methyl group was placed in *ortho*-position. Moreover, the desired products were obtained with moderate yields for aldehydes containing strong electron-withdrawing groups, indicating that this method is suitable for forming P–C bonds. Products with nitro, chlorine, or bromine groups at the *para* position had higher yields compared to those with the groups at the *meta* or *ortho* positions, which may be due to steric and electronic effects. The reaction proceeded via a radical process by forming $Ph_2P(O)H$ (Scheme 16). The reaction failed to give



Scheme 15: Electrochemical P–C bond formation of amides.



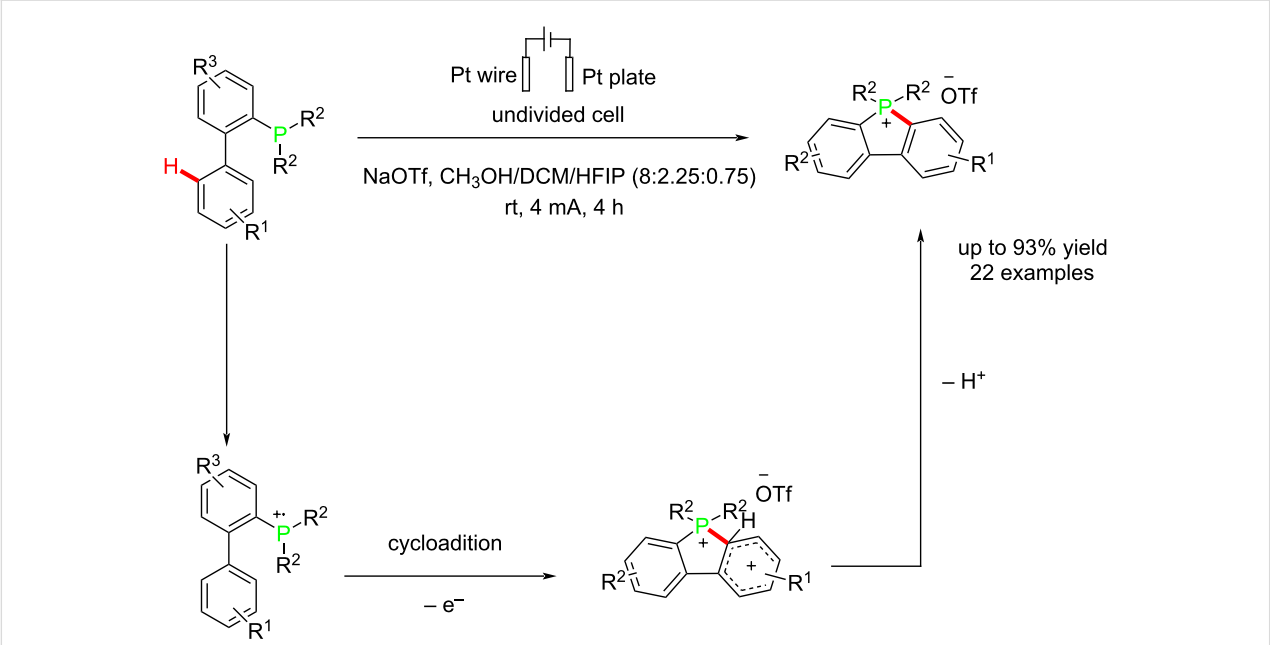
Scheme 16: Electrochemical synthesis of α-hydroxy phosphine oxides.

the corresponding product when using TEMPO in the reaction mixture.

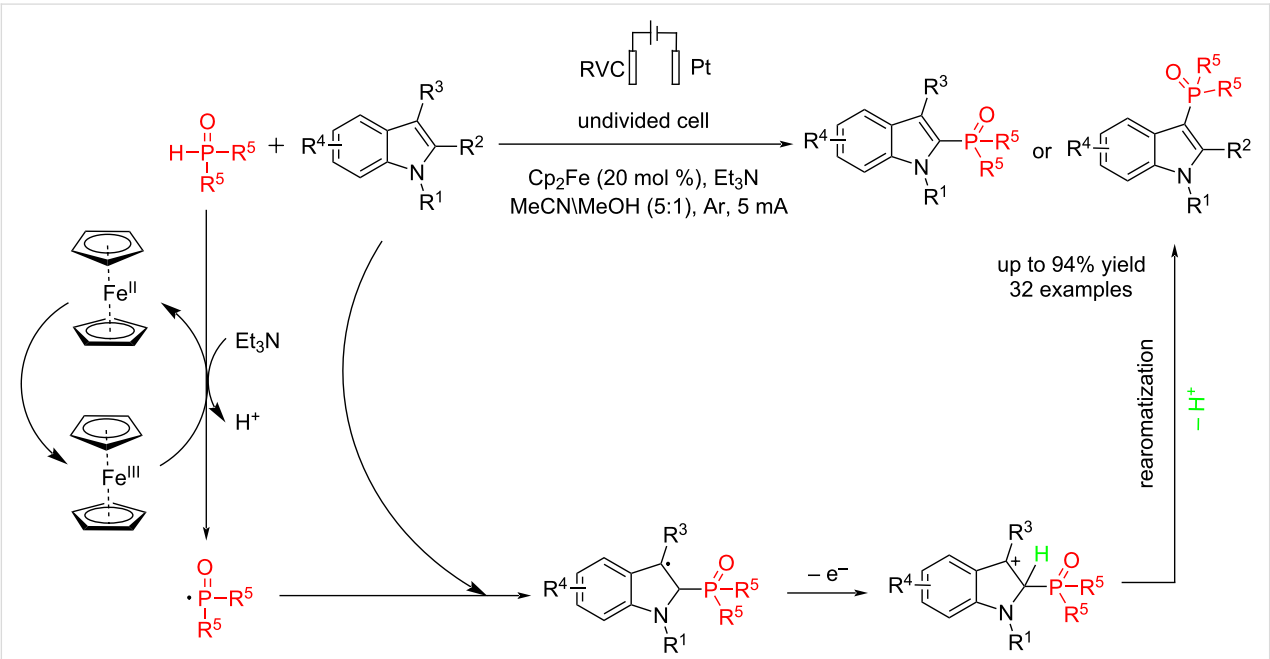
Zhang and co-workers [61] reported an electrochemical process for synthesizing π-conjugated phosphonium salts at room temperature in catalyst/oxidant-free conditions. The reaction was carried out in an undivided cell using a platinum plate as the anode and platinum wire as the cathode at a constant current of 4 mA. The reaction proceeded via an anodic oxidation followed by an internal combination of the formed radical to give the corresponding product (Scheme 17). The oxidation reaction was probably ineffective in the absence of HFIP due to the stability of HFIP's radical cation ions. The efficiency of the reaction was dependent on the electrolyte concentration, with a decrease in efficiency observed at lower concentrations. The reaction proceeded well under nitrogen, indicating that the oxidation process is unrelated to the presence or absence of oxygen. The yields of some products are likely due to the strong electron-withdrawing effects of the electron-withdrawing groups.

In 2024, Wang et al. [62] reported an electrochemical method for the synthesis of phosphorylated indoles in the presence of Cp_2Fe as the mediator under mild reaction conditions without the need for external oxidants. This method improves the scalability of the resulting products, which also exhibit enhanced anticancer activity. The reaction was carried out in an undivided cell where the anode was reticulated vitreous carbon (RVC), and the cathode was platinum. Mechanistic studies revealed that Cp_2Fe plays the main role in the reaction, and the reaction did not proceed without using Cp_2Fe. Replacing the Boc group with an acetyl group significantly decreased the reaction yield. Furthermore, the results showed that the reaction proceeded via a radical phosphorylation process (Scheme 18). Cyclic voltammetry experiments demonstrated that Cp_2Fe is likely to undergo oxidation first due to its lowest oxidation potential among the species.

In 2024, Zhu et al. [63] reported an electrochemical transition-metal and additive-free synthesis of phosphorylated propargyl alcohols at room temperature. The reaction is carried out in an undivided cell using glassy carbon (GC) as an anode and copper foam (CF) as a cathode at a constant current of 14 mA. Experiments confirmed that the trace amount of copper dissolved from the cathode had no catalytic effect on the reaction. The reaction proceeded via anodic oxidation of diphenylphosphine followed by a reaction with alkenes to give corresponding phosphorylated propargyl alcohols (Scheme 19). The reaction yield showed that this method is not sensitive to electron-withdrawing or electron-donating groups at different positions on the aromatic ring. Most likely, the 3-substituted pyridine substrate and the enynes with nitro or carbonyl groups on the aromatic ring did not react in this system due to the incompatibility of the intermediate radicals.



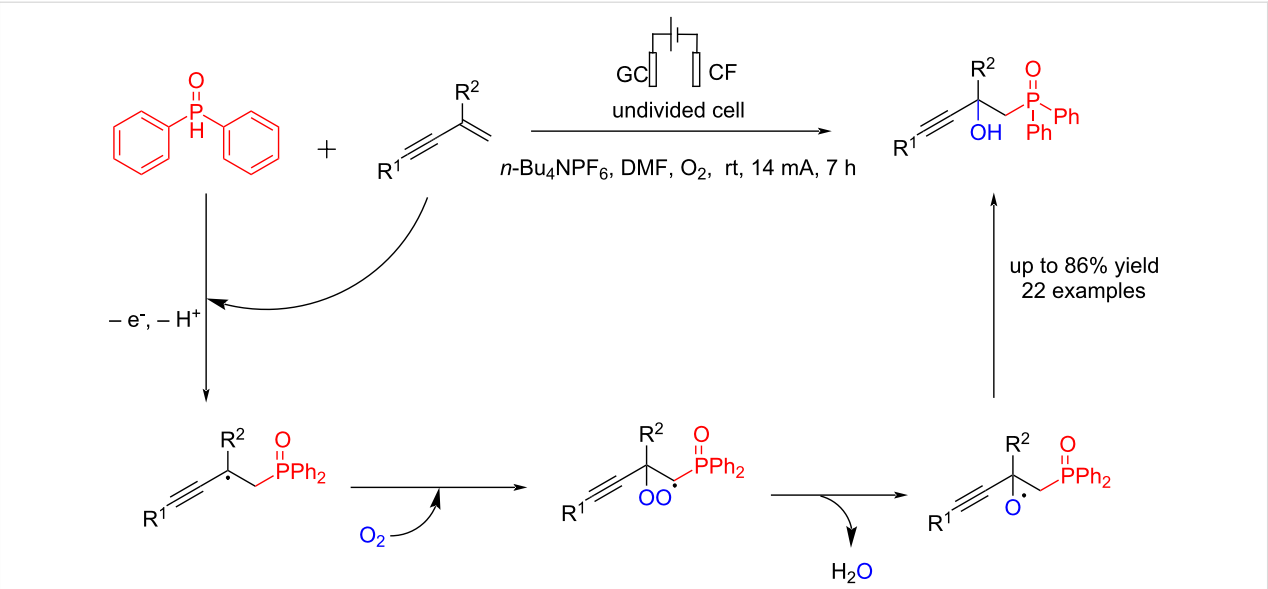
Scheme 17: Electrochemical synthesis of π-conjugated phosphonium salts.



Scheme 18: Electrochemical phosphorylation of indoles.

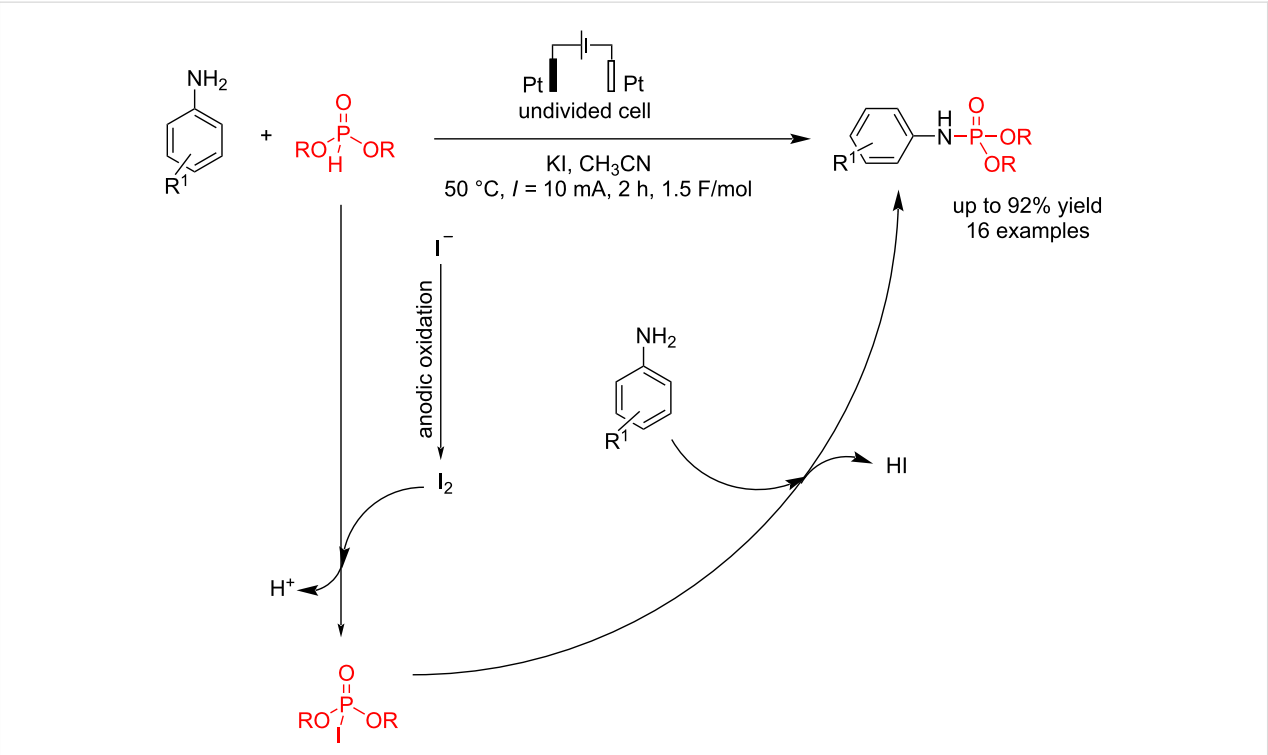
Electrochemical N–P bond formation

Due to the importance of phosphoramidates in medicine and organic synthesis, Zhong et al. [64] reported an electrochemical P–N coupling of amines with dialkyl phosphonates for synthesizing phosphoramidates. The reaction was carried out in an undivided cell at a constant current of 10 mA using platinum electrodes as the anode and cathode and potassium iodide as a key additive. Studies have shown that the choice of solvent significantly impacts the reaction. Studies have shown that the choice of solvent significantly impacts the reaction. CH_3CN exhibits better than CH_3OH, with a wider electrochemical window and better reactant solubility. When the reaction was conducted in CH_3CN using n-Bu_4NPF_6 and n-Bu_4NBF_4 as electrolytes but without iodide salt and in the presence of air, no product was



Scheme 19: Electrochemical synthesis of phosphorylated propargyl alcohols.

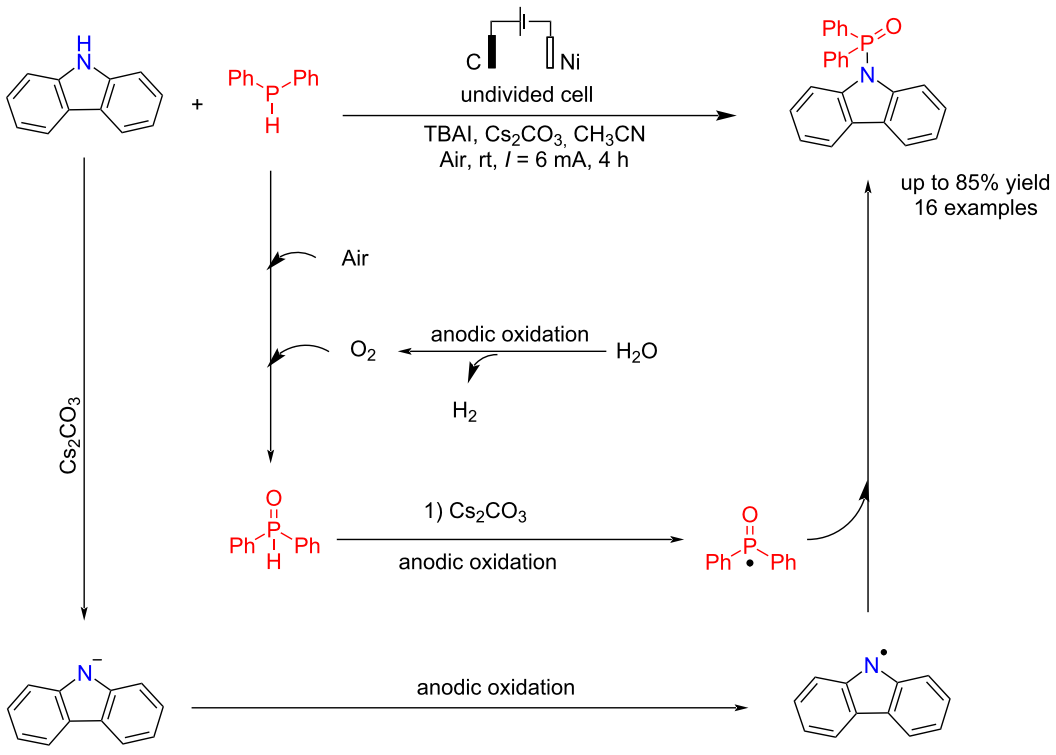
formed. This finding indicates that iodide salt plays a crucial role in driving the reaction and acts as a catalyst in the reaction process. The electronic properties of the substituents on the compounds influenced the reaction yield. Phenol with the –OMe group produced a lower yield than the –Me group. This decrease in yield is likely due to the lower oxidation voltage of the –OMe group, which may lead to the formation of unwanted byproducts. The reaction began with an anodic oxidation of iodide to iodine, followed by a reaction with dialkyl phosphonate to give I–P(O)$(OR)_2$. The final product was formed by a simple nucleophilic substitution of the phosphorus center (Scheme 20).



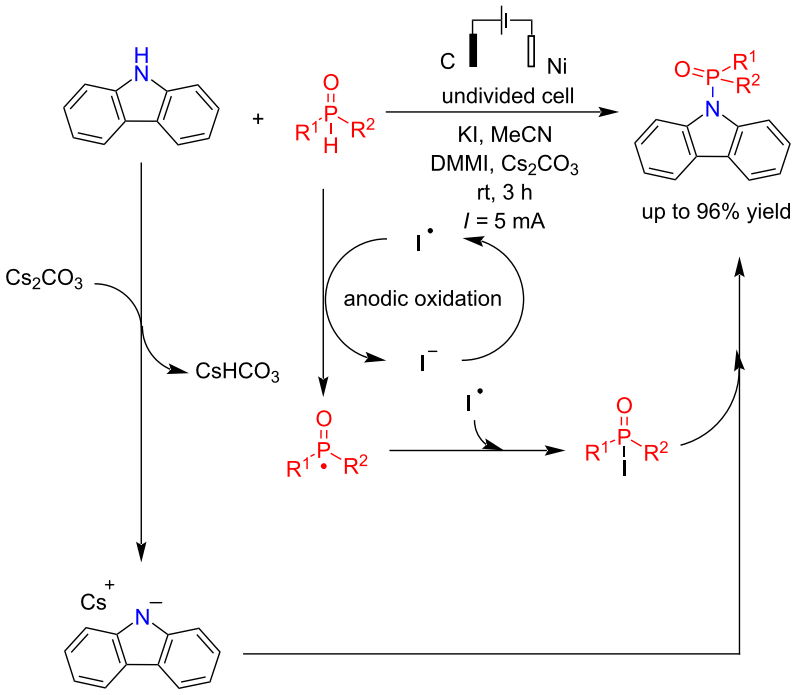
Scheme 20: Electrochemical synthesis of phosphoramidates.

The N–P bond formation is a critical process in organic synthesis due to the preparation of various materials with different biological and medicinal activities. In 2021 Wang et al. [65] reported a novel method for the N–P bond formation of carbazoles with diphenylphosphine using an electrochemical process. The main advantage of this method is its high selectivity, as only a 1:1 ratio of the starting materials was required for the reaction. The reaction was carried out in an undivided cell using TBAI as a key additive and carbon and nickel electrodes as the anode and cathode for 4 h at a constant current. Graphite, platinum, nickel, and reticulated vitreous carbon (RVC) electrodes were examined in this conversion. The platinum electrode did not perform well in the anode, and no reaction was performed. The use of graphite and RVC gave good results. Nickel, graphite, and platinum electrodes were examined as the cathodes. Results showed that platinum and nickel performed better than graphite in the cathode due to their higher conductivity and lower electrical resistance. When platinum and nickel were used as the cathode and graphite as the anode, the efficiencies of the processes were very close to each other. The use of dry acetonitrile as the reaction medium significantly reduced the yield. These results indicate that water plays a crucial role in this reaction, as its decomposition leads to the generation of O_2, the primary oxygen source in the reaction process. A radical process was proposed in the reaction. Diphenylphosphine oxide and carbazole radicals were formed via anodic oxidation in the presence of a base, followed by a coupling reaction to give the final P–N product (Scheme 21).

In another attempt, Liu et al. [66] also reported the electrochemical phosphorylation of carbazoles and indoles in the presence of 1,3-dimethylimidazolium iodide (DMMI) as a mediator in the oxidation–reduction process. The reaction proceeded in an undivided cell using cesium carbonate as a base for 3 h with graphite and platinum electrodes as the anode and cathode, respectively (Scheme 22). In this reaction, a variety of substitutions were examined. The results showed that the reaction proceeded very well with electron-donating groups such as –OMe, –Me, and $–CH_2CN$ and electron-withdrawing groups such as –Cl, –Br, and $–CO_2Me$. It was observed that carbazole derivatives with an extended conjugated system showed enhanced reactivity. Like the above P–N coupling mechanism, the reaction proceeded by an anodic oxidation of iodide to iodine followed by a reaction with dialkylphosphine oxide to give $I–P(O)(R)_2$. The exact mechanism of this coupling reaction is not yet fully understood; however, the possibility of direct radical cross-coupling between the nitrogen radical derived from carbazole and the phosphoryl radical intermediate cannot be completely ruled out.



Scheme 21: Electrochemical reaction of carbazole with diphenylphosphine.



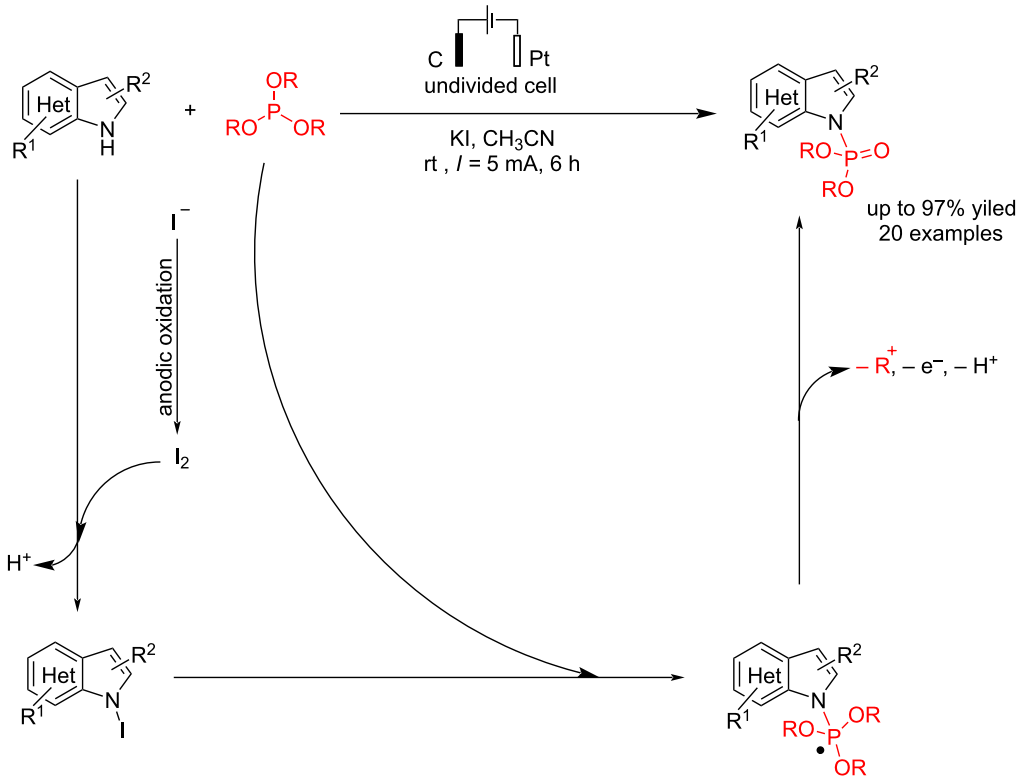
Scheme 22: Electrochemical P–N coupling of carbazole with phosphine oxides.

In another electrosynthesis report, Gao et al. [55] reported similar P–N coupling reactions of indoles with trialkyl phosphites in the presence of potassium iodide as a mediator and electrolyte. The carbon and platinum electrodes were used as the anode and cathode at a constant current of 5 mA for 6 h in acetonitrile as solvent. The results showed that potassium iodide is critical in this reaction, and the reaction failed to give a corresponding product without using KI. This reaction was quickly extended to a wide range of substituted indoles. Moreover, despite significant steric hindrance or the presence of a long alkyl chain, both $P(OiPr)_3$ and $P(On\text{-}Bu)_3$ proved effective in this reaction. In this reaction, the P–N coupling process proceeded via forming an *N*-indole iodide intermediate via anodic oxidation of iodide to iodine, followed by a reaction with indole (Scheme 23). Cyclic voltammetry demonstrated that in the presence of $n\text{-}Bu_4NClO_4$, free indole undergoes oxidation due to its electron-rich nature, forming a radical-cation intermediate. However, when KI was used instead, oxidation of free indole was not observed, indicating a different oxidation pathway. Additionally, under certain low-yield conditions, the C3-phosphorylated product was also formed.

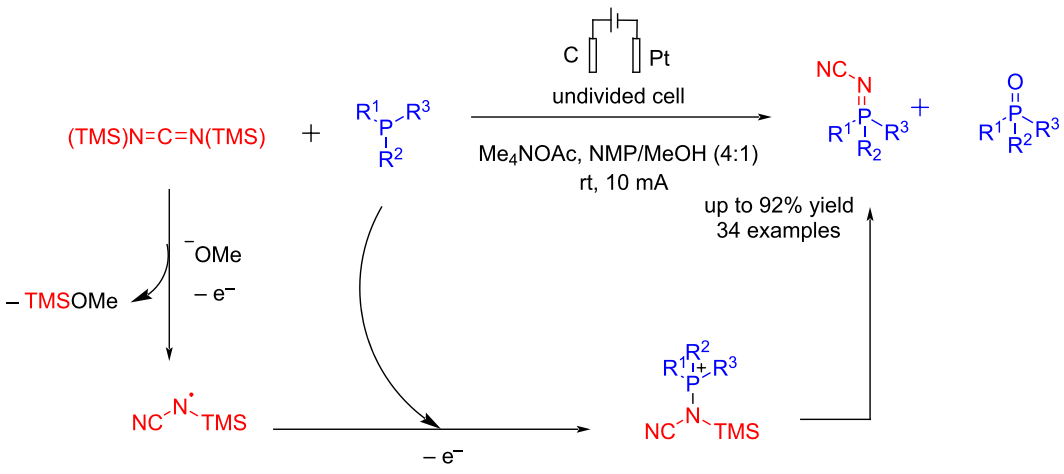
In 2024, Mdluli et al. [67] reported an electrochemical method for synthesizing iminophosphoranes. In this method, iminophosphorane was investigated due to its air stability and the presence of a UV–vis chromophore, which enables the analysis of the reaction via UPLC. This reaction was carried out in an undivided cell using graphite as the anode and platinum foil as the cathode at a constant current of 10 mA. In the presence of a graphite anode, a stainless-steel cathode, and Et_4NBr as the electrolyte, the oxidation of PPh_3 was observed. For optimization of the reaction, an HTe^-Chem reactor was used in the presence of Me_4NOAc as the electrolyte. The use of NMP and Me_4NOAc was beneficial, as in many cases, adding water led to the precipitation of the desired product from the reaction mixture. A wide range of iminophosphoranes were synthesized according to the following mechanism via an anodic trimethylsilyl cyanide radical formation (Scheme 24). The formation of the $Ph_3P{=}O$ as the side product was assumed to be due to the presence of water or oxygen in the reaction mixture, which competes with the aminating reagent.

Electrochemical O–P bond formation

In 2021, Zhong et al. [64] reported an electrochemical coupling reaction of phenols with dialkyl phosphonates. The reaction was carried out in an undivided cell using platinum electrodes in the presence of sodium iodide at a constant current. Various electrodes were examined, and the best results were obtained using platinum electrodes as the anode and cathode (Scheme 25). Studies showed that CH_3CN performed better than CH_3OH due to its wider electrochemical window and better solubility. The results indicated that the electronic properties of substituents had no significant effect on the yield, and all substituted anilines afforded high yields of phosphoramidates. However,



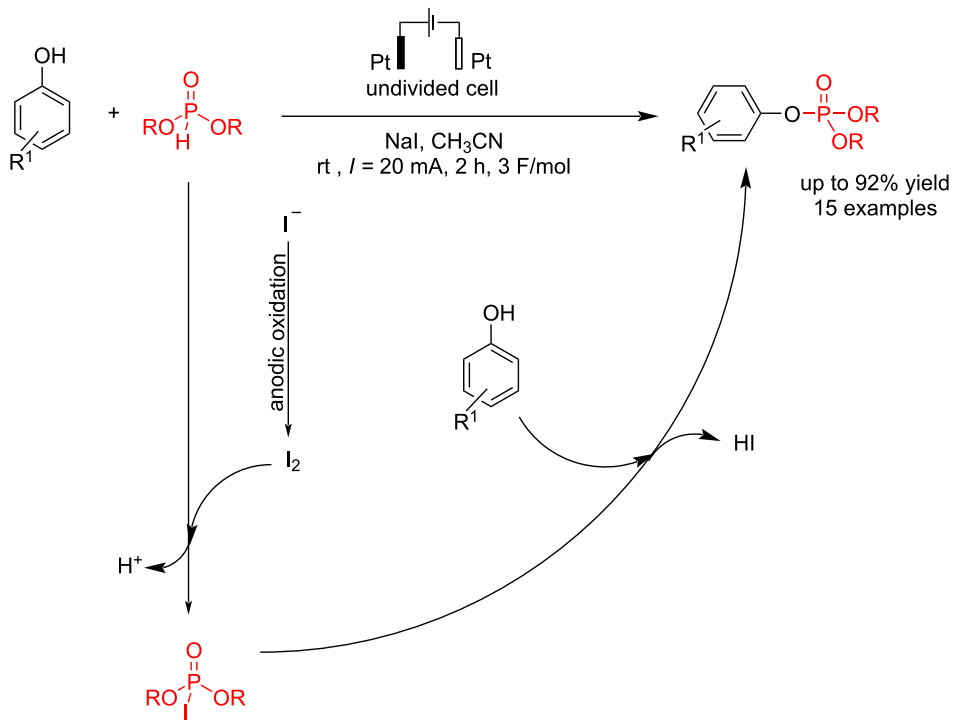
Scheme 23: Electrochemical P–N coupling of indoles with a trialkyl phosphite.



Scheme 24: Electrochemical synthesis of iminophosphoranes.

N-methyl- and *N*-ethylanilines showed lower yields and electron-donating groups led to a reduced yield compared to unsubstituted aniline. Further, KI performed best as the electrolyte and catalyst at 50 °C (Scheme 20). The reaction proceeded with anodic oxidation of iodide to iodine, followed by a reaction with dialkyl phosphite to give I–P(O)(OR)$_2$. The final product was formed by a simple nucleophilic substitution of phenols with I–P(O)(OR)$_2$.

In 2021, Wang et al. [65] presented a report on electrochemical P–O bond formation. In this method, they have reported an electrochemical reaction of alcohols (aliphatic and aromatic)



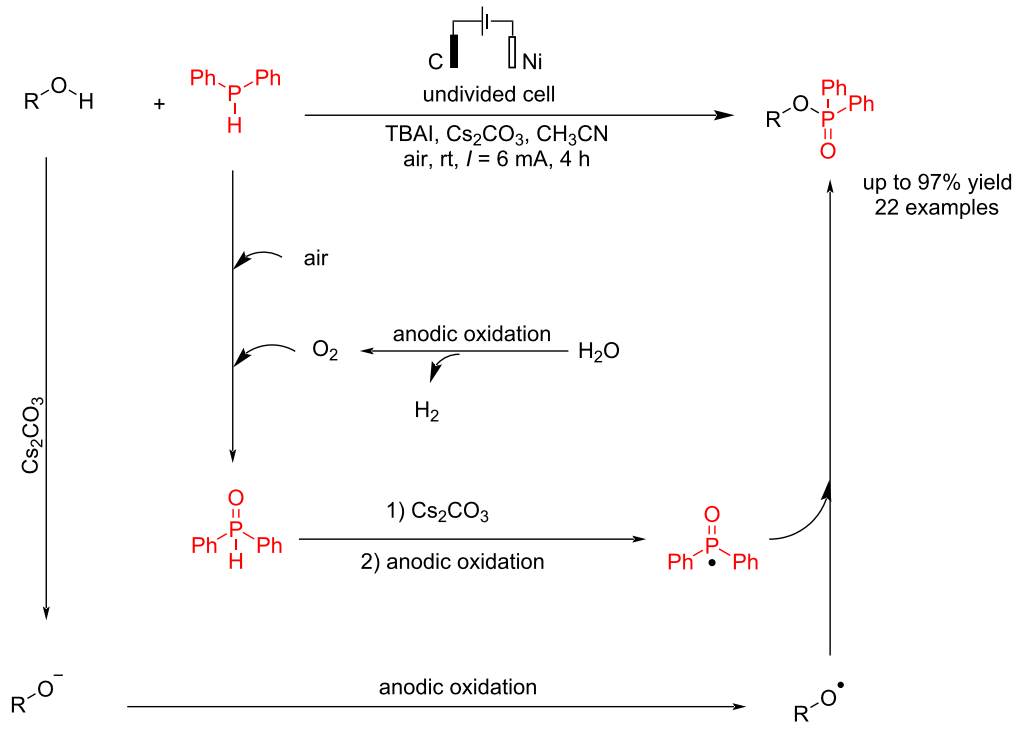
Scheme 25: Electrochemical P–O coupling of phenols with dialkyl phosphonate.

and diphenylphosphine in an undivided cell, using carbon and nickel electrodes as the anode and cathode, respectively, at a constant current for 4 h in the presence of cesium carbonate as a base. Various phenols, including those with electron-neutral, electron-donating, and electron-withdrawing groups, were efficiently converted into the target products in high yields. Phenols containing condensed aromatic and heterocyclic rings were also identified as suitable starting materials. The reaction proceeded via the anodic oxidation of diarylphosphines to diarylphosphine oxides, followed by further anodic oxidation to give phosphine oxide radicals. In the subsequent step treatment of alkoxide radicals (formed via the deprotonation of alcohols with cesium carbonate and anodic oxidation), the phosphine oxide radicals gave a corresponding phosphorylated products (Scheme 26).

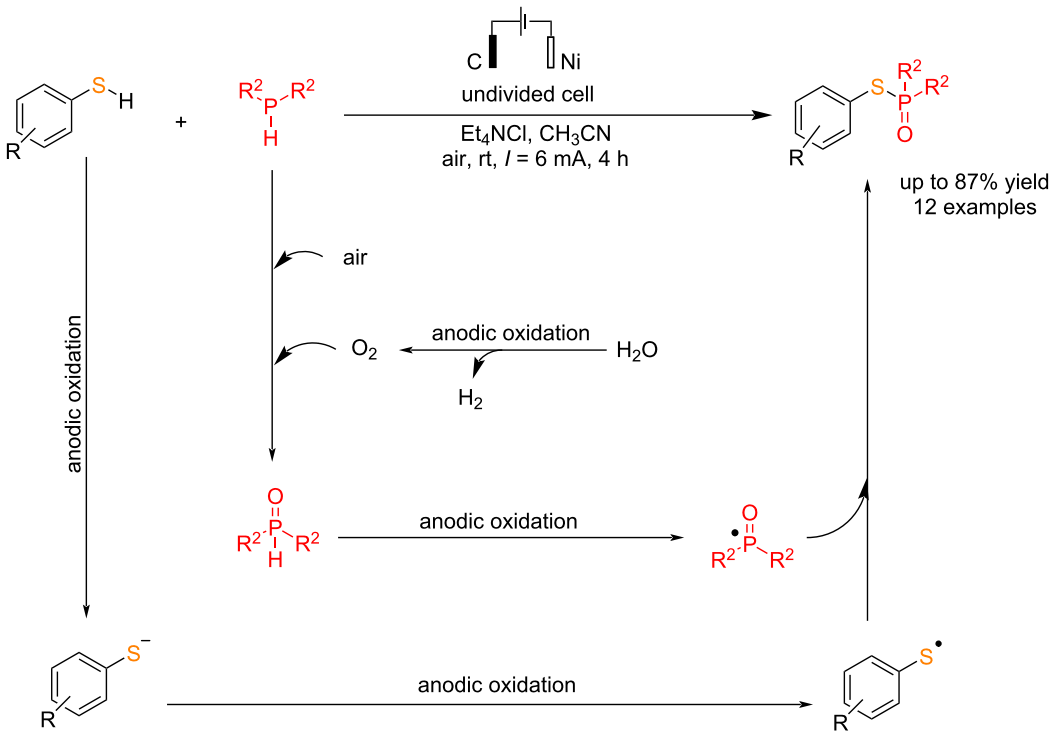
Electrochemical S–P bond formation

Phosphorothioates are essential compounds with broad applications in industry and medicine. Wang et al. [65] reported a novel electrochemical process for direct P–S coupling of thiols with dialkylphosphines. The reaction was carried out in an undivided cell using carbon and nickel electrodes as the anode and cathode in a constant current for 4 h. They have prepared various phosphorothioates in moderate to good yields. Methanol, as an environmentally friendly solvent, provided a satisfactory outcome. Changing the electric current intensity reduced the yield, and using dry acetonitrile also led to a significant decrease in yield. These results indicate that water undergoes decomposition in the reaction, generating oxygen as the primary oxygen source in the system. The reaction proceeded via the anodic oxidation of phosphines to phosphine oxides, followed by further anodic oxidation to give a phosphine oxide radical. In the subsequent step, treatment of the thiol radical (formed via the deprotonation of thiols with cesium carbonate and anodic oxidation) with the phosphine oxide radical gave the corresponding thiophosphorylated product (Scheme 27).

Recently, a novel and one-pot electrochemical oxidation method was reported for synthesizing *S*-(hetero)aryl phosphorothioates without using any oxidants or transition metals at room temperature [68]. The reaction was carried out in an undivided cell. The anode and cathode electrodes were graphite felt (GF) and platinum, respectively, at a constant current of 7 mA. When a platinum plate or a carbon rod was used instead of GF for the anode, and a nickel plate or copper plate was used for the cathode, the efficiency of the reaction decreased (Table 6). Although using other solvents improved the solubility, it reduced the reaction yield. Ammonium thiocyanate is used as a sulfur source in the presence of DBU as a base and n-Bu_4NBF_4 as an electrolyte. When electron-donating groups were present at the C2-benzene ring, the reaction yield was higher than when the



Scheme 26: Electrochemical P–O coupling of alcohols with diphenylphosphine.



Scheme 27: Electrochemical P–S coupling of thiols with dialkylphosphines.

rings contained electron-withdrawing groups. It is suggested that the reaction proceeded via single-electron oxidation of thiocyanate at the anode. DBU was used in the reaction for a simple nucleophilic substitution of phosphonate with a cyanide group in the formed intermediate (Scheme 28).

Table 6: Optimization studies.

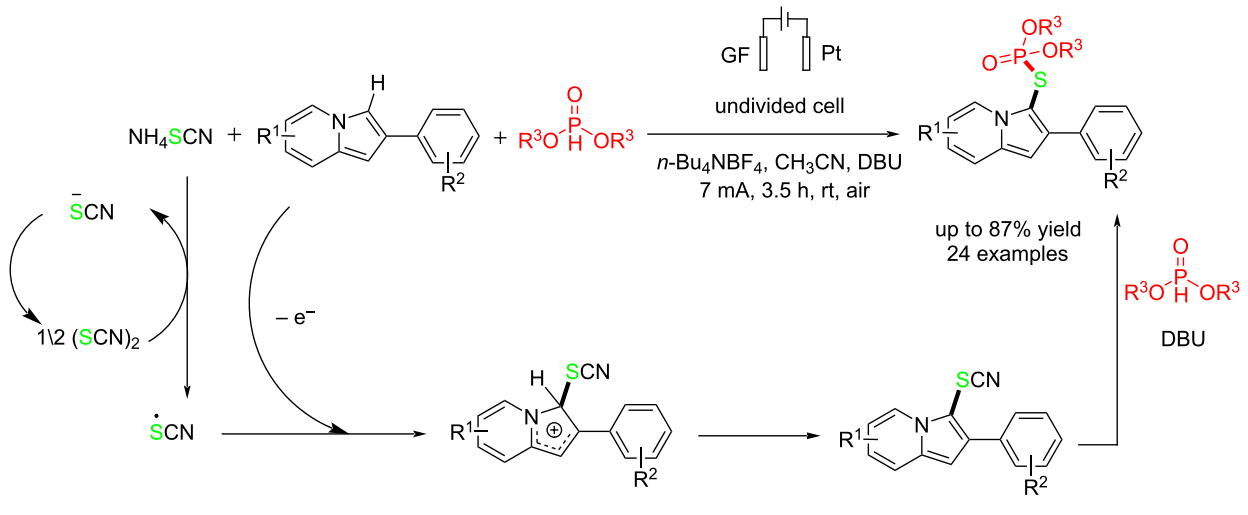
Variation from the standard conditions	Yield (%)
none	83
DMF as the solvent	36
without DBU	n.r.
Pt as the anode	78
C(rod) as the anode	69
Ni as the cathode	67
Cu as the cathode	56

In another study, Ding and co-workers [69] recently reported an electrochemical method for synthesizing *S*-heteroaryl phosphorothioates without using any transition metal catalysts and oxidants at 90 °C. This method is compatible with various functional groups and can be easily scaled up to a gram scale. The reaction was carried out in an undivided cell using platinum electrodes as the anode and cathode. In this method, S_8 was used as a sulfur source and ammonium iodide as a mediator, which has a key role. Based on the control experiments, a nucleophilic substitution is the main pathway for the reaction. The reaction proceeded with electrophilic iodination of aromatic compounds followed by a nucleophilic reaction of the formed phosphorothioate intermediate to give corresponding *S*-heteroaryl phosphorothioates in good to excellent yields (Scheme 29).

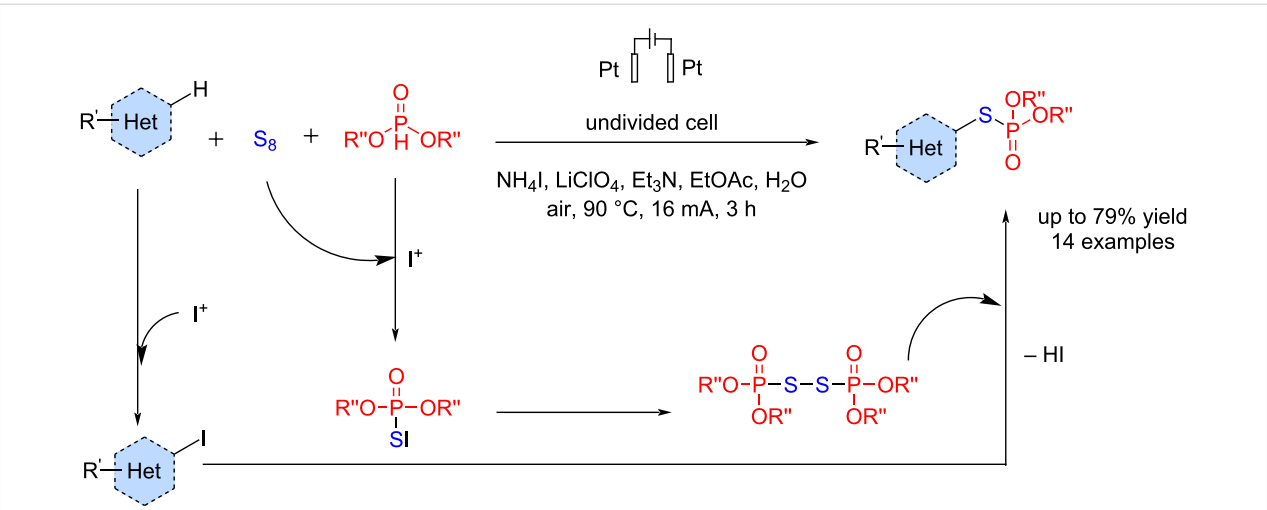
In 2023, Liu et al. [70] reported an interesting electrochemical process for the simultaneous C–H phosphorothiolation and S- to C-[1,4]-phosphoryl migration at room temperature. The reaction was carried out in an undivided cell using a carbon plate as the anode and platinum as the cathode at a constant current of 10 mA in the presence of KBr as a key mediator. Using a mixture of solvents, product **c** was obtained with a lower yield, and product **d**, which was formed via the 1,4-S → C phospho-Fries migration of product **c**, was also obtained in low yield (Table 7). By reducing the current to 5 mA, a mixture of products was obtained, and it also caused issues in the reaction system. The reaction proceeded via an anodic oxidation of bromide to bromine, followed by a reaction with sulfur and dialkylphosphite to give the corresponding dialkylphsophothioate. The reaction proceeded via an electrophilic aromatic substitution in the next step to provide the final product (Scheme 30). The experimental results showed that product **c** was initially formed and then continuously transformed into product **d** via the phospho-Fries rearrangement. This transformation was completed in the presence of Et_3N within 5 hours. Additionally, an excess of S_8 and $(EtO)_2P(O)H$ likely inhibits the occurrence of this rearrangement.

Electrochemical Se–P bond formation

In another study, Gu et al. [71] reported electrochemical P–Se bond formation of the reaction of elemental Se with diethyl phosphonate and aromatic compounds. In this method, potassium iodide acts as a key additive. The reaction is carried out in an undivided cell using graphite and platinum electrodes. Using



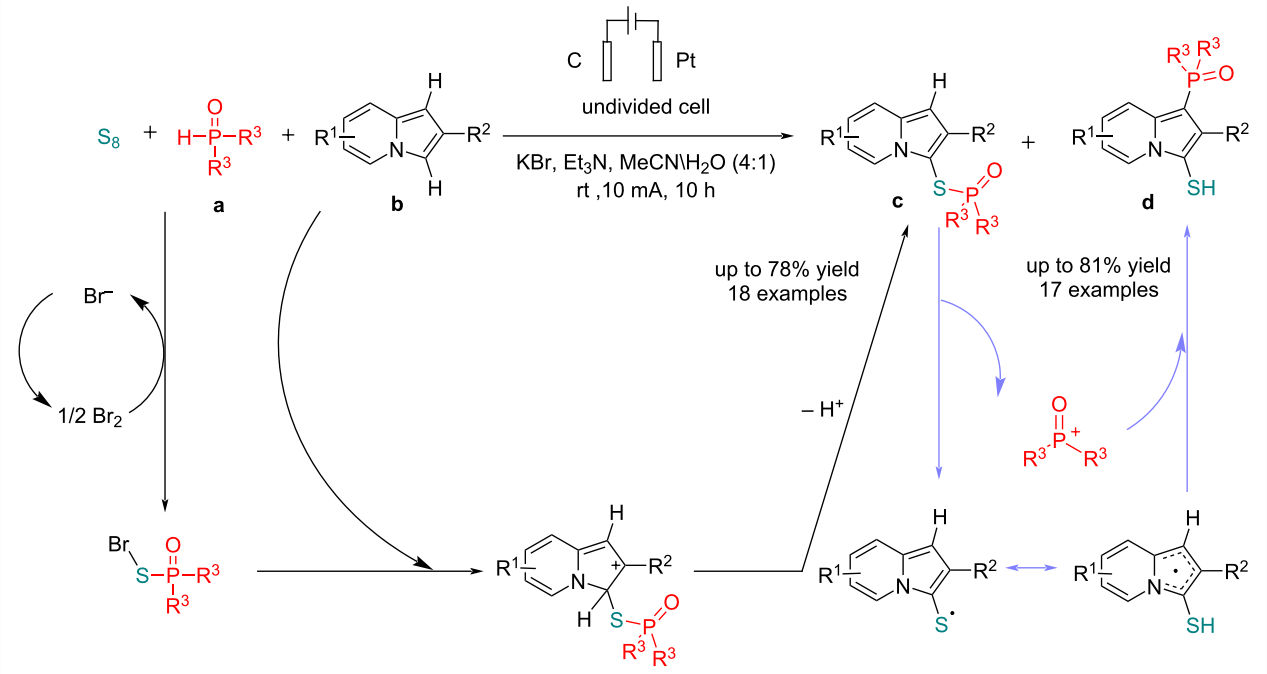
Scheme 28: Electrochemical thiophosphorylation of indolizines.



Scheme 29: Electrosynthesis of *S*-heteroaryl phosphorothioates.

Table 7: Optimization studies.

a/S_8/**b**/base	Variation from the standard conditions	Yield **c** (%)	Yield **d** (%)
1:2.2:2.2:2.2	none	78	–
1:2.2:2.2:2.2	MeOH/H_2O as the solvent	13	10
1:2.2:2.2:2.2	THF/H_2O as the solvent	20	16
1:2.2:2.2:2.2	constant current = 5 mA	27	30
1:1.1:1.1:1.1	none	–	81
1:1.1:1.1:1.1	constant current = 5 mA	25	47

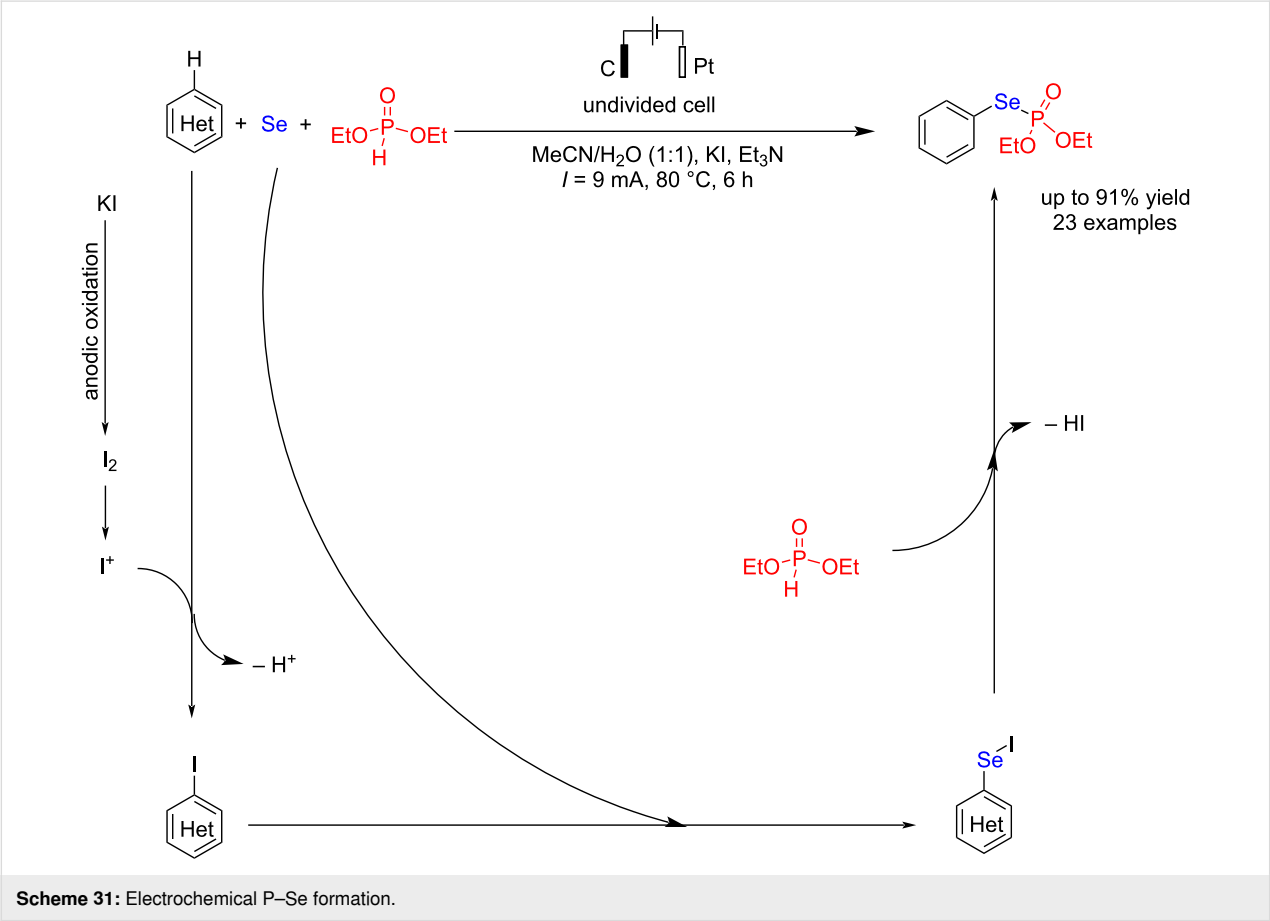


Scheme 30: Electrochemical phosphorylation reactions.

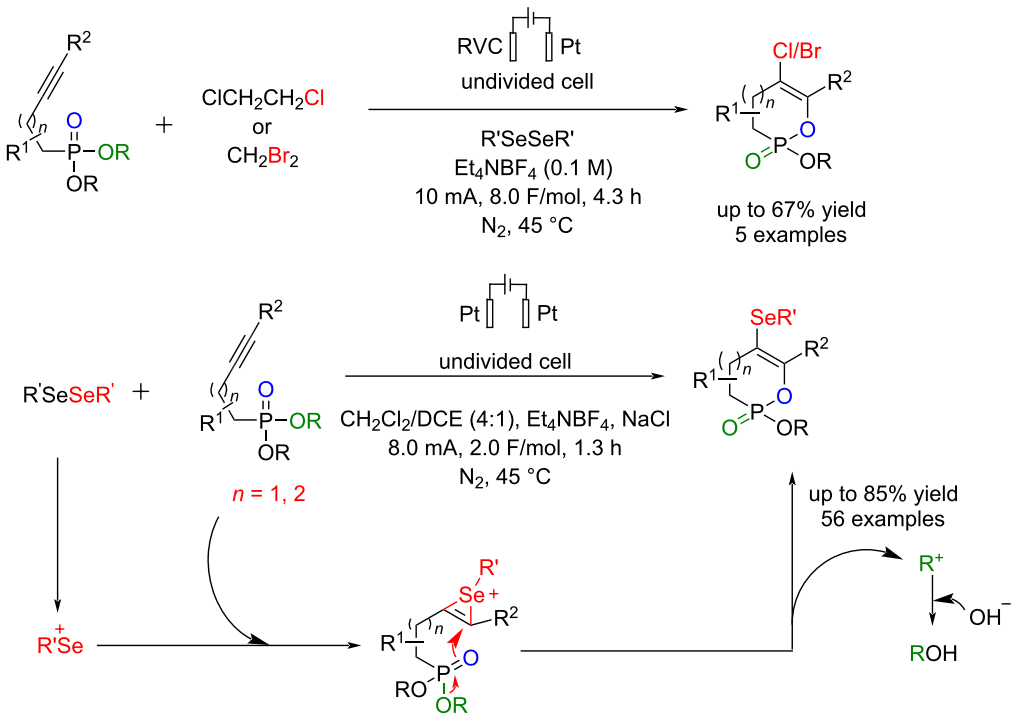
water as a co-solvent in the reaction was essential, as its absence led to a complete loss of efficiency. Lowering the reaction temperature and shortening the reaction time also reduced product yields. In this method, the target phosphoroselenoates were formed with moderate to high yields in the presence of electron-donating groups such as methyl (Me) and methoxy (OMe), as well as electron-withdrawing groups like fluorine (F), chlorine (Cl), bromine (Br), and nitro (NO_2) at the 5-position of the phenyl ring in indole. Studies showed that even unprotected anilines participated in this reaction, yielding the desired product with a 72% yield. Furthermore, anilines bearing electron-donating groups such as methyl or weak electron-withdrawing groups like chlorine at the *ortho* position were efficiently involved in the electrochemical phosphoroselenylation reaction, producing the corresponding products with satisfactory yields. These findings demonstrate this method's broad substrate scope and high functional group compatibility. The P–Se bond formation process proceeded by forming an aryl iodide intermediate via anodic oxidation of iodide to iodine, followed by the iodination reaction of aromatic compounds (Scheme 31). In the next step, elemental selenium was inserted into the aryl iodide bond to form the aryl iodoselenide intermediate for forming the P–Se bond.

Other electrochemical reactions of organophosphorus

Li et al. [72] reported an electrochemical synthesis method for the transition-metal-free cyclization and selenation/halogenation of alkynyl phosphonates at 45 °C under N_2. This method can chemoselectively convert these products into halogen-functionalized cyclic enol phosphonates. The reaction is carried out in an undivided cell using platinum plates as the anode and cathode at a constant current of 8 mA. In addition to serving as an electrolyte, NaCl will likely facilitate the formation of PhSeCl, an active species in this reaction. The reactions proceeded smoothly, regardless of electron-donating or electron-withdrawing groups in the phenyl rings' *ortho*, *meta*, or *para* positions. This method proceeded via an anodic oxidation, followed by intramolecular cyclization (Scheme 32). The key role of anodic oxidation became evident when the annulation product was isolated exclusively from the anode chamber. Based on cyclic voltammetry experiments, the effect of diphenyl diselenide on the oxidative cyclization process was determined, showing that this compound enables the reaction to occur at a significantly lower electrode potential compared to what is required for the direct anodic oxidation of alkynyl phosphonates.

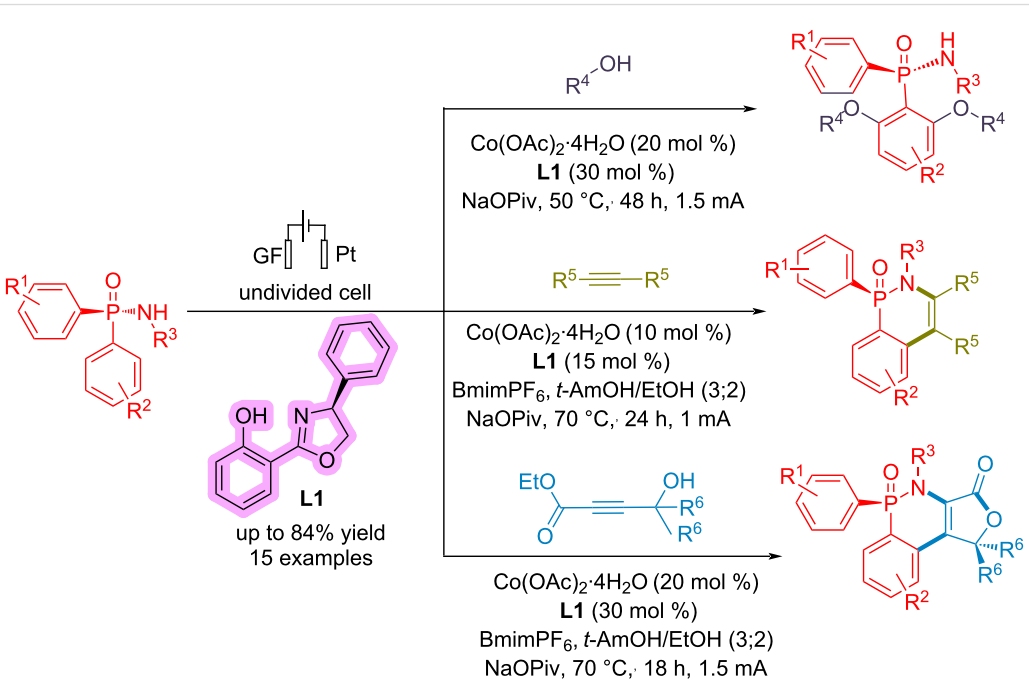


Scheme 31: Electrochemical P–Se formation.



Scheme 32: Electrochemical selenation/halogenation of alkynyl phosphonates.

von Münchow and co-workers [73] reported an electrochemical process for enantioselective aryl C–H bond activation in the presence of a cobalt catalyst. The reaction is carried out in an undivided cell using graphite felt (GF) as an anode and platinum as the cathode at a constant current of 1–1.5 mA (Scheme 33). They did not present any mechanism for the reaction; however, based on their control experiments, they have suggested that electricity is necessary for the reaction, which



Scheme 33: Electrochemical enantioselective aryl C–H bond activation.

makes the reductive elimination pathway easier, and Co undergoes oxidation state changes between Co(II), Co(III), and Co(IV).

Conclusion

Organophosphorous compounds are important materials with a wide range of applications in industry, agrochemicals, and drug design. Therefore, introducing new methods for the preparation of these compounds will remain an interesting research area in organic reactions. This review focuses on electrochemical methods for forming various phosphorus–carbon, phosphorus–nitrogen, phosphorus–oxygen, phosphorus–sulfur, and phosphorus–selenium bonds. The main goal of the electrosynthesis method is to introduce novel and green processes for synthesizing a wide range of organophosphorus compounds. Different types of electrodes were used, and graphite and platinum were the most used. Most of the reactions proceeded via an anodic oxidation of materials, followed by the reaction with other compounds to give the products.

Acknowledgements

The authors gratefully acknowledge support from the Institute for Advanced Studies in Basic Sciences (IASBS), Iran.

ORCID® iDs

Babak Kaboudin - https://orcid.org/0000-0003-0495-0006
Milad Behroozi - https://orcid.org/0000-0003-4151-9610

Data Availability Statement

Data sharing is not applicable as no new data was generated or analyzed in this study.

References

1. Lodh, J.; Paul, S.; Sun, H.; Song, L.; Schöfberger, W.; Roy, S. *Front. Chem. (Lausanne, Switz.)* **2023,** *10,* 956502. doi:10.3389/fchem.2022.956502
2. Leech, M. C.; Lam, K. *Nat. Rev. Chem.* **2022,** *6,* 275–286. doi:10.1038/s41570-022-00372-y
3. Ghosh, M.; Shinde, V. S.; Rueping, M. *Beilstein J. Org. Chem.* **2019,** *15,* 2710–2746. doi:10.3762/bjoc.15.264
4. Yan, M.; Kawamata, Y.; Baran, P. S. *Chem. Rev.* **2017,** *117,* 13230–13319. doi:10.1021/acs.chemrev.7b00397
5. Jiang, Y.; Xu, K.; Zeng, C. *Chem. Rev.* **2018,** *118,* 4485–4540. doi:10.1021/acs.chemrev.7b00271
6. Tang, S.; Liu, Y.; Lei, A. *Chem* **2018,** *4,* 27–45. doi:10.1016/j.chempr.2017.10.001
7. Jutand, A. *Chem. Rev.* **2008,** *108,* 2300–2347. doi:10.1021/cr068072h
8. Wiebe, A.; Gieshoff, T.; Möhle, S.; Rodrigo, E.; Zirbes, M.; Waldvogel, S. R. *Angew. Chem., Int. Ed.* **2018,** *57,* 5594–5619. doi:10.1002/anie.201711060
9. Kaboudin, B.; Behroozi, M.; Sadighi, S. *RSC Adv.* **2022,** *12,* 30466–30479. doi:10.1039/d2ra04087e
10. Wirtanen, T.; Rodrigo, E.; Waldvogel, S. R. *Adv. Synth. Catal.* **2020,** *362,* 2088–2101. doi:10.1002/adsc.202000349
11. Kaboudin, B.; Sadighi, S.; Varmaghani, F.; Behrouzi, L. *J. Electroanal. Chem.* **2024,** *974,* 118739. doi:10.1016/j.jelechem.2024.118739
12. Yuan, Y.; Lei, A. *Nat. Commun.* **2020,** *11,* 802. doi:10.1038/s41467-020-14322-z
13. Sbei, N.; Martins, G. M.; Shirinfar, B.; Ahmed, N. *Chem. Rec.* **2020,** *20,* 1530–1552. doi:10.1002/tcr.202000096
14. Ye, X.; Zhao, P.; Zhang, S.; Zhang, Y.; Wang, Q.; Shan, C.; Wojtas, L.; Guo, H.; Chen, H.; Shi, X. *Angew. Chem., Int. Ed.* **2019,** *58,* 17226–17230. doi:10.1002/anie.201909082
15. Xie, T.; Huang, J.; Li, J.; Peng, L.; Song, J.; Guo, C. *Nat. Commun.* **2023,** *14,* 6749. doi:10.1038/s41467-023-42603-w
16. Liang, H.; Julaiti, Y.; Zhao, C.-G.; Xie, J. *Nat. Synth.* **2023,** *2,* 338–347. doi:10.1038/s44160-022-00219-w
17. Malapit, C. A.; Prater, M. B.; Cabrera-Pardo, J. R.; Li, M.; Pham, T. D.; McFadden, T. P.; Blank, S.; Minteer, S. D. *Chem. Rev.* **2022,** *122,* 3180–3218. doi:10.1021/acs.chemrev.1c00614
18. Ackermann, L. *Acc. Chem. Res.* **2020,** *53,* 84–104. doi:10.1021/acs.accounts.9b00510
19. Li, N.; Sitdikov, R.; Kale, A. P.; Steverlynck, J.; Li, B.; Rueping, M. *Beilstein J. Org. Chem.* **2024,** *20,* 2500–2566. doi:10.3762/bjoc.20.214
20. Zhu, Y.; He, L.; Ni, Y.; Li, G.; Li, D.; Lin, W.; Wang, Q.; Li, L.; Yang, H. *Nanomaterials* **2022,** *12,* 2374. doi:10.3390/nano12142374
21. Yan, Z.; Ji, M.; Xia, J.; Zhu, H. *Adv. Energy Mater.* **2020,** *10,* 1902020. doi:10.1002/aenm.201902020
22. Adamek, J. *Molecules* **2023,** *28,* 4752. doi:10.3390/molecules28124752
23. Neog, K.; Gogoi, P. *Org. Biomol. Chem.* **2020,** *18,* 9549–9561. doi:10.1039/d0ob01988g
24. Yakhvarov, D. G.; Gorbachuk, E. V.; Kagirov, R. M.; Sinyashin, O. G. *Russ. Chem. Bull.* **2012,** *61,* 1300–1312. doi:10.1007/s11172-012-0176-5
25. Budnikova, Y. H.; Dolengovsky, E. L.; Tarasov, M. V.; Gryaznova, T. V. *Front. Chem. (Lausanne, Switz.)* **2022,** *10,* 1054116. doi:10.3389/fchem.2022.1054116
26. Sbei, N.; Martins, G. M.; Shirinfar, B.; Ahmed, N. *Chem. Rec.* **2020,** *20,* 1530–1552. doi:10.1002/tcr.202000096
27. Kaboudin, B.; Daliri, P.; Faghih, S.; Esfandiari, H. *Front. Chem. (Lausanne, Switz.)* **2022,** *10,* 890696. doi:10.3389/fchem.2022.890696
28. Oeser, P.; Tobrman, T. *Molecules* **2024,** *29,* 1593. doi:10.3390/molecules29071593
29. Malysheva, S. F.; Kuimov, V. A.; Arbuzova, S. N. *Russ. J. Gen. Chem.* **2023,** *93* (Suppl. 1), S238–S255. doi:10.1134/s1070363223140293
30. Turhanen, P. A.; Kafarski, P. *Front. Chem. (Lausanne, Switz.)* **2022,** *10,* 1054145. doi:10.3389/fchem.2022.1054145
31. Le Corre, S. S.; Berchel, M.; Couthon-Gourvès, H.; Haelters, J.-P.; Jaffrès, P.-A. *Beilstein J. Org. Chem.* **2014,** *10,* 1166–1196. doi:10.3762/bjoc.10.117
32. Kaboudin, B.; Faghih, S.; Alavi, S.; Naimi-Jamal, M. R.; Fattahi, A. *Synthesis* **2023,** *55,* 121–130. doi:10.1055/a-1941-1242
33. Ye, J.-J.; Yan, B.-X.; Wang, J.-P.; Wen, J.-H.; Zhang, Y.; Qiu, M.-R.; Li, Q.; Zhao, C.-Q. *Org. Chem. Front.* **2020,** *7,* 2063–2068. doi:10.1039/d0qo00453g
34. Kaboudin, B.; Ghashghaee, M.; Fukaya, H.; Yanai, H. *Chem. Commun.* **2023,** *59,* 7076–7079. doi:10.1039/d3cc01669b
35. Berlicki, L.; Rudziska, E.; Mlynarza, P.; Kafarski, P. *Curr. Org. Chem.* **2006,** *10,* 2285–2306. doi:10.2174/138527206778992699
36. Luo, K.; Yang, W.-C.; Wu, L. *Asian J. Org. Chem.* **2017,** *6,* 350–367. doi:10.1002/ajoc.201600512

37. Jasiak, A.; Mielniczak, G.; Owsianik, K.; Koprowski, M.; Krasowska, D.; Drabowicz, J. *J. Org. Chem.* **2019,** *84,* 2619–2625. doi:10.1021/acs.joc.8b03053
38. Smith, C. J.; Smith, C. D.; Nikbin, N.; Ley, S. V.; Baxendale, I. R. *Org. Biomol. Chem.* **2011,** *9,* 1927–1937. doi:10.1039/c0ob00813c
39. Kaboudin, B.; Alipour, S. *Tetrahedron Lett.* **2009,** *50,* 4243–4245. doi:10.1016/j.tetlet.2009.05.016
40. Keglevich, G. *Molecules* **2021,** *26,* 1196. doi:10.3390/molecules26041196
41. Mustafa, D.; Overhulse, J. M.; Kashemirov, B. A.; McKenna, C. E. *Molecules* **2023,** *28,* 3497. doi:10.3390/molecules28083497
42. Keglevich, G.; Grun, A.; Balint, E.; Zsuzsa Kiss, N.; Jablonkai, E. *Curr. Org. Chem.* **2013,** *17,* 545–554. doi:10.2174/1385272811317050009
43. Kargin, Y. M.; Budnikova, Y. G. *Russ. J. Gen. Chem.* **2001,** *71,* 1393–1421. doi:10.1023/a:1013906019685
44. Heard, D. M.; Lennox, A. J. J. *Angew. Chem., Int. Ed.* **2020,** *59,* 18866–18884. doi:10.1002/anie.202005745
45. Fu, K.; Jiang, J.; Zhao, Q.; Wang, N.; Kong, W.; Yu, Y.; Xie, H.; Li, T. *Org. Biomol. Chem.* **2023,** *21,* 1662–1666. doi:10.1039/d2ob01849g
46. Wang, R.; Wang, J.; Zhang, Y.; Wang, B.; Xia, Y.; Xue, F.; Jin, W.; Liu, C. *Adv. Synth. Catal.* **2023,** *365,* 900–905. doi:10.1002/adsc.202201198
47. Zeng, L.; Jiao, Y.; Yan, W.; Wu, Y.; Wang, S.; Wang, P.; Wang, D.; Yang, Q.; Wang, J.; Zhang, H.; Lei, A. *Nat. Synth.* **2023,** *2,* 172–181. doi:10.1038/s44160-022-00197-z
48. Mo, K.; Zhou, X.; Wang, J.; Wu, J.; Zhao, Y. *Org. Lett.* **2023,** *25,* 3956–3960. doi:10.1021/acs.orglett.3c01368
49. Zheng, H.; Liu, C.-H.; Guo, S.-Y.; He, G.-C.; Min, X.-T.; Zhou, B.-C.; Ji, D.-W.; Hu, Y.-C.; Chen, Q.-A. *Nat. Commun.* **2022,** *13,* 3496. doi:10.1038/s41467-022-31178-7
50. Gryaznova, T. V.; Nikanshina, E. O.; Fayzullin, R. R.; Islamov, D. R.; Tarasov, M. V.; Kholin, K. V.; Budnikova, Y. H. *Electrochim. Acta* **2022,** *428,* 140946. doi:10.1016/j.electacta.2022.140946
51. Zhang, S.-K.; Del Vecchio, A.; Kuniyil, R.; Messinis, A. M.; Lin, Z.; Ackermann, L. *Chem* **2021,** *7,* 1379–1392. doi:10.1016/j.chempr.2021.04.009
52. Long, H.; Huang, C.; Zheng, Y.-T.; Li, Z.-Y.; Jie, L.-H.; Song, J.; Zhu, S.; Xu, H.-C. *Nat. Commun.* **2021,** *12,* 6629. doi:10.1038/s41467-021-26960-y
53. Wang, S.; Xue, Q.; Guan, Z.; Ye, Y.; Lei, A. *ACS Catal.* **2021,** *11,* 4295–4300. doi:10.1021/acscatal.1c00549
54. Zhu, P.-W.; Yang, Y.-T.; Li, Y.; Zhu, J.; Wu, L. *Mol. Catal.* **2022,** *517,* 112022. doi:10.1016/j.mcat.2021.112022
55. Deng, Y.; You, S.; Ruan, M.; Wang, Y.; Chen, Z.; Yang, G.; Gao, M. *Adv. Synth. Catal.* **2021,** *363,* 464–469. doi:10.1002/adsc.202000997
56. Ollivier, A.; Sengmany, S.; Rey, M.; Martens, T.; Léonel, E. *Synlett* **2020,** *31,* 1191–1196. doi:10.1055/s-0039-1690899
57. Daili, F.; Ouarti, A.; Pinaud, M.; Kribii, I.; Sengmany, S.; Le Gall, E.; Léonel, E. *Eur. J. Org. Chem.* **2020,** 3452–3455. doi:10.1002/ejoc.202000422
58. Gryaznova, T. V.; Khrizanforov, M. N.; Levitskaya, A. I.; Rizvanov, I. K.; Balakina, M. Yu.; Ivshin, K. A.; Kataeva, O. N.; Budnikova, Y. H. *Organometallics* **2020,** *39,* 2446–2454. doi:10.1021/acs.organomet.0c00247
59. Zhou, X.; Wang, J.; Shen, Y.; Ma, D.; Zhao, Y.; Wu, J. *J. Org. Chem.* **2023,** *88,* 17521–17526. doi:10.1021/acs.joc.3c02017
60. Ma, Y.; Zhang, X.; Ma, C.; Xia, W.; Hu, L.; Dong, X.; Xiong, Y. *J. Org. Chem.* **2023,** *88,* 4264–4272. doi:10.1021/acs.joc.2c02826
61. Zhang, T.; Cai, M.; Zhao, W.; Liu, M.; Jiang, N.; Ge, Q.; Cong, H. *Green Chem.* **2023,** *25,* 1351–1355. doi:10.1039/d2gc04569a
62. Wang, J.; Zhang, Z.; Shen, Y.; Zhao, Y.; Wu, J. *Org. Lett.* **2024,** *26,* 4700–4704. doi:10.1021/acs.orglett.4c01471
63. Zhu, L.; Zhu, P.-W.; Hu, L.-Y.; Lin, S.-Y.; Wu, L.; Zhu, J. *J. Org. Chem.* **2024,** *89,* 10796–10804. doi:10.1021/acs.joc.4c01023
64. Zhong, Z.; Xu, P.; Zhou, A. *Org. Biomol. Chem.* **2021,** *19,* 5342–5347. doi:10.1039/d1ob00779c
65. Wang, R.; Dong, X.; Zhang, Y.; Wang, B.; Xia, Y.; Abdukader, A.; Xue, F.; Jin, W.; Liu, C. *Chem. – Eur. J.* **2021,** *27,* 14931–14935. doi:10.1002/chem.202102262
66. Dong, X.; Wang, R.; Jin, W.; Liu, C. *Org. Lett.* **2020,** *22,* 3062–3066. doi:10.1021/acs.orglett.0c00814
67. Mdluli, V.; Lehnherr, D.; Lam, Y.-h.; Chaudhry, M. T.; Newman, J. A.; DaSilva, J. O.; Regalado, E. L. *Chem. Sci.* **2024,** *15,* 5980–5992. doi:10.1039/d3sc05357a
68. Feng, C.; Wang, H.; She, Y.; Li, M.; Shen, Z. *Tetrahedron* **2024,** *155,* 133911. doi:10.1016/j.tet.2024.133911
69. Ding, S.; Zhang, C.; Zhao, Z.; He, L.; Li, X.; Li, G.; Gu, L. *Tetrahedron* **2024,** *163,* 134131. doi:10.1016/j.tet.2024.134131
70. Liu, X.; Jiang, W.; Huang, C.; Ma, S.; Wang, Q.; Cao, H. *Org. Chem. Front.* **2023,** *10,* 5198–5204. doi:10.1039/d3qo01042b
71. Zhang, C.; Zhou, Y.; Zhao, Z.; Xue, W.; Gu, L. *Chem. Commun.* **2022,** *58,* 13951–13954. doi:10.1039/d2cc05570h
72. Li, B.; Zhou, Y.; Xu, Y.; Li, X.; Li, Z.; Gu, L.; Ma, W.; Mei, R. *J. Org. Chem.* **2023,** *88,* 15414–15427. doi:10.1021/acs.joc.3c01946
73. von Münchow, T.; Dana, S.; Xu, Y.; Yuan, B.; Ackermann, L. *Science* **2023,** *379,* 1036–1042. doi:10.1126/science.adg2866

License and Terms

This is an open access article licensed under the terms of the Beilstein-Institut Open Access License Agreement (https://www.beilstein-journals.org/bjoc/terms), which is identical to the Creative Commons Attribution 4.0 International License (https://creativecommons.org/licenses/by/4.0). The reuse of material under this license requires that the author(s), source and license are credited. Third-party material in this article could be subject to other licenses (typically indicated in the credit line), and in this case, users are required to obtain permission from the license holder to reuse the material.

The definitive version of this article is the electronic one which can be found at: https://doi.org/10.3762/bjoc.21.61

BEILSTEIN JOURNAL OF ORGANIC CHEMISTRY

Chitosan-supported CuI-catalyzed cascade reaction of 2-halobenzoic acids and amidines for the synthesis of quinazolinones

Xuhong Zhao, Weishuang Li*, Mengli Yang, Bojie Li, Yaoyao Zhang, Lizhen Huang* and Lei Zhu*

Full Research Paper

Open Access

Address:
School of Chemistry and Materials Science, Hubei Provincial Engineering Research Center of Key Technologies in Modern Paper and Hygiene Products Manufacturing, Hubei Engineering University, Xiaogan 432000, China

Email:
Weishuang Li* - liweishuang706@hbeu.edu.cn; Lizhen Huang* - hlizhen@hbeu.edu.cn; Lei Zhu* - Lei.zhu@hbeu.edu.cn

* Corresponding author

Keywords:
chitosan-supported CuI catalyst; cyclization reaction; mild conditions; quinazolinone

Beilstein J. Org. Chem. **2025,** *21,* 839–844.
https://doi.org/10.3762/bjoc.21.67

Received: 15 November 2024
Accepted: 15 April 2025
Published: 28 April 2025

This article is part of the thematic issue "Green chemistry III".

Associate Editor: L. Vaccaro



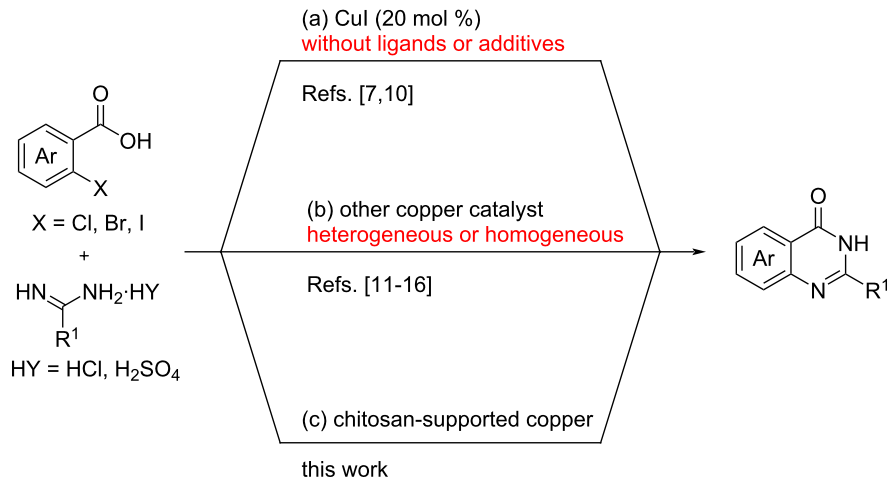
© 2025 Zhao et al.; licensee Beilstein-Institut.
License and terms: see end of document.

Abstract

A chitosan-supported CuI (CS@CuI) catalyst was developed for the synthesis of quinazolinones from 2-halobenzoic acids (including iodine and bromine) and amidines. The reaction proceeds under mild reaction conditions, demonstrating a broad substrate scope (30 examples) and good catalytic efficiency (up to 99% yield).

Introduction

Quinazolinones are not only a key core of nitrogen-containing benzo heterocyclic compounds found in many natural products and bioactive molecules [1-3], but can also be readily converted into other functional compounds under specific conditions [4,5]. Due to their significant biological relevance and potential applications, numerous synthetic methods have been recently developed to synthesize these useful intermediates [6-9]. Among these methods, the cascade reaction between *ortho*-halogen (e.g., chlorine, bromine or iodine) substituted benzoic acids and amidines has become a prominent route to synthesize the corresponding quinazolinones [10-18]. In 2009, Fu and co-workers found that copper(I) could effectively promote this cascade reaction for the synthesis of quinazolinones without the need for additional ligands or additives (Scheme 1a) [7,10]. Since then, various copper-based catalysts, both homogeneous and heterogeneous, have been explored (Scheme 1b) [11-16]. For example, Wang's group developed a magnetically recoverable and reusable Fe_3O_4 nanoparticle-supported copper(I) catalyst with excellent catalytic efficiency for quinazolinone synthesis [11]. In addition, Cai et al. reported that



Scheme 1: Copper-catalyzed cascade reaction of 2-halobenzoic acids and amidines for the synthesis of quinazolinones.

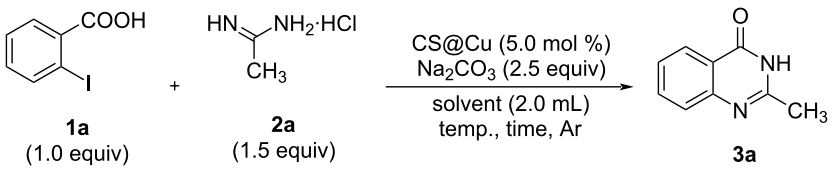
MCM-41-immobilized tridentate nitrogen-supported copper(I) [MCM-41-3N–CuI] served as a highly efficient, reusable heterogeneous catalyst for this cascade reaction, achieving good to excellent yields without any loss of activity even after ten cycles of simple filtration-based recovery [12]. Moreover, a copper catalyst has been shown to function effectively in both organic and aqueous media [13,14]. Furthermore, dicopper(I) complexes can also be used as an effective catalyst in Ullmann-type *N*-arylation/cyclization of 2-bromobenzoic acids with amidines, providing the corresponding quinazolinones in good yields [15]. Despite the high efficiency of the above-mentioned copper catalysts in the synthesis of quinazolinones, and the wide application of the chitosan-supported copper catalyst in various organic transformations [19-21], the use of chitosan-supported copper for quinazolinone synthesis has not been reported. As part of our ongoing research interest in chitosan and chitosan-supported copper catalysts in organic transformations [22-24], we intended to investigate the use of chitosan-supported copper as a catalyst for the synthesis of quinazolinones from 2-halobenzoic acids and amidines under mild reaction conditions (Scheme 1c).

Results and Discussion

The initial reactions commenced with 2-iodobenzoic acid (**1a**, 0.5 mmol, 1.0 equiv) and acetamidine hydrochloride (**2a**, 0.75 mmol, 1.5 equiv) as model substrates, Na_2CO_3 (1.25 mmol, 2.5 equiv) as a base, and chitosan-supported copper (5.0 mol %) as the catalyst under an argon atmosphere (Table 1). First, various solvents were investigated. When nonprotonated solvents such as THF and toluene were used, the yields were relatively low (Table 1, entries 1 and 2, 39 and 27% yields), indicating poor catalytic activity in these solvents. In contrast, using proton solvents (MeOH, iPrOH and H_2O) led to improved yields (Table 1, entries 3–5, 51–60% yields). Notably, the reaction was also successful in water, affording the target product in moderate yield (Table 1, entry 5, 51% yield). Next, to further improve the yield, a mixed solvent of iPrOH and H_2O was examined. The reaction conducted with a solvent ratio of iPrOH/H_2O = 4:1 gave an 83% yield (Table 1, entry 6), while a ratio of iPrOH/H_2O = 9:1 resulted in an 89% yield (Table 1, entry 7). In the optimal solvent (iPrOH/H_2O = 9:1), other chitosan-supported copper catalysts, such as chitosan-supported on CuBr (CS@CuBr), chitosan-supported on $Cu(OAc)_2$ (CS@$Cu(OAc)_2$), chitosan-supported on $Cu(acac)_2$ (CS@$Cu(acac)_2$) and chitosan-supported on $CuSO_4$ (CS@$CuSO_4$) were explored, and the results showed that CS@CuI was the most effective catalyst (Table 1, entries 7–11, 65–89% yields). To further enhance the reaction yield, the reaction temperature was increased to 90 °C, and the target product **3a** was obtained in 96% isolated yield (Table 1, entry 12). Control experiments indicated poor results when no catalyst was used, with the corresponding product obtained only in 31% yield (Table 1, entry 13). When CuI or chitosan alone was used as a catalyst, the reaction occurred but with less efficiency (Table 1, entries 14 and 15, 80 and 40% yields). In addition, when the reaction time was reduced, the yields decreased accordingly (Table 1, entries 16–18, 70–94% yields). Finally, when the reaction was carried out under open air, the catalytic activity decreased and only 45% yield of the target product was obtained (Table 1, entry 19).

With the optimized conditions in hand, we explored the substrate scope of the CS@CuI-catalyzed cascade reactions of 2-halobenzoic acids (including 2-iodobenzoic acid and 2-bromobenzoic acid) with amidines (Scheme 2). Initially, when the amidine substituent (R^2) is a methyl group, we inves-

Table 1: Optimization of reaction conditions[a].



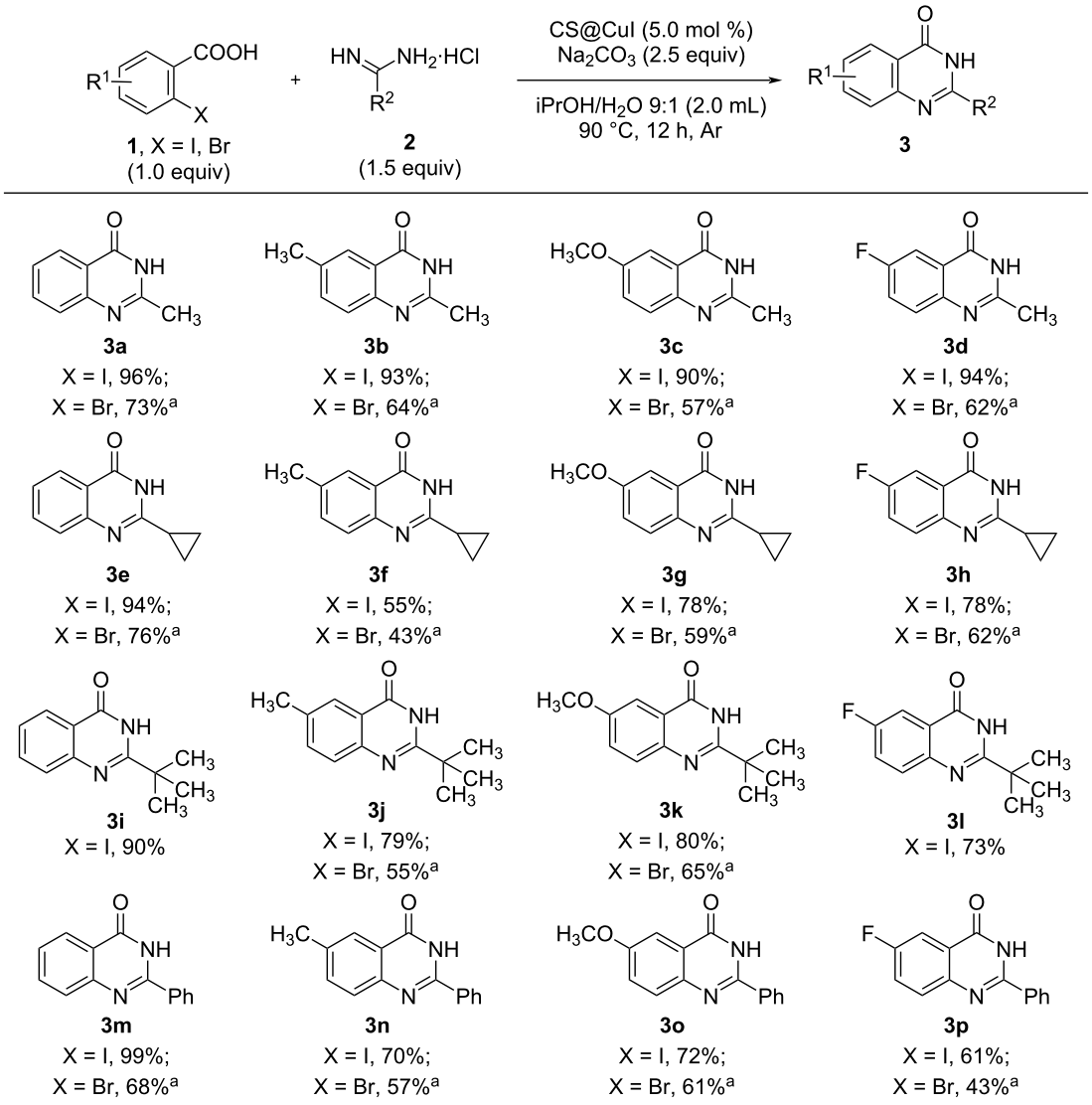
1a (1.0 equiv) + **2a** (1.5 equiv) → **3a**

Entry	CS@Cu	Solvent	Temp. (°C)	Time (h)	Yield (%)[b]
1	CS@CuI	THF	80	12	39
2	CS@CuI	toluene	80	12	27
3	CS@CuI	MeOH	80	12	55
4	CS@CuI	iPrOH	80	12	60
5	CS@CuI	H_2O	80	12	51
6	CS@CuI	iPrOH/H_2O (4:1)	80	12	83
7	CS@CuI	iPrOH/H_2O (9:1)	80	12	89
8	CS@CuBr	iPrOH/H_2O (9:1)	80	12	87
9	CS@Cu(OAc)$_2$	iPrOH/H_2O (9:1)	80	12	65
10	CS@Cu(acac)$_2$	iPrOH/H_2O (9:1)	80	12	65
11	CS@$CuSO_4$	iPrOH/H_2O (9:1)	80	12	67
12	**CS@CuI**	**iPrOH/H_2O (9:1)**	**90**	**12**	**99 (96)[c]**
13	–	iPrOH/H_2O (9:1)	90	12	31
14	CuI	iPrOH/H_2O (9:1)	90	12	80
15	CS	iPrOH/H_2O (9:1)	90	12	40
16	CS@CuI	iPrOH/H_2O (9:1)	90	8	94
17	CS@CuI	iPrOH/H_2O (9:1)	90	5	83
18	CS@CuI	iPrOH/H_2O (9:1)	90	3	70
19[d]	CS@CuI	iPrOH/H_2O (9:1)	90	12	45

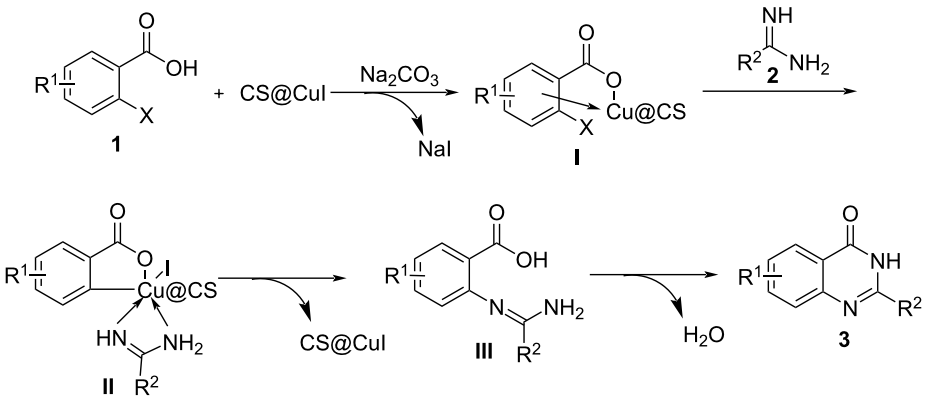
[a]Reaction conditions: **1a** (0.5 mmol, 1.0 equiv), acetamidine hydrochloride **2a** (0.75 mmol, 1.5 equiv), CS@Cu (5.0 mol %), Na_2CO_3 (1.25 mmol, 2.5 equiv), solvent (2.0 mL) at argon atmosphere. [b]The yield was determined by ^{1}H NMR analysis with dibromomethane as an internal standard. [c]Isolated yield in parentheses. [d]The reaction was performed under open air.

tigated the reactions with various substituted 2-halobenzoic acids. The reactivity of 2-iodobenzoic acid derivatives (**3a**–**d**, 90−96% yields) was higher than that of 2-bromobenzoic acid derivatives (**3a**–**d**, 57−73% yields), the electronic properties of the substituents on the benzene ring had little effect on the reactivity. When the amidine substituent (R^2) was changed to a cyclopropyl group, the yields of all reaction decreased, especially when substituents were present on the benzene ring (**3e**–**h**, 55−94% yields for 2-iodobenzoic acid, 43–76% yields for 2-bromobenzoic acid). We then investigated the reactions of different 2-halobenzoic acid derivatives with amidines where R^2 was a *tert*-butyl group. The results showed that 2-bromobenzoic acid derivatives (**3j**–**k**, 55−65% yields) displayed lower activity compared to 2-iodobenzoic acid derivatives (**3i**–**l**, 73−90% yields), with a decrease in reaction activity observed when substituents were presented on the benzene ring. Finally, we examined reactions with 2-halobenzoic acid derivatives where the R^2 substituent was a phenyl group. In this case, the reactivity of 2-iodobenzoic acid derivatives (**3m**–**p**, 61–99% yields) was again superior to that of 2-bromobenzoic acid derivatives (**3m**−**3p**, 43−68% yields). The reactivity of 2-halobenzoic acid without substituents was obviously better than that of substituted derivatives. Overall, these results demonstrate that the reaction has a broad substrate scope, with 2-iodobenzoic acid derivatives showing higher reactivity than 2-bromobenzoic acid derivatives.

Based on previously reported literature [7,13], a mechanism for the copper-catalyzed formation of quinazolinones is proposed in Scheme 3. Initially, the 2-halobenzoic acid **1** coordinates with CS@CuI to form intermediate **I** in the presence of Na_2CO_3, which acts as a base. Subsequently, **I** undergoes oxidative addition and complexation with the amidine **2** to generate intermediate **II**. This intermediate then undergoes reductive elimination to form intermediate **III**, releasing CS@CuI back into the system. Finally, the coupling reaction between the carboxyl and amino groups in **III** yields the target quinazolinone **3**.



Scheme 2: Substrate scope. Reaction conditions: **1** (0.5 mmol, 1.0 equiv), amidines hydrochloride **2** (0.75 mmol, 1.5 equiv), CS@CuI (10.0 mg, ICP: 14.6%, 5.0 mol %), Na_2CO_3 (1.25 mmol, 2.5 equiv), iPrOH/H_2O 9:1 (2.0 mL), 90 °C, 12 h, argon atmosphere; [a]**1** (0.2 mmol), amidine hydrochloride **2** (0.3 mmol, 1.5 equiv), CS@CuI (5.0 mol %), Na_2CO_3 (1.25 mmol, 2.5 equiv), iPrOH/H_2O 9:1 (2.0 mL), 90 °C, 12 h, argon atmosphere.



Scheme 3: Proposed mechanism for the CS@CuI-catalyzed synthesis of quinazolinones.

To demonstrate the practicality of this reaction in organic synthesis, the reaction was scaled up to the gram level. For instance, the desired product **3a** was obtained in 91% yield (1.45 g) when the reaction was conducted on a 10.0 mmol scale under optimized conditions (Scheme 4a). The recyclability of heterogeneous catalysts is a critical factor in assessing their practical utility in transition metal-catalyzed reactions. Therefore, the recyclability of CS@CuI was evaluated in the reaction of 2-iodobenzoic acid (**1a**) with **2a**, as illustrated in Scheme 4b. In each cycle, the recovered CS@CuI was simply centrifuged, filtered, washed, dried, and then reused with fresh substrate under the optimized conditions. The results demonstrate that the catalyst retains good catalytic activity (yields no less than 86%) even after six cycles, and ICP analysis of the filtered aqueous solution after the reaction confirmed no detectable leaching of CuI.

Conclusion

In summary, we have developed a CS@CuI-catalyzed cascade reaction of 2-halobenzoic acids (including iodine and bromine derivatives) and amidines for the synthesis of quinazolinones. This approach features mild reaction conditions, broad substrate scope (30 examples), and high efficiency (up to 99% yield). In a word, this work presents a novel and efficient protocol for the construction of quinazolinones and offers significant research value.

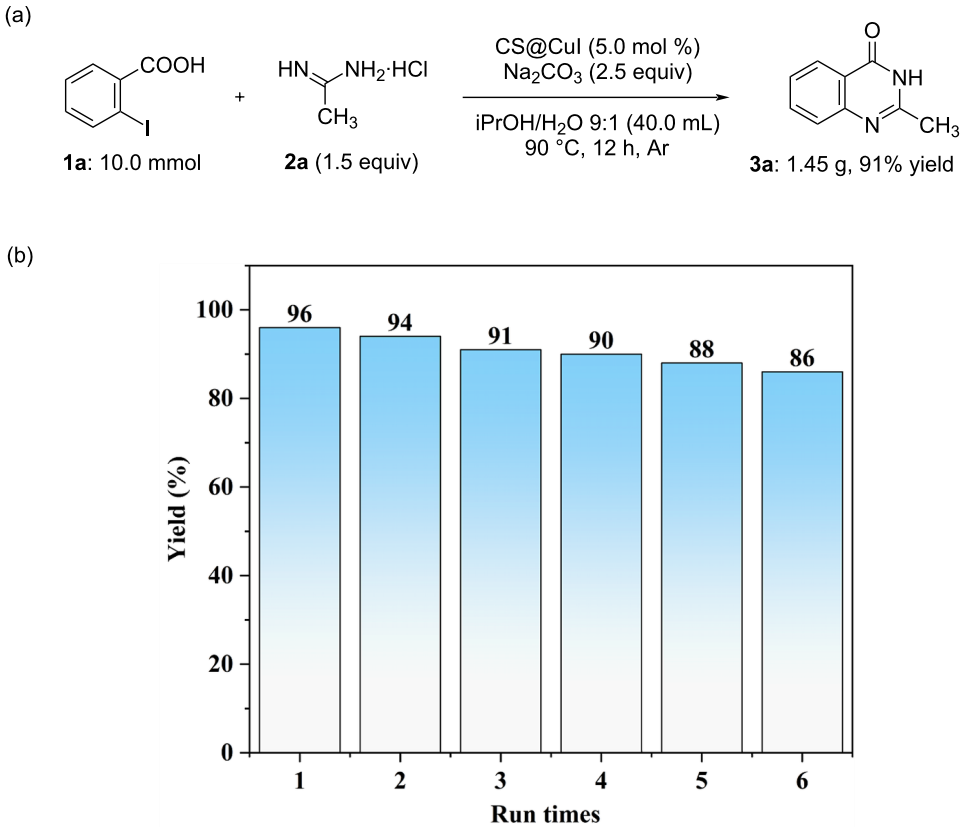
Supporting Information

Supporting Information File 1

Full experimental details, characterization data and copies of NMR spectra of all products.
[https://www.beilstein-journals.org/bjoc/content/supplementary/1860-5397-21-67-S1.pdf]

Funding

This work was financially supported by Project of Science and Technology Research of Hubei Provincial Department of Education (Q20232704, Q20222707), Hubei Provincial Natural Science Foundation of China (2022CFB547, 2023AFA108), Ningxia Hui Autonomous Region Natural Science Foundation of China (2024AAC03316).



Scheme 4: Scaling-up experiment (a) and recyclability of CS@CuI (b).

ORCID® iDs

Lei Zhu - https://orcid.org/0000-0003-4399-1855

Data Availability Statement

All data that supports the findings of this study is available in the published article and/or the supporting information of this article.

Preprint

A non-peer-reviewed version of this article has been previously published as a preprint: https://doi.org/10.3762/bxiv.2024.66.v1

References

1. Szpyrka, E.; Walorczyk, S. *Food Chem.* **2013,** *141,* 3525–3530. doi:10.1016/j.foodchem.2013.06.055
2. Esteve-Turrillas, F. A.; Mercader, J. V.; Parra, J.; Agulló, C.; Abad-Somovilla, A.; Abad-Fuentes, A. *PLoS One* **2015,** *10,* e0134042. doi:10.1371/journal.pone.0134042
3. Lamb, J.; Fischer, E.; Rosillo-Lopez, M.; Salzmann, C. G.; Holland, J. P. *Chem. Sci.* **2019,** *10,* 8880–8888. doi:10.1039/c9sc03736e
4. Chandrika, P. M.; Yakaiah, T.; Rao, A. R. R.; Narsaiah, B.; Reddy, N. C.; Sridhar, V.; Rao, J. V. *Eur. J. Med. Chem.* **2008,** *43,* 846–852. doi:10.1016/j.ejmech.2007.06.010
5. Pang, B.; Wang, Y.; Hao, L.; Wu, G.; Ma, Z.; Ji, Y. *J. Org. Chem.* **2023,** *88,* 143–153. doi:10.1021/acs.joc.2c02006
6. Zhong, J.-J.; To, W.-P.; Liu, Y.; Lu, W.; Che, C.-M. *Chem. Sci.* **2019,** *10,* 4883–4889. doi:10.1039/c8sc05600e
7. Liu, X.; Fu, H.; Jiang, Y.; Zhao, Y. *Angew. Chem., Int. Ed.* **2009,** *48,* 348–351. doi:10.1002/anie.200804675
8. Hao, S.; Yang, J.; Liu, P.; Xu, J.; Yang, C.; Li, F. *Org. Lett.* **2021,** *23,* 2553–2558. doi:10.1021/acs.orglett.1c00475
9. Nguyen, T. B.; Ermolenko, L.; Al-Mourabit, A. *Green Chem.* **2013,** *15,* 2713–2717. doi:10.1039/c3gc41186a
10. Huang, X.; Yang, H.; Fu, H.; Qiao, R.; Zhao, Y. *Synthesis* **2009,** 2679–2688. doi:10.1055/s-0029-1216871
11. Yu, L.; Wang, M.; Li, P.; Wang, L. *Appl. Organomet. Chem.* **2012,** *26,* 576–582. doi:10.1002/aoc.2902
12. He, W.; Zhao, H.; Yao, R.; Cai, M. *RSC Adv.* **2014,** *4,* 50285–50294. doi:10.1039/c4ra09379h
13. Xu, Y.; Xie, Q.; Li, W.; Sun, H.; Wang, Y.; Shao, L. *Tetrahedron* **2015,** *71,* 4853–4858. doi:10.1016/j.tet.2015.05.011
14. Ke, F.; Liu, C.; Zhang, P.; Xu, J.; Chen, X. *Synth. Commun.* **2018,** *48,* 3089–3098. doi:10.1080/00397911.2018.1533974
15. Hung, M.-U.; Liao, B.-S.; Liu, Y.-H.; Peng, S.-M.; Liu, S.-T. *Appl. Organomet. Chem.* **2014,** *28,* 661–665. doi:10.1002/aoc.3177
16. Zhang, X.; Ye, D.; Sun, H.; Guo, D.; Wang, J.; Huang, H.; Zhang, X.; Jiang, H.; Liu, H. *Green Chem.* **2009,** *11,* 1881–1888. doi:10.1039/b916124b
17. Tiwari, A. R.; Bhanage, B. M. *RSC Adv.* **2015,** *5,* 57235–57239. doi:10.1039/c5ra11159e
18. Malasala, S.; Gour, J.; Ahmad, M. N.; Gatadi, S.; Shukla, M.; Kaul, G.; Dasgupta, A.; Madhavi, Y. V.; Chopra, S.; Nanduri, S. *RSC Adv.* **2020,** *10,* 43533–43538. doi:10.1039/d0ra08644d
19. Zhu, L.; Li, B.; Wang, S.; Wang, W.; Wang, L.; Ding, L.; Qin, C. *Polymers (Basel, Switz.)* **2018,** *10,* 385. doi:10.3390/polym10040385
20. Dekamin, M. G.; Kazemi, E.; Karimi, Z.; Mohammadalipoor, M.; Naimi-Jamal, M. R. *Int. J. Biol. Macromol.* **2016,** *93,* 767–774. doi:10.1016/j.ijbiomac.2016.09.012
21. Babamoradi, J.; Ghorbani-Vaghei, R.; Alavinia, S. *Int. J. Biol. Macromol.* **2022,** *209,* 1542–1552. doi:10.1016/j.ijbiomac.2022.04.140
22. Li, B.; Wen, W.; Wen, W.; Guo, H.; Fu, C.; Zhang, Y.; Zhu, L. *Molecules* **2023,** *28,* 5609. doi:10.3390/molecules28145609
23. Wen, W.; Han, B.; Yan, F.; Ding, L.; Li, B.; Wang, L.; Zhu, L. *Nanomaterials* **2018,** *8,* 326. doi:10.3390/nano8050326
24. Chen, S.; Wen, W.; Zhao, X.; Zhang, Z.; Li, W.; Zhang, Y.; Li, B.; Zhu, L. *Molecules* **2022,** *27,* 7962. doi:10.3390/molecules27227962

License and Terms

This is an open access article licensed under the terms of the Beilstein-Institut Open Access License Agreement (https://www.beilstein-journals.org/bjoc/terms), which is identical to the Creative Commons Attribution 4.0 International License (https://creativecommons.org/licenses/by/4.0). The reuse of material under this license requires that the author(s), source and license are credited. Third-party material in this article could be subject to other licenses (typically indicated in the credit line), and in this case, users are required to obtain permission from the license holder to reuse the material.

The definitive version of this article is the electronic one which can be found at: https://doi.org/10.3762/bjoc.21.67

BEILSTEIN JOURNAL OF ORGANIC CHEMISTRY

A multicomponent reaction-initiated synthesis of imidazopyridine-fused isoquinolinones

Ashutosh Nath, John Mark Awad and Wei Zhang*

Full Research Paper

Open Access

Address:
Department of Chemistry, University of Massachusetts Boston, 100 Morrissey Boulevard, Boston, MA 02125, USA

Email:
Wei Zhang* - wei2.zhang@umb.edu

* Corresponding author

Keywords:
Groebke–Blackburn–Bienaymé (GBB); imidazopyridine; intramolecular Diels–Alder (IMDA); isoquinolinone; multicomponent reaction (MCR); re-aromatization

Beilstein J. Org. Chem. **2025,** *21,* 1161–1169.
https://doi.org/10.3762/bjoc.21.92

Received: 20 March 2025
Accepted: 05 June 2025
Published: 13 June 2025

This article is part of the thematic issue "Green chemistry III".

Associate Editor: L. Vaccaro

© 2025 Nath et al.; licensee Beilstein-Institut.
License and terms: see end of document.

Abstract

A new synthetic route initiated with Groebke–Blackburn–Bienaymé (GBB) followed by *N*-acylation, intramolecular Diels–Alder (IMDA), and dehydrative re-aromatization reactions for the synthesis of imidazopyridine-fused isoquinolinones is developed. Gaussian computation analysis on the effect of the substitution groups for the IMDA reaction is performed to understand the reaction mechanism.

Introduction

Multicomponent reactions (MCRs) have intrinsic green chemistry advantages of synthetic efficiency and operational simplicity. Performing post-condensational modifications of MCRs could generate novel and complex molecular scaffolds [1-8]. Some MCR adducts generated from Ugi, Passerini, Gewald, Biginelli, and Groebke–Blackburn–Bienaymé (GBB) reactions have been modified to form chemically diverse heterocyclic scaffolds with potential biological activities [9,10].

Imidazo[1,2-*a*]pyridine and isoquinolinone-kind scaffolds are privileged rings which can be found in drug molecules such as zolimidine [11], zolpidem [12], alpidem and antiemetic drug 5-HT3A antagonist palonosetron [13] (Figure 1). Imidazopyridine-fused isoquinolinones have been developed as HIV inhibitors [14]. The imidazo[1,2-*a*]pyridine ring can be readily synthesized by the GBB reaction [10,15], while the isoquinolinone ring is commonly generated by a cyclative lactamization process. Performing a GBB reaction followed by an intramolecular amidation is a good approach for making imidazopyridine-fused isoquinolinones.

The Veljkovic group employed methyl 2-formylbenzoate for the GBB reaction to form adducts **I** which undergoes intramolecular amidation to afford product **A** (Scheme 1A) [16]. In a patent filed by Tibotec Pharmaceuticals, substituted alkyl isonitriles were used for the GBB reaction followed by the cleavage

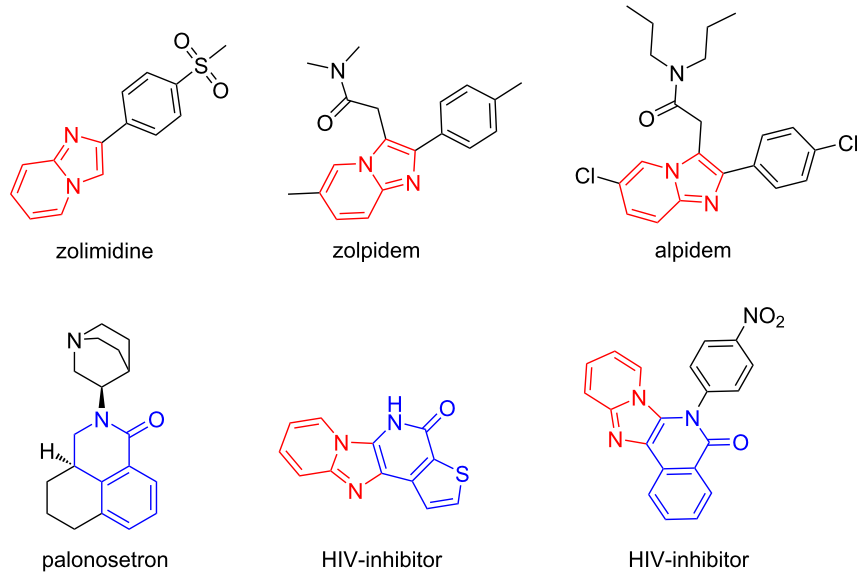
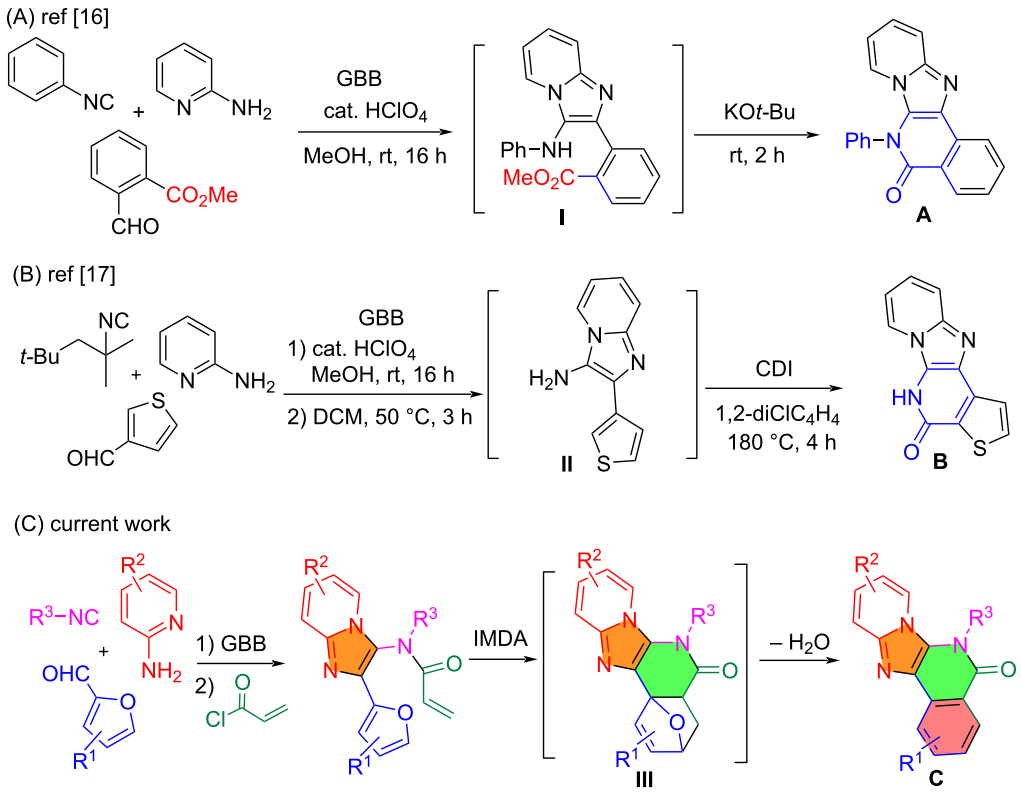


Figure 1: Bioactive compounds bearing imidazopyridine (red) and isoquinolinone-kind (blue) rings.



Scheme 1: GBB-initiated synthesis of imidazopyridine-fused isoquinolinones.

of the alkyl group to give intermediate **II** as a free amine. Annulation of **II** with CDI gave product **B** which is an HIV reverse transcriptase inhibitor (Scheme 1B) [17]. We have reported a three-component [3 + 2] cycloaddition followed by IMDA reaction for making heterocyclic compounds [18]. Presented in this paper is a new synthetic route involving GBB, *N*-acylation and

IMDA reactions for making intermediate **III** followed by dehydrative re-aromatization to give imidazopyridine-fused isoquinolinones **C** (Scheme 1C).

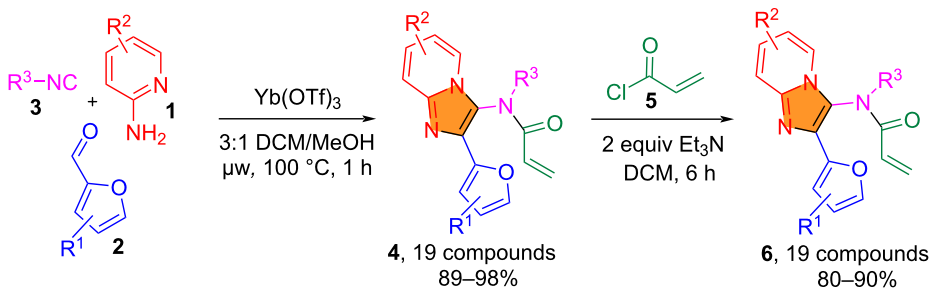
Results and Discussion

Following the reported procedures [10], the initial GBB reaction of aminopyridines **1** (0.5 mmol), isocyanides **3** (1.2 equiv), and furfuraldehydes **2** (1.2 equiv) was conducted in 3:1 CH_2Cl_2/MeOH (4 mL) using $Yb(OTf)_3$ (0.08 equiv) as a Lewis acid catalyst under microwave irradiation at 100 °C for 1 h (Scheme 2). Nineteen distinct adducts **4** were obtained in 89–98% yields. Reactions of **4** with acryloyl chloride (**5**, 1.5 equiv) in the presence of Et_3N (2 equiv) at room temperature in anhydrous CH_2Cl_2 for 6 h afforded 19 *N*-acylated compounds **6** in 80–90% yields [19].

With *N*-acylated GBB adducts **6** in hand, the synthesis of imidazopyridine-fused isoquinolinones **8** was explored by conducting IMDA and spontaneous dehydrative re-aromatization reactions. The IMDA reaction using **6a** as a model compound was systematically evaluated by varying catalysts, solvents, reaction temperatures and times (Table 1). The best conditions were found to use $AlCl_3$ as a catalyst in 1,2-dichlorobenzene at 180 °C for 4 h, which gave **8a** in 85% conversion and 82% isolated yield (Table 1, entry 3). Other solvents like toluene and xylene gave minimal or no product. Different combinations of temperature and reaction time couldn't improve the yield. Among the various Lewis acids tested, $AlCl_3$ gave the best result, while CuCl, $ZnCl_2$, $PdCl_2$ and $Sc(OTf)_3$ showed moderate conversions (30–55%), and $InCl_3$ had the lowest efficiency. Without any Lewis acid we observed no conversion by LC–MS (Table 1, entry 16). During the reaction, IMDA adduct **7a** was detected by LC–MS (Figure S1, Supporting Information File 1), but it was not stable enough for isolation. The structure of **8a** was confirmed by single crystal X-ray diffraction analysis.

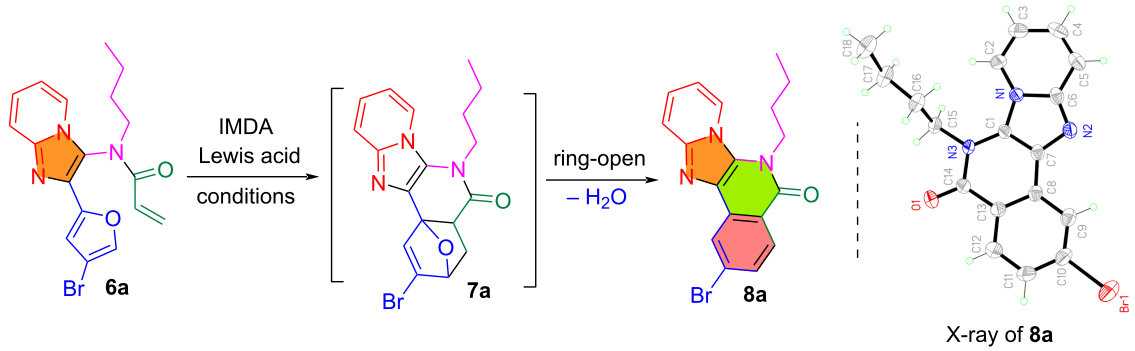
The optimized reaction conditions were used to evaluate the substrate scope of the synthesis of imidazopyridine-fused isoquinolinones **8** (Scheme 3). The R^1 residue on the furan ring was found to have the most significant impact on the IMDA reaction. A bromine atom at the 3- or the 4-position resulted in products **8a–i** in 66–86% yields, while a bromine atom or a methyl group at the 5-position inhibited the IMDA reaction in the preparation of **8j** and **8k**. A comprehensive DFT investigation of reactant **6** was carried out to analyze the transition state of the IMDA reaction for a Br-substituted diene and its charge distribution (Figure 2). The diene has a notable positive charge (+0.318, +0.098, **6a**), (+0.334, +0.082, **6h**) and (+0.316, +0.074, **6r**) whereas the dienophile presents a negative charge (−0.280 to −0.325, **6a**), (−0.280 to −0.327, **6h**) and (−0.280 to −0.327, **6r**), respectively. This structure induces electrostatic repulsion instead of the requisite attraction for a successful interaction between the electron-rich diene and the electron-deficient dienophile, characteristic of Diels–Alder processes. The incorporation of a bromine atom at the 5-position of the diene (+0.306, −0.041, **6j**) complicates the situation. As an electronegative element, Br exerts an inductive electron-withdrawing influence to enhance the electron shortage of the diene. This electronic imbalance reduces the diene's nucleophilicity, rendering it less reactive to the dienophile. The unfeasibility of the IMDA reaction in this system arises from inadequate interatomic distances, electrostatic repulsion from incompatible associated dienophile was conducted [19,20]. Firstly, the charge and the electronic consequences of the 5-Br substitution **6j** were considered, which were found to inhibit the system from attaining the requisite conditions for successful cycloaddition. Secondly, the interatomic distances between the reactive centers of the diene and dienophile are almost similar for all substitutes of **6a**, **6h**, **6r** and **6j**, which, are not ideal effective for IMDA cycloadditions compared to the other substitute cycloadditions.

The R^2 substituent on the imidazopyridine moiety in **6** was found to have a significant electronic impact on the IMDA cycloaddition. When R^2 is a halogen (Br or Cl), it withdraws electron density through its inductive (−I) effect to increase diene reactivity for the cycloaddition to form **7**. For example, **6l**



Scheme 2: GBB reaction and *N*-acylation for the preparation of imidazo[1,2-*a*]pyridines **6**.

Table 1: Optimization of IMDA and re-aromatization reactions for the preparation of **8a**.

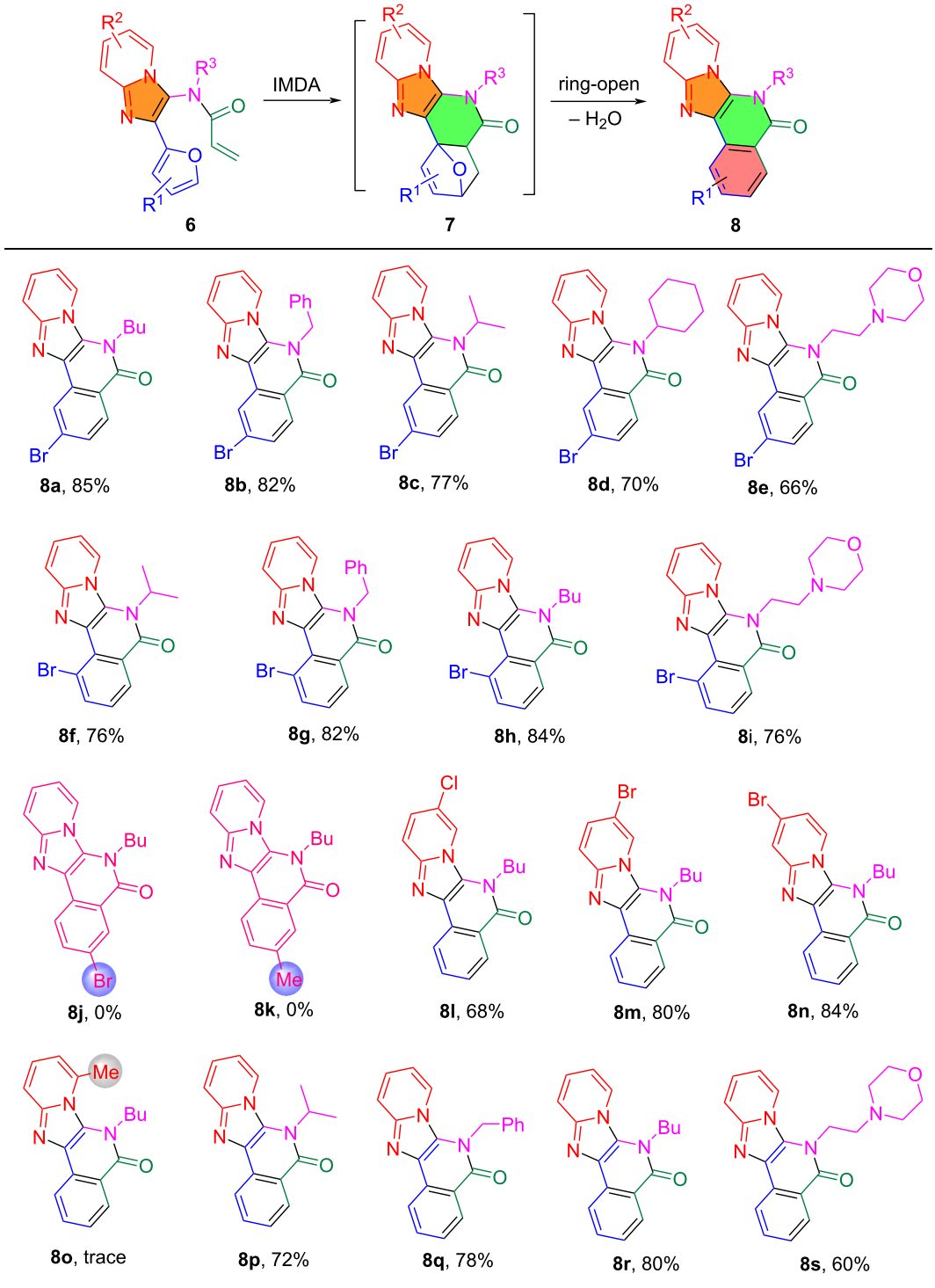


entry	catalyst (10 mol %)	solvent	temp (°C)	time	conversion (%)
1	$AlCl_3$	toluene	120	12 h	0
2	$FeCl_3$	1,2-dichlorobenzene	120 (μw)	1 h	0
3	**$AlCl_3$**	**1,2-dichlorobenzene**	**180**	**4 h**	**85**
4	$AlCl_3$	1,2-dichlorobenzene	180 (μw)	1 h	5
5	$AlCl_3$	1,2-dichlorobenzene	120 (μw)	2 h	15
6	$AlCl_3$	xylene	140	4 h	0
7	$ZnCl_2$	1,2-dichlorobenzene	140	4 h	50
8	CuCl	1,2-dichlorobenzene	180	4 h	55
9	$PdCl_2$	1,2-dichlorobenzene	180	4 h	40
10	CsF	1,2-dichlorobenzene	180	4 h	30
11	$Sc(OTf)_3$	1,2-dichlorobenzene	180	4 h	35
12	$CsCO_3$	1,2-dichlorobenzene	180	4 h	30
13	$InCl_3$	1,2-dichlorobenzene	180	4 h	20
14	$Yb(OTf)_3$	1,2-dichlorobenzene	180	4 h	60
15	$NiCl_2$	1,2-dichlorobenzene	180	4 h	47
16	no catalyst	1,2-dichlorobenzene	180	4 h	0

(R^2 = 6-Cl, 68% yield of **8l**), **6m** (R^2 = 6-Br, 80% yield of **8m**), and **6n** (R^2 = 7-Br, 84% yield of **8n**) are high-yielding substrates. But an electron-donating group in **6o** (R^2 = 5-methyl) lowers the dienophilic nature and gave no product **8o**. The R^3 substituent from isocyanides is an important factor in forming intermediates **7** and promoting dehydrative aromatization for making products **8**. The reactions with R^3 = *n*-butyl resulted in the high yielding formation of **8a**,**h**,**l**,**m**,**n** and **8r** (68–85%), R^3 = phenyl resulted in **8b**,**g** and **8q** in 78–82% yields, R^3 = isopropyl and cyclopentene gave **8c**,**f**,**p** and **8d** in greater than 70% yields, and R^3 = 2-morpholinoethyl gave **8e**,**i** and **8s** in 60–76% yields.

The energy status for the transformation of compound **6a** to **8a** was calculated using the Gaussian 16 software (Figure 3) [21]. The *N*-acylated compound **6a** has a baseline relative energy of 0 kJ/mol, while the transition state of the Diels–Alder (**TS-DA**) reaction presents the highest energy barrier at 1.221 kJ/mol. The DA adduct shows a little lower energy at 1.001 kJ/mol, indicating a smooth transition from the transition state to the product. The final dehydrative ring-opening gives products by decreasing the energy to 0.978 kJ/mol. Computational analysis indicates that the IMDA step has a high energy barrier which needs a catalyst, while the dehydrative re-aromatization step is energetically favorable.

Other than furfural, thiophene-2-carbaldehyde (**2s**) was used for the GBB and *N*-acylation reactions to make **6t** (Scheme 4). The IMDA reaction of **6t** was carried out under the catalysis of $AlCl_3$ in dichlorobenzene at 180 °C for up to 24 h, but no compounds **7t** and **8t** could be detected by LC–MS from the reaction mixture. The X-ray structure of **6t** indicated that the diene and dienophile are perpendicular to each other which prevents them from being properly aligned for the IMDA reaction. The



Scheme 3: Substrate scope for IMDA and dehydrative aromatization in making **8**. Reaction conditions: **6** and $AlCl_3$ (10 mol %) in 1,2-dichlorobenzene at 180 °C for 4 h.

transition state of the IMDA is electronically destabilized by the sulfur group of the thiophene to reduce the diene's reactivity or altering the electrophilicity of the dienophile.

Based on the computational analysis of the transition states, reaction mechanisms for the IMDA and the dehydration re-aromatization process are proposed in Scheme 5. In the

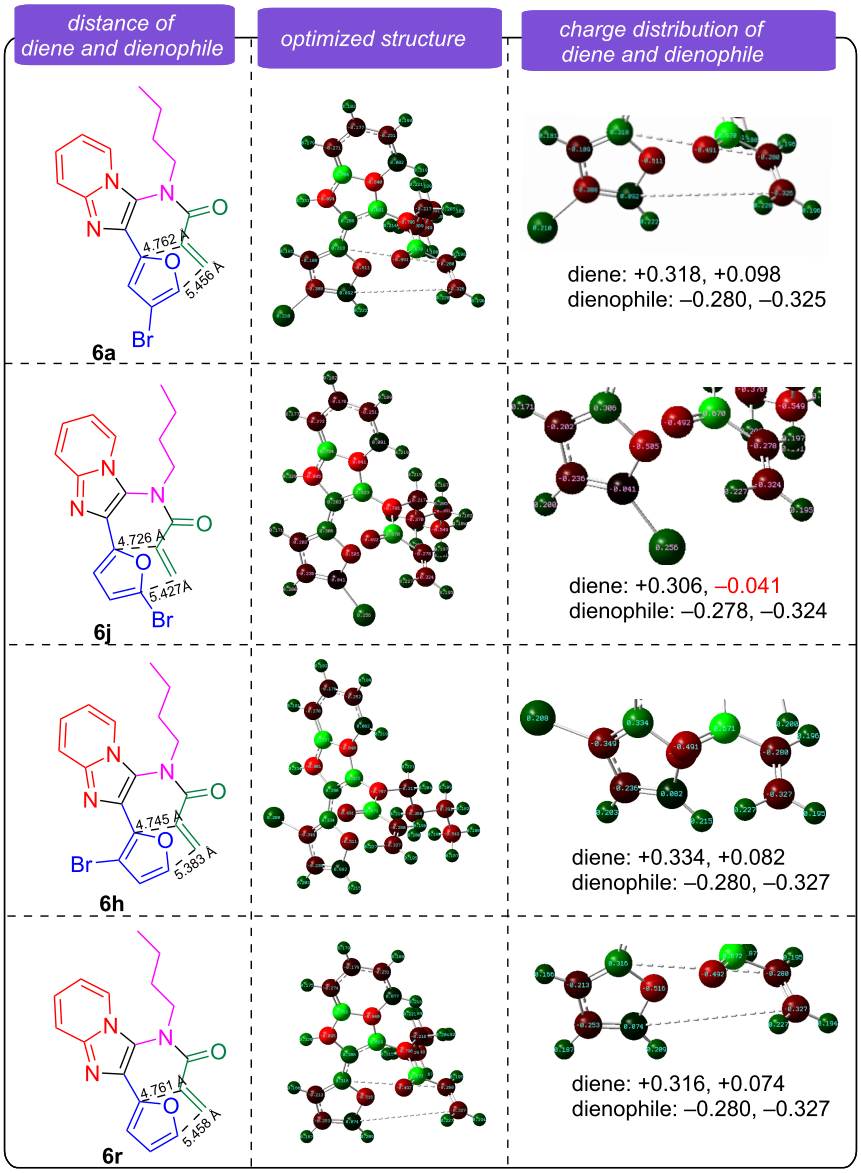


Figure 2: Transition state analysis of IMDA reactions for **6a**, **6j**, **6h** and **6r**.

IMDA reaction for the preparation of intermediate **7**, the carbonyl oxygen interacts with $AlCl_3$, enhancing the electrophilicity and promoting the rearrangement to form stable oxonium ions. The removal of water from **7** is facilitated by protonation, producing reactive carbocations which undergo dehydrative aromatization to produce products **8**.

Conclusion

In summary, we developed a reaction sequence involving GBB, *N*-acylation, IMDA and dehydrative re-aromatization reactions for the synthesis of imidazopyridine-fused isoquinolinones. Computational studies of the IMDA reaction indicated that the position of the R^1 group on the furan ring and the R^2 group on the imidazopyridine moiety have direct electronic impact on the IMDA reaction. This integrated reaction process provided a new avenue for the preparation of heterocyclic scaffolds with potential biological activity.

Experimental

General procedure for the synthesis of intermediates 4 and 6

The GBB reactions for the preparation of imidazo[1,2-*a*]pyridines **4** were conducted using aminopyridines **1**

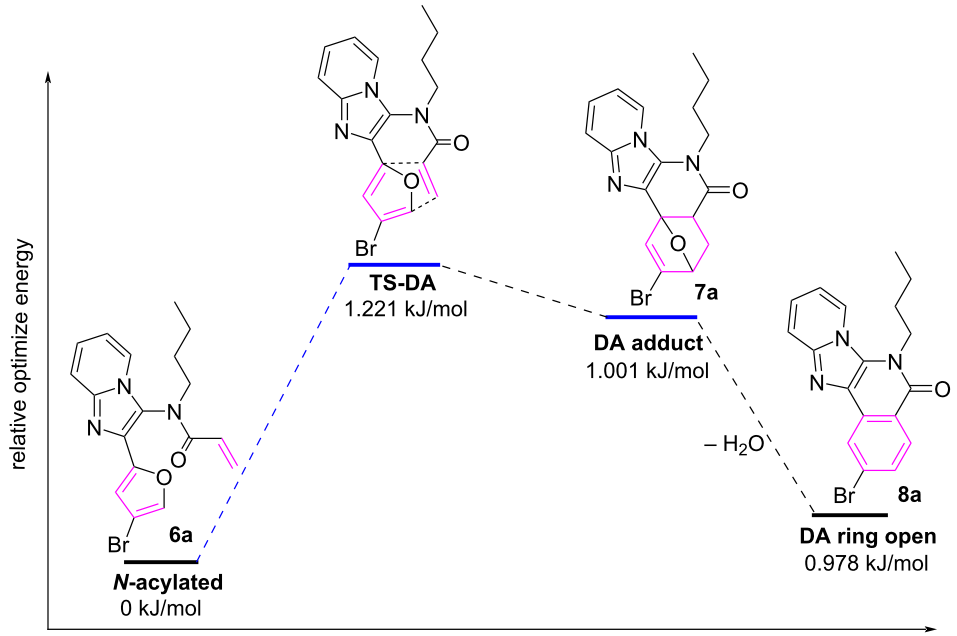
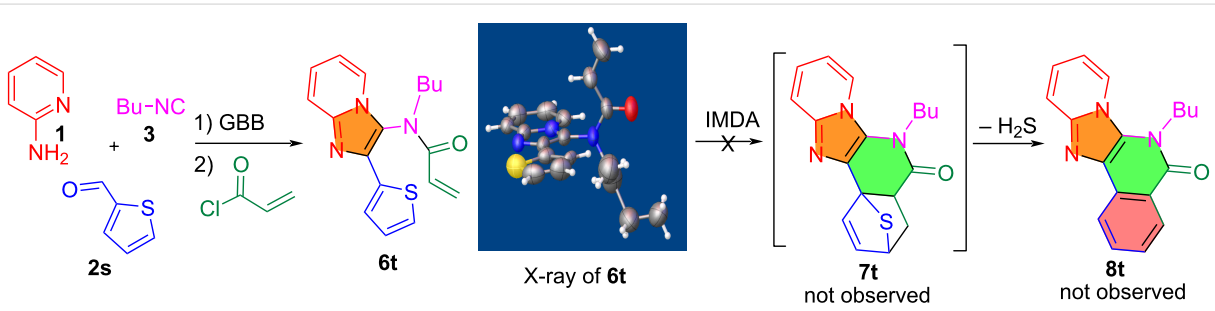
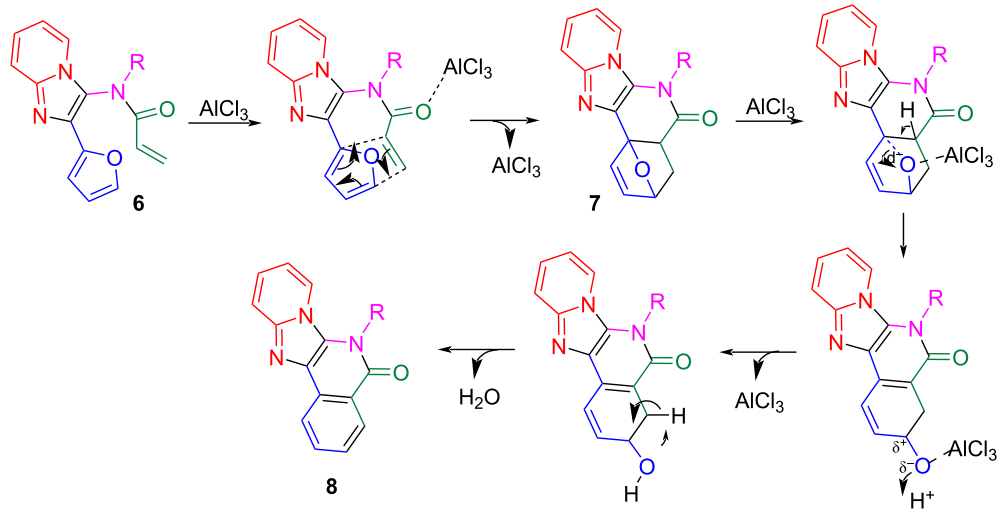


Figure 3: Relative energy diagram for the synthesis of **8a** from **6a**.



Scheme 4: Using thiophene-2-carbaldehyde for the synthesis of **8t**.



Scheme 5: Proposed mechanisms for IMDA reaction and dehydration re-aromatization.

(0.5 mmol), isocyanides **3** (0.6 mmol, 1.2 equiv), and furfuraldehyde **2** (0.6 mmol, 1.2 equiv) in 3:1 DCM/MeOH (4 mL) with $Yb(OTf)_3$ (0.04 mmol, 0.08 equiv) as a Lewis acid catalyst under microwave irradiation at 100 °C for 1 h (Scheme 2, Table S1 in Supporting Information File 1). Nineteen distinct adducts **4** were obtained in 89–98% yields. The reactions of GBB adducts **4** with acryloyl chloride (**5**, 1.5 equiv) in the presence of Et_3N (2 equiv) at room temperature in anhydrous CH_2Cl_2 for 6 h afforded 19 *N*-acylated compounds **6** in 80–90% yields after flash chromatography with 1:6 EtOAc/hexanes (Scheme 2, Table S2 in Supporting Information File 1) [19].

General procedure for the synthesis of products **8**

In the presence of 0.08 equiv of Lewis's acid $AlCl_3$, *N*-acylation products **6** (0.1 mmol) in dichlorobenzene were heated at 180 °C for 4 h (Scheme 3). The reaction mixtures were checked by LC–MS to follow the formation of DA adducts **7** and the ring opening products **8** (Figure S1, Supporting Information File 1). After 4 h, the reaction mixtures were worked up and the crude products were purified by flash chromatography with 30:70 EtOAc/hexanes. Product structures were confirmed by ^1H and ^{13}C NMR analysis and X-ray crystal structure analysis of **8a**.

Density functional theory (DFT) calculations

DFT computations were conducted utilizing Gaussian 16W with the B3LYP functional and the 6-31G(d,p) basis set [21,22]. Geometry optimizations were performed without symmetry restrictions, and frequency analyses verified that all structures represented genuine minima. Charge distributions and interatomic distances were evaluated to determine reaction feasibility, utilizing GaussView for molecular visualization.

Supporting Information

Supporting Information File 1

General reaction procedures, compound characterization data, and copies of NMR spectra.
[https://www.beilstein-journals.org/bjoc/content/supplementary/1860-5397-21-92-S1.pdf]

Conflict of Interest

The authors declare no competing financial interest.

Author Contributions

Ashutosh Nath: data curation; formal analysis; investigation; methodology; software; validation; writing – original draft. John Mark Awad: investigation; methodology; validation; writing – original draft. Wei Zhang: conceptualization; funding acquisition; supervision; writing – review & editing.

ORCID® iDs

Wei Zhang - https://orcid.org/0000-0002-6097-2763

Data Availability Statement

All data that supports the findings of this study is available in the published article and/or the supporting information of this article.

Preprint

A non-peer-reviewed version of this article has been previously published as a preprint: https://doi.org/10.3762/bxiv.2025.20.v1

References

1. Krasavin, M.; Dar'in, D.; Balalaie, S. *Tetrahedron Lett.* **2021,** *86,* 153521. doi:10.1016/j.tetlet.2021.153521
2. Shen, G.-B.; Yu, T.; Zhang, Y.-L.; Ma, L.-P.; Chen, L.; Lu, J.-J.; Meng, T. *J. Heterocycl. Chem.* **2018,** *55,* 814–820. doi:10.1002/jhet.3102
3. Qian, Z.; Yang, A.; An, W.; Yu, T.; Wang, X.; Zhang, Y.; Shen, J.; Meng, T. *RSC Adv.* **2014,** *4,* 50947–50949. doi:10.1039/c4ra09196e
4. Tang, L.; Ren, J.; Ma, Y.; Wang, X.; Chen, L.; Shen, J.; Chen, Y.-L.; Xiong, B. *Tetrahedron Lett.* **2016,** *57,* 2311–2314. doi:10.1016/j.tetlet.2016.04.050
5. Srinivasulu, V.; Khanfar, M.; Omar, H. A.; ElAwady, R.; Sieburth, S. M.; Sebastian, A.; Zaher, D. M.; Al-Marzooq, F.; Hersi, F.; Al-Tel, T. H. *J. Org. Chem.* **2019,** *84,* 14476–14486. doi:10.1021/acs.joc.9b01919
6. Tandi, M.; Sharma, V.; Gopal, B.; Sundriyal, S. *RSC Adv.* **2025,** *15,* 1447–1489. doi:10.1039/d4ra06681b
7. Dömling, A.; Wang, W.; Wang, K. *Chem. Rev.* **2012,** *112,* 3083–3135. doi:10.1021/cr100233r
8. Flores-Reyes, J. C.; Islas-Jácome, A.; González-Zamora, E. *Org. Chem. Front.* **2021,** *8,* 5460–5515. doi:10.1039/d1qo00313e
9. Slobbe, P.; Ruijter, E.; Orru, R. V. A. *Med. Chem. Commun.* **2012,** *3,* 1189–1218. doi:10.1039/c2md20089a
10. Boltjes, A.; Dömling, A. *Eur. J. Org. Chem.* **2019,** 7007–7049. doi:10.1002/ejoc.201901124
11. Cai, Q.; Liu, M.-C.; Mao, B.-M.; Xie, X.; Jia, F.-C.; Zhu, Y.-P.; Wu, A.-X. *Chin. Chem. Lett.* **2015,** *26,* 881–884. doi:10.1016/j.cclet.2014.12.016
12. Erhorn, S. Zolpidem. In *xPharm: The Comprehensive Pharmacology Reference;* Enna, S. J.; Bylund, D. B., Eds.; Elsevier: New York, NY, USA, 2007; pp 1–5. doi:10.1016/b978-008055232-3.62888-0
13. Schneier, F. R.; Carrasco, J. L.; Hollander, E.; Campeas, R.; Fallon, B.; Saoud, J. B.; Feerick, J.; Liebowitz, M. R. *J. Clin. Psychopharmacol.* **1993,** *13,* 150–153. doi:10.1097/00004714-199304000-00011
14. Devi, N.; Rawal, R. K.; Singh, V. *Tetrahedron* **2015,** *71,* 183–232. doi:10.1016/j.tet.2014.10.032
15. Martini, C.; Mardjan, M. I. D.; Basso, A. *Beilstein J. Org. Chem.* **2024,** *20,* 1839–1879. doi:10.3762/bjoc.20.162
16. Veljkovic, I.; Zimmer, R.; Reissig, H.-U.; Brüdgam, I.; Hartl, H. *Synthesis* **2006,** 2677–2684. doi:10.1055/s-2006-942506
17. Kesteleyn, B. R. R.; Schepens, W. B. G. HIV inhibiting 3,4-dihydro-imidazo[4,5-b]pyridin-5-ones. U.S. Patent US 7,994,187 B2, Aug 9, 2011.

18. Lu, Q.; Huang, X.; Song, G.; Sun, C.-M.; Jasinski, J. P.; Keeley, A. C.; Zhang, W. *ACS Comb. Sci.* **2013,** *15,* 350–355. doi:10.1021/co400026s
19. Paulvannan, K.; Stille, J. R. *J. Org. Chem.* **1992,** *57,* 5319–5328. doi:10.1021/jo00046a011
20. Rae, R. L.; Żurek, J. M.; Paterson, M. J.; Bebbington, M. W. P. *Org. Biomol. Chem.* **2013,** *11,* 7946–7952. doi:10.1039/c3ob41616j
21. *Gaussian 16,* Revision C.01; Gaussian, Inc.: Wallingford, CT, 2016.
22. Ali, M. A.; Nath, A.; Islam, M. M.; Shaheed, S. B.; Dibbo, I. N. *RSC Adv.* **2022,** *12,* 11255–11261. doi:10.1039/d2ra00450j

License and Terms

This is an open access article licensed under the terms of the Beilstein-Institut Open Access License Agreement (https://www.beilstein-journals.org/bjoc/terms), which is identical to the Creative Commons Attribution 4.0 International License (https://creativecommons.org/licenses/by/4.0). The reuse of material under this license requires that the author(s), source and license are credited. Third-party material in this article could be subject to other licenses (typically indicated in the credit line), and in this case, users are required to obtain permission from the license holder to reuse the material.

The definitive version of this article is the electronic one which can be found at:
https://doi.org/10.3762/bjoc.21.92

BEILSTEIN JOURNAL OF ORGANIC CHEMISTRY

Recent advances in amidyl radical-mediated photocatalytic direct intermolecular hydrogen atom transfer

Hao-Sen Wang[1,2], Lin Li[2], Xin Chen[3,4], Jian-Li Wu[*1], Kai Sun[*2], Xiao-Lan Chen[2], Ling-Bo Qu[1,3] and Bing Yu[*1]

Review

Open Access

Address:
[1]Medical School, Huanghe Science and Technology College, Zhengzhou, 450006, PR China, [2]College of Chemistry, Zhengzhou University, Zhengzhou 450001, PR China, [3]Institute of Chemistry, Henan Academy of Sciences, Zhengzhou 450002, PR China and [4]National Engineering Research Center of Low-Carbon Processing and Utilization of Forest Biomass, Nanjing Forestry University, Nanjing 210037, PR China

Email:
Jian-Li Wu[*] - wjl@hhstu.edu.cn; Kai Sun[*] - sunkaichem@zzu.edu.cn; Bing Yu[*] - bingyu@zzu.edu.cn

* Corresponding author

Keywords:
amidyl radicals; C–H; HAT reagents; hydrogen-atom-transfer; late-stage functionalization

Beilstein J. Org. Chem. **2025,** *21,* 1306–1323.
https://doi.org/10.3762/bjoc.21.100

Received: 27 March 2025
Accepted: 10 June 2025
Published: 27 June 2025

This article is part of the thematic issue "Green chemistry III".

Associate Editor: L. Vaccaro

© 2025 Wang et al.; licensee Beilstein-Institut.
License and terms: see end of document.

Abstract

In recent years, amidyl radicals have emerged as highly efficient and versatile reagents for hydrogen atom transfer (HAT) in photocatalytic reactions. These radicals display exceptional selectivity and efficiency in abstracting hydrogen atoms from C–H, Si–H, B–H, and Ge–H, positioning them as invaluable tools in synthetic chemistry. This review summarizes the latest advancements in the photocatalyzed generation of amidyl radicals as HAT reagents, with a particular emphasis on their role in the intermolecular HAT process. We highlight key developments, mechanistic insights, and emerging strategies that harness the unique reactivity of amidyl radicals in the selective functionalization of a variety of substrates.

Introduction

C–H bonds are the predominant chemical bonds in organic compounds, and their direct conversion can rapidly and efficiently increase the complexity and functionality of organic molecules. On the other hand, C–H bonds exhibit low reactivity due to their relatively high bond dissociation energy (BDE) (Figure 1a). Therefore, the direct functionalization of C–H bonds is extremely challenging [1-5].

In recent decades, transition-metal-catalyzed C–H bond functionalization demonstrated a decent methodology of organic synthesis. These elegant strategies presented powerful C–H bond transformation toolkits (Figure 1b) [6-8]. One of the exceptions to the perfection is the pre-functionalization of substrates. Current catalytic methodologies predominantly rely on substrate prefunctionalization through directing group (DG) incorpora-

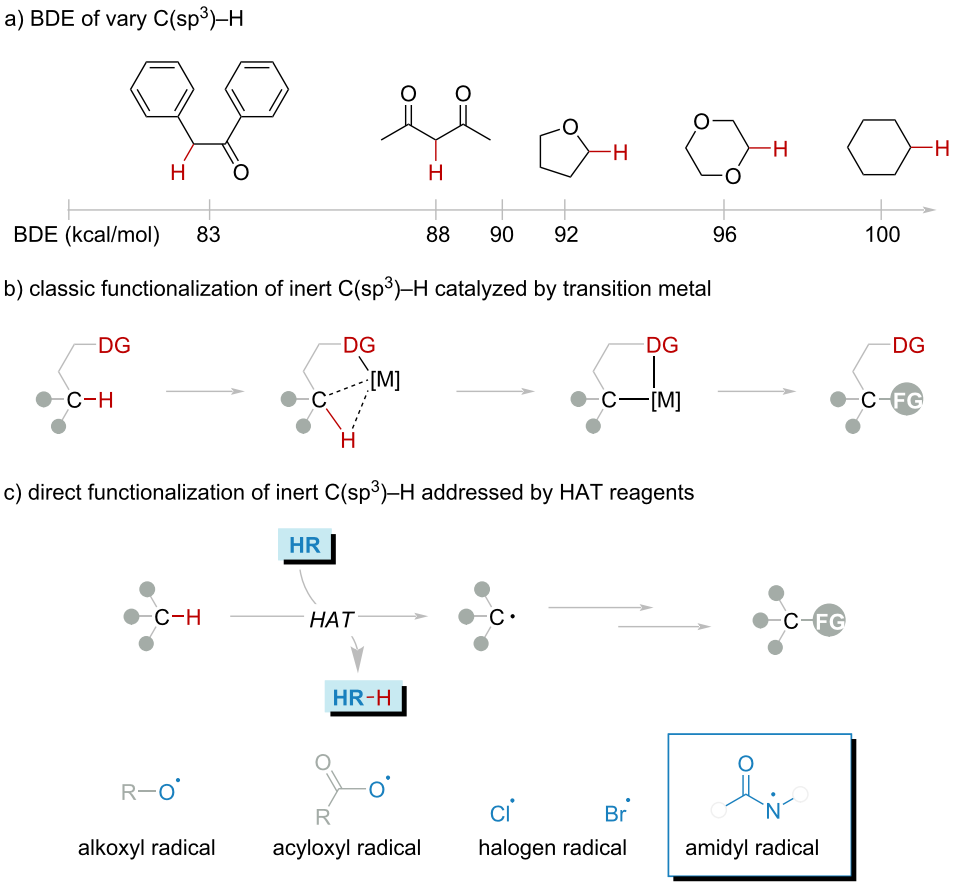


Figure 1: (a) BDE of C–H. (b) Direct functionalization of C–H catalyzed by transition-metal. (c) Direct functionalization of C–H via HAT process.

tion, inevitably necessitating covalent DG-metal coordinative anchoring. This prerequisite fundamentally compromises both atomic efficiency and synthetic practicality, thereby imposing fundamental constraints on the catalytic system's intrinsic sustainability and operational scalability [9,10]. Moreover, a high temperature and additive oxidants are generally required, which would limit the substrate scope.

The hydrogen atom transfer (HAT) process has emerged as a powerful avenue for addressing these challenges, leveraging the HAT reagents to selectively abstract hydrogen atoms from these C–H bonds and directly functionalize these bonds via radical reactions (Figure 1c) [11-18]. This approach involves HAT reagents abstracting hydrogen atoms from C–H bonds to generate highly reactive C-centered radicals, which can subsequently form C–C or C–heteroatom bonds. The incorporation of HAT strategies into the functionalization of C–H bonds represents a significant advancement in synthetic organic chemistry for their high atom economy and step economy.

HAT reagents (HR), including alkoxyl, acyloxyl, halogen radicals, and amidyl (Figure 1c) [19-27], serve as key species for the HAT process. These HR were generated from different HAT reagent precursors (HRP) in a variety of strategies. Among these, amidyl radical HRPs have gained significant attention in recent years due to their ease of HRP synthesis and the relatively green chemistry of generating amidyl radicals. Amidyl radicals offer several advantages that enhance their applicability in organic synthesis:

1) The BDE of amidyl N–H bond is more than 105 kcal/mol, relative to the bond (C–H, Si–H, B–H, and Ge–H) which BDE is lower than 100 kcal/mol (Figure 2a) [28-30]. Almost 5 kcal/mol difference between two species could spontaneously undergo a HAT process. That also justifies the selectivity and efficiency of amidyl radical serving as HAT reagent.

2) Recent research indicated a critical correlation between electronic effects and activation energy modulation during transition state formation. Specifically, donor/acceptor electronic configurations in the substrate could either stabilize or destabilize the transient hybrid state, thereby thermodynamically governing the energy barrier for intermolecular HAT progression. When the partial positive and negative charges of two

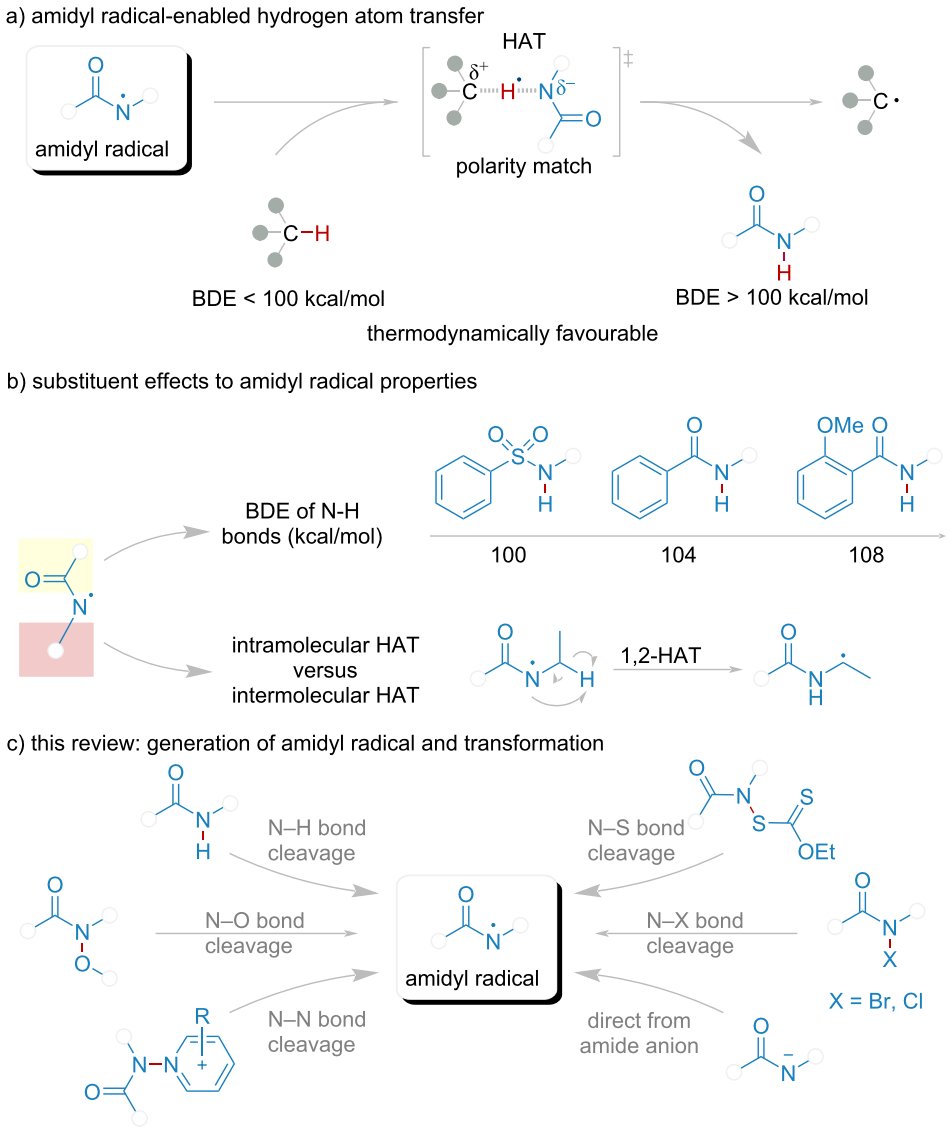


Figure 2: (a) Amidyl radical-enabled hydrogen atom transfer. (b) Substituent effects to amidyl radical properties. (c) This review: generation of amidyl radical and transformation.

species can be stabilized by the electronic effects, these species are considered to be polarity matched during the HAT process. Conversely, when there is a polarity mismatch, the HAT process is likely to be impeded (Figure 2a). C–H bonds predominantly prefer to be nucleophilic, which smoothly facilitates the HAT process with amidyl radical. This effect is also called a polarity match [31-39].

3) Considering the electronic effect, modifying the substituent of the N atom could tune the property of HAT capability (Figure 2b) [40-43]. The electron-withdrawing groups could stabilize the charge of the N-centered radical during the HAT process by decreasing the charge density [44]. Notably, the BDE of N–H in the corresponding amide might be too low to ensure a spontaneous HAT process due to the electronic effect of the substituent. When introducing electron-donating groups to address this contradiction, another vital impact arises, the intramolecular HAT would take place. The amidyl radical would abstract a hydrogen atom from the nearest C–H, i.e., 1,2-HAT. Taken all these together, the substituent group should be decently modified.

In recent years, photocatalysis has been widely adopted due to its green and efficient nature [45-51]. The generation of amidyl radical is implemented by HRP. Six different methods (Figure 2c), which have been developed for visible-light mediated reactions, could generate amidyl radicals from HRP: (a) direct single-electron oxidation of amide HRP in the pres-

ence of photocatalyst and a base via a proton-coupled electron transfer (PCET) process by the cleavage of the N–H bond; (b) single-electron reduction of HRP catalyzed by photocatalyst via a single-electron transfer (SET) process by the cleavage of the N–O bond; (c) direct homolytic cleavage of weak N–S or N–X bonds in HRP initiated in the presence of visible light; (d) the intersystem crossing (ISC) of S_1 to T_1 state directly from the amide anion. This review is organized by bond cleavage type, offering a deep insight in the development of novel methods for amidyl radical-mediated photocatalytic direct intermolecular hydrogen atom transfer.

Although, amidyl radicals employed in many reactions as HAT reagents via heating conditions have been summarized in several studies [52-58]. To advance the research of direct functionalization via HAT processes and the development of green chemistry in photocatalysis, this review will focus on the generation of amidyl radicals and reaction mechanisms and highlight the photocatalyzed reaction characteristics. This review aims to provide researchers with a systematic understanding and strategic toolkit, thereby propelling the development of direct functionalization of C–H, B–H, Si–H, and Ge–H techniques in modern organic synthesis. Most of the photocatalysts used in this review are listed in Figure 3.

Review

Amidyl radical from N–H bond cleavage

N-Alkylbenzamide constitutes the primary structural unit of this class of compounds. The structures of these compounds are relatively simple and readily synthesizable. In these photocatalytic systems, direct single-electron oxidation of the amide HRP occurs in the presence of a photoredox catalyst and a base via a proton-coupled electron transfer process [59-69]. Following this process, the corresponding amidyl radical abstracts a hydrogen atom from the substrate, resulting in the conversion of the amidyl radical back to *N*-alkylbenzamide. This pathway creates a complete cycle in synchrony with the photocatalytic cycle, thereby allowing these HRPs to be consistently employed for catalytic equivalence.

In 2016, Knowles' group independently developed an oxidative photocatalytic system capable of directly generating amidyl radicals from *N*-ethyl-4-methoxybenzamide, utilizing the photocatalyst $[Ir(dF(CF_3)ppy)_2(4,4'\text{-}d(CF_3)bpy)]PF_6$ in combination with a base ($NBu_4OP(O)(OBu)_2$) (Scheme 1) [59]. The generation of amidyl radical **5** involved a stepwise PCET process catalyzed by the combined effect, in the presence of photocatalyst and the base. Subsequently, amidyl radical **5** abstracted a hydrogen atom from substrate **1**. This HAT process returned the

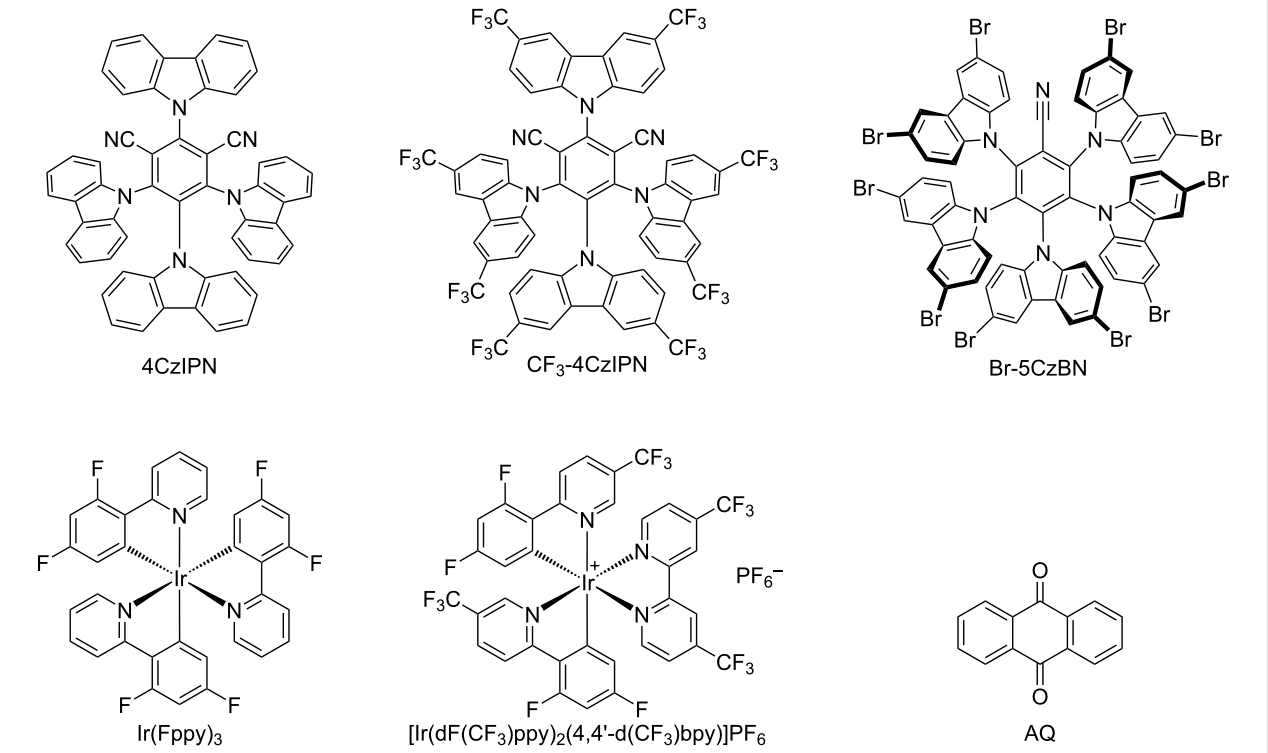
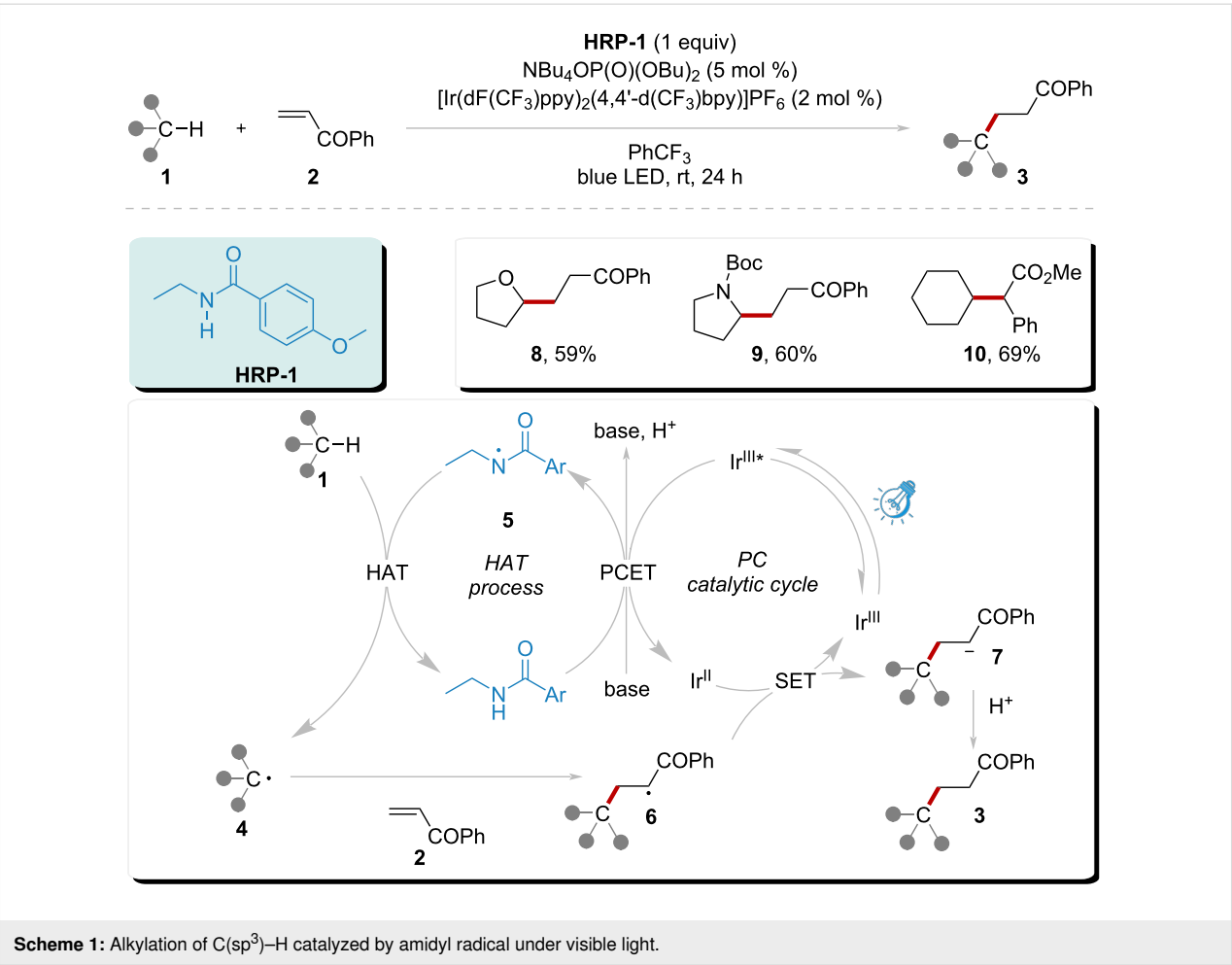


Figure 3: Representative photocatalysts discussed in this review.



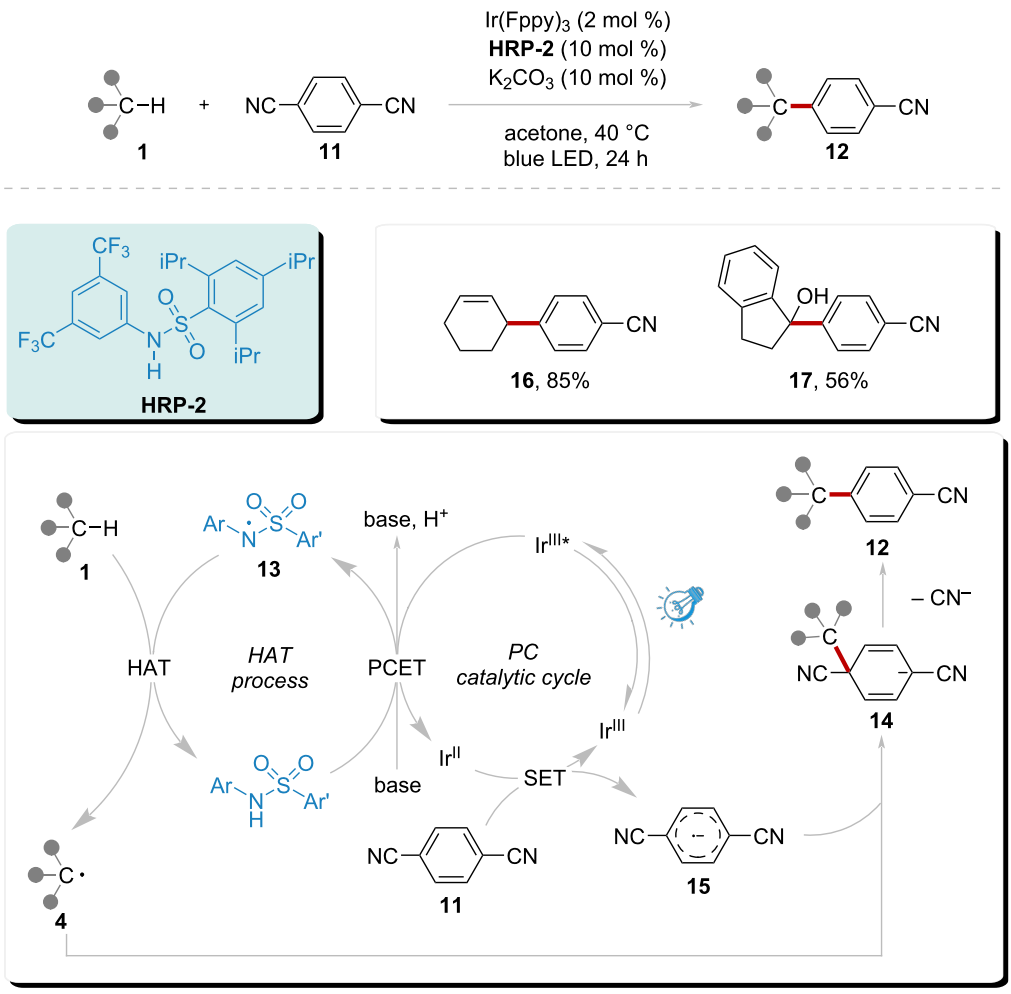
Scheme 1: Alkylation of C(sp^3)–H catalyzed by amidyl radical under visible light.

amidyl radical **5** to **HRP-1**, enabling the continuation of the HAT cycle in synchronization with the photocatalytic cycle. The resulting radical **4** then underwent Giese addition with activated alkenes, leading to the formation of products **8**, **9**, and **10** with 59%, 60%, and 69% yields. This powerful and efficient toolkit effectively overcame the limitations of intramolecular HAT processes.

Building on this strategy, Kanai's group reported a novel HAT method employing a new radical precursor in an oxidative photocatalytic system in 2018 (Scheme 2) [70]. Through a similar oxidative pathway, amidyl radical **13** was generated directly from the amide **HRP-2**, facilitating a smooth HAT process with substrate **1** while simultaneously regenerating **HRP-2**. The resulting radical **4** then participated in an addition reaction with radical anion **15**. The radical anion **15** was reduced by the photocatalyst $Ir(Fppy)_3$ from the reagent **11**. The resulting anion **14** underwent aromatization to release a nitrile anion, subsequently yielding product **12**. This strategy also successfully produced products **16** and **17** with yields of 85% and 56%, respectively, from cycloalkenes and alcohols.

To eliminate the need for noble metal photocatalysts in the system, Duan's group employed 2,4,5,6-tetra-9*H*-carbazol-9-yl-1,3-benzenedicarbonitrile (4CzIPN) as a metal-free photocatalyst (Scheme 3) [71]. This system initiated the formation of amidyl radical **20** from **HRP-3** through a PCET process, involving the oxidation of excited 4CzIPN* and deprotonation by a base. The resulting amidyl radical **20** smoothly abstracted a hydrogen atom from the substrate via a HAT process, generating a radical **4**. This C-centered radical subsequently underwent Giese addition with activated alkenes, resulting in the formation of radical **21**. Radical **21** then oxidized the photocatalyst radical anion to its ground state while simultaneously generating anion **22**. Ultimately, anion **22** yielded product **19** through protonation. This system demonstrated good applicability, achieving yields of 53% to 60% for products **23**, **24**, and **25**.

To further investigate the scope of substrates, Selvakumar's group employed **HRP-4** in combination with 4CzIPN (Scheme 4) [72]. This system examined the applicability of Si–H and Ge–H bonds through a HAT process. As seen in previous strategies, **HRP-4** was converted into amidyl radical



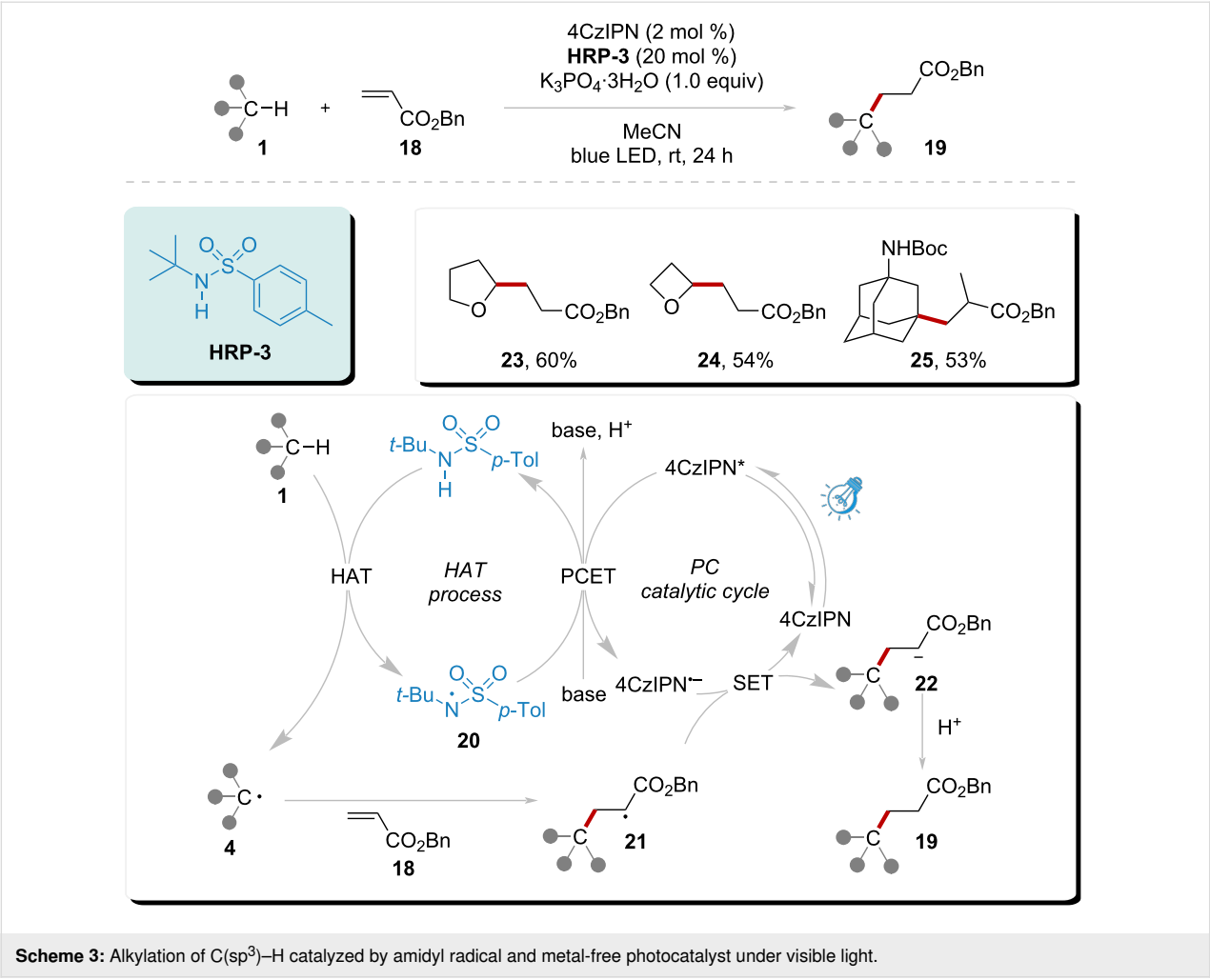
Scheme 2: Direct heteroarylation of C(sp^3)–H catalyzed by amidyl radical under visible light.

29 in the presence of 4CzIPN and a base via a PCET process. Radical **29** subsequently engaged in a HAT process with substrate **26**, generating either a Si radical or a Ge radical **28**. Following this, radical **28** underwent Giese addition with activated alkenes. The reduction of species **31** was efficiently promoted by the PC radical anion. The resulting anion **32** ultimately produced product **27** through protonation. This system demonstrated the significant HAT capability of amidyl radical **29**, as evidenced by the synthesis of products **33**, **34**, and **35** with yields reaching 70% to 78%.

Amidyl radical from N–N bond cleavage

N-Amidopyridinium salts are known to undergo SET reduction, leading to the formation of amidyl radicals. Hong's group has made significant advances in the cleavage of N–N bonds in recent years. Through SET reduction of *N*-amidopyridinium salts to generate amidyl radicals, Hong's group has accomplished various remote functionalizations of C–H bonds via 1,5-hydrogen atom transfer processes [73-76].

In 2021, Hong's group reported a HAT combined with a reverse hydrogen atom transfer (rHAT) system (Scheme 5) [77]. By utilizing anthraquinone (**AQ**) as the HAT photocatalyst, activated **AQ** was able to abstract a hydrogen atom from substrate **1**. The addition of the corresponding radical **4** to **HRP-5** facilitated the release of amidyl radical **36**, which simultaneously produced the final product **35**. Amidyl radical **36** was capable of abstracting hydrogen atoms from both substrate **1** and **AQ**–**H**. The HAT process between substrate **1** and amidyl radical **36** initiated a chain reaction pathway leading to the formation of product **35**. Conversely, the rHAT process between amidyl radical **36** and **AQ**–**H** allowed for the regeneration of the photocatalyst and the completion of the catalytic cycle. Amidyl radical **36** played a central role in this photocatalytic



Scheme 3: Alkylation of C(sp^3)–H catalyzed by amidyl radical and metal-free photocatalyst under visible light.

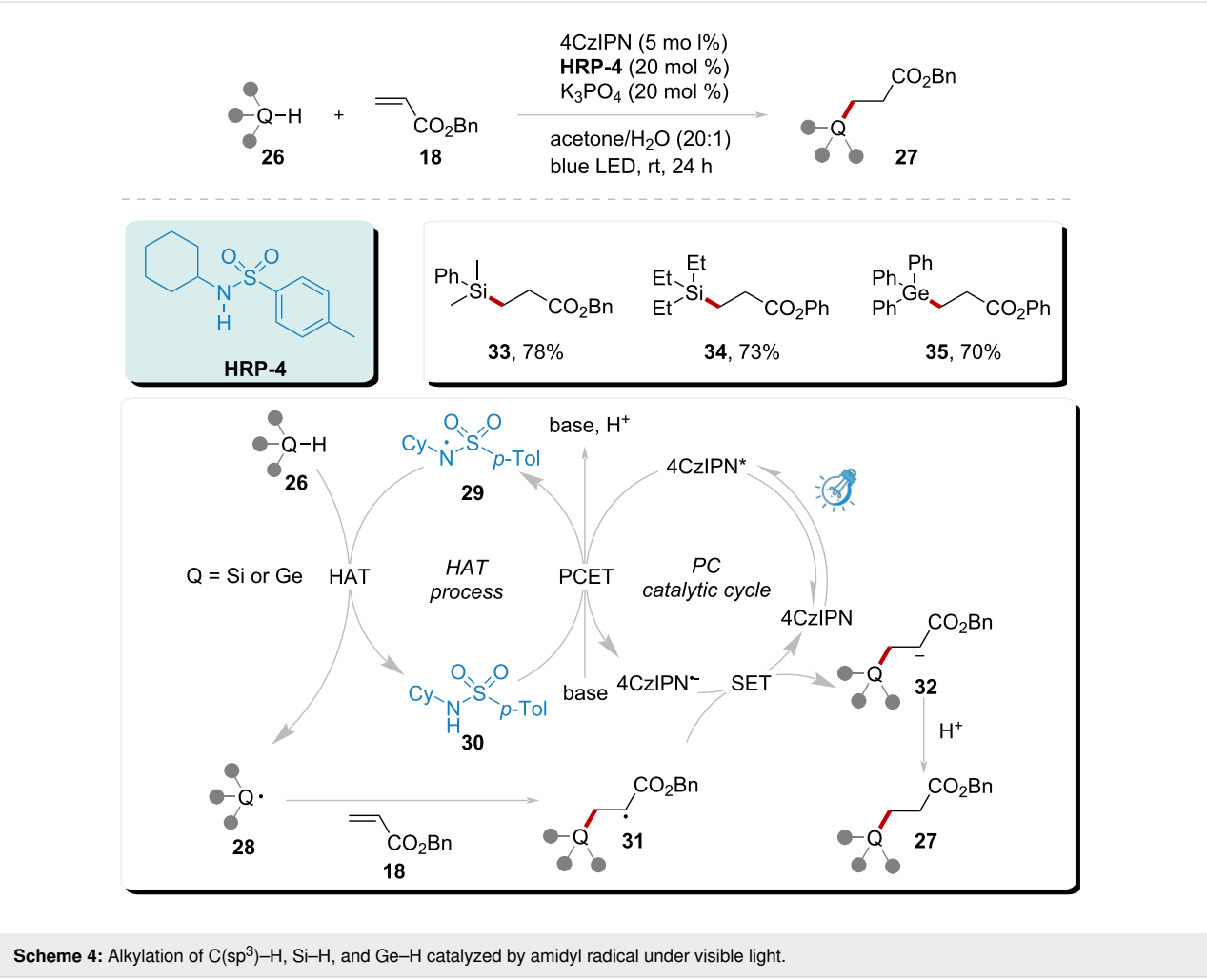
system. This strategy demonstrated good chemical selectivity for the functionalization of pyridine and alkanes, resulting in 55% to 86% yields of products **38**, **39**, **40**, and **41**, respectively.

Amidyl radical from N–O bond cleavage

In 2022, Alexanian's group demonstrated the homolytic cleavage of the N–O bond using *N*-(*tert*-butyl)-*O*-(1-phenylvinyl)-phenylhydroxyamide as a HAT reagent [78,79]. This compound was capable of initiating the formation of amidyl radicals through visible light activation. Although their controlled experiments showed that this method was effective, the use of heating conditions resulted in a higher yield of the corresponding products. This advancement prompted scientists to explore alternative pathways for generating amidyl radicals, as an alternative to the traditional SET reduction of the N–O bond [80-82]. The SET reduction is able to produce amidyl radicals and oxygen anions in the presence of photocatalysts activated by visible light. Two representative cases illustrating this approach were reported in 2023.

Building upon the experiments conducted by Alexanian's group, Yan's group extended the applicability of carborane as a HAT substrate (Scheme 6) [83]. Initially, under optimized conditions, **HRP-6** was employed to generate amidyl radical **45**, which subsequently participates in the HAT process with the carborane substrate. This process results in the formation of borone radical **47**, accompanied by amide **46**. The resultant radical **47** can be intercepted by species **43**, simultaneously releasing radical **48** and product **44**. Radical **48** reacts with **HRP-6**, leading to the regeneration of amidyl radical **45**, the release of byproduct **49**, and the initiation of a chain reaction pathway. Notably, this system could give rise to the formation of the highly applied value products **50**, **51**, and **52**, with the 39% to 60% yields. The work by Yan demonstrated the HAT capabilities of amidyl radical **45** and significantly broadened the substrate scope of amidyl radical-enhanced photocatalytic systems.

The reduction of the N–O bond through traditional SET processes is effectively illustrated by *N*-(acyloxy)phthalimides

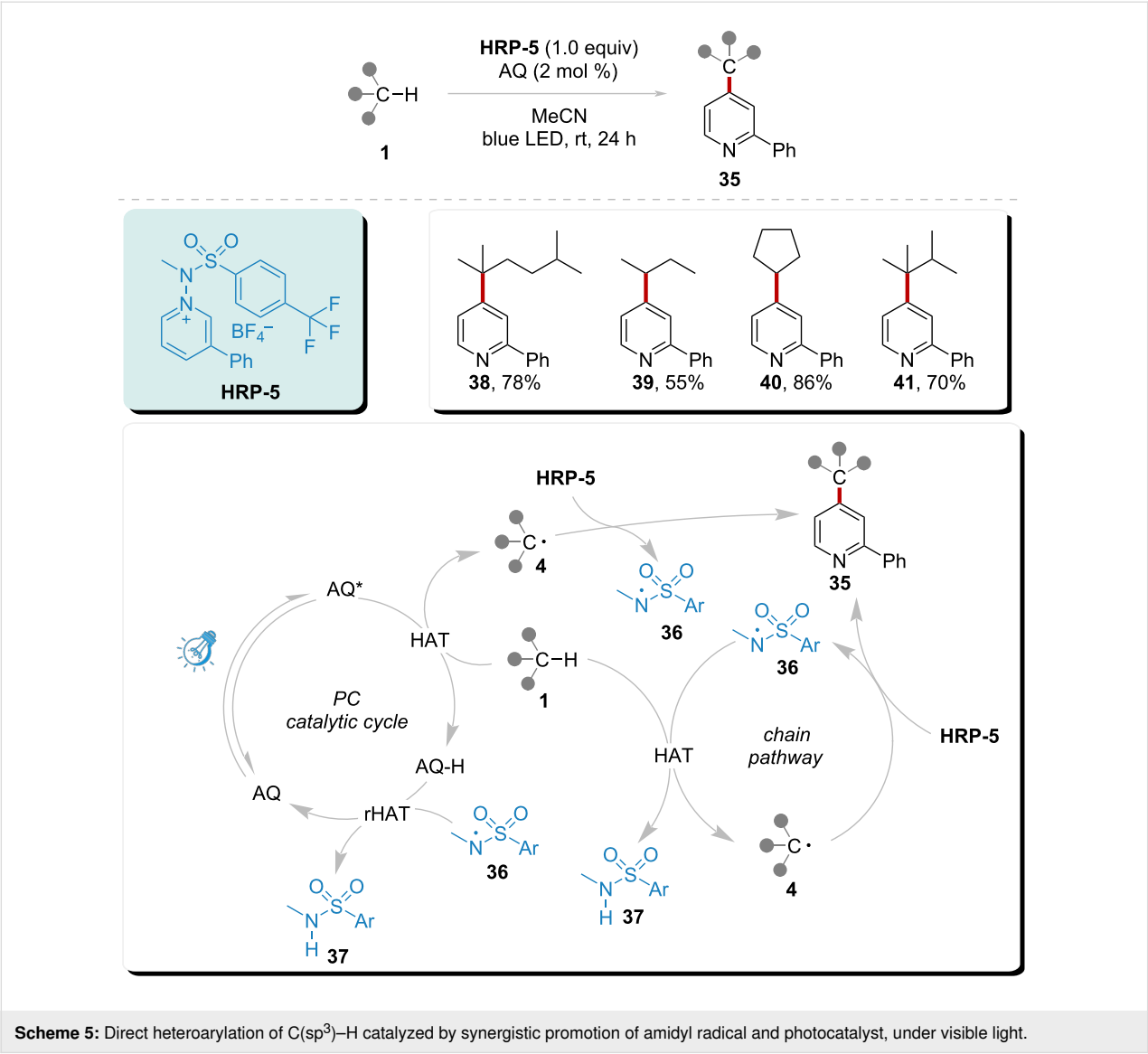


Scheme 4: Alkylation of C(sp^3)–H, Si–H, and Ge–H catalyzed by amidyl radical under visible light.

[84]. These compounds preferentially undergo SET reduction, resulting in the cleavage of the N–O bond. Typically, this cleavage generates an amidyl anion and an O radical [5,85-88]. Conversely, it is also possible for the N–O bond to produce an amidyl radical alongside an O anion.

In 2023, Doyle's group reported a novel system initiated by an off-cycle reductive quenching of the activated CF_3-4CzIPN* species, leading to the generation of a ground state photocatalyst radical anion (Scheme 7) [89]. This radical anion subsequently underwent SET reduction of **HRP-7**, resulting in the liberation of amidyl radical **45**. The amidyl radical **45** efficiently abstracted a hydrogen atom from substrate **1**, yielding radical **4** and byproduct amide **46**. Furthermore, the resultant radical **4** was oxidized by the excited photocatalyst, resulting in the concurrent generation of the carbon cation **55**. This cation was subsequently trapped by a nucleophile, leading to the formation of product **54**. This system demonstrated a broad applicability for the general nucleophilic amination of benzylic C–H bonds. The substrate's scope and selectivity were exemplified by the satisfactory yields of products **55**–**57**, and **58**, which achieved yields of 43–85%.

Inspired by these previous work, Yu's group devised a new photocatalyzed system catalyzed by a newly designed photocatalyst Br-5CzBN. This robust strategy implements direct heteroarylation of C(sp^3)–H and C(sp^3)–H without the presence of strong bases, acids, or oxidants (Scheme 8) [90]. The reaction is initiated by SET reduction of **HRP-8** via excited photocatalyst Br-5CzBN*, subsequently generating HAT reagent **45**, O-anion **64**, and Br-5CzBN$^{+\bullet}$. HAT reagent **45** engages a HAT event with the substrate, converting it into the byproduct **46** and generating a carbon-centered radical **62**. Species **62** is trapped by heteroarene **60**, leading to the formation of the intermediate **63**. This intermediate **63** undergoes SET and proton transfer with the assistance of O-anion **64** and the Br-5CzBN$^{+\bullet}$ radical cation, delivering the final product **61** and regenerating photocatalyst Br-5CzBN. **HRP-8** functions as an oxidizing agent, facilitating the generation of a highly active HAT reagent, while the O-anion **64** serves as a base. This eluci-



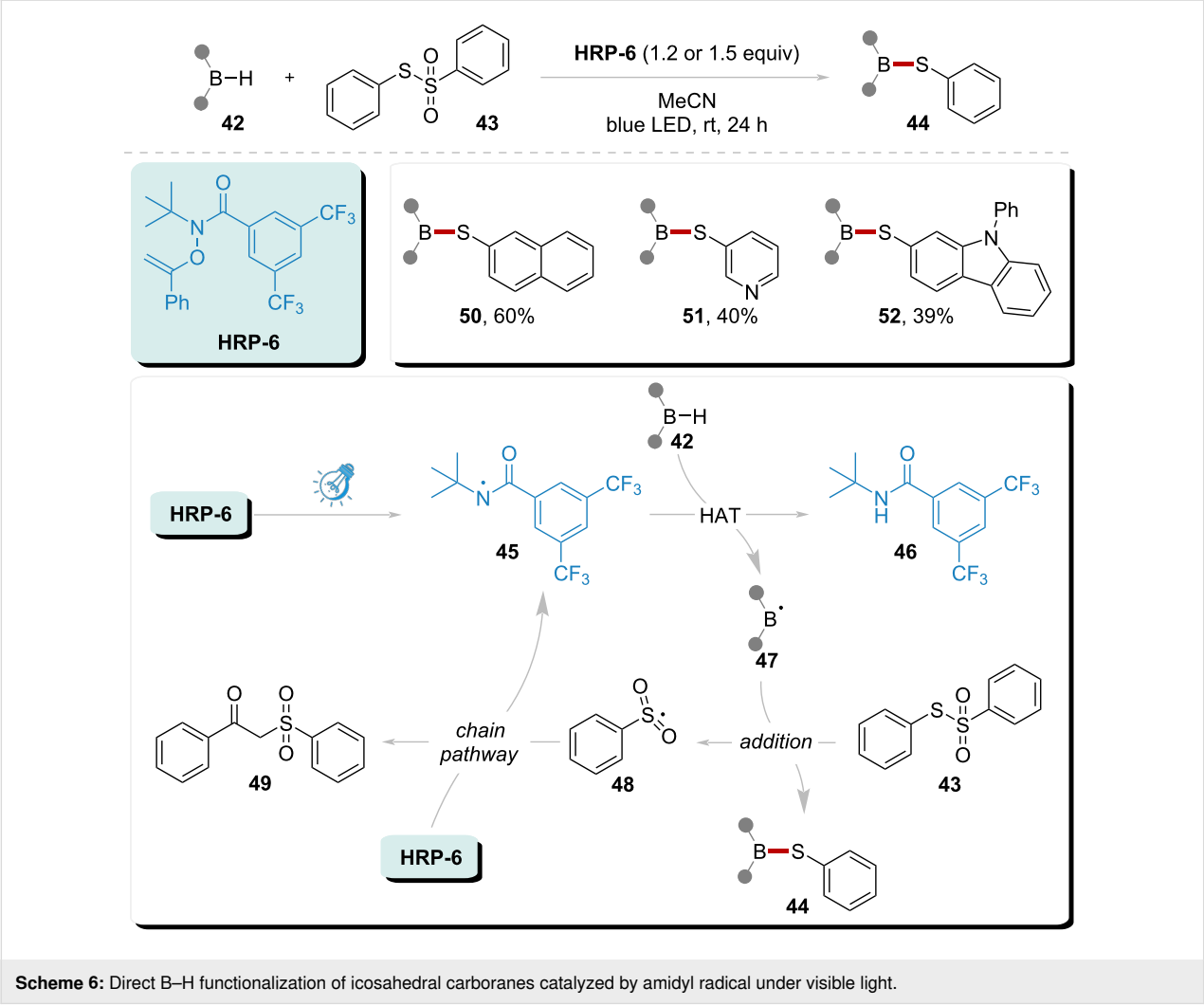
Scheme 5: Direct heteroarylation of C(sp^3)–H catalyzed by synergistic promotion of amidyl radical and photocatalyst, under visible light.

dates the rationale behind the self-sufficiency of this photocatalytic system, obviating the need for supplementary oxidants and bases, thereby enabling broad substrate adaptability. This streamlined approach demonstrates significant potential for extended utility in pharmaceutical late-stage functionalization (LSF), particularly evidenced by the synthetically valuable yields (60–80%) obtained for structurally diversified target molecules **65**–**68** under optimized reaction conditions. In these cases, the high polarity of the radical intermediates of CF_3CH_2OH and 4-methylbenzonitrile, combined with the poor solubility of adamantane, may explain the possible reasons behind the reaction process [91].

Amidyl radical from N–S bond cleavage

The work of Alexanian's group has significantly advanced the field of organic synthesis over recent years, particularly in the area of N–S bond homolytic cleavage [92-94]. Initial studies demonstrated that high-temperature conditions were required to facilitate this reaction; however, such extreme conditions limited the practical applicability of the reactions. To address this limitation, Alexanian's research has shifted toward the principles of green chemistry, utilizing visible light to achieve mild reaction conditions. This approach has not only enhanced the feasibility of the reactions but has also led to the establishment of a comprehensive platform for C–H functionalization through the introduction of the highly versatile xanthyl functional group.

In 2016, Alexanian's group successfully implemented a method for the direct xanthylation of C–H bonds with high selectivity and efficiency (Scheme 9) [95]. This process is initiated through a visible light-triggered chain reaction, involving the homolytic cleavage of **HRP-9**. The liberation of amidyl radical **45** facili-



Scheme 6: Direct B–H functionalization of icosahedral carboranes catalyzed by amidyl radical under visible light.

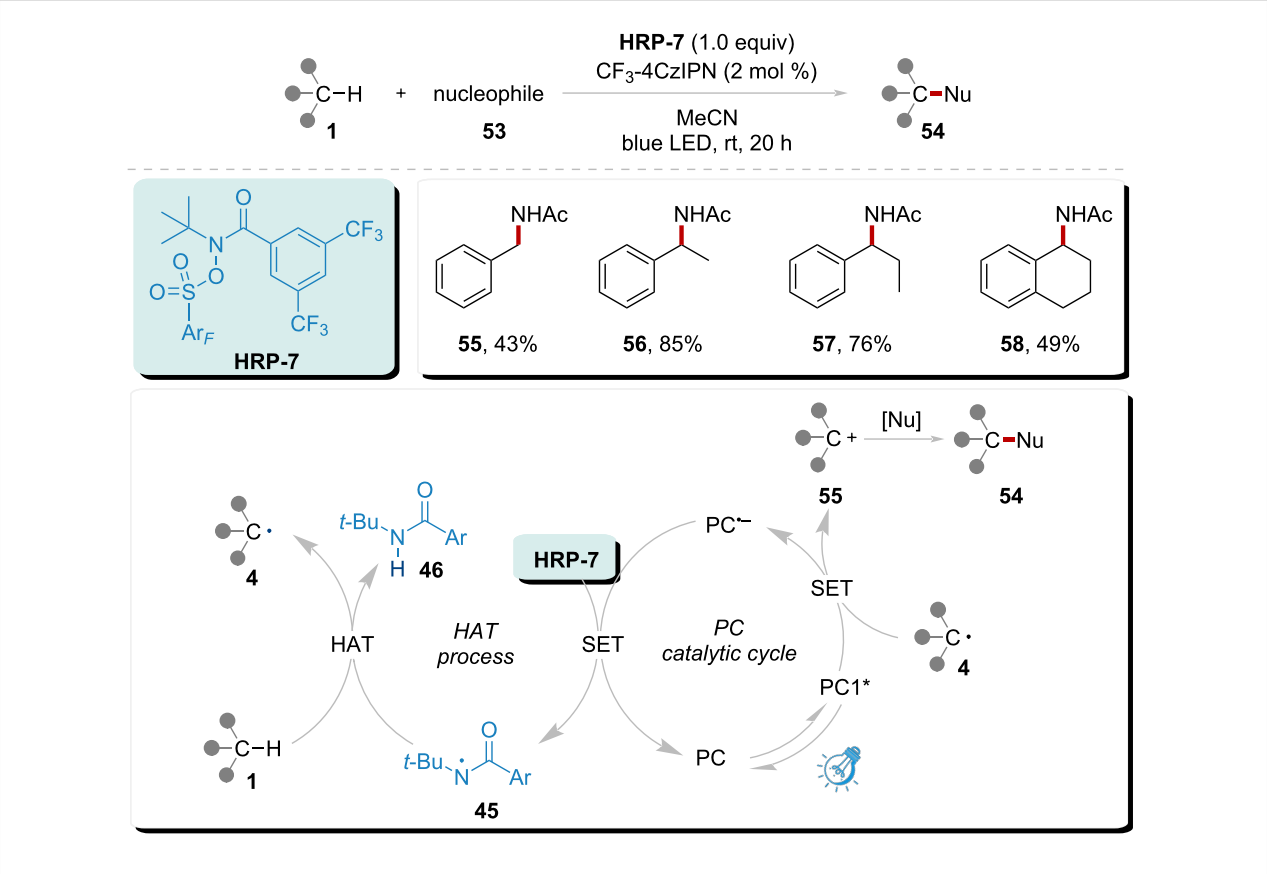
tates hydrogen atom abstraction from the substrate, resulting in the formation of radical **4** and the concurrent generation of by-product **46**. Subsequent trapping of radical **4** by **HRP-9** leads to the generation of product **69**. This methodology demonstrates a broad substrate scope and exhibits significant synthetic utility, particularly for the generation of products **70**, **71**, and **72** with yields ranging from 54% to 59%.

In an effort to evaluate the practicality of visible light-promoted xanthylation, Alexanian's group conducted a regioselective C–H xanthylation of polyolefins (Scheme 10) [96]. Building on previous findings, the **HRP-9** undergoes homolytic N–S cleavage, yielding amidyl radical **45**. This radical effectively abstracts a hydrogen atom from the polyolefin substrate, demonstrating notable regioselectivity. The xanthylation reaction preferentially generates main products **76**, and byproducts (**77** and **78**). Furthermore, the successful implementation of this methodology facilitates the production of a diverse range of functionalized polyolefins, showcasing the applicability of this xanthylated polyolefin in various reactions, including trifluoromethylthiolation, polymer grafting, Michael addition, and epoxide opening.

Amidyl radical from N–X bond cleavage

Direct halogenation of C–H bonds is of significant value in organic synthesis. Introducing a bromine or chlorine atom into aliphatic C–H bonds with high site selectivity and efficiency poses a formidable challenge. Traditional strategies for the halogenation of aliphatic C–H bonds typically rely on biomimetic iron-catalyzed oxidation systems that require electrophilic heterocycles. These limitations hinder the broader application of such systems.

Alexanian's group modified amidyl radical precursors by incorporating halogen atoms, transforming them into bifunctional reagents. The HAT component of amidyl radical precursors was facilitated by amidyl radicals, while halogenation was promoted by the introduced halogen atom [26].



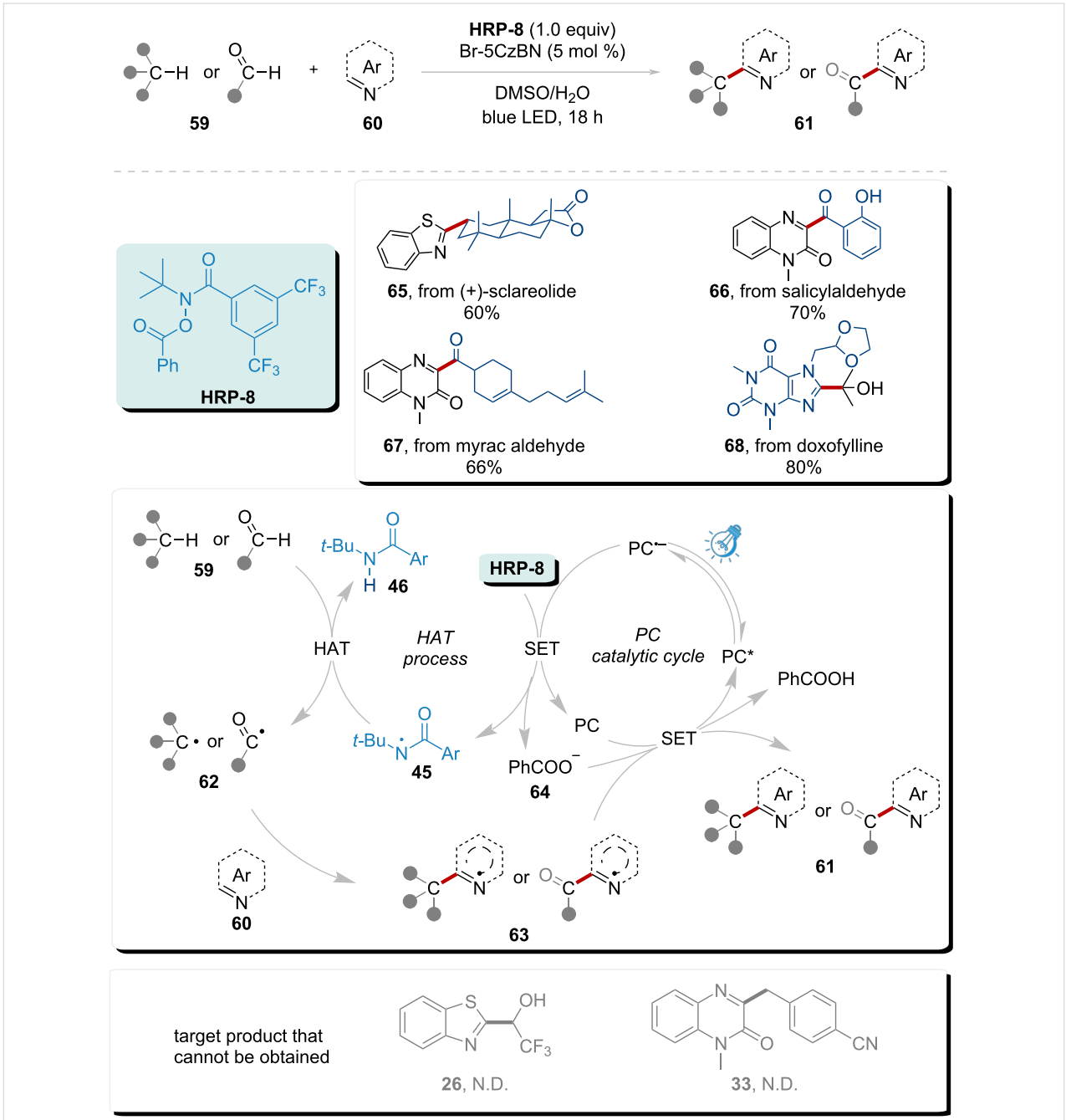
Scheme 7: Nucleophilic amination of C(sp^3)–H enabled by amidyl radical under visible light.

In 2014, Alexanian's group reported a site-selective aliphatic C–H bromination utilizing modified HRP as both the bromination reagent and HAT reagent (Scheme 11) [25]. Initiated by visible light, **HRP-10** underwent homolytic cleavage of the N–Br bond, generating amidyl radical **45**. This amidyl radical subsequently participated in a HAT process with the aliphatic substrate **1**, leading to the formation of radical **4** and byproduct amide **46**. The corresponding radical **4** was then trapped by **HRP-10**, thereby triggering a chain reaction that regenerated amidyl radical **45**. This system effectively examined the site selectivity of aliphatic C–H bromination, yielding products **80**–**82**, and **83** with 54% to 63% yields at selective positions. This bromination system provided a mild reaction environment suitable for aliphatic C–H bonds.

In 2016, Alexanian's group reported a chlorination method for aliphatic C–H bonds with high site selectivity to expand the halogenation capabilities and applicability of their system (Scheme 12) [97]. Consistent with previous experiments, the reaction was initiated by visible light, generating amidyl radical **45** from **HRP-11**. The resulting radical **45** abstracted a hydrogen atom from substrate **1**, simultaneously generating radical **4**. Subsequently, radical **4** was trapped by **HRP-11**, leading to the formation of chlorinated product **84**. In this system, monochlorinated products were obtained with good selectivity, evidenced by yields of 69% and 54% for products **85**, and **86**, respectively. Notably, the natural product sclareolide underwent chlorination with an impressive selectivity, achieving an 82% yield for the product **87**.

Amidyl radical from amide anion

In 2024, Ooi and colleagues established a pivotal advancement in catalytic methodology through the rational design of zwitterionic acridinium amidates. These photoactive amidyl radical precursors demonstrated exceptional HAT reactivity, enabling efficient functionalization of unactivated C–H bonds under mild irradiation conditions (Scheme 13) [98]. The mechanistic pathway initiates with ground-state complexation **90** between **HRP-12** and HFIP via hydrogen bonding. Following visible-light excitation of **90**, intersystem crossing (ISC) from the S1(LE) to T2 state generates the catalytically competent triplet excited state **91**. This N-centered radical species subsequently abstracts a hydrogen atom from substrate **1** through HAT, producing an α-amido-acridinyl radical intermediate **92** and a substrate-derived carbon-centered radical **4**. Radical **4** undergoes regioselective addition to the acceptor, forming transient radical adduct



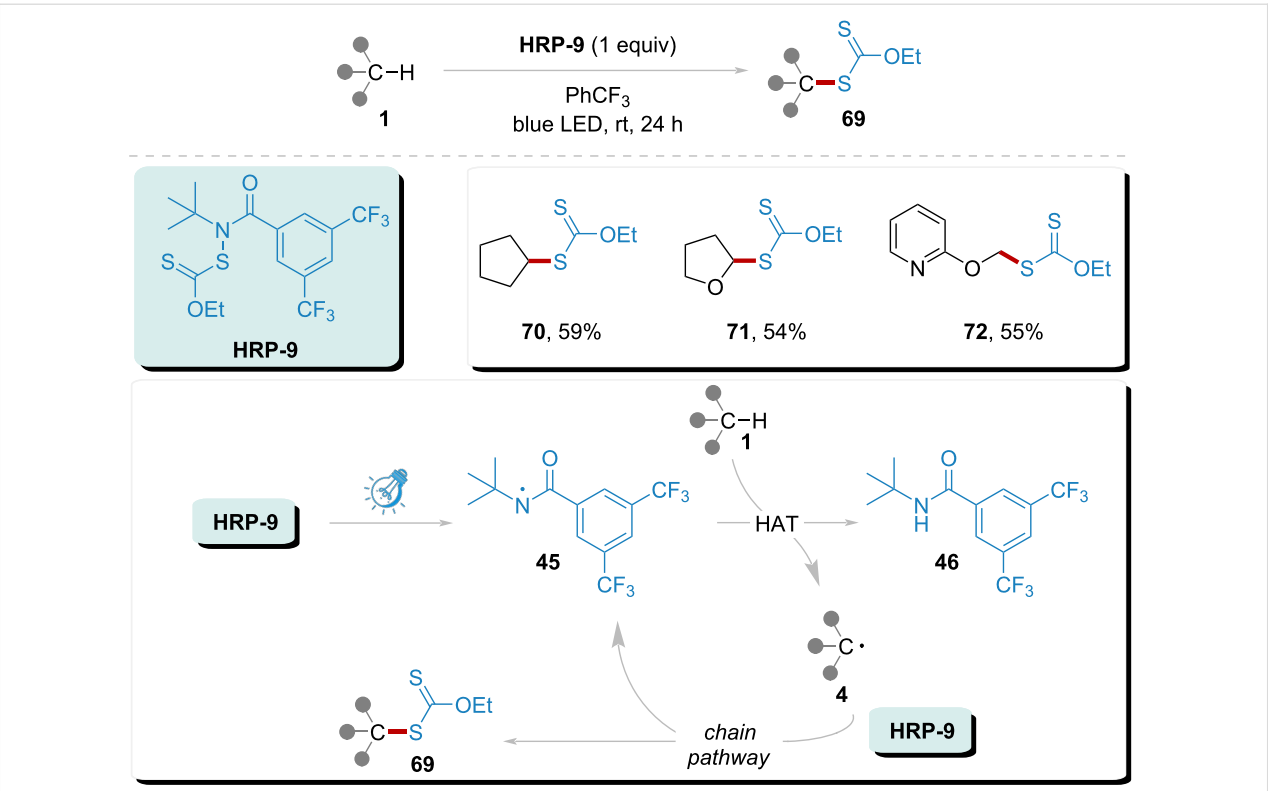
Scheme 8: Direct heteroarylation of C(sp^3)–H and C(sp^3)–H without the presence of strong bases, acids, or oxidants.

93. A concomitant SET from **92** to **93** generates a carbanion, which undergoes either solvent-mediated protonation or direct proton transfer from the acridiniumamide, ultimately delivering product **89** while regenerating the zwitterionic **HRP-12** catalyst.

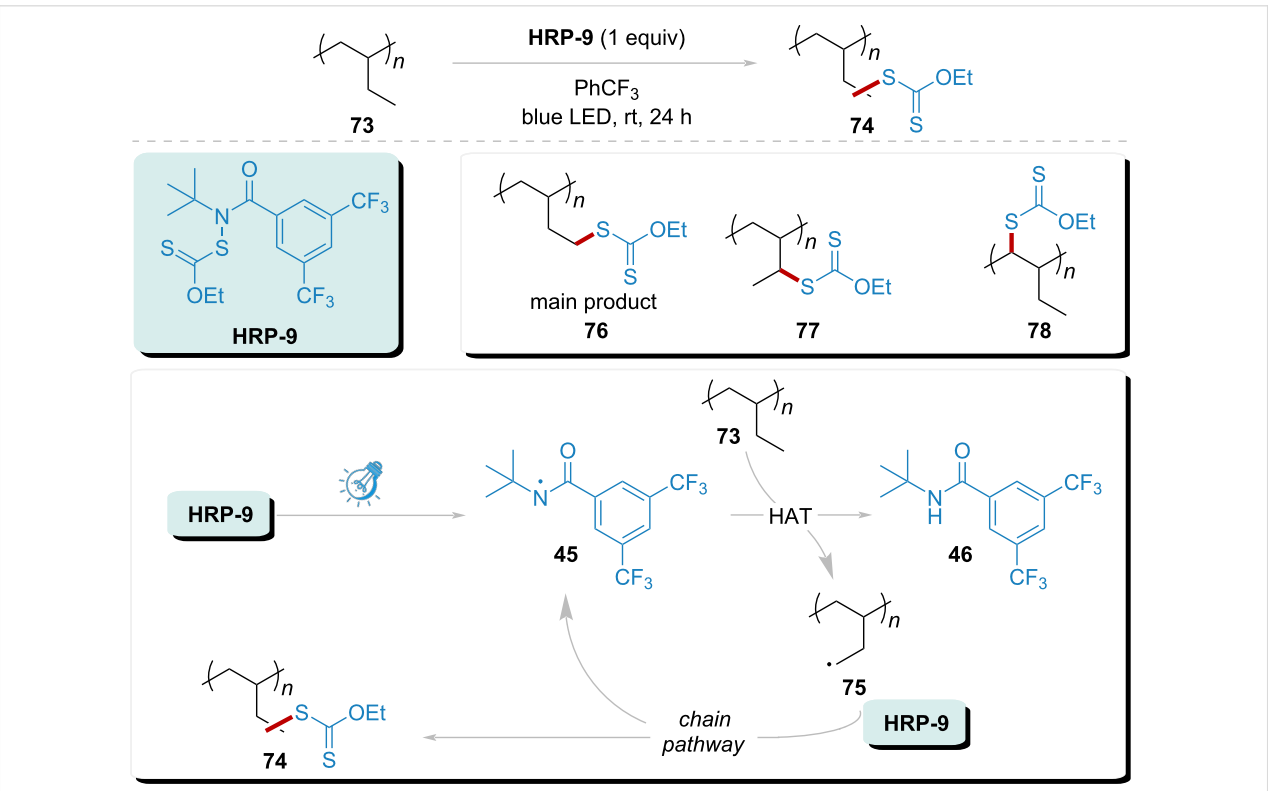
This catalytic platform demonstrated exceptional site selectivity in aliphatic C–H bromination under ambient temperature and visible-light irradiation, achieving site-selective bromination (products **94**–**96**) in 51–99% yields across electronically differentiated positions. The system's operational mildness and functional group tolerance highlight its suitability for late-stage functionalization of complex aliphatic architectures.

Conclusion

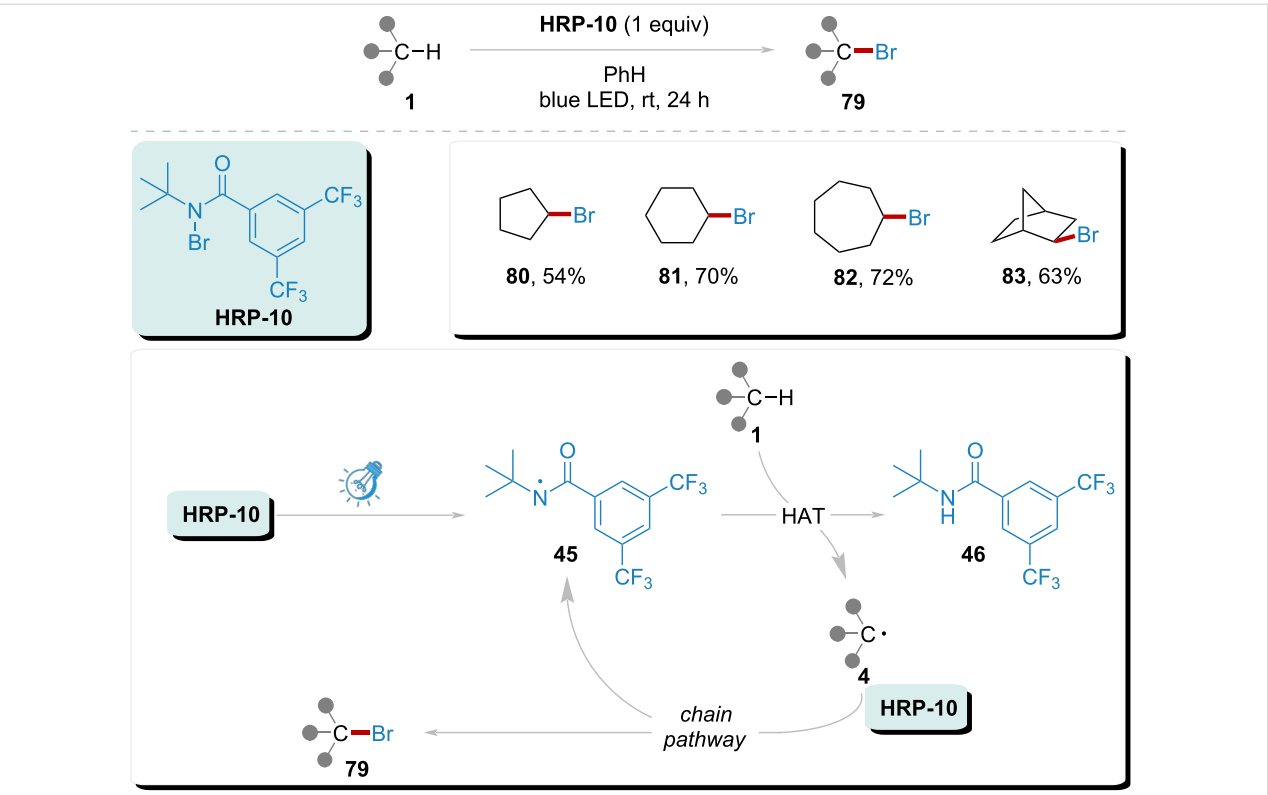
In this review, we highlight recent advances in the use of visible light to enhance amidyl radical-mediated direct intermolecular HAT for the functionalization of C–H, Si–H, Ge–H, and B–H bonds. These robust strategies hold the promise of the direct



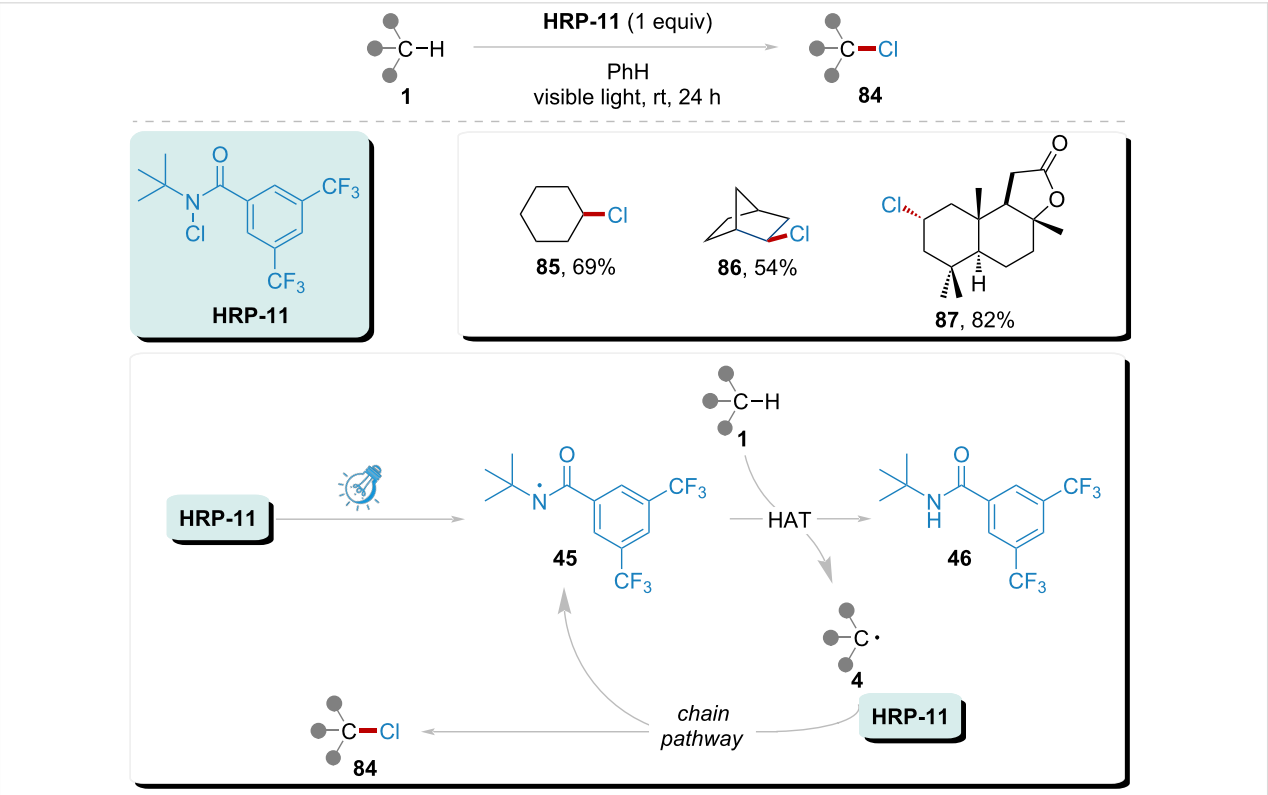
Scheme 9: Xanthylation of C(sp^3)–H addressed by amidyl radical under visible light.



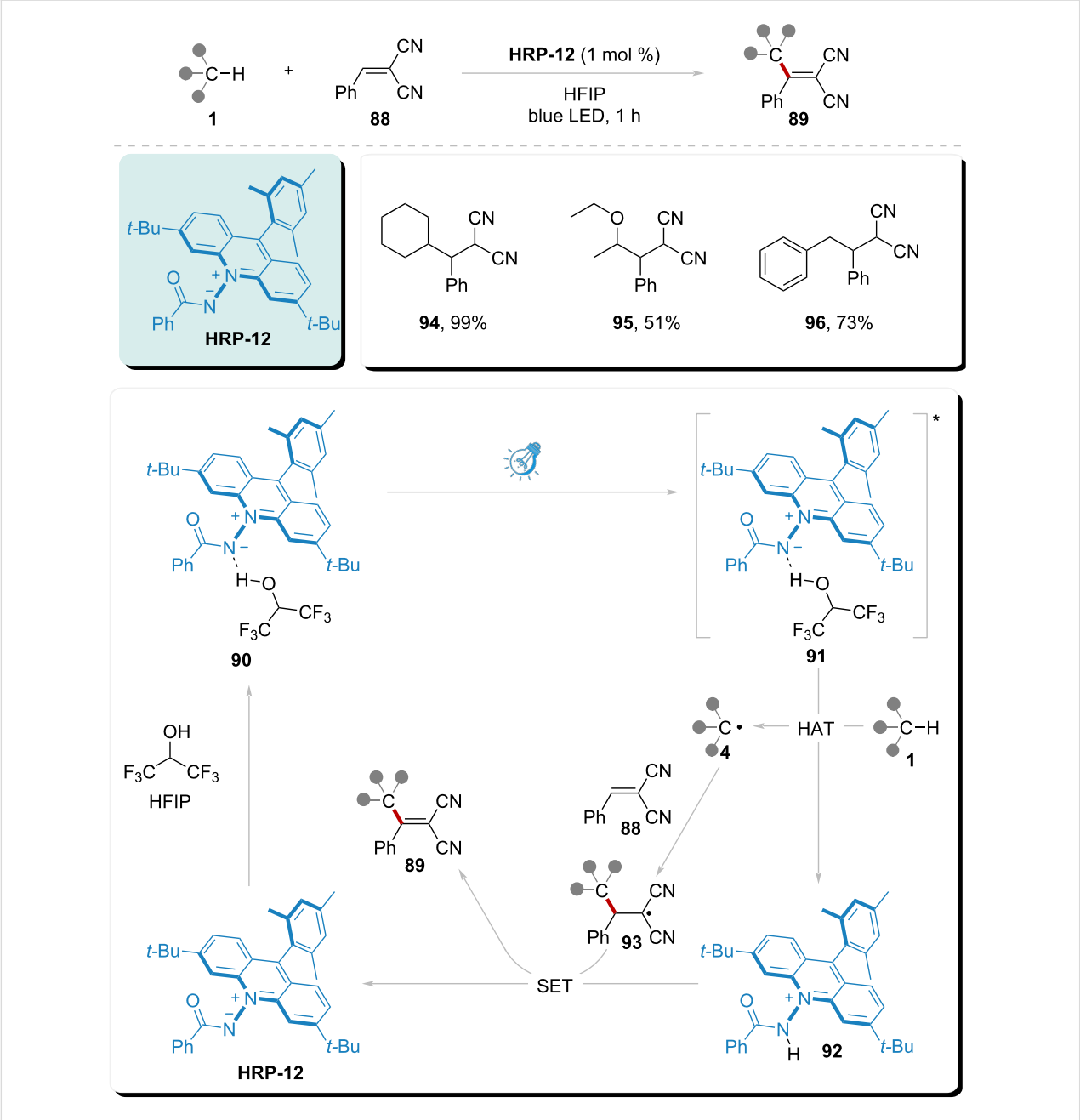
Scheme 10: Xanthylation of C(sp^3)–H in polyolefins addressed by amidyl radical under visible light.



Scheme 11: Site-selective C(sp^3)–H bromination implemented by amidyl radical under visible light.



Scheme 12: Site-selective chlorination of C(sp^3)–H in natural products implemented by amidyl radical under visible light.



Scheme 13: Alkylation of C(sp^3)–H catalyzed by amidyl radical photocatalyst under visible light.

functionalization of these bonds through high selectivity, efficiency, and a stepwise approach.

In the presence of amidyl radicals, hydrogen atoms are directly abstracted from C–H, Si–H, Ge–H, and B–H bonds, leading to the formation of corresponding radicals. We summarize and emphasize notable pioneering experiments in this area. Switchable amidyl radicals provide an effective toolkit for completing hydrogen atom transfer processes. Transitioning from noble metal photocatalysts to organic photocatalysts and from HAT reagents to bifunctional reagents, these remarkable photocatalytic systems have inspired innovations across various fields of organic synthesis methodology.

Despite significant research achievements of amidyl radicals in the photocatalytic transformation of C(sp^3)–H, C(sp^2)–H, S–H, Ge–H, and B–H bonds, they still face considerable challenges in the application of hydrogen abstraction from electron-deficient C–H bonds due to their inherent polarity. Furthermore, amidyl radicals encounter difficulties in regioselectivity when

applied to structurally complex C–H substrates, which limits their utility in modifying intricate molecular architectures. Future advancements are anticipated through structural modifications of amidyl radicals aimed at optimizing their polarity via electronic effects, which may enhance their effectiveness in hydrogen abstraction from electron-deficient substrates. Additionally, strategies to optimize steric effects could improve their regioselectivity in hydrogen abstraction from complex substrates.

Crucially, structural optimization of HRP components could potentially overcome current mechanistic limitations, establishing a generalized platform for hydrogen atom transfer (HAT)-enabled direct functionalization. This advanced methodology would demonstrate unprecedented versatility across diverse bond activation challenges, particularly in C(sp^3)–H, C(sp^2)–H, S–H, Ge–H, and B–H bond transformations. The proposed system architecture emphasizes synergistic reagent cooperation rather than isolated component performance, representing a paradigm shift in photoredox catalysis design principles.

Funding

We acknowledge the financial support from the National Natural Science Foundation of China (21971224 and 22171249), the Science & Technology Innovation Talents in Universities of Henan Province (23HASTIT003), Science and Technology Research and Development Plan Joint Fund of Henan Province (242301420006).

ORCID® iDs

Lin Li - https://orcid.org/0009-0008-2678-5324
Bing Yu - https://orcid.org/0000-0002-2423-1212

Data Availability Statement

Data sharing is not applicable as no new data was generated or analyzed in this study.

References

1. Pratley, C.; Fenner, S.; Murphy, J. A. *Chem. Rev.* **2022,** *122,* 8181–8260. doi:10.1021/acs.chemrev.1c00831
2. Xiong, T.; Zhang, Q. *Chem. Soc. Rev.* **2016,** *45,* 3069–3087. doi:10.1039/c5cs00852b
3. Yu, X.-Y.; Chen, J.-R.; Xiao, W.-J. *Chem. Rev.* **2021,** *121,* 506–561. doi:10.1021/acs.chemrev.0c00030
4. Zhang, J.; Huan, X.-D.; Wang, X.; Li, G.-Q.; Xiao, W.-J.; Chen, J.-R. *Chem. Commun.* **2024,** *60,* 6340–6361. doi:10.1039/d4cc01969e
5. Guo, Y.; Lin, G.; Zhang, M.; Xu, J.; Song, Q. *Nat. Commun.* **2024,** *15,* 7313. doi:10.1038/s41467-024-51334-5
6. Hartwig, J. F. *J. Am. Chem. Soc.* **2016,** *138,* 2–24. doi:10.1021/jacs.5b08707
7. Liu, B.; Romine, A. M.; Rubel, C. Z.; Engle, K. M.; Shi, B.-F. *Chem. Rev.* **2021,** *121,* 14957–15074. doi:10.1021/acs.chemrev.1c00519
8. Mishra, A. A.; Subhedar, D.; Bhanage, B. M. *Chem. Rec.* **2019,** *19,* 1829–1857. doi:10.1002/tcr.201800093
9. He, C.; Whitehurst, W. G.; Gaunt, M. J. *Chem* **2019,** *5,* 1031–1058. doi:10.1016/j.chempr.2018.12.017
10. Zhang, Y.; Qi, Z.-H.; Ruan, G.-Y.; Zhang, Y.; Liu, W.; Wang, Y. *RSC Adv.* **2015,** *5,* 71586–71592. doi:10.1039/c5ra11488h
11. Wu, X.; Zhu, C. *CCS Chem.* **2020,** *2,* 813–828. doi:10.31635/ccschem.020.202000234
12. Maity, B.; Dutta, S.; Cavallo, L. *Chem. Soc. Rev.* **2023,** *52,* 5373–5387. doi:10.1039/d2cs00960a
13. Wang, X.; He, J.; Wang, Y.-N.; Zhao, Z.; Jiang, K.; Yang, W.; Zhang, T.; Jia, S.; Zhong, K.; Niu, L.; Lan, Y. *Chem. Rev.* **2024,** *124,* 10192–10280. doi:10.1021/acs.chemrev.4c00188
14. Hu, X.; Cheng-Sánchez, I.; Kong, W.; Molander, G. A.; Nevado, C. *Nat. Catal.* **2024,** *7,* 655–665. doi:10.1038/s41929-024-01153-0
15. Li, Q.-Y.; Cheng, S.; Ye, Z.; Huang, T.; Yang, F.; Lin, Y.-M.; Gong, L. *Nat. Commun.* **2023,** *14,* 6366. doi:10.1038/s41467-023-42191-9
16. Gong, L. *Nat. Synth.* **2022,** *1,* 915–916. doi:10.1038/s44160-022-00174-6
17. Li, B.; Qin, H.; Yan, K.; Ma, J.; Yang, J.; Wen, J. *Org. Chem. Front.* **2022,** *9,* 6861–6868. doi:10.1039/d2qo01498j
18. Yan, T.; Yang, J.; Yan, K.; Wang, Z.; Li, B.; Wen, J. *Angew. Chem., Int. Ed.* **2024,** *63,* e202405186. doi:10.1002/anie.202405186
19. Kawasaki, T.; Ishida, N.; Murakami, M. *J. Am. Chem. Soc.* **2020,** *142,* 3366–3370. doi:10.1021/jacs.9b13920
20. Ishida, N.; Masuda, Y.; Imamura, Y.; Yamazaki, K.; Murakami, M. *J. Am. Chem. Soc.* **2019,** *141,* 19611–19615. doi:10.1021/jacs.9b12529
21. Wang, Z.; Ji, X.; Han, T.; Deng, G.-J.; Huang, H. *Adv. Synth. Catal.* **2019,** *361,* 5643–5647. doi:10.1002/adsc.201901168
22. Treacy, S. M.; Rovis, T. *J. Am. Chem. Soc.* **2021,** *143,* 2729–2735. doi:10.1021/jacs.1c00687
23. Tu, J.-L.; Hu, A.-M.; Guo, L.; Xia, W. *J. Am. Chem. Soc.* **2023,** *145,* 7600–7611. doi:10.1021/jacs.3c01082
24. Shen, Y.; Gu, Y.; Martin, R. *J. Am. Chem. Soc.* **2018,** *140,* 12200–12209. doi:10.1021/jacs.8b07405
25. Schmidt, V. A.; Quinn, R. K.; Brusoe, A. T.; Alexanian, E. J. *J. Am. Chem. Soc.* **2014,** *136,* 14389–14392. doi:10.1021/ja508469u
26. Carestia, A. M.; Ravelli, D.; Alexanian, E. J. *Chem. Sci.* **2018,** *9,* 5360–5365. doi:10.1039/c8sc01756e
27. Mao, R.; Bera, S.; Turla, A. C.; Hu, X. *J. Am. Chem. Soc.* **2021,** *143,* 14667–14675. doi:10.1021/jacs.1c05874
28. Huang, C.; Qin, Y.-S.; Wang, C.-L.; Xiao, P.; Tang, S.; Liu, H.-J.; Wei, Z.; Cai, H. *Chem. Commun.* **2024,** *60,* 2669–2672. doi:10.1039/d3cc06210d
29. Sonawane, S. C.; Gourkhede, R.; Saini, P.; Ramakrishnan, S.; Balakrishna, M. S. *Chem. Commun.* **2024,** *60,* 6055–6058. doi:10.1039/d4cc01119h
30. Sharma, A. K.; Maseras, F. *Inorg. Chem.* **2024,** *63,* 13801–13806. doi:10.1021/acs.inorgchem.4c01763
31. Roberts, B. P. *Chem. Soc. Rev.* **1999,** *28,* 25–35. doi:10.1039/a804291h
32. Cao, J.; Wang, G.; Gao, L.; Cheng, X.; Li, S. *Chem. Sci.* **2018,** *9,* 3664–3671. doi:10.1039/c7sc05225a
33. Bell, J. D.; Murphy, J. A. *Chem. Soc. Rev.* **2021,** *50,* 9540–9685. doi:10.1039/d1cs00311a

34. Zhang, Y.; Li, K.-D.; Zhou, C.-Q.; Xing, Z.-X.; Huang, H.-M. *Green Chem.* **2024,** *26,* 10434–10440. doi:10.1039/d4gc02879a
35. Pannwitz, A.; Wenger, O. S. *Chem. Commun.* **2019,** *55,* 4004–4014. doi:10.1039/c9cc00821g
36. Latrache, M.; Hoffmann, N. *Chem. Soc. Rev.* **2021,** *50,* 7418–7435. doi:10.1039/d1cs00196e
37. Zhou, R.; Li, J.; Cheo, H. W.; Chua, R.; Zhan, G.; Hou, Z.; Wu, J. *Chem. Sci.* **2019,** *10,* 7340–7344. doi:10.1039/c9sc02818h
38. Su, Y.; Li, Y.; Ganguly, R.; Kinjo, R. *Chem. Sci.* **2017,** *8,* 7419–7423. doi:10.1039/c7sc03528d
39. Zhu, X.; Li, P.; Shi, Q.; Wang, L. *Green Chem.* **2016,** *18,* 6373–6379. doi:10.1039/c6gc01487a
40. Tierney, M. M.; Crespi, S.; Ravelli, D.; Alexanian, E. J. *J. Org. Chem.* **2019,** *84,* 12983–12991. doi:10.1021/acs.joc.9b01774
41. Nanjo, T.; Matsumoto, A.; Oshita, T.; Takemoto, Y. *J. Am. Chem. Soc.* **2023,** *145,* 19067–19075. doi:10.1021/jacs.3c06931
42. Lee, H.; He, T.; Cook, S. P. *Org. Lett.* **2023,** *25,* 1–4. doi:10.1021/acs.orglett.2c02864
43. Gonzalez, M. I.; Gygi, D.; Qin, Y.; Zhu, Q.; Johnson, E. J.; Chen, Y.-S.; Nocera, D. G. *J. Am. Chem. Soc.* **2022,** *144,* 1464–1472. doi:10.1021/jacs.1c13333
44. Li, N.; Li, J.; Qin, M.; Li, J.; Han, J.; Zhu, C.; Li, W.; Xie, J. *Nat. Commun.* **2022,** *13,* 4224. doi:10.1038/s41467-022-31956-3
45. Wu, Y.; Liu, Z.; Li, Y.; Chen, J.; Zhu, X.; Na, P. *Chin. J. Catal.* **2019,** *40,* 60–69. doi:10.1016/s1872-2067(18)63170-5
46. Liu, D.; Chen, S.; Zhang, Y.; Li, R.; Peng, T. *Appl. Catal., B* **2023,** *333,* 122805. doi:10.1016/j.apcatb.2023.122805
47. Wei, Y.; Shahid, M. Z.; Lyu, S.; Sun, W.; Lyu, S. *RSC Adv.* **2021,** *11,* 22618–22624. doi:10.1039/d1ra02958d
48. Ouyang, W.-T.; Jiang, J.; Jiang, Y.-F.; Li, T.; Liu, Y.-Y.; Ji, H.-T.; Ou, L.-J.; He, W.-M. *Chin. Chem. Lett.* **2024,** *35,* 110038. doi:10.1016/j.cclet.2024.110038
49. Xu, Y.-D.; Xing, Y.-M.; Ji, H.-T.; Ou, L.-J.; He, W.-B.; Peng, J.; Wang, J.-S.; Jiang, J.; He, W.-M. *J. Org. Chem.* **2024,** *89,* 17701–17707. doi:10.1021/acs.joc.4c02445
50. Hou, J.-C.; Jiang, J.; Dai, H.; Wang, J.-S.; Li, T.; Chen, X.; He, W.-M. *Sci. China: Chem.* **2025,** *68,* 1945–1951. doi:10.1007/s11426-024-2496-5
51. Zhang, Q.; Zhao, Q.; Wu, X.; Wang, L.; Shen, K.; Hua, Y.; Gao, C.; Zhang, Y.; Peng, M.; Zhao, K. *Chin. Chem. Lett.* **2025,** *36,* 110167. doi:10.1016/j.cclet.2024.110167
52. Guo, J.-J.; Hu, A.; Zuo, Z. *Tetrahedron Lett.* **2018,** *59,* 2103–2111. doi:10.1016/j.tetlet.2018.04.060
53. Chen, H.; Yu, S. *Org. Biomol. Chem.* **2020,** *18,* 4519–4532. doi:10.1039/d0ob00854k
54. Davies, J.; Morcillo, S. P.; Douglas, J. J.; Leonori, D. *Chem. – Eur. J.* **2018,** *24,* 12154–12163. doi:10.1002/chem.201801655
55. Gao, S.; Li, F. *Adv. Funct. Mater.* **2023,** *33,* 2304291. doi:10.1002/adfm.202304291
56. Lasso, J. D.; Castillo-Pazos, D. J.; Li, C.-J. *Chem. Soc. Rev.* **2021,** *50,* 10955–10982. doi:10.1039/d1cs00380a
57. Liang, Y.-F.; Bilal, M.; Tang, L.-Y.; Wang, T.-Z.; Guan, Y.-Q.; Cheng, Z.; Zhu, M.; Wei, J.; Jiao, N. *Chem. Rev.* **2023,** *123,* 12313–12370. doi:10.1021/acs.chemrev.3c00219
58. Bellotti, P.; Huang, H.-M.; Faber, T.; Glorius, F. *Chem. Rev.* **2023,** *123,* 4237–4352. doi:10.1021/acs.chemrev.2c00478
59. Choi, G. J.; Zhu, Q.; Miller, D. C.; Gu, C. J.; Knowles, R. R. *Nature* **2016,** *539,* 268–271. doi:10.1038/nature19811
60. Chu, J. C. K.; Rovis, T. *Nature* **2016,** *539,* 272–275. doi:10.1038/nature19810
61. Li, W.; Sun, B.; Zhang, L.; Mo, F. *Green Chem.* **2023,** *25,* 5030–5034. doi:10.1039/d3gc01426f
62. Wang, C.; Chen, Z.; Sun, J.; Tong, L.; Wang, W.; Song, S.; Li, J. *Nat. Commun.* **2024,** *15,* 5087. doi:10.1038/s41467-024-49337-3
63. Stateman, L. M.; Dare, R. M.; Paneque, A. N.; Nagib, D. A. *Chem* **2022,** *8,* 210–224. doi:10.1016/j.chempr.2021.10.022
64. Ding, W.-W.; Zhou, Y.; Song, S.; Han, Z.-Y. *Org. Lett.* **2022,** *24,* 7350–7354. doi:10.1021/acs.orglett.2c02877
65. Deng, Z.; Zhao, Z.; He, G.; Chen, G. *Org. Lett.* **2021,** *23,* 3631–3635. doi:10.1021/acs.orglett.1c01020
66. Shu, W.; Zhang, H.; Huang, Y. *Org. Lett.* **2019,** *21,* 6107–6111. doi:10.1021/acs.orglett.9b02255
67. Herron, A. N.; Hsu, C.-P.; Yu, J.-Q. *Org. Lett.* **2022,** *24,* 3652–3656. doi:10.1021/acs.orglett.2c01261
68. Chen, Z.; Zhu, W.; Wang, C.; Xu, N.; Jin, Q.; Huang, X.; Song, S.; Li, J. *Org. Chem. Front.* **2023,** *10,* 4709–4717. doi:10.1039/d3qo00931a
69. Fu, X.; Tian, J.; Zhang, M.; Jing, Y.; Liu, Y.; Song, H.; Wang, Q. *Adv. Sci.* **2025,** *12,* 2411744. doi:10.1002/advs.202411744
70. Tanaka, H.; Sakai, K.; Kawamura, A.; Oisaki, K.; Kanai, M. *Chem. Commun.* **2018,** *54,* 3215–3218. doi:10.1039/c7cc09457d
71. Ma, Z.-Y.; Li, M.; Guo, L.-N.; Liu, L.; Wang, D.; Duan, X.-H. *Org. Lett.* **2021,** *23,* 474–479. doi:10.1021/acs.orglett.0c03992
72. Ram Bajya, K.; Kumar, M.; Ansari, A.; Selvakumar, S. *Adv. Synth. Catal.* **2023,** *365,* 976–982. doi:10.1002/adsc.202300040
73. Kim, J.; Kim, Y.-E.; Hong, S. *Angew. Chem., Int. Ed.* **2024,** *63,* e202409561. doi:10.1002/anie.202409561
74. Jung, S.; Lee, H.; Moon, Y.; Jung, H.-Y.; Hong, S. *ACS Catal.* **2019,** *9,* 9891–9896. doi:10.1021/acscatal.9b03367
75. Shin, S.; Lee, S.; Choi, W.; Kim, N.; Hong, S. *Angew. Chem., Int. Ed.* **2021,** *60,* 7873–7879. doi:10.1002/anie.202016156
76. Vellakkaran, M.; Kim, T.; Hong, S. *Angew. Chem., Int. Ed.* **2022,** *61,* e202113658. doi:10.1002/anie.202113658
77. Lee, W.; Jung, S.; Kim, M.; Hong, S. *J. Am. Chem. Soc.* **2021,** *143,* 3003–3012. doi:10.1021/jacs.1c00549
78. Fazekas, T. J.; Alty, J. W.; Neidhart, E. K.; Miller, A. S.; Leibfarth, F. A.; Alexanian, E. J. *Science* **2022,** *375,* 545–550. doi:10.1126/science.abh4308
79. Liang, D.; Chen, J.-R.; Tan, L.-P.; He, Z.-W.; Xiao, W.-J. *J. Am. Chem. Soc.* **2022,** *144,* 6040–6049. doi:10.1021/jacs.2c01116
80. Zhang, B.; Erb, F. R.; Vasilopoulos, A.; Voight, E. A.; Alexanian, E. J. *J. Am. Chem. Soc.* **2023,** *145,* 26540–26544. doi:10.1021/jacs.3c10751
81. Miller, A. S.; Alexanian, E. J. *Chem. Sci.* **2022,** *13,* 11878–11882. doi:10.1039/d2sc04605a
82. Lyu, X.-L.; Huang, S.-S.; Song, H.-J.; Liu, Y.-X.; Wang, Q.-M. *Org. Lett.* **2019,** *21,* 5728–5732. doi:10.1021/acs.orglett.9b02105
83. Ren, H.; Zhang, P.; Xu, J.; Ma, W.; Tu, D.; Lu, C.-s.; Yan, H. *J. Am. Chem. Soc.* **2023,** *145,* 7638–7647. doi:10.1021/jacs.3c01314
84. Fu, M.-C.; Shang, R.; Zhao, B.; Wang, B.; Fu, Y. *Science* **2019,** *363,* 1429–1434. doi:10.1126/science.aav3200
85. Qi, X.-K.; Zheng, M.-J.; Yang, C.; Zhao, Y.; Guo, L.; Xia, W. *J. Am. Chem. Soc.* **2023,** *145,* 16630–16641. doi:10.1021/jacs.3c04073
86. Feng, L.; Guo, L.; Yang, C.; Zhou, J.; Xia, W. *Org. Lett.* **2020,** *22,* 3964–3968. doi:10.1021/acs.orglett.0c01267
87. Zhu, Y.; Gao, H.; Tu, J.-L.; Yang, C.; Guo, L.; Zhao, Y.; Xia, W. *Org. Chem. Front.* **2024,** *11,* 1729–1735. doi:10.1039/d3qo01822a
88. Mu, S.; Guo, Y.; Huang, X.; Luo, Y.; Chen, M.; Xu, J.; Song, Q. *Org. Chem. Front.* **2023,** *10,* 3259–3263. doi:10.1039/d3qo00537b

89. Ruos, M. E.; Kinney, R. G.; Ring, O. T.; Doyle, A. G. *J. Am. Chem. Soc.* **2023,** *145,* 18487–18496. doi:10.1021/jacs.3c04912
90. Wang, H.-S.; Li, H.-C.; Yuan, X.-Y.; Sun, K.; Chen, X.-L.; Qu, L.; Yu, B. *Green Chem.* **2025,** *27,* 4655–4663. doi:10.1039/d4gc06209d
91. Garwood, J. J. A.; Chen, A. D.; Nagib, D. A. *J. Am. Chem. Soc.* **2024,** *146,* 28034–28059. doi:10.1021/jacs.4c06774
92. Na, C. G.; Ravelli, D.; Alexanian, E. J. *J. Am. Chem. Soc.* **2020,** *142,* 44–49. doi:10.1021/jacs.9b10825
93. Williamson, J. B.; Na, C. G.; Johnson, R. R., III; Daniel, W. F. M.; Alexanian, E. J.; Leibfarth, F. A. *J. Am. Chem. Soc.* **2019,** *141,* 12815–12823. doi:10.1021/jacs.9b05799
94. Margrey, K. A.; Czaplyski, W. L.; Nicewicz, D. A.; Alexanian, E. J. *J. Am. Chem. Soc.* **2018,** *140,* 4213–4217. doi:10.1021/jacs.8b00592
95. Czaplyski, W. L.; Na, C. G.; Alexanian, E. J. *J. Am. Chem. Soc.* **2016,** *138,* 13854–13857. doi:10.1021/jacs.6b09414
96. Williamson, J. B.; Czaplyski, W. L.; Alexanian, E. J.; Leibfarth, F. A. *Angew. Chem., Int. Ed.* **2018,** *57,* 6261–6265. doi:10.1002/anie.201803020
97. Quinn, R. K.; Könst, Z. A.; Michalak, S. E.; Schmidt, Y.; Szklarski, A. R.; Flores, A. R.; Nam, S.; Horne, D. A.; Vanderwal, C. D.; Alexanian, E. J. *J. Am. Chem. Soc.* **2016,** *138,* 696–702. doi:10.1021/jacs.5b12308
98. Entgelmeier, L.-M.; Mori, S.; Sendo, S.; Yamaguchi, R.; Suzuki, R.; Yanai, T.; García Mancheño, O.; Ohmatsu, K.; Ooi, T. *Angew. Chem., Int. Ed.* **2024,** *63,* e202404890. doi:10.1002/anie.202404890

License and Terms

This is an open access article licensed under the terms of the Beilstein-Institut Open Access License Agreement (https://www.beilstein-journals.org/bjoc/terms), which is identical to the Creative Commons Attribution 4.0 International License (https://creativecommons.org/licenses/by/4.0). The reuse of material under this license requires that the author(s), source and license are credited. Third-party material in this article could be subject to other licenses (typically indicated in the credit line), and in this case, users are required to obtain permission from the license holder to reuse the material.

The definitive version of this article is the electronic one which can be found at:
https://doi.org/10.3762/bjoc.21.100

BEILSTEIN JOURNAL OF ORGANIC CHEMISTRY

High-pressure activation for the solvent- and catalyst-free syntheses of heterocycles, pharmaceuticals and esters

Kelsey Plasse[1], Valerie Wright[1], Guoshu Xie[1], R. Bernadett Vlocskó[1], Alexander Lazarev[2] and Béla Török[*1]

Full Research Paper

Open Access

Address:
[1]Department of Chemistry, University of Massachusetts Boston, 100 Morrissey Blvd, Boston, MA, USA and [2]Pressure BioSciences Inc., 480 Neponset Street, Unit 10B, Canton, MA, USA

Email:
Béla Török[*] - Bela.Torok@umb.edu

* Corresponding author

Keywords:
acetaminophen; acetylsalicylic acid; benzimidazoles; catalyst-free synthesis; cyclization; esters; high hydrostatic pressure; pyrazoles

Beilstein J. Org. Chem. **2025,** *21,* 1374–1387.
https://doi.org/10.3762/bjoc.21.102

Received: 14 March 2025
Accepted: 11 June 2025
Published: 02 July 2025

This article is part of the thematic issue "Green chemistry III".

Associate Editor: L. Vaccaro



© 2025 Plasse et al.; licensee Beilstein-Institut.
License and terms: see end of document.

Abstract

High hydrostatic pressure (HHP) was found to be an efficient activation method in several catalyst- and solvent-free reactions and has found application for the syntheses of heterocycles and the preparation of active pharmaceutical ingredients (APIs) via acylation and acid- and solvent-free esterification. The reactions were carried out at ambient pressure (control) and under HHP (up to 3.8 kbar) conditions. These representative reactions provided higher yields for the products and HHP enabled truly green processes that are catalyst- and solvent-free, to occur with high yields and producing only non-toxic by-products. A computational study accompanies the experimental data to interpret the outcome of the reactions.

Introduction

Non-traditional activation methods are one of the major driving forces in green synthesis [1,2]. High hydrostatic pressure (HHP) activation, one of such methods, is based on mechanical compression force. The typical pressure range is 2–20 kbar that is orders of magnitude greater than the conditions traditionally employed in chemistry with pressurized gases (0.01–0.1 kbar). The first reports of using HHP were related to food industry applications [3,4], and later in chemical synthesis [5,6]. While the technique had been known since the late 1800s, and it had become popular in materials science and inorganic synthesis, it has largely gone unnoticed as an activation method for organic synthesis. A large number of applications have been reported in solid state, homogeneous and heterogeneous systems to prepare inorganic compounds and materials [7-9]. In contrast, high pressure organic chemistry, or HHP-initiated organic synthesis is still in its infancy. Despite the recent advances [10,11], the HHP applications in this field are still being developed. The first HHP-assisted organic syntheses were reported in the 1970s

[12,13]. Although the mechanism of how pressure enables reactions is not fully elucidated, there is a broad agreement that a decrease in the activation volume ($\Delta V^{\ddagger}$) and reaction volume (ΔV) is the driving force for these reactions [14-16]. A recent computational analysis of high pressure reactions by the extreme pressure polarizable continuum model (XP-PCM) improved the theoretical understanding of the phenomena [17]. In addition, due to the availability of commercially accessible instruments, the applications of HHP in synthetic chemistry have expanded in the past decades. The studied reactions include hydrogenation [18], the addition of enamines to Michael acceptors [19], enantioselective Mannich reactions [20], lipase-catalyzed esterification [21], nitro-aldol [22], Michael [23], and aza-Michael reactions [24,25], Diels–Alder reactions [26,27] and Friedel–Crafts alkylation of indoles [28]. Many high pressure reactions were applied in natural product synthesis [29]. The high pressure protocol was even applied in the elegant syntheses of platencin [30], and steroid derivatives [31]. Despite these encouraging applications, there is a broad area to be developed for the advancement of green synthesis efforts.

Continuing our program on developing environmentally benign synthetic methods [32-35], especially in the realm of high pressure chemistry [36,37], in the present work we demonstrate a variety of new, catalyst- and additional solvent-free applications of HHP to develop green synthesis methods. Here, we describe several cyclization reactions for the preparation of a variety of important heterocycles, the synthesis of well-known APIs, such as acetaminophen and acetylsalicylic acid, a variety of esterification reactions and the successful scale up (up to 100 g scale) of the Paal–Knorr reaction. The use of HHP appears to provide several advantages, for example, resulting in higher reaction rates. Given that every reaction in the present work has been carried out without a catalyst, in many instances this contrast is even greater since the non-pressurized reactions simply did not take place. In other applications when ambient pressure reactions yielded product, HHP still offered a reasonable increase in rates and thus, in yields. In addition to the synthetic advantages, the benefits HHP offers can also translate to green chemistry. The use of HHP extends the scope of solvent-, reagent- and catalyst-free reactions that significantly reduce workup and waste generation. Using water as pressure transmitting fluid, the reaction vessel is immersed in water minimizing fire hazard during the reactions. Finally, most procedures can be carried out at ambient temperature, improving safety and energy efficiency. Energy efficiency is also supported by the nature of the reactions; although pressurizing the system requires energy, once the system is pressurized it does not need energy to maintain it. This can result in remarkable energy saving especially in long reactions. In order to aid the understanding of this technique a schematic design of a high hydrostatic pressure instrument is depicted in Figure 1.

The core of the instrument is the intensifier which generates the required pressure by amplifying the relatively low pressure (about 140 psi) supplied by an air compressor. The intensifier pressurizes the water in the pressure chamber where the sealed

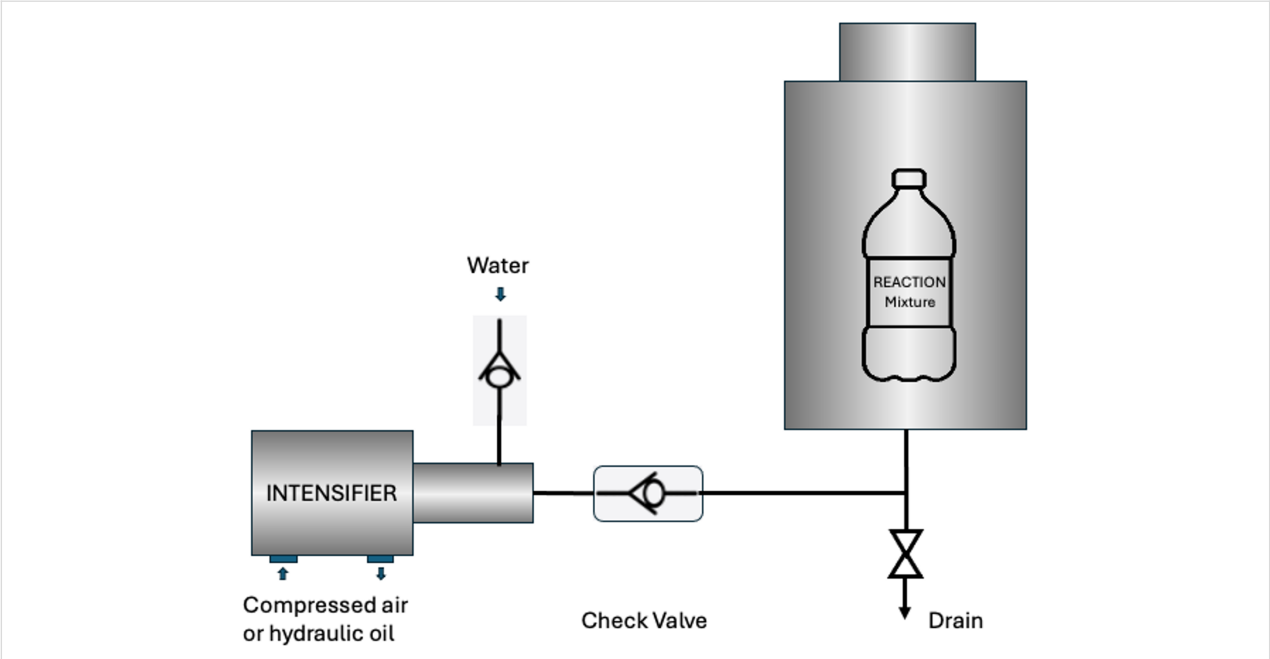


Figure 1: Simplified schematic rendering of a high hydrostatic pressure reactor.

samples are placed. Water is used as a pressure transmitting medium that has relatively low compressibility, readily available, and non-toxic.

Results and Discussion

HHP-assisted synthesis of 1,3-dihydrobenzimidazoles

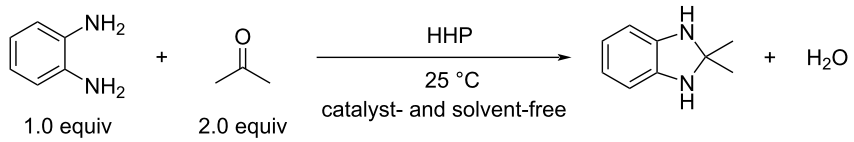
Heterocycles are extremely versatile compounds and are used as building blocks for fine chemicals and conducting polymers or scaffolds for drug synthesis. Among them, 1,3-dihydrobenzimidazoles are widely found in many materials, drug candidates, and catalysts. For instance, they can be used in organic light-emitting diodes (OLEDs) [38], as water-soluble antitrypanosomatid agents [39], or in the synthesis of imidazole-based N-heterocyclic carbene (NHC)–CuCl complexes [40]. However, their synthesis is often tainted by the use of toxic reagents and solvents. In addition, when *o*-phenylenediamine reacts with ketones, the common catalytic methods yield benzodiazepine products [41]. In our case the reaction of *o*-phenylenediamine and acetone was selected as a model reaction. The optimization of the reaction conditions is summarized in Table 1. All reactions were carried out at room temperature without involving any catalyst or additional solvent. While *o*-phenylenediamine is solid, it dissolves well in the reactant acetone, thus the actual reaction mixture remains in a liquid state, making it ideal for HHP-assisted reactions. The first reaction in the optimization effort was the control experiment at atmospheric pressure. Under these conditions, no product formation was observed even after 10 h reaction time. However, 8% of products were generated when 2.8 kbar was applied after only 1 h reaction time. By gradually increasing both pressure and reaction time, higher yields were obtained. The data shows that increasing the pressure up to 3.8 kbar nearly linearly increases the product yield. Meanwhile, the pressure effect appears to work synergistically with reaction time.

The optimization data indicate that the use of HHP resulted in the formation of 1,3-dihydro-2,2-dimethylbenzimidazole (**3a**) in excellent yield (90%) whereas, in contrast, the ambient pressure reaction did not provide any product. The reaction appears to be applicable for other substrates as well, although the yields were lower, which is mainly due to the decomposition of the products (Scheme 1).

HHP-assisted cyclization of chalcones with hydrazines for the synthesis of pyrazoles

The cyclization of 1,3-bifunctional compounds, such chalcones, with two N-containing substrates can yield a variety of valuable heterocycles, including pyrazoles. Accordingly, their syntheses attracted extensive interest, and several green procedures have been published [42]. Many of these reactions still apply catalysts and organic solvents, thus the development of catalyst- and solvent-free processes is desirable. Chalcones are a privileged scaffold in medicinal chemistry and are used for the synthesis of a multitude of products [43]. The cyclization between chalcones and hydrazines usually occur via a C=O/NH_2 condensation and a subsequent NH addition to the C–C double bond, that most commonly require some form of catalysis. Thus, developing catalyst-free processes presents significant challenges, although there are few successful examples in the literature [44]. Similar to the dihydrobenzimidazoles above, the

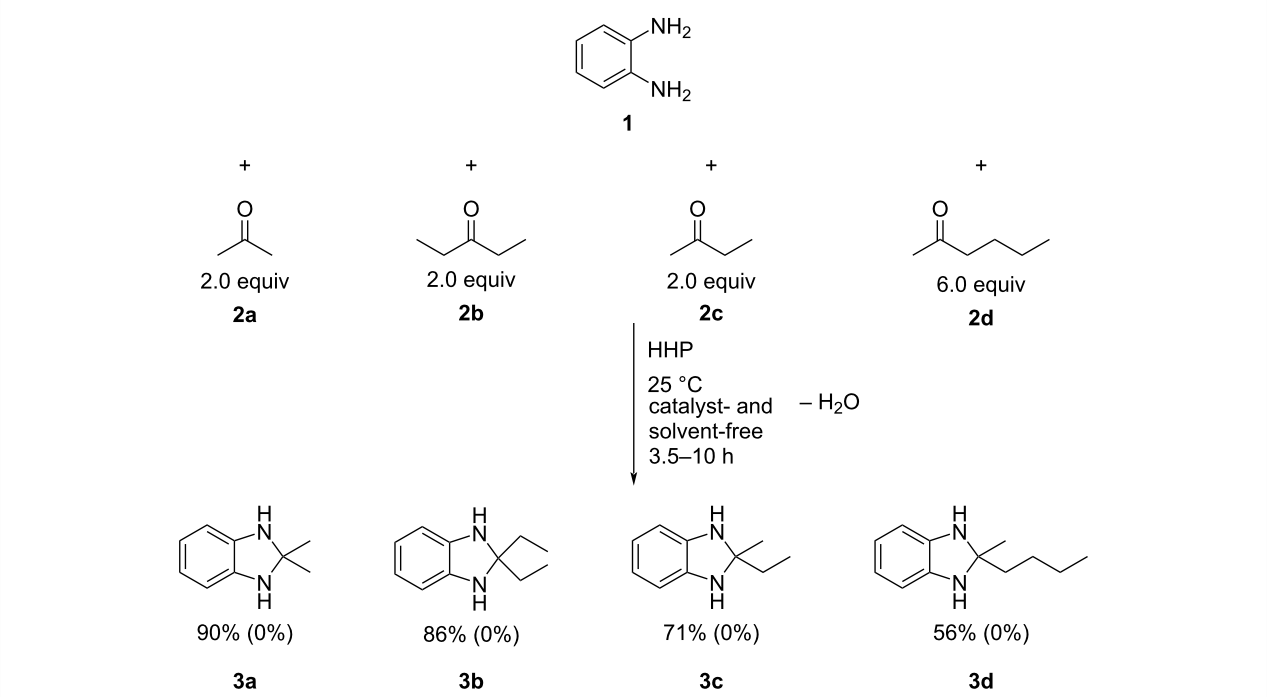
Table 1: Optimization of the HHP-initiated synthesis of 1,3-dihydro-2,2-dimethylbenzimidazole (**3a**).



1.0 equiv (**1**) 2.0 equiv (**2a**) **3a**

Entry	Pressure (kbar)	Time (h)	Yield (%)[a]
1	0.001	10	0
2	2.8	1	8
3	3.4	1	11
4	3.8	1	25
5	3.8	2	32
6	3.8	10	90
7[b]	3.8	10	54

[a]GC yields; [b]1.0 equiv acetone.



Scheme 1: High pressure-initiated synthesis of 1,3-dihydrobenzimidazoles **3a–d**. The yields are GC yields and the numbers in parentheses show the yields of the control reactions (1 bar pressure).

investigations here also started with an optimization of the reaction conditions, including substrate ratio, pressure, and reaction time. The cyclization of chalcone with 3-(trifluoromethyl)phenylhydrazine was selected as a test reaction. This reaction is relatively easy to follow even visually. Once the reaction mixture is subjected to 3.8 kbar pressure, the originally liquid mixture turns to a semisolid, viscous oily product, as shown in Figure 2. The numerical values are presented in Table 2.

The data shows that using excess hydrazine under pressure of 3.8 kbar resulted in the best performance. Based on the opti-

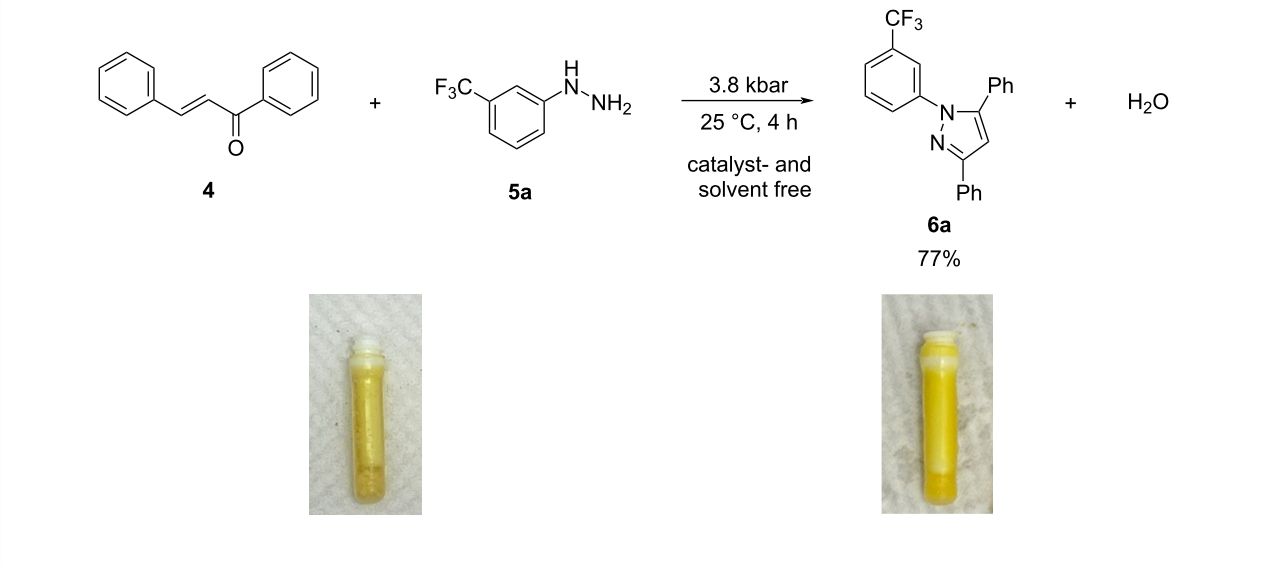
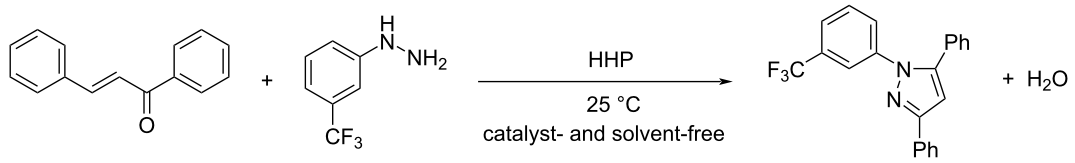


Figure 2: Illustration of the cyclization reaction between chalcone (**4**) and 3-(trifluoromethyl)phenylhydrazine (**5a**) under 3.8 kbar pressure at small (≈150–200 mg) scale reactions.

Table 2: Optimization of the reaction conditions for the synthesis of 3,5-diphenyl-1-(3-(trifluoromethyl)phenyl)-1*H*-pyrazole (**6a**) under ambient pressure (0.001 kbar) and high hydrostatic pressure from chalcone (**4**) and 3-(trifluoromethyl)phenylhydrazine (**5a**).



4 **5a** **6a**

Entry	Molar ratio (chalcone/hydrazine)	Pressure (kbar)	Time (h)	Yield (%)[a]
1	1:2	0.001	4	12
2	1:1	0.7	1	14
3	1:2	1.4	1	12
4	1:1	2.1	1	12
5	1:1	2.8	1	14
6	1:1	3.8	1	56
7	1:3	3.8	1	57
8	1:1	3.8	4	60
9	1:2	3.8	4	78

[a]GC yield.

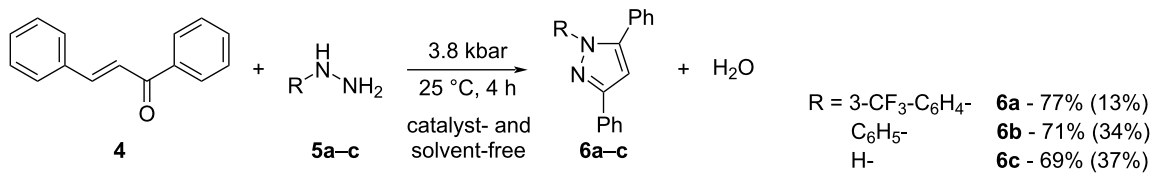
mized data several compounds were subjected to those conditions to provide a representative scope of the reactions and the results are summarized in Scheme 2. For comparison, the yields obtained under ambient pressure (1 bar) are provided in parentheses.

The data show that the reactions readily occur at room temperature providing good yields. Although the reactions do occur at ambient pressure, the pressurized reactions generally provide higher yields under the otherwise same conditions. It also appears that the reactivity of the hydrazine plays a significant role. In the case of the highly reactive hydrazine, the positive effect of HHP is somewhat diminished and only about 10% increase in yield was observed. In contrast, when using substituted phenylhydrazines of lower reactivity HHP results in more significant benefits, for example a nearly 70% higher yield in the case of the chalcone/3-(trifluoromethyl)phenylhydrazine reaction (Scheme 2).

HHP-assisted acylation of NH and OH groups: synthesis of acetaminophen (paracetamol) and acetylsalicylic acid

Tylenol® and Aspirin® are two popular drugs used as pain killers as well as antipyretics [45]. Although their industrial production is straightforward, these syntheses include the use of catalysts and solvents that must be neutralized and recycled. Given the large scale these compounds are prepared at, even a small green improvement in their synthesis might yield great environmental, as well as financial benefits. Thus, these two compounds were selected as model compounds to investigate the potential benefits of the HHP-assisted synthesis. Similar to the other reactions, preliminary optimization experiments have been carried out as described in Table 3.

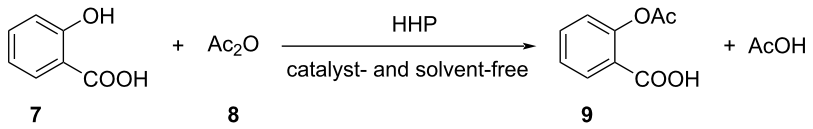
The results clearly indicate that the product yields improve under high pressure conditions. The best performance was ob-



4 **5a–c** **6a–c**

Scheme 2: High pressure-initiated catalyst- and solvent-free synthesis of pyrazoles **6a–c** from chalcone (**4**) and hydrazines **5a–c**. The GC yields at high pressure are shown for each compound, and the numbers in parentheses represent the yields of the respective control reactions at 1 bar pressure. In the case of the unsubstituted hydrazine (NH_2–NH_2), the non-aromatic product, dihydropyrazole, formed.

Table 3: Optimization of the high pressure-assisted catalyst- and additional solvent-free synthesis of acetylsalicylic acid (**9**).



7 **8** **9**

Entry	Molar ratio (**7**/**8**)	Pressure (kbar)	Time (h)	Temperature (°C)	Yield (%)[a]
1	1:2	0.001	0.5	80	30
2	1:1	3.8	1.5	25	6
3	1:2	3.8	1.5	25	8
4	1:1	3.8	12	25	24
5	1:2	3.8	12	25	36
6	1:1	3.8	2	50	36
7	1:2	3.8	2	50	41
8	1:2	3.8	2	80	64
9	1:2	2.8	0.5[b]	80	100

[a]GC yield; [b]30 × 1 min cycles, with 5 s decompression.

tained under pressure cycling conditions as illustrated in Figure 3.

It has been observed that pressure cycling resulted in a quantitative yield after 30 1-min cycles (Table 3, entry 9), that would account for 30 min reaction under pressure, and provides a significantly better yields than the reaction conducted under ambient pressure (30%, Table 3, entry 1) or a 2 h reaction at static higher pressure (64%, Table 3, entry 8). While the exact nature of this phenomenon is not fully understood, it is hypothesized that the pressure cycling protocol causes periodic change in the volume of the reaction vessel that could lead to molecular re-alignments during compression and decompression steps that are beneficial for reaction kinetics.

Under optimized conditions, the products were isolated with good to excellent yields under a catalyst- and solvent-free environment (Scheme 3). The data in Scheme 3 illustrate that HHP provides some advantage in both reactions, more evident in the case of OH acylation. The NH_2 acylation occurred much more rapidly in 10 s at room temperature, while also generating the product nearly quantitatively. The OH group is significantly less reactive under such conditions; therefore, the use of pressure resulted in a more substantial improvement in the OH acylation reaction.

HHP-assisted esterification of alcohols: synthesis of fragrances

Esterification is one of the most common organic reactions and there are a multitude of processes available. However, most require some form of catalysis from simple acids to metal catalysts [46]. Similar to the previous examples, the first step was the optimization of the conditions using the esterification of benzyl alcohol (**12a**) with acetic anhydride (**8**) and acetic acid

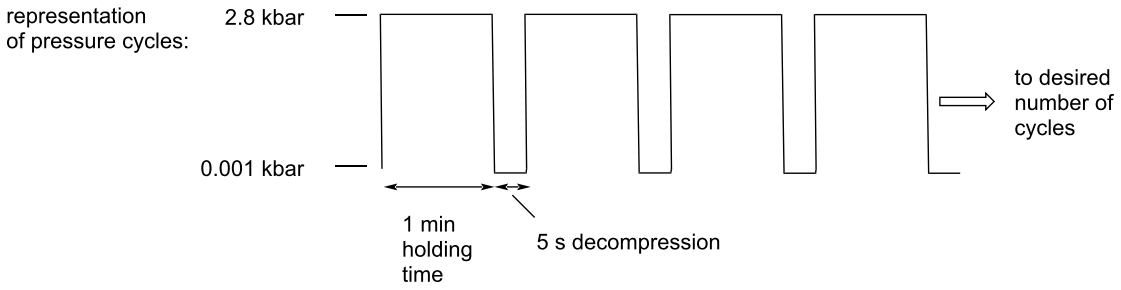
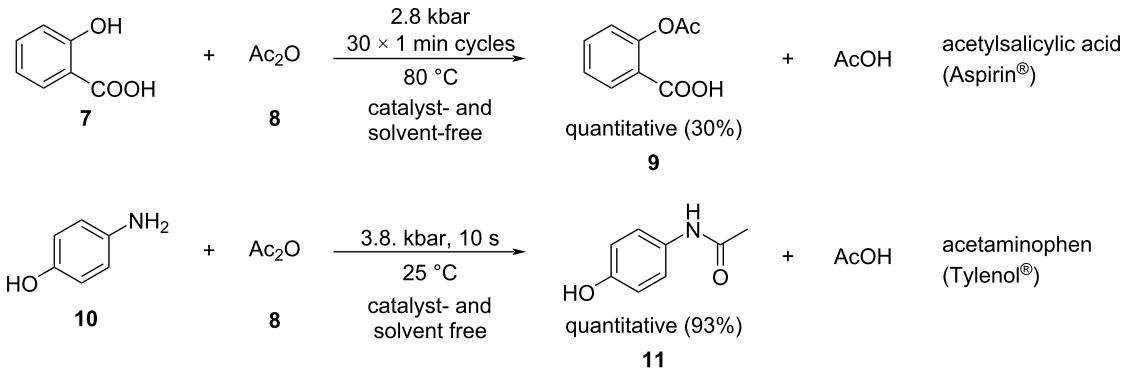


Figure 3: Schematic representation of the cycling experiments: the major variables are the applied pressure, the holding time, the length of decompression and the number of cycles in the sequence.



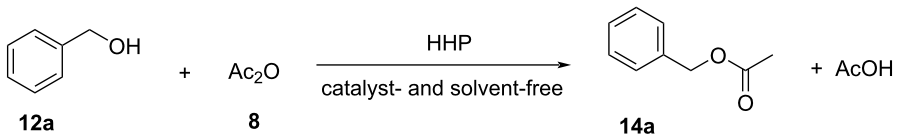
Scheme 3: High pressure-initiated synthesis of the active pharmaceutical ingredients in Tylenol® and Aspirin®. The yields refer to GC yields and the numbers in parentheses represent the yields of the control reactions at 1 bar pressure.

(**13**), respectively. The optimization data are summarized in Table 4.

The data indicates that the use of pressure is beneficial for the esterification reaction. The ambient pressure reaction only yields 52% product (Table 4, entry 1) compared to the 92% obtained under 3.8 kbar. Increasing the ROH/Ac_2O ratio (1:3, Table 4, entry 9) or the reaction time (2 h, Table 4, entry 5) under pressure yielded quantitative product formation. The optimized conditions allowed the extension of the protocol and a selection of alcohols was investigated. The results are illustrated in Scheme 4. For comparison, results obtained from reactions at ambient pressure are given in parentheses.

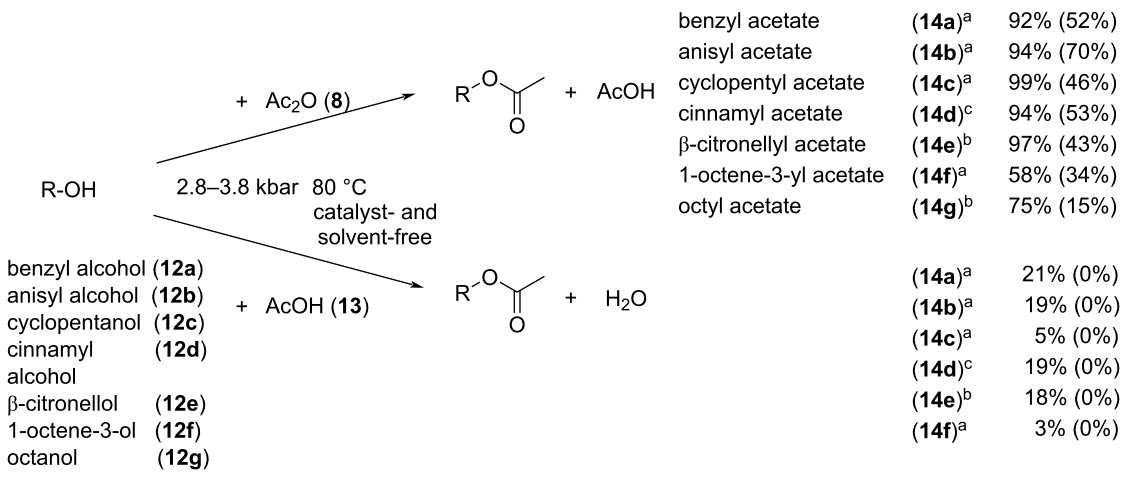
As shown in Table 4 and Scheme 4, the HHP reactions occurred at 50 °C with low to moderate yields, and with nearly quantitative yields at 80 °C. HHP reactions afforded the products in higher yields than those of the control experiments under the same conditions (time, temp. etc.) but only at 1 bar (atmospheric) pressure. It appears that the pressurized reactions provided about 40–60% yield improvements in the same timeframe as the controls. The reactions gave significantly higher yields when using Ac_2O, than with AcOH. However, while the reactions with acetic acid after 1 h under pressure all yielded the expected products to some extent, no product formation was observed at the ambient pressure control reactions.

Table 4: Optimization of the HHP-assisted catalyst-free esterification of benzyl alcohol (**12a**).



Entry	Molar ratio (**12a**/**8**)	Pressure (kbar)	Time (h)	Temperature (°C)	Yield (%)[a]
1	1:2	0.001	1	80	52
2	1:1	3.8	2	50	38
3	1:2	3.8	2	50	46
4	1:1	3.8	2	80	52
5	1:2	3.8	2	80	100
6	1:3	3.8	2	80	100
7	1:1	3.8	1	80	92
8	1:2	3.8	1	80	80
9	1:3	3.8	1	80	100

[a]GC yield.



Scheme 4: High pressure-initiated esterification of alcohols **12a–g** in a catalyst- and additional solvent-free reactions with either acetic anhydride (**8**) or acetic acid (**13**). All reactions were carried out at 80 °C and at (a) 3.8 kbar, 1 h, (b) 2.8 kbar, 30 × 1 min cycles, (c) 2.8 kbar, 40 × 1 min cycles. The yields were determined by GC.

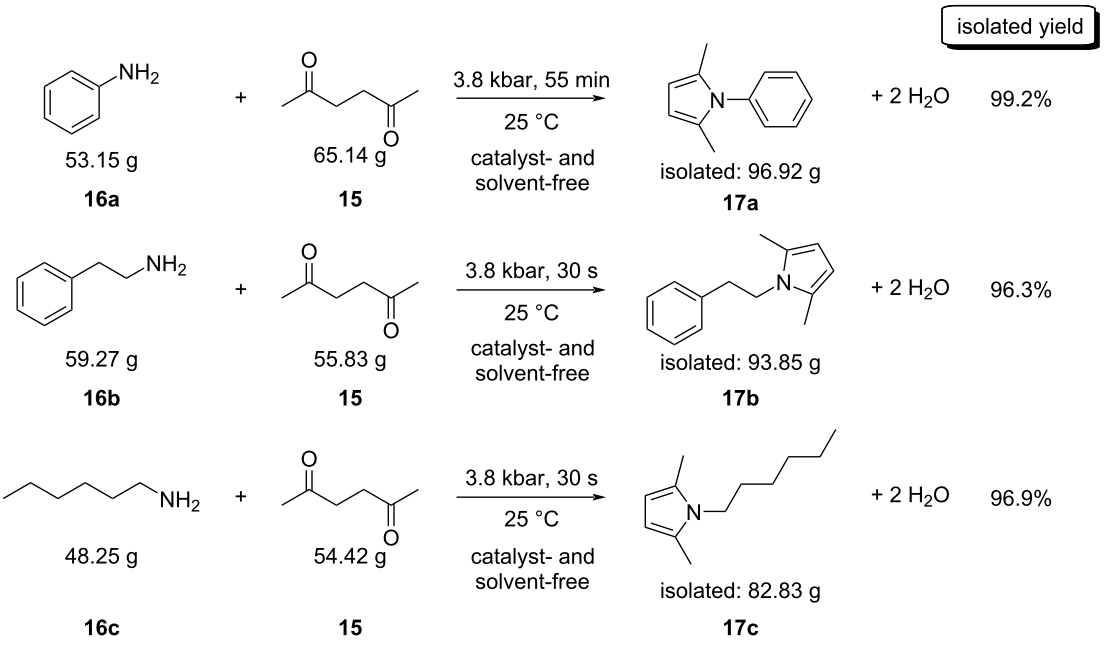
Unlike water and a few elements (silicon, bismuth, gallium, etc.) that tend to form tetrahedral crystal lattices and exhibit lower density upon freezing, most organic compounds are expected to form crystals of higher density, compared to their liquid state. However, phase transitions of the vast majority of organic compounds at high pressure are not yet adequately studied. Data on their behaviour when pressurized are not readily available, except for some long chain aliphatic hydrocarbons, due to their propensity to sedimentation in pressurized oil pipelines. Attempts to correlate known phase transition parameters of reactants and products at atmospheric pressure, such as their respective melting point and boiling point at 1 bar, have not revealed any conclusive trends with respect to the observed reaction yields shown in Scheme 4. While Ac_2O is generally more reactive than AcOH, it is conceivable that the significant difference in esterification yields with acetic anhydride vs. acetic acid is further enhanced due to acetic acid forming solid crystalline state during pressurization even at 80 °C. However, the reaction rate with AcOH is still much improved under high pressure, as none of the alcohols formed any product under 1 bar pressure.

Scale up of the HHP-assisted reactions

The above protocols were carried out at a small scale (mg to g) and thus, an effort was made to investigate the scale-up potential of the HHP-assisted method. Although the HHP-assisted organic syntheses are relatively rare, the large (often ton) scale-capable equipment is readily available in the food industry. Accordingly, industrial level organic syntheses are attainable in a large scale. In an earlier work we already demonstrated that such reactions, e.g. the HHP-assisted Paal–Knorr reaction can be easily scaled up to a multigram level [36]. Although the reaction occurred in catalyst-free systems without pressure the reaction times were 24 h or more [47]. Thus it was attempted to provide some examples for the further scale-up of the Paal–Knorr reaction in a much larger scale, at this time, up to a 100 g level. The experiments were carried out in a 5-L capacity high pressure instrument (Pressure BioSciences) using commercially available low-density polyethylene (LDPE) bottles as reaction vessels and afforded the products with good yields (Scheme 5).

Although the chemically inert nature of reaction vessels is essential, the ductile amorphous property of the material is also of the utmost importance, making the vessel flexible enough to handle the decreasing volume of the reaction mixture under pressure: contrary to a common misconception that liquids are incompressible, a significant (5–12%) decrease in the volume is generally observed at the pressure levels studied here.

The results of these experiments show that the reaction scale can be readily increased to the ≈100 gram level, suggesting that achieving these reactions at even higher scales is reasonable. The reactions occurred in a similar fashion as they did at the mg scale [36] and all reactions produced higher than 96% isolated yield of the product. Where the two alkyl amines were used, the reactions were complete within 30 s of reaction time. Even the less reactive aniline gave nearly quantitative isolated yields in less than an hour, while the 1 bar control reaction yielded no detectable products. In addition to the excellent yields, the products were isolated without any purification, using a simple air-drying process to remove the water that forms as a by-product during the cyclization–aromatization sequence. The gas chromatograms of the three crude products appeared essentially



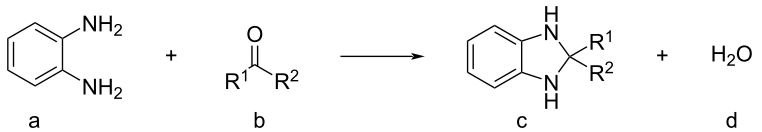
Scheme 5: High pressure-initiated large scale syntheses of *N*-aryl- and *N*-alkylpyrroles at about 100 g scale.

100% pure, neither starting material nor other by-products were observed.

In order to explain the outcome of the above reactions, the reaction volume data (ΔV) was calculated for each reaction. Gaussian 09 was used to carry out the calculations at the b3lyp/6-311++g(d,p) level of theory. The molecular volume of each reactant and product (including all by-products that are part of the reaction scheme) was calculated and the overall volume difference of the starting materials and the products was determined. The obtained values are summarized in Tables 5–10.

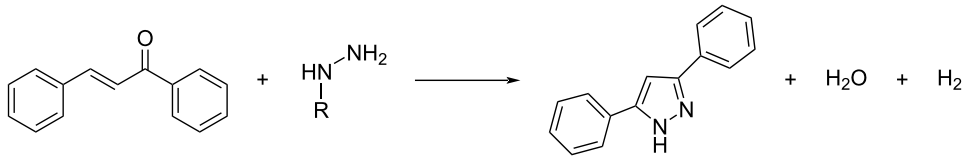
The data in Tables 5–10 indicate that the reaction volumes appear to be in the negative region for the large majority of examples, some being 0 or a small positive number. Based on the theoretical models briefly discussed in the introduction, the negative ΔV values suggest that these reactions respond well to pressurized conditions by improved yields, and increased reaction rates. One must note, however, that ΔV is just one of the characteristic descriptors of high pressure reactions, and full analysis can be obtained by also evaluating the activation volume ($\Delta V^{\ddagger}$) data. Considering that all of the above studied reactions are multistep processes with several elementary steps,

Table 5: Molecular volumes of the reactants and products and the reaction volume (ΔV) for the reaction of *o*-phenylenediamine with ketones to form 1,3-dihydrobenzimidazoles.



Entry	R^1	R^2	V_a (cm^3/mol)	V_b (cm^3/mol)	V_c (cm^3/mol)	V_d (cm^3/mol)	$\Delta V_{(c+d)-(a+b)}$ (cm^3/mol)
1	Me	Me	94	60	130	18	–6
2	Et	Et	94	81	150	18	–7
3	Me	Et	94	66	140	18	–2
4	Me	*n*-Bu	94	100	140	18	–36

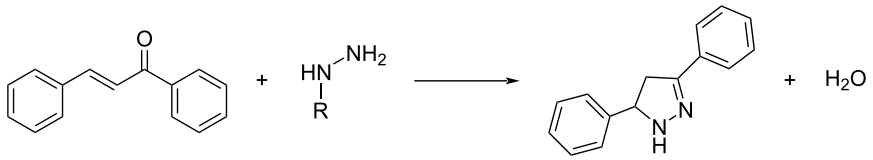
Table 6: Molecular volumes of the reactants and products and the reaction volume (Δ*V*) for the reaction of chalcone with hydrazines to form pyrazoles.



a b c d e

Entry	R	V_a (cm^3/mol)	V_b (cm^3/mol)	V_c (cm^3/mol)	V_d (cm^3/mol)	V_e (cm^3/mol)	$\Delta V_{(c+d)-(a+b)}$ (cm^3/mol)
1	3-CF_3-C_6H_4-	180	110	260	18	13	1
2	C_6H_5-	180	92	230	18	13	–11
3	H-	180	37	160	18	13	–26

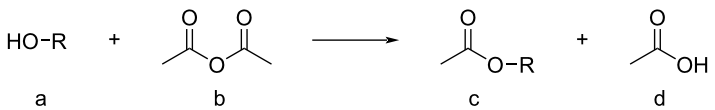
Table 7: Molecular volumes of the reactants and products and the reaction volume (Δ*V*) for the reaction of chalcone with hydrazines to form dihydropyrazoles.



a b c d

Entry	R	V_a (cm^3/mol)	V_b (cm^3/mol)	V_c (cm^3/mol)	V_d (cm^3/mol)	$\Delta V_{(c+d)-(a+b)}$ (cm^3/mol)
1	3-CF_3-C_6H_4-	180	110	270	18	–2
2	C_6H_5-	180	92	230	18	–24
3	H-	180	37	190	18	–9

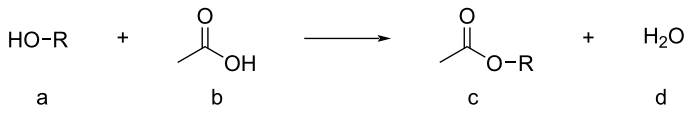
Table 8: Molecular volumes of the reactants and products and the reaction volume (Δ*V*) for the esterification reaction of alcohols with acetic anhydride.



a b c d

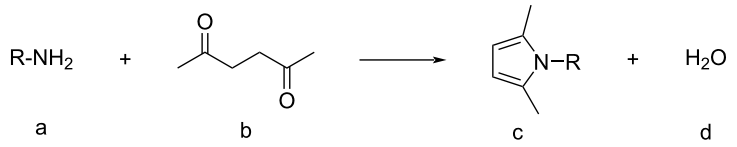
Entry	alcohol	R	V_a (cm^3/mol)	V_b (cm^3/mol)	V_c (cm^3/mol)	V_d (cm^3/mol)	$\Delta V_{(c+d)-(a+b)}$ (cm^3/mol)
1	benzyl alcohol	-$CH_2C_6H_5$	81	73	120	38	4
2	anisyl alcohol	-$CH_2C_6H_4OCH_3$	130	73	140	38	–25
3	cyclopentanol	-C_5H_9	76	73	100	38	–11
4	cinnamyl alcohol	C_6H_5CH=$CHCH_2$-	120	73	140	38	_15
5	β-citronellol	$C_9H_{19}CH_2$-	160	73	180	38	–15
6	1-octene-3-ol	H_2C=$CHCH_2CH$-$(CH_2)_3CH_3$	120	73	140	38	–15
7	octanol	$CH_3(CH_2)_7$-	140	73	190	38	–25

Table 9: Molecular volumes of the reactants and products and the reaction volume (Δ*V*) for the esterification reaction of alcohols with acetic acid.



Entry	alcohol	R	V_a (cm^3/mol)	V_b (cm^3/mol)	V_c (cm^3/mol)	V_d (cm^3/mol)	$\Delta V_{(c+d)-(a+b)}$ (cm^3/mol)
1	benzyl alcohol	$-CH_2C_6H_5$	81	38	120	18	19
2	anisyl alcohol	$-CH_2C_6H_4OCH_3$	130	38	140	18	−10
3	cyclopentanol	$-C_5H_9$	76	38	100	18	4
4	cinnamyl alcohol	$C_6H_5CH{=}CHCH_2-$	120	38	140	18	0
5	β-citronellol	$C_9H_{19}CH_2-$	160	38	180	18	0
6	1-octene-3-ol	$H_2C{=}CHCH_2CH-(CH_2)_3CH_3$	120	38	140	18	0
7	octanol	$CH_3(CH_2)_7-$	140	38	190	18	−10

Table 10: Molecular volumes of the reactants and products and the reaction volume (Δ*V*) for the Paal–Knorr reaction of amines with 2,5-hexanedione.



Entry	R	V_a (cm^3/mol)	V_b (cm^3/mol)	V_c (cm^3/mol)	V_d (cm^3/mol)	$\Delta V_{(c+d)-(a+b)}$ (cm^3/mol)
1	$C_6H_5-(CH_2)_2$	130	93	160	18	−45
2	C_6H_5-	90	93	150	18	−15
3	$CH_3-(CH_2)_5-$	110	93	170	18	−15

the determination of $\Delta V^{\ddagger}$ requires a detailed theoretical reaction mechanism study that is beyond the scope of the current work. Nonetheless, since the Δ*V* values provide clear support for the beneficial effect of pressure, it is reasonable to predict that the activation volumes are also either negative or near zero to explain to observed experimental data.

Conclusion

The high hydrostatic pressure activation has been successfully applied to several reactions; cyclizations of various types, acylations and esterifications. In addition to being efficient at a small scale, the scale up of the Paal–Knorr reaction was also achieved. Compared to the traditional benchtop alternatives the HHP-assisted approach provided several benefits, such as (i) improved reactions rates and yields in catalyst and solvent-free reactions, which enables easy isolation, and simplified work-up procedure; (ii) the neat reactions of the substrates eliminates solvents and thus reduces environmental and hazard impact; (iii) the HHP conditions enable many reactions to proceed at ambient temperature, resulting in convenient, safe, and energy-efficient protocols; and finally, (iv) HHP instruments allow broadly tuneable procedures that include modifying pressure, temperature, reaction time, or pressure cycles to ensure easy process optimization. Based on our earlier publications and the data presented here, it is reasonable to predict that the high-pressure activation strategy will gain broad application possibilities in the future.

Experimental

Materials and methods

Materials: All substrates (aldehydes, hydrazones, alcohols, *p*-aminophenol, salicylic acid, acetic anhydride, acetic acid, hexan-2,5-dione, aniline, hexylamine and 2-phenylethylamine) were purchased from Aldrich and used without any purification.

Ethyl acetate, used to dissolve the products for GC–MS analysis (minimum purity of 99.5%) was purchased from ThermoFisher Scientific. The small scale reactor tubes "PCT MicroTubes" were made of FEP and PTFE Teflon® and obtained from Pressure BioSciences Inc., while the larger scale bulbs and bottles used as reaction vessels were made of low-density polyethylene and purchased from ThermoFisher Scientific.

Analysis: All compounds are common, known entities and they were identified based on their high-resolution mass spectra. The mass spectrometric identification and purity determination of the products have been carried out by using an Agilent 7250 GC-QTOF mass spectrometer operated in electron impact ionization (EI, 70 eV) mode using a 30m long DB-5 type column (J&W Scientific).

General protocols for HHP reactions

The high pressure syntheses can be carried out in two different ways, in manners analogous to ref. [37]. A bench-top Barocycler 2320EXT was used to initiate HHP reactions. (i) *Constant pressure* means that the system is pressurized to the desired pressure that is maintained through the reaction and decompressed, when complete. (ii) *Pressure cycling*. Another, HHP approach is the pressure cycling, when compression–decompression cycles are repeated. In these investigations, 2.8 kbar was selected as applied pressure based on the optimization experiments (Table 3).

General procedure for the catalyst and solvent-free reactions of chalcone with hydrazines under HHP conditions

To a 150 μL high-pressure FEP reaction tube was added chalcone (52.0 mg, 0.25 mmol) and 3-(trifluoromethyl)phenylhydrazine (65 mg, 0.37 mmol) which could just fill up the entire reaction tube, and the tube was sealed by a PTFE PCT MicroCap and secured in the MicroTube carrier to ensure the secure seal. Then, the tube was placed in the chamber compartment of a Barocycler 2320EXT (Pressure BioSciences Inc.). The chamber was filled with water and pressurized up to the desired pressure and the pressure was maintained for the predetermined time. After removing the reaction tube, from the pressure chamber, the product was dissolved in ethyl acetate and the yield was determined by an Agilent 7250 GC-QTOF mass spectrometer operated in electron impact ionization (EI, 70 eV) mode using a 30 m long DB-5 type column (J&W Scientific).

General procedure for the high hydrostatic pressure-initiated catalyst and solvent-free synthesis of 1,3-dihydrobenzimidazoles

The appropriate amount of the reactants was added into a 3.5 mL volume LDPE reaction vial. The well-sealed reaction mixtures were placed into the chamber. Water is filled into the HHP vessel and pressurized to the desired pressure up to 3.8 kbar. After the reactions are completed, the pressure was released and the reaction products are isolated.

General procedure for the catalyst and solvent-free acylation of hydroxyl compounds and *p*-aminophenol under HHP conditions

To a 150 μL high-pressure FEP reaction tube was added the corresponding hydroxy compound or *p*-aminophenol (0.25 mmol) and acetic anhydride or acetic acid in a 1.5 molar excess (0.37 mmol). The tube was sealed by a PTFE PCT MicroCap and secured in the metal MicroTube cassette. Then, the cassette with the reaction tubes was placed in the chamber of the Barocycler. The chamber was pressurized up to the desired pressure which was maintained for the desired time. After depressurizing the pressure chamber, the tubes were removed and the product was isolated by aqueous wash, neutralization with $NaHCO_3$ and then extracted with ethyl acetate. The yield was determined by an Agilent 7250 GC-QTOF mass spectrometer operated in electron impact ionization (EI, 70 eV) mode using a 30m long DB-5 type column (J&W Scientific).

General procedure for the catalyst and solvent-free large-scale reaction of hexan-2,5-dione and aniline under high hydrostatic pressure

To a 100 mL low-density polyethylene (LDPE) bottle was added hexan-2,5-dione (65.14 g, 0.57 mol) and 1.0 equiv aniline (59.27 g, 0.57 mol) to fill up the entire reaction vessel, then the bottle was sealed by an LDPE screw cap. Afterward, the vessel was placed in the chamber compartment of a Pressure BioSciences HHP instrument with a 5 L chamber. The chamber was filled up with water and pressurized up to 3.8 kbar. The reaction mixture was reacted under 3.8 kbar at room temperature for 55 min. After removing the reaction vessel from the pressure chamber, the cap was removed and the solid material was collected and dried by a simple air-drying. After drying 96.92 g of the product was obtained. The purity of the product was determined by an Agilent 7250 GC-QTOF mass spectrometer operated in electron impact ionization (EI, 70 eV) mode using a 30m long DB-5 type column (J&W Scientific).

Computational details

To determine the reaction volume (ΔV), the volumes of the starting materials and products were calculated separately using the Gaussian 09 program suite [48]. Geometry optimizations were performed using density functional theory (DFT) with the Becke three-parameter exchange and Lee–Yang–Parr correlation (B3LYP) functional [49], along with the 6–311++G(d,p) basis set for gas-phase calculations of all compounds. After completing the molecular geometry optimizations, vibrational

frequency calculations were conducted to ensure that none of the optimized structures exhibited imaginary frequencies confirming that all structures corresponded to real local minima on the potential energy surface. For the volume calculations, the Gaussian keyword "volume" was used, which defines the molar volume as the region inside a contour of 0.001 electrons/Bohr^3 density [50].

The reaction volume was calculated as:

$$\Delta V = \Sigma V_{\text{products}} - \Sigma V_{\text{reactants}} \quad (1)$$

Supporting Information

Supporting Information File 1

Materials and methods, spectral data of new compounds, and HRMS spectra of known products.
[https://www.beilstein-journals.org/bjoc/content/supplementary/1860-5397-21-102-S1.pdf]

Acknowledgements

The authors are grateful for the use of the supercomputing facilities managed by the Research Computing Department at the University of Massachusetts Boston.

Funding

Support of this work by the University of Massachusetts Boston and the National Institute of General Medical Sciences of the National Institutes of Health (1R15GM157702-01, BT) is gratefully acknowledged.

Author Contributions

Kelsey Plasse: data curation; investigation; writing – review & editing. Valerie Wright: data curation; investigation; writing – review & editing. Guoshu Xie: data curation; investigation; writing – review & editing. R. Bernadett Vlocskó: data curation; investigation; writing – review & editing. Alexander Lazarev: investigation; methodology; resources; writing – review & editing. Béla Török: conceptualization; funding acquisition; methodology; project administration; resources; writing – original draft; writing – review & editing.

ORCID® iDs

Alexander Lazarev - https://orcid.org/0009-0005-1490-9025
Béla Török - https://orcid.org/0000-0002-5465-9789

Data Availability Statement

All data that supports the findings of this study is available in the published article and/or the supporting information of this article.

References

1. Török, B.; Schäfer, C., Eds. *Non-traditional Activation Methods in Green and Sustainable Applications: Microwaves, Ultrasounds, Photo, Electro and Mechanochemistry and High Hydrostatic Pressure;* Elsevier, 2021. doi:10.1016/b978-0-12-819009-8.09997-7
2. Datta, S.; Sood, A.; Török, M. *Curr. Org. Synth.* **2011,** *8,* 262–280. doi:10.2174/157017911794697330
3. Hite, B. H. *Bull. - W. Va., Agric. Exp. Stn.* **1899,** *58,* 15–35. doi:10.33915/agnic.58
4. Bridgman, P. W. *J. Biol. Chem.* **1914,** *19,* 511–512. doi:10.1016/s0021-9258(18)88287-4
5. Röntgen, W. C. *Annu. Rev. Phys. Chem.* **1892,** *281,* 98–107. doi:10.1002/andp.18922810109
6. Kelm, H., Ed. High Pressure Chemistry; Proceedings of the NATO Advanced Study Institute, Corfu, Greece, Sept 24–Oct 8, 1977; Riedel Publishing Company: Dordrecht, Holland, 1978. doi:10.1007/978-94-009-9888-9
7. Miao, M.; Sun, Y.; Zurek, E.; Lin, H. *Nat. Rev. Chem.* **2020,** *4,* 508–527. doi:10.1038/s41570-020-0213-0
8. Schettino, V.; Bini, R. *Chem. Soc. Rev.* **2007,** *36,* 869–880. doi:10.1039/b515964b
9. McMillan, P. F. *Chem. Soc. Rev.* **2006,** *35,* 855–857. doi:10.1039/b610410j
10. Margetic, D., Ed. *High Pressure Organic Synthesis;* Walter de Gruyter GmbH: Berlin, Germany, 2019. doi:10.1515/9783110556841
11. Rulev, A. Y.; Zubkov, F. I. *Org. Biomol. Chem.* **2022,** *20,* 2320–2355. doi:10.1039/d1ob01423d
12. Xie, G.; Wright, V.; Lazarev, A.; Smejkal, G.; Gross, V.; Török, B. *Green Chem.* **2025,** *27,* 7096–7113. doi:10.1039/d5gc01075f
13. Chataigner, I.; Maddaluno, J. High-Pressure Synthesis: An Eco-friendly Chemistry. In *Activation Methods: Sonochemistry and High Pressure;* Goddard, J.-P.; Malacria, M.; Ollivier, C., Eds.; iSTE Ltd & John Wiley & Sons, Inc., 2019; Vol. 2, pp 96–149. doi:10.1002/9781119687443.ch2
14. Asano, T.; Le Noble, W. J. *Chem. Rev.* **1978,** *78,* 407–489. doi:10.1021/cr60314a004
15. Van Eldik, R.; Asano, T.; Le Noble, W. J. *Chem. Rev.* **1989,** *89,* 549–688. doi:10.1021/cr00093a005
16. Drljaca, A.; Hubbard, C. D.; van Eldik, R.; Asano, T.; Basilevsky, M. V.; le Noble, W. J. *Chem. Rev.* **1998,** *98,* 2167–2290. doi:10.1021/cr970461b
17. Chen, B.; Hoffmann, R.; Cammi, R. *Angew. Chem., Int. Ed.* **2017,** *56,* 11126–11142. doi:10.1002/anie.201705427
18. Tomin, A.; Lazarev, A.; Bere, M. P.; Redjeb, H.; Török, B. *Org. Biomol. Chem.* **2012,** *10,* 7321–7326. doi:10.1039/c2ob25941a
19. Horinouchi, R.; Kamei, K.; Watanabe, R.; Hieda, N.; Tatsumi, N.; Nakano, K.; Ichikawa, Y.; Kotsuki, H. *Eur. J. Org. Chem.* **2015,** 4457–4463. doi:10.1002/ejoc.201500411
20. Hayashi, Y.; Tsuboi, W.; Shoji, M.; Suzuki, N. *J. Am. Chem. Soc.* **2003,** *125,* 11208–11209. doi:10.1021/ja0372513
21. Eisenmenger, M. J.; Reyes-De-Corcuera, J. I. *J. Mol. Catal. B: Enzym.* **2010,** *67,* 36–40. doi:10.1016/j.molcatb.2010.07.002
22. Misumi, Y.; Matsumoto, K. *Angew. Chem., Int. Ed.* **2002,** *41,* 1031–1033. doi:10.1002/1521-3773(20020315)41:6<1031::aid-anie1031>3.0.co;2-k
23. Kwiatkowski, P.; Dudziński, K.; Łyżwa, D. *Org. Lett.* **2011,** *13,* 3624–3627. doi:10.1021/ol201275h

24. Fedotova, A.; Crousse, B.; Chataigner, I.; Maddaluno, J.; Rulev, A. Y.; Legros, J. *J. Org. Chem.* **2015,** *80,* 10375–10379. doi:10.1021/acs.joc.5b01756
25. Rulev, A. Y.; Kotsuki, H.; Maddaluno, J. *Green Chem.* **2012,** *14,* 503–508. doi:10.1039/c2gc16220b
26. Kumamoto, K.; Fukada, I.; Kotsuki, H. *Angew. Chem., Int. Ed.* **2004,** *43,* 2015–2017. doi:10.1002/anie.200353487
27. Loco, D.; Spezia, R.; Cartier, F.; Chataigner, I.; Piquemal, J.-P. *Chem. Commun.* **2020,** *56,* 6632–6635. doi:10.1039/d0cc01938k
28. Łyżwa, D.; Dudziński, K.; Kwiatkowski, P. *Org. Lett.* **2012,** *14,* 1540–1543. doi:10.1021/ol300274u
29. Hugelshofer, C. L.; Magauer, T. *Synthesis* **2014,** *46,* 1279–1296. doi:10.1055/s-0033-1341073
30. Waalboer, D. C. J.; Schaapman, M. C.; van Delft, F. L.; Rutjes, F. P. J. T. *Angew. Chem., Int. Ed.* **2008,** *47,* 6576–6578. doi:10.1002/anie.200802912
31. Blanco-Ania, D.; Aben, R. W. M.; van Berkom, L. W. A.; Scheeren, H. W.; Rutjes, F. P. J. T. *Eur. J. Org. Chem.* **2014,** 1438–1444. doi:10.1002/ejoc.201301511
32. Daştan, A.; Kulkarni, A.; Török, B. *Green Chem.* **2012,** *14,* 17–37. doi:10.1039/c1gc15837f
33. Pandey, G.; Török, B. *Green Chem.* **2017,** *19,* 5390–5395. doi:10.1039/c7gc02804k
34. Schäfer, C.; Ellstrom, C. J.; Cho, H.; Török, B. *Green Chem.* **2017,** *19,* 1230–1234. doi:10.1039/c6gc03032g
35. Kokel, A.; Török, B. *Green Chem.* **2017,** *19,* 2515–2519. doi:10.1039/c7gc00901a
36. Xie, G.; Lazarev, A.; Török, B. *Green Chem.* **2023,** *25,* 1582–1587. doi:10.1039/d2gc04753e
37. Costa, M.; Adhamidhi, F.; Mastyugin, M.; Fusco, A. R.; Lazarev, A.; Zsengeller, Z. K.; Török, M.; Török, B. *Molecules* **2024,** *29,* No. 5287. doi:10.3390/molecules29225287
38. Fan, H.; Zhou, H.; Ren, X.; Zhang, X. . A kind of compound and application thereof and organic electroluminescence device. Chin. Pat. Appl. CN107759527A, March 6, 2018.
39. Boiani, M.; Boiani, L.; Denicola, A.; Torres de Ortiz, S.; Serna, E.; Vera de Bilbao, N.; Sanabria, L.; Yaluff, G.; Nakayama, H.; Rojas de Arias, A.; Vega, C.; Rolan, M.; Gómez-Barrio, A.; Cerecetto, H.; González, M. *J. Med. Chem.* **2006,** *49,* 3215–3224. doi:10.1021/jm0600343
40. Wen, K.; Wang, H.; Chen, J.; Zhang, H.; Cui, X.; Wei, C.; Fan, E.; Sun, Z. *J. Org. Chem.* **2013,** *78,* 3405–3409. doi:10.1021/jo4000477
41. Landge, S. M.; Török, B. *Catal. Lett.* **2008,** *122,* 338–343. doi:10.1007/s10562-007-9385-1
42. Vlocskó, R. B.; Xie, G.; Török, B. *Molecules* **2023,** *28,* No. 4153. doi:10.3390/molecules28104153
43. Zhuang, C.; Zhang, W.; Sheng, C.; Zhang, W.; Xing, C.; Miao, Z. *Chem. Rev.* **2017,** *117,* 7762–7810. doi:10.1021/acs.chemrev.7b00020
44. Mishra, M.; Twardy, D.; Ellstrom, C.; Wheeler, K. A.; Dembinski, R.; Török, B. *Green Chem.* **2019,** *21,* 99–108. doi:10.1039/c8gc02520g
45. Beaver, W. T. *Arch. Intern. Med.* **1981,** *141,* 293–300. doi:10.1001/archinte.1981.00340030025006
46. Liu, M.; Zhang, Z.; Liu, H.; Xie, Z.; Mei, Q.; Han, B. *Sci. Adv.* **2018,** *4,* eaas9319. doi:10.1126/sciadv.aas9319
47. Cho, H.; Madden, R.; Nisanci, B.; Török, B. *Green Chem.* **2015,** *17,* 1088–1099. doi:10.1039/c4gc01523a
48. *Gaussian 09,* Revision A.02; Gaussian, Inc.: Wallingford, CT, 2016.
49. Becke, A. D. *Phys. Rev. A* **1988,** *38,* 3098–3100. doi:10.1103/physreva.38.3098
50. https://gaussian.com/volume/ (accessed March 8, 2025).

License and Terms

This is an open access article licensed under the terms of the Beilstein-Institut Open Access License Agreement (https://www.beilstein-journals.org/bjoc/terms), which is identical to the Creative Commons Attribution 4.0 International License (https://creativecommons.org/licenses/by/4.0). The reuse of material under this license requires that the author(s), source and license are credited. Third-party material in this article could be subject to other licenses (typically indicated in the credit line), and in this case, users are required to obtain permission from the license holder to reuse the material.

The definitive version of this article is the electronic one which can be found at:
https://doi.org/10.3762/bjoc.21.102

BEILSTEIN JOURNAL OF ORGANIC CHEMISTRY

Azide–alkyne cycloaddition (click) reaction in biomass-derived solvent Cyrene™ under one-pot conditions

Zoltán Medgyesi and László T. Mika*

Full Research Paper

Open Access

Address:
Department of Chemical and Environmental Process Engineering, Faculty of Chemical Technology and Biotechnology, Budapest University of Technology and Economics, Műegyetem rkp. 3., H-1111, Budapest, Hungary

Email:
László T. Mika* - laszlo.t.mika@edu.bme.hu

* Corresponding author

Keywords:
alternative solvent; click chemistry; cycloaddition; Cyrene™; 1,2,3-triazoles

Beilstein J. Org. Chem. **2025,** *21,* 1544–1551.
https://doi.org/10.3762/bjoc.21.117

Received: 28 March 2025
Accepted: 14 July 2025
Published: 30 July 2025

This article is part of the thematic issue "Green chemistry III".

Associate Editor: L. Vaccaro

© 2025 Medgyesi and Mika; licensee Beilstein-Institut.
License and terms: see end of document.

Abstract

It was demonstrated that Cyrene™, as a biomass-originated polar aprotic solvent, could be utilized as an alternative reaction medium for one-pot copper(I)-catalyzed azide–alkyne cycloaddition (click or CuAAC) reactions, for the synthesis of various 1,2,3-triazoles under mild conditions. Nineteen products involving *N*-substituted-4-phenyl-1*H*-1,2,3- and 1-allyl-4-substituted-1*H*-1,2,3-triazoles were synthesized under one-pot conditions and isolated with good to excellent yields (50–96%) and purity (>98%). The observed results represent an example that proves that biomass-derived safer solvents can be introduced into a synthetically important transformation exhibiting higher chemical and environmental safety.

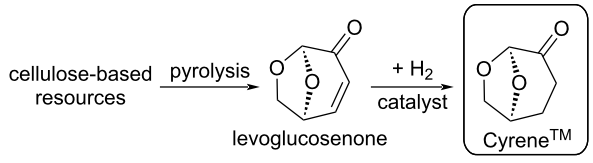
Introduction

In the past few decades, transition-metal-catalyzed coupling and addition reactions have represented one of the most powerful and atom-economical strategies for efficiently assembling new carbon–carbon [1-3] and carbon–heteroatom [4-6] bonds. Thus, it has become the most attractive and facile methodology for creating various complex organic molecular structures from the laboratory to the industrial scale. Among these methods, the copper(I)-catalyzed azide–alkyne cycloaddition (CuAAC) reaction, the so-called click reaction [7], has received substantial attention for the selective synthesis of various 1,2,3-triazoles that are of utmost importance in the synthesis of biologically active compounds such as active pharmaceutical ingredients (APIs) [8-11] and pesticides [12], or metabolic labeling molecules in plant science [13], to name a few important applications. The CuAAC reactions can be easily carried out under mild reaction conditions and exhibit excellent functional group tolerance [7].

While water has been characterized as an ideal solvent for click reactions, the limited solubility of most organic substrates could limit its application. Thus, the transformations of either water-insoluble or solid compounds require a solvent to establish high

reaction performance, i.e. homogeneous solutions with low viscosity. Accordingly, the CuAAC reactions are usually performed in fossil-based common organic reaction media having high vapor pressure, toxicity, flammability, etc., which could result in several serious environmental concerns. According to the FDA guideline [14], common polar aprotic organic solvents used for click reactions such as chlorinated hydrocarbons [15,16], toluene [16], tetrahydrofuran (THF) [17,18], *N*,*N*-dimethylformamide (DMF) [19,20], *N*-methylpyrrolidone (NMP) [21], dimethyl sulfoxide (DMSO) [17,19,22], or acetonitrile [23] are classified into Class 1 and 2, of which applications should be strictly limited, particularly in the pharmaceutical industry. To develop an environmentally benign alternative to this useful method, the identification of an alternative reaction medium is highly desired.

Among the recently characterized biomass-based potential solvents dihydrolevoglucosenone (1*R*,5*S*)-7,8-dioxabicyclo-[3.2.1]octan-2-one, CAS: 53716-82-8) or Cyrene™ (Scheme 1) has received increasing interest over the last few years. It can be produced from cellulose-containing feedstocks, through pyrolysis and a selective hydrogenation of levoglucosenone (Scheme 1). Regarding the market position, the Circa Group announced the production of Cyrene™ of 1 ton/year in 2020, signifying the large-scale production of this new biobased molecule [24]. Cyrene™ is a non-toxic substance with an $LD_{50,oral}$ > 2000 mg/kg (OECD No. 423, acute toxicity method). E(L)C_{50} > 100 mg/L (daphnia and algae), and it is negative in the Ames test [25]. Recently, we determined key physicochemical properties of Cyrene™ and showed that it has a negligible vapor pressure (<9.6 kPa) and low viscosity (<6.8 mPa·s) at typical transition-metal-catalyzed reaction temperatures (30–140 °C) [26].



Scheme 1: Synthesis of Cyrene™ (dihydrolevoglucosenone) from cellulose-based feeds via levoglucosenone (LG).

Cyrene™ has been successfully introduced into homogeneous [26-29] and heterogeneous [30,31] carbon–carbon and carbon–heteroatom bond-forming protocols. Although its reactive carbonyl group could limit its application when a strong base (aldol condensation [29]) or amines (potential Schiff-base formation) are present, a wide range of organic reactions, e.g., urea and amide formation [32,33], amide coupling [34], aldol condensation [35], C–H difluoromethylation [36], aromatic substitution [37], and MOFs synthesis [38] were demonstrated in Cyrene™. Very recently, Fasano and Citarella first reported a CuAAC reaction in Cyrene™ using 10 mol % Cu load, sodium ascorbate as base, and 24 h reaction time [39]. The protocol was successfully applied to synthesize more than 20 1,2,3-triazoles with excellent yields and purity.

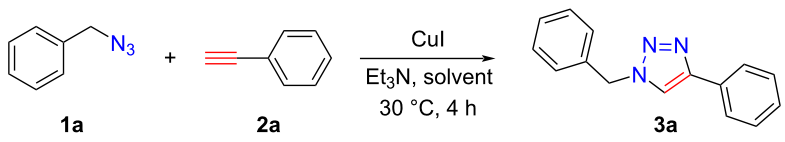
Because the CuAAC reaction is a well-studied transformation, preparing various 1,2,3-triazoles in a less toxic and recyclable medium could further control and reduce the environmental impacts of this synthetically very important transformation.

Herein, we report a study on the copper(I)-catalyzed azide–alkyne cycloaddition (CuAAC) reaction in Cyrene™ under mild conditions.

Results and Discussion

We recently demonstrated that Pd-catalyzed Heck reactions could be performed in Cyrene™ [26]. To extend its applicability, we first compared the typical conventional organic media, selected biomass-derived solvents (i.e., levulinic acid and γ-valerolactone-based solvents), and Cyrene™ in the transformation of 1.15 mmol benzyl azide (**1a**) and 1 mmol phenylacetylene (**2a**) in the presence of 0.01 mmol CuI and 0.1 mmol Et_3N as a model reaction (Scheme 2) under typically used "click conditions" [7].

In common organic solvents, the yields of 1-benzyl-4-phenyl-1*H*-1,2,3-triazole (**3a**) were moderate (DCM, 1,4-dioxane) or low (DMF, NMP, DMSO) (Figure 1). While low conversion was still detected in biomass-originated 2-MeTHF, MeLev, and EtLev established better performance. When their corresponding 4-alkoxy derivatives were applied, moderate (Me-4MeOV) or slightly lower (Et-4EtOV) conversions could be observed. However, significantly higher efficiencies were detected in



Scheme 2: Copper-catalyzed azide–alkyne cycloaddition of benzyl azide (**1a**) and phenylacetylene (**2a**) in various solvents.

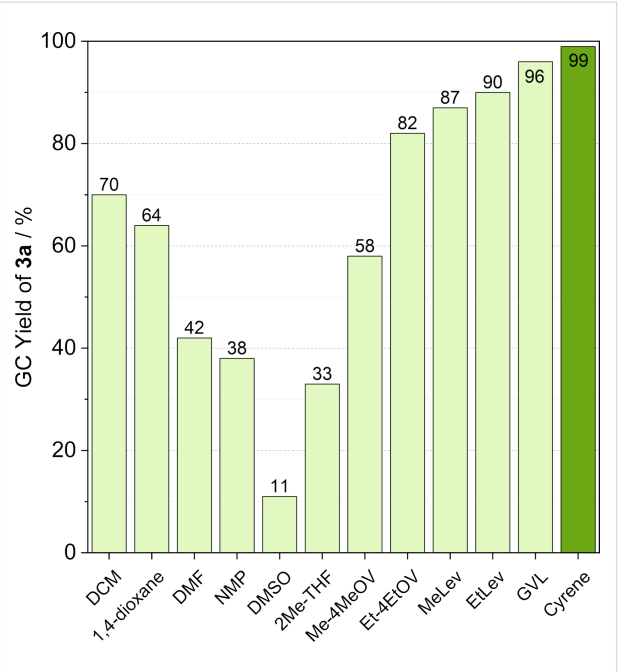


Figure 1: Comparison of various solvents used in the CuAAC reaction. Reaction conditions: 1.15 mmol benzyl azide, 1 mmol phenylacetylene, 2.5 mL solvent, 0.01 mmol CuI, 0.1 mmol Et_3N, T = 30 °C, t = 4 h. DCM: dichloromethane, DMF: *N*,*N*-dimethylformamide, NMP: *N*-methylpyrrolidone, DMSO: dimethyl sulfoxide, 2Me-THF: 2-methyltetrahydrofuran, Me-4MeOV: methyl 4-methoxyvalerate, Et-4EtOV: ethyl 4-ethoxyvalerate, MeLev: methyl levulinate, EtLev: ethyl levulinate, GVL: γ-valerolactone.

GVL and Cyrene™, which clearly verify that both solvents are appropriate for click chemistry.

The source of copper could also have a significant effect on the reaction's performance [40]. Accordingly, both Cu(I) and Cu(II) salts (1 mol % Cu) were tested in the conversion of 1.15 mmol benzyl azide (**1a**) and 1 mmol phenylacetylene (**2a**) in 2.5 mL Cyrene™ at 30 °C. All the selected Cu salts catalyzed the cycloaddition; however, Cu chlorides and oxides resulted in unexpectedly low product yields after 0.5 h. The solubility of Cu oxides was significantly lower in Cyrene™, indicated by a slightly turbid, inhomogeneous initial reaction mixture. Copper(I) bromide, thiocyanate, and acetate also gave low yields. However, CuI afforded almost complete conversion of **1a** under identical conditions (Figure 2). The results are in accordance with those obtained for Cu sources in different solvent systems [40,41].

Although CuAAC reactions can be efficiently performed in water, the moisture content of the organic reaction environment could have a significant effect on the efficiency of a transition-metal-catalyzed reaction. Because Cyrene™ is fully miscible in water, investigating the possible effect of the water content on the reaction was highly desired. We found that a slight decrease

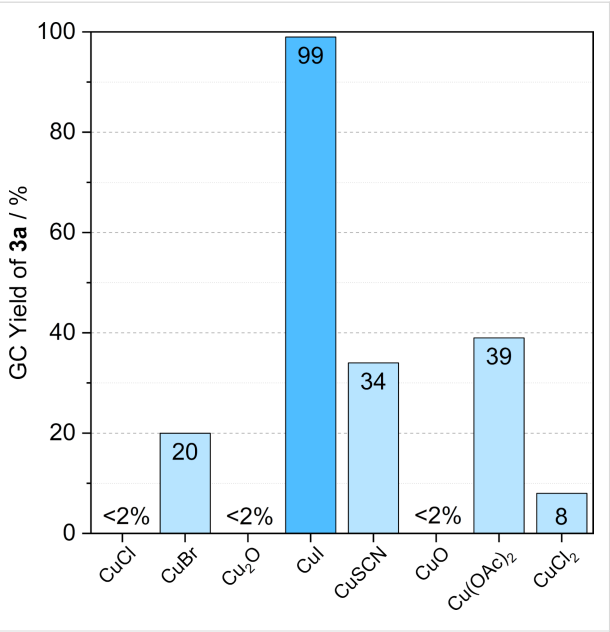


Figure 2: Effect of the Cu source used in the click reaction of benzyl azide (**1a**, 1.15 mmol) and phenylacetylene (**2a**, 1 mmol). Reaction conditions: 2.5 mL Cyrene™, 1 mol % catalyst precursor, 0.1 mmol Et_3N, T = 30 °C, t = 0.5 h.

in formation of product **3a** was detected when the moisture content was varied between 0.05 and 3.0 wt % (Table 1). A higher moisture content reduces the product formation; thus, keeping water content below 1% is necessary to maintain high reaction efficiency. The negative effect could be due to the decreased solubility of **2a** at higher water content [42-44].

Table 1: Effect of the water content on the CuAAC reaction of benzyl azide (**1a**) and phenylacetylene (**2a**).[a]

Entry	Water content/wt %	Yield **3a**[b]/%
1	<0.05	>99
2	1.0	88
3	2.0	86
4	3.0	70
5	4.0	47
6	5.0	29

[a]Reaction conditions: 1.15 mmol benzyl azide (**1a**), 1 mmol phenylacetylene (**2a**), 2.5 mL Cyrene™, 1 mol % CuI, 0.1 mmol Et_3N, T = 30 °C, t = 1 h. [b]GC yield.

Hereafter, the readily available CuI was selected as a catalyst precursor to facilitate click reactions involving benzyl azide (**1a**) and various acetylenes **2b–h** in Cyrene™ at 30 °C for 12 h (Figure 3). It should be noted that all components readily dissolved in Cyrene™, resulting in clear, homogeneous reaction mixtures. With the exception of 3-(1-benzyl-1*H*-1,2,3-triazol-4-

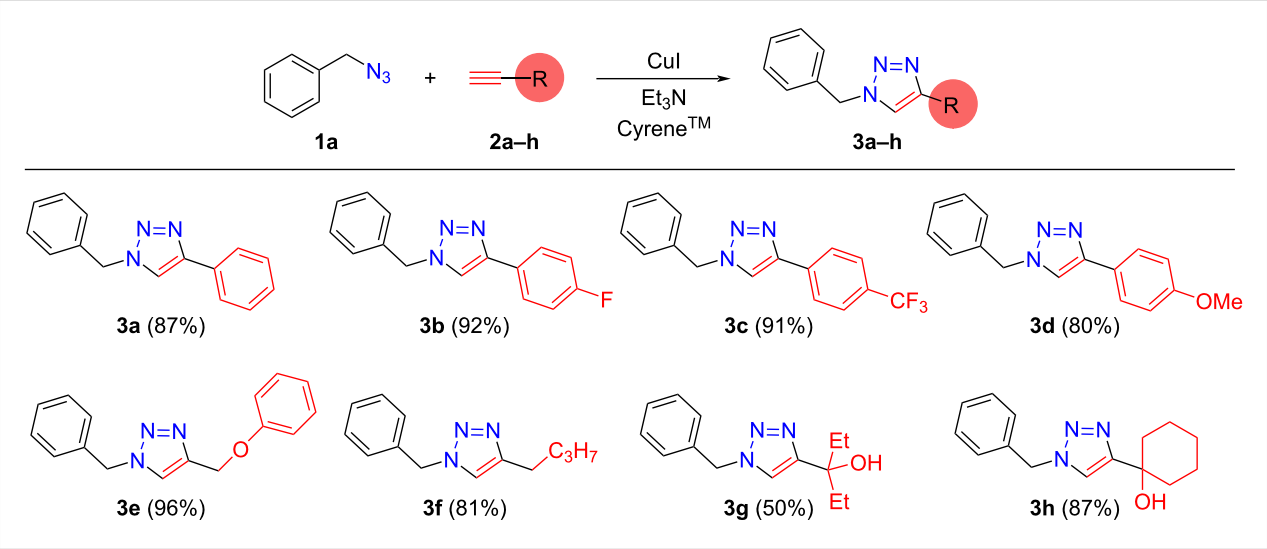


Figure 3: Copper-catalyzed azide–alkyne cycloaddition of benzyl azide (**1a**) and various acetylenes **2a–h** in Cyrene™. Reaction conditions: 1.15 mmol **1a**, 1 mmol **2a–h**, 0.1 mmol Et_3N, 0.01 mmol CuI, 2.5 mL Cyrene™, T = 30 °C, t = 12 h; isolated yields based on **2a–h** are given in parentheses.

yl)pentan-3-ol (**3g**), the isolated 1,2,3-triazole derivatives were generally obtained with good to excellent yields (50–96%). Both electron-withdrawing (fluoro (**3b**) or trifluoromethyl (**3c**)) and electron-donating (methoxy, phenoxy, and alkyl (**3d–h**)) groups were tolerated on the acetylene reaction partner species. In accordance with results reported by Citarella et al. [39], excellent functional group tolerance was verified and the isolated yields are in the same range as reported by Citarella et al. (for **3a**, 90% [39] and 87% [39]). It should be noted that no Cu-catalyzed Glaser-coupling of acetylenes [45] was observed, indicating further the applicability of the present synthetic method.

Due to the excellent solvating power of Cyrene™, the "one-pot" synthesis of 1,2,3-triazoles could be proposed to eliminate the preparation and isolation steps of azide components. This could open an even greener and facile protocol for CuAAC reactions. To demonstrate the one-pot synthesis of 1-benzyl-4-phenyl-1*H*-1,2,3-triazole (**3a**), 1.23 mmol benzyl bromide (**4a**), 1.57 mmol NaN_3, 1.06 mmol phenylacetylene (**2a**), 0.011 mmol CuI, and 0.1 mmol Et_3N were mixed in 2.5 mL of solvent and stirred at 85 °C. After 24 h, GC analysis verified a 90% yield of **3a**, which proves that the CuAAC reaction was completed in Cyrene™ under one-pot conditions. After the work-up procedure, a satisfactory 84% yield of **3a** was obtained. When the one-pot reaction was sequenced, it first involved the synthesis of benzyl azide (**1a**) using 1.17 mmol benzyl bromide (**4a**) and 1.31 mmol NaN_3 at 85 °C. After 8 h, 1.06 mmol phenylacetylene (**2a**), 0.01 mmol CuI, and 0.1 mmol Et_3N were added to initiate the click reaction. The mixture was stirred at 30 °C for 12 h. The GC analysis showed complete conversion, and after the workup procedure, 88% **3a** was isolated with 98.5% purity. It is important to note that there are no differences between the isolated yields (cf. Figure 3 and Figure 4 for **3a**). According to the observation that the consecutive synthesis could be more efficient, the scope of the method was extended to synthesizing various *N*-substituted-4-phenyl-1*H*-1,2,3-triazoles in Cyrene™ (Figure 4). It was shown that the protocol resulted in the formation of products **3a** and **5b–f** with yields of 57–91% depending on the structure of the bromide derivatives. The isolated yields were in the same range as reported by Citarella et al. [39].

The presence of a terminal carbon–carbon double bond in a certain molecular structure could allow for efficient subsequent functionalization via, for example, an addition reaction, opening possibilities for building even more complex molecular skeletons involving 1,2,3-triazole units. Using allyl bromide in the reaction sequence results in the formation of 1-allyl-4-substituted-1*H*-1,2,3-triazoles bearing a terminal C–C double bond moiety. Thus, we attempted to prepare a series of 1-allyl-4-substituted-1*H*-1,2,3-triazoles (Figure 5, **6a–f**) from allyl bromide (**4g**) and selected acetylenes **2a–f**. Similar to the formation of *N*-substituted-4-phenyl-1*H*-1,2,3-triazoles, the method exhibits good functional group tolerance and gives the corresponding products **6a–f** with moderate and/or good isolated yields (52–83%).

Our investigation finally focused on the solvent recovery and reuse, which is a key issue for large-scale applications. When 5 mmol **1a** and 5.75 mmol of **2a** were reacted in the presence of 1 mol % CuI and 0.5 mmol Et_3N at 30 °C for 2 h, a >99.9%

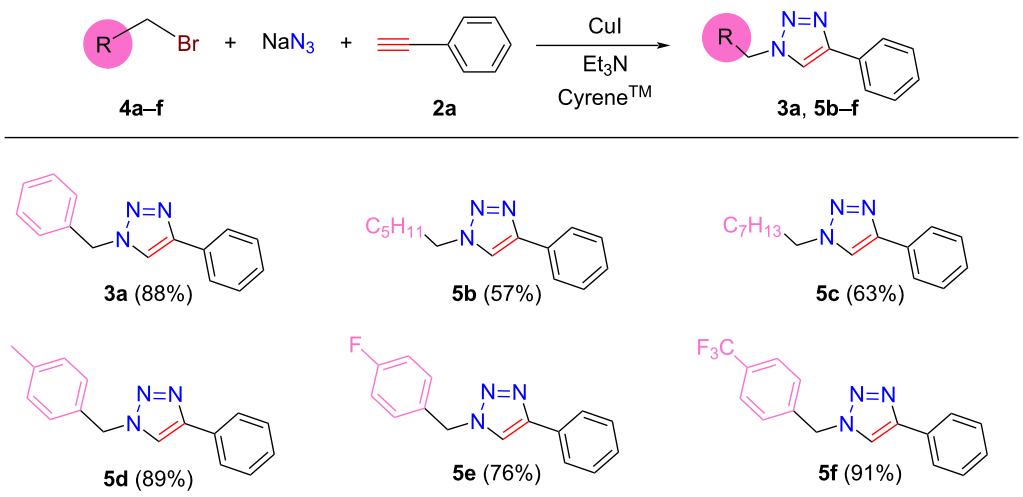


Figure 4: Consecutive synthesis of various *N*-substituted-4-phenyl-1*H*-1,2,3-triazoles in Cyrene™. Reaction conditions: 1st step: 1.15 mmol **4a–e**, and 1.3 mmol NaN_3, 2.5 mL Cyrene™, T = 85 °C, t = 8 h. 2nd step: 1 mmol **2a**, 0.1 mmol Et_3N, 0.01 mmol CuI, T = 30 °C, t = 12 h. Isolated yields based on phenylacetylene (**2a**) are given in parentheses.

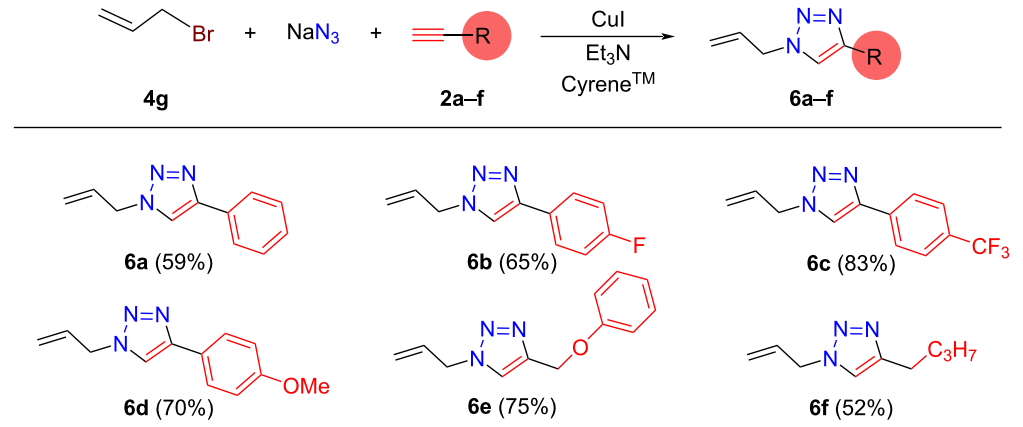


Figure 5: "One-pot" synthesis of various 1-allyl-4-substituted-1*H*-1,2,3-triazoles in Cyrene™. Reaction conditions: 1st step: 1.15 mmol **4g**, 1.3 mmol NaN_3, 2.5 mL Cyrene™, T = 75 °C, t = 24 h. 2nd step: 1 mmol **2a–f**, 0.01, mmol CuI, 0.1 mmol Et_3N, T = 30 °C, t = 12 h. Isolated yields based on corresponding acetylene derivatives are given in parentheses.

conversion was detected. After the reaction, 25 mL of cold water was added to precipitate **3a**, which was subsequently filtered, dried, and isolated with a yield of 93.7%. After the removal of volatile compounds from the aqueous phase by vacuum distillation, 88% of Cyrene™ (13.7 g) was recovered. The reaction was repeated four times with the same procedure under identical conditions (same catalyst and substrate concentration). It was shown that Cyrene™ could be successfully recovered for 4 consecutive runs, which resulted in high conversion of **1a** in each run (Figure 6).

To evaluate and compare the one-pot protocol with published methods, the environmental factor (E-factor) was calculated for the synthesis of **3a**. Considering an average 88% solvent recovery, the E-factor is 76. It is lower than that obtained in the conventional organic medium DMSO (E-factor = 104, [46]) and higher than the one calculated by Citarella (E-factor = 24, [39]) for the Cyrene™-based protocol. However, they used a 15 times higher substrate loading.

Conclusion

In conclusion, we have demonstrated that biomass-derived Cyrene™ can be utilized as an alternative reaction medium for the one-pot copper(I)-catalyzed azide–alkyne cycloaddition (CuAAC) reaction of various acetylenes and azides. Due to the strong solvating power of Cyrene™, a sequenced one-pot syn-

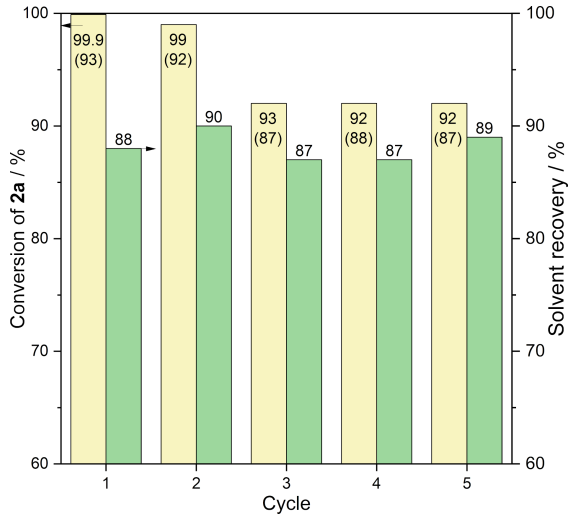


Figure 6: Solvent recovery for the CuAAC reaction of **1a** and **2a**. Reaction conditions: 12.5 mL Cyrene™, 1 mol % CuI, 0.5 mmol Et_3N, T = 30 °C, t = 2 h. Isolated yields are given in parentheses.

thesis of triazoles was successfully demonstrated. The protocol was tested for a wide range of substrates, and successful synthesis and isolation of nineteen 1,2,3-triazole derivatives **3a**–**h**, **5b**–**f**, and **6a–f** with moderate to excellent isolated yields (50–96%) and purity (>98%) was shown.

Experimental

The sources of chemicals are listed in Supporting Information File 1. ^{1}H, ^{13}C, and ^{19}F NMR spectra were collected on a Bruker Avance 300 MHz or Bruker Avance-III 500 MHz instrument and processed by MestReNova v. 14.3.1-31739 (2022) MestreLab Research S. L.

GC analyses were performed on an HP 5890 N Series II instrument with Restek RTX®-50 capillary column (15 m × 0.25 mm × 0.25 μm) using H_2 as a carrier gas. For the analysis, 10 μL of the reaction mixture was dissolved in 1 mL of ethyl acetate, followed by adding 10 μL toluene as the internal standard. Heating profile of GC–FID analysis: The initial temperature was 100 °C and was hold for 0.5 min. Heating rate: 40 °C/min up to the final temperature of 270 °C. The final temperature was held for 4.25 min.

The water content of Cyrene™ was measured on a Methrom 684 KF Coulometer at Balint Analitika Ltd, Budapest, Hungary.

Cyrene™ was purchased from Sigma-Aldrich Kft. Budapest, Hungary. Its purification was performed by vacuum distillation (18–20 mmHg, 114–116 °C) and stored under argon before subsequent use. The purity (>99.99%) was checked by ^{1}H and ^{13}C NMR spectroscopy. ^{1}H NMR (300 MHz, $CDCl_3$, TMS) δ 5.10 (s, 1H, CH), 4.71 (s, 1H, CH), 4.05 (d, J = 7.3 Hz, 1H, CH), 3.96 (t, J = 6.3 Hz, 1H, CH), 2.73–2.02 (m, 4H, CH_2); ^{13}C NMR (75 MHz, $CDCl_3$, TMS) δ 200.3 (CO), 101.5 (CH), 73.1 (CH), 67.6 (CH_2), 31.1 (CH_2), 29.9 (CH_2). The NMR data correspond to the published results.

Methyl 4-methoxyvalerate and ethyl 4-ethoxyvalerate were prepared using the published method [47].

The synthesis of benzyl azide, detailed experimental procedures, and characterization of prepared compounds are reported in Supporting Information File 1.

General procedure for click reaction in Cyrene™

In a 4 mL screw-cap vial, 1.15 mmol of benzyl azide (**1a**), 1 mmol corresponding acetylene, 0.1 equiv Et_3N, and 0.01 mmol CuI, were dissolved in 2.5 mL Cyrene™. The reaction mixture was stirred overnight at a given temperature. After the reaction, 20 mL of cold distilled water was added, followed by intensive stirring. The solid product was filtered, washed with distilled water (3 × 5 mL), and dried until constant weight under the fume hood. The detailed experimental procedure, as well as the characterization of isolated compounds, are provided in Supporting Information File 1.

General procedure for click reaction in Cyrene™ under one-pot conditions

In a 4 mL screw-cap vial, 1.15 mmol of corresponding bromine and 1.3 mmol NaN_3 were dissolved in 2.5 mL Cyrene™ and stirred at a given temperature. After a given reaction time, 1 mmol of the corresponding acetylene compound, 0.1 mmol of Et_3N, and 0.01 mmol of CuI were added to the reaction mixture and reacted for a given time at a given temperature. The work-up procedure is similar to the one given above. The detailed experimental procedure, as well as the characterization of isolated compounds, are provided in Supporting Information File 1.

Supporting Information

Supporting Information File 1

Source of chemicals, detailed experimental procedure, and characterization of isolated compounds.
[https://www.beilstein-journals.org/bjoc/content/supplementary/1860-5397-21-117-S1.pdf]

Acknowledgements

The authors thank Mr. Imre Nyiri at Bálint Analitika Kft. Budapest, Hungary, for the Karl-Fischer test of Cyrene™.

Funding

The Project was supported by the Hungarian National Research Development and Innovation Office – NKFIH under FK 143197 grant. The research reported in this paper is part of project no. BME-EGA-02 with the support provided by the Ministry of Innovation and Technology of Hungary from the National Research Development and Innovation Fund financed under the TKP2021 funding scheme. Zoltán Medgyesi is grateful for the support of the József Varga Foundation, Budapest University of Technology and Economics.

Author Contributions

Zoltán Medgyesi: formal analysis; investigation; writing – original draft. László T. Mika: conceptualization; funding acquisition; project administration; supervision.

ORCID® iDs

László T. Mika - https://orcid.org/0000-0002-8520-0065

Data Availability Statement

All data that supports the findings of this study is available in the published article and/or the supporting information of this article.

Preprint

A non-peer-reviewed version of this article has been previously published as a preprint: https://doi.org/10.3762/bxiv.2025.21.v1

References

1. de Meijere, A.; Diederich, F., Eds. *Metal-Catalyzed Cross-Coupling Reactions;* Wiley-VCH: Weinheim, Germany, 2004. doi:10.1002/9783527619535
2. Jana, R.; Pathak, T. P.; Sigman, M. S. *Chem. Rev.* **2011,** *111,* 1417–1492. doi:10.1021/cr100327p
3. Biffis, A.; Centomo, P.; Del Zotto, A.; Zecca, M. *Chem. Rev.* **2018,** *118,* 2249–2295. doi:10.1021/acs.chemrev.7b00443
4. Beletskaya, I. P.; Ananikov, V. P. *Chem. Rev.* **2022,** *122,* 16110–16293. doi:10.1021/acs.chemrev.1c00836
5. Tamatam, R.; Kim, S.-H.; Shin, D. *Front. Chem. (Lausanne, Switz.)* **2023,** *11,* 1140562. doi:10.3389/fchem.2023.1140562
6. Hsieh, J.-C. *Chem. Rec.* **2021,** *21,* 3370–3381. doi:10.1002/tcr.202100008
7. Kolb, H. C.; Finn, M. G.; Sharpless, K. B. *Angew. Chem., Int. Ed.* **2001,** *40,* 2004–2021. doi:10.1002/1521-3773(20010601)40:11<2004::aid-anie2004>3.0.co;2-5
8. Thirumurugan, P.; Matosiuk, D.; Jozwiak, K. *Chem. Rev.* **2013,** *113,* 4905–4979. doi:10.1021/cr200409f
9. Meldal, M.; Diness, F. *Trends Chem.* **2020,** *2,* 569–584. doi:10.1016/j.trechm.2020.03.007
10. Khandelwal, R.; Vasava, M.; Abhirami, R. B.; Karsharma, M. *Bioorg. Med. Chem. Lett.* **2024,** *112,* 129927. doi:10.1016/j.bmcl.2024.129927
11. Hein, C. D.; Liu, X.-M.; Wang, D. *Pharm. Res.* **2008,** *25,* 2216–2230. doi:10.1007/s11095-008-9616-1
12. Chen, Z.; Jiang, Y.; Xu, C.; Sun, X.; Ma, C.; Xia, Z.; Zhao, H. *Molecules* **2022,** *27,* 4928. doi:10.3390/molecules27154928
13. Chen, M.-M.; Kopittke, P. M.; Zhao, F.-J.; Wang, P. *Trends Plant Sci.* **2024,** *29,* 167–178. doi:10.1016/j.tplants.2023.07.003
14. Q3C – Tables and List guidance for industry. Companion document for the International Council for Harmonisation of Technical Requirements for Pharmaceuticals for Human Use guidance for Industry *Q3C Impurities: Residual Solvents*. https://www.fda.gov/media/71737/download (accessed March 2, 2025).
15. Kovács, S.; Zih-Perényi, K.; Révész, Á.; Novák, Z. *Synthesis* **2012,** *44,* 3722–3730. doi:10.1055/s-0032-1317697
16. Wang, W.; Wei, F.; Ma, Y.; Tung, C.-H.; Xu, Z. *Org. Lett.* **2016,** *18,* 4158–4161. doi:10.1021/acs.orglett.6b02199
17. Wu, L.-Y.; Xie, Y.-X.; Chen, Z.-S.; Niu, Y.-N.; Liang, Y.-M. *Synlett* **2009,** 1453–1456. doi:10.1055/s-0029-1216745
18. Friscourt, F.; Boons, G.-J. *Org. Lett.* **2010,** *12,* 4936–4939. doi:10.1021/ol1022036
19. Xu, M.; Kuang, C.; Wang, Z.; Yang, Q.; Jiang, Y. *Synthesis* **2011,** 223–228. doi:10.1055/s-0030-1258357
20. Coady, D. J.; Bielawski, C. W. *Macromolecules* **2006,** *39,* 8895–8897. doi:10.1021/ma062030d
21. Weterings, J. J.; Khan, S.; van der Heden, G. J.; Drijfhout, J. W.; Melief, C. J. M.; Overkleeft, H. S.; van der Burg, S. H.; Ossendorp, F.; van der Marel, G. A.; Filippov, D. V. *Bioorg. Med. Chem. Lett.* **2006,** *16,* 3258–3261. doi:10.1016/j.bmcl.2006.03.034
22. Kolarovič, A.; Schnürch, M.; Mihovilovic, M. D. *J. Org. Chem.* **2011,** *76,* 2613–2618. doi:10.1021/jo1024927
23. Bandyopadhyay, M.; Bhadra, S.; Pathak, S.; Menon, A. M.; Chopra, D.; Patra, S.; Escorihuela, J.; De, S.; Ganguly, D.; Bhadra, S.; Bera, M. K. *J. Org. Chem.* **2023,** *88,* 15772–15782. doi:10.1021/acs.joc.3c01836
24. Brouwer, T.; Schuur, B. *ACS Sustainable Chem. Eng.* **2020,** *8,* 14807–14817. doi:10.1021/acssuschemeng.0c04159
25. Waaijers-van der Loop, S. L.; Dang, Z.-C.; Rorije, E.; Janssen, N. Toxicity screening of potential bio-based Polar Aprotic Solvents (PAS). Rijksintituut voor Volksgezondheid en Milieu; Minsterie van Volksgesondheid, Welzijn en Sport; December 21, 2018, version 1.0. https://www.rivm.nl/sites/default/files/2019-02/Screening%20van%20potenti%C3%ABle%20polair%20aprotische%20oplosmiddelen.pdf (accessed March 20, 2024).
26. Medgyesi, Z.; Mika, L. T. *ChemPlusChem* **2024,** *89,* e202400379. doi:10.1002/cplu.202400379
27. Camp, J. E. *ChemSusChem* **2018,** *11,* 3048–3055. doi:10.1002/cssc.201801420
28. Sangon, S.; Supanchaiyamat, N.; Sherwood, J.; McElroy, C. R.; Hunt, A. J. *React. Chem. Eng.* **2020,** *5,* 1798–1804. doi:10.1039/d0re00174k
29. Wilson, K. L.; Kennedy, A. R.; Murray, J.; Greatrex, B.; Jamieson, C.; Watson, A. J. B. *Beilstein J. Org. Chem.* **2016,** *12,* 2005–2011. doi:10.3762/bjoc.12.187
30. Stini, N. A.; Gkizis, P. L.; Kokotos, C. G. *Org. Biomol. Chem.* **2023,** *21,* 351–358. doi:10.1039/d2ob02012b
31. Galaverna, R. S.; Fernandes, L. P.; Menezes da Silva, V. H.; de Siervo, A.; Pastre, J. C. *Eur. J. Org. Chem.* **2022,** e202200376. doi:10.1002/ejoc.202200376
32. Bousfield, T. W.; Pearce, K. P. R.; Nyamini, S. B.; Angelis-Dimakis, A.; Camp, J. E. *Green Chem.* **2019,** *21,* 3675–3681. doi:10.1039/c9gc01180c
33. Mistry, L.; Mapesa, K.; Bousfield, T. W.; Camp, J. E. *Green Chem.* **2017,** *19,* 2123–2128. doi:10.1039/c7gc00908a

34. Wilson, K. L.; Murray, J.; Jamieson, C.; Watson, A. J. B. *Org. Biomol. Chem.* **2018,** *16,* 2851–2854. doi:10.1039/c8ob00653a
35. Hughes, L.; McElroy, C. R.; Whitwood, A. C.; Hunt, A. J. *Green Chem.* **2018,** *20,* 4423–4427. doi:10.1039/c8gc01227j
36. Veerabagu, U.; Jaikumar, G.; Lu, F.; Quero, F. *React. Chem. Eng.* **2021,** *6,* 1900–1910. doi:10.1039/d1re00196e
37. Citarella, A.; Cavinato, M.; Amenta, A.; Nardini, M.; Silvani, A.; Passarella, D.; Fasano, V. *Eur. J. Org. Chem.* **2024,** *27,* e202301305. doi:10.1002/ejoc.202301305
38. Zhang, J.; White, G. B.; Ryan, M. D.; Hunt, A. J.; Katz, M. J. *ACS Sustainable Chem. Eng.* **2016,** *4,* 7186–7192. doi:10.1021/acssuschemeng.6b02115
39. Citarella, A.; Fiori, A.; Silvani, A.; Passarella, D.; Fasano, V. *ChemSusChem* **2025,** *18,* e202402538. doi:10.1002/cssc.202402538
40. Meldal, M.; Tornøe, C. W. *Chem. Rev.* **2008,** *108,* 2952–3015. doi:10.1021/cr0783479
41. Liang, L.; Astruc, D. *Coord. Chem. Rev.* **2011,** *255,* 2933–2945. doi:10.1016/j.ccr.2011.06.028
42. Singh, H.; Sindhu, J.; Khurana, J. M. *RSC Adv.* **2013,** *3,* 22360–22366. doi:10.1039/c3ra44440f
43. Alonso, F.; Moglie, Y.; Radivoy, G.; Yus, M. *Adv. Synth. Catal.* **2010,** *352,* 3208–3214. doi:10.1002/adsc.201000637
44. Castro-Godoy, W. D.; Heredia, A. A.; Schmidt, L. C.; Argüello, J. E. *RSC Adv.* **2017,** *7,* 33967–33973. doi:10.1039/c7ra06390c
45. Glaser, C. *Justus Liebigs Ann. Chem.* **1870,** *154,* 137–171. doi:10.1002/jlac.18701540202
46. Calculation performed by Citarella et al. in ref. [39].
47. Fegyverneki, D.; Orha, L.; Láng, G.; Horváth, I. T. *Tetrahedron* **2010,** *66,* 1078–1081. doi:10.1016/j.tet.2009.11.013

License and Terms

This is an open access article licensed under the terms of the Beilstein-Institut Open Access License Agreement (https://www.beilstein-journals.org/bjoc/terms), which is identical to the Creative Commons Attribution 4.0 International License (https://creativecommons.org/licenses/by/4.0). The reuse of material under this license requires that the author(s), source and license are credited. Third-party material in this article could be subject to other licenses (typically indicated in the credit line), and in this case, users are required to obtain permission from the license holder to reuse the material.

The definitive version of this article is the electronic one which can be found at:
https://doi.org/10.3762/bjoc.21.117

BEILSTEIN JOURNAL OF ORGANIC CHEMISTRY

Fe-catalyzed efficient synthesis of 2,4- and 4-substituted quinolines via C(sp^2)–C(sp^2) bond scission of styrenes

Prafull A. Jagtap, Manish M. Petkar, Vaishnavi R. Sawant and Bhalchandra M. Bhanage*

Full Research Paper

Open Access

Address:
Department of Chemistry, Institute of Chemical Technology, Mumbai-400019, India

Email:
Bhalchandra M. Bhanage* - bm.bhanage@ictmumbai.edu.in

* Corresponding author

Keywords:
C–C activation; C–H annulation; iron metal catalysis; quinolines; styrene

Beilstein J. Org. Chem. **2025,** *21,* 1799–1807.
https://doi.org/10.3762/bjoc.21.142

Received: 07 May 2025
Accepted: 20 August 2025
Published: 05 September 2025

This article is part of the thematic issue "Green chemistry III: Technologies shaping future directions in synthesis".

Associate Editor: L. Vaccaro

© 2025 Jagtap et al.; licensee Beilstein-Institut.
License and terms: see end of document.

Abstract

Herein, we report a highly efficient, environmentally benign protocol for the domino synthesis of 2,4-disubstituted and 4-substituted quinoline molecules. The developed strategy involves an earth-abundant Fe-catalyzed C(sp^2)–C(sp^2) bond cleavage of styrene, followed by the hydroamination of the cleaved synthons with arylamines and subsequent C–H annulation to yield two valuable quinoline derivatives. Key features of this protocol include the use of O_2 as an ideal, green oxidant, operational simplicity and scalability, high atom- and step-economy, and cost-effectiveness, collectively enabling the single-step synthesis of two medicinally relevant N-heterocycles in excellent combined yields.

Introduction

Quinolines are one of the essential heteroaromatic motifs that play a crucial role across diverse scientific fields due to their wide range of applications. In contemporary medicine, quinoline derivatives frequently appear in active pharmaceutical ingredients, therapeutic agents, and agrochemical formulations [1-9]. Around 60% of recently FDA-approved drugs contain heterocyclic compounds, with quinoline recognized as a key structural motif due to its significant anticancer, antifungal, antibacterial, and anti-inflammatory activities [10-13]. In the field of optoelectronics, especially with 2,4-diarylquinoline derivatives, extensive studies have highlighted their applicability in organic light-emitting diode (OLED) systems as functional materials [14,15] and cutting-edge fluorescent probes for sensing and bioimaging applications (Figure 1) [16,17]. Quinoline-derived metal complexes have also demonstrated broad utility, functioning as effective catalysts in organic synthesis and finding applications across medicinal chemistry, materials science, photovoltaics, and chemical sensing [18].

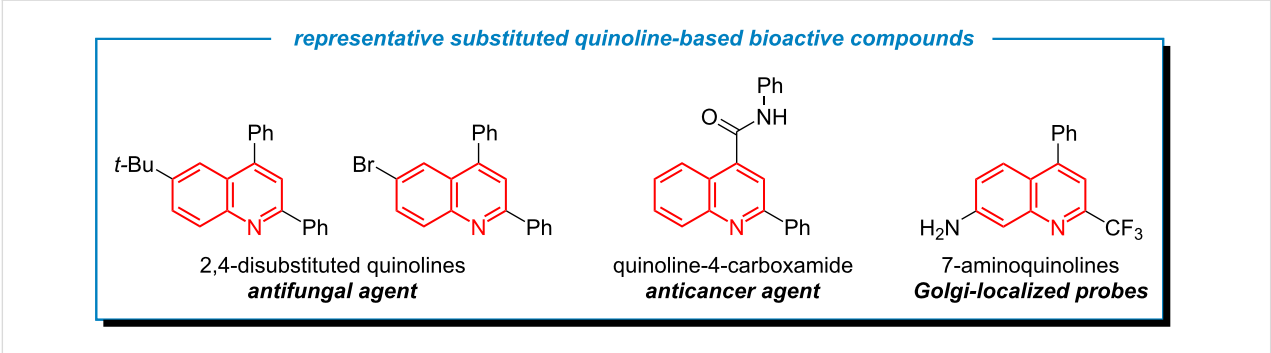
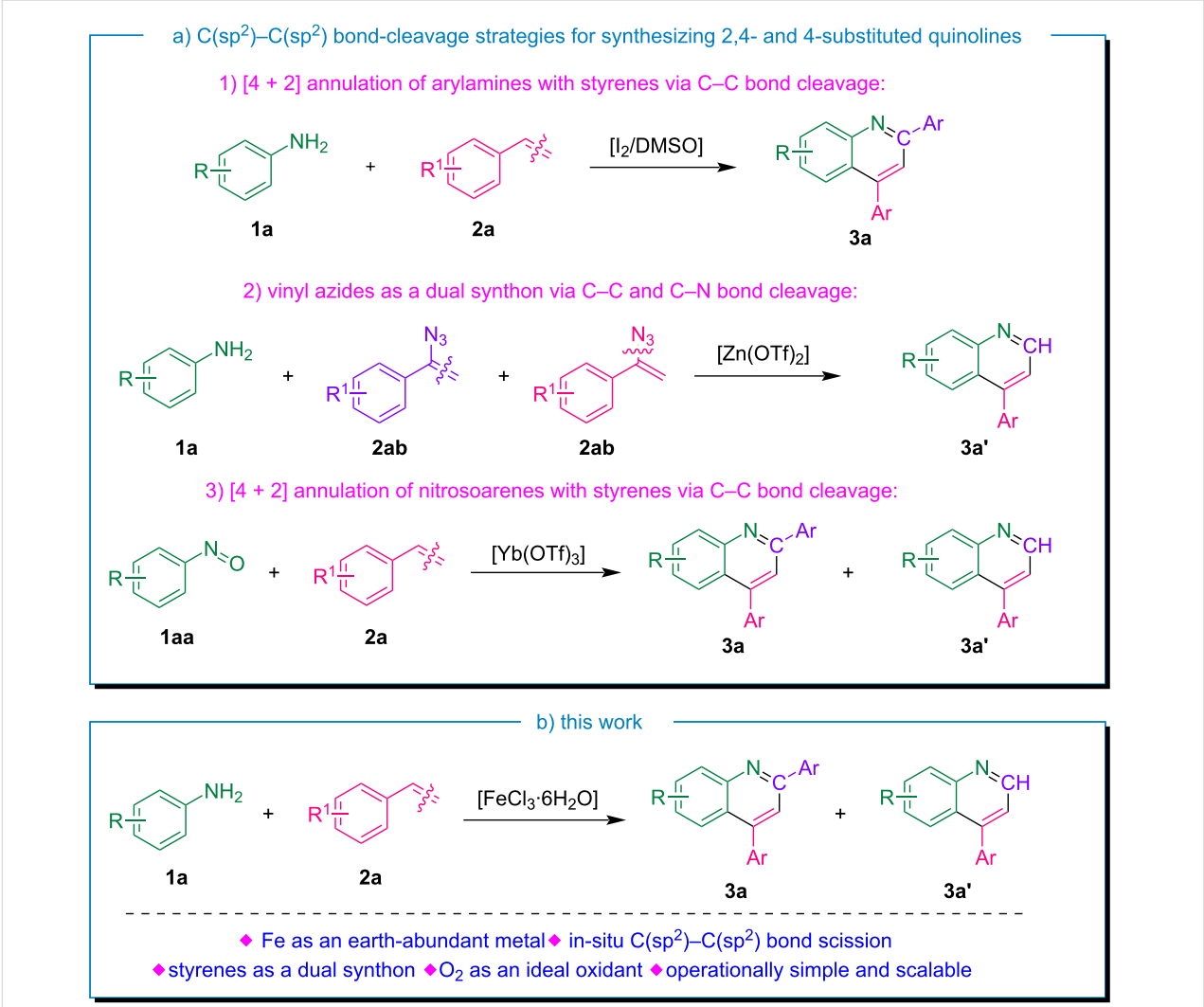


Figure 1: Representative examples of bioactive quinolines.

Due to its wide range of applications, several methods for synthesizing substituted quinoline derivatives have been developed in recent decades, based on mechanisms such as Conrad–Limpach–Knorr [19], Friedländer [20], Doebner–Miller [21], Pfitzinger [22], Skraup [23], Povarov [24], and Combes [25]. However, these methods often require multiple synthetic steps and demanding conditions such as elevated temperatures, strong acidic or basic environments, and the use of expensive metal catalysts, which limit their broader applicability. To overcome these limitations, numerous catalytic strategies have been explored in recent decades for the synthesis of structurally diverse quinolines. Among them, transition-metal-catalyzed multicomponent reactions (MCRs) have emerged as particularly effective for constructing complex quinoline-based heterocycles [26-28]. Catalytic pathways such as cycloaddition, tandem annulation, intramolecular cyclization, and cross-coupling reactions are commonly employed under thermal conditions, utilizing metal catalysts based on Pd, Ru, Au, Cu, and Fe to access a wide array of substituted quinoline frameworks [29-38].

Conversely, in light of climate change and the ongoing energy crisis, there is an urgent need to reform energy and chemical production by prioritizing environmentally sustainable methods that are both practical and broadly implementable. Styrenes are industrially important bulk chemicals [39], with an estimated global production of approximately 30 million tons annually [40]. Their low cost and widespread availability make them highly valuable as fundamental building blocks in organic synthesis. Over the past few decades, the direct functionalization of styrenes has emerged as a prominent research area due to its promising industrial relevance. Oxidative cleavage of alkenes to yield carbonyl compounds is one of the key transformations in synthetic organic chemistry [41,42]. Over the past two decades, this field has witnessed significant advancements, primarily through the use of organic oxidants and transition-metal catalysts. One of the key transformations in organic synthesis is the selective oxidative cleavage of alkenes to yield ketones or aldehydes [43-47]. Traditionally, such transformations have been achieved using various oxidizing agents, transition-metal-based systems, organo- and biocatalysts, as well as enzymatic processes. Among these, molecular oxygen stands out as a greener and more sustainable oxidant due to its natural abundance, low cost, and environmentally friendly properties, making it an appealing option for both academic research and industrial applications. Recently, some advanced strategies have been developed for cleavage of alkenes [48-51].

Owing to the abundance and versatile applications of styrenes in diverse fields of organic chemistry, some strategies have recently been developed for synthesizing 2,4-disubstituted and 4-substituted quinoline derivatives via the $C(sp^2)$–$C(sp^2)$ bond-scission approach. A summary of known procedures for synthesizing these derivatives via $C(sp^2)$–$C(sp^2)$ bond cleavage is presented in Scheme 1a. In 2015, Shah et al. documented the first two-component, metal-free approach for accessing 2,4-disubstituted quinolines [52]. They employed an I_2/DMSO-facilitated C–C bond-scission strategy of styrenes, followed by C–N bond formation and subsequent [4 + 2] annulation. Jiang and co-workers developed a method for synthesizing 4-substituted quinolines using vinyl azides as dual synthons, facilitating both the C–C and C–N bond cleavage [53]. In this work, the authors used a stoichiometric amount of $Zn(OTf)_3$ as a Lewis acid catalyst and air as the oxidant for the reaction. Jana and colleagues demonstrated an atom-efficient pseudo-three-component C–H annulation reaction catalyzed by Yb and Cu, which involved nitrosoarenes and styrene or epoxystyrene as coupling partners to yield substituted aryl quinolines [54]. However, the methods discussed in the literature often have limitations, such as reliance on stoichiometric amounts of reagents, expensive metal triflates, poor atom economy, and long reaction times. Moreover, many existing methodologies suffer from poor atom utilization, leading to increased waste and reduced overall efficiency, which can be challenging to manage, especially when scaling up.



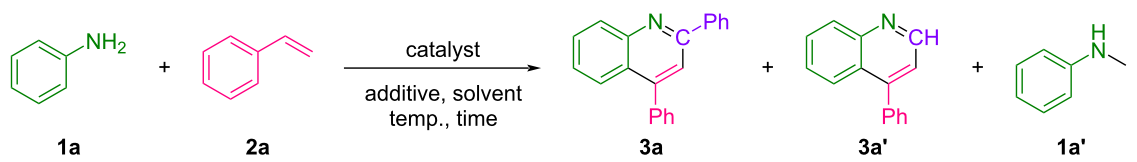
Scheme 1: C(sp^2)–C(sp^2) bond-cleavage strategies for quinoline synthesis.

Building on previous studies, we envisioned a novel reaction system that facilitates the C(sp^2)–C(sp^2) bond cleavage of styrene, leading to the in situ generation of two valuable intermediates that act as dual synthons for the synthesis of 2,4- and 4-substituted quinolines. As part of our ongoing efforts to develop innovative C–C and C–H activation strategies for constructing nitrogen-containing heterocycles [55,56], we herein report the first example of the earth-abundant iron-catalyzed oxidative cleavage of C(sp^2)–C(sp^2) bonds of styrenes and further utilization of the intermediates as dual synthons for the synthesis of two essential quinoline moieties as shown in Scheme 1b.

Results and Discussion

To validate our hypothesis, we commenced our investigation by employing arylamine **1a** and styrene (**2a**) as model substrates. The optimized reaction conditions are presented in Table 1. Building upon our previous studies, where we investigated how solvent selection can influence the selective formation of quinoline scaffolds, the present C–H annulation reaction of aniline (**1a**) with styrene (**2a**) was initially carried out in TFE (trifluoroethanol) as solvent in the presence of 25 mol % $FeCl_3·6H_2O$ as a catalyst and 1.5 equiv of TFA (trifluoroacetic acid) as an additive (Table 1, entry 1). For this reaction, 12% of 2,4-disubstituted quinolone **3a** along with 36% of 4-substituted quinolone **3a′** were observed during GC and GC–MS analysis, and the structures of both quinoline moieties were identified by ^{1}H and ^{13}C NMR spectroscopy. Encouraged by this result, we next examined the feasibility of the reaction with methanol as solvent (Table 1, entry 2). We were delighted to observe that, in methanol, the reaction proceeded smoothly, affording 41% and 51% isolated yields of **3a** and **3a′**, respectively. We further explored the effect of other catalysts on the reaction. As listed in Table 1, entries 3–6, among the Lewis acids surveyed, $FeCl_3·6H_2O$ provided the best results (Table 1, entry 2). A further reduction in

Table 1: Optimization of reaction conditions.[a]



1a **2a** **3a** **3a'** **1a'**

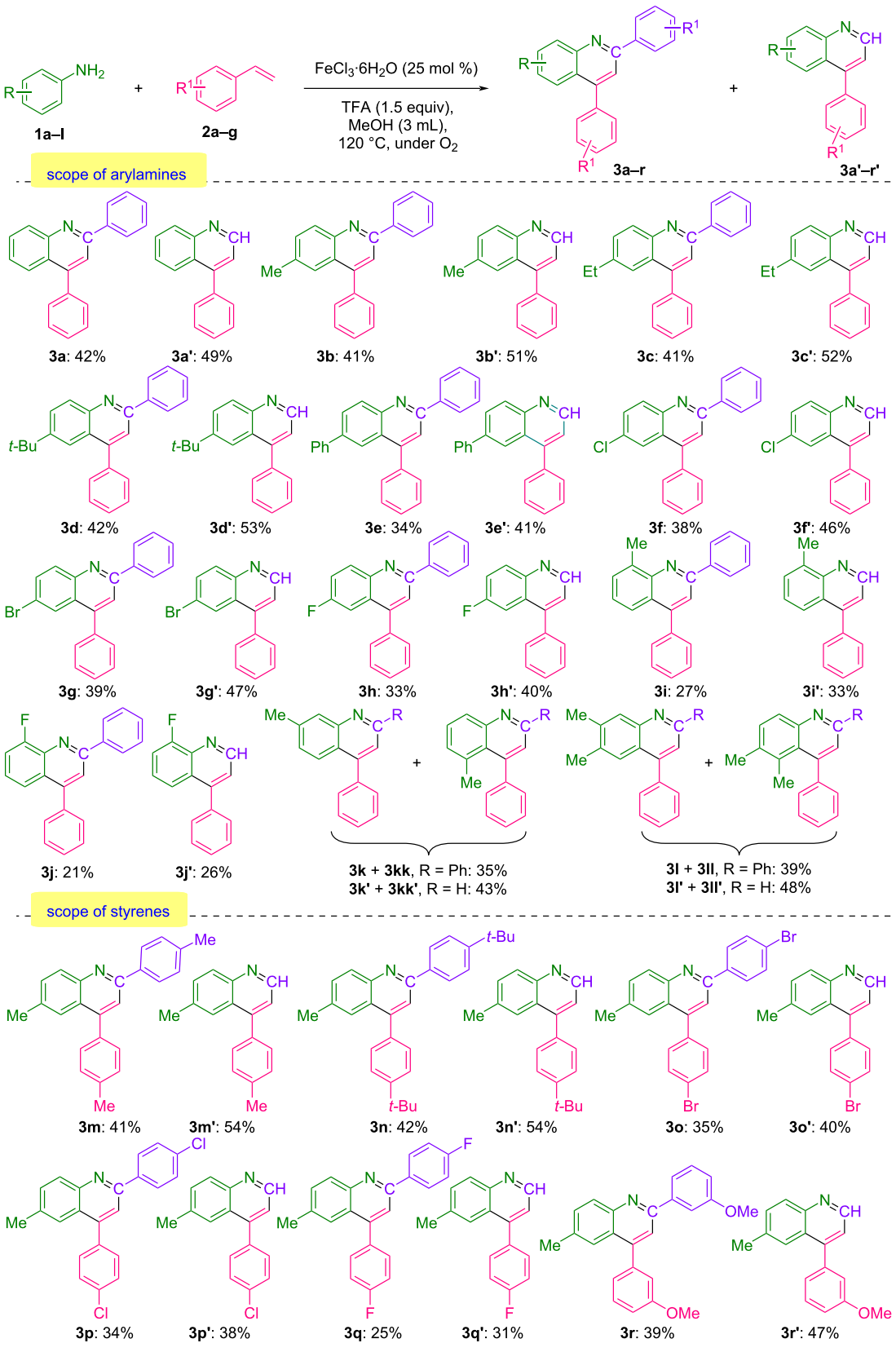
Entry	Catalyst	Additive	Solvent	Conv. (%)[b]	Selectivity (%)[b]			
					3a	**3a′**	**1a′**	**1a′′**
1	$FeCl_3·6H_2O$	TFA	TFE	94	12	36	–	–
2	$FeCl_3·6H_2O$	TFA	MeOH	100	44 (41)[c]	56 (51)[c]	–	–
3	$FeCl_3$	TFA	MeOH	96	46	48	–	6
4	$FeBr_3$	TFA	MeOH	89	37	42	6	15
5	$FeCl_2·4H_2O$	TFA	MeOH	94	50	47	3	–
6	$Fe(OAc)_2$	TFA	MeOH	82	34	45	4	17
7[d]	$FeCl_3·6H_2O$	TFA	MeOH	99	41	55	4	–
8[e]	$FeCl_3·6H_2O$	TFA	MeOH	78	45	50	5	–
9	–	TFA	MeOH	10	–	–	–	100
10	$FeCl_3·6H_2O$	AcOH	MeOH	92	37	58	5	–
11	$FeCl_3·6H_2O$	TsOH	MeOH	91	35	59	1	5
12[f]	$FeCl_3·6H_2O$	TFA	MeOH	96	40	56	4	–
13	$FeCl_3·6H_2O$	–	MeOH	56	40	47	8	5
14[g]	$FeCl_3·6H_2O$	TFA	MeOH	84	40	58	2	–
15[h]	$FeCl_3·6H_2O$	TFA	MeOH	75	32	36	10	22

[a]Reaction conditions: **1a** (0.5 mmol, 1 equiv), **2a** (2.2 equiv), catalyst (25 mol %), TFA (1.5 equiv), in solvent (2 mL), and allowed to stir under an O_2 (≈1 atm). at 120 °C for 24 h; [b]conversion and selectivity were determined through GC and GC–MS analysis; [c]isolated yields after column chromatography; [d]20 mol % $FeCl_3·6H_2O$; [e]10 mol % $FeCl_3·6H_2O$; [f]1 equiv TFA; [g]100 °C; [h]1 equiv $K_2S_2O_8$ as oxidant instead of O_2, (**1a′′**: other side products of **1a**).

catalyst loading from 25 mol % to 20 mol % and 10 mol % resulted in a noticeable decrease in both selectivity and conversion efficiency (Table 1, entries 7 and 8). This is likely due to insufficient C(sp^2)–C(sp^2) bond cleavage as well as inadequate Lewis acid activation of *N*-methylaniline (**1a′**), which hinders its further cyclization into the final product **3a′**.

The reaction, when conducted in the absence of a catalyst, failed to proceed, thereby highlighting the crucial role of catalytic activation in facilitating the transformation under the given reaction conditions (Table 1, entry 9). The effect of additives on this transformation was then investigated, and it was found that utilizing AcOH and TsOH additives instead of TFA failed to reach optimal yields (Table 1, entries 10 and 11). A noticeable decrease in yield was observed when the amount of trifluoroacetic acid (TFA) was reduced from 1.5 equiv to 1.0 equiv (Table 1, entry 12). Consequently, in the absence of the additive, the yield was significantly diminished due to the incomplete consumption of **1a** (Table 1, entry 13). Lowering the temperature to 100 °C considerably reduced both the conversion and selectivity (Table 1, entry 14). Furthermore, when $K_2S_2O_8$ was used as the oxidizing agent instead of O_2, a considerable drop in both conversion and selectivity was observed.

Having identified satisfactory conditions, we sought to examine the scope and generality of this methodology. As summarized in Scheme 2, we initially investigated the scope and effect of arylamine functionalities on this transformation. Under optimized reaction conditions, arylamines bearing either electron-rich or electron-deficient substituents at the *para*-position demonstrated good tolerance, producing both mono- and disubstituted quinolines with high overall yields. Substrates bearing electron-rich groups at *para*-position such as -Me, -Et, and –*t*-Bu (**1b–d**) showed excellent compatibility, producing both 2,4-disubstituted quinolines **3b–d** and 4-substituted quinolines **3b′–d′** with consistently high combined yields, ranging from 92% to 95%. Probably due to steric hindrance, when the phenyl group was attached to the *para*-position of the aniline (**1e**), the corresponding products **3e** along with **3e′** could be obtained in 75% yields. Electron-deficient groups at the *para*-position, such as -Cl, -Br, and -F (**1f–h**), were next evaluated using the optimized conditions, resulting in the isolation of the correspond-



Scheme 2: Substrate scope of various arylamines and styrenes.

ing quinolines **3f**–**h** and their 4-substituted analogs **3f′**–**h′** with satisfactory yields ranging from 73% to 86%. *ortho*-Substituted arylamines **1i** and **1j** showed sensitivity, likely due to steric hindrance, leading to a moderate combined yield. Moreover, when the *meta*-substituted arylamine **1k** was reacted under standard conditions, regioisomeric forms of quinolines were observed during GC and GC–MS analysis. Nearly identical results were obtained when 3,4-dimethylaniline (**1l**) was used.

An additional effort was made to broaden the scope of this transformation by exploring various functionalities on the styrene substrate as well. Styrene with an electron-rich group at *para*-position such as -Me and –*t*-Bu (**2b** and **2c**) also reacted smoothly to afford the corresponding quinolines **3m** and **3n** along with **3m′** and **3n′** in high yields. Slightly lower yields were observed when styrenes bearing electron-withdrawing substituents (**2d** and **2f**) were examined, giving the final products ranging from 56% to 75% isolated yields. Nevertheless, *meta*-substituted styrene (**2g**) was also evaluated in this reaction, resulting in the formation of both **3r** and **3r′**, which were obtained in 86% combined yield.

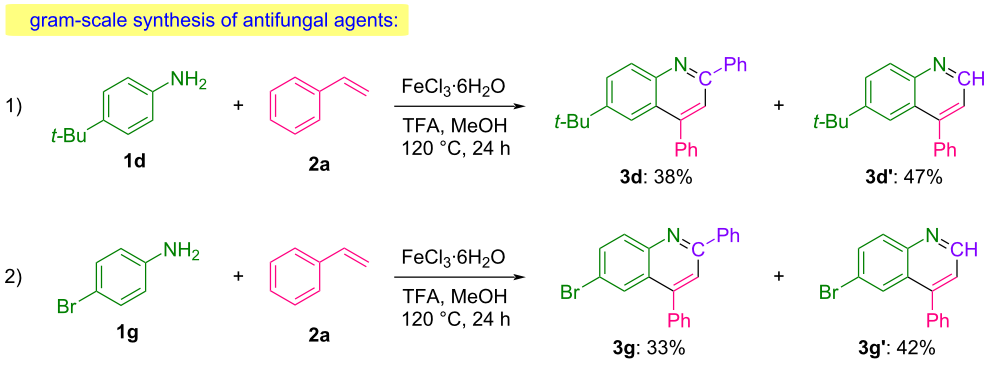
Gram-scale studies were conducted to further demonstrate the synthetic potential and practical utility of the developed methodology.

The biologically significant compounds 6-(*tert*-butyl)-2,4-diphenylquinoline (**3d**) and 6-bromo-2,4-diphenylquinoline (**3g**), both recognized for their antifungal activity [10], were successfully synthesized on a gram scale, showcasing the scalability and efficiency of the process (Scheme 3).

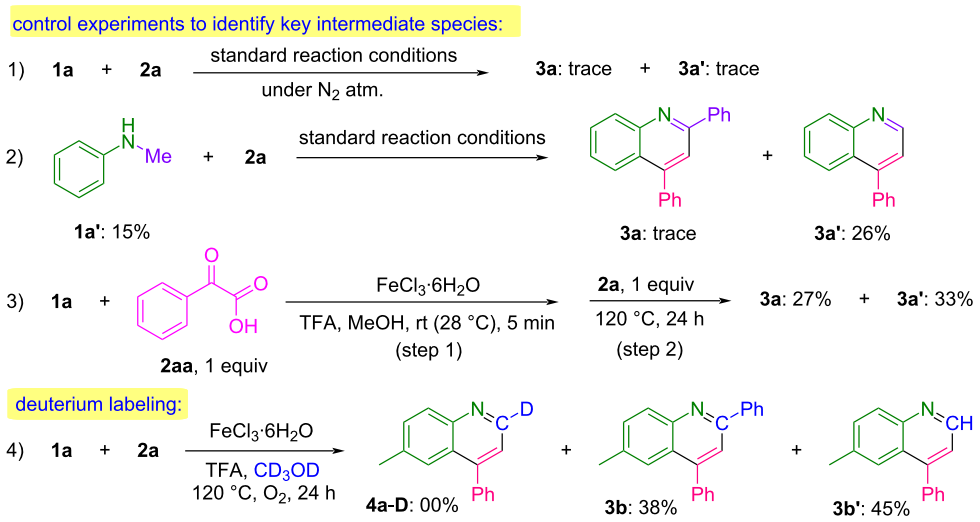
After having demonstrated the broad substrate compatibility and the synthetic potential of this protocol, a set of control experiments was conducted to gain insight into the reaction mechanism, as depicted in Scheme 4.

To clarify the significance of oxidative conditions, the standard reaction was initially conducted under an inert atmosphere by replacing oxygen with nitrogen (reaction 1). Under these conditions, the reaction led to a complete suppression in the yield of **3a** and **3a′**. The above results reveal that O_2 plays a remarkable role in this transformation. Subsequently, the reaction was performed using *N*-methylaniline (**1a′**) under the optimized conditions (reaction 2), which afforded product **3a′** in 26% yield. Then, in reaction 3, a one-pot, two-step reaction involving phenylglyoxalic acid (**2aa**) was carried out. In step 1, compounds **1a** and **2aa** were stirred at room temperature for 5 minutes in the presence of a catalyst and an additive. Subsequently, in step 2, styrene (**2a**) was added, and the reaction mixture was stirred at 120 °C for 24 hours, resulting in the formation of 27% of **3a** along with 33% of **3a′**. To further investigate the role of the solvent in the reaction mechanism, a deuterium-labeling experiment was performed by reacting **1a** with **2a** in deuterated methanol (CD_3OD) under standard conditions. In this reaction, **4a-D** was not detected, indicating that methanol is not utilized as a C1 source.

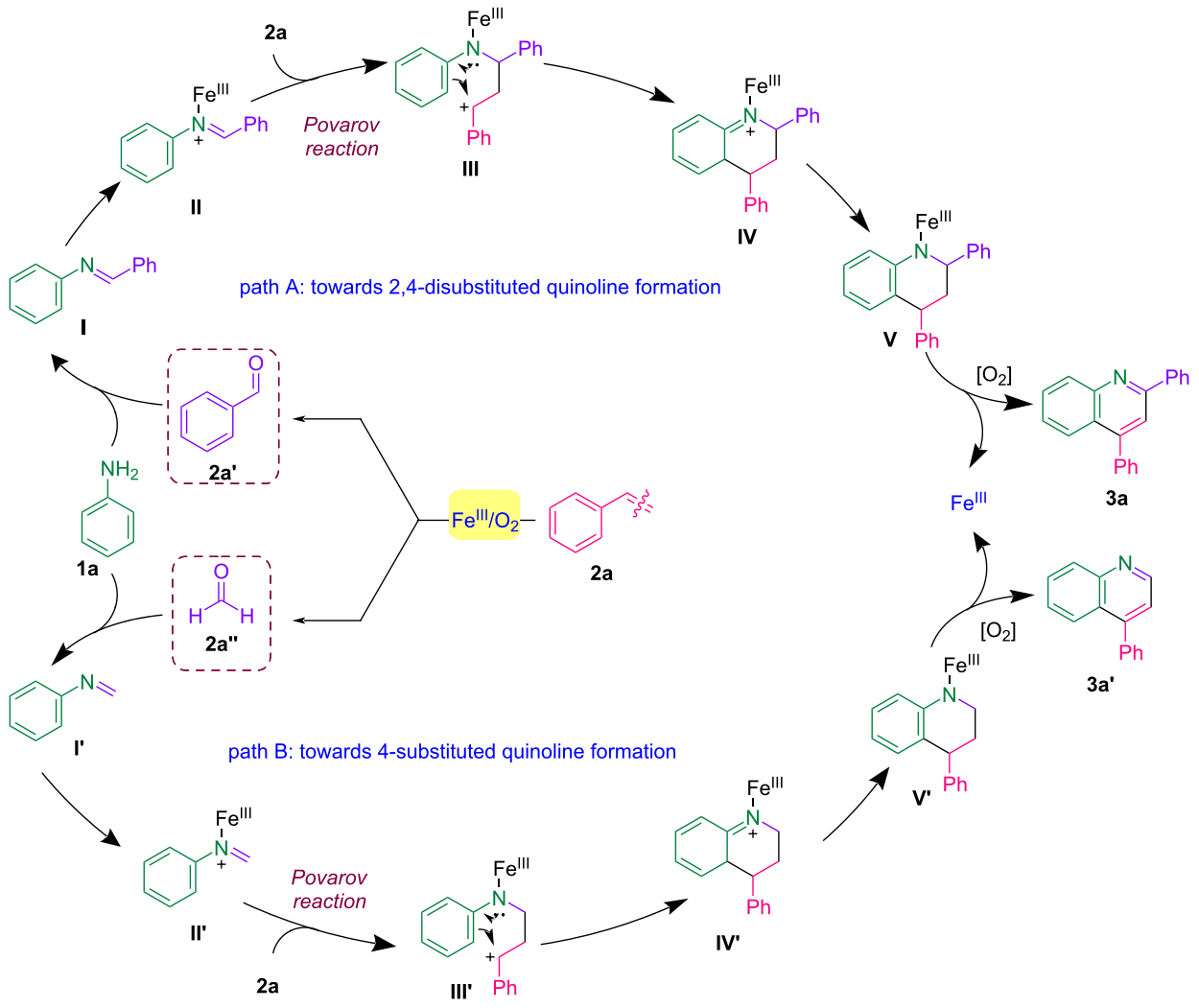
Considering this experimental evidence and existing literature [54,57], a plausible mechanism is depicted in Scheme 5. The reaction likely proceeds through forming benzaldehyde (**2a′**) (detected during GC–MS analysis) and formaldehyde (**2a″**) via C–C bond scission of styrene in the presence of Fe^{III}/O_2, possibly through a 1,2-addition of O_2 to styrene [49,58-60]. This in-situ generated aldehyde species then undergoes condensation with the amine **1a**, leading to the formation of the corresponding imines **I** and **I′**, as supported by the detection of imine **I** during GC–MS analysis. Both imines coordinate with the Lewis acid Fe^{III} forming intermediates **II** and **II′** with enhanced electrophilicity, respectively. Another equivalent of styrene (**2a**) attacks the electrophilic carbon, leading to the formation of intermediates **III** and **III′**. Subsequent electrophilic cyclization/C–H annulation of the aromatic amine, followed by



Scheme 3: Scale-up studies for the synthesis of antifungal agents.



Scheme 4: Mechanistic investigations.



Scheme 5: Plausible reaction mechanism.

aromatization, afford intermediates **V** and **V′**. The oxidative dehydrogenation of intermediates **V** and **V′** then results in the formation of products **3a** and **3a′** and the regeneration of the Fe^{III} species. An alternative mechanism involving a concerted [4 + 2] cycloaddition between the aza-butadiene moiety in **II** and the alkene, leading to intermediate **IV**, cannot be ruled out.

Conclusion

In summary, we have successfully developed a highly efficient method for the oxidative C–C bond cleavage of styrenes, catalyzed by earth-abundant iron, followed by the in-situ utilization of the resulting cleaved synthon in a domino process to synthesize highly substituted quinoline derivatives. We have demonstrated that this process can efficiently convert readily available feedstocks, including a broad range of styrenes and arylamines, into valuable quinolines with good to excellent yields under environmentally benign and mild reaction conditions. The successful execution of a scale-up reaction to synthesize single-step antifungal agents emphasizes the significant synthetic potential of this approach in chemical synthesis and drug discovery.

Supporting Information

Supporting Information File 1

Experimental section, characterization of synthesized compounds, and copies of spectra.
[https://www.beilstein-journals.org/bjoc/content/supplementary/1860-5397-21-142-S1.pdf]

Funding

P.A.J. gratefully acknowledges the Chhatrapati Shahu Maharaj Research Training and Human Development Institute (SARTHI), Pune, India, for the Senior Research Fellowship.

Author Contributions

Prafull A. Jagtap: conceptualization; data curation; formal analysis; investigation; methodology; software; validation; visualization; writing – original draft; writing – review & editing. Manish M. Petkar: data curation; formal analysis; investigation. Vaishnavi R. Sawant: data curation; formal analysis; investigation. Bhalchandra M. Bhanage: project administration; resources; supervision; validation; writing – review & editing.

ORCID® iDs

Prafull A. Jagtap - https://orcid.org/0000-0002-9576-629X
Bhalchandra M. Bhanage - https://orcid.org/0000-0001-9538-3339

Data Availability Statement

All data that supports the findings of this study is available in the published article and/or the supporting information of this article.

References

1. Eswaran, S.; Adhikari, A. V.; Chowdhury, I. H.; Pal, N. K.; Thomas, K. D. *Eur. J. Med. Chem.* **2010,** *45,* 3374–3383. doi:10.1016/j.ejmech.2010.04.022
2. Dorababu, A. *Arch. Pharm. (Weinheim, Ger.)* **2021,** *354,* 2000232. doi:10.1002/ardp.202000232
3. Ferreira, L. M.; García-García, P.; García, P. A.; Castro, M. Á. *Eur. J. Pharm. Sci.* **2025,** *209,* 107097. doi:10.1016/j.ejps.2025.107097
4. Tanwar, B.; Kumar, A.; Yogeeswari, P.; Sriram, D.; Chakraborti, A. K. *Bioorg. Med. Chem. Lett.* **2016,** *26,* 5960–5966. doi:10.1016/j.bmcl.2016.10.082
5. Pissinate, K.; Villela, A. D.; Rodrigues-Junior, V.; Giacobbo, B. C.; Grams, E. S.; Abbadi, B. L.; Trindade, R. V.; Roesler Nery, L.; Bonan, C. D.; Back, D. F.; Campos, M. M.; Basso, L. A.; Santos, D. S.; Machado, P. *ACS Med. Chem. Lett.* **2016,** *7,* 235–239. doi:10.1021/acsmedchemlett.5b00324
6. Kaur, R.; Kumar, K. *Eur. J. Med. Chem.* **2021,** *215,* 113220. doi:10.1016/j.ejmech.2021.113220
7. Utreja, D.; Salotra, R.; Kaur, G.; Sharma, S.; Kaushal, S. *Curr. Org. Chem.* **2023,** *26,* 1895–1913. doi:10.2174/1385272827666221219101902
8. Hollomon, D. W.; Wheeler, I.; Dixon, K.; Longhurst, C.; Skylakakis, G. *Pestic. Sci.* **1997,** *51,* 347–351. doi:10.1002/(sici)1096-9063(199711)51:3<347::aid-ps651>3.0.co;2-3
9. Khan, S. U.; Nawaz, T.; Alam, O.; Khan, D.; Fahad, S.; Saud, S.; Lu, K. *Appl. Biochem. Biotechnol.* **2025,** *197,* 2097–2119. doi:10.1007/s12010-024-05164-2
10. Liberto, N. A.; Simões, J. B.; de Paiva Silva, S.; da Silva, C. J.; Modolo, L. V.; de Fátima, Â.; Silva, L. M.; Derita, M.; Zacchino, S.; Zuñiga, O. M. P.; Romanelli, G. P.; Fernandes, S. A. *Bioorg. Med. Chem.* **2017,** *25,* 1153–1162. doi:10.1016/j.bmc.2016.12.023
11. Chen, X.; Sun, W.; Huang, S.; Zhang, H.; Lin, G.; Li, H.; Qiao, J.; Li, L.; Yang, S. *J. Med. Chem.* **2020,** *63,* 10474–10495. doi:10.1021/acs.jmedchem.0c01183
12. Kumaraswamy, B.; Hemalatha, K.; Pal, R.; Matada, G. S. P.; Hosamani, K. R.; Aayishamma, I.; Aishwarya, N. V. S. S. *Eur. J. Med. Chem.* **2024,** *275,* 116561. doi:10.1016/j.ejmech.2024.116561
13. da Silva, F. F.; Paz, J. D.; Rambo, R. S.; Gonçalves, G. A.; Muniz, M. N.; de Matos Czeczot, A.; Perelló, M. A.; Berger, A.; González, L. C.; Duarte, L. S.; da Silva, A. B.; Ferreira, C. A. S.; de Oliveira, S. D.; Moura, S.; Bizarro, C. V.; Basso, L. A.; Machado, P. *J. Med. Chem.* **2024,** *67,* 21781–21794. doi:10.1021/acs.jmedchem.4c01302
14. Kumar, V.; Gohain, M.; Van Tonder, J. H.; Ponra, S.; Bezuindenhoudt, B. C. B.; Ntwaeaborwa, O. M.; Swart, H. C. *Opt. Mater. (Amsterdam, Neth.)* **2015,** *50,* 275–281. doi:10.1016/j.optmat.2015.11.009
15. Dai, W.; Niu, X.; Wu, X.; Ren, Y.; Zhang, Y.; Li, G.; Su, H.; Lei, Y.; Xiao, J.; Shi, J.; Tong, B.; Cai, Z.; Dong, Y. *Angew. Chem., Int. Ed.* **2022,** *61,* e202200236. doi:10.1002/anie.202200236
16. Chen, J.; Liu, H.; Yang, L.; Jiang, J.; Bi, G.; Zhang, G.; Li, G.; Chen, X. *ACS Med. Chem. Lett.* **2019,** *10,* 954–959. doi:10.1021/acsmedchemlett.9b00118

17. Liu, T.; Chen, Y.-N.; Tan, D.-X.; Han, F.-S. *J. Organomet. Chem.* **2022,** *977,* 122453. doi:10.1016/j.jorganchem.2022.122453
18. Kumar, R.; Thakur, A.; Sachin; Chandra, D.; Kumar Dhiman, A.; Kumar Verma, P.; Sharma, U. *Coord. Chem. Rev.* **2024,** *499,* 215453. doi:10.1016/j.ccr.2023.215453
19. Conrad, M.; Limpach, L. *Ber. Dtsch. Chem. Ges.* **1887,** *20,* 944–948. doi:10.1002/cber.188702001215
20. Friedlaender, P. *Ber. Dtsch. Chem. Ges.* **1882,** *15,* 2572–2575. doi:10.1002/cber.188201502219
21. Doebner, O.; v. Miller, W. *Ber. Dtsch. Chem. Ges.* **1881,** *14,* 2812–2817. doi:10.1002/cber.188101402258
22. Buu-Hoi, N. P.; Royer, R.; Xuong, N. D.; Jacquignon, P. *J. Org. Chem.* **1953,** *18,* 1209–1224. doi:10.1021/jo50015a019
23. Manske, R. H. F.; Kulka, M. *Org. React.* **1953,** *7,* 59–98. doi:10.1002/0471264180.or007.02
24. Povarov, L. S.; Grigos, V. I.; Mikhailov, B. M. *Bull. Acad. Sci. USSR, Div. Chem. Sci. (Engl. Transl.)* **1963,** *12,* 1878–1880. doi:10.1007/bf00843814
25. Born, J. L. *J. Org. Chem.* **1972,** *37,* 3952–3953. doi:10.1021/jo00797a045
26. Mandal, A.; Khan, A. T. *Org. Biomol. Chem.* **2024,** *22,* 2339–2358. doi:10.1039/d4ob00034j
27. Wang, Y.; Chen, C.; Peng, J.; Li, M. *Angew. Chem., Int. Ed.* **2013,** *52,* 5323–5327. doi:10.1002/anie.201300586
28. Naidoo, S.; Jeena, V. *Synthesis* **2017,** *49,* 2621–2631. doi:10.1055/s-0036-1588176
29. Liu, B.; Gao, H.; Yu, Y.; Wu, W.; Jiang, H. *J. Org. Chem.* **2013,** *78,* 10319–10328. doi:10.1021/jo401707j
30. Chen, P.; Nan, J.; Hu, Y.; Ma, Q.; Ma, Y. *Org. Lett.* **2019,** *21,* 4812–4815. doi:10.1021/acs.orglett.9b01702
31. Li, J.; Zhang, J.; Yang, H.; Jiang, G. *J. Org. Chem.* **2017,** *82,* 3284–3290. doi:10.1021/acs.joc.6b03064
32. Oh, K. H.; Kim, J. G.; Park, J. K. *Org. Lett.* **2017,** *19,* 3994–3997. doi:10.1021/acs.orglett.7b01701
33. Zhao, X.; Wang, G.; Hashmi, A. S. K. *Chem. Commun.* **2024,** *60,* 6999–7016. doi:10.1039/d4cc01915f
34. Li, M.; Zheng, J.; Hu, W.; Li, C.; Li, J.; Fang, S.; Jiang, H.; Wu, W. *Org. Lett.* **2018,** *20,* 7245–7248. doi:10.1021/acs.orglett.8b03165
35. Sakai, N.; Tamura, K.; Shimamura, K.; Ikeda, R.; Konakahara, T. *Org. Lett.* **2012,** *14,* 836–839. doi:10.1021/ol203360g
36. Wang, Z.-H.; Shen, L.-W.; Yang, P.; You, Y.; Zhao, J.-Q.; Yuan, W.-C. *J. Org. Chem.* **2022,** *87,* 5804–5816. doi:10.1021/acs.joc.2c00128
37. Zhong, M.; Sun, S.; Cheng, J.; Shao, Y. *J. Org. Chem.* **2016,** *81,* 10825–10831. doi:10.1021/acs.joc.6b01910
38. Jagtap, P. A.; Bhanage, B. M. *Asian J. Org. Chem.* **2025,** *14,* e202500343. doi:10.1002/ajoc.202500343
39. Vaughan, B. A.; Webster-Gardiner, M. S.; Cundari, T. R.; Gunnoe, T. B. *Science* **2015,** *348,* 421–424. doi:10.1126/science.aaa2260
40. Frye, A.; Liu, J.; Neal, L.; Li, F. *ACS Sustainable Chem. Eng.* **2024,** *12,* 14059–14069. doi:10.1021/acssuschemeng.4c05165
41. Liang, Y.-F.; Bilal, M.; Tang, L.-Y.; Wang, T.-Z.; Guan, Y.-Q.; Cheng, Z.; Zhu, M.; Wei, J.; Jiao, N. *Chem. Rev.* **2023,** *123,* 12313–12370. doi:10.1021/acs.chemrev.3c00219
42. Urgoitia, G.; SanMartin, R.; Herrero, M. T.; Domínguez, E. *ACS Catal.* **2017,** *7,* 3050–3060. doi:10.1021/acscatal.6b03654
43. Wan, J.-P.; Gao, Y.; Wei, L. *Chem. – Asian J.* **2016,** *11,* 2092–2102. doi:10.1002/asia.201600671
44. Imada, Y.; Okada, Y.; Noguchi, K.; Chiba, K. *Angew. Chem., Int. Ed.* **2019,** *58,* 125–129. doi:10.1002/anie.201809454
45. Cheng, Z.; Jin, W.; Liu, C. *Org. Chem. Front.* **2019,** *6,* 841–845. doi:10.1039/c8qo01412d
46. Cousin, T.; Chatel, G.; Kardos, N.; Andrioletti, B.; Draye, M. *Catal. Sci. Technol.* **2019,** *9,* 5256–5278. doi:10.1039/c9cy01269a
47. Song, T.; Ma, Z.; Ren, P.; Yuan, Y.; Xiao, J.; Yang, Y. *ACS Catal.* **2020,** *10,* 4617–4629. doi:10.1021/acscatal.9b05197
48. Huang, Z.; Guan, R.; Shanmugam, M.; Bennett, E. L.; Robertson, C. M.; Brookfield, A.; McInnes, E. J. L.; Xiao, J. *J. Am. Chem. Soc.* **2021,** *143,* 10005–10013. doi:10.1021/jacs.1c05757
49. Ou, J.; He, S.; Wang, W.; Tan, H.; Liu, K. *Org. Chem. Front.* **2021,** *8,* 3102–3109. doi:10.1039/d1qo00175b
50. Ruffoni, A.; Hampton, C.; Simonetti, M.; Leonori, D. *Nature* **2022,** *610,* 81–86. doi:10.1038/s41586-022-05211-0
51. Wise, D. E.; Gogarnoiu, E. S.; Duke, A. D.; Paolillo, J. M.; Vacala, T. L.; Hussain, W. A.; Parasram, M. *J. Am. Chem. Soc.* **2022,** *144,* 15437–15442. doi:10.1021/jacs.2c05648
52. Deshidi, R.; Devari, S.; Shah, B. A. *Org. Chem. Front.* **2015,** *2,* 515–519. doi:10.1039/c5qo00010f
53. Cen, J.; Li, J.; Zhang, Y.; Zhu, Z.; Yang, S.; Jiang, H. *Org. Lett.* **2018,** *20,* 4434–4438. doi:10.1021/acs.orglett.8b01718
54. Purkait, A.; Saha, S.; Ghosh, S.; Jana, C. K. *Chem. Commun.* **2020,** *56,* 15032–15035. doi:10.1039/d0cc02650f
55. Jagtap, P. A.; Sawant, V. R.; Bhanage, B. M. *ChemCatChem* **2024,** *16,* e202400979. doi:10.1002/cctc.202400979
56. Jagtap, P. A.; Lokolkar, M. S.; Bhanage, B. M. *J. Org. Chem.* **2023,** *88,* 10960–10973. doi:10.1021/acs.joc.3c00954
57. Gandeepan, P.; Rajamalli, P.; Cheng, C.-H. *Asian J. Org. Chem.* **2014,** *3,* 303–308. doi:10.1002/ajoc.201300262
58. Gonzalez-de-Castro, A.; Xiao, J. *J. Am. Chem. Soc.* **2015,** *137,* 8206–8218. doi:10.1021/jacs.5b03956
59. Barton, D. H. R.; Wang, T.-L. *Tetrahedron Lett.* **1994,** *35,* 1519–1522. doi:10.1016/s0040-4039(00)76747-5
60. Liang, Y.-F.; Jiao, N. *Acc. Chem. Res.* **2017,** *50,* 1640–1653. doi:10.1021/acs.accounts.7b00108

License and Terms

This is an open access article licensed under the terms of the Beilstein-Institut Open Access License Agreement (https://www.beilstein-journals.org/bjoc/terms), which is identical to the Creative Commons Attribution 4.0 International License (https://creativecommons.org/licenses/by/4.0). The reuse of material under this license requires that the author(s), source and license are credited. Third-party material in this article could be subject to other licenses (typically indicated in the credit line), and in this case, users are required to obtain permission from the license holder to reuse the material.

The definitive version of this article is the electronic one which can be found at:
https://doi.org/10.3762/bjoc.21.142

BEILSTEIN JOURNAL OF ORGANIC CHEMISTRY

Stereoselective electrochemical intramolecular imino-pinacol reaction: a straightforward entry to enantiopure piperazines

Margherita Gazzotti, Fabrizio Medici*, Valerio Chiroli, Laura Raimondi, Sergio Rossi and Maurizio Benaglia*

Full Research Paper

Open Access

Address:
Dipartimento di Chimica, Università degli Studi di Milano, via Golgi 19, IT-20133 Milano, Italy

Email:
Fabrizio Medici* - fabrizio.medici@unimi.it; Maurizio Benaglia* - maurizio.benaglia@unimi.it

* Corresponding author

Keywords:
chiral piperazines; electrosynthesis; flow chemistry; green chemistry; imino-pinacol coupling

Beilstein J. Org. Chem. **2025,** *21,* 1897–1908.
https://doi.org/10.3762/bjoc.21.147

Received: 24 May 2025
Accepted: 04 September 2025
Published: 12 September 2025

This article is part of the thematic issue "Green chemistry III: Technologies shaping future directions in synthesis".

Associate Editor: L. Vaccaro

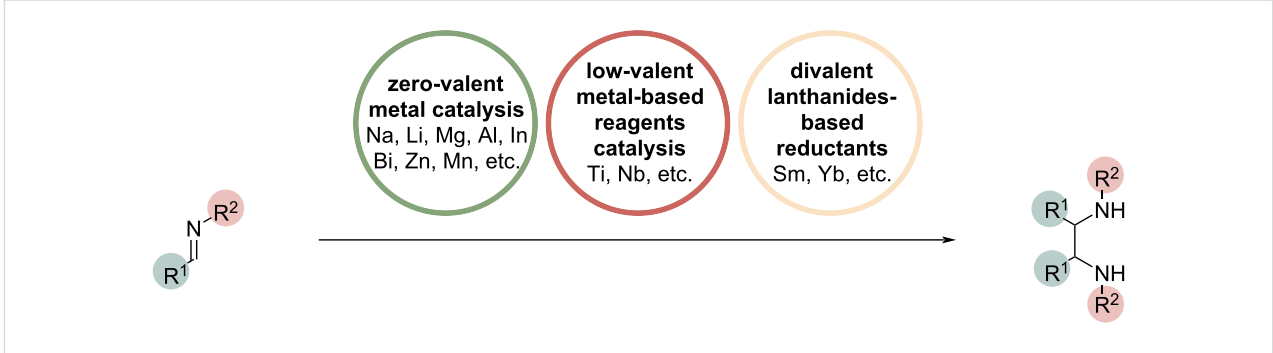
© 2025 Gazzotti et al.; licensee Beilstein-Institut.
License and terms: see end of document.

Abstract

The stereoselective electroreductive intramolecular coupling of chiral diimines of aromatic aldehydes with *trans*-1,2-diaminocyclohexane for the synthesis of enantiopure tetrasubstituted piperazines has been investigated by an electrochemical approach. The methodology was successfully developed under both batch and continuous flow conditions, and afforded enantiomerically pure products with complete stereoselectivity. Substrates bearing electron-donating or electron-withdrawing groups on the aromatic rings provided good to excellent yields, indicating that both types of substituents are well tolerated under the reaction conditions. Although modest yields were obtained under flow conditions, the continuous process afforded higher productivities and space-time yields than the batch reactions due to a short residence time. This work provides a mild, efficient, and scalable alternative to traditional methods for the synthesis of tetrasubstituted enantiopure piperazines, with potential applications in the preparation of chiral ligands.

Introduction

Vicinal diamines represent a highly valuable class of compounds that, over the past decades, have found widespread application in natural products, agrochemicals, and pharmacologically active compounds. Enantiomerically pure 1,2-diamines and their derivatives are also increasingly used in stereoselective synthesis, particularly as chiral auxiliaries or as ligands for metal complexes in asymmetric catalysis [1]. Metal-based reductants represent the most established approach to imino-pinacol coupling (Scheme 1), with zero-valent metals traditionally employed as reductants and various strategies extensively explored [2]. The use of alkali metals [3-5], as lithium and sodium, and alkaline earth metals [6], as magnesium, are characteristic of the earliest versions of this transformation. Several metals from the p- and the d-blocks of the periodic table, such



Scheme 1: Synthesis of vicinal diamines via imino-pinacol coupling in the presence of metal-based reductants.

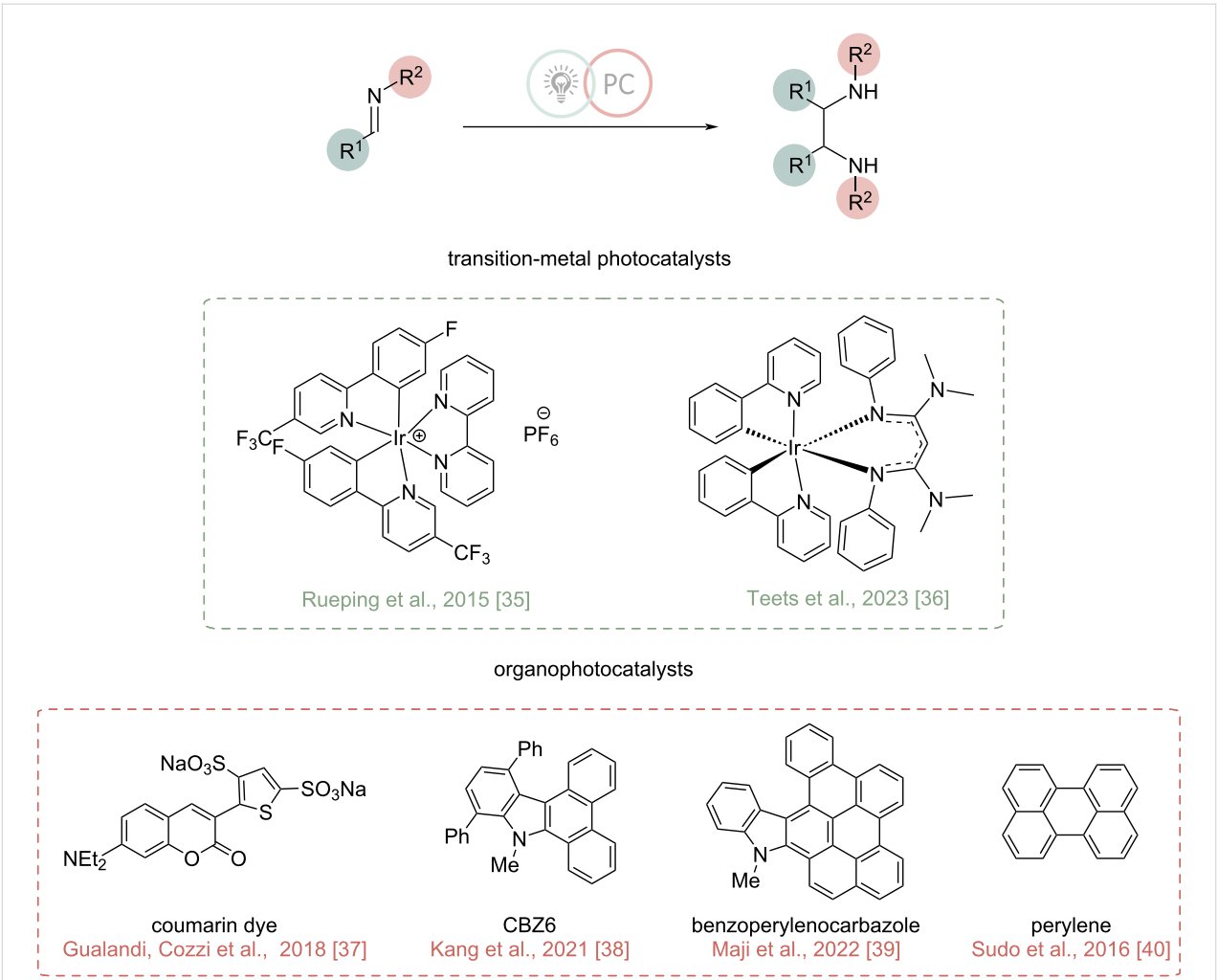
as aluminum [7], indium [8], bismuth [7], zinc [9-17], and manganese [18,19], were later studied. The use of zinc, in particular, has attracted significant attention in this context due to its flexibility, efficiency, and practical applicability. Since the late 1980s, many research groups have investigated the use of in situ-generated low-valent titanium [20-25] and niobium [26] reagents to promote the pinacol-type coupling of imines. Among the metal-based reducing agents explored for this transformation, divalent lanthanide-based reductants derived from samarium and ytterbium have received significant attention since the early 90's [27-34].

Although traditional well-established procedures for the imino-pinacol coupling reaction are efficient, they often require more than stoichiometric amounts of metal reductants and produce significant quantities of metal waste, which in some cases can present considerable environmental and safety concerns. To mitigate this issue, more sustainable approaches, such as photochemical and electrochemical methods, have been explored. Over the past two decades a variety of light-promoted imino-pinacol coupling reactions have been developed, involving the use of catalytic transition-metal complexes [35,36], organic dyes [37-39], and polyaromatic compounds [40,41] as photocatalysts (Scheme 2). The combination of photoredox catalysis with imine activation enabled the reductive coupling of imines under mild reaction conditions, providing direct access to benzyl and aryl vicinal diamines with good to excellent yields.

Organic electrochemistry represents an attractive and sustainable alternative; however, unfortunately, the electrochemical application is limited to only a few examples (Scheme 3). The electroreductive coupling of imines was first reported in the early 20th century by Law [42]. However, this initial method led to the formation of vicinal diamines with low to moderate yields and required geometrically complex divided cells. In 1989, a more efficient procedure was introduced by Torii et al. [43], who simplified the process by using $PbBr_2$, TFA and THF, in a beaker-type undivided cell equipped with two platinum electrodes. This approach afforded vicinal diamines for different *N*-benzyl benzaldimines in moderate to good yields. In 1991, Shono's research group described the electroreductive intramolecular coupling of aromatic diimines, carried out in DMF in the presence of methanesulfonic acid in a divided cell equipped with a lead cathode, a carbon rod anode, and a ceramic diaphragm [44]. This method was found to be effective for synthesizing *trans*-2,3-diarylpiperazines through the intramolecular reductive coupling of 1,2-diimines and seven- and eight-membered heterocycles which were obtained in moderate to good yields via the cyclization of 1,3- and 1,4-diimines.

Later, in 2001, Yudin and co-workers described the parallel reductive coupling of aldimines using a spatially addressable electrosynthesis platform, which employed a stainless steel cathode, a sacrificial aluminum anode and a procedure adapted from Torii's earlier work including the use of $PbBr_2$, TFA, and Bu_4NBr [45]. Under these conditions, parallel electrosynthesis allowed the synthesis of up to 16 vicinal diamines in good yields in 30 minutes. To the best of our knowledge, the most recent example of electroreductive coupling of imines was reported in 2025 by Wang's research group [46], who described a new electrochemical procedure to provide vicinal diamines involving the use of Sn electrodes as both anode and cathode in a divided cell, $Mn(OAc)_3{\cdot}2H_2O$ as additive and *n*-Bu_4NOAc as electrolyte. Under these conditions, using aldehydes and amines as starting materials to form the imines in situ resulted in a wide range of diamines, obtained in moderate to good yields.

Inspired by these works, we aimed to investigate and optimize the stereoselective electrochemical intramolecular imino-pinacol coupling reaction under both batch and continuous flow conditions as a direct approach to enantiopure scaffolds that are commonly used as chiral ligands. In this context we report the development of a more sustainable method – which avoids the use of lead bromide or lead electrodes – employing an undivided cell with two glassy carbon electrodes for the electroreductive intramolecular coupling of aromatic diimines



Scheme 2: Light-promoted imino-pinacol coupling for the synthesis of vicinal diamines.

(Scheme 4). This methodology has been successfully applied to the synthesis of enantiopure tetrasubstituted piperazines, featuring both electron-withdrawing and electron-donating groups on the aromatic rings.

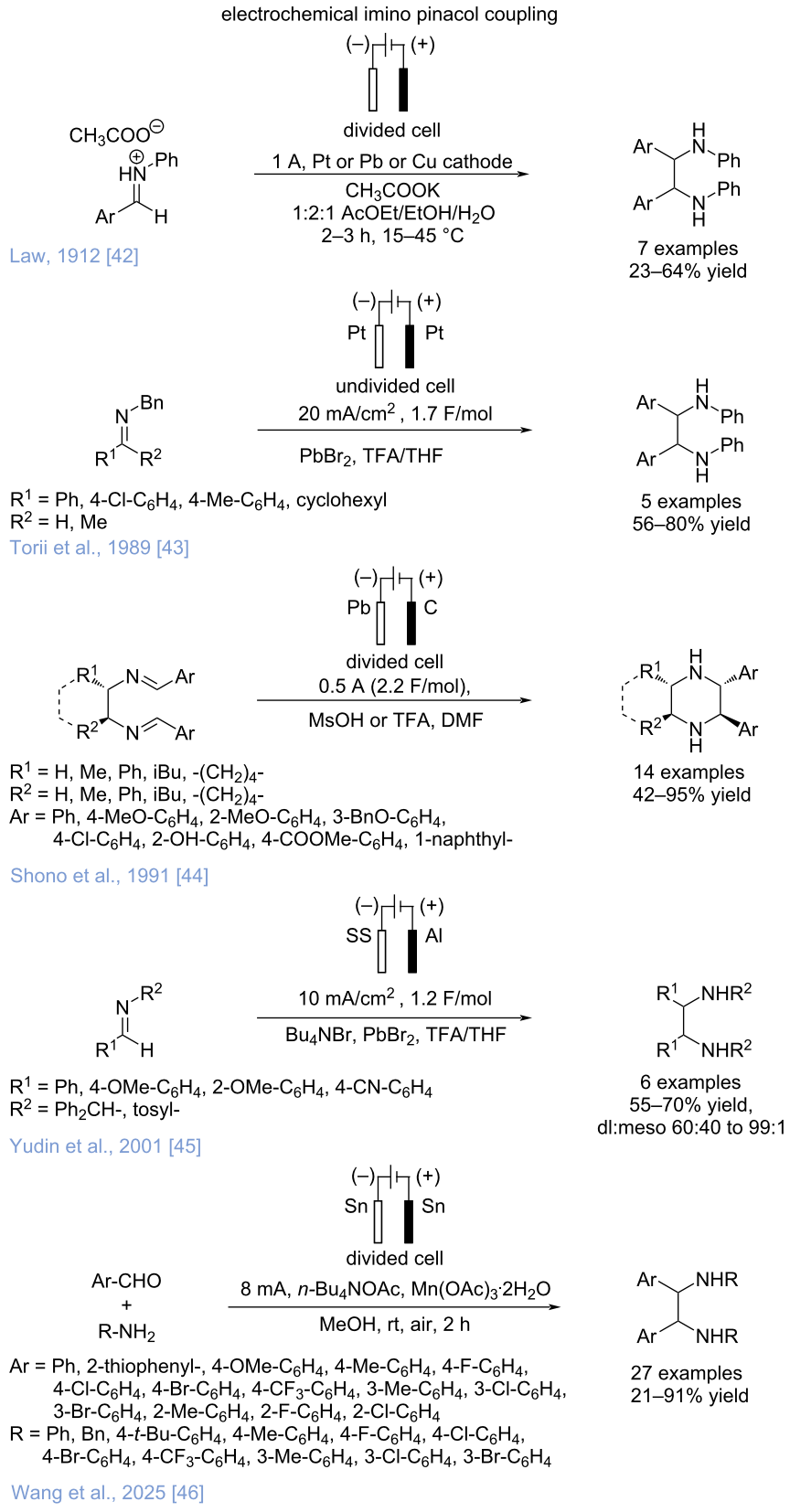
Results and Discussion

The stereoselective electroreductive intramolecular coupling of chiral diimines of aromatic aldehydes with *trans*-1,2-diaminocyclohexane was initially investigated under traditional batch conditions through a series of screening experiments designed to find the optimal reaction conditions.

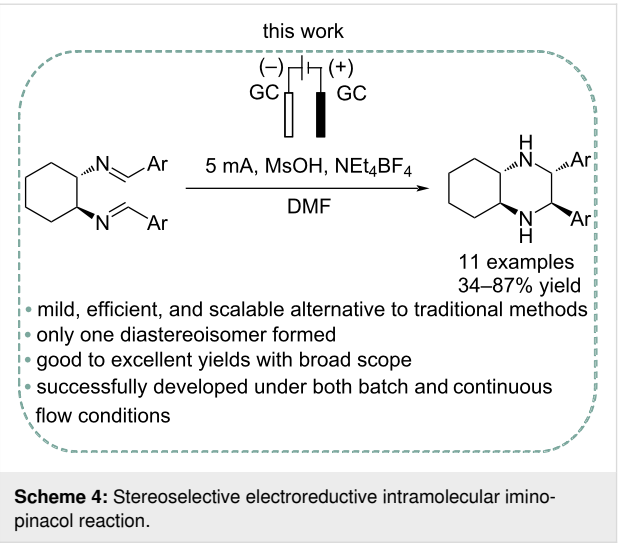
Diimine **1a** was selected as model substrate for the intramolecular coupling reaction and a screening of reaction parameters such as solvents, electrodes materials, electrolytes, total charges, and concentrations of the reaction mixture was performed. All optimization studies were carried out using 0.5 mmol of **1a** in the presence of methanesulfonic acid in an undivided cell (5 mL volume) equipped with two electrodes under galvanostatic conditions (constant current 5 mA, 2.5 mA/cm^2) and the results are summarized in Table 1.

Using platinum electrodes and NEt_4BF_4 as electrolyte, the tetrasubstituted piperazine **2a** was obtained as a single stereoisomer in 51% yield in CH_3CN, which increased to 68% when DMF was used (Table 1, entry 2). The replacement of the platinum anode with graphite or zinc (Table 1, entries 4 and 5) had no significant effect on the yield. Similarly, increasing the total charge from 2.2 to 2.5 F/mol (Table 1, entries 6 and 7) resulted in only marginal changes. Doubling the substrate concentration (Table 1, entry 7) also failed to provide a significant advantage in terms of yield, leading to the formation of the desired product in 64% yield.

The replacement of both working cathode and counter anode to stainless steel electrodes caused a decrement of the yield to 47%



Scheme 3: Historical perspective on electrochemical imino-coupling protocols.



Scheme 4: Stereoselective electroreductive intramolecular imino-pinacol reaction.

(Table 1, entry 8), while with two glassy carbon electrodes desired product **2a** was isolated in 85% yield (Table 1, entry 9).

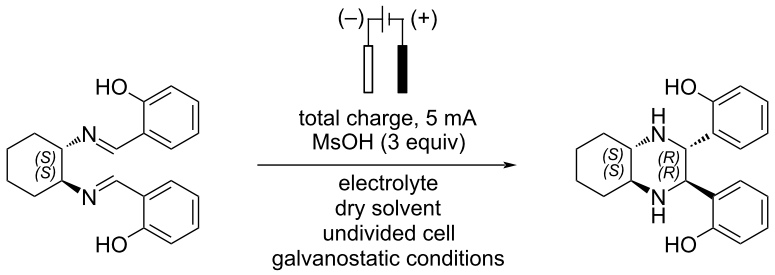
Reducing the electrolyte loading from 2.6 to 1.3 equivalents significantly affected the reaction outcome, leading to a noticeable decrease in the yield suggesting that sufficient ionic conductivity is crucial to achieve efficient conversion (Table 1, entry 10).

Lastly, replacing tetraethylammonium tetrafluoroborate with tetrabutylammonium tetrafluoroborate resulted in a negligible reduction of the chemical efficiency (Table 1, entry 9 vs 11).

As demonstrated by Shono and co-workers [44], the presence of a strong protic acid, such as methanesulfonic acid, MsOH, is essential to promote the intramolecular coupling. A control experiment revealed that when the electroreduction of **1a** was performed in the absence of MsOH (Table 1, entry 3), no formation of the desired product was observed and the starting diimine **1a** was quantitatively recovered.

The optimized reaction conditions, consisting in the use of GC electrodes, NEt_4BF_4 (2.6 equiv) as electrolyte, MsOH (3 equiv) as additive, constant current of 5 mA (2.5 mA/cm^2), total charge of 2.2 F/mol, dry DMF as solvent (0.125 M), were then applied to evaluate the scope of the reaction. Under these conditions a small library of chiral enantiopure tetrasubstituted piper-

Table 1: Screening of the imino-pinacol reaction conditions.



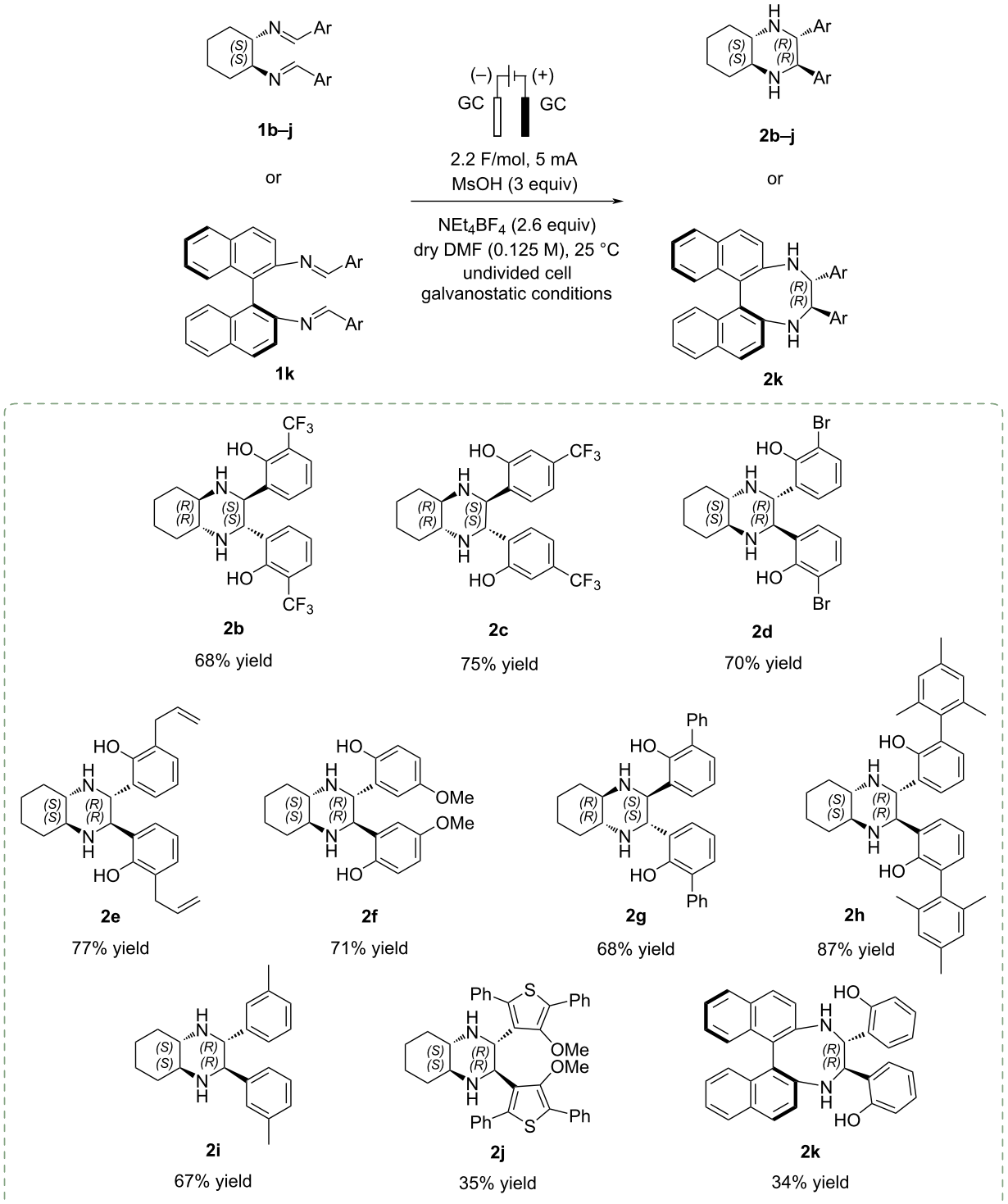
1a **2a**

Entry	Working (cathode)	Counter (anode)	Electrolyte	Electrolyte equivalents	Total charge (F/mol)	Solvent	Substrate concentration (M)	Yield **2a** (%)[a]
1	Pt	Pt	NEt_4BF_4	2.6	2.2	MeCN	0.125	51
2	Pt	Pt	NEt_4BF_4	2.6	2.2	DMF	0.125	68
3[b]	Pt	Pt	NEt_4BF_4	2.6	2.2	DMF	0.125	–
4	Pt	Gr	NEt_4BF_4	2.6	2.2	DMF	0.125	64
5	Pt	Zn	NEt_4BF_4	2.6	2.2	DMF	0.125	64
6	Pt	Zn	NEt_4BF_4	2.6	2.5	DMF	0.125	61
7	Pt	Zn	NEt_4BF_4	2.6	2.5	DMF	0.250	64
8	SS	SS	NEt_4BF_4	2.6	2.2	DMF	0.125	47
9	**GC**	**GC**	**NEt_4BF_4**	**2.6**	**2.2**	**DMF**	**0.125**	**85**
10	GC	GC	NEt_4BF_4	1.3	2.2	DMF	0.125	50
11	GC	GC	NBu_4BF_4	2.6	2.2	DMF	0.125	72

[a]Isolated yields. Reactions were performed on a 0.5 mmol scale. [b]Reaction performed without MsOH.

azines **2b**–**j** bearing both electron-withdrawing and electron-donating substituents, was synthetized. The results are summarized in Scheme 5.

The chiral tetrasubstituted piperazines **2b**–**j** were obtained as a single, enantiopure diastereoisomer from diimines **1b**–**j**, prepared from the enantiopure *trans*-1,2-diaminocyclohexane and



Scheme 5: Scope of the imino-pinacol coupling reaction. Reaction conditions: GC electrodes, NEt_4BF_4 (2.6 equiv), MsOH (3 equiv), constant current 5 mA (2.5 mA/cm^2), total charge 2.2 F/mol, dry DMF (0.125 M). Yields reported are isolated yields. Reactions were performed on a 0.5 mmol scale.

aromatic aldehydes, in good to excellent yields. Substrates bearing electron-withdrawing groups such as trifluoromethyl (**2b**,**c**) and bromine (**2d**), as well as electron-donating groups like methoxy (**2f**), aryl/alkyl (**2h**,**i**), and alkenyl substituents (**2e**), were well tolerated. Notably, the sterically hindered derivative **2h** was isolated with the highest yield of 87% indicating that bulky *ortho*-substituents on the aromatic rings do not influence the electrochemical cyclization process.

In contrast, more complex and extended heterocyclic electron-rich π-systems such as compound **2j** was obtained in 35% yield only, presumably as a result of electronic factors affecting the efficiency of the initial radical formation [47].

To further extend the scope of this methodology, the *trans*-1,2-diaminocyclohexane was replaced with (*S*)-1,1′-binaphthyl-2,2′-diamine. Under the optimized conditions, the corresponding cyclic product **2k** was obtained in 34% yield, consistent with previous observations reporting reduced efficiency as the ring size increases [44].

To confirm the absolute configuration of the piperazine formed, a pure sample of compound **2b** derived from (1*R*,2*R*)-*trans*-diaminocyclohexane was crystallized from a chloroform solution resulting in the formation of white crystals suitable for single crystal X-ray diffraction studies. The absolute configuration of the product was unambiguously determined, by XRD analysis, to be (2*S*,3*S*,4a*R*,8a*R*)-**2b** as shown in Figure 1.

Following the promising results obtained from the batch approach, the electroreductive coupling was investigated under continuous flow conditions [48-50], with the aim to improve process efficiency and in view of a possible scale up of the reaction [51,52]. Flow experiments were performed using the commercially available pre-configured Syrris-Asia electrochemical flow module, a user-friendly solution for continuous flow electrochemical synthesis which is part of the Asia platform [53].

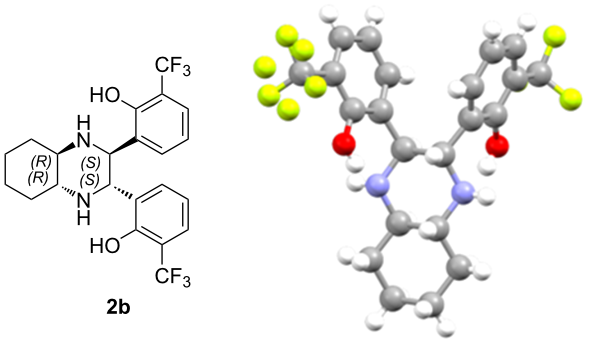
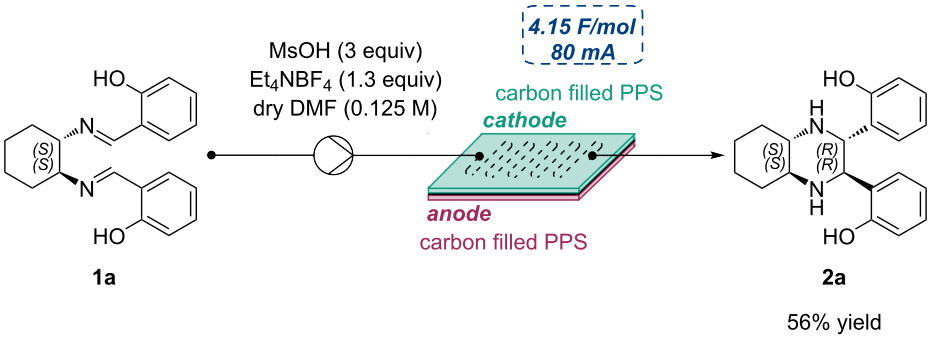


Figure 1: X-ray determined structure of chiral piperazine **2b**.

A comprehensive optimization of the flow reaction conditions was carried out using the model substrate **1a** systematically varying key parameters such as the working electrodes, the current intensity, the total charge, the flow rate, and the equivalents of the employed electrolyte. Following this in-depth screening, optimal conditions were identified: Carbon filled PPS electrodes, a constant current of 80 mA, a total charge of 4.15 F/mol, a flow rate of 96 µL/min, and 1.3 equivalents of NEt_4BF_4 as electrolyte. Under these optimized conditions, the desired tetrasubstituted piperazine **2a** was obtained as single stereoisomer in 56% yield with a residence time of 2.34 minutes (Scheme 6).

Although the yield appears lower compared to the batch process, it is important to highlight that the reaction time has been reduced by nearly a factor of 150, resulting in a substantial increase in terms of productivity, which is 6.2 times higher than the batch protocol. Moreover, the significantly shorter residence time in the flow setup led to an improved space-time yield (STY), a key metric for comparing reactors of different volumes. Under these conditions, the STY of the flow process was 112.2 times higher than that achieved in the batch reactor (Table 2).



Scheme 6: Continuous flow synthesis of piperazine **2a**. The yield was determined by ^{1}H NMR spectroscopy using 1,3,5-trimethoxybenzene as internal standard. Reactions were performed on a 0.1 mmol scale.

Table 2: Comparison of productivity and space-time yield of batch and flow processes for the synthesis of piperazine **2a**.

Entry	Method	Productivity[a] (mmol/h)	Productivity rel. factor	STY[b] (mmol/mL*h)	STY rel. factor
1	batch	0.065	1	0.016	1
2	flow	0.403	6.2	1.795	112.2

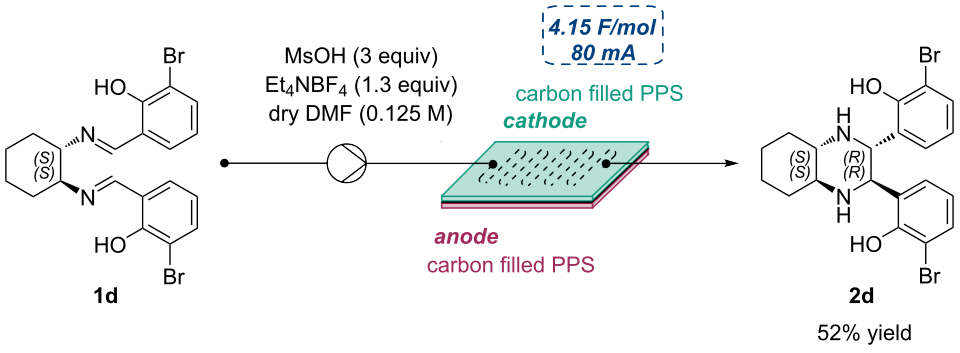
[a]Productivity: moles of product divided by the collection time required to collect the product obtained by the reaction of 0.5 mmol of diimine **1a**.
[b]Space-time yield: moles of product in the reactor, divided by residence time and reactor volume (for details on calculations see Supporting Information File 1).

The scalability of the reaction was further demonstrated by performing the electroreduction of diimine **1d** on a 2.5 mmol scale under flow conditions. Compound **2d** was obtained in 52% isolated yield achieving productivity and STY values that were 10.4 and 184.7 times higher, respectively, compared to those obtained in the batch reaction (Table 3).

To gain a deeper understanding of the mechanism behind the observed reaction, a plausible reaction pathway is proposed, as illustrated in Scheme 7. The process presumably involves the activation of the diimine substrate **1a** by methanesulfonic acid, which acts as a strong Brønsted acid to selectively protonate the imine nitrogen atoms. This protonation step increases the electrophilicity of the adjacent imine carbons by inductive effect, leading to the formation of a highly reactive diiminium intermediate **4a**. When formed, compound **4a** is electrochemically reduced to give the carbon-centered diradical intermediate **5a** and the spatial proximity of these two radical centers allows a rapid intramolecular radical–radical coupling resulting in the formation of the desired piperazine **2a**. The feasibility of this mechanism is supported by literature precedents involving electroreduction of activated imines and diiminium species [19]. Furthermore, control experiments conducted in the absence of methanesulfonic acid (Table 1, entry 3) resulted in no observable product formation, highlighting the acid activation in driving this transformation.

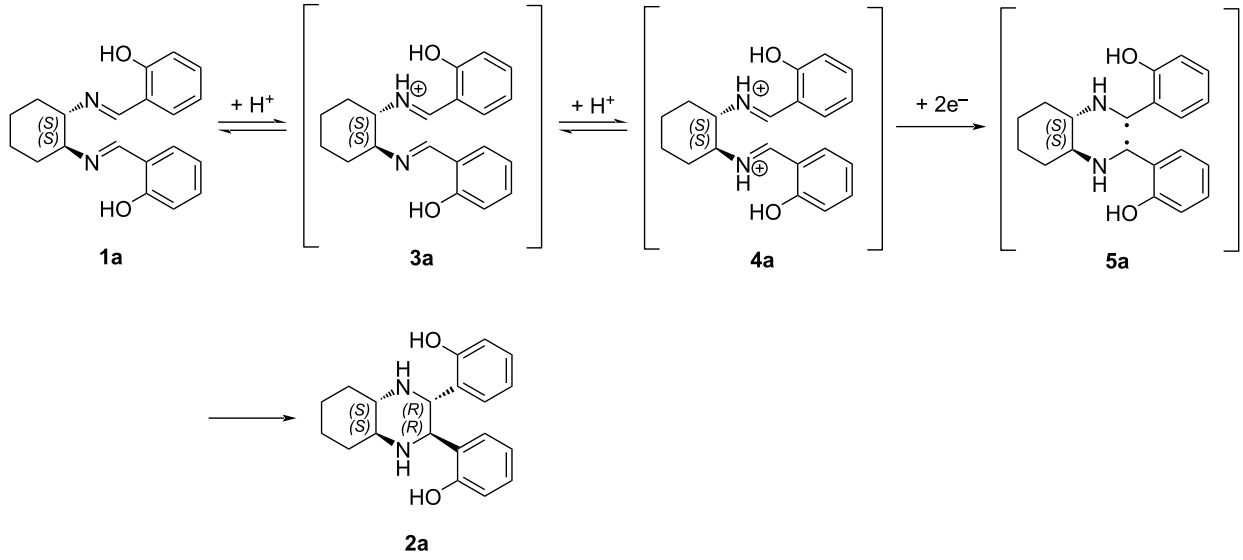
Cyclic voltammetry measurements were also carried out in order to evaluate the electrochemical redox properties of the species involved in the process and to provide evidence for the behavior of the monoprotonated and the bisprotonated diimines, **3a** and **4a** (Scheme 8). The cyclic voltammogram of the starting diimine **1a** shows one distinct reductive peak at −1.75 V. Upon addition of one equivalent of MsOH, monoprotonated species **3a** is formed, and a shift of the reduction peak to −1.92 V was observed. Subsequent addition of a second equivalent of acid leads to the formation of the bisprotonated species **4a**, and as consequence, a shift of the reduction peak to −1.82 V was ob-

Table 3: Comparison of productivity and space-time yield of batch and flow processes for the synthesis of piperazine **2d**.

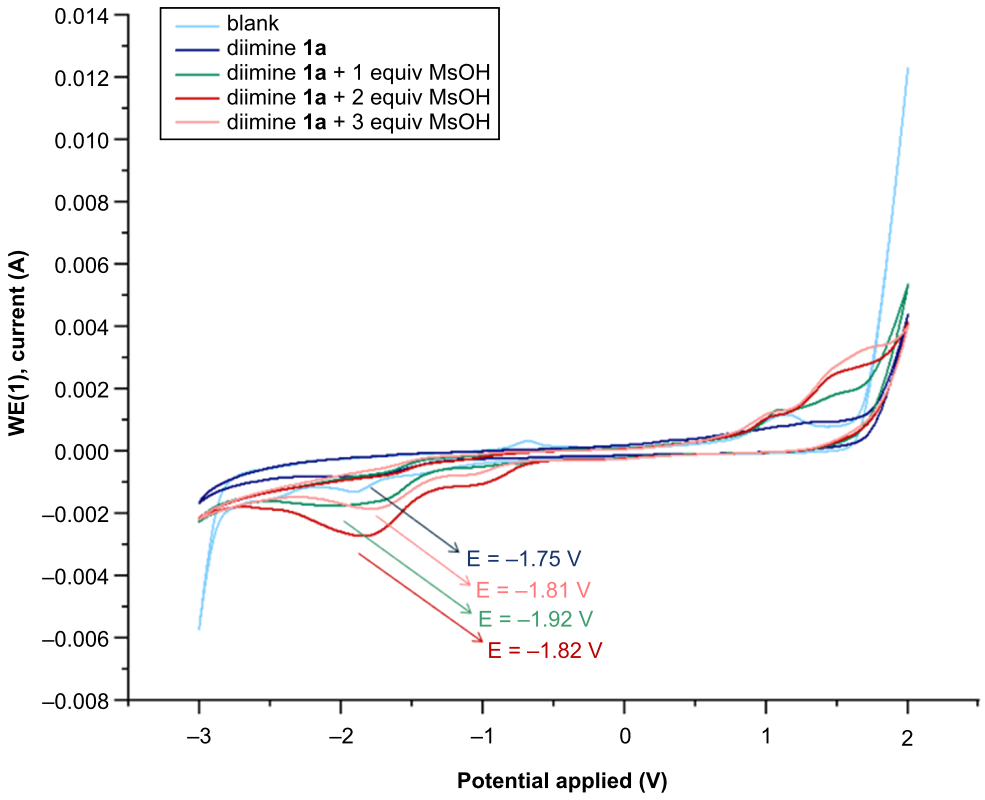


Entry	Method	Productivity[a] (mmol/h)	Productivity rel. factor	STY [b] (mmol/mL*h)	STY rel. factor
1	batch	0.036	1	0.009	1
2	flow	0.374	10.4	1.662	184.7

[a]Productivity: moles of product divided by the collection time required to collect the product obtained by the reaction of 0.5 mmol of diimine **1d**.
[b]Space-time yield: moles of product in the reactor, divided by residence time and reactor volume (for details on calculations please see Supporting Information File 1).



Scheme 7: Proposed reaction mechanism.



Scheme 8: Cyclic voltammetry investigation. Cyclic voltammetry of a 0.325 M solution of Et_4NBF_4 in DMF (light-blue line). Cyclic voltammetry of diimine **1a** (10 mM) recorded in a 0.325 M solution of Et_4NBF_4 in DMF (dark-blue line). Cyclic voltammetry of diimine **1a** (10 mM) in presence of 1 equiv of methanesulfonic acid (10 mM) recorded in a 0.325 M solution of Et_4NBF_4 in DMF (green line). Cyclic voltammetry of diimine **1a** (10 mM) in presence of 2 equiv of methanesulfonic acid (20 mM) recorded in a 0.325 M solution of Et_4NBF_4 in DMF (dark-red line). Cyclic voltammetry of diimine **1a** (10 mM) in presence of 3 equiv of methanesulfonic acid (30 mM) recorded in a 0.325 M solution of Et_4NBF_4 in DMF (light-red line). Glassy carbon as working, glassy carbon as counter, and Ag/AgCl as reference electrodes with 0.1 V/s as scan rate.

served. However, the addition of three equivalents of methanesulfonic acid (corresponding to the typical reaction conditions) results in a decrease in the intensity of the reduction peak at −1.81 V. This observation is presumably associated with the initiation of the SET reduction process, which leads to the consumption of the diiminium salt **4a** and to the formation of the diradical intermediate **5a**.

Conclusion

In conclusion, we have successfully developed a simple and mild electroreductive, stereoselective intramolecular coupling of aromatic diimines, performed under batch and flow conditions. The reaction provided good to excellent yields across a wide range of substrates with both electron-withdrawing and electron-donating groups being well tolerated. As a result, a series of chiral enantiopure tetrasubstituted piperazines was efficiently synthetized. Significantly higher productivities and space-time yields were achieved under continuous conditions compared to the batch process. Furthermore, the scalability of the reaction was successfully demonstrated, highlighting its potential for larger-scale applications.

Experimental

General procedure in-batch electrochemical imino-pinacol coupling

In a flame-dried, undivided cell equipped with two GC electrodes and a stirring bar, diimine (0.5 mmol, 1 equiv) and NEt_4BF_4 (1.3 mmol, 2.6 equiv) were added, followed by two vacuum–nitrogen cycles. Under nitrogen atmosphere, dry DMF (0.125 M) and methanesulfonic acid (1.5 mmol, 3 equiv) were then added to the electrochemical cell. The reaction mixture was degassed by bubbling with argon for 20 minutes under vigorous stirring. The undivided cell was then connected to the Autolab power supply and stirred at 25 °C under galvanostatic conditions at 5 mA (2.5 mA/cm^2) until a total charge of 2.2 F/mol was delivered. The reaction mixture was poured into a beaker with 10 mL of distilled water, and a saturated solution of $NaHCO_3$ was added to adjust the pH to ≈7. 10 mL of ethyl acetate were then added, and the two phases were separated. The aqueous phase was then extracted with CH_2Cl_2 (3 × 10 mL). The combined organic layers were dried over Na_2SO_4, filtered and concentrated under vacuum. The reaction crude was purified by flash column chromatography on silica gel (*n*-hexane/ethyl acetate 8:2) to give the desired pure product.

General procedure for in-flow electrochemical imino-pinacol coupling

Diimine (1 equiv) and NEt_4BF_4 (1.3 equiv) were added in a flame-dried Erlenmeyer flask with a stirring bar, followed by two vacuum–nitrogen cycles. Under nitrogen atmosphere, dry DMF (0.125 M) and methanesulfonic acid (3 equiv) were then added to the reaction mixture, which was degassed by bubbling with argon for 20 minutes under vigorous stirring. In-flow experiments were performed using the Asia (Syrris) modular system with two carbon filled PPS electrodes, a constant current of 80 mA, a flow rate of 96 μL/min, a residence time of 2.34 minutes, and 1.3 equivalents of NEt_4BF_4. The experiments were conducted until a total charge of 4.15 F/mol was delivered. The reaction mixture was then poured into a beaker with distilled water, and a saturated solution of $NaHCO_3$ was added to adjust the pH to ≈7. Ethyl acetate was added, and the two phases were separated. The aqueous phase was then extracted three times with CH_2Cl_2. The combined organic layers were dried over Na_2SO_4, filtered and concentrated under vacuum. Yields were calculated on the reaction crude by ^{1}H NMR spectroscopy using 1,3,5-trimethoxybenzene as internal standard. In the case of the large-scale reaction the crude was purified through flash column chromatography on silica gel to give the isolated pure product.

Supporting Information

Supporting Information File 1

Synthetic procedures and physical data for the new compounds, copies of ^{1}H and ^{13}C NMR spectra of the prepared compounds.
[https://www.beilstein-journals.org/bjoc/content/supplementary/1860-5397-21-147-S1.pdf]

Acknowledgements

The authors thank Prof. A. Puglisi (Università degli Studi di Milano) for valuable discussions. For the single-crystal X-ray diffraction analysis the Unitech COSPECT (Università degli Studi di Milano) for provision of beamtime and Prof. Leonardo Lo Presti for structure solution and refinement are acknowledged.

Funding

The authors thank MUSA – Multilayered Urban Sustainability Action – project, funded by the European Union – NextGenerationEU, under the National Recovery and Resilience Plan (NRRP) Mission 4 Component 2 Investment Line 1.5: Strengthening of research structures and creation of R&D "innovation ecosystems", set up of "territorial leaders in R&D". M. Benaglia thanks MUR for the project PRIN 2022 ""Flow chemistry, photo and organocatalysis: powerful tools for the development of technology-driven sustainable strategies to alfa and beta amination of carbonyls and carboxylic acids derivatives-

TECHNO", financed by EU - Next Generation EU, Mission 4 Component 1 CUP G53D23003280006. M. Gazzotti thanks Università degli Studi di Milano for a PhD fellowship.

Author Contributions

Margherita Gazzotti: investigation; visualization; writing – review & editing. Fabrizio Medici: conceptualization; investigation; methodology; writing – review & editing. Valerio Chiroli: data curation; investigation; validation. Laura Raimondi: data curation; methodology; writing – review & editing. Sergio Rossi: methodology; supervision; writing – review & editing. Maurizio Benaglia: conceptualization; funding acquisition; methodology; supervision; writing – original draft; writing – review & editing.

ORCID® iDs

Margherita Gazzotti - https://orcid.org/0009-0008-5930-4371
Fabrizio Medici - https://orcid.org/0000-0003-1356-7244
Laura Raimondi - https://orcid.org/0000-0002-7314-1387
Sergio Rossi - https://orcid.org/0000-0002-2694-9535
Maurizio Benaglia - https://orcid.org/0000-0002-9568-9642

Data Availability Statement

Data generated and analyzed during this study is available from the corresponding author upon reasonable request.

Preprint

A non-peer-reviewed version of this article has been previously published as a preprint: https://doi.org/10.3762/bxiv.2025.34.v1

References

1. Lucet, D.; Le Gall, T.; Mioskowski, C. *Angew. Chem., Int. Ed.* **1998,** *37,* 2580–2627. doi:10.1002/(sici)1521-3773(19981016)37:19<2580::aid-anie2580>3.0.co;2-l
2. Faugeroux, V.; Genisson, Y. *Curr. Org. Chem.* **2008,** *12,* 751–773. doi:10.2174/138527208784567188
3. Eisch, J. J.; Kaska, D. D.; Peterson, C. J. *J. Org. Chem.* **1966,** *31,* 453–456. doi:10.1021/jo01340a024
4. Smith, J. G.; Veach, C. D. *Can. J. Chem.* **1966,** *44,* 2497–2502. doi:10.1139/v66-376
5. Smith, J. G.; Ho, I. *J. Org. Chem.* **1972,** *37,* 653–656. doi:10.1021/jo00969a027
6. Mercer, G. J.; Sturdy, M.; Jensen, D. R.; Sigman, M. S. *Tetrahedron* **2005,** *61,* 6418–6424. doi:10.1016/j.tet.2005.03.124
7. Baruah, B.; Prajapati, D.; Sandhu, J. S. *Tetrahedron Lett.* **1995,** *36,* 6747–6750. doi:10.1016/00404-0399(50)1331-b
8. Kalyanam, N.; Rao, G. V. *Tetrahedron Lett.* **1993,** *34,* 1647–1648. doi:10.1016/0040-4039(93)85031-q
9. Vellemäe, E.; Tšubrik, O.; Mäeorg, S.; Mäeorg, U. *J. Chem. Res.* **2006,** 149–150. doi:10.3184/030823406776330792
10. Hatano, B.; Tachikawa, T.; Mori, T.; Nagahashi, K.; Kijima, T. *Tetrahedron Lett.* **2011,** *52,* 3467–3469. doi:10.1016/j.tetlet.2011.04.104
11. Shimizu, M.; Iida, T.; Fujisawa, T. *Chem. Lett.* **1995,** *24,* 609–610. doi:10.1246/cl.1995.609
12. Alexakis, A.; Aujard, I.; Mangeney, P. *Synlett* **1998,** 873–874. doi:10.1055/s-1998-1790
13. Hesemann, P.; Moreau, J. J. E.; Soto, T. *Synth. Commun.* **2003,** *33,* 183–189. doi:10.1081/scc-120015698
14. Khan, N. H.; Zuberi, R. K.; Siddiqui, A. A. *Synth. Commun.* **1980,** *10,* 363–371. doi:10.1080/00397918008061825
15. Shono, T.; Kise, N.; Oike, H.; Yoshimoto, M.; Okazaki, E. *Tetrahedron Lett.* **1992,** *33,* 5559–5562. doi:10.1016/s0040-4039(00)61145-0
16. Sakai, T.; Korenaga, T.; Washio, N.; Nishio, Y.; Minami, S.; Ema, T. *Bull. Chem. Soc. Jpn.* **2004,** *77,* 1001–1008. doi:10.1246/bcsj.77.1001
17. Dutta, M. P.; Baruah, B.; Boruah, A.; Prajapati, D.; Sandhu, J. S. *Synlett* **1998,** 857–858. doi:10.1055/s-1998-1800
18. Rieke, R. D.; Kim, S.-H. *J. Org. Chem.* **1998,** *63,* 5235–5239. doi:10.1021/jo971942y
19. Mercer, G. J.; Sigman, M. S. *Org. Lett.* **2003,** *5,* 1591–1594. doi:10.1021/ol034469l
20. Shimizu, M.; Inayoshi, K.; Sahara, T. *Org. Biomol. Chem.* **2005,** *3,* 2237–2238. doi:10.1039/b505335h
21. Kumar, A.; Samuelson, A. G. *Eur. J. Org. Chem.* **2011,** 951–959. doi:10.1002/ejoc.201001256
22. Talukdar, S.; Banerji, A. *J. Org. Chem.* **1998,** *63,* 3468–3470. doi:10.1021/jo9716892
23. Mangeney, P.; Tejero, T.; Alexakis, A.; Grosjean, F.; Normant, J. *Synthesis* **1988,** 255–257. doi:10.1055/s-1988-27536
24. Periasamy, M.; Srinivas, G.; Karunakar, G. V.; Bharathi, P. *Tetrahedron Lett.* **1999,** *40,* 7577–7580. doi:10.1016/s0040-4039(99)01609-3
25. Periasamy, M.; Srinivas, G.; Suresh, S. *Tetrahedron Lett.* **2001,** *42,* 7123–7125. doi:10.1016/s0040-4039(01)01480-0
26. Arai, S.; Takita, S.; Nishida, A. *Eur. J. Org. Chem.* **2005,** 5262–5267. doi:10.1002/ejoc.200500301
27. Banik, B. K.; Zegrocka, O.; Banik, I.; Hackfeld, L.; Becker, F. F. *Tetrahedron Lett.* **1999,** *40,* 6731–6734. doi:10.1016/s0040-4039(99)01395-7
28. Yanada, R.; Negoro, N.; Okaniwa, M.; Miwa, Y.; Taga, T.; Yanada, K.; Fujita, T. *Synlett* **1999,** 537–540. doi:10.1055/s-1999-2695
29. Kawaji, T.; Hayashi, K.; Hashimoto, I.; Matsumoto, T.; Thiemann, T.; Mataka, S. *Tetrahedron Lett.* **2005,** *46,* 5277–5279. doi:10.1016/j.tetlet.2005.06.038
30. Annunziata, R.; Benaglia, M.; Caporale, M.; Raimondi, L. *Tetrahedron: Asymmetry* **2002,** *13,* 2727–2734. doi:10.1016/s0957-4166(02)00748-6
31. Imamoto, T.; Nishimura, S. *Chem. Lett.* **1990,** *19,* 1141–1142. doi:10.1246/cl.1990.1141
32. Kim, M.; Knettle, B. W.; Dahlén, A.; Hilmersson, G.; Flowers, R. A., II. *Tetrahedron* **2003,** *59,* 10397–10402. doi:10.1016/j.tet.2003.06.004
33. Dahlén, A.; Prasad, E.; Flowers, R. A., II; Hilmersson, G. *Chem. – Eur. J.* **2005,** *11,* 3279–3284. doi:10.1002/chem.200401320
34. Taniguchi, Y.; Kuno, T.; Nakahashi, M.; Takaki, K.; Fujiwara, Y. *Appl. Organomet. Chem.* **1995,** *9,* 491–503. doi:10.1002/aoc.590090519
35. Nakajima, M.; Fava, E.; Loescher, S.; Jiang, Z.; Rueping, M. *Angew. Chem., Int. Ed.* **2015,** *54,* 8828–8832. doi:10.1002/anie.201501556
36. Dang, V. Q.; Teets, T. S. *Chem. Sci.* **2023,** *14,* 9526–9532. doi:10.1039/d3sc03000h

37. Gualandi, A.; Rodeghiero, G.; Della Rocca, E.; Bertoni, F.; Marchini, M.; Perciaccante, R.; Jansen, T. P.; Ceroni, P.; Cozzi, P. G. *Chem. Commun.* **2018,** *54,* 10044–10047. doi:10.1039/c8cc04048f
38. Wang, H.; Qu, J.-P.; Kang, Y.-B. *Org. Lett.* **2021,** *23,* 2900–2903. doi:10.1021/acs.orglett.1c00537
39. Kundu, S.; Roy, L.; Maji, M. S. *Org. Lett.* **2022,** *24,* 9001–9006. doi:10.1021/acs.orglett.2c03600
40. Okamoto, S.; Kojiyama, K.; Tsujioka, H.; Sudo, A. *Chem. Commun.* **2016,** *52,* 11339–11342. doi:10.1039/c6cc05867a
41. Okamoto, S.; Ariki, R.; Tsujioka, H.; Sudo, A. *J. Org. Chem.* **2017,** *82,* 9731–9736. doi:10.1021/acs.joc.7b01838
42. Law, H. D. *J. Chem. Soc., Trans.* **1912,** *101,* 154–166. doi:10.1039/ct9120100154
43. Tanaka, H.; Nakahara, T.; Dhimane, H.; Torii, S. *Synlett* **1989,** 51–52. doi:10.1055/s-1989-34700
44. Shono, T.; Kise, N.; Shirakawa, E.; Matsumoto, H.; Okazaki, E. *J. Org. Chem.* **1991,** *56,* 3063–3067. doi:10.1021/jo00009a026
45. Siu, T.; Li, W.; Yudin, A. K. *J. Comb. Chem.* **2001,** *3,* 554–558. doi:10.1021/cc0100159
46. Cui, W.; Xu, X.; Zhang, C.; Wang, D.; Yang, Y.; Wang, Q.; Wang, J. *J. Org. Chem.* **2025,** *90,* 3659–3664. doi:10.1021/acs.joc.4c02994
47. When the reaction was attempted with the diimines derived from the 2-pyridinecarboxaldehyde and the 3-pyridinecarboxaldehyde, it resulted in extensive decomposition of the starting materials.
48. Capaldo, L.; Wen, Z.; Noël, T. *Chem. Sci.* **2023,** *14,* 4230–4247. doi:10.1039/d3sc00992k
49. Atobe, M.; Tateno, H.; Matsumura, Y. *Chem. Rev.* **2018,** *118,* 4541–4572. doi:10.1021/acs.chemrev.7b00353
50. Elsherbini, M.; Wirth, T. *Acc. Chem. Res.* **2019,** *52,* 3287–3296. doi:10.1021/acs.accounts.9b00497
51. Noël, T.; Cao, Y.; Laudadio, G. *Acc. Chem. Res.* **2019,** *52,* 2858–2869. doi:10.1021/acs.accounts.9b00412
52. Cantillo, D. *Curr. Opin. Electrochem.* **2024,** *44,* 101459. doi:10.1016/j.coelec.2024.101459
53. Asia premium flow chemistry system for modular efficiency in systems chemistry. http://www.syrris.com.

License and Terms

This is an open access article licensed under the terms of the Beilstein-Institut Open Access License Agreement (https://www.beilstein-journals.org/bjoc/terms), which is identical to the Creative Commons Attribution 4.0 International License (https://creativecommons.org/licenses/by/4.0). The reuse of material under this license requires that the author(s), source and license are credited. Third-party material in this article could be subject to other licenses (typically indicated in the credit line), and in this case, users are required to obtain permission from the license holder to reuse the material.

The definitive version of this article is the electronic one which can be found at:
https://doi.org/10.3762/bjoc.21.147

BEILSTEIN JOURNAL OF ORGANIC CHEMISTRY

C2 to C6 biobased carbonyl platforms for fine chemistry

Jingjing Jiang[1,§], Muhammad Noman Haider Tariq[2,§], Florence Popowycz[*1], Yanlong Gu[*2] and Yves Queneau[*1]

Review

Open Access

Address:
[1]Université Lyon 1, INSA Lyon, CNRS, CPE Lyon, ICBMS, UMR5246, 69622 Villeurbanne, France and [2]Institute of Physical Chemistry and Industrial Catalysis, School of Chemistry and Chemical Engineering, Huazhong University of Science and Technology, 1037 Luoyu road, Wuhan 430074, China

Email:
Florence Popowycz[*] - Florence.Popowycz@insa-lyon.fr; Yanlong Gu[*] - klgyl@hust.edu.cn; Yves Queneau[*] - Yves.Queneau@insa-lyon.fr

* Corresponding author
§ Equal contributors in the work and should both received any equivalent benefit related to first-authorship

Keywords:
aldehydes; biobased chemistry; biomass; carbonyl; fine chemicals; ketones; multicomponent; platforms; sustainability

Beilstein J. Org. Chem. **2025,** *21,* 2103–2172.
https://doi.org/10.3762/bjoc.21.165

Received: 27 May 2025
Accepted: 19 September 2025
Published: 15 October 2025

This article is part of the thematic issue "Green chemistry III: Technologies shaping future directions in synthesis".

Associate Editor: L. Vaccaro



© 2025 Jiang et al.; licensee Beilstein-Institut.
License and terms: see end of document.

Abstract

The carbonyl group is central in organic synthesis, thanks to its ability to undergo a vast range of different chemical transformations on its carbon center or at the neighboring positions. Due to the high level of oxygen content in biomass, small molecules arising from biomass often possess a carbonyl group. This is why biobased platform molecules possessing a carbonyl group, either under the form of an aldehyde, a ketone, an acid or an ester, play a dominant role in biobased chemistry. This review aims at illustrating how the chemistry of biobased carbonyl platform molecules with backbones from C_2 to C_6 offers opportunities to reach all kinds of chemical architectures, sometimes even complex ones benefiting from the ability of the carbonyl group to be involved in multicomponent reactions.

Introduction

Shifting towards sustainable practices in the chemical industry relies on continued advancement of green chemistry sciences which aim to minimize the global environmental impact while maintaining the efficiency of the chemical processes [1]. Green Chemistry principles outlined by Anastas and Warner in their work “Green Chemistry: Theory and Practice (2000)” [2] notably highlight atom economy, waste minimization and the use of renewable feedstock as pillars of sustainable chemistry [3-6]. Indeed, the use of biobased feedstocks provide a promising substitute for traditional petroleum-based resources [7]. Particularly lignocellulosic materials have emerged as a key source of producing fine chemicals and fuels [8,9], relying on the advances in catalytic processes dedicated to the conversion of biomass-derived platform molecules [10,11]. Recent studies

have also highlighted the potential of biobased aromatic compounds as sustainable alternatives to their fossil-derived counterparts [12-15]. Developing biobased solvents [16,17] and platform chemicals from biomass shows how renewable carbon sources can replace non-renewable chemicals in important industrial processes [18-20].

Many, if not most, biobased platform molecules contain carbonyl groups. Carbonyl compounds have unique electrophilic and nucleophilic reactivity which make them central players in organic synthesis. Therefore, synthetic chemists can base strategies on the existing reactivity of carbonyl compounds for defining novel routes converting biobased platform molecules containing carbonyl groups to prepare fine organic chemicals [21,22]. Following this approach, researchers can obtain diverse downstream products from biomass, with efforts for using clean and sustainable conditions in terms of solvents, reagents and catalysts. The topic of biomass conversion has been explored in multiple perspectives [23-27], and the purpose of the present review is to offer a specific viewpoint by focusing on the reactivity of biobased platform molecules containing carbonyl groups. This review, which does not pretend to be comprehensive, attempts to highlight the central role of carbonyl-containing biobased platform molecules notably those having a C_2 to C_6 backbone shown in Figure 1, and illustrating their high-value conversion methods towards fine chemicals.

Review

C_2 biobased carbonyl platforms

Glycolaldehyde

Developing accesses from biomass to structures such as glycolic acid (GA) and glycolaldehyde (GCA) with high atomic economy is challenging. Hu et al. reported a new route for the synthesis of GA and GCA using activated carbon deposited Cu catalysts and different biomass-derived polyols as feedstock with exceptionally high atom utilization ≈93% and up to 90% yield (Scheme 1) [28].

Glycolaldehyde (GCA), the smallest sugar molecule, was used by Sels et al. for the synthesis of amines by replacing the current toxic pathway based on ethylene oxide and dichloroethane [29]. Due to the high reactivity of α-hydroxycarbonyls, the main

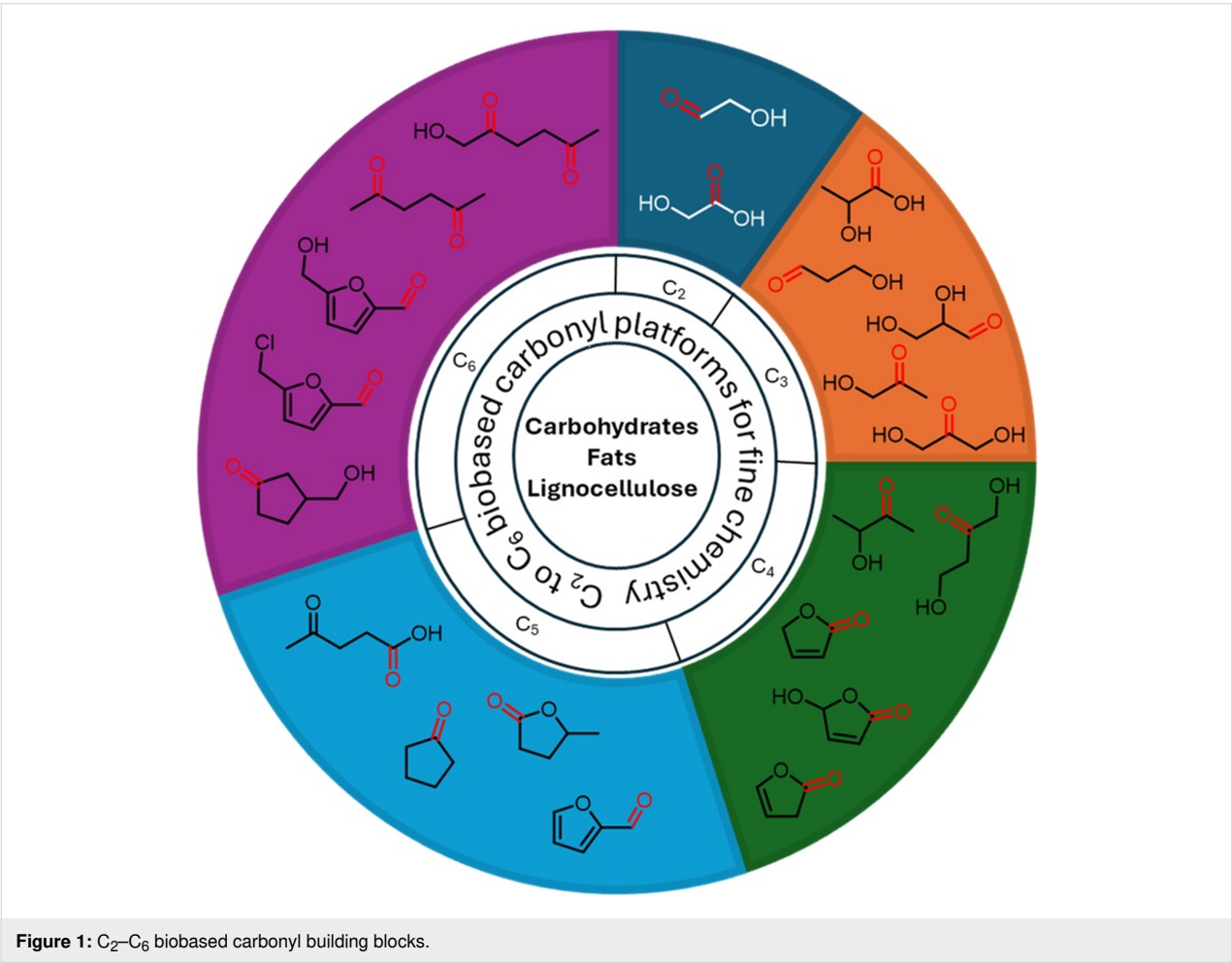
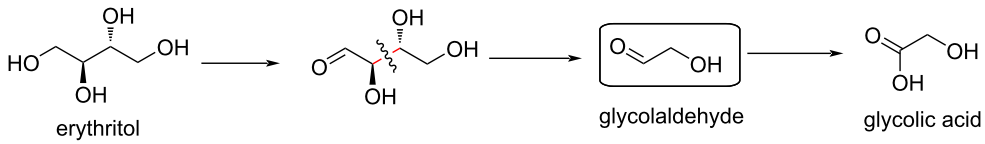


Figure 1: C_2–C_6 biobased carbonyl building blocks.

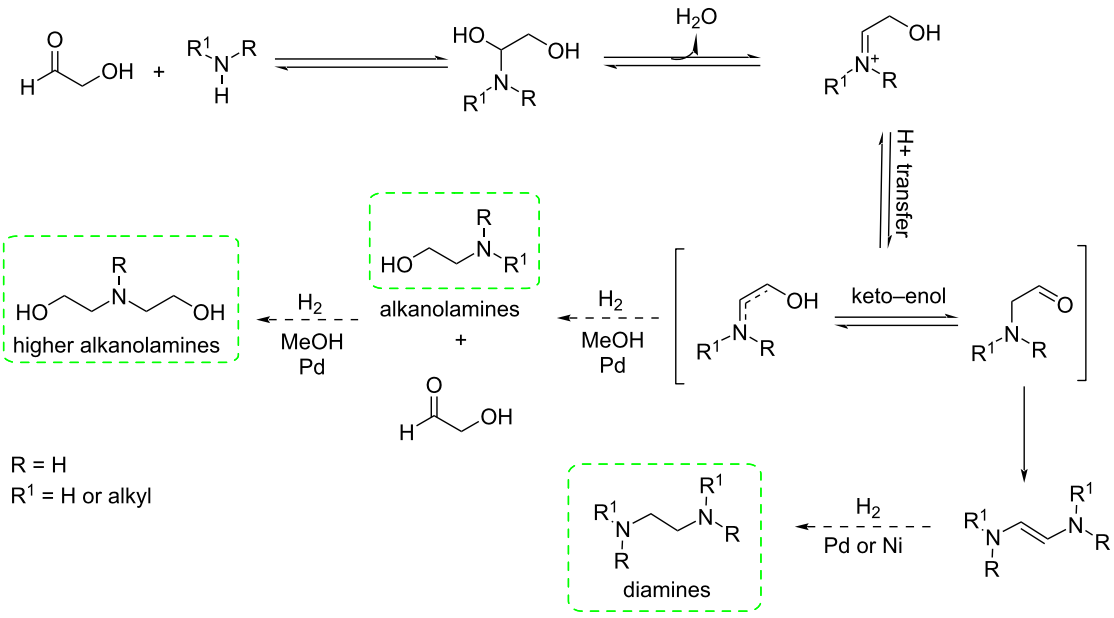


Scheme 1: Proposed (2 + 2) route to glycolaldehyde and glycolic acid from erythritol by Cu/AC catalyst (AC = activated carbon).

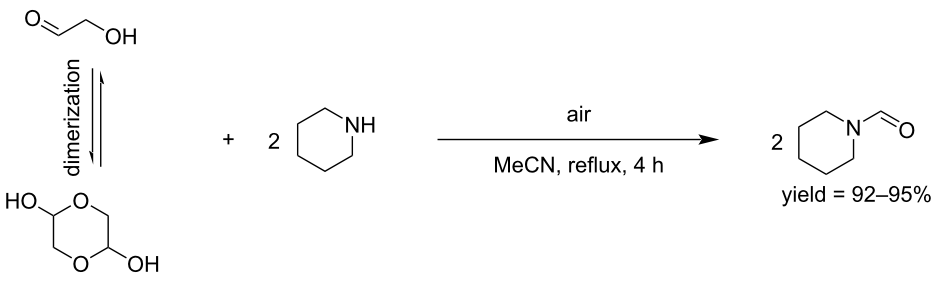
issue in this reductive amination reaction [30] was to control the cascade of consecutive and parallel reactions. The use of methanol as solvent and Pd as catalyst played a vital role for achieving a high yield. Efficient subsequent esterification and quaternarization to diesterquat fabric softeners demonstrated that high-value chemicals could be produced fully biobased from GCA as the starting platform (Scheme 2).

GCA can also be used as a C_1 building block for the *N*-formylation of secondary amines to formamides under catalyst-free conditions and air as oxidant. This method was applied to different aromatic and aliphatic (both cyclic and acyclic) amines (Scheme 3) [31].

Already in 1955, Parham and Reiff reported the synthesis and conversion of a glycolaldehyde acetal (hydroxy acetal). The first step was the reaction of sodium benzyloxide with bromo acetals giving the hydroxy acetals in 75–82% yield. The intermediate ether was converted to the hydroxy acetal with sodium in liquid ammonia in good yield (70%). The



Scheme 2: Reductive amination of GCA.

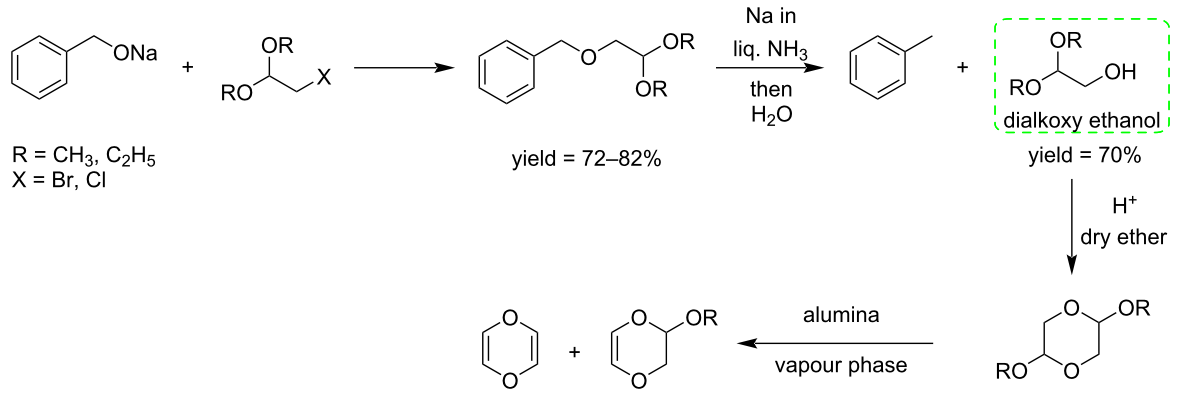


Scheme 3: *N*-Formylation of secondary amines by reaction with GCA.

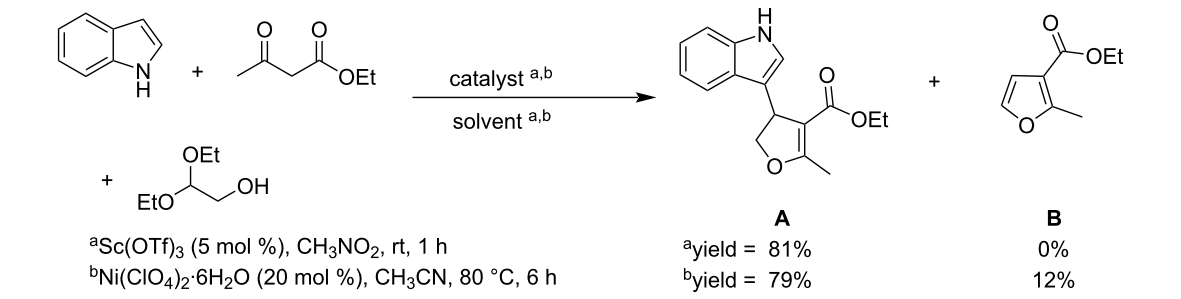
hydroxy acetal then evolves towards cyclic acetals (Scheme 4) [32].

Exploring methods for the conversion of glycolaldehyde (GCA) to 3-(indol-3-yl)-2,3-dihydrofurans in organic solvents, Gu et al. reported a three-component reaction combining GCA, ethyl acetoacetate as 1,3-dicarbonyl component and indole. Using glycolaldehyde acetal as source of glycolaldehyde, two catalytic systems, namely $Sc(OTf)_3$/nitromethane and $Ni(ClO_4)_2{\cdot}6H_2O$/acetonitrile, resulted in good yields. When using directly the aqueous solution of glycolaldehyde, these latter conditions were unproductive, whereas the deep eutectic solvent (DES) system $FeCl_3{\cdot}6H_2O$/meglumine (*N*-methylglucamine) was found effective. This DES system proved to be a fully water compatible medium for the three-component conversion of glycolaldehyde, allowing the synthesis of a variety of 3-(indol-3-yl)-2,3-dihydrofurans in good yields. Interestingly, the DES ($FeCl_3{\cdot}6H_2O$/meglumine) system can be recycled without significant loss of activity (Scheme 5) [33].

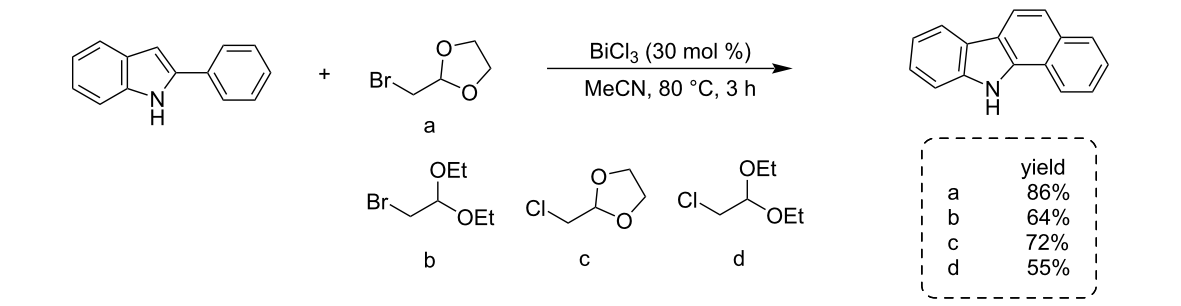
α-Bromoacetaldehyde derivatives (Scheme 6, structures a–d) and 2-phenylindoles were used to synthesize benzo[*a*]carbazoles. The reaction reported by the Gu research group was



Scheme 4: Synthesis and conversion of hydroxy acetals to cyclic acetals.



Scheme 5: Synthesis of 3-(indol-3-yl)-2,3-dihydrofurans via three-component reaction of glycolaldehyde, indole and ethyl acetoacetate.



Scheme 6: $BiCl_3$-catalyzed synthesis of benzo[*a*]carbazoles from 2-arylindoles and α-bromoacetaldehyde ethylene acetal.

speeded up by bismuth trichloride ($BiCl_3$). The Friedel–Crafts alkylation products were then converted into an intermediate tryptaldehyde that underwent intramolecular olefination to form the targeted product [34].

Glycolic acid (GA)

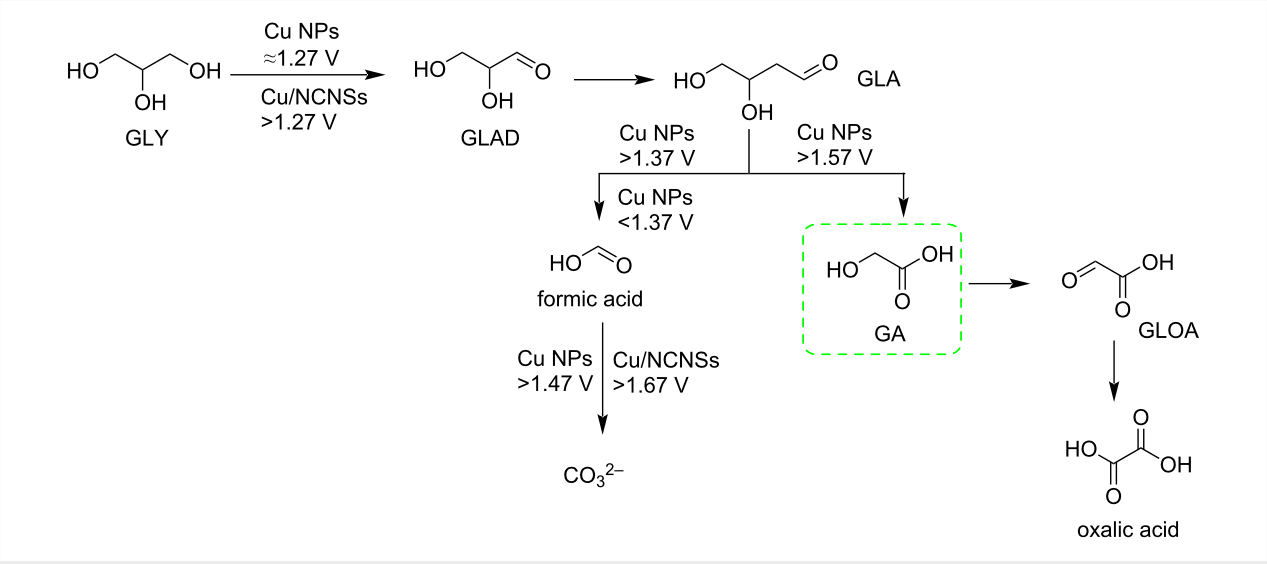
The growing impact of fossil fuel consumption has heightened the need for advancing renewable energy technologies. One promising strategy for sustainable energy development involves the electrochemical oxidation of biomass-derived feedstocks. Recent work by Shen et al. demonstrates that glycolic acid (GA), also referred to as hydroxyacetic acid, can be synthesized from glycerol (GLY) using a copper single-atom electrocatalyst supported on nitrogen-doped carbon nanosheets (Cu/NCNSs). This catalyst exhibits high activity for the oxidation of various substrates, including GLY, gluconic acid (GLU), 5-hydroxymethylfurfural (HMF), benzyl alcohol (BA), furfuryl alcohol (FA), and ethylene glycol (EG) (Scheme 7) [35].

Park et al. reported the valorization of C_1 molecules (CH_4, CO_2, and CO) upgraded to the industrially important C_2 chemical glycolic acid (GA) in a sustainable way. In the first step all the C_1 source molecules are converted into formaldehyde. Metabolic engineering of *E. coli*-based biocatalysts allowed to avoid side reactions and promoted exclusive transformation of formaldehyde into glycolic acid. The use of *E. coli* K-12 strains as host cells and paraformaldehyde as the starting material, led to production of GA with high conversion even at rather high concentrations (Scheme 8) [36]. Using a Cu^{II}-based single ion catalyst, Brückner and Shi synthesized value added formamides by treating amines with different C_2 and C_3 platform molecules like GA, glyceraldehyde (GLAD), and 1,3- dihydroxyacetone (DHA) (Scheme 9) [37].

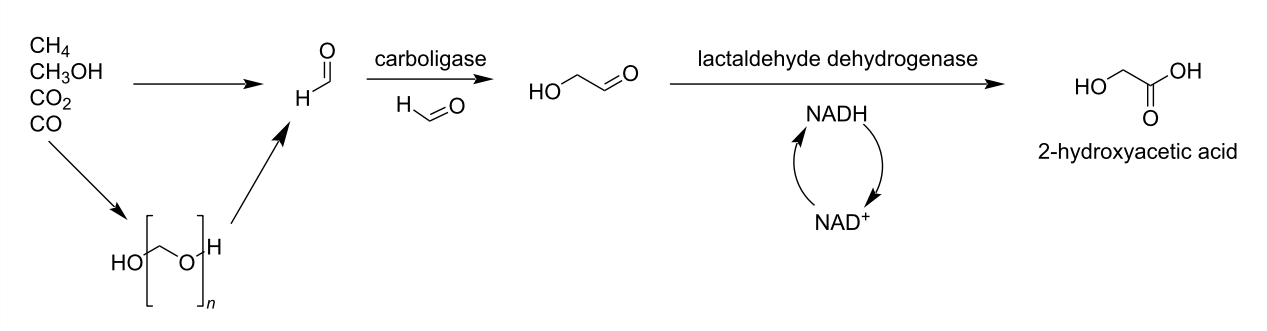
C_3 biobased carbonyl platforms

Lactic acid (LA)

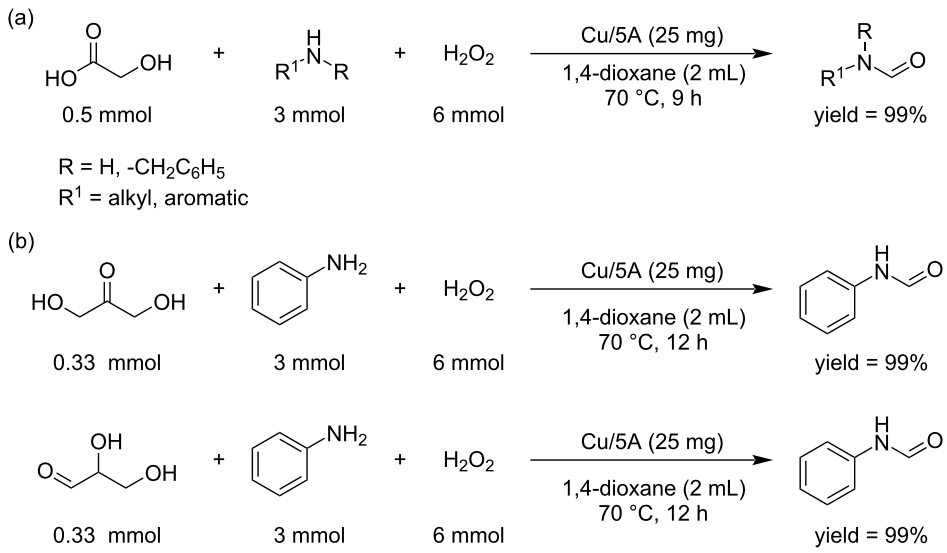
Propanoic (or propionic) acid (PA), a valuable chemical used in the feed and food industry, is produced by petrochemical pro-



Scheme 7: Cu/NCNSs-based conversion of glycerol to glycolic acid and other short biobased acids.



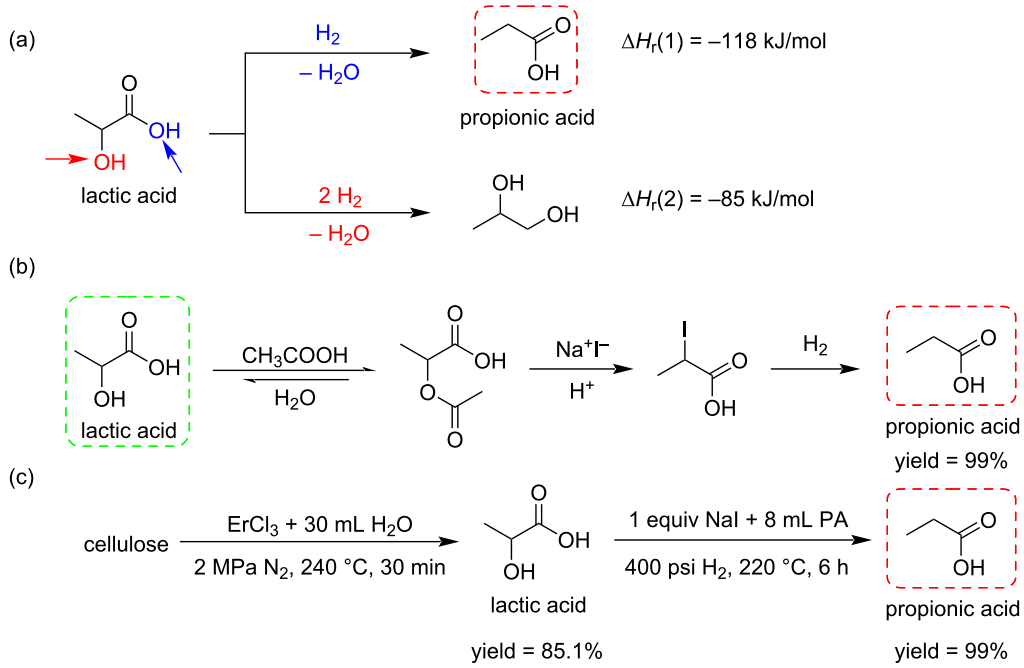
Scheme 8: *E. coli*-based biotransformation of C_1 source molecules (CH_4, CO_2 and CO) towards C_2 glycolic acid.



Scheme 9: *N*-Formylation of amines with C_2 (a) or C_3 (b) biomass-based feedstocks.

cesses. Its synthesis from biobased lactic acid (LA) offers an access from renewable resources. However, this conversion is difficult due to the high activation energy required for the hydrogenation reaction removing the hydroxy group at the α-position of the carboxyl group (Scheme 10) [38]. Yang and his team reported a metal-free catalytic system for the conversion of LA to PA (Scheme 10a). The use of NaI as catalyst and PA itself as solvent allowed to simplify the product separation process, giving yields up to 99% (Scheme 10b) [39]. This strategy offers a green and efficient approach to synthesize PA from biomass resources. The synthesis of PA was also achieved in a two-step process from cellulose (Scheme 10c) [40].

The use of biobased monomers is receiving tremendous attention in the field of bioplastic materials. Polylactic acid (PLA) and polyglycolic acid (PGA) are most important examples of



Scheme 10: Methods for the formation of propanoic acid (PA) from lactic acid (LA).

biopolymers exhibiting interesting biodegradability properties [41]. The co-polymerization of PLA with glycolic acid was reported by Ayyoob and Kim [42]. High molecular weight polylactic-*co*-glycolic acid (PLGA) was obtained by the direct condensation and co-polymerization of both monomers promoted by a bicatalytic system including stannous chloride ($SnCl_2{\cdot}2H_2O$) and methane sulfonic acid (MSA). PLGA films were prepared by the solvent casting technique, for which the presence of glycolic acid was found to increase their wettability (Scheme 11).

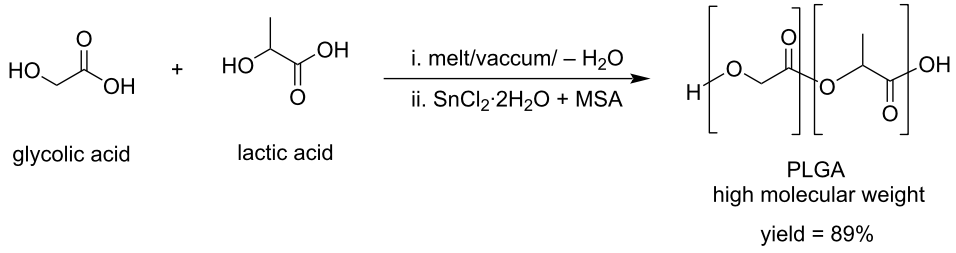
The group of Gupta et al. investigated the kinetics of the oxidation by tetrachloroaurate(III) in acetic acid–sodium acetate buffer medium of some neutralized α-hydroxy acids, including glycolic acid (GA), lactic acid (LA), α-hydroxybutyric acid (IB), mandelic acid (MA), atrolactic acid (ALA), and benzylic acid (BA). These acids were oxidized and gave formaldehyde, acetaldehyde, acetone, benzaldehyde, acetophenone, and benzophenone, respectively. By increasing pH and concentration, the rate of the reactions increased, but decreased upon increasing the amount of Cl^- ions (Scheme 12) [43].

Many other studies have concerned lactic acid (LA) because of its low cost and versatile reactivity owing to the presence of one hydroxy group and one carboxylic group. Zhou et al. [44] summarized the selective catalytic (chemical or biological) pathways for the conversion of lactic acid towards different commodity chemicals which includes acrylic acid [45-50], pentane-2,3-dione [51,52], pyruvic acid [53-55], 1,2-propanediol [56-59], PLA [60-64], acetaldehyde [49,51], ethyl lactate [65-68] and propanoic acid (Figure 2) [49,69,70].

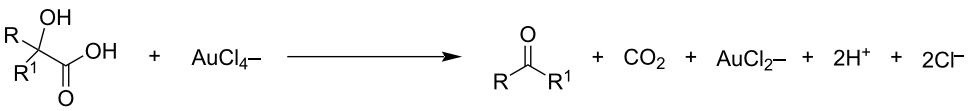
3-Hydroxypropanal (3-HPO) and 2,3-dihydroxypropanal (2,3-HPO)

Xu et al. reported the cross-aldol reaction of formaldehyde and acetaldehyde for the synthesis of 3-hydroxypropanal and further reduction to 1,3-propanediol (PDO). The reaction was promoted by X-$5Mg/SiO_2$ and Mg/SiO_2 (X = Mn, Co, Ni, Fe) catalysts synthesized by the sol–gel method. The $5Mg/SiO_2$ catalyst showed the highest activity in terms of selectivity and yield because of its suitable basic and acidic density. The addition of Mn to the $5Mg/SiO_2$ (1Mn-$5Mg/SiO_2$) catalyst as week acidic side increased the selectivity towards 3-HPA. According to reaction kinetics studies, the cross-aldol reaction of formaldehyde and acetaldehyde gives a higher yield of 3-HPO than the self-aldol reaction of acetaldehyde. Moreover, Raney nickel was applied successfully for the conversion of 3-HPO to 1,3-PDO with good yield and about 90% conversion rate of 3-HPO (Scheme 13) [71].

The Bobleter and Feather groups investigated the reaction mechanism of the conversion of these C_3 compounds. The acid-



Scheme 11: Co-polymerization of biobased lactic acid and glycolic acid via a bicatalytic process.



	yield
$R = R^1 = H$ for glycolic acid	88%
$R = CH_3$, $R^1 = H$ for lactic acid	89%
$R = R^1 = -CH_3$ for α-hydroxyisobutyric acid	80%
$R = -C_6H_5$, $R^1 = H$ for mandelic acid	94%
$R = -C_6H_5$, $R^1 = -CH_3$ for atrolactic acid	85%
$R = R^1 = -C_6H_5$ for benzilic acid	91%

Scheme 12: Oxidation of α-hydroxy acids by tetrachloroaurate(III) in acetic acid–sodium acetate buffer medium.

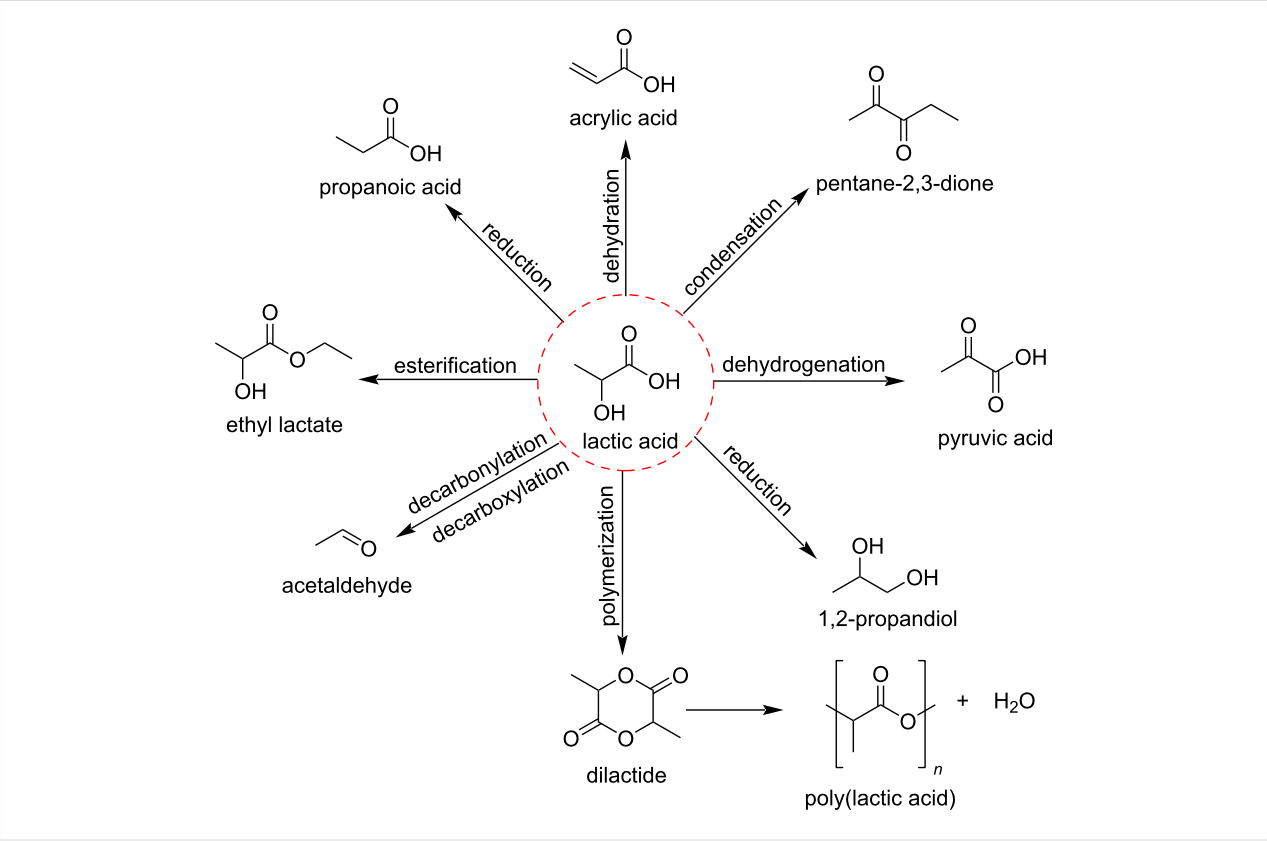
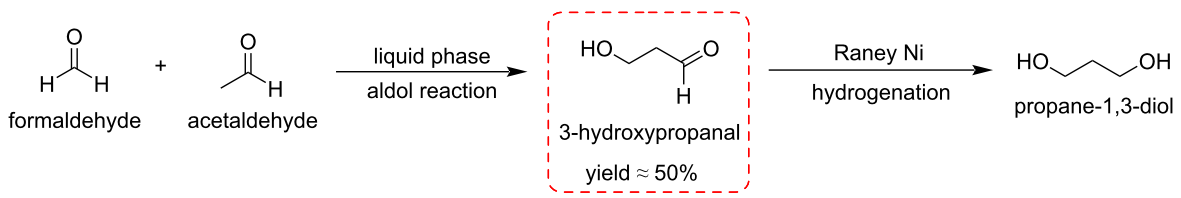


Figure 2: Selective catalytic pathways for the conversion of lactic acid (LA).



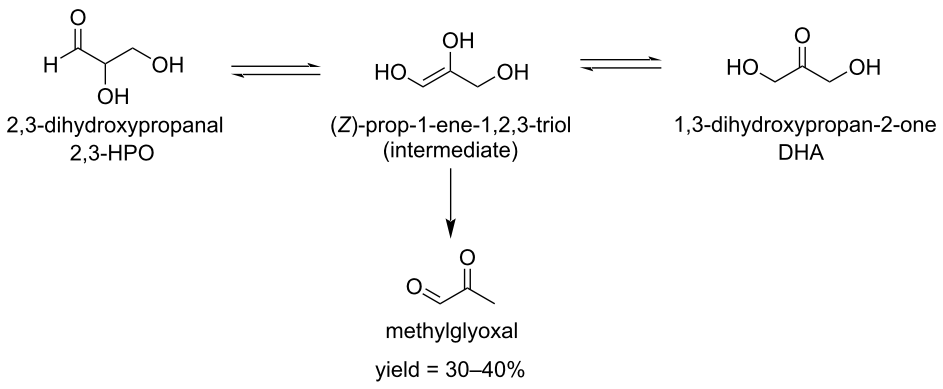
Scheme 13: Synthesis of 1,3-PDO via cross-aldol reaction between formaldehyde and acetaldehyde to 3-hydroxypropanal followed by hydrogenation.

catalyzed equilibrium between 1,3-dihydroxy-2-propane and 2,3-dihydroxypropanal involves an ene-triol intermediate which leads to methylglyoxal by a dehydration reaction at temperatures between 180–240 °C in a maximum yield of about 30–40% (Scheme 14) [72,73].

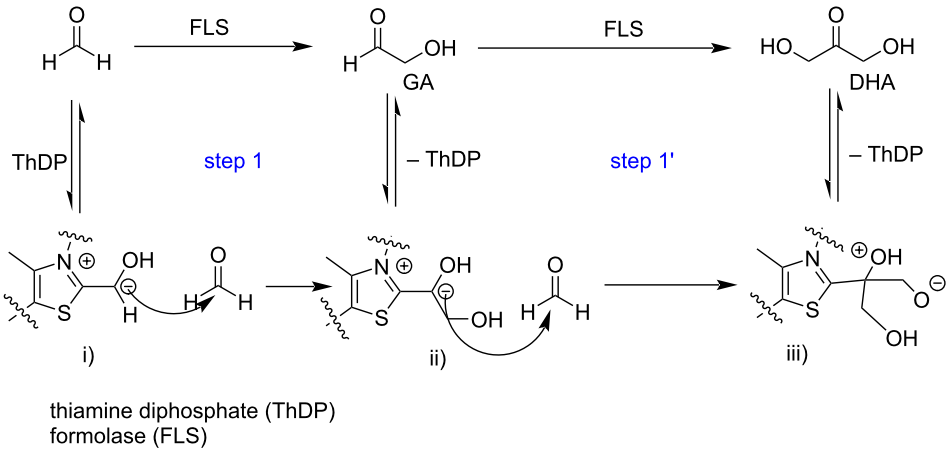
Dihydroxyacetone (DHA)

The formose process is the conversion of formaldehyde to glycolaldehyde and 1,3-dihydroxy-2-propanone (dihydroxyacetone, DHA). A computational protein-directed evolution allowed to create "formolase" (FLS), an enzyme able to catalyze the formose process. Various teams investigated the kinetics of the reaction and the entire carbon uptake allowing to select the best computationally modified enzyme profile depending on the formaldehyde amount and guiding future efforts to improve this pathway (Scheme 15) [74-76].

Tang et al. recently reported the environmentally friendly production of glyceraldehyde and dihydroxyacetone from using glycerol through photocatalytic oxidation under visible light using a $Cu^{\delta+}$-decorated WO_3 photocatalyst in the presence of hydrogen peroxide (H_2O_2) [77]. The presence of the photocatalyst provokes an impressive five-fold rise in the conversion rate (3.81 mmol/g) without compromising the high selectivity towards the two trioses (glyceraldehyde, 46.4%, and dihydroxyacetone, 32.9%). Okamoto and co-workers developed a new



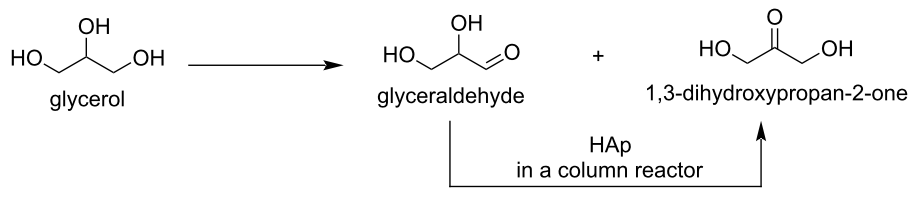
Scheme 14: Hydrothermal conversion of 1,3-dihydroxy-2-propane and 2,3-dihydroxypropanal to methylglyoxal.



Scheme 15: FLS-catalyzed formose reaction to synthesize GA and DHA.

hydroxyapatite (HAp)-loaded flow system for the atom economical preparation of dihydroxyacetone (DHA) in good yield from aqueous glyceraldehyde (Scheme 16) [78].

Transformation of 1,3-dihydroxy-2-propanone (dihydroxyacetone, DHA) has been a very popular topic for many years, using a variety of reactions like isomerizations and dehydra-



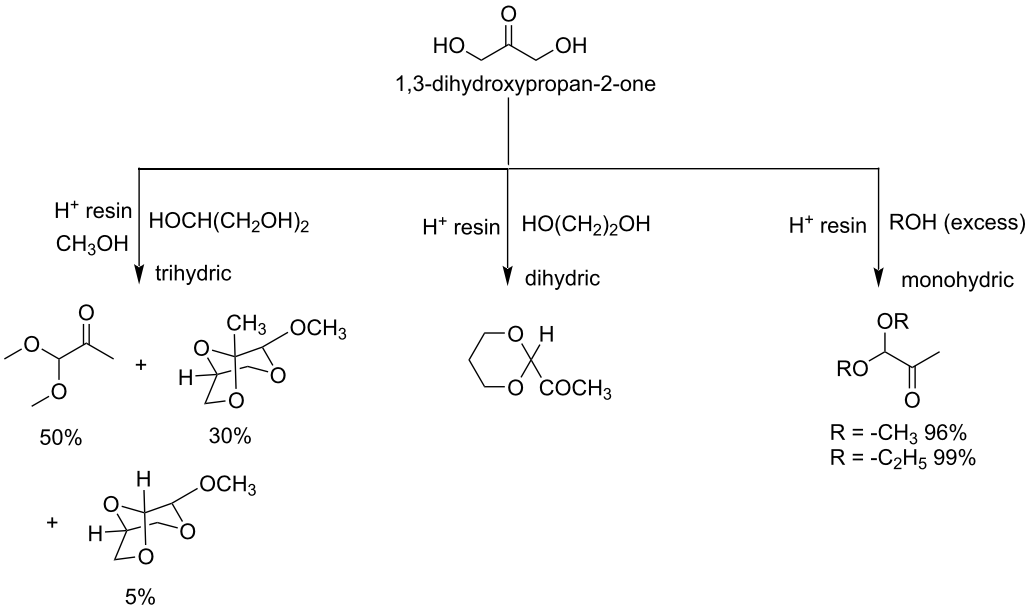
Entry	temp. (°C)	flow rate (mL/min)	yield (%)
1	25	0.1	1
2	55	0.1	19
3	85	0.1	85
4	85	1	16
5	85	0.01	>99

Scheme 16: GCA and DHA oxidation products of glycerol and isomerization of GCA to DHA under flow conditions using a hydroxyapatite (Hap)-packed column.

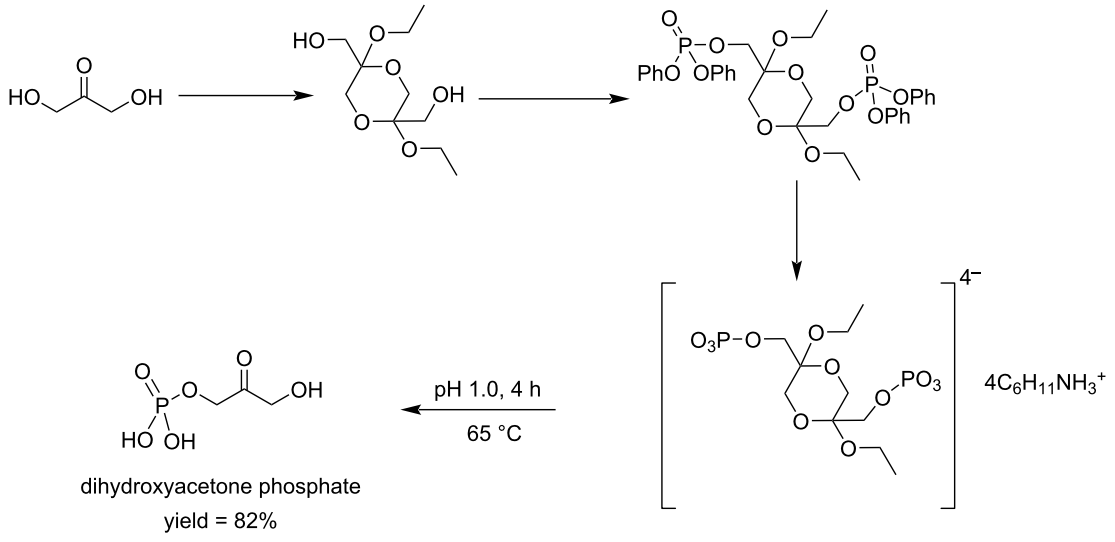
tions [79-81]. Keto acetals have been observed as by-products, such as in the work reported by Gupta investigating the acid-catalyzed reactions of DHA with various alcohols (Scheme 17) [82].

Colbran and colleagues reported the conversion of DHA to dihydroxyacetone phosphate in four steps in 27% overall yield [83]. In their synthesis the cyclic acetal (2,5-diethoxy-1,4-dioxane-2,5-diyl)dimethanol or its dimethoxy analog was esterified with diphenyl phosphorochloridate in pyridine to give (2,5-diethoxy-1,4-dioxane-2,5-diyl)bis(methylene) tetraphenyl bis(phosphate). Subsequent removal of the phenyl groups through hydrogenolysis, neutralization with cyclohexylamine and treatment with ion-exchange resin led to dihydroxyacetone phosphate. This 4-step method was more efficient than the previously reported dismutation of fructose-1,6-diphosphate [84] and 3-chloro-1,3-propanediol [85] which required more than nine steps and gave only 15% yield. No remaining acetal was found in the final product (Scheme 18).

The production of lactic acid from dihydroxyacetone or its derivative pyruvaldehyde was investigated on large scale to eval-



Scheme 17: Acid-catalyzed reactions of DHA with alcohols.



Scheme 18: Synthesis of dihydroxyacetone phosphate from dihydroxyacetone.

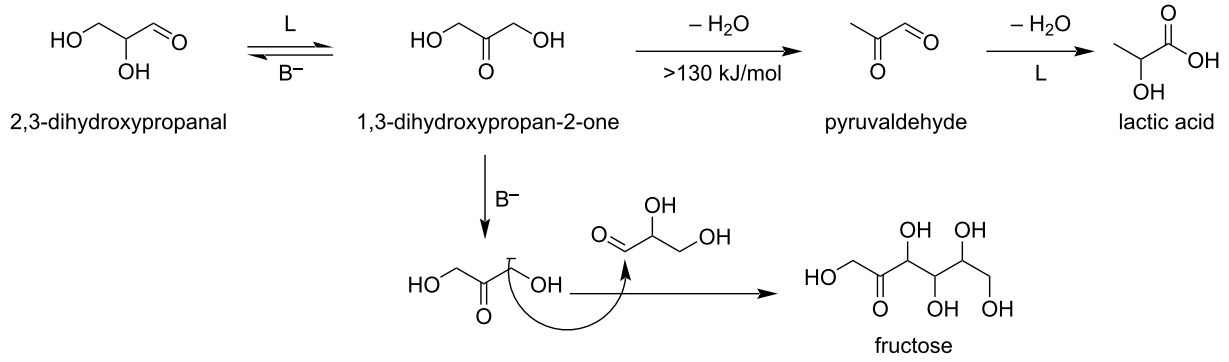
uate the water tolerance of Lewis acid sites of several solid catalysts [86-92]. Essayem and co-workers reported the conversion of DHA with the help of TiO_2-based catalysts having dual properties. Two parallel pathways are as follows: on one hand the catalyst Lewis acidic sites promote the formation of pyruvaldehyde and lactic acid (LA) by a two-step reaction, while the catalyst Lewis base sites produce fructose (Scheme 19) [93].

Shi et al. [94] reported a novel strategy to synthesize glycolic acid (GA), a very important building block of biodegradable polymers as already stressed in the C_2 section. The catalytic one-pot synthesis of GA and co-synthesis of formamides and formates was achieved in particularly good yield by selective oxidation of DHA using a Cu/Al_2O_3 catalyst with single active Cu^{II} species at room temperature without using a base (Scheme 20).

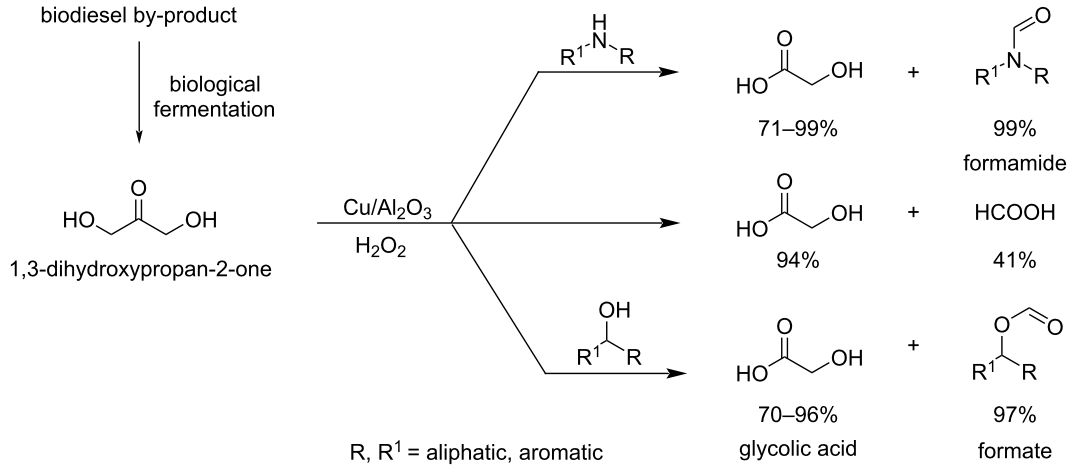
1-Hydroxypropan-2-one

Gu et al. reported the [3 + 2] cyclization reaction of 1-hydroxypropan-2-one with acylacetonitrile towards furan derivatives using a $Sc(OTf)_3$ catalyst. C_2-based bifunctional acetals, such as glycolaldehyde diethyl acetal, α-bromoacetaldehyde acetal, and 1,4-dithiane-2,5-diol also take part in the reaction as counterpart reagents. The well-known fungicide fenfuram was prepared using this process. Antifungal activity assays against four general plant fungi demonstrated that several of the synthesized new furan products exhibited also broad and strong biological activities (Scheme 21) [95].

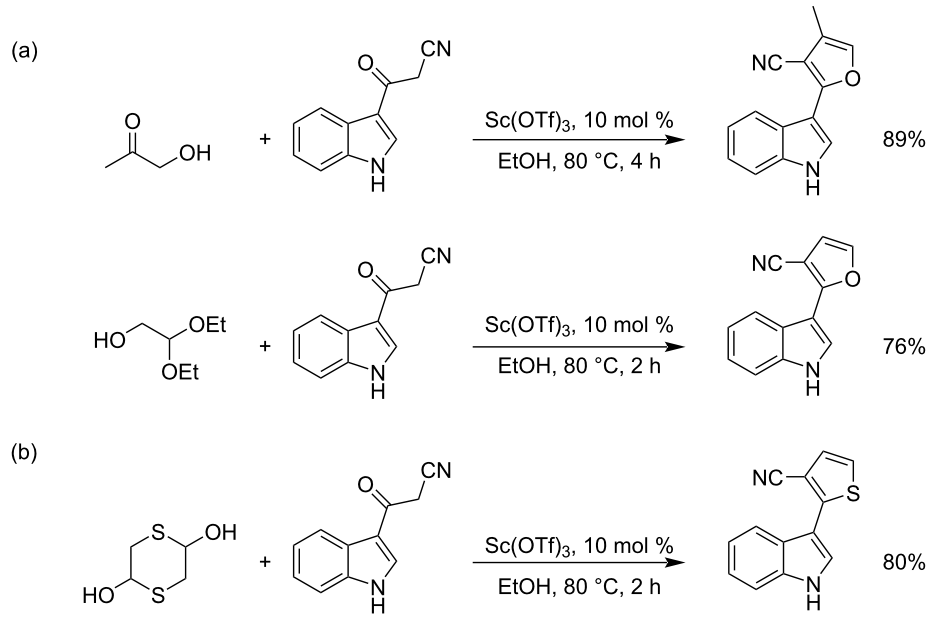
A metal-free efficient strategy was developed by the Gu group for the synthesis of benzo[*a*]carbazole (a very important scaffold in the pharmaceutical industry) from the commercially available 2-phenylindole and bio-renewable 1-hydroxypropan-2-one (acetol) using a sulfone-containing Brønsted acidic medium as catalyst. The process was applied to a number of substituted 2-phenylindoles and hydroxyketones. The catalyst could be recovered and reused five times without decreasing its selectivity and activity. Mechanistically, the reaction involves a Heyns-type rearrangement and subsequent intramolecular olefination (Scheme 22) [96].



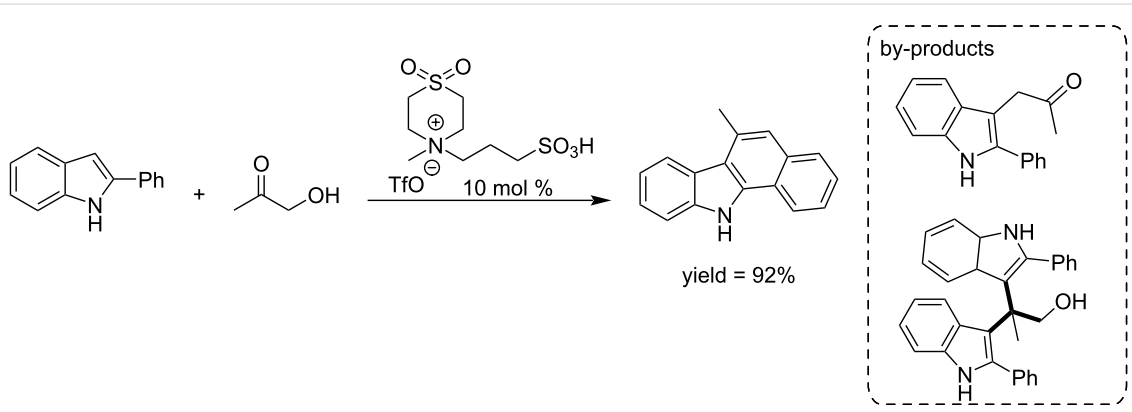
Scheme 19: Bifunctional acid–base catalyst DHA conversion into lactic acid via pyruvaldehyde or fructose formation.



Scheme 20: Catalytic one-pot synthesis of GA and co-synthesis of formamides and formates from DHA.



Scheme 21: (a) Synthesis of furan derivatives and (b) synthesis of thiophene derivative by cascade [3 + 2] annulation.

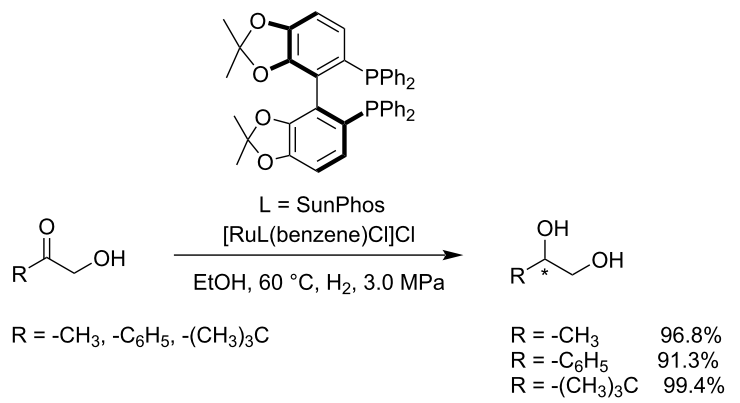


Scheme 22: Brønsted acidic ionic liquid catalyzed synthesis of benzo[*a*]carbazole from renewable acetol and 2-phenylindoles.

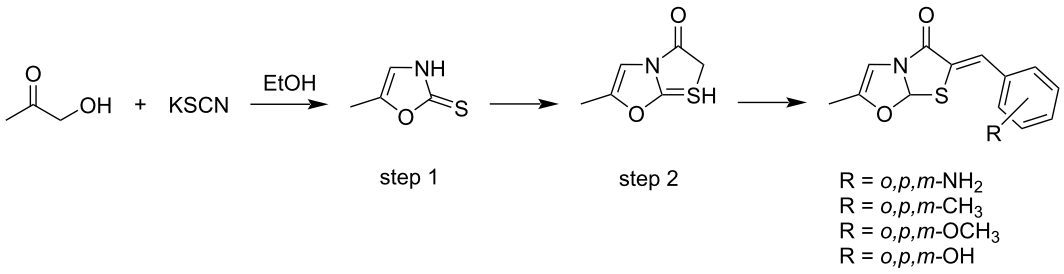
Arandia et al. reported the application of the aqueous-phase reforming (APR) technology for the production of light hydrocarbons and hydrogen in a single step from aqueous organic phases [97] containing 1-hydroxypropan-2-one (acetol), ethanol, benzene-1,2-diol (catechol), acetic acid or mixtures thereof. The process was conducted over various Ni-based catalysts including Ni/CeO_2-γAl_2O_3, spinal $NiAl_2O_4$ and Ni/La_2O_3-αAl_2O_3, at 230 °C and 3.2 MPa. Using a chiral catalyst composed of $[RuCl_2(benzene)]_2$ and SunPhos, an effective asymmetric hydrogenation of α-hydroxy ketones was reported, yielding chiral terminal 1,2-diols in up to 99% ee. This Ru-catalyzed asymmetric hydrogenation process of α-hydroxy ketones opens up a new pathway for the production of chiral terminal 1,2-diols (Scheme 23) [98].

Kini and Mathews reported the synthesis of novel oxazole derivatives such as 6-(substituted benzylidene)-2-methylthiazolo[2,3-*b*]oxazol-5(6*H*)-one by reacting 1-hydroxypropan-2-one and KSCN in ethanol for further evaluation of their anticancerous activity by MTT assays (Scheme 24) [99].

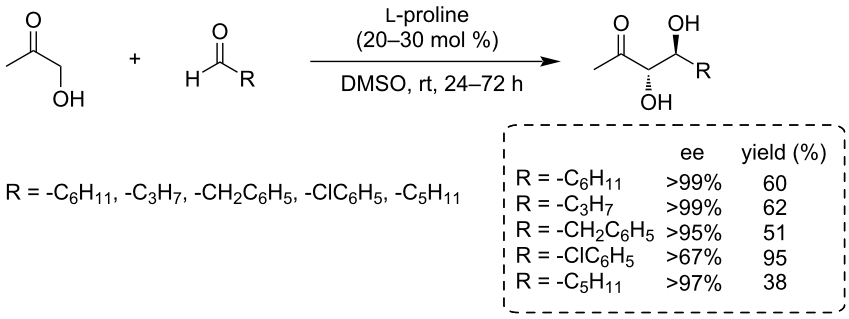
Notz and List reported the synthesis of *anti*-diols in good yield from 1-hydroxypropan-2-one and different (aromatic and aliphatic) substituted aldehydes using a new strategy using L-proline as a catalyst (Scheme 25) [100]. The C–C-bond formation between biomass-based feedstock by aldol condensation reactions of furfural with 1-hydroxyacetone has been reported by Subrahmanyam and co-workers (Scheme 26) [101].



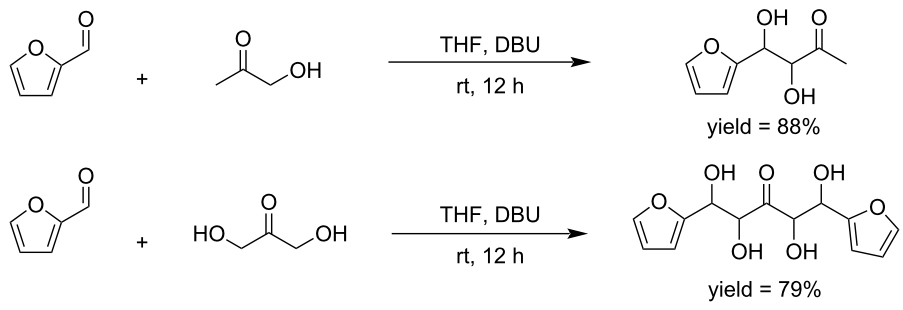
Scheme 23: Asymmetric hydrogenation of α-hydroxy ketones to 1,2-diols.



Scheme 24: Synthesis of novel 6-(substituted benzylidene)-2-methylthiazolo [2,3-*b*]oxazol-5(6*H*)-one from 1-hydroxypropan-2-one.



Scheme 25: L-Proline-catalyzed synthesis of *anti*-diols from hydroxyacetone and aldehydes.



Scheme 26: C–C-bond-formation reactions of a biomass-based feedstock aromatic aldehyde (C_5) and hydroxyacetone (C_3).

C_4 biobased carbonyl platforms

Acetoin

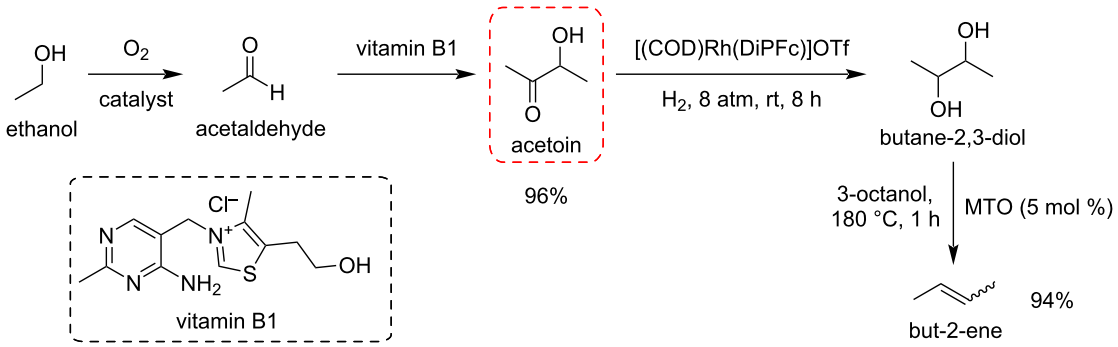
Acetoin is a very important C_4 biomass-based molecule and widely used building block in the food industry as flavoring compound. It can be synthesized from diacetyl by reduction using enzymes such as *Aerobacter aerogenes* [102] or thiamine diphosphate-dependent lyase (ThdP-lyase) [103]. The biotechnological production of chiral acetoin was reported by Meng and co-workers [104]. Zhang and his team [105] reported the synthesis of bulk C_4 chemicals from bioethanol via intermediate formation of acetoin in the presence of simple, environmentally benign, cheap and readily available natural vitamin B1 salts as the key step. Acetoin was further converted to C_4 bulk chemicals such as 2,3-butanediol and butene (Scheme 27).

1,4-Dihydroxybutan-2-one

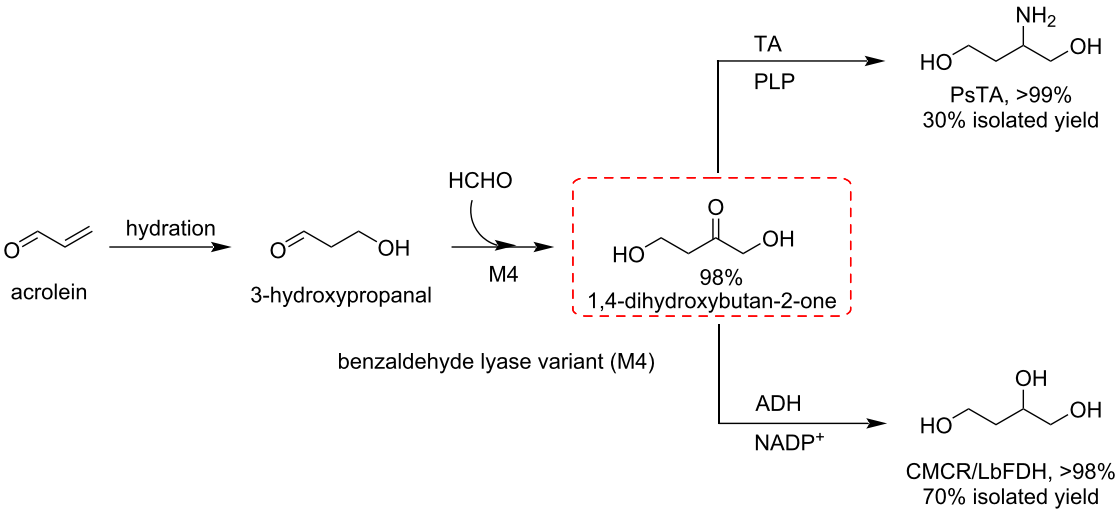
1,4-Dihydroxybutan-2-one is a key intermediate for the synthesis of different polyols such as 2-aminobutane-1,4-diol. Ma and co-workers synthesized 1,4-dihydroxybutan-2-one by a benzaldehyde lyase-catalyzed reaction of formaldehyde with 3-hydroxypropanal [106]. Another report depicts a new M4-catalyzed reaction between acrolein and formaldehyde for the synthesis of 1,4-dihydroxybutan-2-one, which was further converted into 1,2,4-butanetriol and 2-aminobutane-1,4-diol (Scheme 28) [107].

Matsumura et al. [108] reported the biocatalytic conversion of butane-1,2,4-triol into 1,4-dihydroxybutan-2-one. This work dealt with the conversion of *sec*-hydroxy groups to carbonyl derivatives by methanol yeast, *Candida boidinii* KK912, a cheaper and simpler process compared to other methods. The product is a kind of tetrose with biological and industrial relevance (Scheme 29).

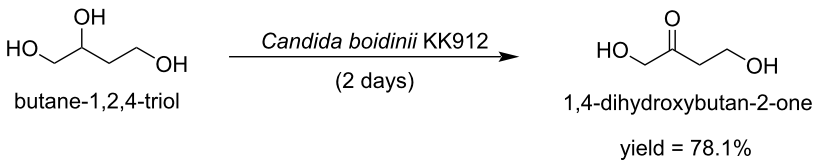
Waymouth et al. [109] reported the regio- and chemoselective oxidation of vicinal polyols using [2,9-dimethyl-1,10-phenan-



Scheme 27: Ethanol upgrading to C_4 bulk chemicals via the thiamine (VB1)-catalyzed acetoin condensation.



Scheme 28: One-pot sequential chemoenzymatic synthesis of 2-aminobutane-1,4-diol and 1,2,4-butanetriol via 1,4-dihydroxybutan-2-one.

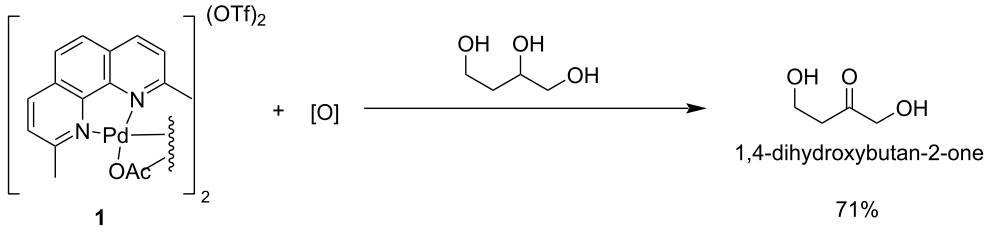


Scheme 29: Synthesis of 1,4-dihydroxybutan-2-one by microbial transformation.

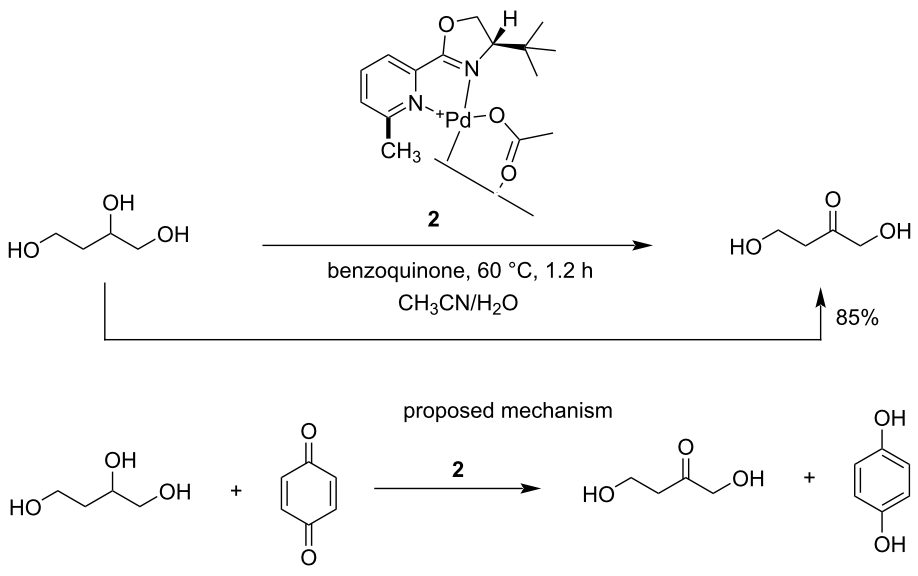
throline = neocuproine)Pd(OAc)]$_2$(OTf)$_2$] (**1**) as catalyst. The formation of α-hydroxyketones occurs very rapidly under mild conditions. The catalyst **1** oxidizes the vicinal diols to the corresponding hydroxy ketones faster than other alcohols. Primary alcohols and 1,5-diols are oxidized to yield secondary alcohols and cyclic lactones, respectively (Scheme 30). A high chemo- and regioselectivity was observed for the oxidation of 1,2-diols, triols and tetraols using the chiral palladium-based catalyst **2** bearing a pyridinyl oxazoline (pyOX) ligand (Scheme 31) [110].

5-Hydroxy-2(5*H*)-furanone (HFO)

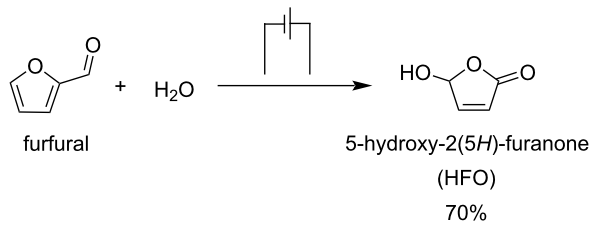
5-Hydroxy-2(5*H*)-furanone (HFO) is an interesting C_4 platform which is formed from furfural by oxidation. Han and co-workers developed an electrocatalytic strategy for the synthesis of HFO from furfural [111]. The very important and key bioactive compound HFO was formed by using water as an oxygen source and chalcogenides such as CuS, ZnS, or PbS as electrocatalysts. CuS nanosheets gave the best performance, with high selectivity towards HFO (83%) and high conversion of furfural (70%) (Scheme 32).



Scheme 30: Conversion of polyols by [neocuproine)Pd(OAc)]$_2$(OTf)$_2$] to α-hydroxy ketones.



Scheme 31: Chemoselective oxidation of alcohols with chiral palladium-based catalyst **2**.

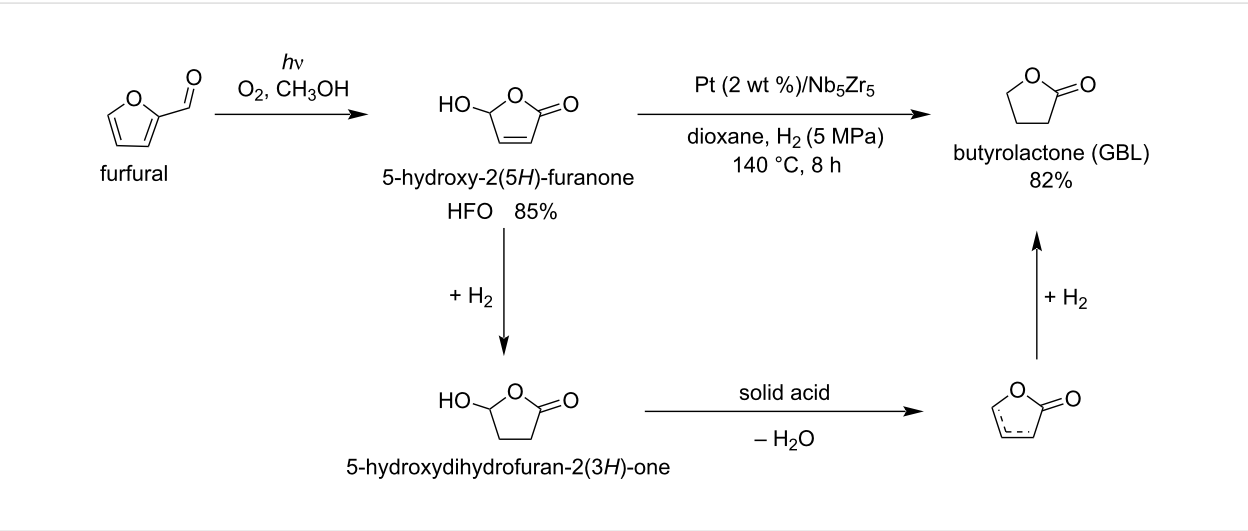


Scheme 32: Electrochemical transformation of furfural to 5-hydroxy-2(5*H*)-furanone (HFO).

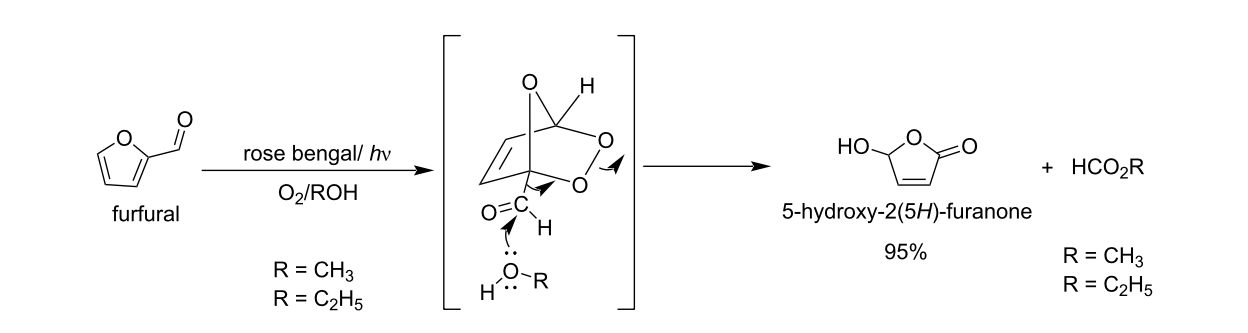
Yuan et al. [112] reported the synthesis of γ-butyrolactone (GBL) by the hydrodeoxygenation of HFO prepared by photocatalytic conversion of furfural. HFO is converted to GBL by two pathways: the first one is dehydration over mesoporous solid acids and the second one is a metal-catalyzed hydrogenation. HFO was obtained in 85% yield and its conversion rate to GBL was about 97%. Different bifunctional Pt-based solid acids were used. An overall GBL yield of 82.7% from furfural was obtained (Scheme 33).

Gollnick and Griesbeck reported the tetraphenylporphin-photosensitized oxygenations of furan and derivatives in non-polar aprotic solvents, yielding the corresponding monomeric unsaturated secondary ozonides through a (4 + 2) cycloaddition of singlet oxygen onto the diene linkage of the furan ring. The attack of a hydroxy group on the carbonyl group of the ozonide triggers the formation of HFO in high yields (>90%) (Scheme 34) [113-115].

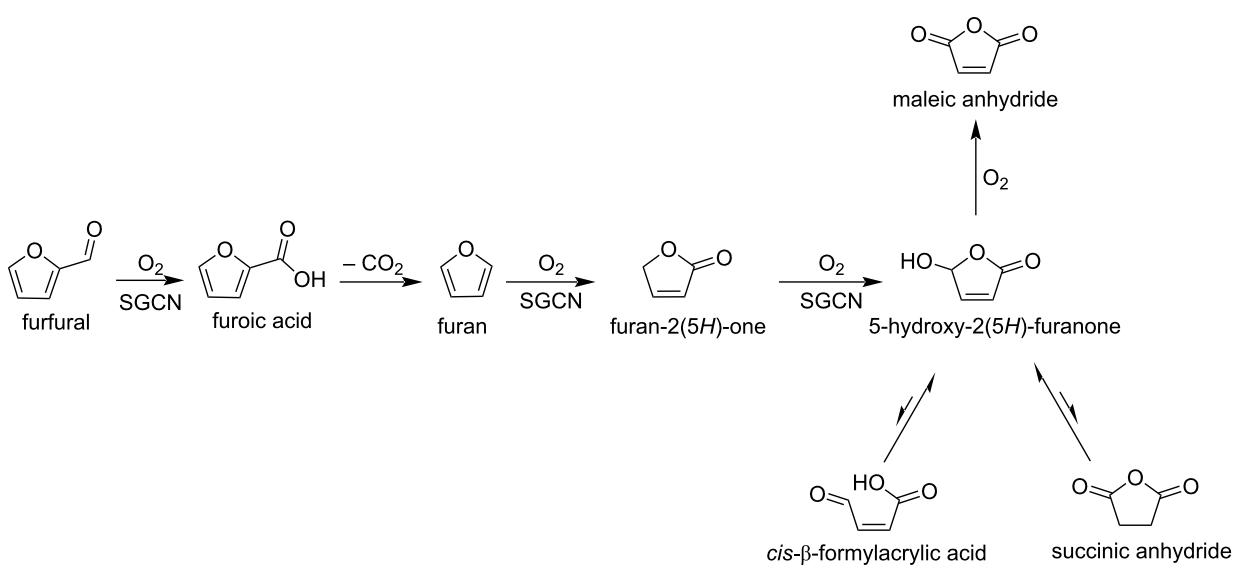
Kailasam and co-workers reported a heterogeneous photocatalytic oxidation of furfural towards HFO and maleic anhydride (MAN) [116]. This conversion is performed under simulated solar light and molecular O_2 as the oxidant, and mesoporous carbon nitride (SGCN) as the photocatalyst. The latter showed excellent photoconversion (>95%) of furfural with 33% and 42% selectivity of HFO and MAN, respectively (Scheme 35). Xiao et al. developed this method and suggested that the Fe_2B_2 can be used as electrocatalyst for the production of furanoic acid and HFO with potentials of −0.15 V and −0.93 V, respectively [117].



Scheme 33: Selective hydrodeoxygenation of HFO and oxidation to γ-butyrolactone (GBL).



Scheme 34: Photosensitized oxygenation of furan towards HFO via ozonide intermediates.



Scheme 35: Conversion of furfural to HFO and MAN by using mesoporous carbon nitride (SGCN) as photocatalyst.

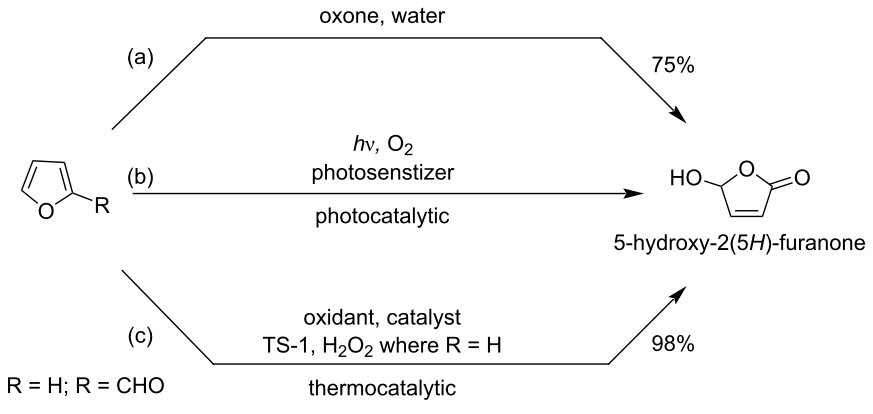
Chavan et al. reported a simple and efficient method for the synthesis of HFO from furan by using oxone as oxidant (Scheme 36a) [118]. Before this study Kumar et al. also synthesized HFO from furan by thermocatalytic oxidation (Scheme 36b) [119]. Salomon and co-workers reported the conversion of 2-substituted furans to HFO using $NaClO_2$ as oxidizing agent (Scheme 36c) [120].

The conversion of furfural to HFO by a dye-sensitized photooxidation reaction with oxygen in alcoholic medium has also been reported (Scheme 37) [121,122].

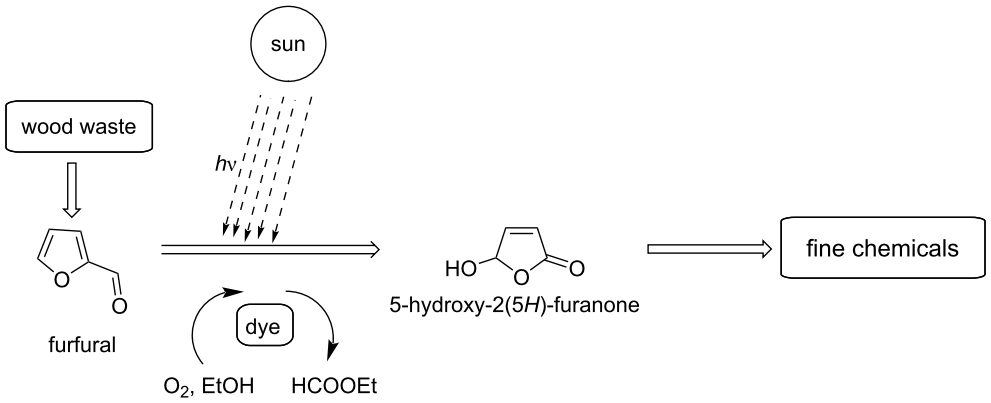
Riguet synthesized γ-lactams through a Ugi 4-center 3-component reaction (U-4C-3CR) protocol. HFO was used as the electrophile in the Friedel–Crafts (FC) alkylation reactions of indole catalyzed by diphenylprolinol silyl ether. The high reactivity of HFO permitted that a limited loading of catalyst could be employed. The reduction of the Friedel–Crafts adduct gave the targeted indoyl lactones with good yield (Scheme 38) [123].

Bos and Riguet reported the one pot synthesis of α,γ-substituted chiral γ-lactones from HFO. The reaction involves the enantioselective organocatalyzed transfer of boronic acid to HFO followed by an intramolecular diastereoselective Passerini-type reaction. Varying the boronic acid enabled to reach high yields (Scheme 39) [124].

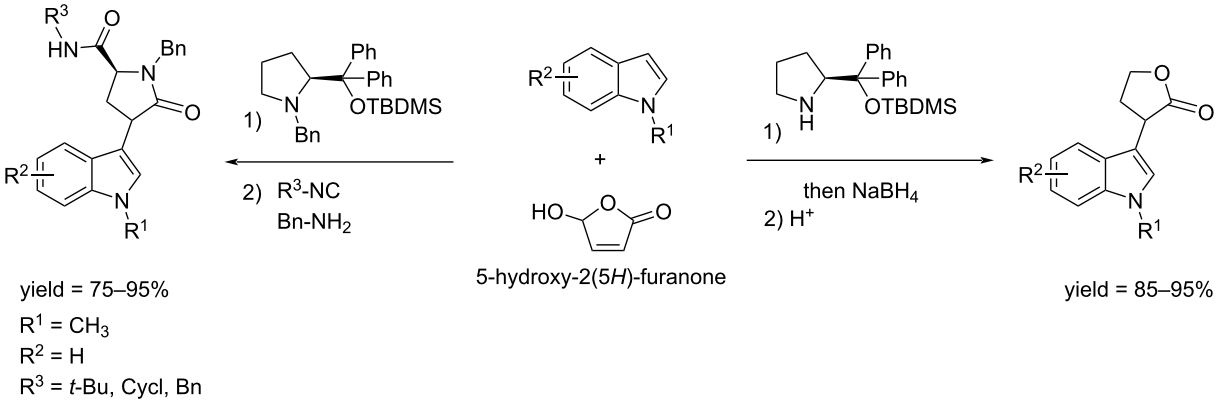
The tautomeric transformation of HFO to *cis*-β-formylacrylic acid was reported by Strizhov et al. [125]. The liable equilibrium transformation requires precisely pH-controlled condi-



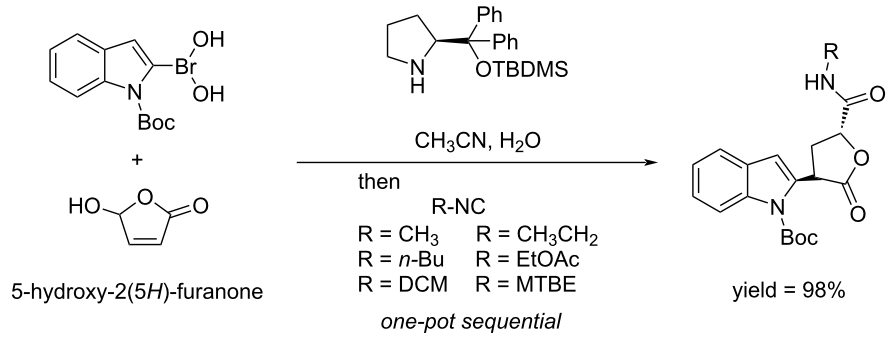
Scheme 36: Synthesis of HFO from furan derivatives.



Scheme 37: Photooxidation of furfural to 5-hydroxy-2(5*H*)-furanone (HFO).



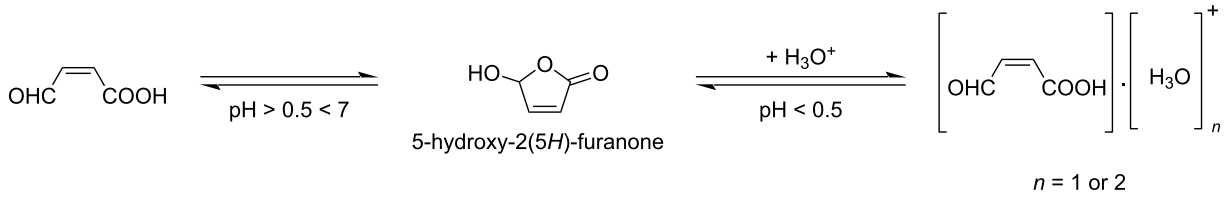
Scheme 38: Synthesis of Friedel–Crafts indole adduct from HFO.



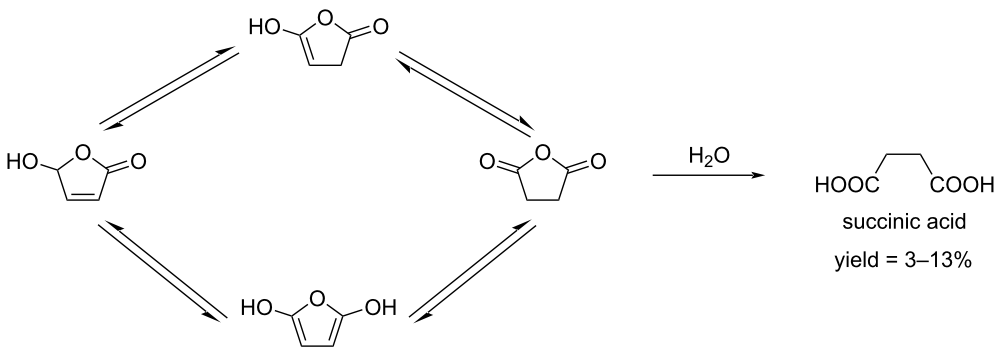
Scheme 39: Conversion of HFO to α,γ-substituted chiral γ-lactones.

tions. In neutral medium, the furanone is in the form of its cis tautomer, while upon a slight increase in the pH, its cyclic original tautomer undergoes a ring opening with the formation of protonated forms (Scheme 40). HFO can be hydrolyzed to succinic acid, however, it is a slow process in aqueous solution. In NaOH solution at pH 9–10, a complete conversion of HFO to succinic acid is rapidly achieved (Scheme 41) [126].

Substitution and condensation reactions of HFO (crude from furfural oxidation without isolation) produce 5,5'-oxybis(furan-

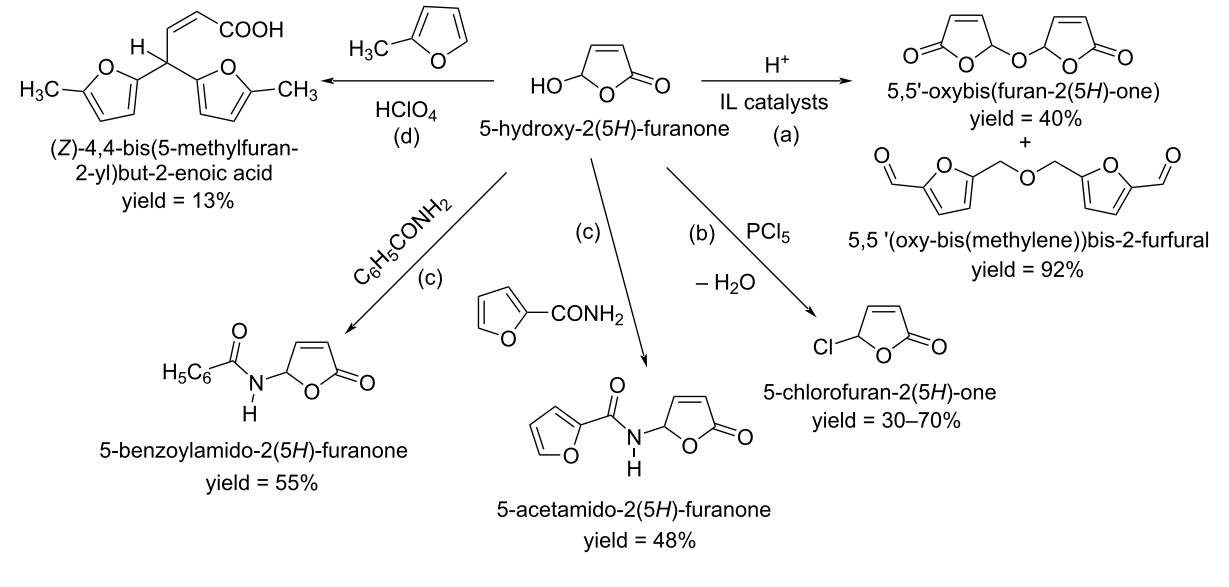


Scheme 40: Tautomeric transformation of HFO to formylacrylic acid.



Scheme 41: Hydrolysis of HFO to succinic acid in aqueous solution.

2(5*H*)-one) and 5,5 '-(oxybis(methylene))bis-2-furfural [127-129] (Scheme 42, path a). The antimicrobial agent 5-chloro-2(5*H*)-furanone was synthesized by reaction of HFO with thionyl chloride in 30% yield [130], or with phosphorus chloride in 70% yield (Scheme 42, path b) [131]. 5-Acetamido-2(5*H*)-furanone is obtained in 20–40% yield when acetamide reacts with 5-bromo- or 5-ethoxy-2(5*H*)-furanone [132-135], while 5-acetamido-2(5*H*)-furanone and 5-benzoylamido-2(5*H*)-furanone were obtained in 48% and 55% yield, respectively, by reaction of HFO with benzoic acid amide or furan-2-carbox-



Scheme 42: Substitution and condensation reactions of 5-hydroxy-2(5*H*)-furanone (HFO).

amide in 1:1 molar ratio at 70 °C for 4–8 h (Scheme 42, path c) [132]. The reaction of HFO with 2-methylfuran in a 1:2.2 molar ratio in diethyl ether solution at room temperature in the presence of catalytic amounts of perchloric acid for 5 hours led to the formation of *gem*-bis-4,4-(5-methyl-2-furyl)-2-butenoic acid in 13% yield (Scheme 42, path d) [131].

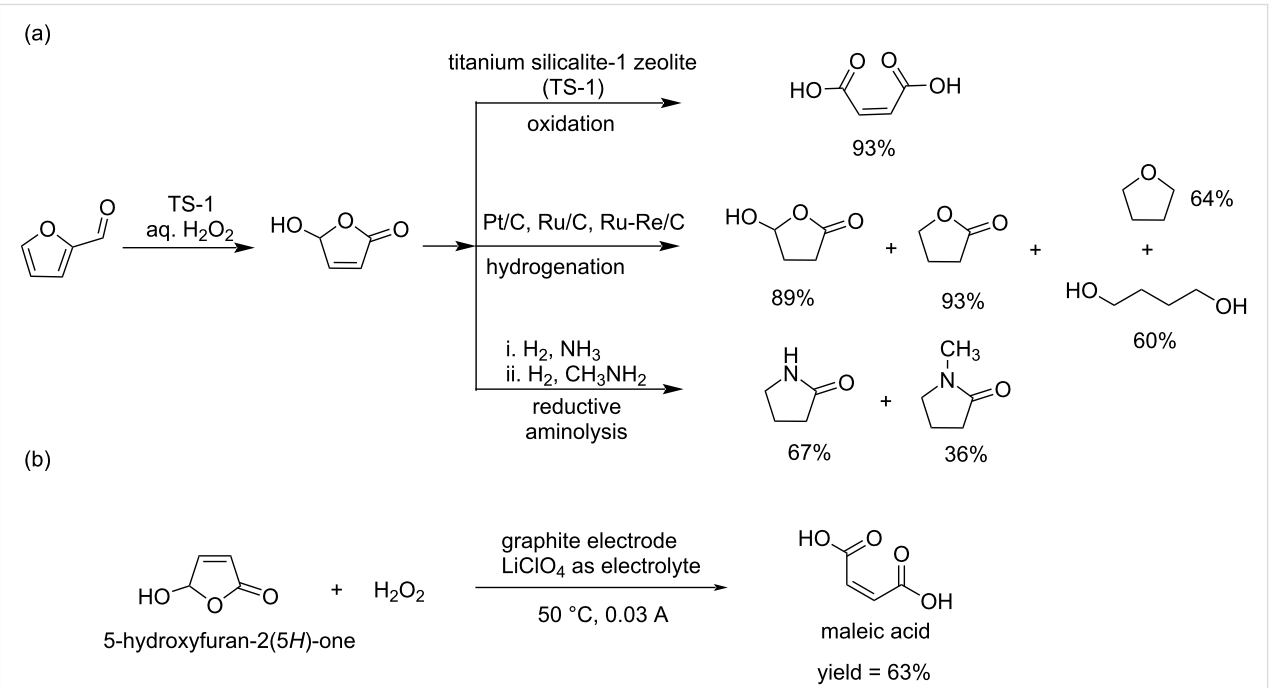
Industrial chemicals with four carbon structures like pyrrolidines, 1,4-butanediol, maleic acid, and butyrolactone are often petroleum-based. However, developing sustainable biomass-derived routes for these compounds remains challenging. In a significant advancement, Shrotri et al. demonstrated an efficient catalytic process for synthesizing C_4 chemicals from biomass-derived hydroxymethylfurfural (HMF) using a TS-1 catalyst under mild reaction conditions [136]. Their work showed that HFO, when processed at moderate temperatures (100–150 °C), could be selectively converted into valuable C_4 products with remarkable yields: maleic acid and γ-butyrolactone were both obtained in 93% yield, while 1,4-butanediol, tetrahydrofuran, and 2-pyrrolidone were produced in 60%, 64%, and 67% yields, respectively (Scheme 43a). In this field, Badovskaya and co-workers chose the anodic oxidation of HFO with H_2O_2 using electrodes made of graphite and $LiClO_4$ as supporting electrolyte at 50 °C and 0.03 A current, providing maleic acid in 63% yield (Scheme 43b) [129].

There are other important conversions of HFO serving as a C_4 building block applied in the synthesis of many different substances. These are summarized in Figure 3 below [120,137-147].

Other furanones

Several other furanones are key intermediates towards important chemicals. For example, the direct oxidation of furfural under aerobic conditions provides maleic anhydride via the successive oxidative decarboxylation of furfural to furan, the oxidation of furan to furanone, and the final oxidation of furanone to maleic anhydride in the presence of VO_x/Al_2O_3 catalysts (Scheme 44, route a) [148]. When using a vanadium phosphorus oxide catalyst (VPO), furoic acid was also found to be a key intermediate (Scheme 44, route b) [149]. A photocatalytic access to succinic anhydride from furoic acid using catalytic porphyrin H_2TPP in the presence of O_2 and light was also reported [150].

Yang and Lv reported the oxidation of furfural to succinic acid in 88% yield under mild conditions using modified hydrophilic acidic metal-free graphene oxide (GO) as solid acid catalyst and H_2O_2 as an oxidant [151]. The suitable acidity of the SO_3H group on the graphene oxide support is crucial for the selectivity of the oxidation. The use of the Lewis acidic Sn-Beta was also reported for this reaction providing succinic acid in 53% yield. Sn-Beta accelerated the Baeyer–Villiger oxidation of furfural to the 2(3*H*)-furanone intermediate by activating furfural (Scheme 45) [152]. Two methods, one using CO under palladium catalysis, and one using electrocatalysis and CO_2



Scheme 43: (a) Conversion of HFO towards valuable C_4 chemicals and (b) anodic oxidation of 5-hydroxy-2(5*H*)-furanone to maleic acid.

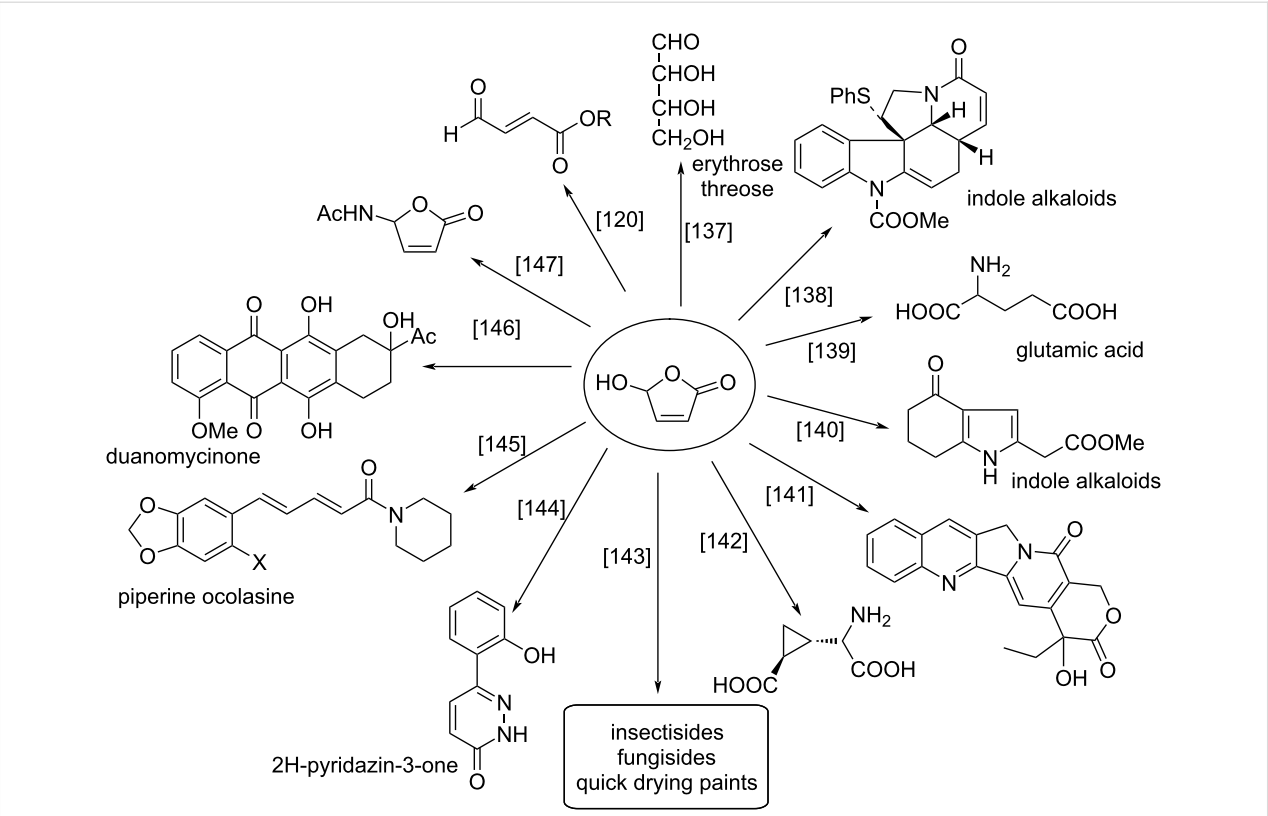
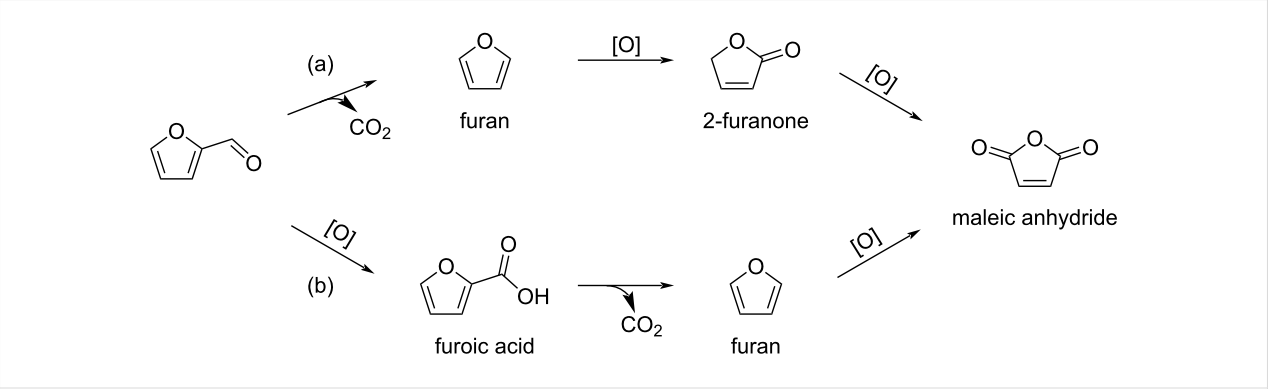


Figure 3: Conversion of HFO towards other natural and synthetic substances.



Scheme 44: Conversion of furfural to maleic anhydride (reaction a: VO_x/Al_2O_3; reaction b: VPO).

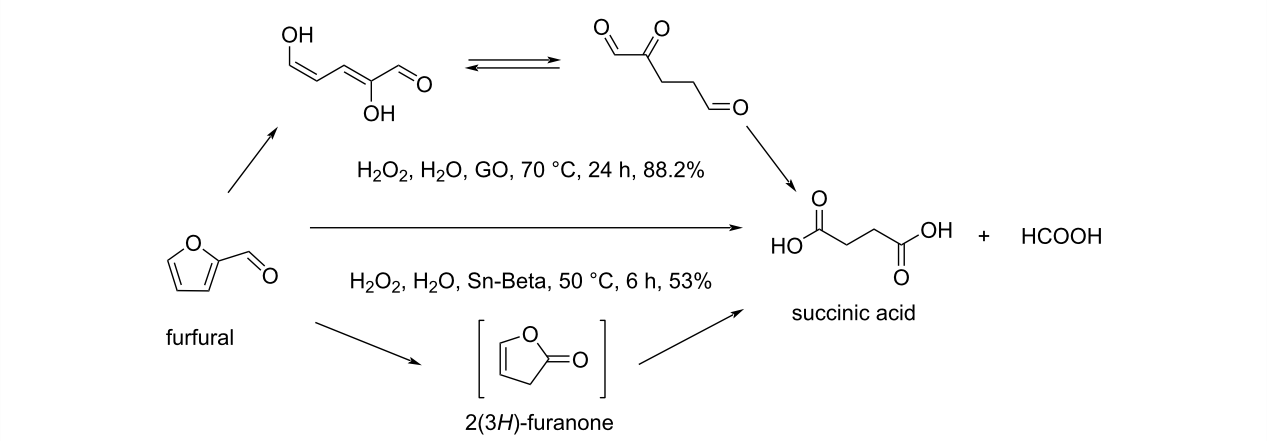
have been reported to produce furandicarboxylic acid (FDCA) from bromofuroic acid [153,154].

A combined electro-, photo-, and biocatalytic approach to several different C_4 chemicals from furfural, including maleic acid, D-malic acid, L-malic acid, fumaric acid, and L-aspartic acid has been reported (Scheme 46). Maleic acid was produced in 97% yield through the electrochemical oxidation of furfural with 4-acetamido-2,2,6,6-tetramethylpiperidine-*N*-oxyl (ACT) and the photooxygenation with eosin Y (EY). Maleic acid was then selectively converted to D-malic acid, L-malic acid, fumaric acid and L-aspartic acid by biocatalysis in 91%, 79%, 94%, 97% yield, respectively, in the presence of enzymes such as maleate hydratase, maleate *cis–trans* isomerase, fumarase, or L-aspartase [155].

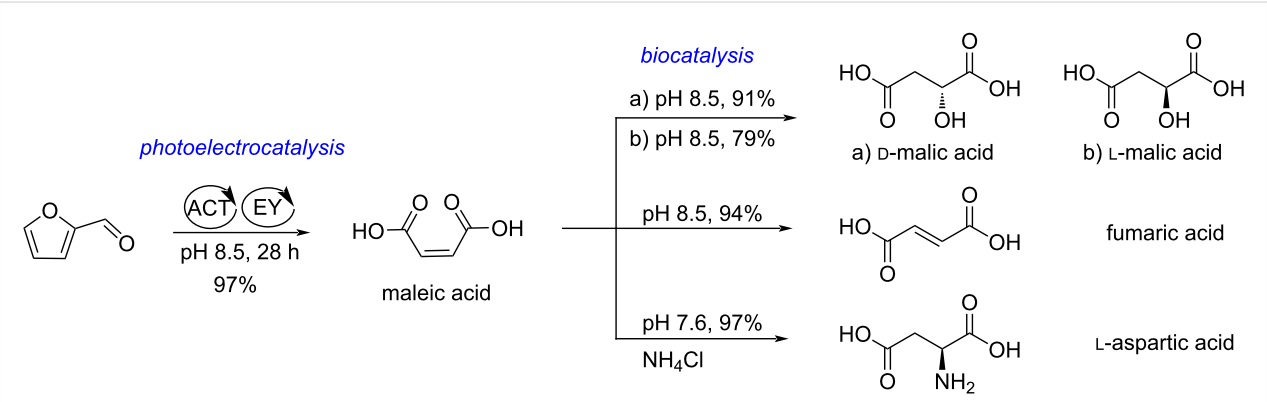
C_5 biobased carbonyl platforms

Furfural

Furfural is a versatile biobased C_5 platform molecule which plays an important role in the biorefining industry. It was first



Scheme 45: Conversion of furfural into succinic acid.

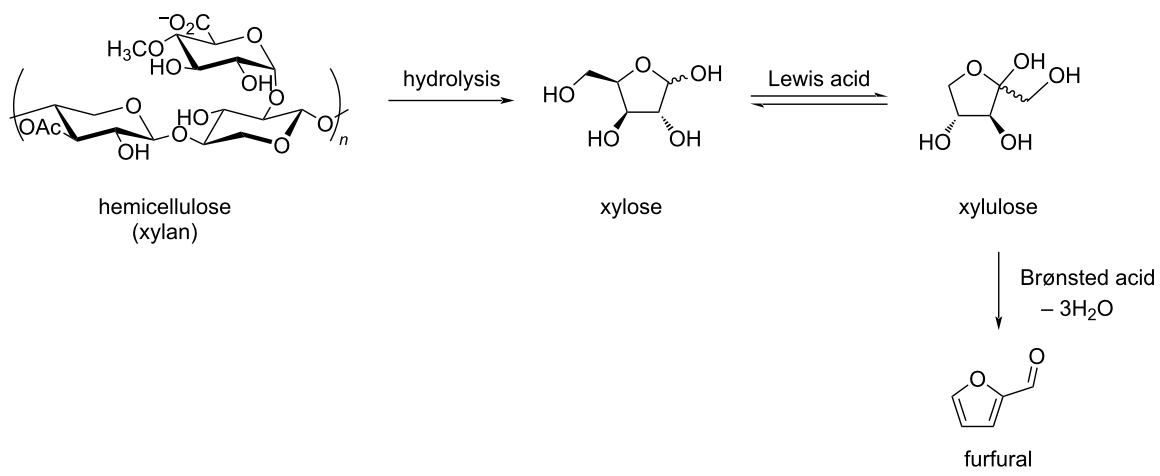


Scheme 46: Electro-, photo-, and biocatalysis for one-pot selective conversions of furfural into C_4 chemicals.

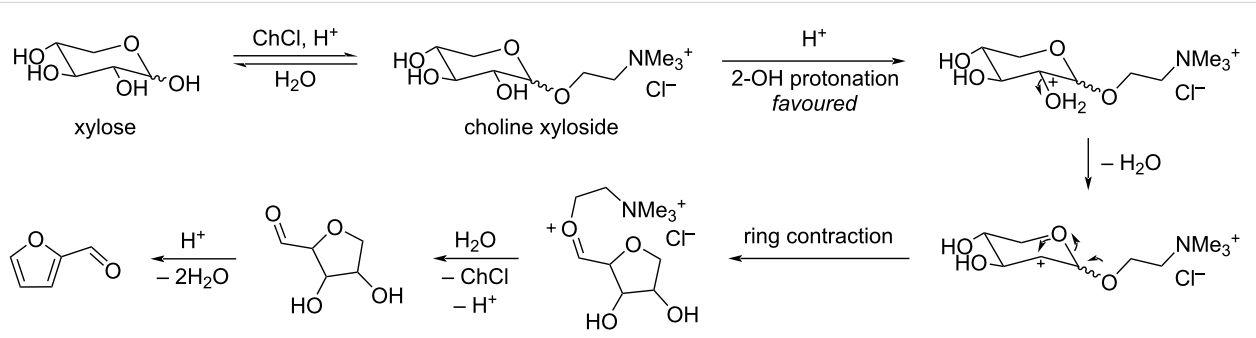
isolated in 1832 by the German chemist Johann Wolfgang Döbereiner, and its structure was determined in 1901 by German chemist Carl Harries. In 1922, the Quaker Oats Company produced furfural on a large scale using oat hulls. Since, many efforts have addressed several issues of the original industrial process, such as low yield, high energy consumption, difficult treatment of acidic aqueous waste and other wastes. Furfural is now produced on an industrial scale in batch or continuous reactors from lignocellulosic resources such as bagasse, corncobs, stalks, switchgrass and hardwoods [156-162], thanks to preliminary selective dissolution and depolymerization of hemicellulose into pentose sugars. Deep eutectic solvents were recently shown to allow fractionation of lignin and production of furfural from lignocelluloses [163]. The hydrolysis and dehydration process of hemicellulose can be accomplished in water or in aqueous-based biphasic systems in the presence of mineral acids (such as H_2SO_4, HCl) and organic acids (such as HCOOH, CH_3SO_3H). The acid catalysts used for furfural production range from homogeneous catalysts such as mineral acids, organic acids, metal salts (with high availability and low costs) to heterogeneous ones such as zeolites, metal oxides, sulfonated polymers, carbon-based solid acids. The latter allow to overcome the problems of separation encountered with homogeneous catalysis. The mechanism first involves the isomerization of xylose into xylulose under Lewis acid-type catalysis, and the subsequent dehydration of xylulose into furfural under Brønsted acid-type catalysis (Scheme 47).

Humins are naturally formed in all processes involving the acid-catalyzed degradation of carbohydrates [164,165]. Attempts to improve the balance between furfural and humins in high feed of starting xylose have been reported, for example by addition of choline chloride which is beneficial to the transformation of xylose to furfural in the presence of HCl (Scheme 48). The faster furfural formation rate is due to the formation of an intermediate choline xyloside which undergoes easier dehydration than xylose itself [166].

The examples given in the following sections illustrate the extremely vast range of reported transformations [160,167-176]



Scheme 47: Production route of furfural from hemicellulose.

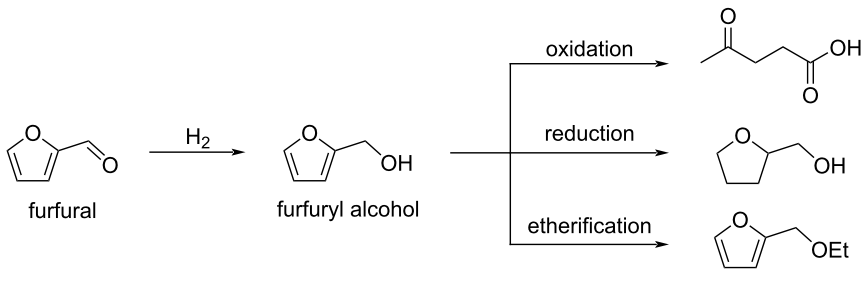


Scheme 48: Mechanism for xylose dehydration to furfural through a choline xyloside intermediate.

of furfural toward useful biobased functional compounds or intermediates with applications in fuels, polymer chemistry and fine organic synthesis (CH activation, Piancatelli rearrangement, etc.).

Conversion of furfural to alcohols, aldehydes and ketones: One of the most important transformations of furfural is its hydrogenation to produce furfuryl alcohol. This latter is a versatile intermediate for the production of resins, coatings, polymers and used as a solvent. It can also be converted into other chemicals through oxidative cleavage, over-reduction and etherification (Scheme 49) [177].

Zhang et al. reported the use of Lewis acid–base bifunctional catalyst (Zr-β zeolite and K_2CO_3) in the Meerwein–Ponndorf–Verley reduction of a concentrated furfural



Scheme 49: Conversion of furfural to furfuryl alcohol and its derivatives.

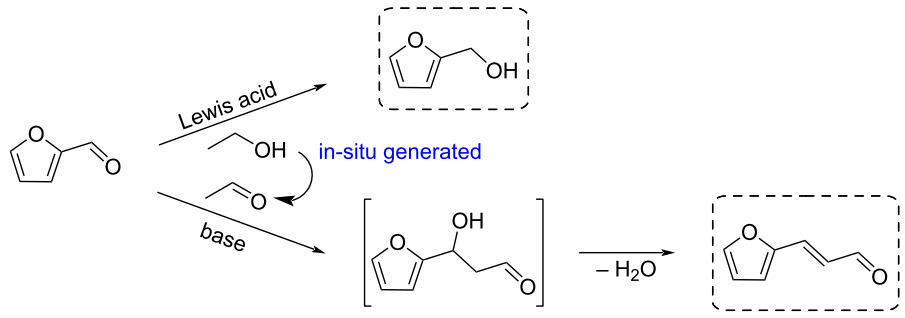
solution (17.3–80.5 wt % in ethanol) combined with in situ cross-aldol condensation with acetaldehyde and crotonization. Ethanol was used as hydrogen donor for the Meerwein–Ponndorf–Verley reduction, while acetaldehyde is generated in situ by ethanol oxidation (Scheme 50). The equilibrium allows furfural to be simultaneously converted into furfuryl alcohol and 3-(2-furyl)acrolein in one pot through a redox reaction. The highest mass conversion rate of furfural can reach up to 95.3 $g \cdot L^{-1} \cdot h^{-1}$ [178].

While furfural oxidation is an important way to reach C_4 platforms such as HFO [(see section 5-Hydroxy-2(5*H*)-furanone (HFO)], interesting C_5 platforms can also be obtained. An example is the work by Shi et al. who reported the aerobic oxidative condensation of furfural with linear alcohols using Cu_2O–LiOH catalytic system or under oxygen, thus achieving a carbon-chain increase from C_5 to C_{7-11} with potential applications in the field of liquid fuels. The conversion of furfural is up to 99.9%, while the selectivity of the corresponding aldehyde is up to 96.9%. The catalyst could be recovered and reused five times without significant loss of activity (Scheme 51) [179].

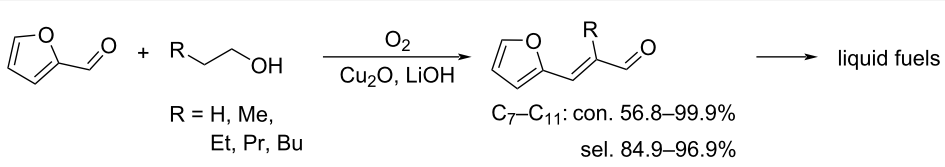
Furfural can be converted to 2-pentanone via simultaneous hydrodeoxygenation, ring-opening, and hydrogenation reactions under catalysis by a bimetallic Cu–Ni/SBA-15 catalyst in a fixed-bed continuous flow reactor. The moderate acidity and the hierarchical tube-type porous nature of SBA-15, as well as the adsorption energy on the surface of 10Cu–5Ni/SBA-15 catalyst, are the key parameters for giving 2-pentanone with high selectivity (78%) (Scheme 52) [180].

Wang developed a new route for the production of jet fuel precursors through the electrocatalytic highly selective coupling reaction of furfural and levulinic acid. The Ni^{2+} species serves as the active site for the coupling process (Scheme 53) [181]. A similar strategy involving phenolic compounds and furfural allowed the production of bicyclic alkanes, used as fuel additives, by hydrodeoxygenation catalyzed by iridium/rhenium oxide supported on silica [182].

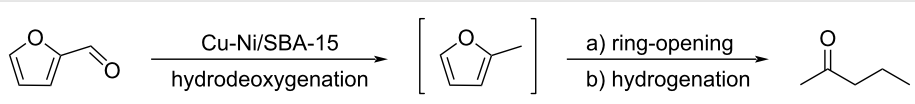
Conversion of furfural to amines: The synthesis of *m*-xylylenediamine from furfural and acrylonitrile through a Diels–Alder/aromatization sequence was developed by Wischet and Jérôme [183]. 2-(Furan-2-yl)-1,3-dioxolane with higher reactivity was generated through the acetalization of furfural with ethylene glycol, and converted to Diels–Alder cycloadducts in the presence of acrylonitrile at 60 °C. Treatment of the Diels–Alder adduct in basic conditions allowed the rearomatiza-



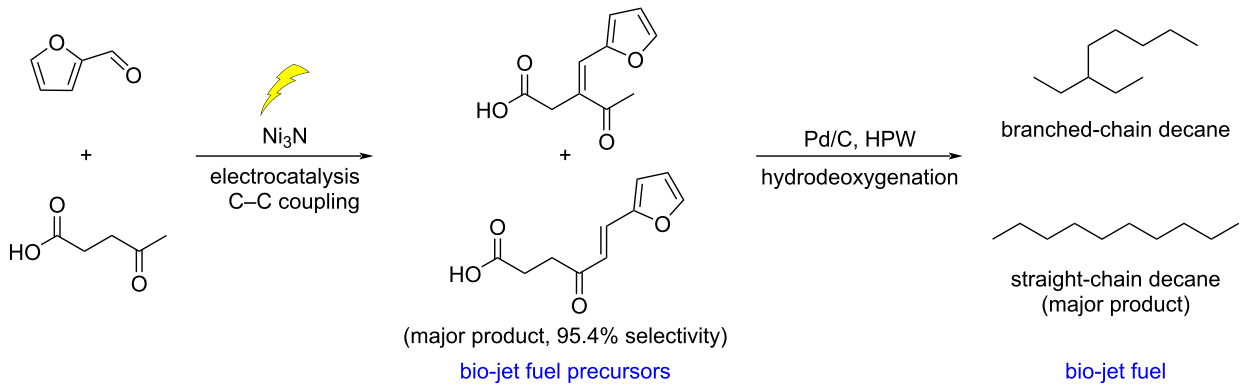
Scheme 50: Conversion of furfural to furfuryl alcohol and 3-(2-furyl)acrolein.



Scheme 51: The aerobic oxidative condensation of biomass-derived furfural and linear alcohols.



Scheme 52: The single-step synthesis of 2-pentanone from furfural.

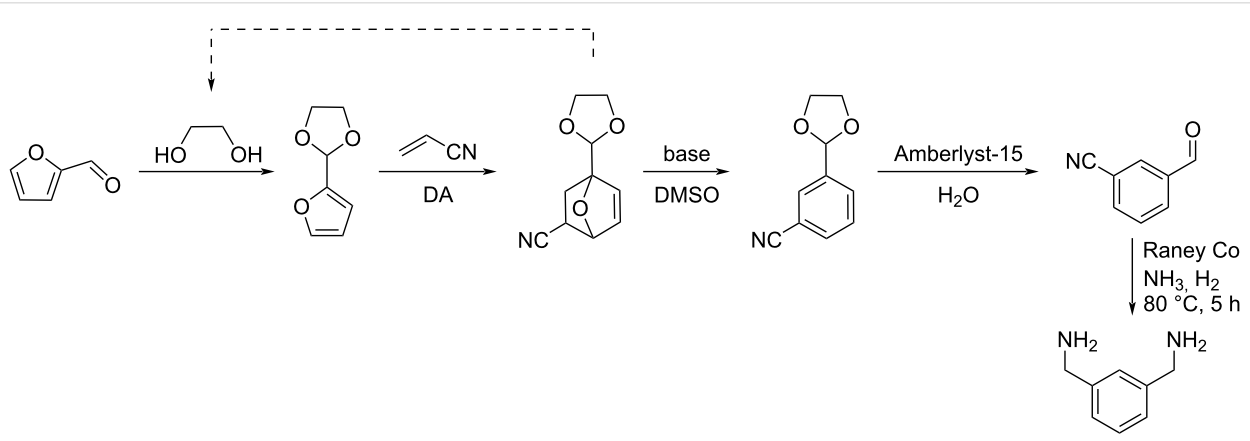


Scheme 53: Electrocatalytic coupling reaction of furfural and levulinic acid.

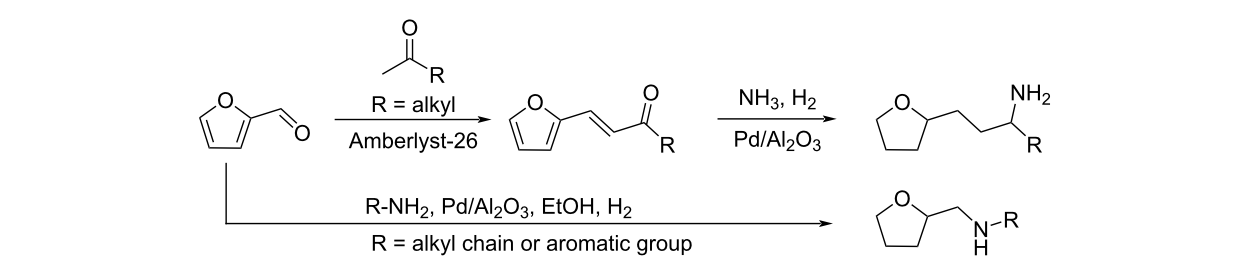
tion of the system in favor of *meta* isomer. Acidic cleavage followed by reductive amination afforded *m*-xylylenediamine (Scheme 54).

Tetrahydrofuran-derived amines were prepared from furfural via a one-pot two-step reaction. The condensation of furfural with ketones over Amberlyst-26 as catalyst produced intermediate furan-derived enones. Subsequent reductive amination was performed in the presence of ammonia or amines and Pd/Al_2O_3 under H_2 pressure, providing the tetrahydrofuran-derived amines [184]. The same catalytic system could allow the one-pot preparation of tetrahydrofuran-derived secondary and tertiary amines from furfural and amines with total reduction of the aromatic ring, as reported by Pera-Titus and De Oliveira Vigier (Scheme 55) [185].

A 2018 study reported the aza-Piancatelli reaction of furfural and secondary amines in deep eutectic solvent based on the



Scheme 54: Conversion of furfural to *m*-xylylenediamine.



Scheme 55: Conversion of furfural to tetrahydrofuran-derived amines.

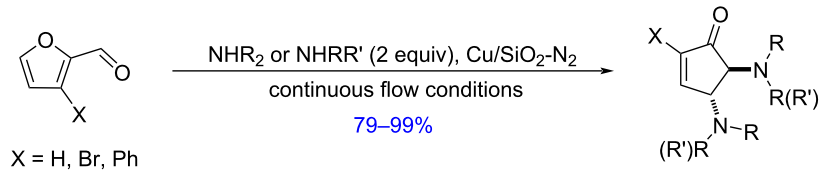
ChCl–urea mixture furnishing *trans*-4,5-diamino-cyclopent-2-enones and 2,4-diaminocyclopent-2-enones [186]. In 2021, Coelho and Afonso prepared a silica-supported copper catalyst (Cu/SiO_2-N_2) by impregnation with copper nitrate, and used it for the reaction of furfural with secondary amines (alkyl, cyclic and aromatic) to produce *trans*-4,5-diaminocyclopent-2-enones in hexane/isopropanol solvent mixture under continuous flow conditions (Scheme 56). The scope could be extended to 2-substituted *trans*-4,5-diaminocyclopent-2-enones by using 3-substituted furfurals [187]. A copper triflate-based analogous strategy was also reported [188].

Conversion of furfural to pyrrole and proline: Zhou and Yan reported a route bridging commercial biomass feedstock with high-value *N*-containing chemicals through pyrrole as a hub molecule. Furfural was converted into pyrrole in 75% yield via tandem decarbonylation–amination reactions over tailor-designed Pd@S-1 and H-beta zeolite catalytic system, exhibiting high resistance to coking in presence of NH_3. Subsequent carboxylation with CO_2 and hydrogenation over Rh/C as catalyst led to racemic proline, an important precursor for pharmaceuticals, in quantitative yield. D-Proline was then obtained in 50% yield and 99% ee after kinetic resolution using *Escherichia coli* (Scheme 57) [189].

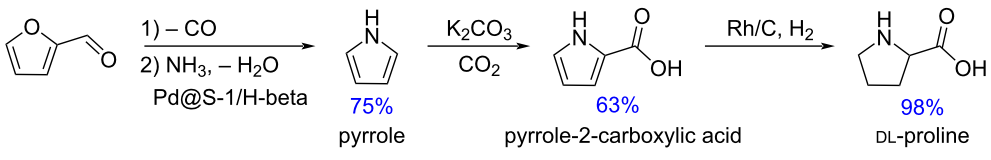
Other reactions: Yamamoto synthesized 6-hydroxy-2-(trifluoromethyl)-2*H*-pyran-3(6*H*)-ones from furfural via trifluoromethylation using the Ruppert–Prakash reagent ($TMSCF_3$), followed by a photo-Achmatowicz reaction. Then, through acetylation and subsequent base-mediated oxidopyrylium [5 + 2] cycloaddition reactions, 1-(trifluoromethyl)-8-oxabicyclo[3.2.1]oct-3-en-2-ones were prepared (Scheme 58) [190].

Chu and Webster reported the photocatalyzed synthesis of furfural-derived diacids from furfural [191,192]. Furfural first was reacted with malonic acid to produce *trans*-3-(2-furyl)acrylic acid in a Knoevenagel reaction, which was then converted into cyclobutane-containing diacids through a [2 + 2] photoreaction. *cis*-3,4-Di(furan-2-yl)cyclobutane-1,2-dicarboxylic acid (CBDA-2) prepared under blacklight UV irradiation was proven to be thermally, chemically and sunlight stable. The esterification of *trans*-3-(2-furyl)acrylic acid with ethanol, provided (1α,2α,3β,4β)-2,4-di(furan-2-yl)cyclobutane-1,3-dicarboxylic acid (CBDA-5) via a solvent-free [2 + 2] photodimerization from ethyl 2-furanacrylate and subsequent hydrolysis (Scheme 59).

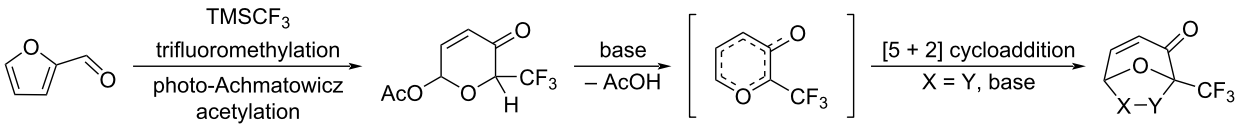
Furfural was employed as starting scaffold in a protocol developed to form acetals as fuel additives. The acyclic acetal is generated in situ from crude furfural with propanol in dimethyl carbonate using a nanoporous aluminosilicate material Al-13-(3.18) as catalyst, and then undergoes transacetalization with glycerol to produce a mixture of corresponding dioxane and dioxolane products (Scheme 60) [193].



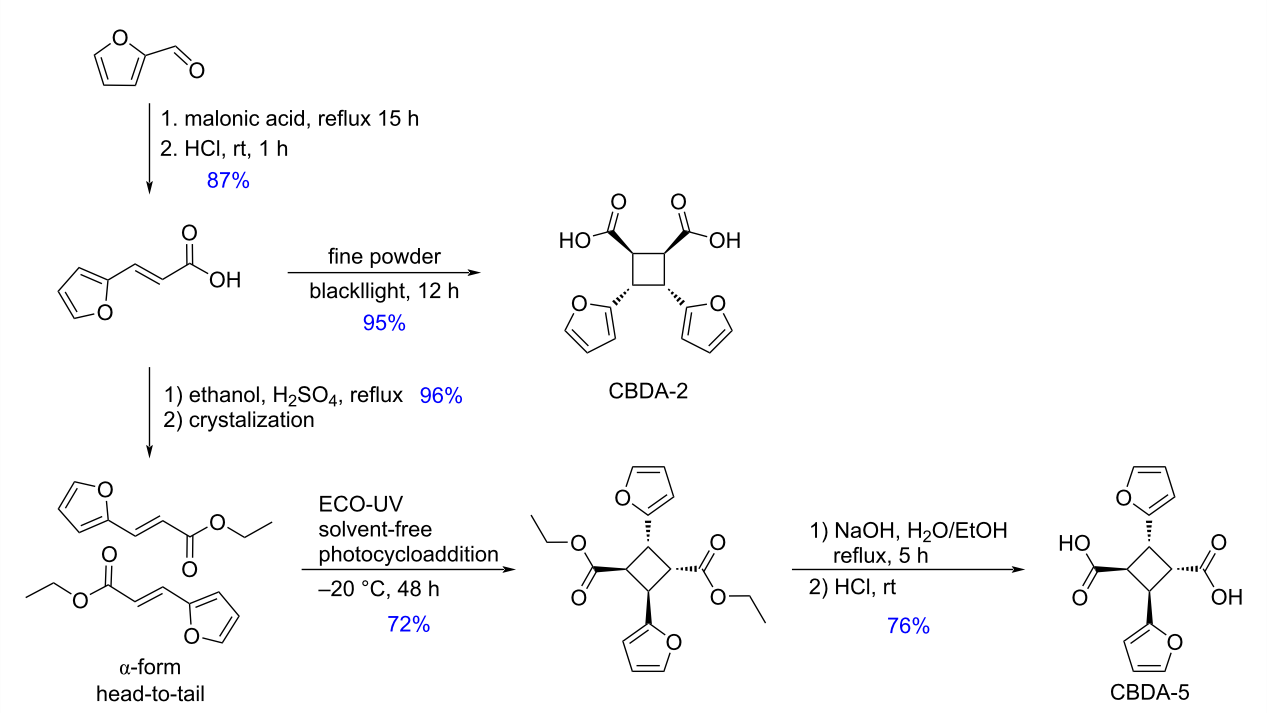
Scheme 56: Formation of *trans*-4,5-diamino-cyclopent-2-enones from furfural.



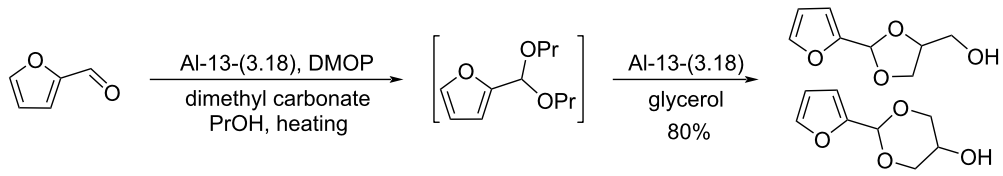
Scheme 57: Production of pyrrole and proline from furfural.



Scheme 58: Synthesis of 1-(trifluoromethyl)-8-oxabicyclo[3.2.1]oct-3-en-2-ones from furfural.



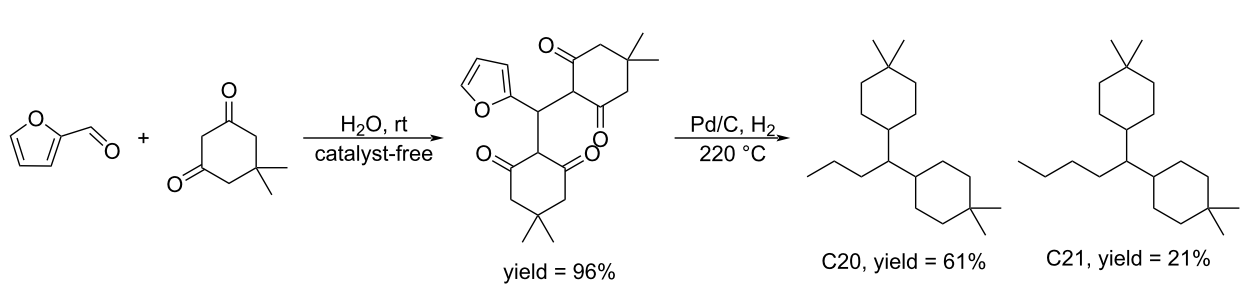
Scheme 59: Conversion of furfural to furfural-derived diacids.



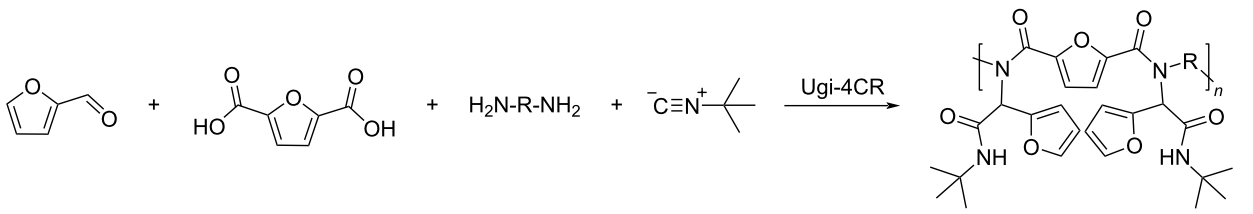
Scheme 60: A telescope protocol derived from furfural and glycerol.

Another strategy was proposed to synthesize potential aviation biofuels from furfural and 5,5-dimethyl 1,3-cyclohexanedione in water or under solvent-free conditions (Scheme 61). The obtained hydrocarbons exhibited higher density (0.78–0.88 g/cm^3) and higher net heat of combustion (44.0–46.0 MJ/kg) than some commonly commercial fuels [194].

Multicomponent reactions involving the reactivity of furfural are also noteworthy. A Ugi four-component polymerization was developed to synthesize photoluminescence-active polyamides from renewable furfural and 2,5-furandicarboxylic acid with diamine and isocyanide (Scheme 62). The intramolecular hydrogen bonding between the secondary amide and furan oxygen



Scheme 61: A tandem cyclization of furfural and 5,5-dimethyl-1,3-cyclohexanedione.



Scheme 62: A Ugi four-component reaction to construct furfural-based polyamides.

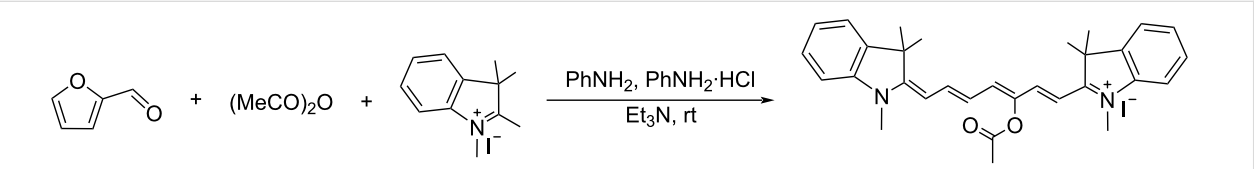
atom promote the strong fluorescence of the polyamides. These furfural-based polyamides possess unusual intrinsic luminescence and high and selective affinity towards Fe^{2+} and Fe^{3+} metal ions, which could be used as fluorescent probes in the biomedical field [195].

Heptamethine cyanine Cy7 is a very important class of intermediates in the fields of biology and photomedicine. The introduction of substituents to the seven-methine carbon chain of Cy7 influences its optical properties and ability to interact with biomolecules. A one-pot synthesis of γ-acyloxy-Cy7 from renewable furfural, simple anhydrides, and a quaternary ammonium salt under smooth conditions was reported (Scheme 63). Partial γ-acyloxy-Cy7 possesses a high fluorescence quantum yield and high photothermal conversion efficiency in PBS, two pivotal parameters in fluorescence imaging and image-guided photothermal therapy [196].

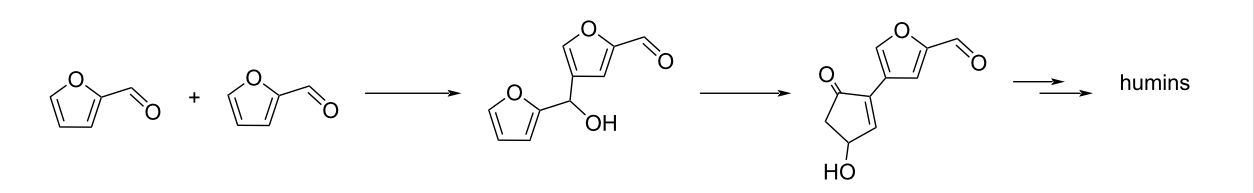
A dimerization of furfural has been found to occur at the early stage of formation of humins, arising from a nucleophilic attack of a furan carbon atom of one furfural molecule onto the aldehyde of a second one, giving 2-(4-furfur-2-al)-4-hydroxy-2-cyloepenten-1-one (Scheme 64), resulting from a Piancatelli rearrangement. This latter can further evolve towards more complex humin precursors by etherification and aldol reactions [197].

Cyclopentanone (CPN)

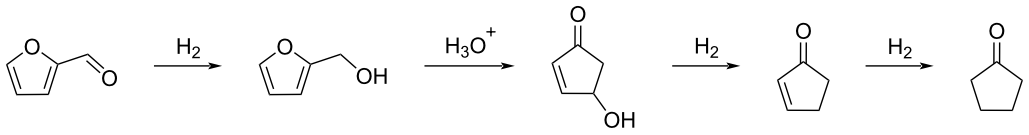
Cyclopentanone (CPN) can be prepared by catalytic hydrogenation and Piancatelli rearrangement of furfural (Scheme 65). This is a biobased alternative to the fossil-based process relying on the intramolecular decarboxylative cyclization of adipic acid. In the biobased reaction from furfural to CPN, the key points influencing the selectivity and yield are the choice of metal catalyst, hydrogen pressure and supporting acidic materials [168,198]. When carried out in aqueous medium, the reaction was found to provide better selectivity by limiting the generation of other hydrogenation products than in organic solvents [199]. Since this new route to CPN from furfural was reported in 2012, many catalysts have been proposed for promoting this reaction. Recent works include heterogeneous systems based on cobalt [200], nickel [201], copper [202] or palladium [203]. Biobased CPN can also be directly obtained from C-5 carbohydrates. For example, Zhang and Li recently reported a two-step route directly from xylose (or hemicellulose) going through cyclopentenone as intermediate. A subsequent hydrodeoxygenation/dehydrogenation sequence led to cyclopentadiene, or methylcyclopentadiene upon additional aldol condensation with



Scheme 63: One-pot synthesis of γ-acyloxy-Cy7 from furfural.



Scheme 64: Dimerization–Piancatelli sequence toward humins precursors from furfural.



Scheme 65: Conversion of furfural to CPN.

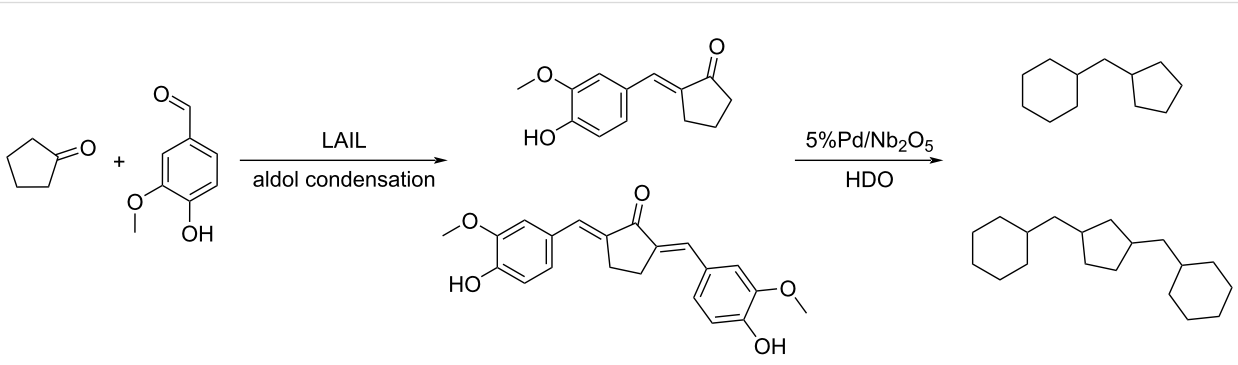
in situ generated formaldehyde, both highly useful intermediates for the production of high-energy-density rocket fuels and polymers [204].

Conversion of CPN to hydrocarbons: CPN can be used as a precursor to produce high-octane diesel or jet fuel additives through aldol condensation/hydrogenation sequences. The acyclic or cyclic chain hydrocarbons can be formed under hydrodeoxygenation conditions after aldol extension of the C–C chain. Dimers and trimers can be obtained from CPN by self-condensation and converted to C_{10} and C_{15} alkane fuels (bicyclopentane, tricyclic alkane and spirocyclic alkane) through hydrodeoxygenation [205-210].

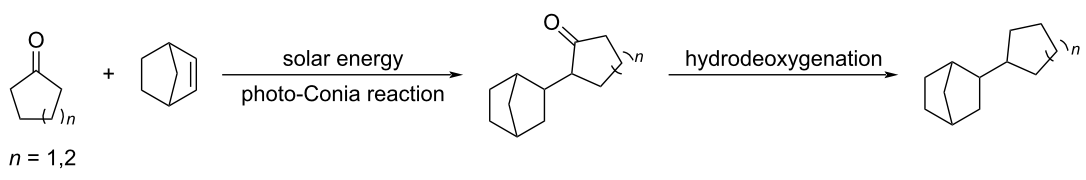
A cycloalkane with a density of 0.89 g/cm^3 and a freezing point below −60 °C was prepared from CPN and lignin-derived vanillin. An overall yield of 95.2% of mono- and di-condensation products was obtained at 100 °C over ethanolamine lactate ionic liquid (LAIL). The condensation products were converted into jet fuels range cycloalkanes through aqueous phase hydrodeoxygenation (HDO) by using 5% Pd/Nb_2O_5 catalyst (Scheme 66) [211].

A new route to novel high-performance aviation fuels driven by solar energy such as non-symmetrical polycyclic hydrocarbons has been proposed by using a photosensitized Conia reaction of ketones and norbornene (Scheme 67) [212]. The hydrocarbons derived from CPN and cyclohexanone endow high density of 0.935 and 0.941 g mL^{-1}, respectively, much higher than conventional aviation kerosene (0.78 g mL^{-1}).

Conversion of CPN to cyclopentylamines and alcohols: Gong and Wang revealed the potential of cobalt oxide catalysts for the production of primary amines via reductive amination of CPN (Scheme 68) [213]. CoO species with oxygen vacancies on the surface have a unique ability to dissociate NH_3 and generate hydrogen-like species ($NH_2^{\delta-}$), thus accelerating the ammonolysis of the Schiff base to produce the corresponding primary amine. Cyclopentylamine was generated from CPN in 96% yield over a core-shell-structured Co@CoO catalyst at

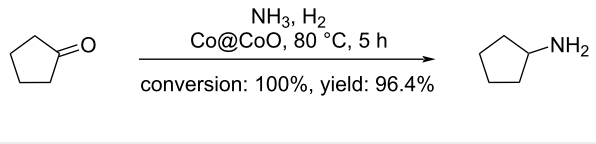


Scheme 66: Synthesis of jet fuels range cycloalkanes from CPN and lignin-derived vanillin.



Scheme 67: Solar-energy-driven synthesis of high-density biofuels from CPN.

80 °C under 0.3 MPa NH_3 and 2 MPa H_2. The reaction could be carried for 10 catalytic cycles without deactivation.

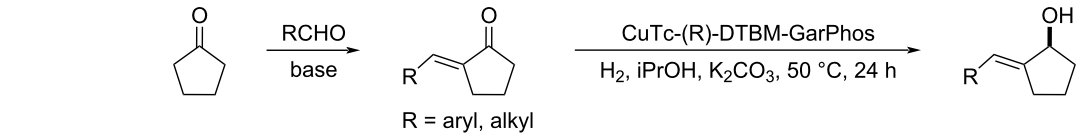


Scheme 68: Reductive amination of CPN to cyclopentylamine.

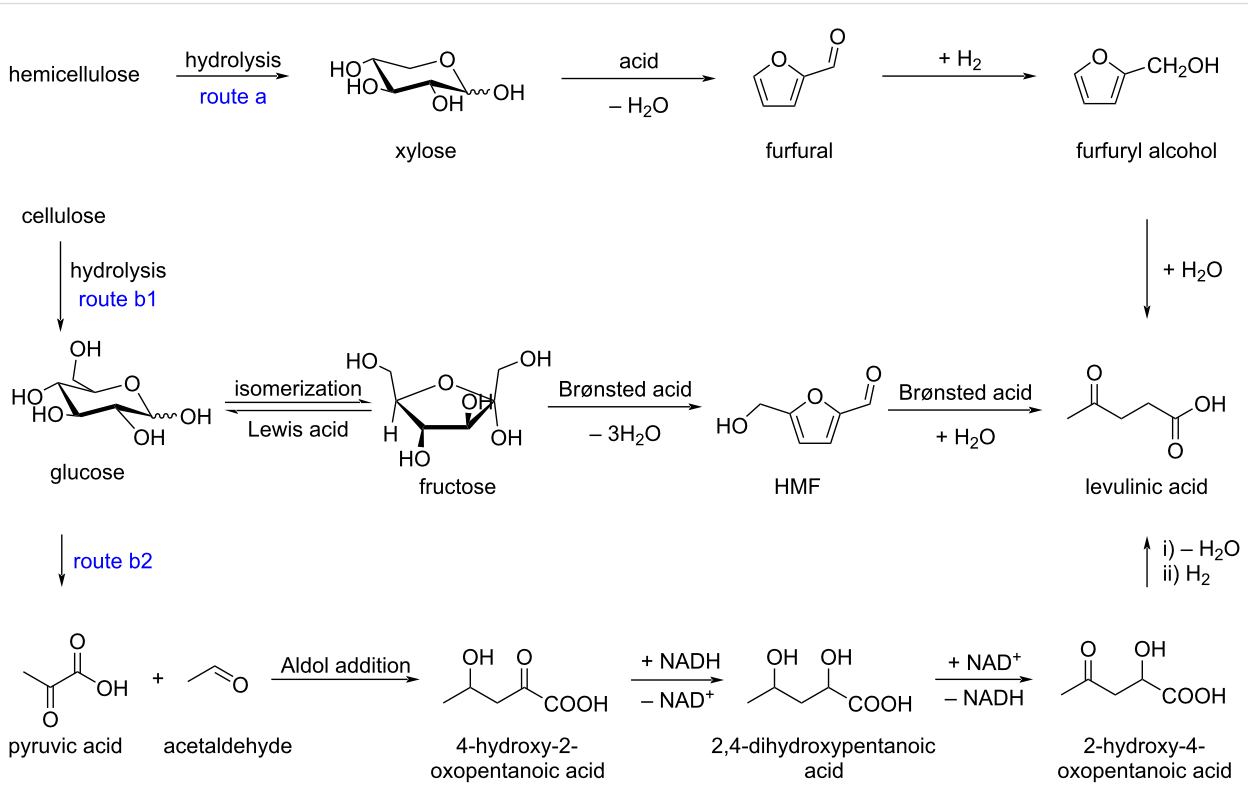
Zhang developed a transition-metal copper-catalyzed chemoselective asymmetric hydrogenation of the carbonyl group in exocyclic α,β-unsaturated cyclopentanones. Chiral exocyclic allylic pentanols (a versatile scaffold for bioactive molecules) with up to 99% yield and 96% ee were prepared (Scheme 69). The large electron-donating groups of 3,5-di-*t*ert-butyl-4-methoxyphenyl (DTBM) improved the activities of the Cu^I–thiophene-2-carboxylate catalyst (CuTc) while the use of (*R*)-DTBM-GarPhos as the chiral ligand led to excellent enantioselective induction during the hydrogenation step. Higher H_2 pressure could promote the regeneration of Cu–H species [214].

Levulinic acid (LEV)

Levulinic acid is a biodegradable C_5 carboxylic acid with high potential as a platform chemical in the field of polymers, fuels, pharmaceuticals or high added value chemicals [215-223]. Its first commercial production began in the 1940s. Its preparation from biomass involves several different possible pathways. One is the C_5 sugar route starting from xylose as an example, relying on acid hydrolysis of hemicellulose, dehydration to furfural, hydrogenation into furfuryl alcohol and final hydrolysis to levulinic acid (Scheme 70, route a). The second route is the acid-catalyzed multistep conversion of polysaccharides into C_6



Scheme 69: Asymmetric hydrogenation of C=O bonds of exocyclic α,β-unsaturated cyclopentanones.



Scheme 70: Preparation of levulinic acid via the C_5 route (route a) or C_6 route (routes b1 and b2).

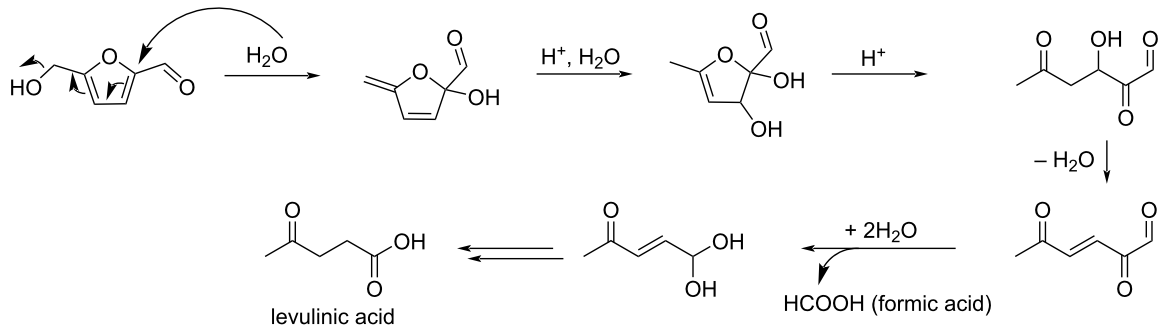
monosaccharides (glucose and fructose), followed by dehydration to 5-HMF, and then rehydration into levulinic acid (Scheme 70, route b1). It is now preferred considering raw material costs, process efficiency and market demand. Alternatively, C_6 monosaccharides can also be fermented to produce pyruvic acid and acetaldehyde, which combine by an aldol reaction and lead to levulinic acid by isomerization and hydrogenation (Scheme 70, route b2).

The accepted mechanism of the rehydration of HMF under acidic conditions leading to the formation of levulinic acid and formic acid proposed by Horvat [224] is depicted in Scheme 71.

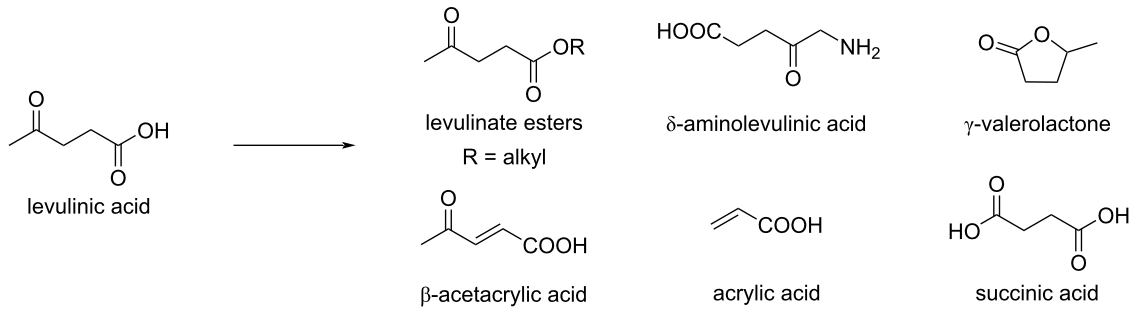
Levulinic acid can be converted into various derivatives, such as esters, amides, lactones, acrylic acid, etc. (Scheme 72) and is therefore a key intermediate in the synthesis of pharmaceuticals, agrochemicals, and other specialty chemicals. Levulinate esters, used as a solvent or as biofuels, are obtained by esterification under acid catalysis, e.g., with a sulfuric acid-modified ultrastable Zeolite Y (SY) [225] or Pd_{NPs}-TiO_2/Al_2O_3/SiO_2 [226].

Conversion to other carboxylic acids: Valeric acid (VA) and valerate esters (VEs), also named pentanoic acid or esters, are targeted as fuel additives and value-added chemicals. They are obtained by hydrogenation of levulinic acid using a wide range of noble or non-noble metal catalysts [227]. For example, treatment of levulinic acid under vapor phase in a continuous fixed-bed with bifunctional mesoporous SBA-15 doped with metals such as Nb, Ti, and Zr having hydrogenation centers and acidic sites led to VA, with GVL and alkyl levulinates obtained as by-products [228]. Xue and Wu reported the electrocatalytic reduction of levulinic acid to VA using a nanocrystalline PbO–In_2O_3 composite material as working electrode in an H-type electrolytic cell [229], while Shen used bimetallic In–Pb electrocatalysts [230], and Tao applied a β-PbO/Pb electrode [231]. Another example reported by the Akula group developed a direct conversion of levulinic acid to VA at 270 °C and ambient H_2 pressure in a continuous flow fixed-bed reactor (Scheme 73) in the presence of Brønsted-acidic material H-ZSM-5-supported W-modified Ni catalyst. The mechanism involves a ring opening of GVL at the Brønsted acidic sites, while the β-proton abstraction occurs on the support surface basic sites [232].

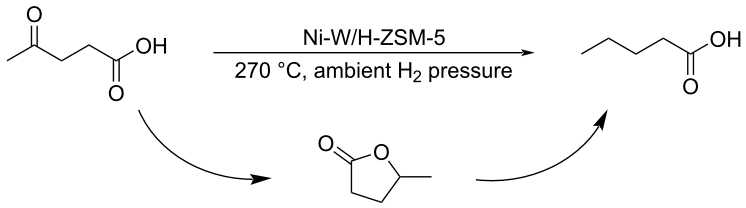
Catalytic aerobic oxidation of levulinic acid towards dicarboxylic acids is a way to obtain monomers for the manufacture of biobased polymers. For example, citramalic acid was obtained with up to 95% selectivity over acetic acid and succinic



Scheme 71: Mechanism of the rehydration of HMF to levulinic acid and formic acid.

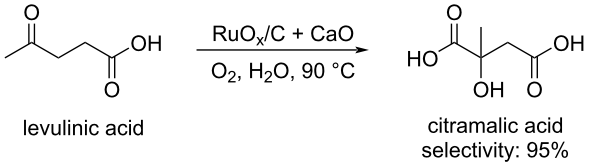


Scheme 72: Important levulinic acid-derived chemicals.



Scheme 73: Direct conversion of levulinic acid to pentanoic acid.

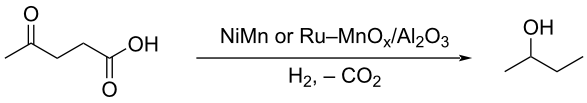
acid using a low-cost reusable heterogeneous RuO_x/C and CaO binary catalyst at 90 °C (Scheme 74) [233]. Levulinic acid can also be efficiently converted into succinic acid [234,235].



Scheme 74: Catalytic aerobic oxidation of levulinic acid to citramalic acid.

Conversion to 1,4-pentanediol or 2-butanol: 1,4-Pentanediol, a useful raw material for the synthesis of polyesters, biofuels and other chemicals, can be obtained from LEV by catalytic hydrogenation. Non-noble metal hydrogenation catalysts are generally more challenging in promoting the conversion of levulinic acid to 1,4-pentanediol because they are more prone to corrosion compared with noble-metal catalysts. This has encouraged the design of highly active and more stable heterogeneous non-noble metal-based catalysts able to tolerate the presence of carboxylic acids, such as those listed in Scheme 75 [236-240].

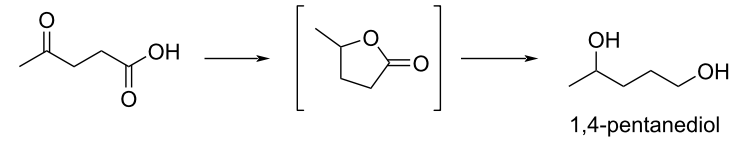
In 2021, Wang reported the high efficiency of the non-precious bimetallic catalyst Ni–Mn in the selective hydrogenolysis of levulinic acid to 2-butanol in 82.5% yield under 5 MPa H_2 at 240 °C (Scheme 76) [241]. The high basicity of the Ni–Mn catalyst results in a good affinity with the C=O or COOH groups of levulinic acid-derived molecules. The same group later reported a more active heterogeneous catalyst, Ru–MnO_x/Al_2O_3, providing 2-butanol with yields up to 98.8% [242].



Scheme 76: Selective production of 2-butanol through hydrogenolysis of levulinic acid.

Conversion to 2-methyltetrahydrofuran: 2-Methyltetrahydrofuran is a promising biofuel with high energy density, high stability and low miscibility with water. Investigations of the catalytic transformation of levulinic acid to 2-methyltetrahydrofuran over bimetallic NiCo/γ-Al_2O_3 catalyst or Ni phyllosilicates have shown that high temperature, high pressure and low selectivity are still important limitations [243,244].

Reductive amination of levulinic acid: The reductive amination of levulinic acid and its esters leads to the formation of *N*-substituted 5-methyl-2-pyrrolidinones (5MPs) which are used in many fields including pharmaceutical and dye industries. Zhang reviewed the synthesis of 5MPs from levulinates and dif-



conditions: a) Ru-MoO_x/AC, 70 °C, 4 MPa H_2, continuous fixed-bed reactor. Yield: 96.7%
b) Au/TiO_2, 200 °C, 50 bar H_2, 4 h, microwave reactor. 100%
c) hcp-Co@G400, 220 °C, 5 MPa H_2, 24 h. 89.5%
d) 0.5CuCo@N-CNT, 160 °C, 5 MPa H_2, 12 h. 87.8%
e) Ru-(0.47)MoOx/TiO_2, 110 °C, 40 bar H_2, 6 h. 91%

Scheme 75: Conversion of levulinic acid to 1,4-pentanediol (a) see ref. [236]; b) see ref. [237]; c) see ref. [238]; d) see ref. [239]; e) see ref. [240]).

ferent substituted amines under metal catalysis or catalyst-free conditions, using hydrosilane, formic acid, hydrogen, MeOH or HCOOH/Et_3N as reducing sources [245]. The type and recyclability of catalysts, the nature of supports, reaction conditions, and reactors play important roles in the sustainability of the conversion of levulinic acid to 5MPs. A well-accepted route from levulinic acid to 5MPs is shown in Scheme 77.

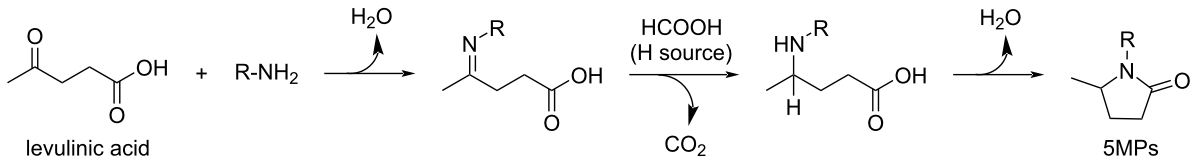
Recent examples of LEV to 5MPs conversions include the use of a ruthenium ion supported on ionic liquid immobilized into graphene oxide (Ru@GOIL), polyvinylpyrrolidone-stabilized metal nanoparticles (Ir–PVP), palladium catalysts synthesized via wet impregnation or Co–M bimetallic C–N doped catalyst (Co–Zr@Chitosan-20) [246-249]. An efficient method for preparing *N*-free 5-methyl-2-pyrrolidone from levulinic acid was developed by Li and Yang using formamide as nitrogen source and formic acid as hydrogen source via transfer hydroamination/amidation and cyclization under quasi solvent-free and catalyst-free conditions [250]. Song and Han designed TiO_2 nanosheets-supported Pt nanoparticles (Pt/P-TiO_2) as porous heterogeneous catalysts with high acidity and low electron density at the Pt sites. Using H_2 as the hydrogen source, such catalysts exhibited high activity for the conversion of LEV to 5MP, being able to promote the formation of a variety of *N*-substituted pyrrolidones at room temperature in excellent yields [251]. In 2022, Liu and Wei synthesized *N*-substituted 5-methyl-2-pyrrolidinones from levulinic acid/esters and various amines in high yields (80–99%) over 0.05 mol % of an N-doped mesoporous carbon-supported Ru catalyst (Ru/NMC) at 120 °C and 1.5 MPa H_2 [252].

Liu and Wang reported the selective reductive amination/cyclization of levulinic acid with primary arylamines in the presence of polymethylhydrosiloxane (PMHS) to *N*-substituted arylpyrroles in a yield range of 35–93%. The 18-crown-6 ether coordinates the cesium ion, thus increasing the nucleophilicity of the fluoride anion. The F^- anion contributes to the activation of the hydrosilane during the reduction step (Scheme 78) [253].

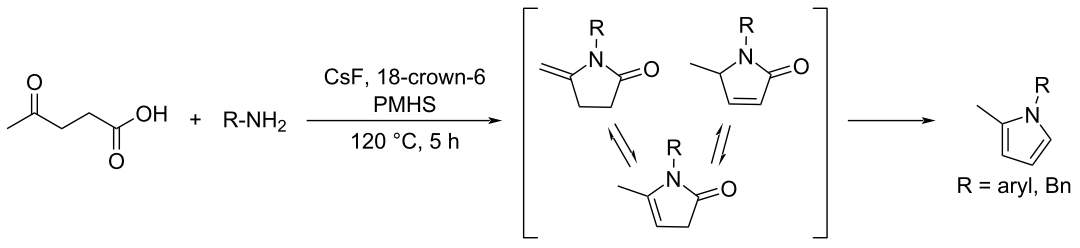
The asymmetric reductive amination of levulinic acid with ammonium acetate can be achieved using commercially available chiral Ru/bisphosphine catalysts, giving 5MPs with excellent enantioselectivity (97% ee) and isolated yield (85%). The chiral 5MPs can then be further functionalized by *N*-alkylation without loss of enantioselectivity (Scheme 79) [254].

Xu and Zheng prepared a non-natural chiral γ-amino acid from levulinic acid in biocatalytic conditions using an engineered amine dehydrogenase *Pm*AmDH$_{I80T/P224S/E296G}$, obtained from a thermophilic bacterium (*Pm*AmDH) by direct evolution in the presence of NaDH. This process leads to (*S*)-4-aminopentanoic acid with >99% ee and 90% yield at 40 °C, and an 18-fold increase in the catalytic efficiency compared with the wild-type enzyme (Scheme 80) [255].

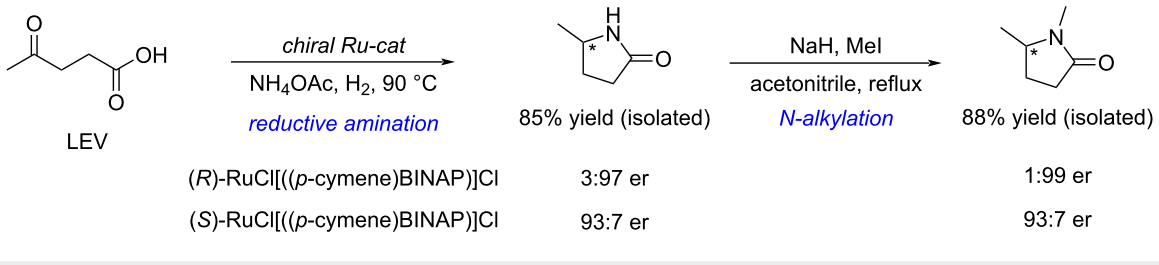
Huang and Lu reported that levulinic acid and hydrazine hydrate can react without a catalyst and in quantitative yield within few minutes in water at room temperature to form the 4,5-dihydro-6-methylpyridazin-3(2*H*)-one (DHMP) platform, in a fashion similar to a click reaction. DHMP can be further selectively converted into pyrrolidine and (alkyl)-pyridazinone



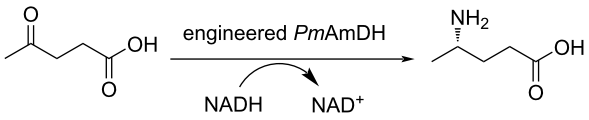
Scheme 77: General reaction pathways proposed for the formation of 5MPs from levulinic acid.



Scheme 78: Selective reductive amination of levulinic acid to *N*-substituted pyrroles.



Scheme 79: Reductive amination of levulinic acid to chiral pyrrolidinone.



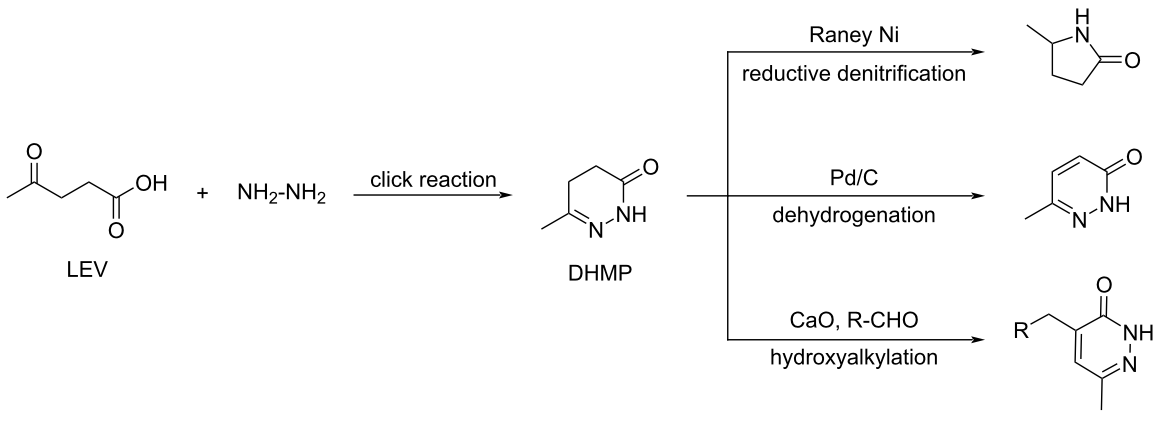
Scheme 80: Reductive amination of levulinic acid to non-natural chiral γ-amino acid.

through reductive denitrification, dehydrogenation and hydroxyalkylation reactions (Scheme 81) [256].

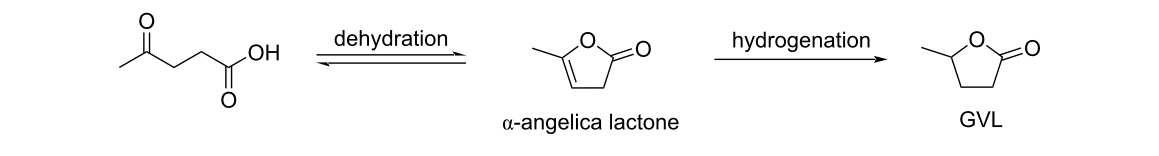
γ-Valerolactone (GVL)

γ-Valerolactone (GVL) is a representative cyclic ester derived from levulinic acid that is commonly used as a biobased solvent with high boiling point (207 °C) able to replace NMP or DMF, and as a chemical platform in various industrial applications [257]. Catalytic production of GVL relies on a dehydration–hydrogenation sequence from levulinic acid via an α-angelica lactone intermediate (Scheme 82) [258]. This has been a hot topic in the past decade with many efficient strategies using various catalysts involving metals such as platinum [259,260], ruthenium [261], titanium [262] or copper [263] as well as other bimetallic species (Ni/Ru, Ni/Mo, Ni/Zn, etc.) [264-268] or in alternative solvents [269].

Studies targeting enantiomerically enriched γ-valerolactone have been also reported. For example, the Bhanage group reported the use of a ruthenium-catalyzed asymmetric transfer hydrogenation of levulinic acid to (*R*)-γ-valerolactone with 93% enantiomeric excess (ee). Using *N*-methylpiperidine with formic acid as an available hydrogen donor and Noyori's chiral catalyst (Ru-(*R*,*R*)-TsDPEN), this route led to 98% LEV



Scheme 81: Nitrogen-containing chemicals derived from levulinic acid.

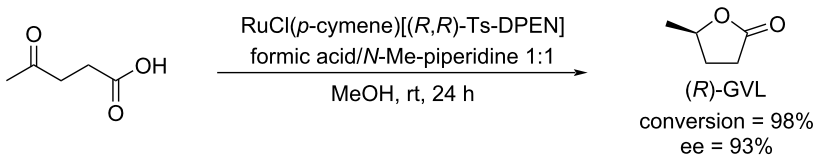


Scheme 82: Preparation of GVL from levulinic acid by dehydration and hydrogenation.

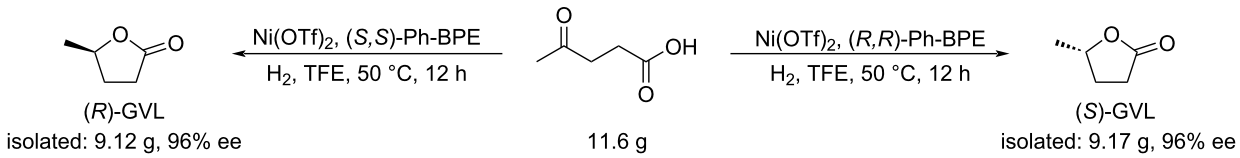
conversion. The direct transformation of LEV obtained from a "raw biomass" resource such as rice husk and corn straw, to optically active GVL was performed by asymmetric hydrogenation with good enantioselectivity (82% ee) (Scheme 83) [270]. Deng and Fu reported the nickel-catalyzed asymmetric hydrogenation of aliphatic ketoacids to chiral γ- and δ-alkyl-substituted lactones. A robust and highly active homogeneous chiral nickel–phosphine catalyst ($Ni(OTf)_2$ with (*S*,*S*)-Ph-BPE) as chiral ligand afforded the chiral lactones in up to 98% yield with 95% ee. A ten-gram scale reaction from LEV to chiral GVL (96% ee) was achieved in the presence of only 0.02 mol % catalyst loading (Scheme 84). (*S*)-GVL could be also obtained by using (*R,R*)-Ph-BPE [271]. The same group used a nickel–phosphine complex [272] or a combination of nickel phosphine complex and metal triflate, both in solvent-free conditions [273].

Uses of GVL in polymer chemistry: GVL is a useful building block for the synthesis of polyesters and other polymers. Kalevaru and de Vries reported the ring-opening reaction of GVL with methanol over ZrO_2/SiO_2 as catalyst in a continuous gas-phase process with 95% conversion towards methyl 2-, 3-, and 4-pentenoate (81% in favor of M4P). Methyl 4-pentenoate was then converted into methyl 5-formylvalerate with 90% selectivity, leading to subsequent generation of ε-caprolactam (the monomer of nylon-6) via reductive amination and ring closure (Scheme 85) [274].

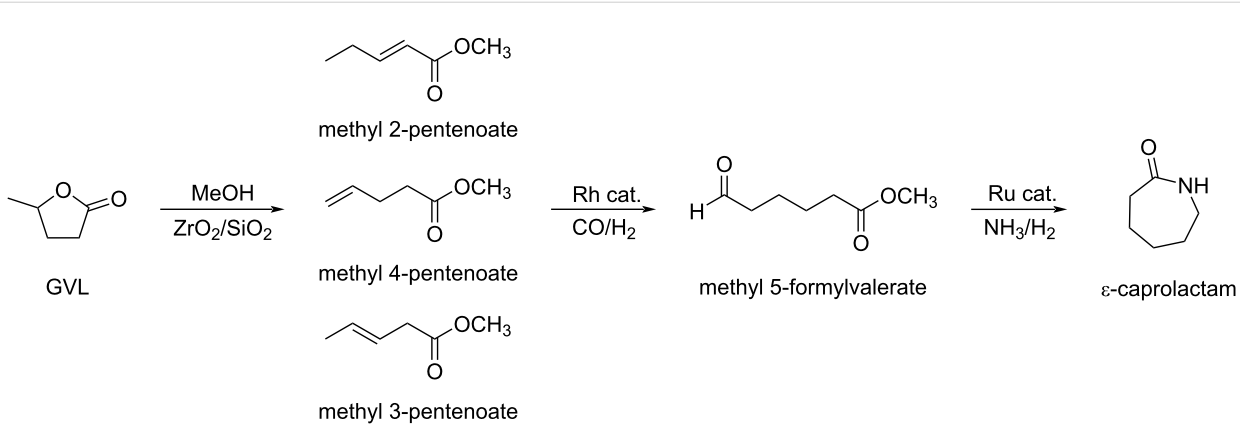
Kim and Han developed a protocol for the synthesis of nylon 6.6 from GVL. After esterification of GVL to methyl-3-pentenoate, subsequent metathesis of methyl-3-pentenoate afforded dimethyl hexenedioate. Upon hydrogenation, this alkene was converted into dimethyl adipate, which, under



Scheme 83: Ruthenium-catalyzed levulinic acid to chiral γ-valerolactone.



Scheme 84: Catalytic asymmetric hydrogenation of levulinic acid to chiral GVL.



Scheme 85: Three steps synthesis of ε-caprolactam from GVL.

hydrolysis provided adipic acid. The final step was the polymerization of adipic acid to nylon 6,6 in the presence of 1,6-hexanediamine (Scheme 86) [275].

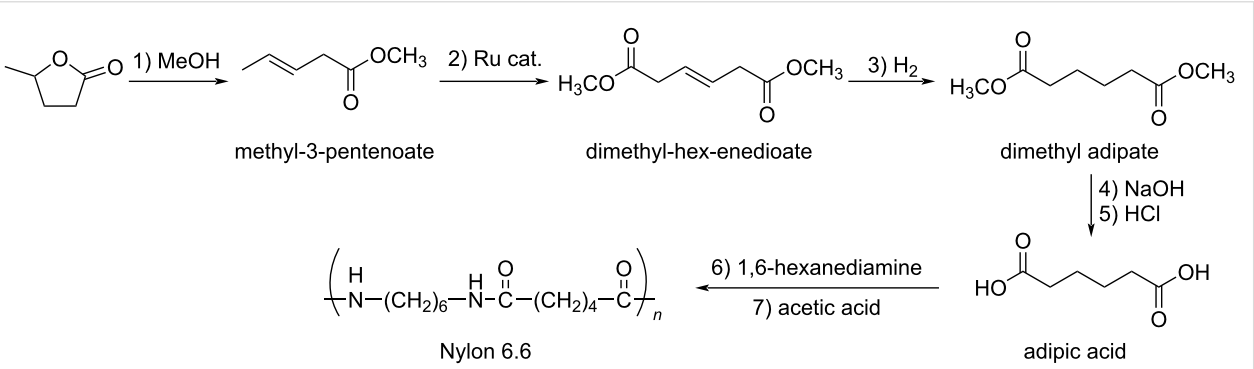
GVL can be transformed into α-methylene-γ-valerolactone (MeGVL), an interesting monomer, that can provide a material with properties similar to the widely used poly(methyl)methacrylate when subjected to visible-light-induced polymerization. Under the action of a base like a beta (Si/Al = 150) zeolite, MeGVL can be formed by nucleophilic attack of the carbon atom at α-position of GVL on formic acid, arising from the decomposition of trioxane (Scheme 87) [276].

Hong reported the conversion of GVL to polythioesters via the isomerization-driven ring-opening polymerization (IROP) of thionolactone intermediates (TnGVL) using $[Et_3O]^+[B(C_6F_5)_4]^-$ as cationic initiator [277,278]. The enantiopure TnGVL undergoes an inversion of configuration during the IROP process through a S_N2 ring-opening mechanism. The method provided a highly isotactic semi-crystalline thermoplastic (Scheme 88).

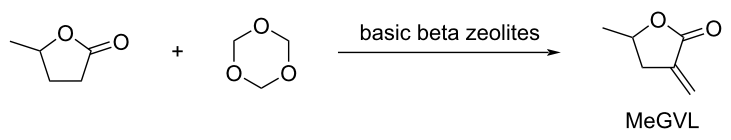
Ionic liquids from GVL

Ionic liquids are innovative environmentally benign reaction media due to their extremely low vapor pressure and easily tunable properties. In 2018, Mika synthesized GVL-based ionic liquids from GVL and tetrabutylphosphonium [TBP] or tetraphenylphosphonium [TPP] hydroxides in excellent yield (Scheme 89). These phosphonium-based ionic liquids showed better thermal stability than their ammonium analogues. Their usefulness was illustrated in industrially important transformations such as the copper-catalyzed Ullmann-type coupling reaction [279] or the Sonogashira coupling of aryl iodides and functionalized acetylenes [280].

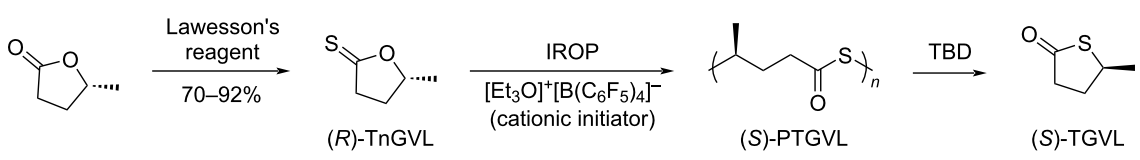
GVL towards biofuels: An important application of GVL is to produce butene by decarboxylation reaction for liquid fuels application. For example, Xin and Zhang reported a one-pot conversion of GVL to butene in 98% yield with 99.5% GVL conversion involving the catalytic decarboxylation of GVL at 300 °C in the presence of high aluminum content beta zeolite (Scheme 90) [281].



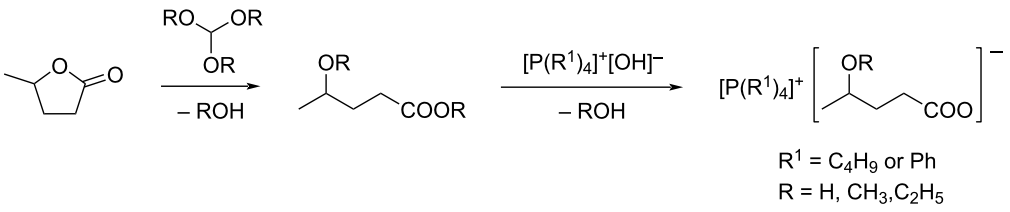
Scheme 86: Multistep synthesis of nylon 6,6 from GVL.



Scheme 87: Preparation of MeGVL by α-alkylation of GVL.



Scheme 88: Ring-opening polymerization of five-membered lactones.

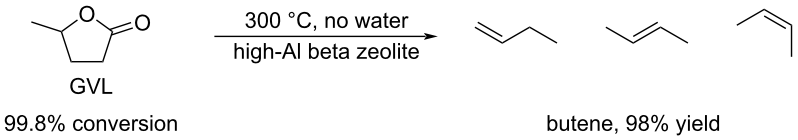


Scheme 89: Synthesis of GVL-based ionic liquids.

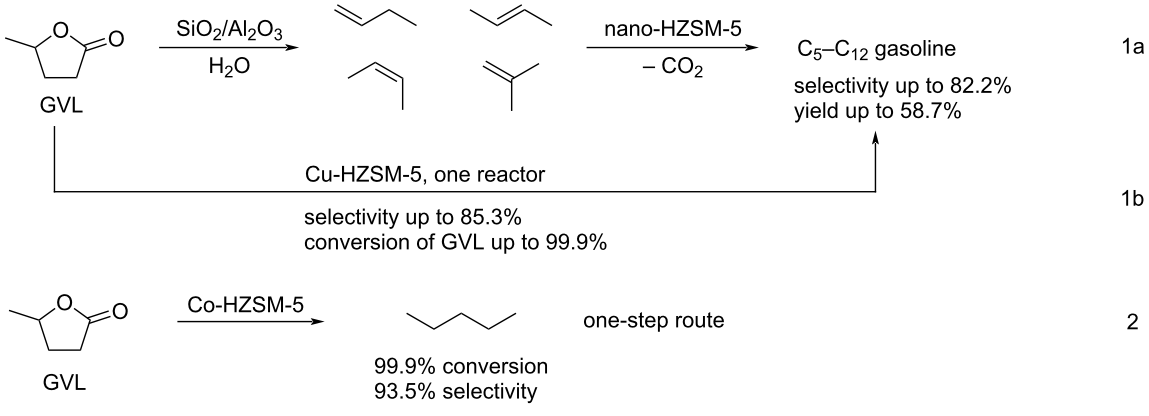
Zeng and Ding targeted C_5–C_{12} gasoline range fuels from GVL in an integrated two-stage fixed-bed catalytic system. In this process, GVL was first converted to a mixture of butene isomers via a ring-opening–decarboxylation sequence, which then oligomerized to gasoline fuels over a nano-HZSM-5 zeolite catalyst (Scheme 91, 1a) [282]. The same team proposed a direct one-step Cu/HZSM-5 (Si/Al ratio of 15)-catalyzed selective conversion of GVL to C_5–C_{12} hydrocarbon fuels (Scheme 91, 1b) or to pentane fuels (Scheme 91, 2) [283,284].

Other reactions of GVL: The Csp^3–O bond of GVL can be cleaved leading to a pentenoic acid intermediate, which can then be hydrogenated into ethyl valerate. In this sequence, which is promoted by a H-ZSM-5 supported Ni catalyst, pentenoic acid (not isolated) was generated in situ and was rapidly hydrogenated and esterified to ethyl valerate with 92% selectivity in the vapor phase (Scheme 92) [285]. Bertero reported the one-pot production of pentyl valerate with high conversion (83.5%) and selectivity (87.8%) in liquid phase over a SiO_2/Al_2O_3-supported Ni-based catalyst (Ni/SA-I) at 523 K under 10 bar of H_2 [286]. Using SiO_2/Al_2O_3-supported Pt-based catalysts with moderate metal loading (1%), a 90% yield of pentyl valerate was obtained with 100% conversion of GVL at 523 K and 10 bar of H_2. This process resulted in a high productivity in pentyl valerate (300 $mmol/g_M \cdot h$) [287].

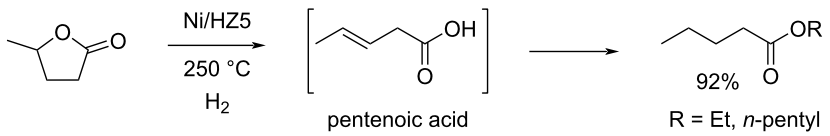
Alkaline hydrolysis of GVL produces 4-hydroxycarboxylic acid salts. These latter can be used in lipase-catalyzed stereoselective acylation of the 4-hydroxy group [288]. Using CALB (Novozym 435) as lipase, (*R*)-4-acyloxypentanoic acids were obtained in a moderate yield (<50%) from racemic GVL after acid hydrolysis of the intermediate salt, with (*R*)-GVL as by-product (Scheme 93).



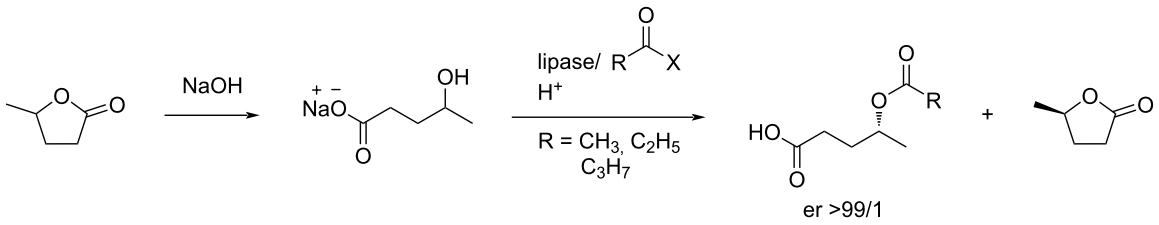
Scheme 90: Preparation of butene isomers from GVL under Lewis acid conditions.



Scheme 91: Construction of C_5–C_{12} fuels from GVL over nano-HZSM-5 catalysts.

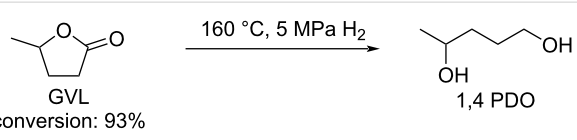


Scheme 92: Preparation of alkyl valerate from GVL via ring opening/reduction/esterification sequence.



Scheme 93: Construction of 4-acyloxypentanoic acids from GVL.

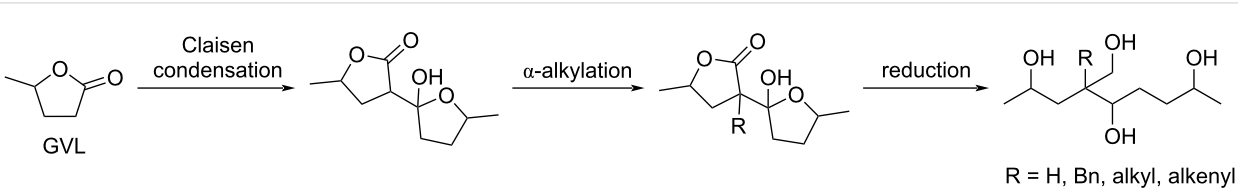
The hydrogenation of GVL to pentanediol by bifunctional $Cu_x/Mg_{3-x}AlO$ nanocatalysts (x = 0.5, 1, 1.5, 2) with excellent catalytic performance has been reported (Scheme 94). Thanks to synergistic effects of the well-dispersed active Cu nanoparticles and the relevant surface basic sites, the process provided 1,4-pentanediol (PDO) with a selectivity over 99% and a GVL conversion of 93% at 160 °C and 5MPa H_2 [289]. Another highly selective and efficient protocol using a Cu/SiO_2 triethoxyoctylsilane-modified catalyst was reported by Cappelletti [290].



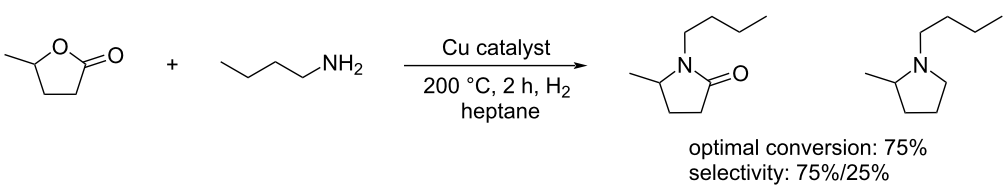
Scheme 94: Synthesis of 1,4-pentanediol (PDO) from GVL.

The self-Claisen condensation of GVL in the presence of *t*-BuOK at 25 °C provided a novel cyclic hemiketal platform in 85% yield. Alkylation and reduction of such cyclic hemiketals led to polyols with long chains ranging from C_{10} to C_{21} (Scheme 95) [291].

N-Alkylpyrrolidones, which are promising solvent alternatives to NMP, can be derived from GVL. In an effort aiming at avoiding noble-metal catalysts and high hydrogen pressure, the Zaccheria group has applied a CuO/Al_2O_3 catalyst which allowed the conversion of GVL to *N*-alkylpyrrolidone solvents at a 10-bar hydrogen pressure (Scheme 96) [292].



Scheme 95: Construction of novel cyclic hemiketal platforms via self-Claisen condensation of GVL.



Scheme 96: Copper-catalyzed lactamization of GVL.

C_6 biobased carbonyl platforms

5-Hydroxymethylfurfural (HMF)

5-Hydroxymethylfurfural (HMF) arises from C_6 carbohydrates (or their polymers) or crude lignocellulosic raw materials [293-298]. HMF has been added to the updated "Top potential value-added chemicals" list in 2010 by Bozell and Petersen [215] considering its functional versatility and wide range of applications in fine chemistry. Extensive recent literature publications and reviews demonstrate the importance of HMF in modern chemistry [299-302]. Its moderate thermal and chemical stability either under acidic or basic conditions is responsible for the formation of levulinic acid (see section Levulinic acid (LEV), Cannizzaro products (such as 2,5-dihydroxymethylfurfural (DHMF) and 5-hydroxymethylfuranoic acid (HMFA)), oligomerization or humins [303,304].

Regarding HMF oxidation, a major topic is the path towards new biobased polymers via the furandicarboxylic (FDCA) platform, when combined with diols or diamines (Figure 4) [8,305-311]. Other oxidation products such as diformylfuran (DFF), hydroxymethyl-2-furanoic acid (HMFA), 5-formyl-2-furancarboxylic acid (FFCA) are also interesting intermediates, as well as the corresponding diamide, resulting in numerous studies and reviews on HMF (Figure 4) [312-320]. Several HMF-derived monomers attest its versatile role in polymer chemistry [321-323]. On the reduction side, many useful chemical intermediates, such as dihydroxymethylfuran (DHMF), (hydroxymethyl)tetrahydrofurfural (HMTHFF), methylfurfurylalcohol (MFA), dimethylfuran (DMF), dihydroxymethyltetrahydrofuran (DHMTHF), and dimethyltetrahydrofuran (DMTHF) can be also produced by reduction/hydrogenation processes [324-327]. The Piancatelli rearrangement of furylmethanols is a route towards cyclopentenones such as 4-hydroxy-4-(hydroxymethyl)cyclopentenone (HHCPN) or 3-(hydroxy-methyl)cyclopentanone (HCPN) [168,328,329]. It is important to note that biocatalytic approaches have also been investigated for both the oxidation and reduction senses [172,330,331].

Because many reports have reviewed the formation of the HMF-derived scaffolds (Figure 4), this section will focus on transformations towards alternative fine chemicals, notably through cascade or multicomponent reactions.

Combining atom-economic strategies with biobased platforms offers very interesting options for the innovative design of complex fine chemicals. Queneau and Popowycz investigated the reactivity of HMF in Biginelli reactions, preparing a series of functionalized dihydropyrimidinones in 30–86% yield. The reaction of HMF with ethyl acetoacetate (1 equiv) and urea or thiourea (1 equiv) at 80–100 °C using a catalytic loading of the Lewis acid $ZnCl_2$ (20 mol %), provided respectively 82% and 42% of the corresponding dihydropyrimidinones (Scheme 97) [332]. Afradi et al. designed a nanocatalyst comprising aspartic acid-loaded starch-functionalized Mn/Fe/Ca ferrite magnetic nanoparticles for the efficient synthesis of dihydropyrimidine derivatives in solvent-free conditions [333].

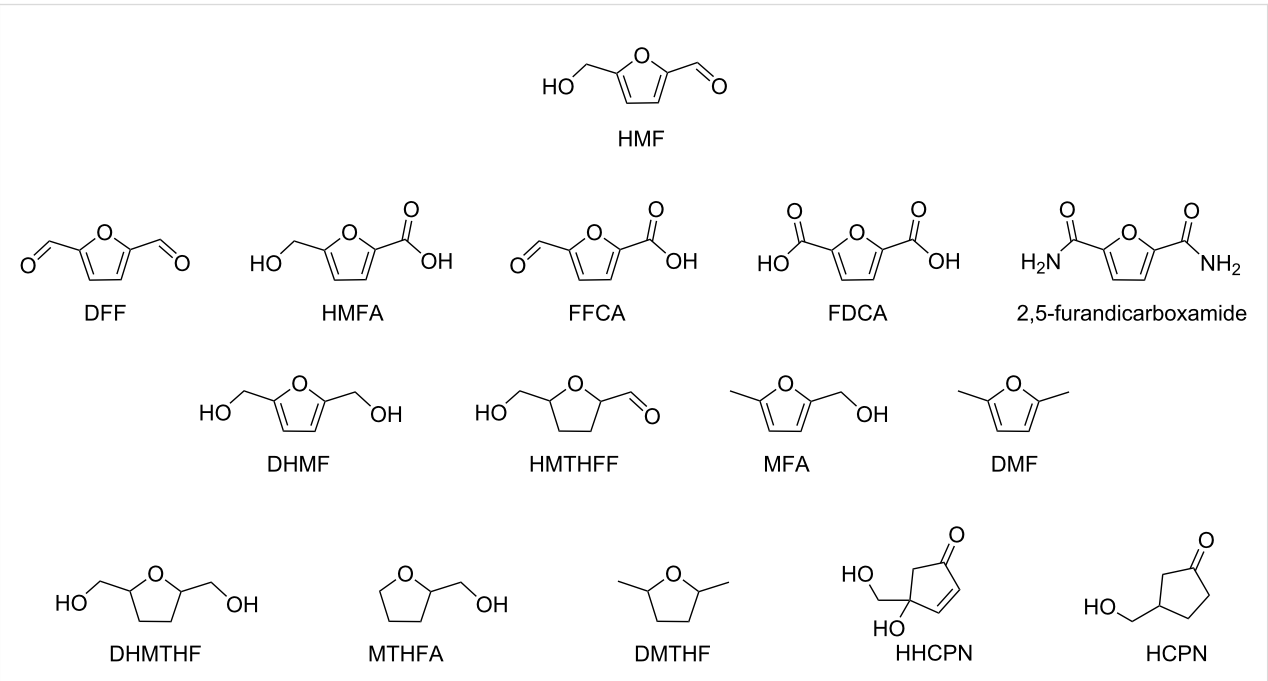
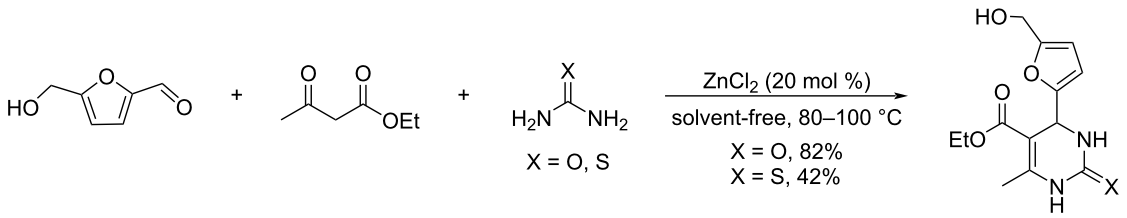


Figure 4: Main scaffolds obtained from HMF.



Scheme 97: Biginelli reactions towards HMF-containing dihydropyrimidinones.

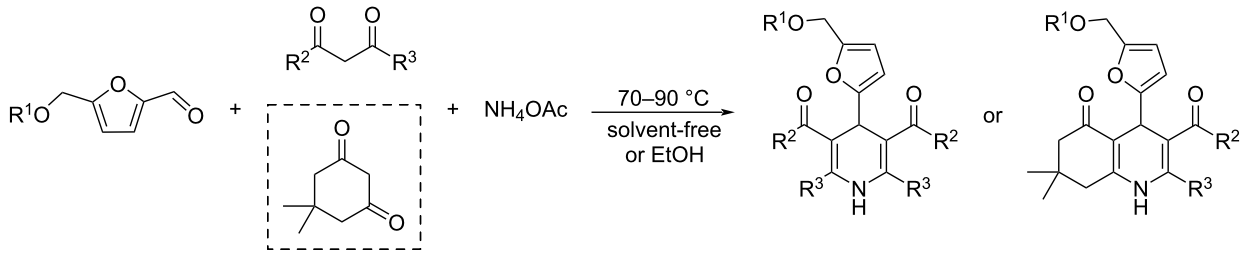
Queneau and Popowycz also recently reported the use of HMF in the Hantzsch dihydropyridine synthesis in the absence of any additional catalyst. The strategy was applied to a scope of β-dicarbonyl molecules in a three-component procedure leading to a series of symmetrical 1,4-dihydropyridines derived from 5-HMF and in a 4-component protocol which efficiently provided the corresponding unsymmetrical dihydropyridines under remarkably mild conditions (Scheme 98) [334].

Another multicomponent process involving HMF is the Kabachnik–Fields reaction which provides a variety of furan-based α-aminophosphonates in moderate to excellent yields (31–91%), using a catalytic quantity of iodine in the biobased solvent 2-methyltetrahydrofuran (2-MeTHF). A scope of aliphatic and aromatic amines and various dialkyl phosphonates were well tolerated in this reaction (Scheme 99) [335].

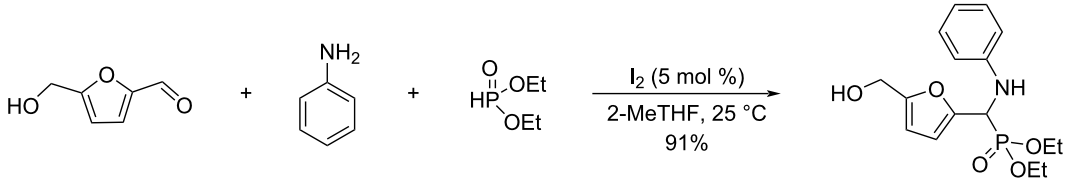
In 2018, Chen and Wu reported a copper-catalyzed four-component reaction to build oxazolidinones from furfurals, CO_2, terminal aromatic alkynes and primary aliphatic amines. A series of 1,3-oxazolidin-2-ones were obtained in 17–84% yield when CuI was used as catalyst. As an example, 50% yield of the 1,3-oxazolidin-2-one product was produced by the reaction of HMF, CO_2, propylamine, and phenylacetylene (Scheme 100) [336].

Rhodamine-furan hybrids were synthesized via one-pot stereoselective reaction in solvent-free conditions by Sabahi-Agabager. Starting from biobased furanic aldehydes (HMF, CMF, furfural), ethyl bromoacetate, carbon disulfide and phenethylamine, a 75% yield of rhodamine-furan hybrids was obtained at room temperature in the presence of Et_3N (Scheme 101) [337].

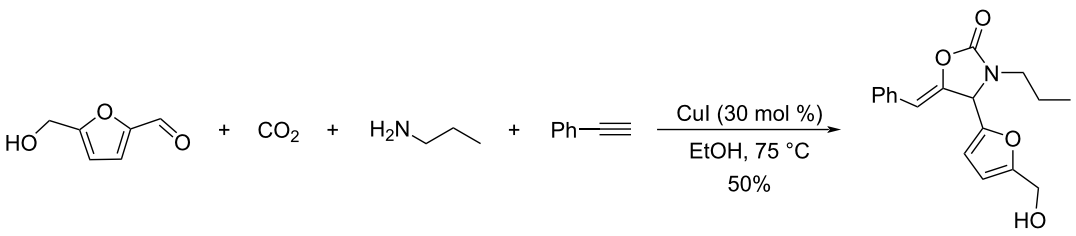
López and Porcal investigated the reactivity of HMF in the three-component Groebke–Blackburn–Bienaymé reaction. In the presence of 20 mol % of trifluoroacetic acid, the reaction of HMF with cyclic amidines (5- or 6-membered) and isocyanides



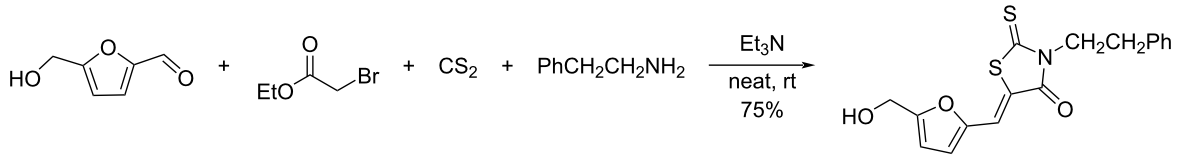
Scheme 98: Hantzsch dihydropyridine synthesis involving HMF.



Scheme 99: The Kabachnik–Fields reaction involving HMF.



Scheme 100: Construction of oxazolidinone from HMF.



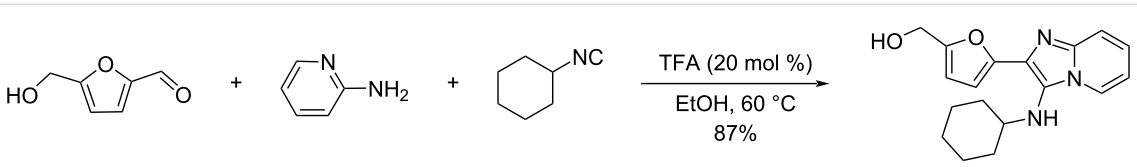
Scheme 101: Construction of rhodamine-furan hybrids from HMF.

afforded a library of new imidazoheterocycles. The best yield (87%) was obtained for the case of 2-aminopyridine and isocyanocyclohexane at 60 °C (Scheme 102) [338].

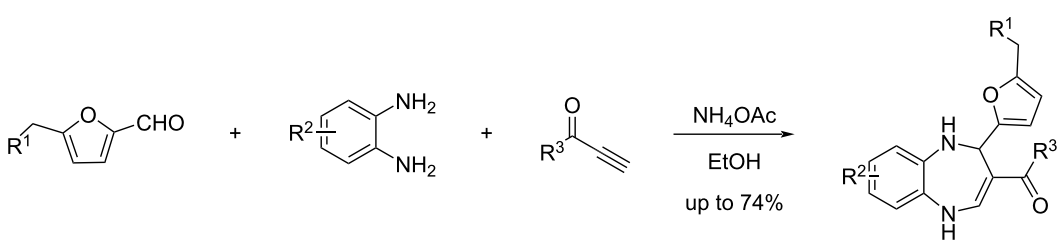
A [4 + 2 + 1] cycloaddition strategy towards 1,5-benzodiazepines involving HMF was developed by the Queneau and Popowycz group with yields up to 74% by using ammonium acetate as both a mild catalyst and a source of nitrogen, in ethanol as a green solvent. The reaction scope was extended to various substituted diamines, alkynones/alkyl alkynoates, and furan aldehydes leading to a wide range of novel benzodiazepines (Scheme 103) [339].

HMF reactivity was investigated in several other MCRs. For example, Yang and Wu reported the use of *N*-heterocyclic carbene catalysis for the reaction of HMF with an alkene and a perfluoroalkyl reagent in the presence of Cs_2CO_3, providing access to the corresponding α-aryl-β-perfluoroalkyl products (Scheme 104). HMF led to a lower 43% yield compared to benzaldehyde (81%) and furfural (75%) [340].

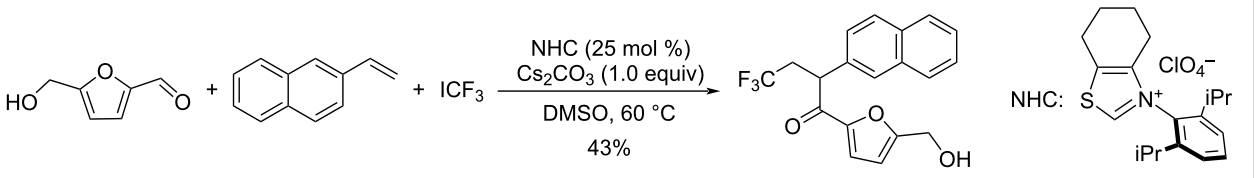
The multicomponent reaction combining electron-rich aromatic aldehydes, sulfoxonium ylides and Meldrum's acid can be performed in the presence of *N*,*N*-diisopropylethylamine to produce *trans*-β,γ-disubstituted-γ-butyrolactones in good yields



Scheme 102: A Groebke–Blackburn–Bienaymé reaction involving HMF.



Scheme 103: HMF-containing benzodiazepines by [4 + 2 + 1] cycloadditions.

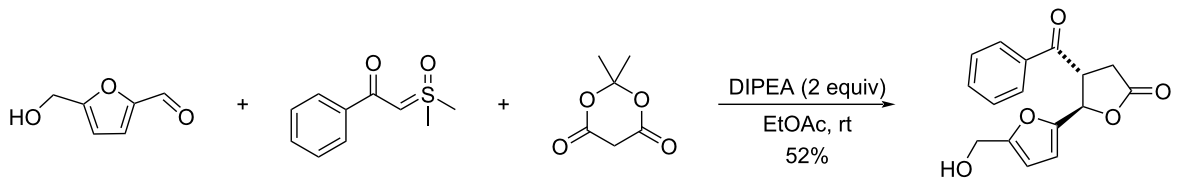


Scheme 104: Synthesis of fluorinated analogues of α-aryl ketones.

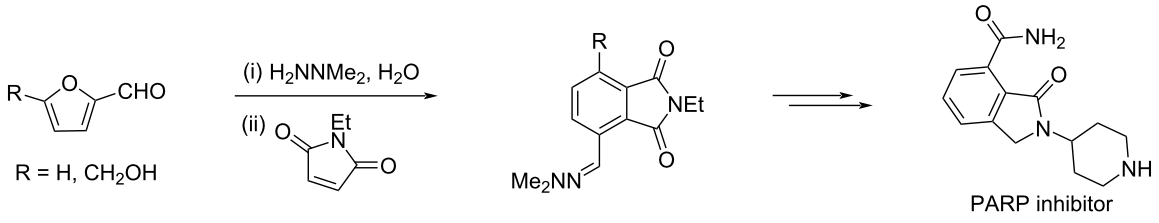
(65–98%). In this process reported by Ma and Peng [341], HMF led to only a 52% yield of the target product due to competitive reaction of the free hydroxy group in HMF with Meldrum's acid (Scheme 105).

A one-pot three-step cascade reaction involving HMF and other furanic aldehydes in the presence of dimethylhydrazine and phthalimide provides polysubstituted aromatics in water. The intermediate hydrazone formed from the aldehyde and dimethylhydrazine underwent in situ cycloaddition with the dienophile, before aromatization. This protocol afforded a range of polysubstituted aromatic compounds in high yields (up to 97%) and was employed to prepare a poly(ADP-ribose) polymerase (PARP) inhibitor (Scheme 106) [342].

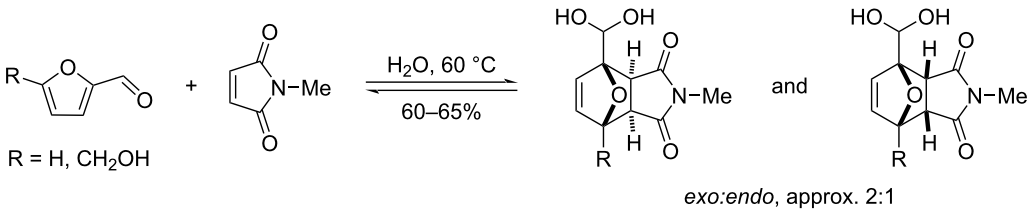
Several studies have concerned pericyclic cycloadditions involving HMF as diene component. For example, Bruijnincx reported a direct Diels–Alder reaction of HMF or furfural with *N*-methylmaleimide in aqueous medium to produce geminal diol products in 60 to 65% yield. Water is thought to pull the equilibrium toward the product side by chemically trapping the Diels–Alder adducts by hydratation (Scheme 107) [343].



Scheme 105: Synthesis of HMF derived disubstituted γ-butyrolactone.



Scheme 106: Functionalized aromatics from furfural and HMF.



Scheme 107: Diels–Alder adducts from HMF or furfural with *N*-methylmaleimide.

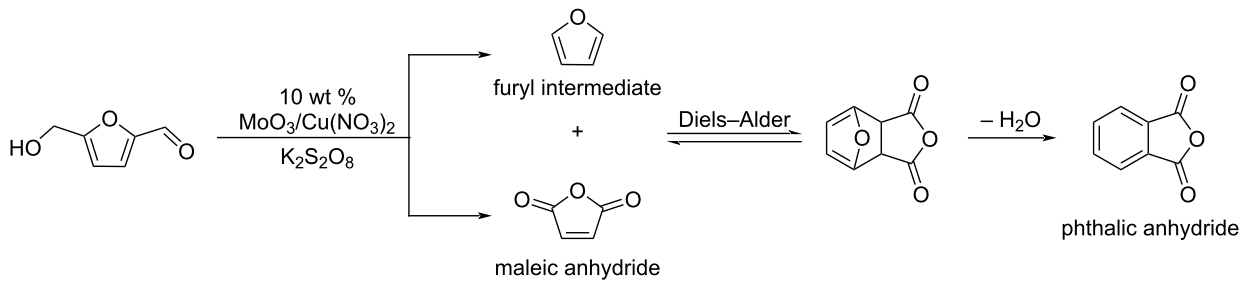
Sun reported the one-pot synthesis of phthalic anhydride by Diels–Alder reaction between HMF and maleic anhydride, promoted by a synergistic combination of MoO_3 and $Cu(NO_3)_2$ catalysts. HMF can provide both partners of this Diels–Alder reaction, either by decarbonylation to an active furyl intermediate, and by oxidation to maleic anhydride. Subsequent dehydration of the DA adduct provided phthalic anhydride in 63% yield (Scheme 108) [344].

He and Guo reported the first photocatalyzed polymerization of HMF for the preparation of photo-generated humins (L-H) (Scheme 109). The L-H containing HMF and 5-hydroxy-4-ketopentenoic acid were generated by reacting HMF under illumination in presence of a low molecular weight humin (LMW-H) made from spoiled HMF residues. The resulting product allowed the preparation of furan-based polymers by Diels–Alder reaction with bismaleimidodiphenylmethane. A detailed physicochemical characterization indicated that the polymer DA-L-H had self-healing properties, and a recovery efficiency reaching 92.8% [345].

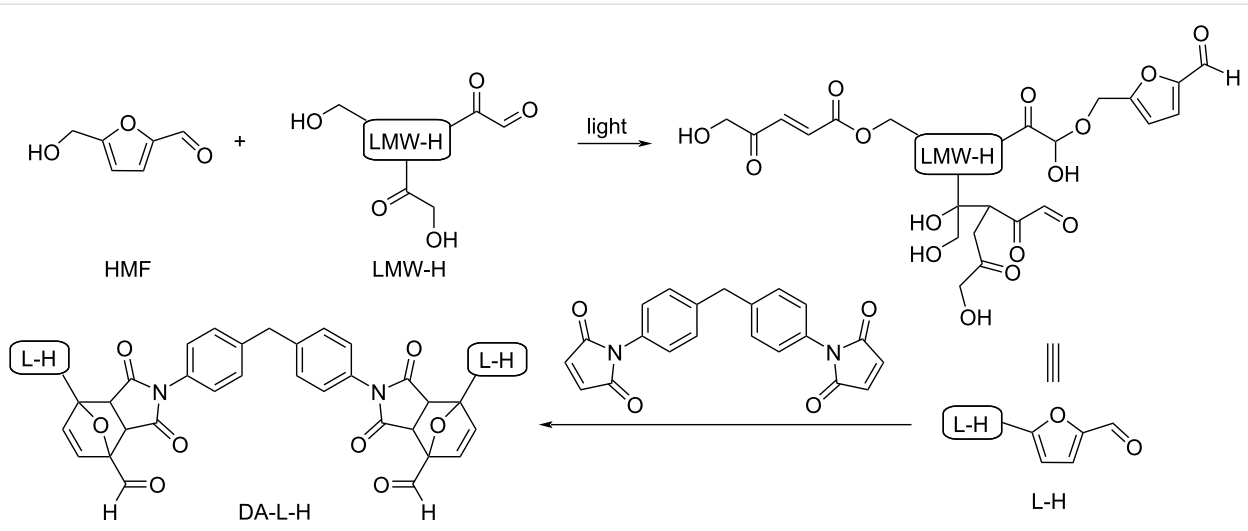
Reaction of HMF with alanine methyl ester hydrochloride in the presence of Et_3N afforded HMF-derived iminoesters. By using the (*R*)-Fesulphos/$Cu(CH_3CN)_4PF_6$ complex as a catalyst, the asymmetric 1,3-dipolar cycloaddition of the iminoester with activated alkenes provided enantiomerically enriched heterocyclic scaffolds in 41–87% yield and high enantioselectivity (79–99% ee) (Scheme 110) [346].

Queneau reported the synthesis of 3-furanylisoxazolidines by a dipolar cycloaddition of HMF-based nitrones with electron-deficient olefins in yields up to 84% for the stepwise reaction or 75% for the one-pot reaction. For example, *N*-methylhydroxylamine hydrochloride and HMF were condensed in isopropanol to form the corresponding nitrone, which underwent subsequently a cycloaddition with methyl acrylate in isopropanol to provide a regioisomeric mixture of 3,4-substituted and 3,5-substituted isoxazolidines in 84% yield (Scheme 111) [347].

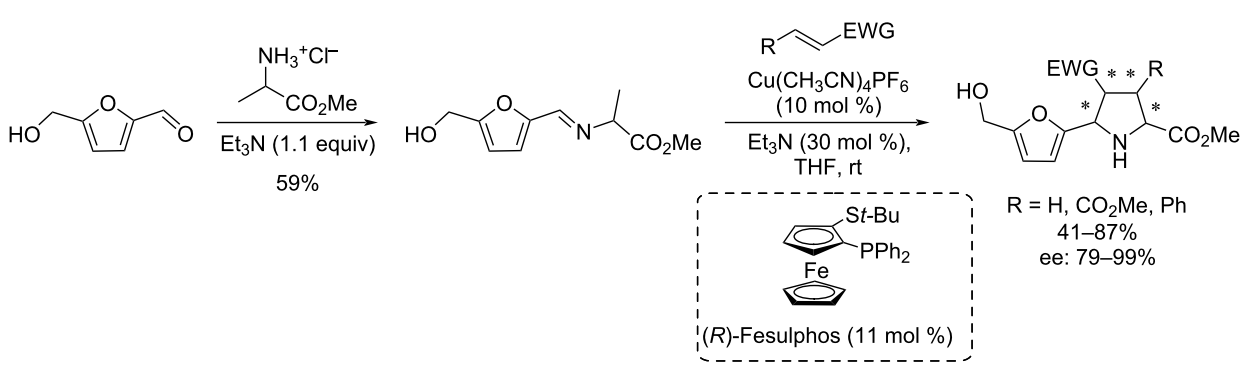
Novel aminated lactone-fused cyclopenten-2-ones were prepared by reaction of the Knoevenagel product arising from



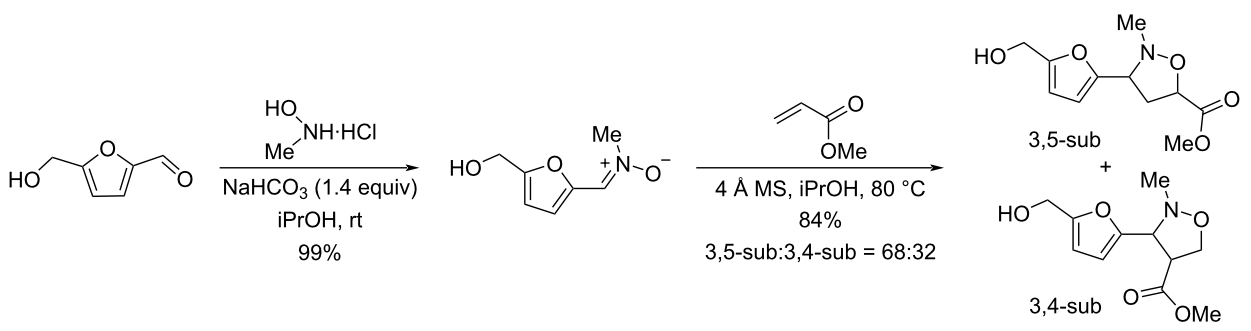
Scheme 108: Pathway of the one-pot conversion of HMF into phthalic anhydride.



Scheme 109: Photocatalyzed preparation of humins (L-H) from HMF mixed with spoiled HMF residues (LMW-H) and further cycloadditions with bismaleimide.



Scheme 110: Asymmetric dipolar cycloadditions on HMF.



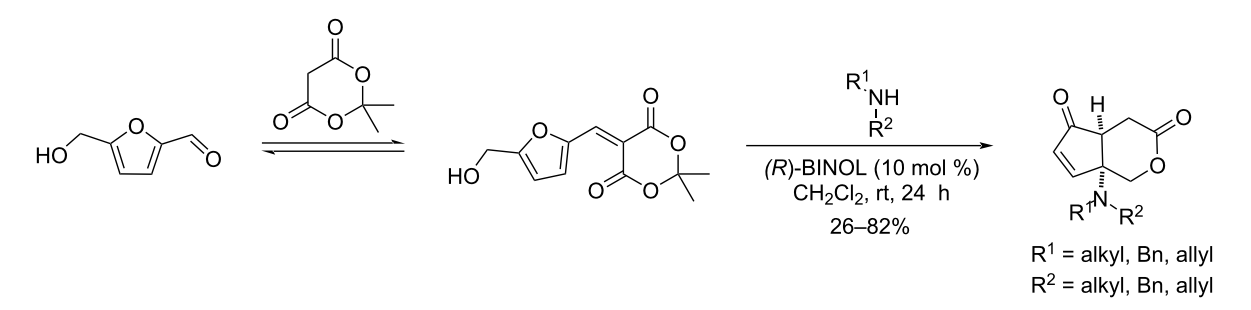
Scheme 111: Dipolar cycloadditions of HMF based nitrones to 3,4- and 3,5-substituted isoxazolidines.

Meldrum's acid and HMF with a wide range of secondary amines. Through a furan ring-opening–cyclization–lactonization cascade process (closely related to the Piancatelli reaction), highly functionalized δ-lactone-fused cyclopenten-2-ones were formed in 26–82% yields under the promotion of (*R*)-BINOL acting as a weak Brønsted acid (Scheme 112) [348].

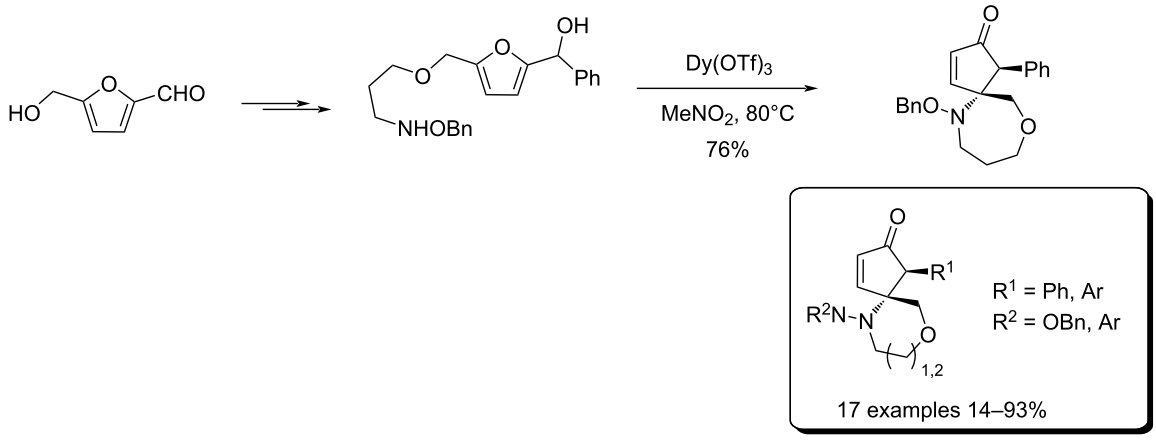
Moebs-Sanchez and Popowycz recently reported a dysprosium triflate-catalyzed aza-Piancatelli reaction from HMF-derived intermediates forming cyclopentenone aza-spirocycles. A wide scope of novel 5,6- and 5,7-spirobicyclic scaffolds were prepared with yields up to 93% (Scheme 113) [349].

The cross-aldol condensation of HMF, furfural and acetone can generate C_{13}–C_{15} condensation products which are biofuels and polymer precursors [350]. Several solid metal catalysts and different ratios of starting materials were tested for comparing the reactivity of HMF and furfural in this process (Scheme 114).

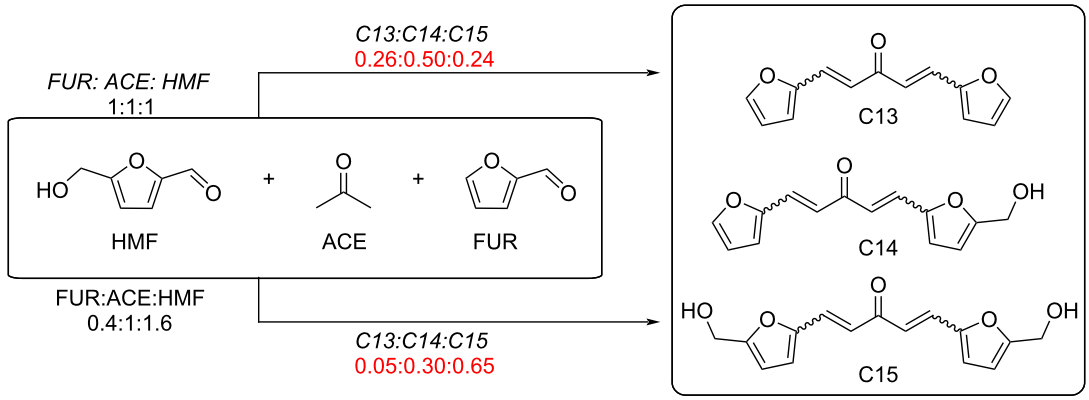
Ketones with enolizable α-H atoms can be coupled with HMF in alkaline medium to form new C–C bonds via cross-aldol condensation reaction. Examples include the use of alkyl ketones, cycloalkanones, and α,β-unsaturated ketones. Recently, Vigier used choline chloride to convert a carbohydrate feedstock into HMF which was then condensed with methyl isobutyl ketone



Scheme 112: Production of δ-lactone-fused cyclopenten-2-ones from HMF.



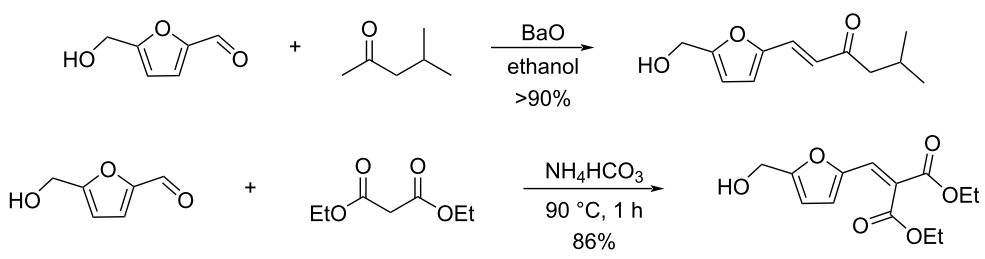
Scheme 113: Aza-Piancatelli access to aza-spirocycles from HMF-derived intermediates.



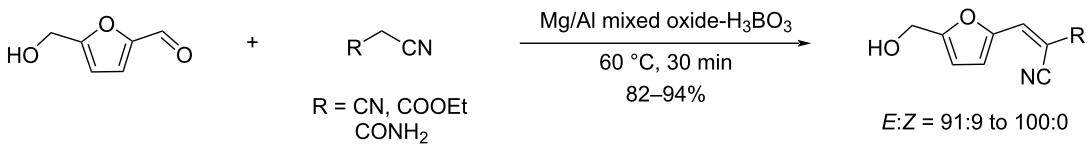
Scheme 114: Cross-condensation of furfural, acetone and HMF into C_{13}, C_{14} and C_{15} products.

(MIBK) in the presence of alkaline barium oxide as catalyst, affording 1-(5-(hydroxymethyl)furan-2-yl)-5-methylhex-1-en-3-one with yield over 90% [351]. Schijndel also reported a Knoevenagel condensation of furan aldehydes and diethyl malonate in the presence of ammonium bicarbonate giving a 86% yield of the HMF-derived condensation product [352] (Scheme 115).

Mancipe and Luque reported the use of a boric acid deposited on hydrotalcite catalyst for the Knoevenagel condensation of HMF with active methylene compounds to afford a series of HMF derivatives containing an acrylonitrile moiety. The acid–base catalytic sites accelerate the reaction leading to high yields (82–94%) and high (*E*)-isomer selectivity (91:9 to 100:0) of the condensation products (Scheme 116) [353].



Scheme 115: Base-catalyzed aldol condensation/dehydration sequences from HMF.

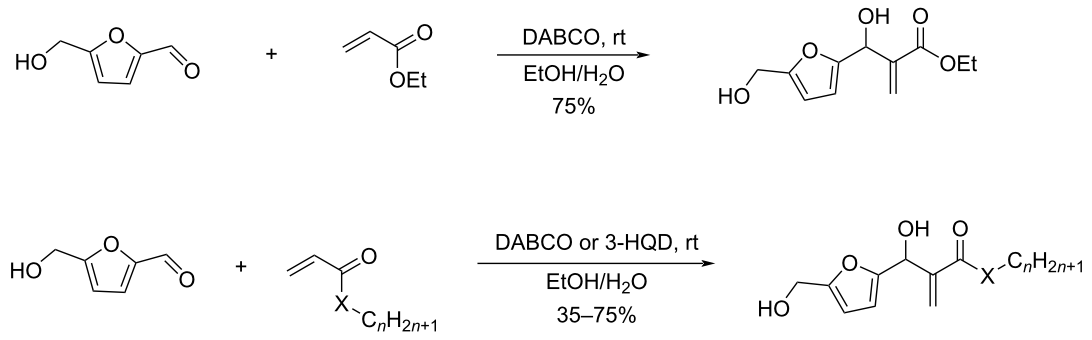


Scheme 116: Condensation of HMF and active methylene nitrile.

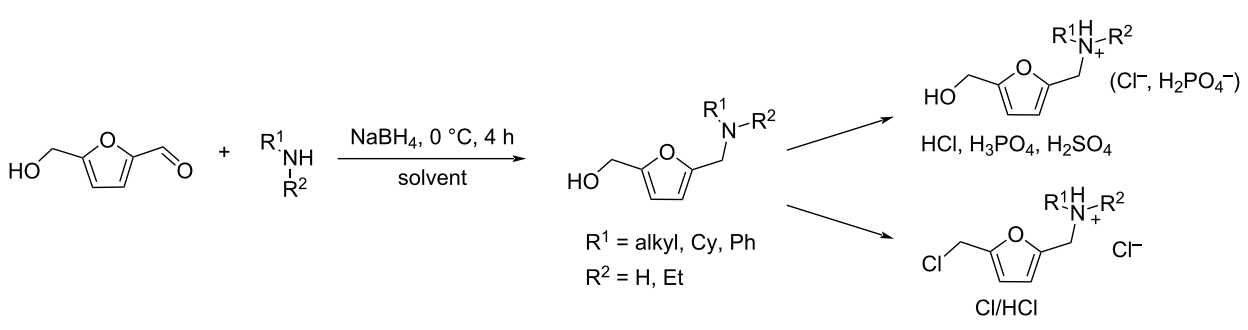
Another carbon–carbon-bond formation involving the aldehyde group of HMF is the Morita–Baylis–Hillman (MBH) reaction. Queneau showed that the reaction with acrylates in the presence of DABCO can take place in a combination of biobased solvents such as EtOH/H_2O 1:1 (v/v) to replace traditional solvents, with yields up to 90% after 24 h [354]. The strategy was later applied to the preparation of original biobased amphiphiles from hydrophobic alkenes. These amphiphiles were shown to emulsify both polar and apolar oils, providing W/O and O/W emulsions, suggesting that they could be used as relevant alternatives to traditional petroleum-based polyethoxylated surfactants (Scheme 117) [355].

Finally, several strategies based on the reductive amination of HMF have been reported. For example, Ananikov synthesized a series of multifunctional protic ammonium ionic liquids with various inorganic anions by reductive amination of HMF with various amines (Scheme 118). The salts were studied with respect to their solvent properties. Interestingly, the ionic liquids containing sulfate anions have the ability to dissolve cellulose. Regarding the biological properties, the introduction of a chlorine substituent into the side chain of the furfural unit is beneficial to the bactericidal effect. A study on physicochemical properties indicated that most of these ionic liquids were stable when stored for more than six months [356].

Heterogeneous monometallic (Ni, Co, Ru, Pd, Pt, Rh) and bimetallic (Ni/Cu, Ni/Mn) catalysts have been shown to be efficient for the reductive amination of HMF [357,358]. A recent application towards surfactant precursors has been reported by Iborra and Corma, using a non-noble metal (NNM) catalyst based on monodisperse cobalt nanoparticles coated with a few



Scheme 117: MBH reactions involving HMF.



Scheme 118: Synthesis of HMF-derived ionic liquids.

layers of carbon (NNM@C). Subsequent lipase-catalyzed acylation using carboxylic acids afforded the aminoesters, one step away from cationic surfactants by amine quaternization (Scheme 119) [359]. This strategy provided additional methods towards biobased furanic surfactants for which two reviews were reported in 2022 [173,360].

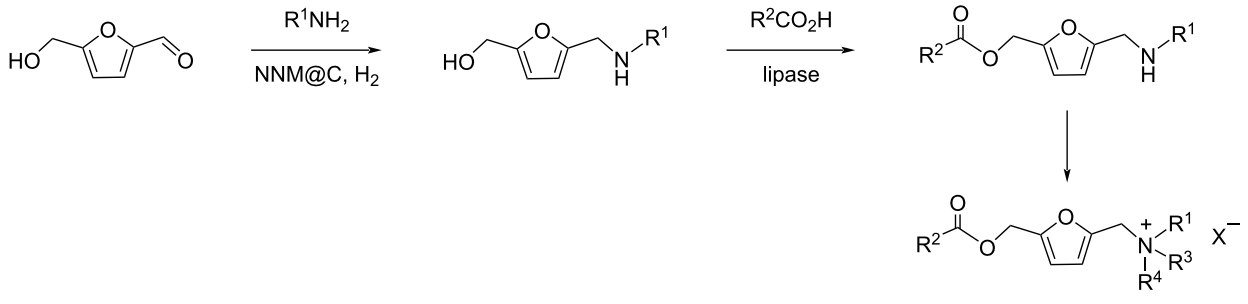
5-(Chloromethyl)furfural (CMF)

5-(Chloromethyl)furfural (CMF) can be obtained from raw biomass such as bagasse, cassava wastes, corn stover, bamboo powder or a variety of pure carbohydrates, such as glucose, sucrose, fructose, cellulose. CMF has gained popularity thanks to the pioneering work and accounts reported by Mascal, showing the potential of this alternative platform for monomers, biofuels and specialty chemicals [361,362]. Several other groups have contributed to the topic, and a few more in-depth perspectives on the synthesis and applications of CMF and other 5-(halomethyl)furfurals have been reported [363,364]. A popular system to access CMF is the use of HCl as chlorinating agent in dichloroethane, which can be achieved from HMF (Scheme 120), but also from glucose, sucrose or cellulose. Compared to HMF, the main differences are the higher stability of CMF under acidic conditions and its easier extractability from the medium due to a higher lipophilicity. In the following we give a brief and non-comprehensive overview of CMF downstream chemistry illustrating its usefulness towards fine chemicals.

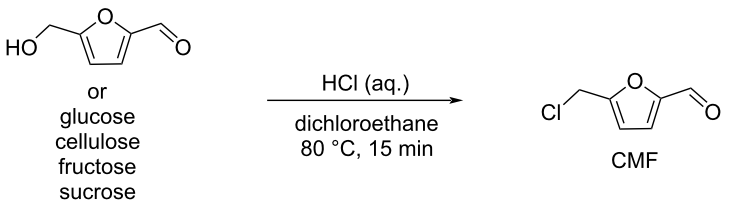
CMF can be used as a stable intermediate for the production of HMF, levulinic acid and alkyl levulinate (EL and BL) via hydrolysis or alcoholysis (Scheme 121) [365]. HMF is obtained in 86% yield from CMF in boiling water for only 30 seconds, while heating CMF in dilute hydrochloric acid at 150 °C for 5 h or without acid at 190 °C leads to levulinic in high yield. If alcohols are added, high yields of alkyl levulinates are directly obtained.

2,5-Diformylfuran (DFF) can be obtained in 81% yield from CMF in DMSO, as proposed by Estrine and Le Bras [366] or in 54% yield over the combined pyridine *N*-oxide and $Cu(OTf)_2$ catalyst when using acetonitrile under microwave irradiation as reported by Afonso [367]. CMF can be also directly oxidized to 5-(chloromethyl)furan-2-carbonyl chloride (CMFCC) or converted to furan-2,5-dicarbonyl chloride (FDCC) via the formation of intermediate 2,5-diformylfuran (DFF) after reaction with *tert*-butyl hypochlorite (*t*-BuOCl) (Scheme 122) [368]. Being conveniently derivatizable acid chlorides, CMFCC and FDCC are highly versatile intermediates for the production of furans presenting a carboxylic acid function or other downstream chemical precursors of polymers and biofuels.

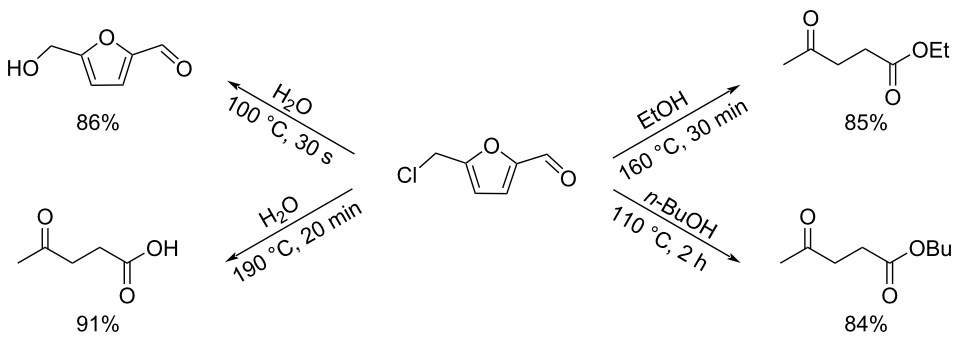
Suh has shown that CMF can be derivatized towards BHMF, using a stepwise hydrolysis and hydrogenation via HMF over mesoporous Cu/Al_2O_3 (meso-CuA-kg) under H_2 pressure



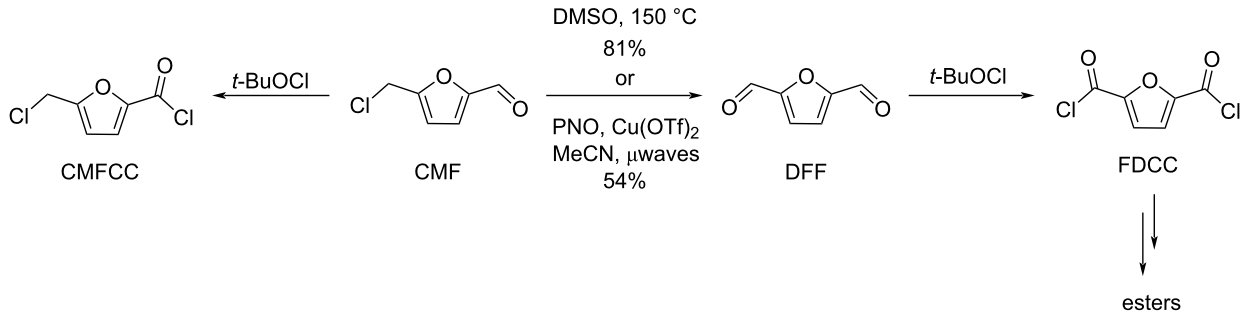
Scheme 119: Reductive amination/enzymatic acylation sequence towards HMF-based surfactants.



Scheme 120: The formation of 5-chloromethylfurfural (CMF).



Scheme 121: Conversion of CMF to HMF, levulinic acid, and alkyl levulinates.

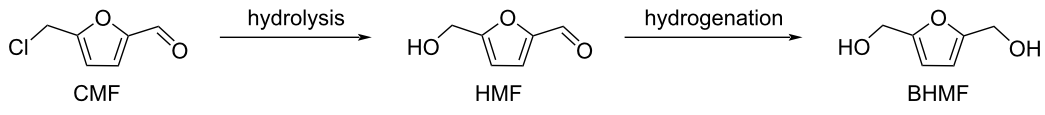


Scheme 122: Conversion of CMF to CMFCC and FDCC.

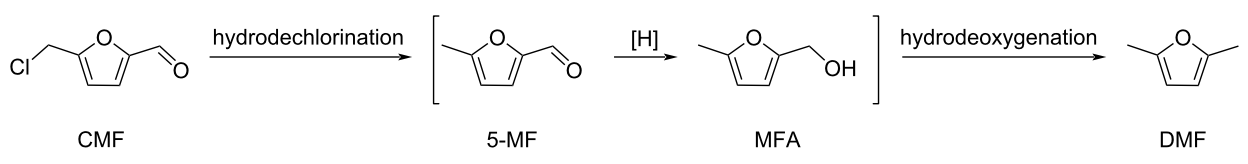
[369]. Recently, Zeng reported the one-pot consecutive hydrolysis and hydrogenation of CMF to BHMF in aqueous phase in 69% overall yield. Under the synergistic effect of Ru and Cu_2O species, 91% BHMF was obtained directly from CMF over Ru/CuO_x as catalyst at 60 °C and 4 MPa H_2 without isolation of the intermediate HMF [370] (Scheme 123).

Zeng has reported the reduction of CMF to 2,5-dimethylfuran (DMF) under mild conditions using a Cl-modified Pd catalysts (Pd/CNTs) and 2 MPa of H_2 affording 92% yield after 15 min at 30 °C (Scheme 124) [371].

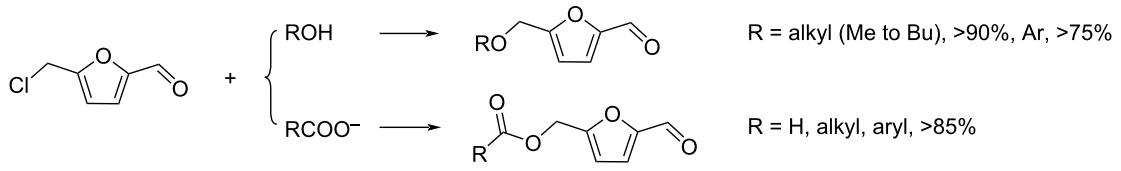
The substitution of the chlorine atom of CMF by nucleophiles produces either ethers [372,373] or esters [374] from alcohols or carboxylic acids, respectively, allowing the preparation of a library of functionalized furanic aldehydes (Scheme 125). For example, Dutta [372] and Sudarsanam [374] recently synthesized a series of alkyl/aryl-substituted HMF esters in high yields



Scheme 123: Conversion of CMF to BHMF.



Scheme 124: Conversion of CMF to DMF.



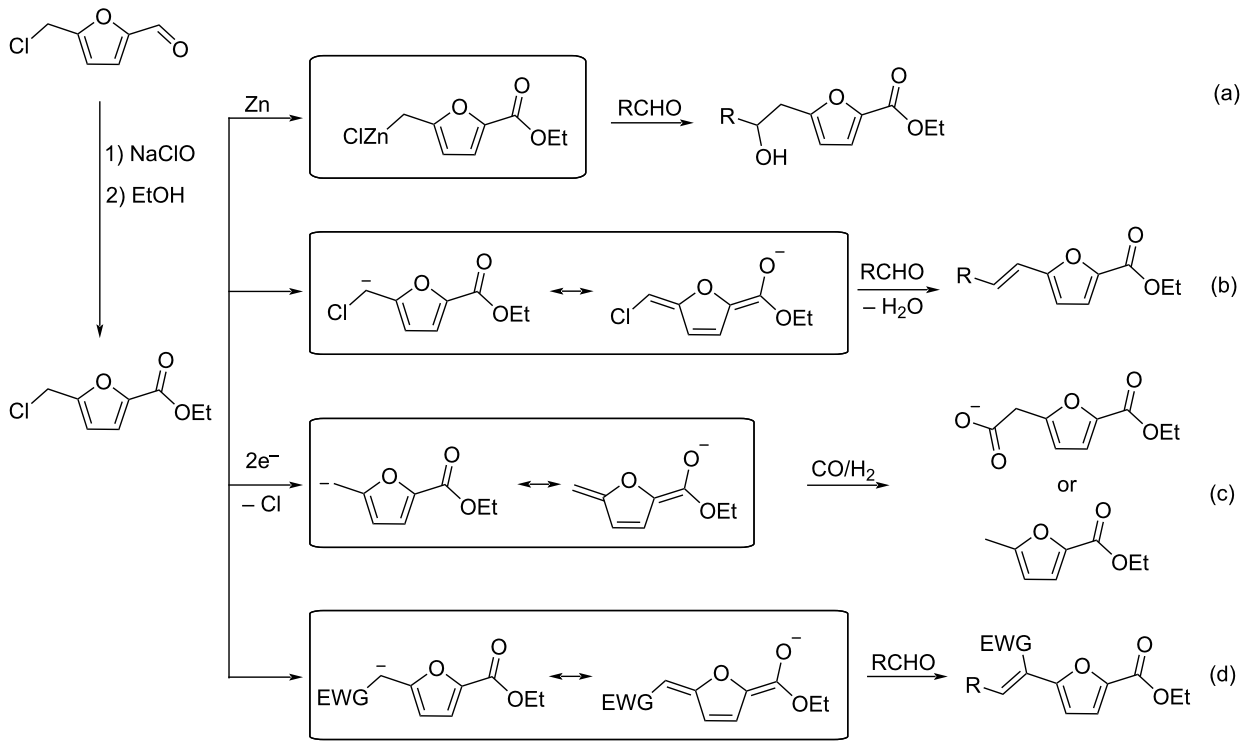
Scheme 125: CMF chlorine atom substitutions toward HMF ethers and esters.

(>85%) by reacting CMF and various carboxylic acids in the presence of a triethylammonium salt under solvent-free conditions (80 °C, 1.5 h). The two-step process from cellulose allowed the preparation of 5-(acetoxymethyl)furfural in an overall yield of nearly 65%.

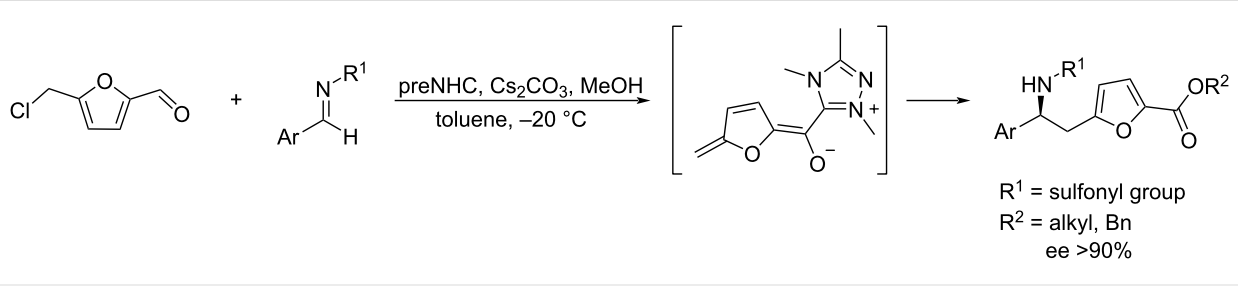
Carbon nucleophiles can also substitute the chlorine atom of CMF. For example, Zn metal insertion into the C–Cl bond of ethyl 5-(chloromethyl)furan-2-carboxylate can produce organozinc furoate esters able to react with a range of aldehydes (Scheme 126, reaction a) [375]. Alternatively, in a Reformatsky-type process, deprotonation of the 5-(chloromethyl)furoate esters and reaction with aldehydes followed by dehydration results in the formation conjugated alkenyl furoates which have applications in dyes or epoxy resin fields (Scheme 126, reaction b) [376]. The furylogous enolate anion resulting from the electrochemical reductive cleavage of ethyl 5-(chloromethyl)furan-2-carboxylate derived from CMF can react with carbon dioxide to yield 5-(carboxymethyl)furan-2-carboxylate, a useful intermediate towards the fuel additive 5-methylfuran-2-carboxylate commercially referred to as "Ethyl 408" (Scheme 126, reaction c) [377]. Similarly, furoate esters derived from CMF can undergo nucleophilic substitution with cyanide to produce furylogous cyanoacetic esters, employed for the design of biobased dyes (Scheme 126, reaction d) [378].

Gao and Ye reported the bifunctional-NHC-catalyzed enantioselective Mannich-type reaction involving CMF (Scheme 127). The products were obtained in high yields and enantioselectivities with excellent functional group tolerance [379].

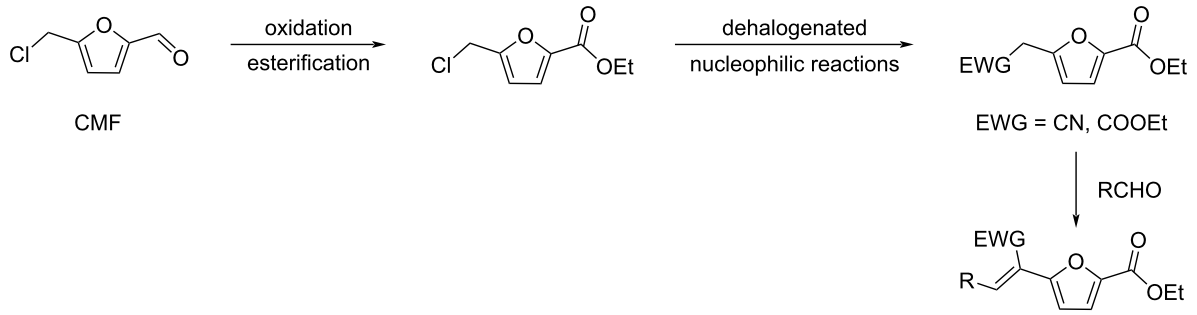
Biobased dyes have been obtained by introducing strong chromophores on the furanoate scaffold through the Knoevenagel reaction of CMF with aldehydes (Scheme 128).



Scheme 126: Introduction of carbon nucleophiles in CMF.



Scheme 127: NHC-catalyzed remote enantioselective Mannich-type reactions of CMF.



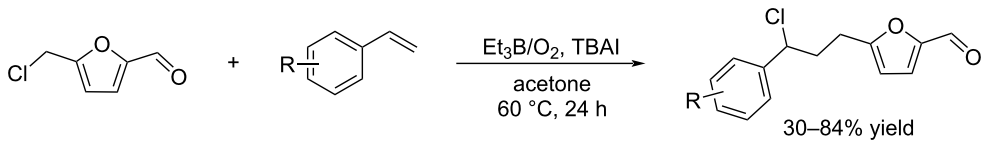
Scheme 128: Conversion of CMF to promising biomass-derived dyes.

The reaction of furylogous malonate or furylogous cyanoacetate and biomass-derived aldehydes produced brightly colored products from the yellow to red region of the spectrum, exhibiting good color properties and color fastness on selected fabrics [378].

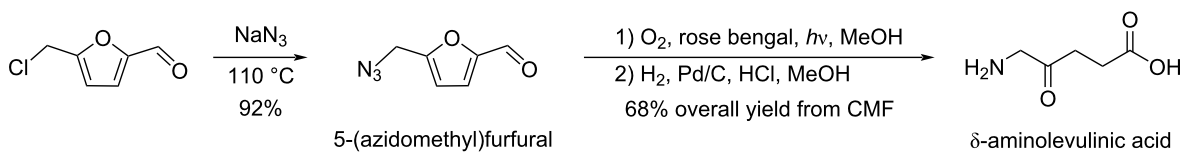
Rehbein and Brasholz have reported the first radical transformation at the benzylic chloromethyl group of CMF. A series of atom transfer radical addition products were obtained by reacting CMF with styrenes under triethylborane (Et_3B)/O_2 system (Scheme 129) [380].

CMF can also react with sodium azide as applied in a synthesis of δ-aminolevulinic acid, an important agricultural and pharmaceutical intermediate. The reaction of CMF and NaN_3 led to the formation of 5-(azidomethyl)furfural. Subsequent photooxidation by irradiation with singlet oxygen, ring opening of the furan and subsequent catalytic hydrogenation resulted in the formation of δ-aminolevulinic acid in 68% yield (Scheme 130) [362].

The substitution of the chlorine atom of CMF by a sulfur atom has also been reported like in a four-step synthesis of ranitidine,



Scheme 129: Radical transformation of CMF with styrenes.

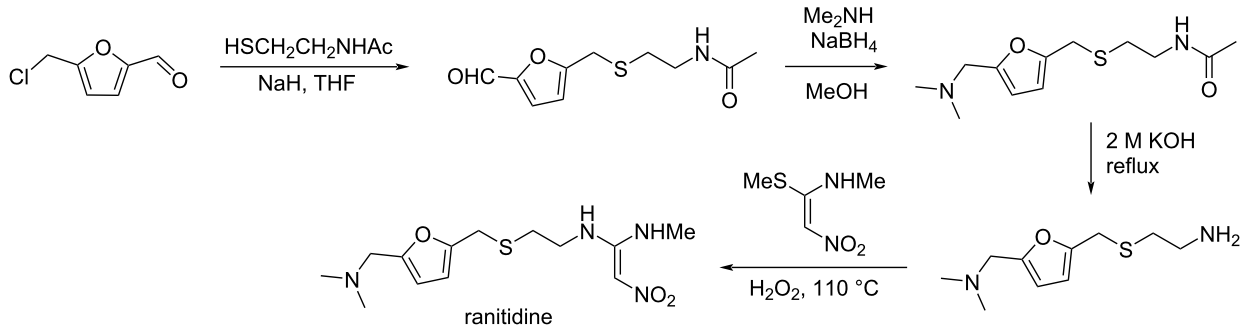


Scheme 130: Synthesis of natural herbicide δ-aminolevulinic acid from CMF.

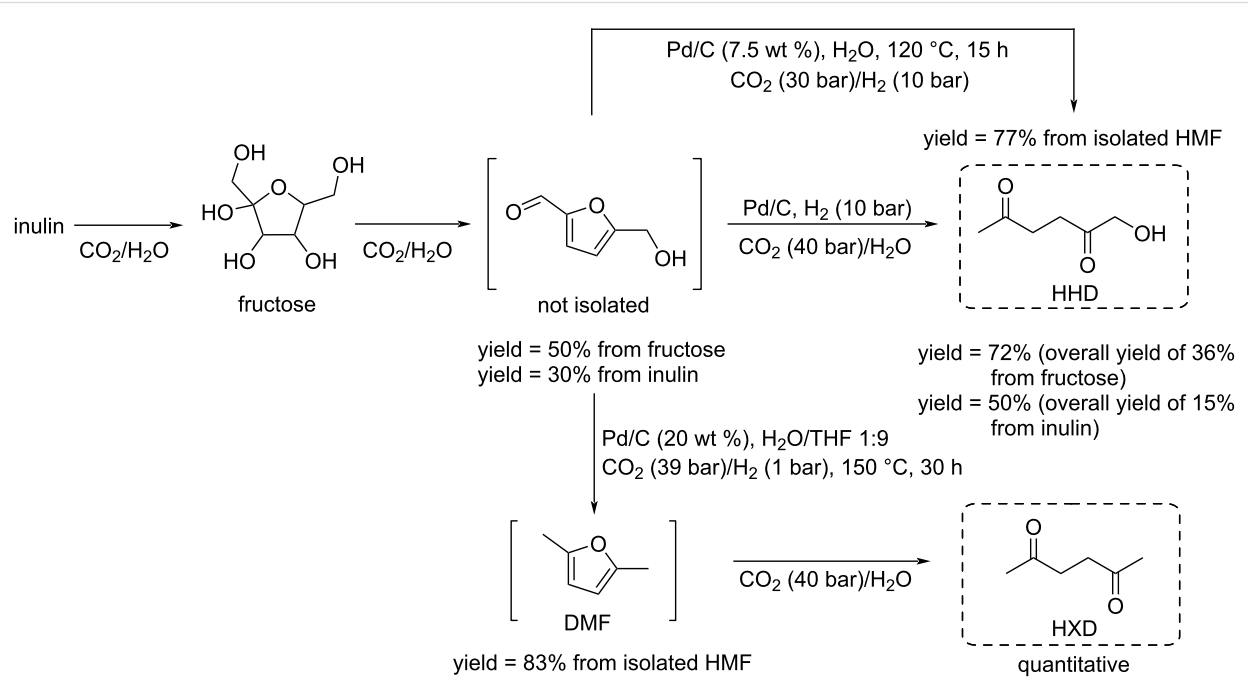
a histamine H_2 receptor antagonists used to treat conditions related to excess stomach acid production. Once the sulfide bond was formed, the (dimethylamino)methyl group was introduced through reductive amination of the aldehyde group (Scheme 131) [381]. Removal of the acetyl group by treatment with KOH led to the previously reported amino intermediate [382] which afforded ranitidine by addition–elimination reaction on 1-methylthio-1-methylamino-2-nitroethylene in overall 68% yield from CMF.

1-Hydroxy-2,5-hexanedione (HHD) and 2,5-hexanedione (HXD)

Linear diketones such as 1-hydroxyhexane-2,5-dione (HHD) or 2,5-hexanedione (HXD) are promising next-generation biomass-derived platform molecules [383,384]. Many conditions have been developed for the catalytic hydrogenation of HMF to HHD using various metals (Pd, Ir, Ru, Rh, Au, Ni-based). For example, Jérome and De Campo reported the one-pot production of HHD directly from carbohydrates (fructose and inulin) through a bifunctional catalytic process using the dual Pd/C/H_2-CO_2/H_2O system, which afforded HHD in 36% and 15% yields, respectively. Pd/C-catalyzed hydrogenation of HMF provided HHD with up to 77% yield. 2,5-Hexanedione (HXD) could be obtained through another route in high yield via 2,5-dimethylfuran (DMF) (Scheme 132) [385]. When using a Pd/C and Amberlyst-15 system, fructose and inulin were found to be converted into HHD in yields of 55% and 27%, respectively [386].



Scheme 131: Four step synthesis of the drug ranitidine from CMF.

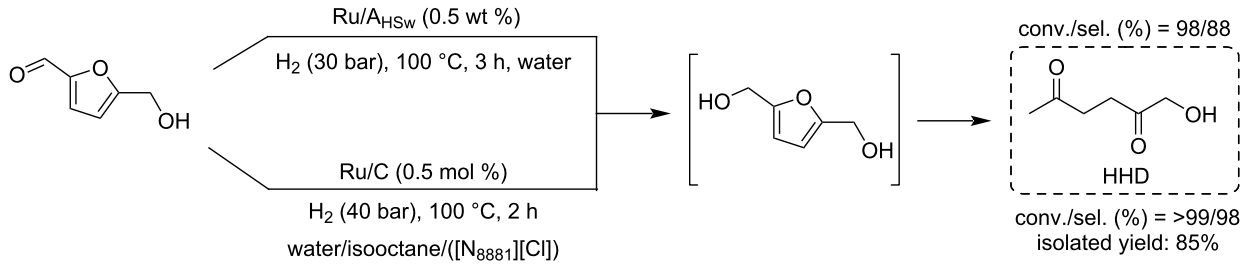


Scheme 132: Pd/CO_2 cooperative catalysis for the production of HHD and HXD.

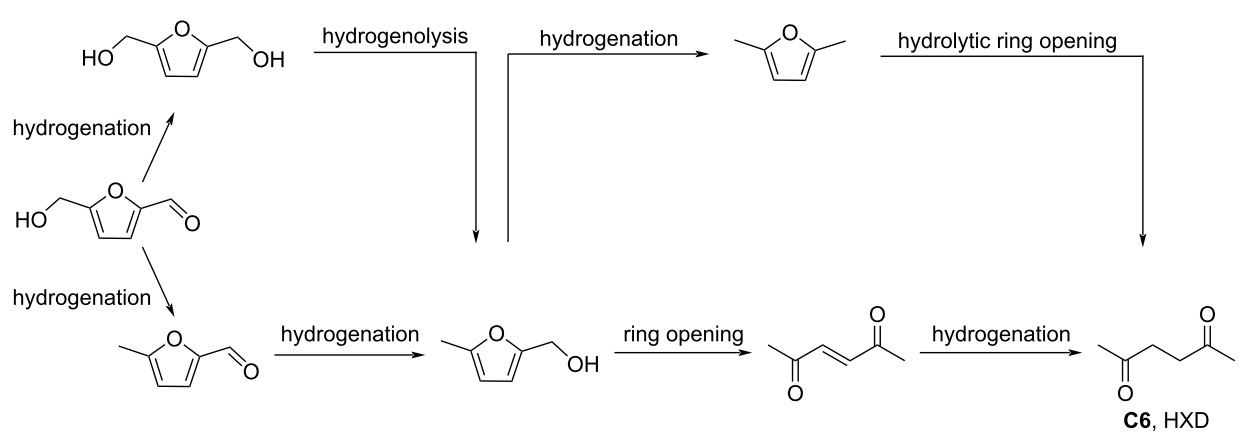
Signoretto reported the hydrogenation of HMF to HHD using a Ru catalyst supported on biochar obtained by pyrolysis of hazelnut shells (Ru/A_{HSw}), a sustainable and inexpensive catalyst. An 88% selectivity for HHD was observed with full conversion of HMF at 30 atm of H_2 (Scheme 133) [387]. In 2023, Selva published a method for the preparation of HHD from HMF by Ru/C catalysis in an ionic liquid-assisted three-phase system consisting of water, isooctane and methyltrioctylammonium chloride ($[N_{8881}][Cl]$), providing HDD with 98% selectivity and 85% isolated yield with full conversion of HMF (>99%). The separation of the product and catalyst (Ru/C) could be easily achieved by adjusting the ratio of the multiphase components (Scheme 133) [388].

2,5-Hexanedione (HXD) could be directly obtained from HMF, DMF or cellulose via acid-catalyzed hydrolysis and metal-catalyzed hydrogenolysis. An iodine-modified Pd catalyst PdI/Al_2O_3 promoted the hydrogenative ring opening of HMF in water at 110 °C under 4.0 MPa H_2, providing HXD in 93% yield [389], while a Pd/Ti_3AlC_2 catalyst promoted the same conversion in water and 4.0 MPa H_2 at only 90 °C [390]. The heterogeneous catalyst cobalt disulfide (CoS_2) with imperfect spherical (A-CoS_2) showed high activity in the hydrogenolysis of HMF to HXD with a yield of 81.5 wt % at 200 °C under H_2 pressure (2 MPa) in MeOH. When applied directly to cellulose, an 11.8 wt % yield of HXD was obtained under these conditions [391]. Various homogeneous acidic catalysts such as $Al_2(SO_4)_3$, $AlCl_3$, $Fe_2(SO_4)_3$, $FeCl_3$, $SnCl_4$, H_2SO_4 and supported noble-metal catalysts (Pd/C, Pt/C, and Ru/C) were tested in the one-pot catalytic conversion of cellulose to HXD developed by Liu and Shu [392]. The combination of $Al_2(SO_4)_3$ with Pd/C exhibited the highest catalytic activity, avoiding excessive hydrogenation of furan intermediates, with an 80% yield of HXD obtained in H_2O/THF at 190 °C and H_2 (2 MPa). Glucose and sucrose gave 91% and 83% yield of HXD at 200 °C and H_2 (2 MPa), respectively. A proposed pathway for the formation of HXD from 5-HMF is shown in Scheme 134.

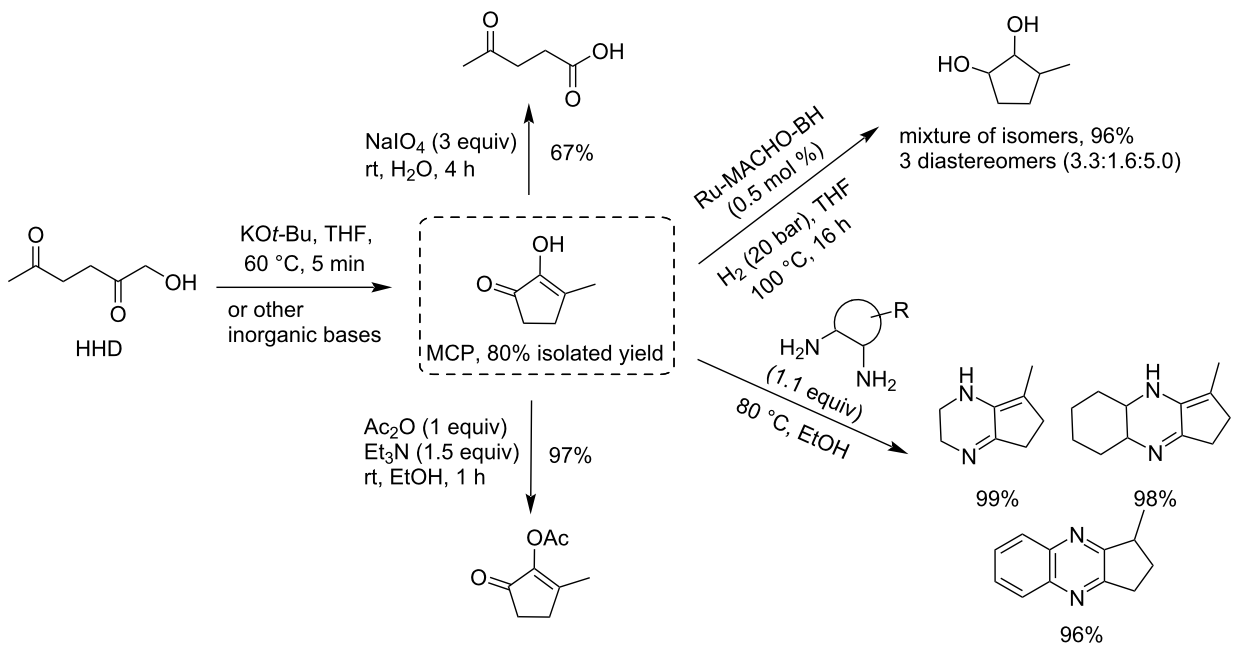
Conversions of HHD: HHD can be further converted into 2-hydroxy-3-methylcyclopent-2-enone (MCP) via intramolecular aldol reactions. In 2018, de Vries developed an efficient base-catalyzed process for the conversion of HHD into MCP. MCP is a hub chemical which can be further transformed into levulinic acid, enol acetate, diol and *N*-heterocyclic compounds through oxidative ring cleavage, acetylation, hydrogenation, and condensation reactions, respectively (Scheme 135) [393].



Scheme 133: Different ruthenium (Ru) catalysts for the ring-opening of 5-HMF to HHD.



Scheme 134: Proposed pathways for preparing HXD from HMF.



Scheme 135: MCP formation and uses.

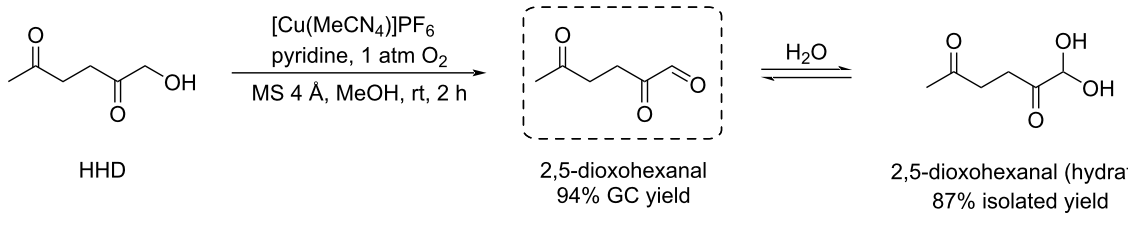
In 2022, de Vries reported the selective Cu(I)-catalyzed oxidation of α-hydroxy ketones to α-keto aldehydes. A 94% GC yield of 2,5-dioxohexanal was obtained from HHD under oxygen atmosphere in the presence of $[Cu(MeCN)_4]PF_6$ (5 mol %), pyridine (10 mol %) and 4 Å molecular sieves (MS). The aqueous work-up of the reaction resulted in the formation of the α-keto aldehyde hydrate in 87% isolated yield (Scheme 136) [394].

This HHD-2,5-dioxohexanal route was also used by the same team to access a wide range of *N*-alkyl and *N*-aryl-3-hydroxypyridinium salts with various functional groups in good yields (up to 82% yield) in the presence of trifluoroacetic acid (Scheme 137). The salts can be used as intermediates in the synthesis of some nitrogen-containing scaffolds [395].

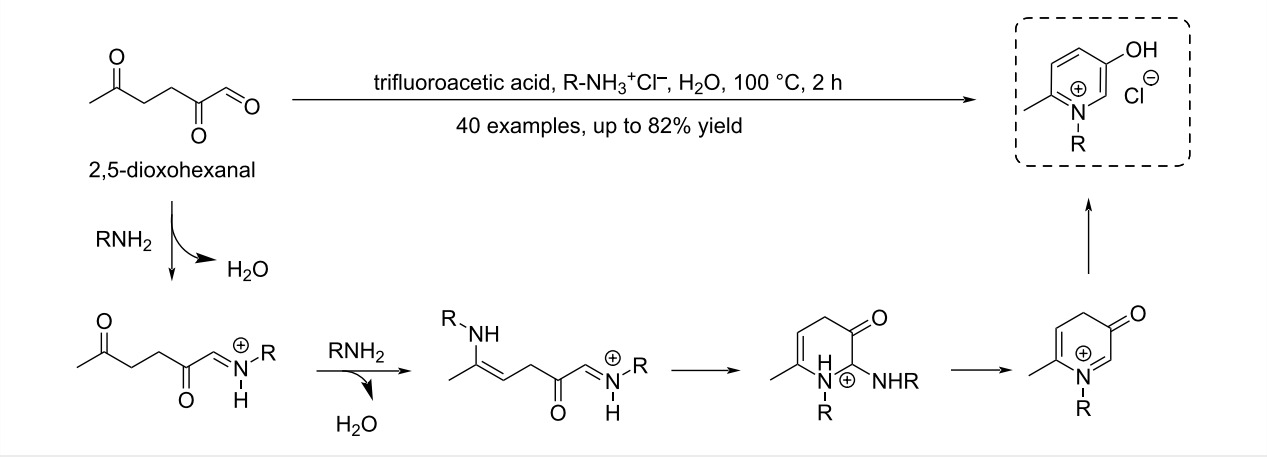
HHD total hydrogenation to 1,2,5-hexanetriol was achieved by de Vries using a Ru-MACHO-BH catalyst (0.5 mol %) under 30 atm H_2 at 100 °C in 18 hours in isopropanol as solvent with nearly quantitative yield (Scheme 138A) [396]. Alternatively, Yang proposed a Ru/C catalyst for the same reaction, giving 1,2,5-hexanetriol in 66% yield with 95% selectivity and 99% conversion of HHD under mild reaction conditions (Scheme 138B) [397].

Conversions of HXD: 3-Methylcyclopent-2-enone (MCP) can be obtained from HXD in 97% yield by cyclization promoted by sodium carbonate in a toluene/H_2O biphasic system. Subsequent dimerization of MCP under ultraviolet irradiation provided polycyclic C_{12} diketones which were hydrodeoxygenated under acidic zeolite H-Y and commercial Ru/C catalysis, leading to a high-density C_{12} polycycloalkane mixture with low freezing point consistent with the usage as aviation fuel (Scheme 139) [398].

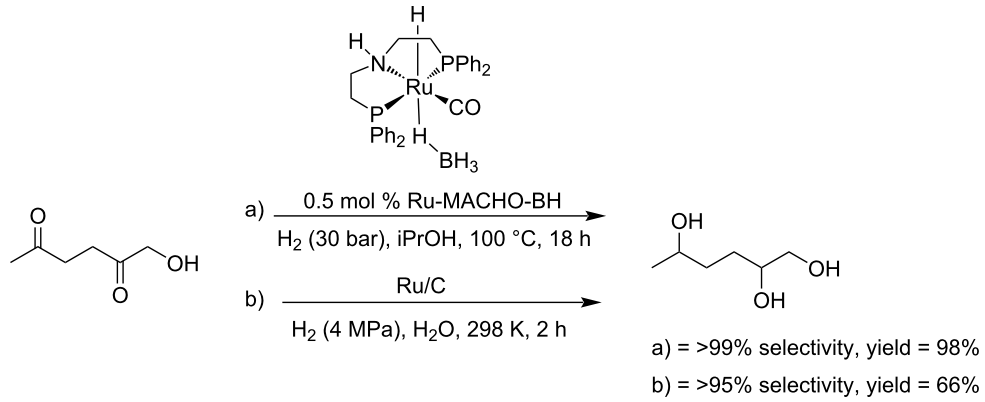
Yan and Chen synthesized the 2,5-hexadione glycerol ketal (HDGK) by reaction of HXD and glycerol, and used it as a



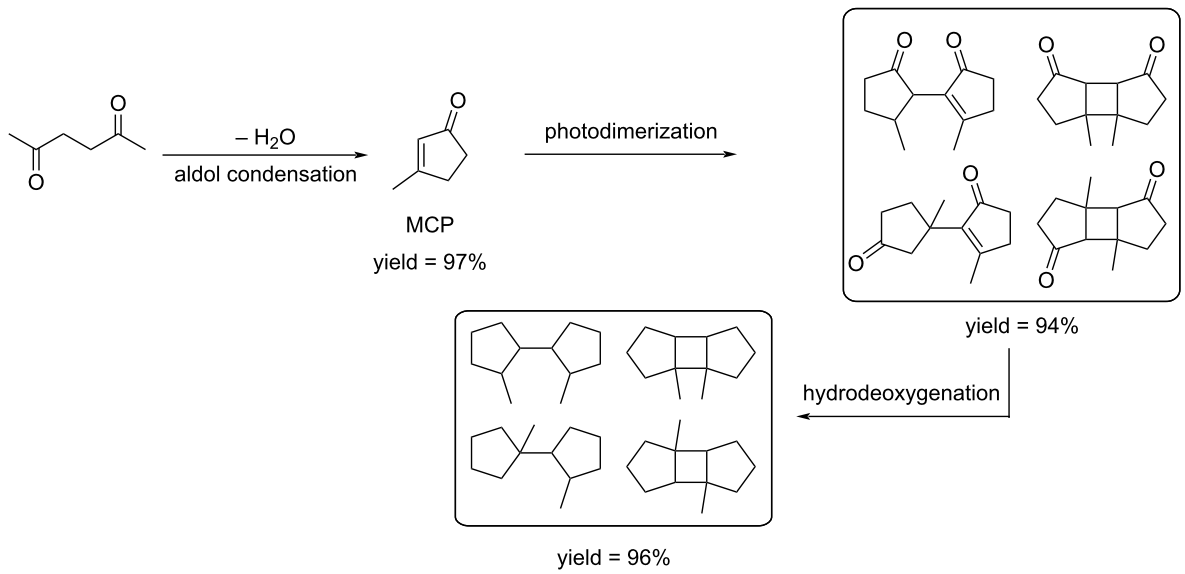
Scheme 136: Cu(I)-catalyzed highly selective oxidation of HHD to 2,5-dioxohexanal.



Scheme 137: Synthesis of *N*-substituted 3-hydroxypyridinium salts from 2,5-dioxohexanal.



Scheme 138: Ru catalyzed hydrogenations of HHD to 1,2,5-hexanetriol (a) see ref. [396]; b) see ref. [397]).



Scheme 139: Aviation fuel range quadricyclanes produced by HXD.

chain extender and crosslinking agent to prepare KCPU-*x*, a dynamic covalent cross-linked polyurethane elastomer (Scheme 140) [399]. The incorporation of a cyclic ketal structure improved the stability, dielectric properties, and healing efficiency of these polyurethane elastomers.

HXD can react with serinol to form 2-(2,5-dimethyl-1*H*-pyrrol-1-yl)-1,3-propanediol (serinol pyrrole, SP) which was used as a high efficiency coupling agent between silica and unsaturated polymer chains in elastomer composites for tires, applicable on the industrial scale (Scheme 141) [400].

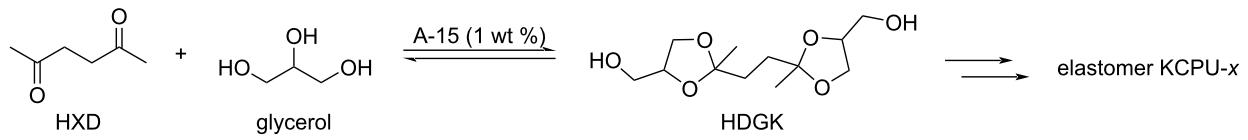
A series of pyrroles, among which some are important intermediates in drug design, has been obtained in 55–89% yields by the cascade reaction of nitroarenes with HXD over a carbon-based iron heterogeneous catalyst (Fe@NSiC) using HCOOH/DBU as reducing agent (Scheme 142) [401].

Efficient upgrading of cellulose into *p*-xylene (PX) was reported through intermediate HXD by Chu et al. [402]. Following a new two-step route (Scheme 143), an 64% overall yield of HXD and DMF was obtained from cellulose, and PX was obtained in 55% yield from this mixture using a solid acid like SnPO-1.75 as catalyst at 275 °C and 2 MPa H_2.

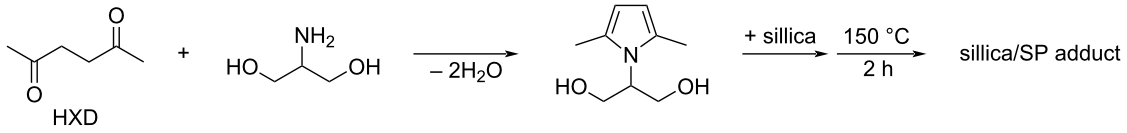
3-(Hydroxymethyl)cyclopentanone (HCPN)

3-(Hydroxymethyl)cyclopentanone (HCPN) can be obtained from HMF, usually involving the hydrogenation of HMF to 2,5-dihydroxymethylfurfural (DHMF), and subsequent Piancatelli rearrangement to 4-hydroxy-4-(hydroxymethyl)cyclopentenone followed by hydrogenation to HCPN (Scheme 144) [168,328].

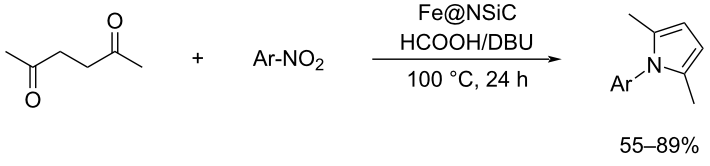
The first reported conversion of HMF to HCPN in 2014 used metal oxide-supported Au nanoparticles as catalysts, with Au/Nb_2O_5 providing the best yield (86%) in the presence of H_2



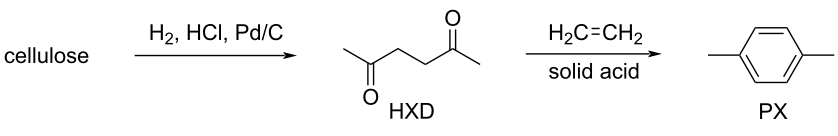
Scheme 140: Synthesis of HDGK from HXD and glycerol as a chain extender.



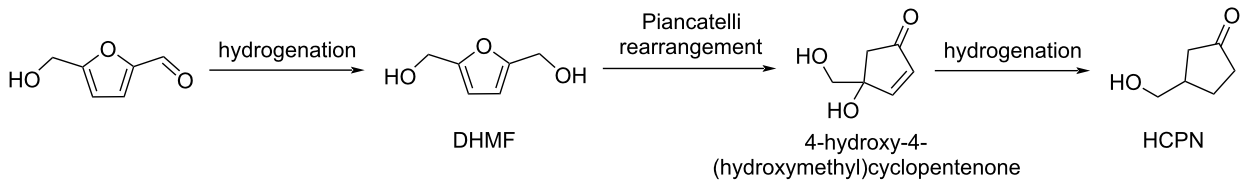
Scheme 141: Synthesis of serinol pyrrole from HXD and serinol.



Scheme 142: Synthesis of pyrroles from HXD and nitroarenes.



Scheme 143: Two-step production of PX from cellulose *via* HXD.

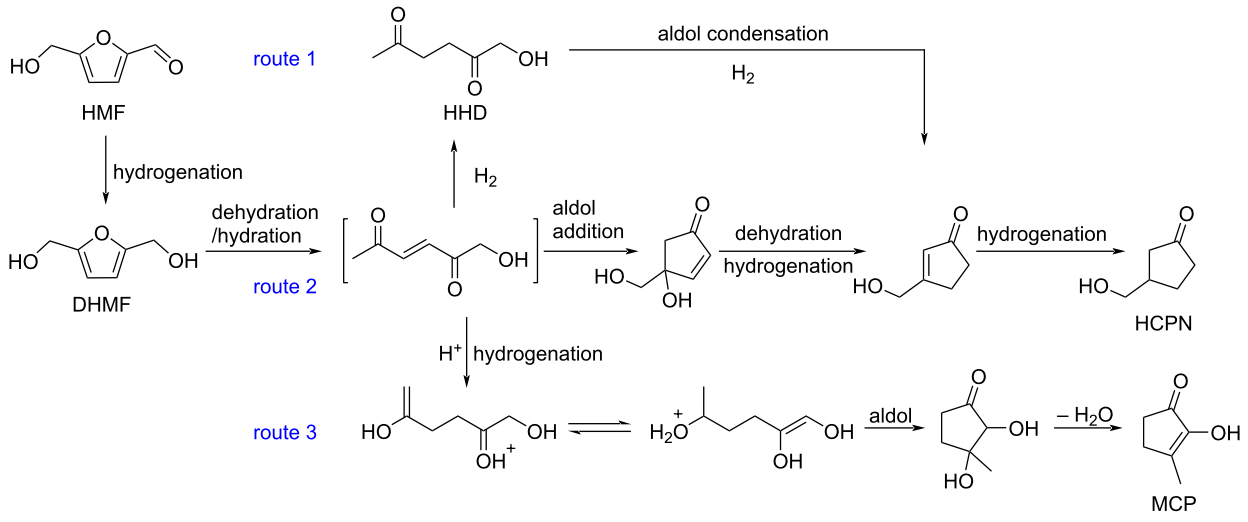


Scheme 144: Preparation of HCPN from HMF via hydrogenation and ring rearrangement.

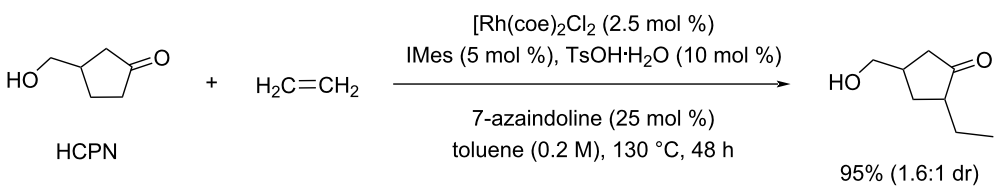
(8 MPa) at 140 °C [403]. Since then, several other supports such as SiO_2, Al_2O_3, Al_2O_3 pyrochlore composites, MOFs, and DMC (double-metal cyanide) have been used for Pt, Pb, Ir catalysts and a palladium bifunctional catalysis method has been reported [404,405]. In 2016, Rosseinsky reported a first non-noble-metal-catalyst derived from Ni/Al layered double hydroxides (Ni-on-Al_2O_3), that afforded an 81% yield of HCPN from HMF [406]. Subsequently, other non-noble-metal-based bimetallic catalysts were applied for this transformation such as Cu-Al_2O_3, Ni-Cu/MOF and Ni-Fe/Al_2O_3 [407-410].

While route 1 and route 2 mechanisms shown in Scheme 145 were previously proposed for the conversion of HMF to HCPN, Deng and Fu expressed doubts about the involvement of intermediate 1-hydroxy-2,5-hexanedione (HHD). They considered that Brønsted acid catalysis promotes the formation of HHD and subsequently 3-methylcyclopenten-2-ol-1-one (MCP) instead of HCPN (Scheme 145, route 3), while Lewis acids facilitate the production of a precursor of HHD, then generating HCPN [411].

HCPN can undergo all typical reactions of ketones, and only two have been selected here, an alkylation and a reductive amination. In 2014, Dong reported the regioselective α-alkylation of HCPN using ethylene as the alkylating agent in the presence of chlorobis(cyclooctene)rhodium(I) dimer $[Rh(coe)_2Cl]_2$, 1,3-bis(2,4,6-trimethylphenyl)imidazole-2-ylidene (IMes), *p*-toluenesulfonic acid monohydrate ($TsOH{\cdot}H_2O$), and 7-azaindoline, leading to α-ethylated HCPN in 95% isolated yield (1.6:1 dr) (Scheme 146) [412].



Scheme 145: Suggested pathways from HMF to HCPN.



Scheme 146: α-Alkylation of HCPN with ethylene gas.

An efficient one-pot cascade conversion of HMF promoted by the $Ni_{0.5}Co_{0.5}$@C catalytic system formed 3-(hydroxymethyl)cyclopentylamine through reductive amination of HCPN with ammonia at 140 °C and 20 bar H_2 for 8 h, with 97% selectivity and full conversion of HCPN (Scheme 147) [413].

Levoglucosenone (LGO) and dihydrolevoglucosenone (H_2LGO or Cyrene®)

Levoglucosenone (LGO) and its fully hydrogenated derivative, dihydrolevoglucosenone (H_2LGO), commercially known under the trademark Cyrene®, are two highly promising biobased C_6 platform molecules. Derived from renewable cellulosic resources, these compounds offer versatile and sustainable scaffolds for the synthesis of a wide range of value-added chemicals, materials, and pharmaceuticals (Scheme 148). LGO, which arises from cellulose by pyrolysis [414-416], or levoglucosan [417] exhibits a bicyclic structure possessing three reactive functions, namely an acetal, a ketone and its conjugated double bond. The selective hydrogenation of the double bond can produce the corresponding saturated ketone dihydrolevoglucosenone (H_2LGO, Cyrene®) [418], which has intensively been studied as a sustainable alternative to classical aprotic dipolar solvents [419-422].

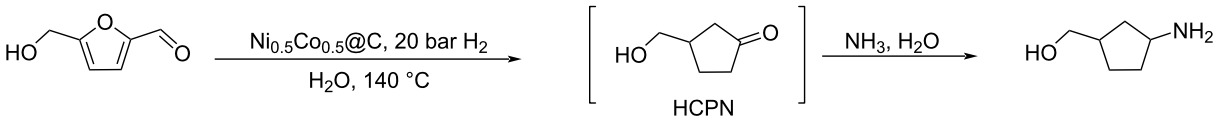
Both LGO and Cyrene® molecules offer a wide range of transformations towards intermediates enabling innovative design in fine chemistry and polymer science [423-425]. The following sections highlight the versatility and practical utility of LGO and Cyrene® through selected recent examples, demonstrating their potential as valuable intermediates in sustainable synthesis.

LGO can be oxidized to (*S*)-γ-hydroxymethyl-α,β-butenolide (HBO) and its formate ester under Baeyer–Villiger conditions (Scheme 149). Hydrolysis of the formate FBO allows a complete transformation of LGO to HBO. When applied to Cyrene®, the reaction leads to the corresponding hydrogenated (*S*)-γ-(hydroxymethyl)butyrolactone (2H-HBO) [426]. The Allais group has reported yields up to 72% on a kilogram scale synthesis, employing aqueous hydrogen peroxide as both the solvent and the oxidizing agent [427]. The sterically hindered bicyclic diol 2H-HBO-HBO can be obtained from LGO through a sustainable two-step process involving LGO homocoupling followed by Baeyer–Villiger oxidation [428]. Several polymers have been obtained after acryloylation or methacryloylation of the OH group [429]. Starting from Cyrene®, Miller and Allais designed a methylated derivative of HBO. After protection of the hydroxy group as a tetrahydropyranyl (THP) acetal giving the intermediate 2-THP-2H-HBO, the α-methylenated derivative (M-THP-2H-HBO) was obtained by reaction of its enolate with paraformaldehyde. This latter was found to slowly oligomerize [430].

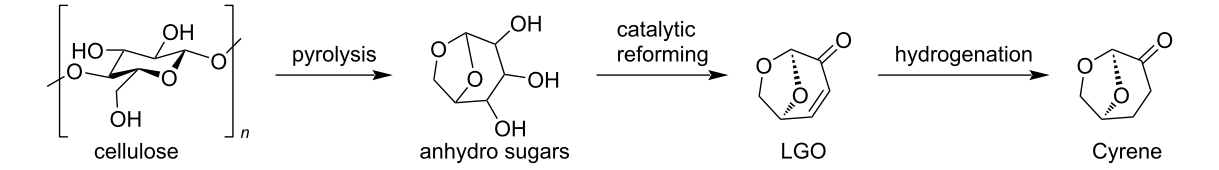
If the hydrogenation of LGO is continued further after formation of Cyrene®, the ketone is reduced and levoglucosanol (Lgol) is formed. For example, in the presence of Pd/C and HCOOH as hydrogen source, the Lgol yield can reach 95% at 180 °C [431]. A methacrylic monomer (*m*-Cyrene®) formed from Lgol was found to undergo rapid polymerization or copolymerization in the presence of AIBN and in Cyrene® as solvent (Scheme 150) [429].

Tetrahydrofurandimethanol (THFDM) and 1,6-hexanediol could be prepared from Lgol via complete hydrogenation/hydrogenolysis [432]. Huber reported a conversion of Lgol to THFDM with 78% overall selectivity to 1,6-hexanediol at 150 °C using a bifunctional $Pd/SiO_2/Al_2O_3$ catalyst (Scheme 151) [433].

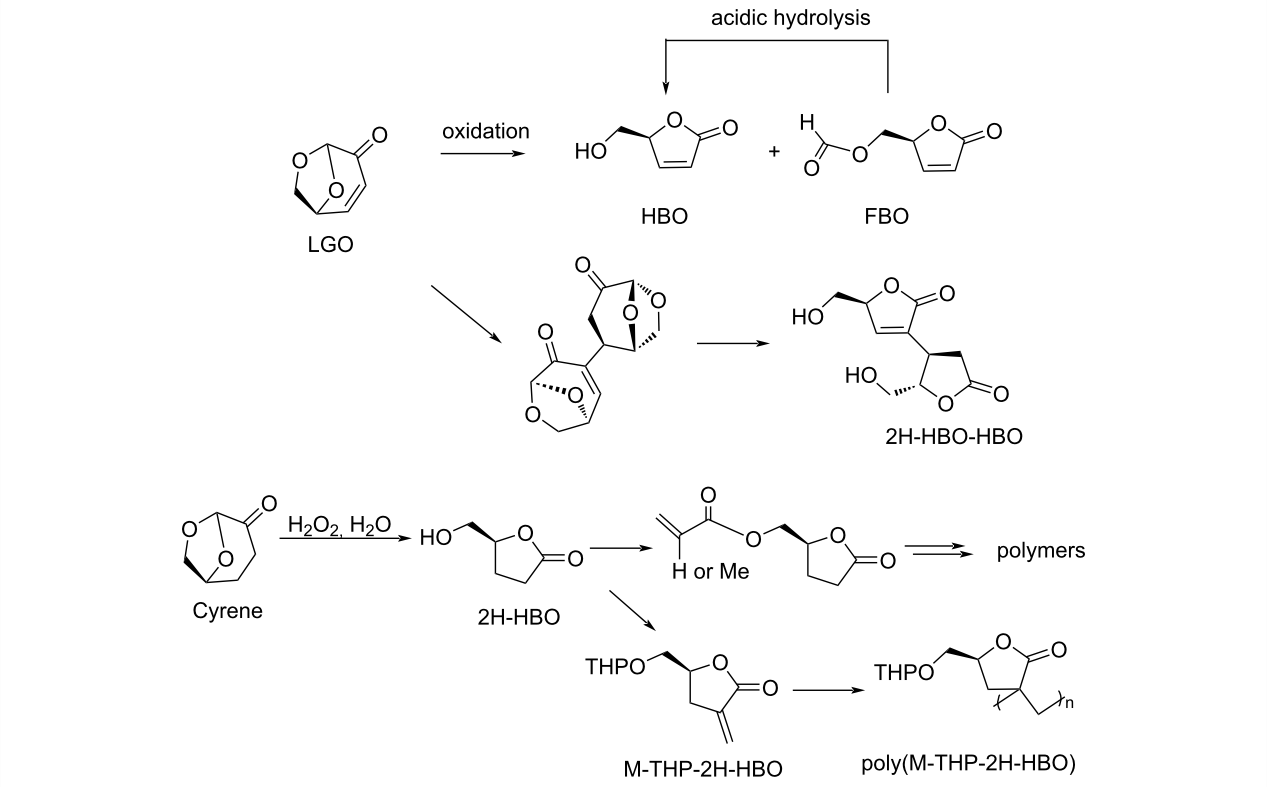
A recent example of reversible addition–fragmentation chain transfer (RAFT) copolymerization of LGO and butadiene or 2-



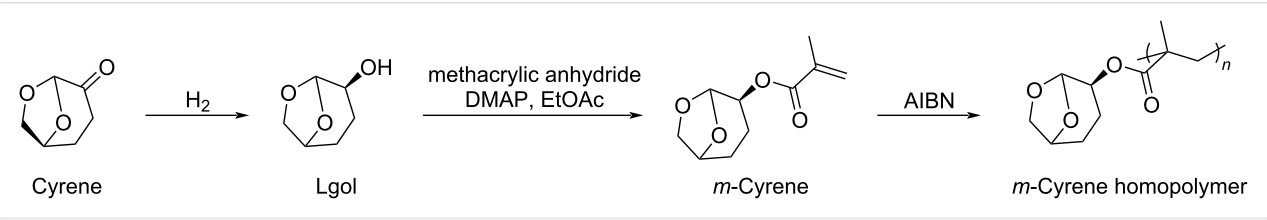
Scheme 147: Synthesis of 3-(hydroxymethyl)cyclopentylamine from HMF via reductive amination of HCPN.



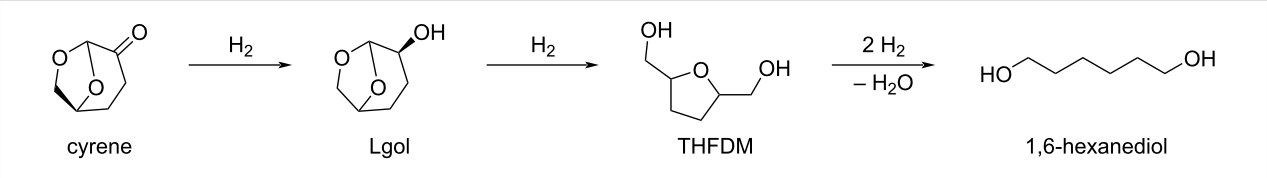
Scheme 148: Production of LGO and Cyrene® from biomass.



Scheme 149: Synthesis of HBO from LGO and other applications.



Scheme 150: Construction of *m*-Cyrene® homopolymer.

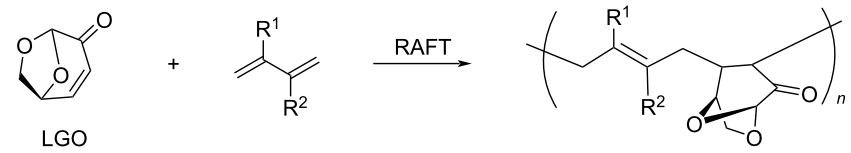


Scheme 151: Conversion of Cyrene® to THFDM and 1,6-hexanediol.

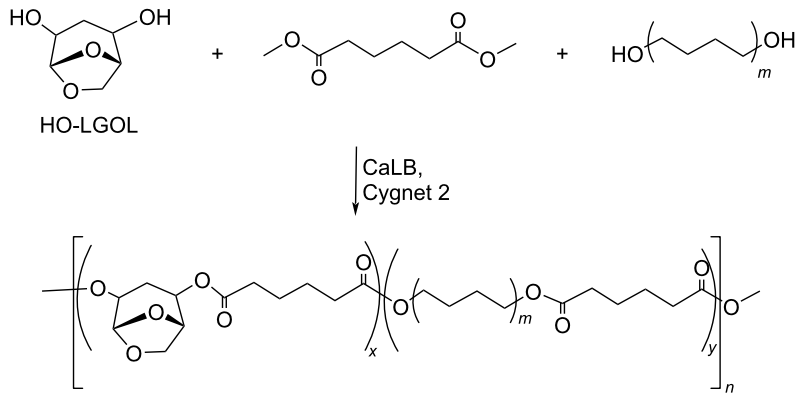
or 3-methyl derivatives was reported by the Choi group (Scheme 152). Conversions of LGO and butadiene up to 80% were observed, leading to polymers having a high degree of alternation and exhibiting excellent thermal stability [434].

Another interesting example of the use of LGO in polymer science was recently reported by Warne and Pellis, who used the diol obtained by hydration and reduction of LGO in combination with butane-1,4-diol for polycondensation with dimethyl adipate in the green solvent dioxolane Cygnet 2 under biocatalytic conditions (*Candida antartica* lipase B CaLB) (Scheme 153). Longer diols such as 1,8-octanediol or 1,12-dodecanediol were also used [435].

In the presence of a catalytic quantity of K_3PO_4, the self-condensation of Cyrene® gave the corresponding product in 81.3%

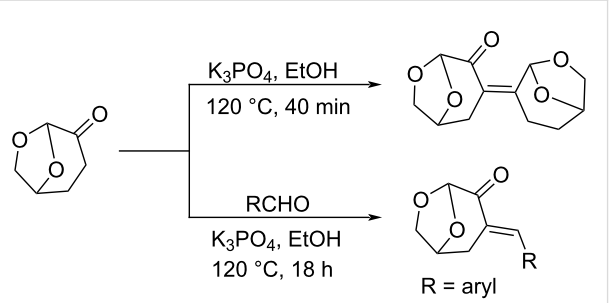


Scheme 152: RAFT co-polymerization of LGO and butadienes.



Scheme 153: Polycondensation of HO-LGOL and diols with dimethyl adipate.

yield at 120 °C for 40 min. The Claisen–Schmidt reaction of Cyrene® with aromatic and heteroaromatic aldehydes offered a wide range of yields, up to 95% at 120 °C after 18 h (Scheme 154) [436].

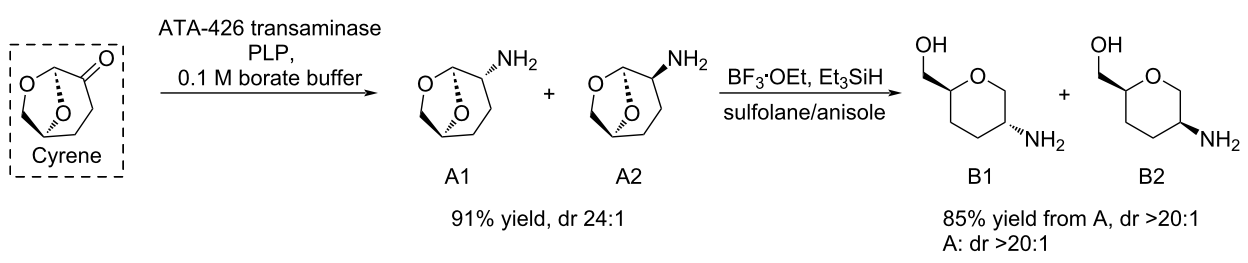


Scheme 154: Self-condensation of Cyrene® and Claisen–Schmidt reactions.

Cyrene® has also been used as a starting chiral building block for applications in drug design. For example, 5-amino-2-hydroxymethyltetrahydropyran (B1), an intermediate in the synthesis of bioactive compounds, was synthesized via a two-step, protecting-group-free, process [437]. Cyrene® underwent an enzyme-catalyzed (ATA-426) transamination followed by reductive acetal opening. ATA-426 provided the chiral cyclohexylamine intermediates **A1** and **A2** with high selectivity (24:1) and 91% yield. Hydroxy-amino derivatives **B1** and **B2** were obtained from **A1** and **A2** in 85% yield with a high diastereoselectivity (>20:1). This two-step process replaced the reported nine-step synthesis of **B1** from tri-*O*-acetyl-D-glucal and resulted in a more than 27% yield improvement (Scheme 155).

Conclusion

The valorization of biobased carbonyl compounds represents a pivotal strategy in the transition towards a greener and sustain-



Scheme 155: Synthesis of 5-amino-2-(hydroxymethyl)tetrahydropyran from Cyrene®.

able biobased chemical industry. The low-molecular-weight intermediates derived from renewable biomass resources exhibit versatile reactivity and serve as crucial building blocks for a wide array of value-added chemicals, fuels, and other materials. Significant advances in catalytic technologies, reaction engineering, and process integration have enabled efficient transformations of biobased aldehydes, ketones, and related compounds into higher-value products such as alcohols, acids, esters, polymers, and fine chemicals. The remarkable structural diversity offered by biobased carbonyl compounds, and the immense variety of chemical reactions that carbonyl compounds can undergo, create an extremely powerful opportunity for accessing all kinds of chemical architectures, including complex ones. Despite the recent progress in the field, efforts must be continued for tackling the remaining challenges, notably achieving always higher selectivity, catalytic stability, and process scalability under economically and environmentally favorable conditions. This will constitute the basis for future biobased access to all types of chemical products.

List of Abbreviations

The abbreviations used in the text and schemes are collected in Table 1.

Table 1: List of abbreviations.

Name	Abbreviation
ALA	atrolactic acid
BA	benzylic acid
CMF	5-(chloromethyl)furfural
CMFCC	5-(chloromethyl)-furan-2-carbonyl chloride
DES	deep eutectic solvent
DFF	2,5-diformyfuran
DHA	dihydroxyacetone
DHM	dihydroxymethylfuran
DHMF	2,5-dihydroxymethylfurfural
DHMTHF	dihydroxymethyltetrahydrofuran,
DMF	2,5-dimethylfuran
DMTHF	dimethyltetrahydrofuran
EG	ethylene glycol
EL and BL	ethyl levulinate and butyl levulinate
FA	furfuryl alcohol
FDCA	furandicarboxylic
FDCC	furan-2,5-dicarbonyl chloride
FFCA	5-formyl-2-furancarboxylic acid
GA	glycolic acid
GBL	γ-butyrolactone
GCA	glycolaldehyde
GLAD	glyceraldehyde
GLY	glycerol
GVL	γ-valerolactone
H_2LGO	dihydrolevoglucosenone
Hap	hydroxyapatite
HBO	(*S*)-γ-hydroxymethyl-α,β-butenolide
HCPN	3-(hydroxymethyl)cyclopentanone
HCPN	3-(hydroxymethyl)cyclopentanone
HDGK	2,5-hexadione glycerol ketal
HFO	2-hydroxy-2(5*H*)-furanone
2H-HBO	(*S*)-γ-hydroxymethyl butyrolactone
HHCPN	4-hydroxy-4-(hydroxymethyl)cyclopent-2-en-1-one
HHD	1-hydroxyhexane-2,5-dione
HMCP	2-hydroxy-3-methylcyclopent-2-enone
HMF	5-hydroxymethylfurfural
HMFA	5-hydroxymethylfuranoic acid
HMTHFF	hydroxymethyltetrahydrofurfural
2,3-HPO	2,3-dihydroxypropanal
3-HPO	3-hydroxypropanal
HXD	2,5-hexanedione
IB	α-hydroxyisobutyric acid
LA	lactic acid
LEV	levulinic acid
LGO	levoglucosenone
Lgol	levoglucosanol
LMW-H	low-molecular-weight humin
MA	mandelic acid
MAN	maleic anhydride
MCP	3-methylcyclopent-2-enone
2-MeTHF	2-methyltetrahydrofuran
MFA	methylfurfurylalcohol,
MS	molecular sieves
MSA	methane sulfonic acid
M-THP-2H-HBO	α-methylenated derivative
NADH	nicotinamide dinucleotide
PA	propanoic acid
PDO	1,3-propanediol
PGA	polyglycolic acid
PLA	polylactic acid
PLGA	polylactic-*co*-glycolic acid
PX	*p*-xylene
RAFT	reversible addition–fragmentation chain transfer
SGCN	mesoporous graphite carbon nitride
TBD	1,5,7-triazabicyclo[4.4.0]dec-5-ene
ThdP-lyase	thiamine diphosphate-dependent lyase
THFDM	tetrahydrofurandimethanol
THP	2-tetrahydropyranyl
TS-1	titanium silicalite catalyst
TsOH·H_2O	*p*-toluenesulfonic acid monohydrate
U-4C-3CR	Ugi 4-center 3-component reaction
VA	valeric acid
VEs	valerate esters

Funding

The authors gratefully acknowledge the financial support from the National Natural Science Foundation of China (22372064 and 22572063), Ordos Key Research and Development Project (2022EEDSKJZDZX003), Key Research and Development and Technology Transfer Projects of Inner Mongolia Autonomous Region of China (2025KJHZ0008), the Innovation and Talent Recruitment Base of New Energy Chemistry and Device (B21003) and the HUST Academic Frontier Youth Team (2019QYTD06) for the financial support. Financial support from to CNRS and MESRI is gratefully acknowledged. The authors also thank the China Scholarship Council program for a scholarship to JJ.

Author Contributions

Jingjing Jiang: conceptualization; methodology; visualization; writing – original draft. Muhammad Noman Haider Tariq: conceptualization; methodology; visualization; writing – original draft. Florence Popowycz: conceptualization; formal analysis; funding acquisition; investigation; methodology; project administration; resources; supervision; validation; writing – review & editing. Yanlong Gu: conceptualization; formal analysis; funding acquisition; investigation; methodology; project administration; resources; supervision; validation; visualization; writing – review & editing. Yves Queneau: conceptualization; formal analysis; funding acquisition; investigation; methodology; project administration; resources; supervision; validation; visualization; writing – review & editing.

ORCID® iDs

Jingjing Jiang - https://orcid.org/0000-0003-3021-6219
Muhammad Noman Haider Tariq - https://orcid.org/0000-0002-5064-642X
Florence Popowycz - https://orcid.org/0000-0002-0297-295X
Yanlong Gu - https://orcid.org/0000-0001-5130-3026
Yves Queneau - https://orcid.org/0000-0003-4052-061X

Data Availability Statement

Data sharing is not applicable as no new data was generated or analyzed in this study.

References

1. Sheldon, R. A. *Green Chem.* **2014,** *16,* 950–963. doi:10.1039/c3gc41935e
2. Anastas, P. T.; Warner, J. C. *Green Chemistry: Theory and Practice;* Oxford University Press: Oxford, UK, 2000. doi:10.1093/oso/9780198506980.001.0001
3. Trost, B. M. *Science* **1991,** *254,* 1471–1477. doi:10.1126/science.1962206
4. Sheldon, R. A. *Chem. Ind. (London)* **1992,** 903–906.
5. Kümmerer, K.; Clark, J. H.; Zuin, V. G. *Science* **2020,** *367,* 369–370. doi:10.1126/science.aba4979
6. Anastas, P. T.; Zimmerman, J. B. *Green Chem.* **2019,** *21,* 6545–6566. doi:10.1039/c9gc01293a
7. He, M.; Sun, Y.; Han, B. *Angew. Chem., Int. Ed.* **2013,** *52,* 9620–9633. doi:10.1002/anie.201209384
8. Isikgor, F. H.; Becer, C. R. *Polym. Chem.* **2015,** *6,* 4497–4559. doi:10.1039/c5py00263j
9. Jang, Y.-S.; Kim, B.; Shin, J. H.; Choi, Y. J.; Choi, S.; Song, C. W.; Lee, J.; Park, H. G.; Lee, S. Y. *Biotechnol. Bioeng.* **2012,** *109,* 2437–2459. doi:10.1002/bit.24599
10. Mika, L. T.; Cséfalvay, E.; Németh, Á. *Chem. Rev.* **2018,** *118,* 505–613. doi:10.1021/acs.chemrev.7b00395
11. Corma, A.; Iborra, S.; Velty, A. *Chem. Rev.* **2007,** *107,* 2411–2502. doi:10.1021/cr050989d
12. Zimmerman, J. B.; Anastas, P. T.; Erythropel, H. C.; Leitner, W. *Science* **2020,** *367,* 397–400. doi:10.1126/science.aay3060
13. Ganesh, K. N.; Zhang, D.; Miller, S. J.; Rossen, K.; Chirik, P. J.; Kozlowski, M. C.; Zimmerman, J. B.; Brooks, B. W.; Savage, P. E.; Allen, D. T.; Voutchkova-Kostal, A. M. *ACS Omega* **2021,** *6,* 16254–16258. doi:10.1021/acsomega.1c03011
14. Schaub, T. *Chem. – Eur. J.* **2021,** *27,* 1865–1869. doi:10.1002/chem.202003544
15. Nising, C. F.; von Nussbaum, F. *Eur. J. Org. Chem.* **2022,** e202200439. doi:10.1002/ejoc.202200439
16. Wegelin, S.; Meier, M. A. R. *Curr. Opin. Green Sustainable Chem.* **2024,** *47,* 100931. doi:10.1016/j.cogsc.2024.100931
17. Gandeepan, P.; Kaplaneris, N.; Santoro, S.; Vaccaro, L.; Ackermann, L. *ACS Sustainable Chem. Eng.* **2019,** *7,* 8023–8040. doi:10.1021/acssuschemeng.9b00226
18. López, G. V.; Porcal, W. *Pure Appl. Chem.* **2024,** *96,* 1271–1277. doi:10.1515/pac-2024-0230
19. Queneau, Y.; Han, B. *Innovation* **2022,** *3,* 100184. doi:10.1016/j.xinn.2021.100184
20. Zuiderveen, E. A. R.; Kuipers, K. J. J.; Caldeira, C.; Hanssen, S. V.; van der Hulst, M. K.; de Jonge, M. M. J.; Vlysidis, A.; van Zelm, R.; Sala, S.; Huijbregts, M. A. J. *Nat. Commun.* **2023,** *14,* 8521. doi:10.1038/s41467-023-43797-9
21. Nair, L. G.; Verma, P. *Biomass Bioenergy* **2024,** *191,* 107454. doi:10.1016/j.biombioe.2024.107454
22. Keijer, T.; Bakker, V.; Slootweg, J. C. *Nat. Chem.* **2019,** *11,* 190–195. doi:10.1038/s41557-019-0226-9
23. Ryu, H. W.; Kim, D. H.; Jae, J.; Lam, S. S.; Park, E. D.; Park, Y.-K. *Bioresour. Technol.* **2020,** *310,* 123473. doi:10.1016/j.biortech.2020.123473
24. Wong, S. S.; Shu, R.; Zhang, J.; Liu, H.; Yan, N. *Chem. Soc. Rev.* **2020,** *49,* 5510–5560. doi:10.1039/d0cs00134a
25. Gérardy, R.; Debecker, D. P.; Estager, J.; Luis, P.; Monbaliu, J.-C. M. *Chem. Rev.* **2020,** *120,* 7219–7347. doi:10.1021/acs.chemrev.9b00846
26. Wang, J.; Fu, J.; Zhao, Z.; Bing, L.; Xi, F.; Wang, F.; Dong, J.; Wang, S.; Lin, G.; Yin, Y.; Hu, Q. *Innovation* **2023,** *4,* 100423. doi:10.1016/j.xinn.2023.100423
27. López, G. V.; Porcal, W. *Pure Appl. Chem.* **2024,** *96,* 1271–1277. doi:10.1515/pac-2024-0230
28. Li, J.; Yang, R.; Xu, S.; Zhou, C.; Xiao, Y.; Hu, C.; Tsang, D. C. W. *Appl. Catal., B* **2022,** *317,* 121785. doi:10.1016/j.apcatb.2022.121785
29. Faveere, W.; Mihaylov, T.; Pelckmans, M.; Moonen, K.; Gillis-D'Hamers, F.; Bosschaerts, R.; Pierloot, K.; Sels, B. F. *ACS Catal.* **2020,** *10,* 391–404. doi:10.1021/acscatal.9b02437

30. Liang, G.; Wang, A.; Li, L.; Xu, G.; Yan, N.; Zhang, T. *Angew. Chem., Int. Ed.* **2017,** *56,* 3050–3054. doi:10.1002/anie.201610964
31. Flynn, M. T.; Liu, X.; Dell'Acqua, A.; Rabeah, J.; Brückner, A.; Baráth, E.; Tin, S.; de Vries, J. G. *ChemSusChem* **2022,** *15,* e202201264. doi:10.1002/cssc.202201264
32. Parham, W. E.; Reiff, H. E. *J. Am. Chem. Soc.* **1955,** *77,* 6391–6393. doi:10.1021/ja01628a108
33. Xu, J.; Huang, W.; Bai, R.; Queneau, Y.; Jérôme, F.; Gu, Y. *Green Chem.* **2019,** *21,* 2061–2069. doi:10.1039/c8gc04000a
34. Wu, F.; Huang, W.; Yiliqi; Yang, J.; Gu, Y. *Adv. Synth. Catal.* **2018,** *360,* 3318–3330. doi:10.1002/adsc.201800669
35. Zhou, Y.; Slater, T. J. A.; Luo, X.; Shen, Y. *Appl. Catal., B* **2023,** *324,* 122218. doi:10.1016/j.apcatb.2022.122218
36. Jo, H.-J.; Yu, H.; Cheon, H.; Kim, J.-H.; Kim, G. Y.; Kim, B. S.; Kim, J.-S.; Park, J.-B. *ACS Sustainable Chem. Eng.* **2023,** *11,* 1078–1086. doi:10.1021/acssuschemeng.2c05936
37. Dai, X.; Wang, X.; Rabeah, J.; Kreyenschulte, C.; Brückner, A.; Shi, F. *Chem. – Eur. J.* **2021,** *27,* 16889–16895. doi:10.1002/chem.202102300
38. Huo, Z.; Xiao, J.; Ren, D.; Jin, F.; Wang, T.; Yao, G. *Green Chem.* **2017,** *19,* 1308–1314. doi:10.1039/c6gc03036j
39. Liu, S.; Feng, H.; Li, T.; Wang, Y.; Rong, N.; Yang, W. *Green Chem.* **2020,** *22,* 7468–7475. doi:10.1039/d0gc02676j
40. Lei, X.; Wang, F.-F.; Liu, C.-L.; Yang, R.-Z.; Dong, W.-S. *Appl. Catal., A* **2014,** *482,* 78–83. doi:10.1016/j.apcata.2014.05.029
41. Jem, K. J.; Tan, B. *Adv. Ind. Eng. Polym. Res.* **2020,** *3,* 60–70. doi:10.1016/j.aiepr.2020.01.002
42. Ayyoob, M.; Kim, Y. J. *Polymers (Basel, Switz.)* **2018,** *10,* 1132. doi:10.3390/polym10101132
43. Sen Gupta, K. K.; Pal, B.; Sen, P. K. *Int. J. Chem. Kinet.* **1999,** *31,* 873–882. doi:10.1002/(sici)1097-4601(1999)31:12<873::aid-kin6>3.0.co;2-z
44. Fan, Y. X.; Zhou, C. H.; Zhu, X. H. *Catal. Rev.: Sci. Eng.* **2009,** *51,* 293–324. doi:10.1080/01614940903048513
45. Lira, C. T.; McCrackin, P. J. *Ind. Eng. Chem. Res.* **1993,** *32,* 2608–2613. doi:10.1021/ie00023a025
46. Paparizos, C.; Shaw, W. G.; Dolhyj, S. R. Catalytic conversion of lactic acid and ammonium lactate to acrylic acid. Eur. Patent EP0181718B1, Nov 22, 1988.
47. Mok, W. S. L.; Antal, M. J., Jr.; Jones, M., Jr. *J. Org. Chem.* **1989,** *54,* 4596–4602. doi:10.1021/jo00280a027
48. Zhang, X.; Lin, L.; Zhang, T.; Liu, H.; Zhang, X. *Chem. Eng. J.* **2016,** *284,* 934–941. doi:10.1016/j.cej.2015.09.039
49. Gunter, G. C.; Langford, R. H.; Jackson, J. E.; Miller, D. J. *Ind. Eng. Chem. Res.* **1995,** *34,* 974–980. doi:10.1021/ie00042a035
50. Wadley, D. C.; Tam, M. S.; Kokitkar, P. B.; Jackson, J. E.; Miller, D. J. *J. Catal.* **1997,** *165,* 162–171. doi:10.1006/jcat.1997.1484
51. Miller, D. J.; Jackson, J. E.; Langford, R. H.; Gunter, G. C.; Tam, M. S.; Kokitkar, P. B. Process for the preparation of 2, 3-pentanedione. U.S. Pat. Appl. US5,731,471 A, March 24, 1998.
52. Gunter, G. C.; Miller, D. J.; Jackson, J. E. *J. Catal.* **1994,** *148,* 252–260. doi:10.1006/jcat.1994.1206
53. Ai, M. *Appl. Catal., A* **2002,** *234,* 235–243. doi:10.1016/s0926-860x(02)00229-6
54. Ai, M. *Appl. Catal., A* **2002,** *232,* 1–6. doi:10.1016/s0926-860x(02)00097-2
55. Minniti, G.; Cerone, R.; De Toni, E. *Am. Biotechnol. Lab.* **2000,** *18,* 25–26.
56. Oude Elferink, S. J. W. H.; Krooneman, J.; Gottschal, J. C.; Spoelstra, S. F.; Faber, F.; Driehuis, F. *Appl. Environ. Microbiol.* **2001,** *67,* 125–132. doi:10.1128/aem.67.1.125-132.2001
57. Chen, Y.; Miller, D. J.; Jackson, J. E. *Ind. Eng. Chem. Res.* **2007,** *46,* 3334–3340. doi:10.1021/ie0614632
58. Simonov, M. N.; Simakova, I. L.; Minyukova, T. P.; Khassin, A. A. *Russ. Chem. Bull.* **2009,** *58,* 1114–1118. doi:10.1007/s11172-009-0144-x
59. Simonov, M. N.; Simakova, I. L.; Parmon, V. N. *React. Kinet. Catal. Lett.* **2009,** *97,* 157–162. doi:10.1007/s11144-009-0005-5
60. Cortright, R. D.; Sanchez-Castillo, M.; Dumesic, J. A. *Appl. Catal., B* **2002,** *39,* 353–359. doi:10.1016/s0926-3373(02)00121-2
61. Lipinsky, E.; Sinclair, R. *Chem. Eng. Prog.* **1986,** *82,* 26–32.
62. Datta, R.; Tsai, S.-P.; Bonsignore, P.; Moon, S.-H.; Frank, J. R. *FEMS Microbiol. Rev.* **1995,** *16,* 221–231. doi:10.1111/j.1574-6976.1995.tb00168.x
63. Vaidya, A. N.; Pandey, R. A.; Mudliar, S.; Kumar, M. S.; Chakrabarti, T.; Devotta, S. *Crit. Rev. Environ. Sci. Technol.* **2005,** *35,* 429–467. doi:10.1080/10643380590966181
64. Wang, H.; Sun, X.; Seib, P. *J. Appl. Polym. Sci.* **2003,** *90,* 3683–3689. doi:10.1002/app.13001
65. Nikles, S. M.; Piao, M.; Lane, A. M.; Nikles, D. E. *Green Chem.* **2001,** *3,* 109–113. doi:10.1039/b101147m
66. Tretjak, S.; Burtin, E.; Teissier, R. Continuous production of ethyl lactate method. WO Patent WO2004/052825, June 11, 2004.
67. He, W.; Zhang, B.; Liu, P.; Sun, X.; Zhang, S. *Chin. J. Catal.* **2006,** *27,* 527–531. doi:10.1016/s1872-2067(06)60030-2
68. Asthana, N.; Kolah, A.; Vu, D. T.; Lira, C. T.; Miller, D. J. *Org. Process Res. Dev.* **2005,** *9,* 599–607. doi:10.1021/op0500640
69. Ahern, W. P.; Andrist, D. F.; Skogerson, L. E. Fermentation of whey to produce propionic acid. U.S. Pat. Appl. US4,743,453 A, May 10, 1988.
70. Odell, B.; Earlam, G.; Cole-Hamilton, D. J. *J. Organomet. Chem.* **1985,** *290,* 241–248. doi:10.1016/0022-328x(85)87436-2
71. Jiang, S.; Li, Z.; Zhao, L.; Sun, M.; Zhang, X.; Yang, D.; Xu, G. *ACS Sustainable Chem. Eng.* **2022,** *10,* 2355–2367. doi:10.1021/acssuschemeng.1c06393
72. Bonn, G.; Rinderer, M.; Bobleter, O. *J. Carbohydr. Chem.* **1985,** *4,* 67–77. doi:10.1080/07328308508062949
73. Lookhart, G. L.; Feather, M. S. *Carbohydr. Res.* **1978,** *60,* 259–265. doi:10.1016/s0008-6215(78)80033-0
74. Poust, S.; Piety, J.; Bar-Even, A.; Louw, C.; Baker, D.; Keasling, J. D.; Siegel, J. B. *ChemBioChem* **2015,** *16,* 1950–1954. doi:10.1002/cbic.201500228
75. Siegel, J. B.; Smith, A. L.; Poust, S.; Wargacki, A. J.; Bar-Even, A.; Louw, C.; Shen, B. W.; Eiben, C. B.; Tran, H. M.; Noor, E.; Gallaher, J. L.; Bale, J.; Yoshikuni, Y.; Gelb, M. H.; Keasling, J. D.; Stoddard, B. L.; Lidstrom, M. E.; Baker, D. *Proc. Natl. Acad. Sci. U. S. A.* **2015,** *112,* 3704–3709. doi:10.1073/pnas.1500545112
76. Yang, J.; Sun, S.; Men, Y.; Zeng, Y.; Zhu, Y.; Sun, Y.; Ma, Y. *Catal. Sci. Technol.* **2017,** *7,* 3459–3463. doi:10.1039/c7cy01062a
77. Xiong, L.; Yu, Z.; Cao, H.; Guan, W.; Su, Y.; Pan, X.; Zhang, L.; Liu, X.; Wang, A.; Tang, J. *Angew. Chem., Int. Ed.* **2024,** *63,* e202318461. doi:10.1002/anie.202318461
78. Usami, K.; Xiao, K.; Okamoto, A. *ACS Sustainable Chem. Eng.* **2019,** *7,* 3372–3377. doi:10.1021/acssuschemeng.8b05574
79. Fedoroňko, M.; Königstein, J. *Collect. Czech. Chem. Commun.* **1969,** *34,* 3881–3894. doi:10.1135/cccc19693881

80. Prey, V.; Waldmann, E.; Berbalk, H.; Sommer, F. *Monatsh. Chem.* **1954,** *85,* 1186–1190. doi:10.1007/bf00899873
81. Lemieux, R. U. Rearrangements and Isomerizations in Carbohydrate Chemistry. In *Molecular rearrangements;* De Mayo, P., Ed.; Interscience Publishers: New York, NY, USA, 1964; p 709.
82. Gupta, S. K. *J. Org. Chem.* **1976,** *41,* 2642–2646. doi:10.1021/jo00877a030
83. Colbran, R. L.; Jones, J. K. N.; Matheson, N. K.; Rozema, I. *Carbohydr. Res.* **1967,** *4,* 355–358. doi:10.1016/s0008-6215(00)80190-1
84. Meyerhof, O.; Lohmann, K. *Biochem. Z.* **1934,** *271,* 89–110.
85. Ballou, C. E.; Fischer, H. O. L. *J. Am. Chem. Soc.* **1956,** *78,* 1659–1661. doi:10.1021/ja01589a045
86. Jolimaitre, E.; Delcroix, D.; Essayem, N.; Pinel, C.; Besson, M. *Catal. Sci. Technol.* **2018,** *8,* 1349–1356. doi:10.1039/c7cy02385e
87. Hossain, M. A.; Mills, K. N.; Molley, A. M.; Rahaman, M. S.; Tulaphol, S.; Lalvani, S. B.; Dong, J.; Sunkara, M. K.; Sathitsuksanoh, N. *Appl. Catal., A* **2021,** *611,* 117979. doi:10.1016/j.apcata.2020.117979
88. Koito, Y.; Nakajima, K.; Kitano, M.; Hara, M. *Chem. Lett.* **2013,** *42,* 873–875. doi:10.1246/cl.130319
89. Albuquerque, E. M.; Borges, L. E. P.; Fraga, M. A.; Sievers, C. *ChemCatChem* **2017,** *9,* 2675–2683. doi:10.1002/cctc.201700305
90. Santos, K. M. A.; Albuquerque, E. M.; Borges, L. E. P.; Fraga, M. A. *Mol. Catal.* **2018,** *458,* 198–205. doi:10.1016/j.mcat.2017.12.010
91. Innocenti, G.; Papadopoulos, E.; Fornasari, G.; Cavani, F.; Medford, A. J.; Sievers, C. *ACS Catal.* **2020,** *10,* 11936–11950. doi:10.1021/acscatal.0c03761
92. Nakajima, K.; Noma, R.; Kitano, M.; Hara, M. *J. Phys. Chem. C* **2013,** *117,* 16028–16033. doi:10.1021/jp404523r
93. Abdouli, I.; Dappozze, F.; Eternot, M.; Guillard, C.; Essayem, N. *Molecules* **2022,** *27,* 8172. doi:10.3390/molecules27238172
94. Dai, X.; Adomeit, S.; Rabeah, J.; Kreyenschulte, C.; Brückner, A.; Wang, H.; Shi, F. *Angew. Chem., Int. Ed.* **2019,** *58,* 5251–5255. doi:10.1002/anie.201814050
95. Huang, W.; Liu, F.; Wang, K.; Sidorenko, A.; Bei, M.; Zhang, Z.; Fang, W.; Li, M.; Gu, Y.; Ke, S. *Green Synth. Catal.* **2022,** *3,* 380–384. doi:10.1016/j.gresc.2022.04.008
96. Li, M.; Wu, F.; Gu, Y. *Chin. J. Catal.* **2019,** *40,* 1135–1140. doi:10.1016/s1872-2067(19)63370-x
97. Arandia, A.; Coronado, I.; Remiro, A.; Gayubo, A. G.; Reinikainen, M. *Int. J. Hydrogen Energy* **2019,** *44,* 13157–13168. doi:10.1016/j.ijhydene.2019.04.007
98. Xu, H.; Meng, Q.-H.; Zhang, Z.-G. *Chin. J. Chem.* **2008,** *26,* 1656–1658. doi:10.1002/cjoc.200890299
99. Kini, D. D.; Mathews, J. E. *Int. J. Pharm. Sci. Res.* **2020,** *11,* 2199–2205. doi:10.13040/ijpsr.0975-8232.11(5).2199-05
100. Notz, W.; List, B. *J. Am. Chem. Soc.* **2000,** *122,* 7386–7387. doi:10.1021/ja001460v
101. Subrahmanyam, A. V.; Thayumanavan, S.; Huber, G. W. *ChemSusChem* **2010,** *3,* 1158–1161. doi:10.1002/cssc.201000136
102. Bryn, K.; Hetland, Ø.; Størmer, F. C. *Eur. J. Biochem.* **1971,** *18,* 116–119. doi:10.1111/j.1432-1033.1971.tb01221.x
103. Kochius, S.; Paetzold, M.; Scholz, A.; Merkens, H.; Vogel, A.; Ansorge-Schumacher, M.; Hollmann, F.; Schrader, J.; Holtmann, D. *J. Mol. Catal. B: Enzym.* **2014,** *103,* 61–66. doi:10.1016/j.molcatb.2013.08.016
104. Meng, W.; Ma, C.; Xu, P.; Gao, C. *Trends Biotechnol.* **2022,** *40,* 958–973. doi:10.1016/j.tibtech.2022.01.008
105. Lu, T.; Li, X.; Gu, L.; Zhang, Y. *ChemSusChem* **2014,** *7,* 2423–2426. doi:10.1002/cssc.201402396
106. Li, Y.; Yao, P.; Zhang, S.; Feng, J.; Su, H.; Liu, X.; Sheng, X.; Wu, Q.; Zhu, D.; Ma, Y. *Chem Catal.* **2023,** *3,* 100467. doi:10.1016/j.checat.2022.11.006
107. Cao, C.; Wu, Q. *Chem Catal.* **2023,** *3,* 100494. doi:10.1016/j.checat.2022.100494
108. Matsumura, S.; Kawamori, T.; Yoshikawa, S. *Chem. Lett.* **1991,** *20,* 729–730. doi:10.1246/cl.1991.729
109. Chung, K.; Banik, S. M.; De Crisci, A. G.; Pearson, D. M.; Blake, T. R.; Olsson, J. V.; Ingram, A. J.; Zare, R. N.; Waymouth, R. M. *J. Am. Chem. Soc.* **2013,** *135,* 7593–7602. doi:10.1021/ja4008694
110. De Crisci, A. G.; Chung, K.; Oliver, A. G.; Solis-Ibarra, D.; Waymouth, R. M. *Organometallics* **2013,** *32,* 2257–2266. doi:10.1021/om4001549
111. Wu, H.; Song, J.; Liu, H.; Xie, Z.; Xie, C.; Hu, Y.; Huang, X.; Hua, M.; Han, B. *Chem. Sci.* **2019,** *10,* 4692–4698. doi:10.1039/c9sc00322c
112. Chen, B.; Li, F.; Yuan, G. *RSC Adv.* **2017,** *7,* 21145–21152. doi:10.1039/c7ra03205f
113. Gollnick, K.; Griesbeck, A. *Tetrahedron* **1985,** *41,* 2057–2068. doi:10.1016/s0040-4020(01)96576-7
114. Zeitsch, K. J. *The chemistry and technology of furfural and its many by-products*, Vol. 13; Elsevier, 2000.
115. Gassama, A.; Ernenwein, C.; Hoffmann, N. *ChemSusChem* **2009,** *2,* 1130–1137. doi:10.1002/cssc.200900150
116. Chauhan, D. K.; Battula, V. R.; Giri, A.; Patra, A.; Kailasam, K. *Catal. Sci. Technol.* **2022,** *12,* 144–153. doi:10.1039/d1cy01681d
117. Xiao, Y.; Shen, C.; Zhang, W.; Zhang, M.; Zhang, H.; Shao, T.; Xiong, Z.; Ding, Y.; Hao, S.; Liu, L.; Chen, Y.; Li, J. *Small* **2023,** *19,* 2205876. doi:10.1002/smll.202205876
118. Chavan, S. P.; Kadam, A. L. *Results Chem.* **2021,** *3,* 100170. doi:10.1016/j.rechem.2021.100170
119. Kumar, P.; Pandey, R. K. *Green Chem.* **2000,** *2,* 29–32. doi:10.1039/a907690e
120. Annangudi, S. P.; Sun, M. J.; Salomon, R. G. *Synlett* **2005,** 1468–1470. doi:10.1055/s-2005-869833
121. Esser, P.; Pohlmann, B.; Scharf, H.-D. *Angew. Chem., Int. Ed. Engl.* **1994,** *33,* 2009–2023. doi:10.1002/anie.199420091
122. Schenck, G. O. *Justus Liebigs Ann. Chem.* **1953,** *584,* 156–176. doi:10.1002/jlac.19535840111
123. Riguet, E. *J. Org. Chem.* **2011,** *76,* 8143–8150. doi:10.1021/jo201184p
124. Bos, M.; Riguet, E. *J. Org. Chem.* **2014,** *79,* 10881–10889. doi:10.1021/jo501908z
125. Strizhov, N. K.; Poskonin, V. V.; Badovskaya, L. A.; Kupina, E. P. *Russ. J. Org. Chem.* **2002,** *38,* 251–255. doi:10.1023/a:1015578003374
126. Poskonin, V. V.; Badovskaya, L. A. *Chem. Heterocycl. Compd.* **2003,** *39,* 594–597. doi:10.1023/a:1025137914137
127. Schroeter, S. H.; Appel, R.; Brammer, R.; Schenck, G. O. *Justus Liebigs Ann. Chem.* **1966,** *697,* 42–61. doi:10.1002/jlac.19666970104
128. Sun, W.; Xu, J.; Li, L.; Liu, Z.; Xiao, Z.; An, Q.; Huang, J. *Mol. Catal.* **2025,** *573,* 114842. doi:10.1016/j.mcat.2025.114842
129. Badovskaya, L. A.; Poskonin, V. V.; Tyukhteneva, Z. I.; Kozhina, N. D. *Russ. J. Gen. Chem.* **2021,** *91,* 133–153. doi:10.1134/s1070363221020018
130. Flanagan, P.; Norster, E.; Carrubba, R.; Heck, R. Method for effecting continuous combustion of carbonaceous fuel. U.S. Pat. Appl. US4,118,171 A, July 6, 1978.

131. Poskonin, V.; Badovskaya, L.; Butin, A. *Russ. J. Org. Chem.* **1997,** *33,* 515–519.
132. Kubota, Y.; Tatsuno, T. *Chem. Pharm. Bull.* **1971,** *19,* 1226–1233. doi:10.1248/cpb.19.1226
133. White, E. P. *J. Chem. Soc. C* **1967,** 346–347. doi:10.1039/j39670000346
134. Gratz, J. A.; Cook, C. E.; Wall, M. E. *Org. Prep. Proced.* **1970,** *2,* 51–52. doi:10.1080/00304947009458418
135. Burkhardt, H. J.; Lundin, R. E.; McFadden, W. H. *Tetrahedron* **1968,** *24,* 1225–1229. doi:10.1016/0040-4020(68)88071-8
136. Palai, Y. N.; Fukuoka, A.; Shrotri, A. *ACS Catal.* **2024,** *14,* 2545–2551. doi:10.1021/acscatal.3c04872
137. Fariña, F.; Parellada, M. *An. Quim., Ser. C* **1983,** *79,* 165–168.
138. Magnus, P.; Cairns, P. M. *J. Am. Chem. Soc.* **1986,** *108,* 217–221. doi:10.1021/ja00262a006
139. Magnus, P.; Cairns, P. M.; Chung, S. K. *Tetrahedron Lett.* **1985,** *26,* 1963–1966. doi:10.1016/s0040-4039(00)98352-7
140. Landor, S. R.; Landor, P. D.; Kalli, M. *J. Chem. Soc., Perkin Trans. 1* **1983,** 2921–2925. doi:10.1039/p19830002921
141. Meyers, A. I.; Nolen, R. L.; Collington, E. W.; Narwid, T. A.; Strickland, R. C. *J. Org. Chem.* **1973,** *38,* 1974–1982. doi:10.1021/jo00951a003
142. Walraven, H. G. M.; Pandit, U. K. *Tetrahedron* **1980,** *36,* 321–327. doi:10.1016/0040-4020(80)80022-6
143. Yuste, F.; Sanchez-Obregon, R. *J. Org. Chem.* **1982,** *47,* 3665–3668. doi:10.1021/jo00140a015
144. Roush, W. R.; Blizzard, T. A. *J. Org. Chem.* **1984,** *49,* 1772–1783. doi:10.1021/jo00184a021
145. Hauser, F. M.; Prasanna, S. *J. Am. Chem. Soc.* **1981,** *103,* 6378–6386. doi:10.1021/ja00411a019
146. Scharf, H.-D.; Janus, J. *Tetrahedron* **1979,** *35,* 385–387. doi:10.1016/0040-4020(79)80076-9
147. de Lange, B.; van Bolhuis, F.; Feringa, B. L. *Tetrahedron* **1989,** *45,* 6799–6818. doi:10.1016/s0040-4020(01)89149-3
148. Alonso-Fagúndez, N.; Granados, M. L.; Mariscal, R.; Ojeda, M. *ChemSusChem* **2012,** *5,* 1984–1990. doi:10.1002/cssc.201200167
149. Li, X.; Ko, J.; Zhang, Y. *ChemSusChem* **2018,** *11,* 612–618. doi:10.1002/cssc.201701866
150. Gao, X.; Tong, X.; Zhang, Y.; Xue, S. *iScience* **2023,** *26,* 107203. doi:10.1016/j.isci.2023.107203
151. Zhu, W.; Tao, F.; Chen, S.; Li, M.; Yang, Y.; Lv, G. *ACS Sustainable Chem. Eng.* **2019,** *7,* 296–305. doi:10.1021/acssuschemeng.8b03373
152. Palai, Y. N.; Shrotri, A.; Fukuoka, A. *ACS Catal.* **2022,** *12,* 3534–3542. doi:10.1021/acscatal.1c05348
153. Shen, G.; Shi, J.; Lei, Y.; Fu, C.; Chen, Z.; Andrioletti, B.; Yin, G. *Ind. Eng. Chem. Res.* **2019,** *58,* 22951–22957. doi:10.1021/acs.iecr.9b05134
154. Lee, M. Y.; Koo, J. W.; Jang, J. H.; In Jo, Y.; Yeo, J. B.; Kim, J. E.; Hong, J. S.; Kim, J. H.; Choi, S.; Nam, K. T. *ACS Sustainable Chem. Eng.* **2025,** *13,* 2845–2852. doi:10.1021/acssuschemeng.4c08861
155. Lu, G.-H.; Zong, M.-H.; Li, N. *ACS Catal.* **2023,** *13,* 1371–1380. doi:10.1021/acscatal.2c05458
156. Ricciardi, L.; Verboom, W.; Lange, J.-P.; Huskens, J. *Sustainable Energy Fuels* **2022,** *6,* 11–28. doi:10.1039/d1se01572a
157. Xu, C.; Paone, E.; Rodríguez-Padrón, D.; Luque, R.; Mauriello, F. *Chem. Soc. Rev.* **2020,** *49,* 4273–4306. doi:10.1039/d0cs00041h
158. Zhang, T.; Li, W.; Xiao, H.; Jin, Y.; Wu, S. *Bioresour. Technol.* **2022,** *354,* 127126. doi:10.1016/j.biortech.2022.127126
159. Cousin, E.; Namhaed, K.; Pérès, Y.; Cognet, P.; Delmas, M.; Hermansyah, H.; Gozan, M.; Alaba, P. A.; Aroua, M. K. *Sci. Total Environ.* **2022,** *847,* 157599. doi:10.1016/j.scitotenv.2022.157599
160. Kumar, A.; Chauhan, A. S.; Bains, R.; Das, P. *Green Chem.* **2023,** *25,* 849–870. doi:10.1039/d2gc03999k
161. Lange, J.-P. *Catal. Today* **2024,** *435,* 114726. doi:10.1016/j.cattod.2024.114726
162. Yong, K. J.; Wu, T. Y.; Lee, C. B. T. L.; Lee, Z. J.; Liu, Q.; Jahim, J. M.; Zhou, Q.; Zhang, L. *Biomass Bioenergy* **2022,** *161,* 106458. doi:10.1016/j.biombioe.2022.106458
163. Liu, L.; Li, Q.; Wan, C. *Green Chem.* **2025,** *27,* 1519–1528. doi:10.1039/d4gc02874k
164. de Jong, E.; Mascal, M.; Constant, S.; Claessen, T.; Tosi, P.; Mija, A. *Green Chem.* **2025,** *27,* 3136–3166. doi:10.1039/d4gc06244b
165. Soukup-Carne, D.; Hillman, B.; Parlett, C. M. A.; Fan, X.; Esteban, J. *React. Chem. Eng.* **2025,** *10,* 839–855. doi:10.1039/d4re00572d
166. Jiang, S.; Verrier, C.; Ahmar, M.; Lai, J.; Ma, C.; Muller, E.; Queneau, Y.; Pera-Titus, M.; Jérôme, F.; De Oliveira Vigier, K. *Green Chem.* **2018,** *20,* 5104–5110. doi:10.1039/c8gc02260g
167. Bielski, R.; Grynkiewicz, G. *Green Chem.* **2021,** *23,* 7458–7487. doi:10.1039/d1gc02402g
168. Dutta, S.; Bhat, N. S. *ACS Omega* **2021,** *6,* 35145–35172. doi:10.1021/acsomega.1c05861
169. Gupta, K.; Rai, R. K.; Singh, S. K. *ChemCatChem* **2018,** *10,* 2326–2349. doi:10.1002/cctc.201701754
170. Jaswal, A.; Singh, P. P.; Mondal, T. *Green Chem.* **2022,** *24,* 510–551. doi:10.1039/d1gc03278j
171. Li, N.; Zong, M.-H. *ACS Catal.* **2022,** *12,* 10080–10114. doi:10.1021/acscatal.2c02912
172. Kumar Vaidyanathan, V.; Saikia, K.; Senthil Kumar, P.; Karanam Rathankumar, A.; Rangasamy, G.; Dattatraya Saratale, G. *Bioresour. Technol.* **2023,** *378,* 128975. doi:10.1016/j.biortech.2023.128975
173. Yue, X. Y.; Queneau, Y. *ChemSusChem* **2022,** *15,* e202102660. doi:10.1002/cssc.202102660
174. Gandini, A.; Lacerda, T. M. *Macromol. Mater. Eng.* **2022,** *307,* 2100902. doi:10.1002/mame.202100902
175. Mori, A.; Curpanen, S.; Pezzetta, C.; Perez-Luna, A.; Poli, G.; Oble, J. *Eur. J. Org. Chem.* **2022,** e202200727. doi:10.1002/ejoc.202200727
176. Zhu, J.; Yin, G. *ACS Catal.* **2021,** *11,* 10058–10083. doi:10.1021/acscatal.1c01989
177. An, Z.; Li, J. *Green Chem.* **2022,** *24,* 1780–1808. doi:10.1039/d1gc04440k
178. Li, G.; Jiao, W.; Sun, Z.; Zhao, Y.; Shi, Z.; Yan, Y.; Feng, L.; Zhang, Y.; Tang, Y. *ACS Sustainable Chem. Eng.* **2018,** *6,* 4316–4320. doi:10.1021/acssuschemeng.7b04770
179. Shi, J.; Tong, X.; Wang, S.; Xue, S. *ACS Catal.* **2022,** *12,* 6029–6035. doi:10.1021/acscatal.2c01257
180. Singh, G.; Khan, T. S.; Samanta, C.; Bal, R.; Bordoloi, A. *Biomass Bioenergy* **2022,** *156,* 106321. doi:10.1016/j.biombioe.2021.106321
181. Wu, J.; Xu, L.; Li, Y.; Dong, C.-L.; Lu, Y.; Nga, T. T. T.; Kong, Z.; Li, S.; Zou, Y.; Wang, S. *J. Am. Chem. Soc.* **2022,** *144,* 23649–23656. doi:10.1021/jacs.2c11153
182. Huang, S.; Luo, X.; Li, J.; Liu, S.; Shuai, L. *Green Chem.* **2024,** *26,* 4043–4050. doi:10.1039/d4gc00105b
183. Scodeller, I.; Mansouri, S.; Morvan, D.; Muller, E.; de Oliveira Vigier, K.; Wischert, R.; Jérôme, F. *Angew. Chem., Int. Ed.* **2018,** *57,* 10510–10514. doi:10.1002/anie.201803828

184. Jiang, S.; Ma, C.; Muller, E.; Pera-Titus, M.; Jérôme, F.; De Oliveira Vigier, K. *ACS Catal.* **2019,** *9,* 8893–8902. doi:10.1021/acscatal.9b03413
185. Jiang, S.; Muller, E.; Jerôme, F.; Pera-Titus, M.; De Oliveira Vigier, K. *Green Chem.* **2020,** *22,* 1832–1836. doi:10.1039/d0gc00119h
186. Di Gioia, M. L.; Nardi, M.; Costanzo, P.; De Nino, A.; Maiuolo, L.; Oliverio, M.; Procopio, A. *Molecules* **2018,** *23,* 1891. doi:10.3390/molecules23081891
187. Gomes, R. F. A.; Cavaca, L. A. S.; Gonçalves, J. M.; Ramos, R.; Peixoto, A. F.; Arias-Serrano, B. I.; Afonso, C. A. M. *ACS Sustainable Chem. Eng.* **2021,** *9,* 16038–16043. doi:10.1021/acssuschemeng.1c00884
188. Gomes, R. F. A.; Esteves, N. R.; Coelho, J. A. S.; Afonso, C. A. M. *J. Org. Chem.* **2018,** *83,* 7509–7513. doi:10.1021/acs.joc.7b02931
189. Song, S.; Fung Kin Yuen, V.; Di, L.; Sun, Q.; Zhou, K.; Yan, N. *Angew. Chem., Int. Ed.* **2020,** *59,* 19846–19850. doi:10.1002/anie.202006315
190. Yamamoto, Y.; Nakazato, Y.; Tadano, R.; Yasui, T. *J. Org. Chem.* **2022,** *87,* 10216–10228. doi:10.1021/acs.joc.2c01189
191. Wang, Z.; Scheuring, M.; Mabin, M.; Shahni, R.; Wang, Z. D.; Ugrinov, A.; Butz, J.; Chu, Q. R. *ACS Sustainable Chem. Eng.* **2020,** *8,* 8909–8917. doi:10.1021/acssuschemeng.0c00708
192. Wang, Z. D.; Elliott, Q.; Wang, Z.; Setien, R. A.; Puttkammer, J.; Ugrinov, A.; Lee, J.; Webster, D. C.; Chu, Q. R. *ACS Sustainable Chem. Eng.* **2018,** *6,* 8136–8141. doi:10.1021/acssuschemeng.8b02415
193. Bailey, L. A.; Bere, T.; Davies, T. E.; Taylor, S. H.; Graham, A. E. *ACS Sustainable Chem. Eng.* **2022,** *10,* 13759–13764. doi:10.1021/acssuschemeng.2c03968
194. Wang, Y.; Li, Z.; Li, Q.; Wang, H. *ACS Omega* **2022,** *7,* 19158–19165. doi:10.1021/acsomega.1c07241
195. Wang, X.; Liu, C.; Xing, Z.; Suo, H.; Qu, R.; Li, Q.; Qin, Y. *Macromolecules* **2022,** *55,* 8857–8865. doi:10.1021/acs.macromol.2c01214
196. Yang, Y.; Fan, Z.; Dong, Q.; Sun, W.; Zhang, X.; Guan, L.; Wang, L. *ACS Sustainable Chem. Eng.* **2022,** *10,* 2282–2288. doi:10.1021/acssuschemeng.1c08048
197. Yang, R.; Zhang, H.; Li, X.; Ye, X.; Liu, L. *ACS Sustainable Chem. Eng.* **2024,** *12,* 12378–12385. doi:10.1021/acssuschemeng.4c02672
198. Baldenhofer, R.; Lange, J.-P.; Kersten, S. R. A.; Ruiz, M. P. *ChemSusChem* **2024,** *17,* e202400108. doi:10.1002/cssc.202400108
199. Hronec, M.; Fulajtarová, K. *Catal. Commun.* **2012,** *24,* 100–104. doi:10.1016/j.catcom.2012.03.020
200. Li, H.; Liu, J.; Cai, C.; Wang, H.; Huang, Y.; Wang, C.; Ma, L. *Fuel* **2023,** *332,* 126057. doi:10.1016/j.fuel.2022.126057
201. Balaga, R.; Balla, P.; Zhang, X.; Ramineni, K.; Du, H.; Lingalwar, S.; Perupogu, V.; Zhang, Z. C. *Catalysts* **2023,** *13,* 580. doi:10.3390/catal13030580
202. Zhang, S.; Ma, H.; Sun, Y.; Liu, X.; Zhang, M.; Luo, Y.; Gao, J.; Xu, J. *Chin. J. Catal.* **2021,** *42,* 2216–2224. doi:10.1016/s1872-2067(21)63842-1
203. Gao, X.; Ding, Y.; Peng, L.; Yang, D.; Wan, X.; Zhou, C.; Liu, W.; Dai, Y.; Yang, Y. *Fuel* **2022,** *314,* 123074. doi:10.1016/j.fuel.2021.123074
204. Yu, Z.; Zou, Z.; Wang, R.; Li, G.; Wang, A.; Cong, Y.; Zhang, T.; Li, N. *Angew. Chem., Int. Ed.* **2023,** *62,* e202300008. doi:10.1002/anie.202300008
205. Li, X.; Sun, J.; Shao, S.; Hu, X.; Cai, Y. *Fuel Process. Technol.* **2021,** *215,* 106768. doi:10.1016/j.fuproc.2021.106768
206. Li, Z.; Li, Q.; Wang, Y.; Zhang, J.; Wang, H. *Energy Fuels* **2021,** *35,* 6691–6699. doi:10.1021/acs.energyfuels.1c00185
207. Ti, L.; Sheng, X.; Jia, H.; Han, W.; Ping, Q.; Yang, J.; Li, N. *Mol. Catal.* **2023,** *535,* 112869. doi:10.1016/j.mcat.2022.112869
208. Wang, W.; Zhang, X.; Jiang, Z.; Cui, Y.; Kang, Q.; Zhao, X.; Zhang, Q.; Ma, L. *Fuel* **2022,** *321,* 124114. doi:10.1016/j.fuel.2022.124114
209. Xu, Q.; Sheng, X.; Jia, H.; Li, N.; Zhang, J.; Shi, H.; Niu, M.; Ping, Q. *ChemCatChem* **2021,** *13,* 916–923. doi:10.1002/cctc.202001538
210. Xu, Q.; Sheng, X.; Li, N.; Zhang, J.; Shi, H.; Niu, M.; Ping, Q.; Li, N. *ACS Sustainable Chem. Eng.* **2021,** *9,* 8232–8237. doi:10.1021/acssuschemeng.1c02270
211. Zhang, X.; Song, M.; Liu, J.; Zhang, Q.; Chen, L.; Ma, L. *J. Energy Chem.* **2023,** *79,* 22–30. doi:10.1016/j.jechem.2022.12.017
212. Xie, J.; Liang, Y.; Yang, B.; Zhang, J.; Xie, J.; Zou, J.-J.; Zhang, Q. *Fuel* **2023,** *340,* 127539. doi:10.1016/j.fuel.2023.127539
213. Guo, W.; Wang, Z.-Q.; Xiang, S.; Jing, Y.; Liu, X.; Guo, Y.; Gong, X.-Q.; Wang, Y. *Chin. J. Catal.* **2023,** *47,* 181–190. doi:10.1016/s1872-2067(22)64196-2
214. Guan, J.; Chen, J.; Luo, Y.; Guo, L.; Zhang, W. *Angew. Chem., Int. Ed.* **2023,** *62,* e202306380. doi:10.1002/anie.202306380
215. Bozell, J. J.; Petersen, G. R. *Green Chem.* **2010,** *12,* 539–554. doi:10.1039/b922014c
216. Kang, S.; Fu, J.; Zhang, G. *Renewable Sustainable Energy Rev.* **2018,** *94,* 340–362. doi:10.1016/j.rser.2018.06.016
217. Di Menno Di Bucchianico, D.; Wang, Y.; Buvat, J.-C.; Pan, Y.; Casson Moreno, V.; Leveneur, S. *Green Chem.* **2022,** *24,* 614–646. doi:10.1039/d1gc02457d
218. Xu, W.-P.; Chen, X.-F.; Guo, H.-J.; Li, H.-L.; Zhang, H.-R.; Xiong, L.; Chen, X.-D. *J. Chem. Technol. Biotechnol.* **2021,** *96,* 3009–3024. doi:10.1002/jctb.6810
219. Yan, L.; Yao, Q.; Fu, Y. *Green Chem.* **2017,** *19,* 5527–5547. doi:10.1039/c7gc02503c
220. Kumar, A.; Shende, D. Z.; Wasewar, K. L. *Mater. Today: Proc.* **2020,** *29,* 790–793. doi:10.1016/j.matpr.2020.04.749
221. Zhang, M.; Wang, N.; Liu, J.; Wang, C.; Xu, Y.; Ma, L. *Crit. Rev. Biotechnol.* **2022,** *42,* 220–253. doi:10.1080/07388551.2021.1939261
222. Badgujar, K. C.; Badgujar, V. C.; Bhanage, B. M. *Fuel Process. Technol.* **2020,** *197,* 106213. doi:10.1016/j.fuproc.2019.106213
223. Hayes, G. C.; Becer, C. R. *Polym. Chem.* **2020,** *11,* 4068–4077. doi:10.1039/d0py00705f
224. Horvat, J.; Klaić, B.; Metelko, B.; Šunjić, V. *Tetrahedron Lett.* **1985,** *26,* 2111–2114. doi:10.1016/s0040-4039(00)94793-2
225. Gautam, P.; Barman, S.; Ali, A. *ChemistrySelect* **2022,** *7,* e202203044. doi:10.1002/slct.202203044
226. Ntshibongo, S.; Maumela, M.; Bingwa, N. *Inorg. Chem. Commun.* **2022,** *146,* 110101. doi:10.1016/j.inoche.2022.110101
227. Pothu, R.; Gundeboyina, R.; Boddula, R.; Perugopu, V.; Ma, J. *New J. Chem.* **2022,** *46,* 5907–5921. doi:10.1039/d1nj05777d
228. Pothu, R.; Mitta, H.; Boddula, R.; Balla, P.; Gundeboyina, R.; Perugopu, V.; Ma, J. *Mater. Sci. Energy Technol.* **2022,** *5,* 391–398. doi:10.1016/j.mset.2022.09.006
229. Yuan, T.; Chu, M.; Zhang, K.; Jia, S.; Han, S.; Zhai, J.; Wang, H.; Xue, T.; Wu, H. *ChemistrySelect* **2022,** *7,* e202201624. doi:10.1002/slct.202201624
230. Zhang, Y.; Wang, X.; Shen, Y. *Fuel* **2023,** *342,* 127787. doi:10.1016/j.fuel.2023.127787

231. Liu, J.; Tao, S. *Appl. Surf. Sci.* **2023,** *616,* 156464. doi:10.1016/j.apsusc.2023.156464
232. Velisoju, V. K.; Gutta, N.; Tardio, J.; Bhargava, S. K.; Vankudoth, K.; Chatla, A.; Medak, S.; Akula, V. *Appl. Catal., A* **2018,** *550,* 142–150. doi:10.1016/j.apcata.2017.11.008
233. Song, L.; Wang, R.; Che, L.; Jiang, Y.; Zhou, M.; Zhao, Y.; Pang, J.; Jiang, M.; Zhou, G.; Zheng, M.; Zhang, T. *ACS Catal.* **2021,** *11,* 11588–11596. doi:10.1021/acscatal.1c02531
234. Dutta, S.; Wu, L.; Mascal, M. *Green Chem.* **2015,** *17,* 2335–2338. doi:10.1039/c5gc00098j
235. Carnevali, D.; Rigamonti, M. G.; Tabanelli, T.; Patience, G. S.; Cavani, F. *Appl. Catal., A* **2018,** *563,* 98–104. doi:10.1016/j.apcata.2018.06.034
236. Cui, J.; Tan, J.; Zhu, Y.; Cheng, F. *ChemSusChem* **2018,** *11,* 1316–1320. doi:10.1002/cssc.201800038
237. Bucciol, F.; Tabasso, S.; Grillo, G.; Menegazzo, F.; Signoretto, M.; Manzoli, M.; Cravotto, G. *J. Catal.* **2019,** *380,* 267–277. doi:10.1016/j.jcat.2019.09.041
238. Gao, X.; Zhu, S.; Dong, M.; Fan, W. *J. Catal.* **2021,** *399,* 201–211. doi:10.1016/j.jcat.2021.05.013
239. Wei, Y.; Lu, J.; Zhang, S.; Wu, C.; Nong, X.; Li, J.; Liu, C.-L.; Dong, W.-S. *Chem. Commun.* **2023,** *59,* 2477–2480. doi:10.1039/d2cc06252f
240. Rodiansono; Azzahra, A. S.; Dewi, H. P.; Adilina, I. B.; Sembiring, K. C. *Catal. Sci. Technol.* **2023,** *13,* 4466–4476. doi:10.1039/d3cy00544e
241. Chen, L.; Liu, Y.; Gu, C.; Feng, G.; Zhang, X.; Liu, J.; Zhang, Q.; Wang, C.; Ma, L. *ACS Sustainable Chem. Eng.* **2021,** *9,* 15603–15611. doi:10.1021/acssuschemeng.1c05771
242. Liu, Y.; Gu, C.; Chen, L.; Zhou, W.; Liao, Y.; Wang, C.; Ma, L. *ACS Appl. Mater. Interfaces* **2023,** *15,* 4184–4193. doi:10.1021/acsami.2c22045
243. Gu, C.; Chen, L.; Liu, Y.; Zhang, X.; Liu, J.; Zhang, Q.; Wang, C.; Ma, L. *Mol. Catal.* **2022,** *524,* 112317. doi:10.1016/j.mcat.2022.112317
244. Lu, K.; Li, Z.; Hai, C.; Li, J.; Liu, C.-L.; Dong, W.-S. *Sustainable Energy Fuels* **2022,** *6,* 3425–3434. doi:10.1039/d2se00330a
245. Jiang, Y.; Li, Z.; Li, Y.; Chen, L.; Zhang, H.; Li, H.; Yang, S. *Fuel* **2023,** *334,* 126629. doi:10.1016/j.fuel.2022.126629
246. Raut, A. B.; Shende, V. S.; Sasaki, T.; Bhanage, B. M. *J. Catal.* **2020,** *383,* 206–214. doi:10.1016/j.jcat.2020.01.020
247. Chaudhari, C.; Shiraishi, M.; Nishida, Y.; Sato, K.; Nagaoka, K. *Green Chem.* **2020,** *22,* 7760–7764. doi:10.1039/d0gc01725f
248. Louven, Y.; Haus, M. O.; Konrad, M.; Hofmann, J. P.; Palkovits, R. *Green Chem.* **2020,** *22,* 4532–4540. doi:10.1039/d0gc01043j
249. Wu, P. -d.; Li, H.; Fang, Z. *Adv. Sustainable Syst.* **2022,** *6,* 2100321. doi:10.1002/adsu.202100321
250. Wu, H.; Dai, W.; Saravanamurugan, S.; Li, H.; Yang, S. *ACS Sustainable Chem. Eng.* **2019,** *7,* 10207–10213. doi:10.1021/acssuschemeng.9b00412
251. Xie, C.; Song, J.; Wu, H.; Hu, Y.; Liu, H.; Zhang, Z.; Zhang, P.; Chen, B.; Han, B. *J. Am. Chem. Soc.* **2019,** *141,* 4002–4009. doi:10.1021/jacs.8b13024
252. Wang, Y.; Wu, H.; Wang, J.; Zhang, K.; Liu, Y.; Wei, Z. *ACS Sustainable Chem. Eng.* **2022,** *10,* 17274–17285. doi:10.1021/acssuschemeng.2c05579
253. Wu, C.; Lou, M.; Sun, M.; Wang, H.; Li, Z.; Qiu, J.; Wang, J.; Liu, Z. *Green Energy Environ.* **2023,** *8,* 438–443. doi:10.1016/j.gee.2021.04.010
254. Chakrabortty, S.; Zheng, S.; Kallmeier, F.; Baráth, E.; Tin, S.; de Vries, J. G. *ChemSusChem* **2023,** *16,* e202202353. doi:10.1002/cssc.202202353
255. Cai, R.-F.; Liu, L.; Chen, F.-F.; Li, A.; Xu, J.-H.; Zheng, G.-W. *ACS Sustainable Chem. Eng.* **2020,** *8,* 17054–17061. doi:10.1021/acssuschemeng.0c04647
256. Chen, J.-Y.; Huang, Y.-B.; Hu, B.; Li, K.-M.; Zhang, J.-L.; Zhang, X.; Yan, X.-Y.; Lu, Q. *Green Chem.* **2023,** *25,* 2672–2680. doi:10.1039/d3gc00213f
257. Kerkel, F.; Markiewicz, M.; Stolte, S.; Müller, E.; Kunz, W. *Green Chem.* **2021,** *23,* 2962–2976. doi:10.1039/d0gc04353b
258. Dutta, S.; Yu, I. K. M.; Tsang, D. C. W.; Ng, Y. H.; Ok, Y. S.; Sherwood, J.; Clark, J. H. *Chem. Eng. J.* **2019,** *372,* 992–1006. doi:10.1016/j.cej.2019.04.199
259. Meng, F.; Yang, X.; Zhao, S.; Li, Z.; Zhang, G.; Qi, Y.; Chu, S.; Wang, G.; Zhang, J.; Qin, Y.; Zhang, B. *Appl. Catal., B* **2023,** *324,* 122236. doi:10.1016/j.apcatb.2022.122236
260. Siddiqui, N.; Pendem, C.; Goyal, R.; Khatun, R.; Khan, T. S.; Samanta, C.; Chiang, K.; Shah, K.; Ali Haider, M.; Bal, R. *Fuel* **2022,** *323,* 124272. doi:10.1016/j.fuel.2022.124272
261. Bounoukta, C. E.; Megías-Sayago, C.; Rendón, N.; Ammari, F.; Penkova, A.; Ivanova, S.; Centeno, M. Á.; Odriozola, J. A. *Sustainable Energy Fuels* **2023,** *7,* 857–867. doi:10.1039/d2se01503j
262. Roa, D. A.; Garcia, J. J. *J. Catal.* **2022,** *413,* 1028–1033. doi:10.1016/j.jcat.2022.08.013
263. Wu, Y.; Wang, H.; Peng, J.; Zhang, J.; Ding, M. *Chem. Eng. J.* **2023,** *454,* 140156. doi:10.1016/j.cej.2022.140156
264. Manal, A. K.; Advani, J. H.; Srivastava, R. *ChemCatChem* **2022,** *14,* e202200576. doi:10.1002/cctc.202200576
265. Tang, Y.; Fu, J.; Wang, Y.; Guo, H.; Qi, X. *Fuel Process. Technol.* **2023,** *240,* 107559. doi:10.1016/j.fuproc.2022.107559
266. Wang, X.; Qi, X.; Qiu, M.; Shen, F.; Yang, J.; Shen, B. *Fuel* **2023,** *341,* 127720. doi:10.1016/j.fuel.2023.127720
267. Zhang, G.; Ma, L.; Dong, Y.; Fang, Y.; Kong, X. *Fuel* **2023,** *333,* 126400. doi:10.1016/j.fuel.2022.126400
268. Huang, R.; Liu, H.; Zhang, J.; Cheng, Y.; He, L.; Peng, L. *Renewable Energy* **2022,** *200,* 234–243. doi:10.1016/j.renene.2022.09.105
269. Kondawar, S.; Rode, C. *Curr. Opin. Green Sustainable Chem.* **2022,** *35,* 100607. doi:10.1016/j.cogsc.2022.100607
270. Shende, V. S.; Raut, A. B.; Raghav, P.; Kelkar, A. A.; Bhanage, B. M. *ACS Omega* **2019,** *4,* 19491–19498. doi:10.1021/acsomega.9b03424
271. Deng, C.-Q.; Liu, J.; Luo, J.-H.; Gan, L.-J.; Deng, J.; Fu, Y. *Angew. Chem., Int. Ed.* **2022,** *61,* e202115983. doi:10.1002/anie.202115983
272. Zada, B.; Zhu, R.; Wang, B.; Liu, J.; Deng, J.; Fu, Y. *Green Chem.* **2020,** *22,* 3427–3432. doi:10.1039/d0gc00763c
273. Gan, L.; Deng, C.; Deng, J. *Green Chem.* **2022,** *24,* 3143–3151. doi:10.1039/d2gc00518b
274. Marckwordt, A.; El Ouahabi, F.; Amani, H.; Tin, S.; Kalevaru, N. V.; Kamer, P. C. J.; Wohlrab, S.; de Vries, J. G. *Angew. Chem., Int. Ed.* **2019,** *58,* 3486–3490. doi:10.1002/anie.201812954
275. Choi, M.; Byun, J.; Park, H.; Jeong, K.; Kim, S. M.; Han, J. *Biomass Bioenergy* **2022,** *162,* 106503. doi:10.1016/j.biombioe.2022.106503
276. Al-Naji, M.; Puértolas, B.; Kumru, B.; Cruz, D.; Bäumel, M.; Schmidt, B. V. K. J.; Tarakina, N. V.; Pérez-Ramírez, J. *ChemSusChem* **2019,** *12,* 2628–2636. doi:10.1002/cssc.201900418

277. Xia, Y.; Yuan, P.; Zhang, Y.; Sun, Y.; Hong, M. *Angew. Chem., Int. Ed.* **2023,** *62,* e202217812. doi:10.1002/anie.202217812
278. Yuan, P.; Sun, Y.; Xu, X.; Luo, Y.; Hong, M. *Nat. Chem.* **2022,** *14,* 294–303. doi:10.1038/s41557-021-00817-9
279. Orha, L.; Tukacs, J. M.; Kollár, L.; Mika, L. T. *Beilstein J. Org. Chem.* **2019,** *15,* 2907–2913. doi:10.3762/bjoc.15.284
280. Orha, L.; Tukacs, J. M.; Gyarmati, B.; Szilágyi, A.; Kollár, L.; Mika, L. T. *ACS Sustainable Chem. Eng.* **2018,** *6,* 5097–5104. doi:10.1021/acssuschemeng.7b04775
281. Wang, X.; Zeng, J.; Lu, X.; Xin, J.; Zhang, S. *Ind. Eng. Chem. Res.* **2019,** *58,* 11841–11848. doi:10.1021/acs.iecr.9b01604
282. Wang, H.; Wu, Y.; Jin, T.; Dong, C.; Peng, J.; Du, H.; Zeng, Y.; Ding, M. *Mol. Catal.* **2020,** *498,* 111267. doi:10.1016/j.mcat.2020.111267
283. Wang, H.; Wu, Y.; Li, Y.; Peng, J.; Gu, X.-K.; Ding, M. *Appl. Catal., B* **2021,** *296,* 120338. doi:10.1016/j.apcatb.2021.120338
284. Wang, H.; Wu, Y.; Li, Y.; Peng, J.; Gu, X.-K.; Ding, M. *Green Chem.* **2021,** *23,* 4780–4789. doi:10.1039/d1gc01062j
285. Velisoju, V. K.; Jampaiah, D.; Gutta, N.; Bentrup, U.; Brückner, A.; Bhargava, S. K.; Akula, V. *ChemCatChem* **2020,** *12,* 1341–1349. doi:10.1002/cctc.201901966
286. Martínez Figueredo, K. G.; Segobia, D. J.; Bertero, N. M. *Catal. Commun.* **2020,** *144,* 106087. doi:10.1016/j.catcom.2020.106087
287. Martínez Figueredo, K. G.; Virgilio, E. M.; Segobia, D. J.; Bertero, N. M. *ChemPlusChem* **2021,** *86,* 1342–1346. doi:10.1002/cplu.202100249
288. Parve, J.; Kudryašova, M.; Shalima, T.; Villo, L.; Liblikas, I.; Reile, I.; Pehk, T.; Gathergood, N.; Aav, R.; Vares, L.; Parve, O. *ACS Sustainable Chem. Eng.* **2021,** *9,* 1494–1499. doi:10.1021/acssuschemeng.0c07918
289. Wu, J.; Gao, G.; Li, Y.; Sun, P.; Wang, J.; Li, F. *Appl. Catal., B* **2019,** *245,* 251–261. doi:10.1016/j.apcatb.2018.12.068
290. Cavuoto, D.; Ravasio, N.; Zaccheria, F.; Marelli, M.; Cappelletti, G.; Campisi, S.; Gervasini, A. *Mol. Catal.* **2022,** *528,* 112462. doi:10.1016/j.mcat.2022.112462
291. Santos, C. S.; Soares, C. C. S. P.; Vieira, A. S.; Burtoloso, A. C. B. *Green Chem.* **2019,** *21,* 6441–6450. doi:10.1039/c9gc03343b
292. Cavuoto, D.; Gervasini, A.; Zaccheria, F.; Scotti, N.; Marelli, M.; Bisio, C.; Begni, F.; Ravasio, N. *Catal. Today* **2023,** *418,* 114104. doi:10.1016/j.cattod.2023.114104
293. van Putten, R.-J.; van der Waal, J. C.; de Jong, E.; Rasrendra, C. B.; Heeres, H. J.; de Vries, J. G. *Chem. Rev.* **2013,** *113,* 1499–1597. doi:10.1021/cr300182k
294. Shen, G.; Andrioletti, B.; Queneau, Y. *Curr. Opin. Green Sustainable Chem.* **2020,** *26,* 100384. doi:10.1016/j.cogsc.2020.100384
295. Karimi, S.; Binglin, C.; Shekaari, H. *React. Chem. Eng.* **2024,** *9,* 1550–1559. doi:10.1039/d4re00056k
296. Qiu, B.; Hu, W.; Zhang, D.; Shen, B.; Wang, Y.; Chu, H. *Fuel* **2024,** *375,* 132568. doi:10.1016/j.fuel.2024.132568
297. Guo, H.; Ma, X.; Chen, Z.; Guo, J.; Lu, J. *RSC Adv.* **2025,** *15,* 3664–3671. doi:10.1039/d5ra00020c
298. Shi, Y.; Zhou, Z.; Tana, T.; Su, C.; Zhu, H. Y.; Bissember, A. C.; Huang, J.; Han, P.; Sarina, S. *ACS Catal.* **2025,** *15,* 2950–2958. doi:10.1021/acscatal.4c07293
299. Fan, W.; Verrier, C.; Queneau, Y.; Popowycz, F. *Curr. Org. Synth.* **2019,** *16,* 583–614. doi:10.2174/1570179416666190412164738
300. Chen, C.; Lv, M.; Hu, H.; Huai, L.; Zhu, B.; Fan, S.; Wang, Q.; Zhang, J. *Adv. Mater. (Weinheim, Ger.)* **2024,** *36,* 2311464. doi:10.1002/adma.202311464
301. Jiang, Z.; Zeng, Y.; Hu, D.; Guo, R.; Yan, K.; Luque, R. *Green Chem.* **2023,** *25,* 871–892. doi:10.1039/d2gc03444a
302. Sohail, A.; Wattanakit, C. *Curr. Opin. Electrochem.* **2025,** *49,* 101628. doi:10.1016/j.coelec.2024.101628
303. Subbiah, S.; Simeonov, S. P.; Esperança, J. M. S. S.; Rebelo, L. P. N.; Afonso, C. A. M. *Green Chem.* **2013,** *15,* 2849–2853. doi:10.1039/c3gc40930a
304. Shen, H.; Shan, H.; Liu, L. *ChemSusChem* **2020,** *13,* 513–519. doi:10.1002/cssc.201902799
305. Krebs, M. L.; Bodach, A.; Wang, C.; Schüth, F. *Green Chem.* **2023,** *25,* 1797–1802. doi:10.1039/d2gc04732b
306. Singhal, S.; Agarwal, S.; Mudoi, M. P.; Singhal, N.; Singh, R. *Biomass Convers. Biorefin.* **2023,** *13,* 15619–15636. doi:10.1007/s13399-021-01871-6
307. Zhang, Z.; Huber, G. W. *Chem. Soc. Rev.* **2018,** *47,* 1351–1390. doi:10.1039/c7cs00213k
308. Su, T.; Zhao, D.; Wang, Y.; Lü, H.; Varma, R. S.; Len, C. *ChemSusChem* **2021,** *14,* 266–280. doi:10.1002/cssc.202002232
309. Li, X.-L.; Zhu, R.; Xu, H.-J. *ACS Sustainable Chem. Eng.* **2025,** *13,* 2223–2259. doi:10.1021/acssuschemeng.4c09659
310. Xie, W.; Zhang, Y.; Zheng, H.; Lyu, P.; Ke, X.; Li, T.; Fang, H.; Sun, Y.; Dong, J.; Lin, L.; Wang, C.; Tang, X. *ACS Catal.* **2024,** *14,* 17510–17524. doi:10.1021/acscatal.4c05864
311. Zhang, Y.; Cui, H.; Xia, H. *ChemSusChem* **2025,** *18,* e202401390. doi:10.1002/cssc.202401390
312. Hoang Tran, P. *ChemSusChem* **2022,** *15,* e202200220. doi:10.1002/cssc.202200220
313. Zhang, W.; Qian, H.; Hou, Q.; Ju, M. *Green Chem.* **2023,** *25,* 893–914. doi:10.1039/d2gc03953b
314. Guo, L.; Zhang, X.; Gan, L.; Pan, L.; Shi, C.; Huang, Z.-F.; Zhang, X.; Zou, J.-J. *Adv. Sci.* **2023,** *10,* 2205540. doi:10.1002/advs.202205540
315. Lecona-Vargas, C. S.; Dumont, M.-J. *Ind. Eng. Chem. Res.* **2024,** *63,* 16222–16246. doi:10.1021/acs.iecr.4c01673
316. An, Y.; Lei, T.; Jiang, W.; Pang, H. *Green Chem.* **2024,** *26,* 10739–10773. doi:10.1039/d4gc03597f
317. Duan, Y.; Lu, X.; Fan, O.; Xu, H.; Zhang, Z.; Si, C.; Xu, T.; Du, H.; Li, X. *ChemSusChem* **2025,** *18,* e202401487. doi:10.1002/cssc.202401487
318. Oyegoke, T.; Dumeignil, F.; E.-Yakubu Jibril, B.; Michel, C.; Wojcieszak, R. *Catal. Sci. Technol.* **2024,** *14,* 6761–6774. doi:10.1039/d4cy00821a
319. Xie, C.; Jiang, Z.; Pang, Y.; Xiao, C.; Song, J. *Green Chem.* **2024,** *26,* 6886–6899. doi:10.1039/d4gc01621a
320. Li, X.; Ma, J.; Jia, X.; Xia, F.; Huang, Y.; Xu, Y.; Xu, J. *ACS Sustainable Chem. Eng.* **2018,** *6,* 8048–8054. doi:10.1021/acssuschemeng.8b01617
321. Annatelli, M.; Sánchez-Velandia, J. E.; Mazzi, G.; Pandeirada, S. V.; Giannakoudakis, D.; Rautiainen, S.; Esposito, A.; Thiyagarajan, S.; Richel, A.; Triantafyllidis, K. S.; Robert, T.; Guigo, N.; Sousa, A. F.; García-Verdugo, E.; Aricò, F. *Green Chem.* **2024,** *26,* 8894–8941. doi:10.1039/d4gc00784k
322. Ceyhan, K.; Gröger, H. *ACS Sustainable Chem. Eng.* **2025,** *13,* 2355–2367. doi:10.1021/acssuschemeng.4c08067
323. Arias, K. S.; Garcia-Ortiz, A.; Climent, M. J.; Corma, A.; Iborra, S. *ACS Sustainable Chem. Eng.* **2018,** *6,* 4239–4245. doi:10.1021/acssuschemeng.7b04685

324. Xia, H.; Li, J.; Zhou, M. *Energies (Basel, Switz.)* **2023,** *16,* 6793. doi:10.3390/en16196793
325. Wan, Y.; Lee, J.-M. *ChemSusChem* **2022,** *15,* e202102041. doi:10.1002/cssc.202102041
326. Gautam, R.; Li, H.; Saravanamurugan, S. *ChemCatChem* **2024,** *16,* e202400691. doi:10.1002/cctc.202400691
327. Yang, Y.; Wang, Y.; Li, S.; Shen, X.; Chen, B.; Liu, H.; Han, B. *Green Chem.* **2020,** *22,* 4937–4942. doi:10.1039/d0gc01587c
328. Verrier, C.; Moebs-Sanchez, S.; Queneau, Y.; Popowycz, F. *Org. Biomol. Chem.* **2018,** *16,* 676–687. doi:10.1039/c7ob02962d
329. Dutta, S. *ChemPlusChem* **2025,** *90,* e202400568. doi:10.1002/cplu.202400568
330. Wu, Q.; Zong, M.-H.; Li, N. *ACS Sustainable Chem. Eng.* **2024,** *12,* 17869–17877. doi:10.1021/acssuschemeng.4c07651
331. Zhang, Z.-G.; Shen, X.; Jiang, S.-K.; Lin, J.-C.; Yi, Y.; Ji, X.-J. *J. Agric. Food Chem.* **2025,** *73,* 2266–2278. doi:10.1021/acs.jafc.4c11258
332. Fan, W.; Queneau, Y.; Popowycz, F. *Green Chem.* **2018,** *20,* 485–492. doi:10.1039/c7gc03425c
333. Afradi, N.; Foroughifar, N.; Pasdar, H.; Qomi, M. *Res. Chem. Intermed.* **2019,** *45,* 3251–3271. doi:10.1007/s11164-019-03791-7
334. Jiang, J.; Queneau, Y.; Popowycz, F. *ChemSusChem* **2024,** *17,* e202301782. doi:10.1002/cssc.202301782
335. Fan, W.; Queneau, Y.; Popowycz, F. *RSC Adv.* **2018,** *8,* 31496–31501. doi:10.1039/c8ra05983g
336. Wu, Q.; Chen, J.; Guo, X.; Xu, Y. *Eur. J. Org. Chem.* **2018,** 3105–3113. doi:10.1002/ejoc.201800461
337. Sabahi-Agabager, L.; Nasiri, F. *J. Sulfur Chem.* **2020,** *41,* 170–181. doi:10.1080/17415993.2019.1702196
338. de la Sovera, V.; López, G. V.; Porcal, W. *Eur. J. Org. Chem.* **2022,** e202101369. doi:10.1002/ejoc.202101369
339. Jiang, J.; Queneau, Y.; Popowycz, F. *Eur. J. Org. Chem.* **2023,** *26,* e202300144. doi:10.1002/ejoc.202300144
340. Yang, H.-B.; Wang, Z.-H.; Li, J.-M.; Wu, C. *Chem. Commun.* **2020,** *56,* 3801–3804. doi:10.1039/d0cc00293c
341. Li, S.-S.; Qin, Q.; Qi, Z.; Yang, L.-M.; Kang, Y.; Zhang, X.-Z.; Ma, A.-J.; Peng, J.-B. *Org. Chem. Front.* **2021,** *8,* 3069–3075. doi:10.1039/d1qo00303h
342. Higson, S.; Subrizi, F.; Sheppard, T. D.; Hailes, H. C. *Green Chem.* **2016,** *18,* 1855–1858. doi:10.1039/c5gc02935j
343. Cioc, R. C.; Lutz, M.; Pidko, E. A.; Crockatt, M.; van der Waal, J. C.; Bruijnincx, P. C. A. *Green Chem.* **2021,** *23,* 367–373. doi:10.1039/d0gc03558k
344. Jia, W.; Sun, Y.; Zuo, M.; Feng, Y.; Tang, X.; Zeng, X.; Lin, L. *ChemSusChem* **2020,** *13,* 640–646. doi:10.1002/cssc.201902590
345. Zhang, W.; Zhang, H.; Feng, Y.; Ma, T.; Liu, F.; Zhao, S.; Yang, J.; Li, Y.; Ji, D.; Tang, W.; Li, X.; Fang, Z.; He, W.; Guo, K. *ACS Sustainable Chem. Eng.* **2023,** *11,* 4595–4605. doi:10.1021/acssuschemeng.2c06150
346. Cristóbal, C.; Corral, C.; Carretero, J. C.; Ribagorda, M.; Adrio, J. *Chem. Commun.* **2023,** *59,* 4336–4339. doi:10.1039/d3cc00499f
347. Wang, L.; Verrier, C.; Ahmar, M.; Queneau, Y. *Green Chem.* **2020,** *22,* 7907–7912. doi:10.1039/d0gc03004j
348. Gomes, R. F. A.; Coelho, J. A. S.; Afonso, C. A. M. *ChemSusChem* **2019,** *12,* 420–425. doi:10.1002/cssc.201802537
349. Larduinat, M.; Dokmak, E.; Verrier, C.; Moebs-Sanchez, S.; Popowycz, F. *J. Org. Chem.* **2024,** *89,* 9661–9665. doi:10.1021/acs.joc.4c00495
350. Tampieri, A.; Föttinger, K.; Barrabés, N.; Medina, F. *Appl. Catal., B* **2022,** *319,* 121889. doi:10.1016/j.apcatb.2022.121889
351. Ramdani, W.; Rabadán González, I.; Benbakoura, N.; Ahmar, M.; Verrier, C.; Queneau, Y.; Pera-Titus, M.; Jérôme, F.; De Oliveira Vigier, K. *ChemCatChem* **2023,** *15,* e202300044. doi:10.1002/cctc.202300044
352. van Schijndel, J.; Canalle, L. A.; Molendijk, D.; Meuldijk, J. *Synlett* **2018,** *29,* 1983–1988. doi:10.1055/s-0037-1610235
353. Mancipe, S.; Castillo, J.-C.; Brijaldo, M. H.; López, V. P.; Rojas, H.; Macías, M. A.; Portilla, J.; Romanelli, G. P.; Martínez, J. J.; Luque, R. *ACS Sustainable Chem. Eng.* **2022,** *10,* 12602–12612. doi:10.1021/acssuschemeng.2c03209
354. Tan, J.-N.; Ahmar, M.; Queneau, Y. *RSC Adv.* **2015,** *5,* 69238–69242. doi:10.1039/c5ra14554f
355. Ontiveros, J. F.; Wang, L.; Chatel, K.; Yue, X.; Tan, J.-N.; Ali-Rachedi, F.; Ahmar, M.; Verrier, C.; Fusina, A.; Nardello-Rataj, V.; Queneau, Y. *ACS Sustainable Chem. Eng.* **2021,** *9,* 16977–16988. doi:10.1021/acssuschemeng.1c05371
356. Seitkalieva, M. M.; Vavina, A. V.; Posvyatenko, A. V.; Egorova, K. S.; Kashin, A. S.; Gordeev, E. G.; Strukova, E. N.; Romashov, L. V.; Ananikov, V. P. *ACS Sustainable Chem. Eng.* **2021,** *9,* 3552–3570. doi:10.1021/acssuschemeng.0c08790
357. Hu, Q.; Jiang, S.; Wu, Y.; Xu, H.; Li, G.; Zhou, Y.; Wang, J. *ChemSusChem* **2022,** *15,* e202200192. doi:10.1002/cssc.202200192
358. Karve, V. V.; Sun, D. T.; Trukhina, O.; Yang, S.; Oveisi, E.; Luterbacher, J.; Queen, W. L. *Green Chem.* **2020,** *22,* 368–378. doi:10.1039/c9gc03140e
359. Moriana Herraiz, C.; Arias, K. S.; Climent, M. J.; Iborra, S.; Corma, A. *Green Chem.* **2024,** *26,* 9118–9131. doi:10.1039/d4gc00425f
360. Velty, A.; Iborra, S.; Corma, A. *ChemSusChem* **2022,** *15,* e202200181. doi:10.1002/cssc.202200181
361. Mascal, M. *ChemSusChem* **2015,** *8,* 3391–3395. doi:10.1002/cssc.201500940
362. Mascal, M. *ACS Sustainable Chem. Eng.* **2019,** *7,* 5588–5601. doi:10.1021/acssuschemeng.8b06553
363. Bueno Morón, J.; Arbore, F.; van Klink, G. P. M.; Mascal, M.; Gruter, G.-J. M. *ChemSusChem* **2024,** *17,* e202400495. doi:10.1002/cssc.202400495
364. Karimi, S.; Gharouni Fattah, S.; Li, Z.; Zuo, M.; Nasrollahzadeh, M.; Zeng, X. *Green Chem.* **2025,** *27,* 379–402. doi:10.1039/d4gc04609a
365. Mascal, M.; Nikitin, E. B. *Green Chem.* **2010,** *12,* 370–373. doi:10.1039/b918922j
366. Laugel, C.; Estrine, B.; Le Bras, J.; Hoffmann, N.; Marinkovic, S.; Muzart, J. *ChemCatChem* **2014,** *6,* 1195–1198. doi:10.1002/cctc.201400023
367. Vicente, A. I.; Coelho, J. A. S.; Simeonov, S. P.; Lazarova, H. I.; Popova, M. D.; Afonso, C. A. M. *Molecules* **2017,** *22,* 329. doi:10.3390/molecules22020329
368. Dutta, S.; Wu, L.; Mascal, M. *Green Chem.* **2015,** *17,* 3737–3739. doi:10.1039/c5gc00936g
369. Park, D.; Lee, S.; Kim, J.; Yeong Ryu, G.; Suh, Y.-W. *ChemPlusChem* **2022,** *87,* e202200166. doi:10.1002/cplu.202200166
370. Chen, B.; Feng, Y.; Ma, S.; Xie, W.; Yan, G.; Li, Z.; Sperry, J.; Yang, S.; Tang, X.; Sun, Y.; Lin, L.; Zeng, X. *J. Energy Chem.* **2023,** *76,* 421–428. doi:10.1016/j.jechem.2022.10.005
371. Chen, B.; Feng, Y.; Huang, R.; Yang, S.; Li, Z.; Sperry, J.; Yang, S.; Tang, X.; Sun, Y.; Lin, L.; Zeng, X. *Appl. Catal., B* **2022,** *318,* 121842. doi:10.1016/j.apcatb.2022.121842
372. Onkarappa, S. B.; Dutta, S. *ChemistrySelect* **2019,** *4,* 5540–5543. doi:10.1002/slct.201900279

373. Khachatryan, D. S.; Razinov, A. L.; Kolotaev, A. V.; Belus´, S. K.; Matevosyan, K. R. *Russ. Chem. Bull.* **2015,** *64,* 395–404. doi:10.1007/s11172-015-0875-9
374. Bhat, N. S.; Hegde, S. L.; Dutta, S.; Sudarsanam, P. *ACS Sustainable Chem. Eng.* **2022,** *10,* 5803–5809. doi:10.1021/acssuschemeng.1c08571
375. Miao, H.; Ling, H.; Shevchenko, N.; Mascal, M. *Organometallics* **2021,** *40,* 3952–3957. doi:10.1021/acs.organomet.1c00528
376. Miao, H.; Shevchenko, N.; Otsuki, A. L.; Mascal, M. *ChemSusChem* **2021,** *14,* 303–305. doi:10.1002/cssc.202001718
377. Ling, H.; Miao, H.; Cao, Z.; Mascal, M. *ChemSusChem* **2023,** *16,* e202201787. doi:10.1002/cssc.202201787
378. Miao, H.; Ling, H.; Wei, J.; Mascal, M. *ACS Sustainable Chem. Eng.* **2023,** *11,* 1502–1507. doi:10.1021/acssuschemeng.2c06209
379. Gao, Y.-Y.; Zhang, C.-L.; Jin, M.-L.; Gao, Z.-H.; Ye, S. *Angew. Chem., Int. Ed.* **2023,** *62,* e202301126. doi:10.1002/anie.202301126
380. Dasi, R.; Schmidhuber, D.; Gronbach, L. M.; Rehbein, J.; Brasholz, M. *Org. Biomol. Chem.* **2021,** *19,* 1626–1631. doi:10.1039/d1ob00013f
381. Mascal, M.; Dutta, S. *Green Chem.* **2011,** *13,* 3101–3102. doi:10.1039/c1gc15537g
382. Khanna, J. M.; Kumar, N.; Khera, B.; Ray, P. C. Process for the manufacture of pharmaceutical grade ranitidine base. U.S. Patent US5,696,275, Dec 9, 1997.
383. Wozniak, B.; Tin, S.; de Vries, J. G. *Chem. Sci.* **2019,** *10,* 6024–6034. doi:10.1039/c9sc01309a
384. Yu, Z.; Guo, M.; Wang, J.; Xiong, J.; Li, X.; Zhang, R.; Qiao, Y.; Han, J.; Lu, X. *Green Chem.* **2023,** *25,* 833–848. doi:10.1039/d2gc04310f
385. Liu, F.; Audemar, M.; De Oliveira Vigier, K.; Clacens, J.-M.; De Campo, F.; Jérôme, F. *ChemSusChem* **2014,** *7,* 2089–2093. doi:10.1002/cssc.201402221
386. liu, F.; Audemar, M.; De Oliveira Vigier, K.; Clacens, J.-M.; De Campo, F.; Jérôme, F. *Green Chem.* **2014,** *16,* 4110–4114. doi:10.1039/c4gc01158a
387. Longo, L.; Taghavi, S.; Ghedini, E.; Menegazzo, F.; Di Michele, A.; Cruciani, G.; Signoretto, M. *ChemSusChem* **2022,** *15,* e202200437. doi:10.1002/cssc.202200437
388. Polidoro, D.; Mihai, I. E.; Perosa, A.; Selva, M. *ACS Sustainable Chem. Eng.* **2023,** *11,* 2520–2530. doi:10.1021/acssuschemeng.2c06692
389. Tong, Z.; Li, X.; Zhu, J.; Chen, S.; Dai, G.; Deng, Q.; Wang, J.; Yang, W.; Zeng, Z.; Zou, J.-J. *ChemSusChem* **2022,** *15,* e202102444. doi:10.1002/cssc.202102444
390. Deng, Q.; Zhou, R.; Zhang, Y.-C.; Li, X.; Li, J.; Tu, S.; Sheng, G.; Wang, J.; Zeng, Z.; Yoskamtorn, T.; Edman Tsang, S. C. *Angew. Chem., Int. Ed.* **2023,** *62,* e202211461. doi:10.1002/anie.202211461
391. Wu, G.; Yang, H.; Gao, W.; Wang, K.; Penzik, M. V.; Kozlov, A. N.; Li, B.; Huang, Y.; Zhang, S.; Zhang, H. *J. Anal. Appl. Pyrolysis* **2022,** *167,* 105659. doi:10.1016/j.jaap.2022.105659
392. Shi, N.; Zhu, T.; Zhang, H.; Huang, H.; Zhou, L.; Liu, Y.; Shu, R. *ACS Omega* **2023,** *8,* 11574–11582. doi:10.1021/acsomega.3c00708
393. Wozniak, B.; Spannenberg, A.; Li, Y.; Hinze, S.; de Vries, J. G. *ChemSusChem* **2018,** *11,* 356–359. doi:10.1002/cssc.201702100
394. Zheng, S.; Smit, W.; Spannenberg, A.; Tin, S.; de Vries, J. G. *Chem. Commun.* **2022,** *58,* 4639–4642. doi:10.1039/d2cc00773h
395. Zheng, S.; Chakrabortty, S.; Baráth, E.; Tin, S.; de Vries, J. G. *ACS Sustainable Chem. Eng.* **2022,** *10,* 15642–15647. doi:10.1021/acssuschemeng.2c05307
396. Wozniak, B.; Li, Y.; Tin, S.; de Vries, J. G. *Green Chem.* **2018,** *20,* 4433–4437. doi:10.1039/c8gc02387e
397. Zhang, C.; Li, Y.; Lv, X.; Gao, X.; Duan, Y.; Sui, D.; Yang, Y. *ChemistrySelect* **2022,** *7,* e202103797. doi:10.1002/slct.202103797
398. Liu, C.; Hu, Y.-C.; Yu, Z.; Li, G.; Wang, A.; Cong, Y.; Wang, X.; Li, N. *ACS Sustainable Chem. Eng.* **2022,** *10,* 17221–17229. doi:10.1021/acssuschemeng.2c05128
399. Dong, J.; Yan, H.; Lv, X.; Wang, Z.; Rao, Z.; Zhu, B.; Wu, J.; Zhou, Y.; Chen, H. *J. Mater. Chem. C* **2023,** *11,* 1369–1380. doi:10.1039/d2tc04603b
400. Locatelli, D.; Bernardi, A.; Rubino, L. R.; Gallo, S.; Vitale, A.; Bongiovanni, R.; Barbera, V.; Galimberti, M. *ACS Sustainable Chem. Eng.* **2023,** *11,* 2713–2726. doi:10.1021/acssuschemeng.2c04617
401. Lin, Y.; Wang, F.; Ren, E.; Zhu, F.; Zhang, Q.; Lu, G.-P. *J. Catal.* **2022,** *416,* 39–46. doi:10.1016/j.jcat.2022.10.017
402. Chu, H.; Feng, X.; Wu, X.; Song, J.; Shen, C.; Tan, T. *ACS Sustainable Chem. Eng.* **2023,** *11,* 177–186. doi:10.1021/acssuschemeng.2c05191
403. Ohyama, J.; Kanao, R.; Esaki, A.; Satsuma, A. *Chem. Commun.* **2014,** *50,* 5633–5636. doi:10.1039/c3cc49591d
404. Deng, Q.; Gao, R.; Li, X.; Wang, J.; Zeng, Z.; Zou, J.-J.; Deng, S. *ACS Catal.* **2020,** *10,* 7355–7366. doi:10.1021/acscatal.0c01666
405. Gao, R.; Li, X.; Guo, L.; Tong, Z.; Deng, Q.; Wang, J.; Zeng, Z.; Zou, J.-J.; Deng, S. *Appl. Catal., A* **2021,** *612,* 117985. doi:10.1016/j.apcata.2020.117985
406. Perret, N.; Grigoropoulos, A.; Zanella, M.; Manning, T. D.; Claridge, J. B.; Rosseinsky, M. J. *ChemSusChem* **2016,** *9,* 521–531. doi:10.1002/cssc.201501225
407. Ramos, R.; Grigoropoulos, A.; Perret, N.; Zanella, M.; Katsoulidis, A. P.; Manning, T. D.; Claridge, J. B.; Rosseinsky, M. J. *Green Chem.* **2017,** *19,* 1701–1713. doi:10.1039/c7gc00315c
408. Zhang, S.; Ma, H.; Sun, Y.; Luo, Y.; Liu, X.; Zhang, M.; Gao, J.; Xu, J. *Green Chem.* **2019,** *21,* 1702–1709. doi:10.1039/c8gc04009e
409. Li, J.; Feng, Y.; Wang, H.; Tang, X.; Sun, Y.; Zeng, X.; Lin, L. *Mol. Catal.* **2021,** *505,* 111505. doi:10.1016/j.mcat.2021.111505
410. Morales, M. V.; Conesa, J. M.; Guerrero-Ruiz, A.; Rodríguez-Ramos, I. *Carbon* **2021,** *182,* 265–275. doi:10.1016/j.carbon.2021.06.007
411. Xu, Y.-J.; Shi, J.; Wu, W.-P.; Zhu, R.; Li, X.-L.; Deng, J.; Fu, Y. *Appl. Catal., A* **2017,** *543,* 266–273. doi:10.1016/j.apcata.2017.07.004
412. Mo, F.; Dong, G. *Science* **2014,** *345,* 68–72. doi:10.1126/science.1254465
413. Hurtado, B.; Arias, K. S.; Climent, M. J.; Concepción, P.; Corma, A.; Iborra, S. *ChemSusChem* **2022,** *15,* e202200194. doi:10.1002/cssc.202200194
414. Allais, F. *Curr. Opin. Green Sustainable Chem.* **2023,** *40,* 100744. doi:10.1016/j.cogsc.2022.100744
415. He, J.; Liu, M.; Huang, K.; Walker, T. W.; Maravelias, C. T.; Dumesic, J. A.; Huber, G. W. *Green Chem.* **2017,** *19,* 3642–3653. doi:10.1039/c7gc01688c
416. Lamb, O.; Puschnig, J.; Glover, S.; Greatrex, B. W. *ChemSusChem* **2025,** *18,* e202402292. doi:10.1002/cssc.202402292
417. Oyola-Rivera, O.; He, J.; Huber, G. W.; Dumesic, J. A.; Cardona-Martínez, N. *Green Chem.* **2019,** *21,* 4988–4999. doi:10.1039/c9gc01526d
418. Camp, J. E. *ChemSusChem* **2018,** *11,* 3048–3055. doi:10.1002/cssc.201801420
419. Kong, D.; Dolzhenko, A. V. *Sustainable Chem. Pharm.* **2022,** *25,* 100591. doi:10.1016/j.scp.2021.100591

420. Warne, C. M.; Fadlallah, S.; Whitwood, A. C.; Sherwood, J.; Mouterde, L. M. M.; Allais, F.; Guebitz, G. M.; McElroy, C. R.; Pellis, A. *Green Chem. Lett. Rev.* **2023,** *16,* 2154573. doi:10.1080/17518253.2022.2154573
421. Citarella, A.; Amenta, A.; Passarella, D.; Micale, N. *Int. J. Mol. Sci.* **2022,** *23,* 15960. doi:10.3390/ijms232415960
422. Stini, N. A.; Gkizis, P. L.; Kokotos, C. G. *Green Chem.* **2022,** *24,* 6435–6449. doi:10.1039/d2gc02332f
423. Ayoub, N.; Toufaily, J.; Guénin, E.; Enderlin, G. *ChemSusChem* **2022,** *15,* e202102606. doi:10.1002/cssc.202102606
424. Comba, M. B.; Tsai, Y.-h.; Sarotti, A. M.; Mangione, M. I.; Suárez, A. G.; Spanevello, R. A. *Eur. J. Org. Chem.* **2018,** 590–604. doi:10.1002/ejoc.201701227
425. Stanfield, M. K.; Terry, R. S.; Smith, J. A.; Thickett, S. C. *Polym. Chem.* **2023,** *14,* 4949–4956. doi:10.1039/d3py01019h
426. Cummings, A.; Rice, C.; Sheldrake, G. N.; Murnaghan, C. W. J. *Eur. J. Org. Chem.* **2025,** *28,* e202401320. doi:10.1002/ejoc.202401320
427. Bonneau, G.; Peru, A. A. M.; Flourat, A. L.; Allais, F. *Green Chem.* **2018,** *20,* 2455–2458. doi:10.1039/c8gc00553b
428. Diot-Néant, F.; Mouterde, L.; Fadlallah, S.; Miller, S. A.; Allais, F. *ChemSusChem* **2020,** *13,* 2613–2620. doi:10.1002/cssc.202000680
429. Ray, P.; Hughes, T.; Smith, C.; Hibbert, M.; Saito, K.; Simon, G. P. *Polym. Chem.* **2019,** *10,* 3334–3341. doi:10.1039/c9py00353c
430. Diot-Néant, F.; Rastoder, E.; Miller, S. A.; Allais, F. *ACS Sustainable Chem. Eng.* **2018,** *6,* 17284–17293. doi:10.1021/acssuschemeng.8b04707
431. Huang, X.; Liu, T.; Wang, J.; Wei, F.; Ran, J.; Kudo, S. *J. Energy Inst.* **2020,** *93,* 2505–2510. doi:10.1016/j.joei.2020.08.010
432. De bruyn, M.; Sener, C.; Petrolini, D. D.; McClelland, D. J.; He, J.; Ball, M. R.; Liu, Y.; Martins, L.; Dumesic, J. A.; Huber, G. W.; Weckhuysen, B. M. *Green Chem.* **2019,** *21,* 5000–5007. doi:10.1039/c9gc00564a
433. Krishna, S. H.; McClelland, D. J.; Rashke, Q. A.; Dumesic, J. A.; Huber, G. W. *Green Chem.* **2017,** *19,* 1278–1285. doi:10.1039/c6gc03028a
434. Wu, L.; Kim, H.; Choi, T.-L. *J. Am. Chem. Soc.* **2025,** *147,* 11682–11687. doi:10.1021/jacs.5c02397
435. Lombardo, G.; Warne, C. M.; Damonte, G.; Todea, A.; Nagy, L.; Guebitz, G. M.; Allais, F.; Fadlallah, S.; Pellis, A. *ACS Sustainable Chem. Eng.* **2025,** *13,* 4068–4077. doi:10.1021/acssuschemeng.4c10010
436. Hughes, L.; McElroy, C. R.; Whitwood, A. C.; Hunt, A. J. *Green Chem.* **2018,** *20,* 4423–4427. doi:10.1039/c8gc01227j
437. Kuhl, N.; Turnbull, B. W. H.; Ji, Y.; Larson, R. T.; Shevlin, M.; Prier, C. K.; Chung, C. K.; Desmond, R.; Guetschow, E.; He, C. Q.; Itoh, T.; Kuethe, J. T.; Newman, J. A.; Reibarkh, M.; Rivera, N. R.; Shang, G.; Wang, Z.; Zewge, D.; Thaisrivongs, D. A. *Green Chem.* **2023,** *25,* 606–613. doi:10.1039/d2gc04117k

License and Terms

This is an open access article licensed under the terms of the Beilstein-Institut Open Access License Agreement (https://www.beilstein-journals.org/bjoc/terms), which is identical to the Creative Commons Attribution 4.0 International License (https://creativecommons.org/licenses/by/4.0). The reuse of material under this license requires that the author(s), source and license are credited. Third-party material in this article could be subject to other licenses (typically indicated in the credit line), and in this case, users are required to obtain permission from the license holder to reuse the material.

The definitive version of this article is the electronic one which can be found at:
https://doi.org/10.3762/bjoc.21.165

BEILSTEIN JOURNAL OF ORGANIC CHEMISTRY

The high potential of methyl laurate as a recyclable competitor to conventional toxic solvents in [3 + 2] cycloaddition reactions

Ayhan Yıldırım* and Mustafa Göker

Full Research Paper

Open Access

Address:
Department of Chemistry, Bursa Uludağ University, Bursa 16059, Turkey

Email:
Ayhan Yıldırım* - yildirim@uludag.edu.tr

* Corresponding author

Keywords:
cycloaddition; fused isoxazolidines; renewable solvent; reusable solvent; *trans*-diastereoselectivity

Beilstein J. Org. Chem. **2025,** *21,* 2389–2415.
https://doi.org/10.3762/bjoc.21.184

Received: 11 June 2025
Accepted: 24 October 2025
Published: 05 November 2025

This article is part of the thematic issue "Green chemistry III: Technologies shaping future directions in synthesis".

Associate Editor: L. Vaccaro

© 2025 Yıldırım and Göker; licensee Beilstein-Institut.
License and terms: see end of document.

Abstract

In the present study, 21 fused isoxazolidines were synthesized in yields ranging from good to excellent. Methyl laurate was identified as the easily accessible optimal solvent medium for the reaction, and the related compounds were obtained through straightforward isolation techniques in a relatively short time frame (5–80 minutes). A comprehensive investigation was conducted utilizing various web platforms, encompassing ecological and environmental risk assessments, toxicity, pesticide similarity, and biodegradability of methyl laurate in comparison with a series of conventional organic solvents, water, some fatty acids and their derivatives. The findings of this investigation revealed that methyl laurate exhibited better green solvent properties when evaluated against other solvents.

Introduction

It is an established fact that a significant number of conventional organic solvents, which are widely utilized in both industrial and academic contexts, have deleterious effects on human and environmental health [1-3]. There is an ongoing and intensive research effort to identify new biocompatible alternatives to replace these existing solvents and many of the criteria that a solvent must meet to be considered green have been well defined in different sources [4,5]. In order to fulfil this requirement, a considerable number of green solvents of various classes have been developed for a range of applications, including the extraction of natural compounds [6-9], food analysis [10-12], pharmacology [13-15], and organic synthesis [16-19]. Despite the advent of environmentally friendly green solvents that have been discovered to be applicable in numerous modern organic chemical transformations, difficulties often arise in the recovery and reuse of these solvents following the completion of the reaction. Moreover, some of these solvents have been observed to degrade under conditions that are particularly severe

[20]. For instance, although ionic liquids are well-known green solvent alternatives with superior properties compared to conventional organic solvents, their recovery from the reaction medium can be quite troublesome [21,22]. It is evident that this class of solvents may be accompanied by a number of drawbacks. For instance, they are frequently expensive, exhibit negligible or non-existent biodegradability, and there is a lack of data concerning their potential toxicity. Conversely, while water is regarded as a promising biocompatible solvent alternative in numerous chemical transformations, there are several challenges associated with product isolation that must be addressed [23]. Consequently, it is evident that the endeavor to identify an optimal green solvent for both industrial and academic applications must persist.

In the modern world, one of the main goals of an increasing number of chemists interested in the design and synthesis of versatile organic molecules is to develop atom-efficient, multicomponent, low-cost, and environmentally benign synthetic strategies for these molecules. In the context of these strategies, it would be judicious to consider cycloaddition reactions of the [3 + 2] type, a field in which Smith and Huisgen are recognized as pioneers [24,25]. In the field of heterocyclic chemistry, the [3 + 2] type of cycloaddition reaction is a widely employed method for the formation of the five-membered isoxazolidine ring motif, which displays a range of biologically active properties [26-30]. It is notable that the fused pyrrolo-isoxazolidines represent a particularly versatile class of heterocyclic compounds and intermediates, which have been demonstrated to exhibit a wide range of biological activities [26,28,31-35]. The validity of the atom-efficient methodology under discussion has been demonstrated in experimental research; its efficacy in facilitating the rapid formation of multifunctional complex molecules being in contradistinction to the time- and labor-intensive nature of traditional multistep synthesis strategies. For instance, this methodology has been demonstrated to be highly advantageous in the synthesis of numerous pharmaceutical compounds, biological probes, insecticides, alkaloids, and other intricate natural compounds consisting of a combination of isoxazolidine rings [36-41]. It has been demonstrated that such cycloaddition reactions are also employed in the efficient preparation of biologically active molecules, including nucleosides, β-lactam class antibiotics, peptides, and amino acids, as well as sugars (Figure 1) [42-48].

More specifically cycloaddition reactions of nitrones (1,3-dipoles) with *N*-aryl-substituted maleimides (electron-poor dipolarophiles) are a highly popular and versatile method for the formation of regio- and stereoselective pyrrolo-isoxazolidine-fused ring scaffolds. From the standpoint of organic chemistry, it is evident that these compounds can be efficiently converted into a variety of versatile organic intermediates through the application of ring-opening reactions [49-52]. In addition to the aforementioned useful properties, the current methods for the preparation of such cyclic compounds and/or their fused cyclic systems typically necessitate the use of toxic solvents, including chloroform, benzene, toluene etc. [32,53-59]. Indeed, the selection of conventional organic solvents, including benzene, toluene and chloroform, for the [3 + 2] cycloaddition reactions between nitrones and diverse dipolarophiles has not been predicated on any criteria other than their inertness [60]. Conversely, certain studies have reported that the effects of organic solvents in such reactions are negligible, and that an increase in solvent polarity results in a decrease in rate constants. This phenomenon is attributed to the lower polarity of the transition state in comparison to that of the initial compounds [61]. Furthermore, these methods often require harsh reaction conditions, prolonged reaction times, and laborious purification techniques [62-64]. Synthesis of pyrrolo-isoxazolidines utilizing nitrosoarenes via the multicomponent strategy is indeed feasible [65,66]. In a similar manner, Chakraborty obtained diastereomer products, primarily in cis configuration, from the cycloaddition reaction of a fluoro or a furyl-based nitrone with some maleimides via a mechanochemical route in a solvent-free medium [67,68]. The development of environmentally friendly green methodologies for the preparation of heterocyclic compounds via such cycloaddition reactions is a significant and ongoing research area that should not be overlooked [69]. However, these methods are accompanied by the inevitability of long reaction times or the use of toxic organic solvents. Such negative aspects encountered during the synthe-

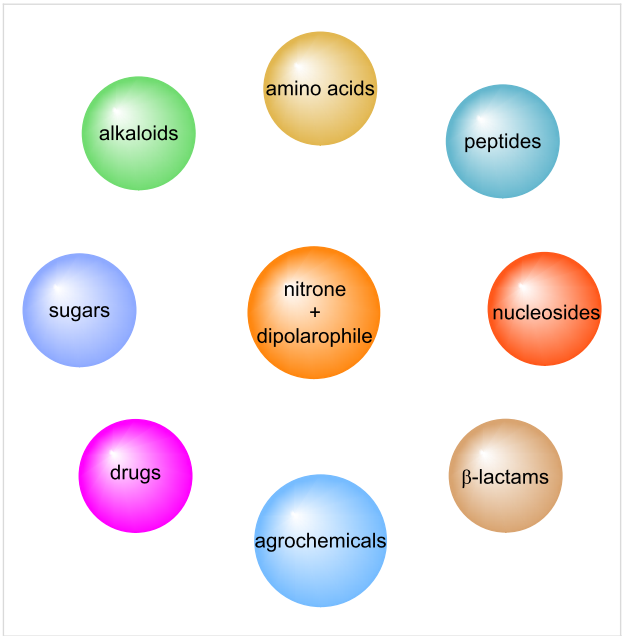


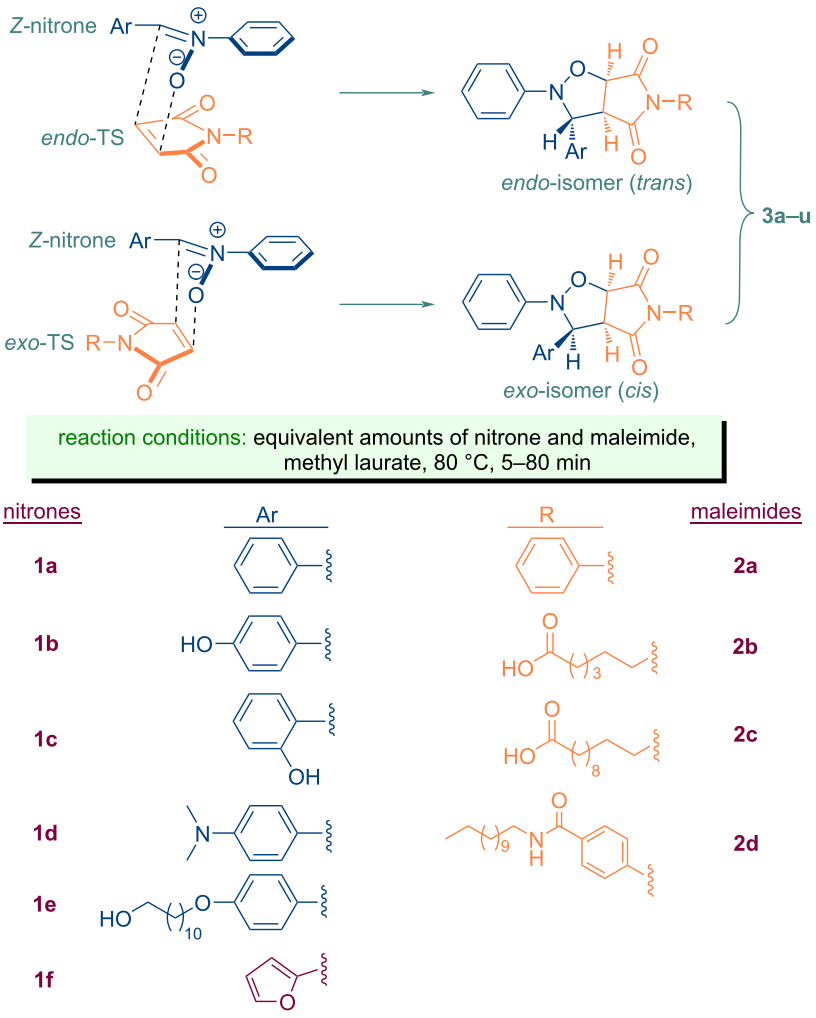
Figure 1: Versatile compounds via cycloaddition reactions.

sis of these compounds prompted us to seek alternative, environmentally benign, renewable, and reusable solvents [70]. It is therefore a basic tenet of *Green Chemistry* to replace the conventional organic solvents, which are flammable and generate toxic volatile components and are costly, with readily accessible and biocompatible alternatives [71]. Indeed, the utilization of eco-friendly bio-based solvents in a multitude of organic chemical transformations [72-74], industrial processes [5,75,76], and pharmaceutical applications [13,77] has recently gained significant prevalence. In view of the aforementioned considerations, the focus of our current research is on more environmentally friendly 1,3-dipoar cycloaddition reactions of nitrones with *N*-arylmaleimides to synthesize a series of pyrrolo-isoxazolidines.

In this context, an investigation was conducted into the potential of vegetable oils and certain derivatives to serve as biocompatible solvents in cycloaddition reaction contexts. This investigation involved a comparative analysis of these vegetable oils and derivatives with water and a range of commonly employed organic solvents in organic transformations.

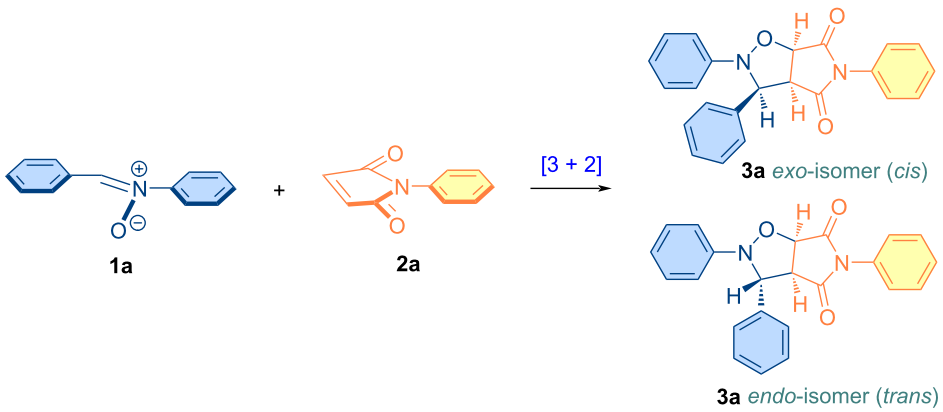
Results and Discussion

The requisite starting compounds, nitrones **1a–f** and a selection of *N*-substituted maleimide derivatives **2b–d** were successfully synthesized in accordance with procedures previously documented in the literature (Scheme 1) [28,78-85]. In this study, the reaction between simple starting compounds *C*,*N*-diphenylnitrone and *N*-phenylmaleimide was selected as the model cycloaddition reaction. A series of bio-based materials were subsequently employed to ascertain the most appropriate green solvent for the specified cycloaddition reaction, with the findings presented in Table 1. As evidenced by the data presented in the table, the majority of the selected vegetable oils and their two derivatives are viable candidates for use as solvents in the proposed reaction. Concurrently, the reaction was carried out in



Scheme 1: Molecular structures of parent compounds **1a–f**, **2a–d** and cycloadducts **3a–u**.

Table 1: Optimization of the [3 + 2] cycloaddition conditions for the synthesis of pyrrolo[3,4-*d*]isoxazolidine **3a** (*cis* + *trans* isomers).



Entry	Solvent	Time (min)	Temperature (°C)	Yield (%)[a]
1	sunflower oil	10	80	89
2	coconut oil	10	80	91
3	olive oil	10	80	75
4	hazelnut oil	10	80	92
5	walnut oil	10	80	87
6	castor oil	10	80	53
7	oleic acid	10	80	87
8	methyl laurate	10	80	100
9	methyl laurate	5	80	100 (*cis*/*trans* 28:72)
10	water[b]	10	80	51
11	solvent free	10	80	42
12	solvent free	60	80	53

[a]The yields were obtained by precipitation of the relevant product from the reaction medium with a suitable solvent. [b]The yield was obtained by means of extraction with EtOAc and subsequent precipitation with hexane.

a solvent-free environment, and the product yields obtained in two distinct time periods are presented in Table 1 (entries 11 and 12). As can be deduced from these results, the reaction is found to be more sluggish in a solvent-free environment. Therefore, as evidenced in Table 1 (entries 8 and 9), methyl laurate is the most suitable solvent candidate for the reaction between nitrones and maleimides. Accordingly, methyl laurate, which facilitates the completion of this reaction in a relatively short time frame (approximately five minutes), was selected as the primary solvent for the isoxazolidine derivatives that are planned to be synthesized in this study.

In recent times, research into the evaluation of ecological and environmental risks posed by various organic compounds and solvents has gained increased significance. In silico models have emerged as a valuable tool, offering rapid and cost-effective solutions when experimental data is not readily available, particularly those that are web-integrated [86]. The predicted physical properties of methyl laurate, as determined by the *ADMETLab 3.0* platform [87] are illustrated in Figure 2a. Conversely, the oral toxicity values of methyl laurate, in conjunction with toluene and chloroform – two conventional solvents that are commonly employed in [3 + 2] cycloaddition reactions were calculated with *ProTox 3.0* (a webserver for the prediction of toxicity of chemicals) [88], as shown in Figure 2b. As illustrated in the figure, the LD_{50} value, which serves as a measure of the toxicity of these solvents, exhibits the highest value for methyl laurate and can be characterized as the solvent with the lowest toxicity. Furthermore, the results for the organic solvents many of which are not environmentally friendly and widely used in other synthesis reactions have been presented in Figure 3. The solvent potential of these solvents in the [3 + 2] cycloaddition reaction was investigated in the context of this study. As demonstrated in Figure 3, the toxicity class estimated for methyl laurate categorizes it as a potential environmentally friendly solvent. The *OSIRIS PropertyExplorer* program was employed to conduct toxicity risk assessments of methyl laurate, the results of which demonstrated that this solvent does

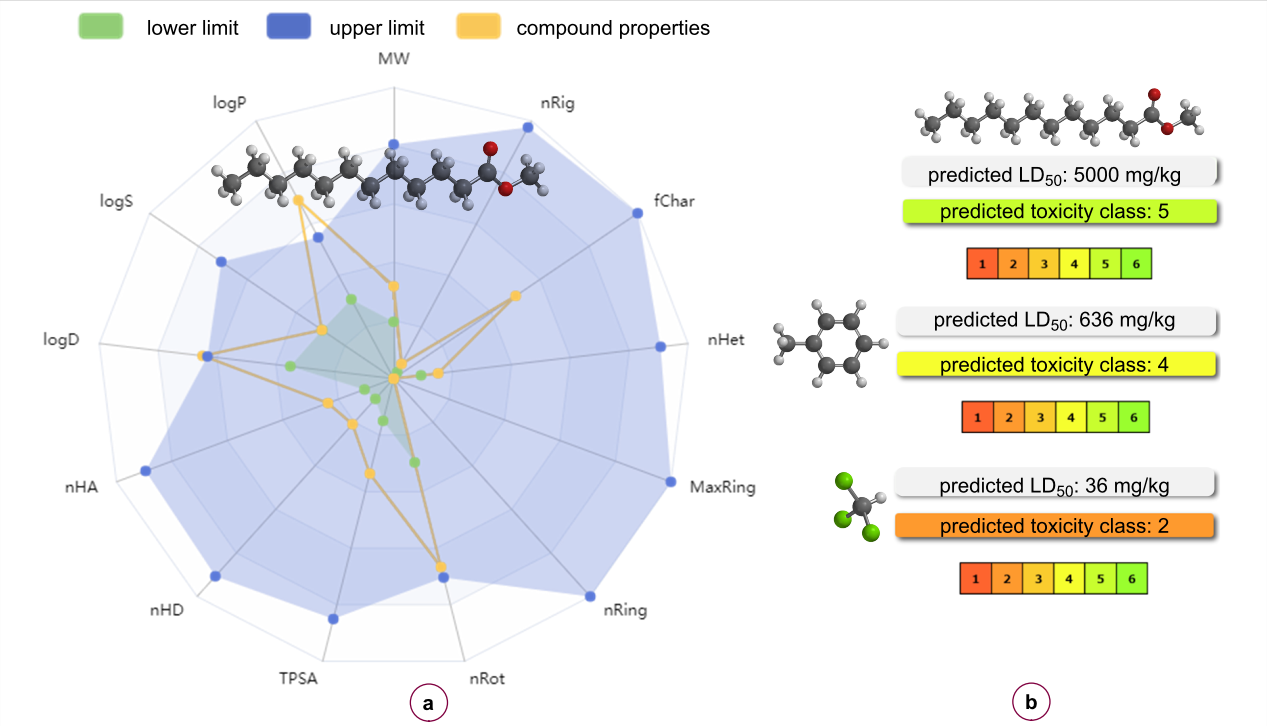


Figure 2: a) Radar view of the physical properties of methyl laurate. b) Oral toxicity values of methyl laurate, toluene, and chloroform, respectively.

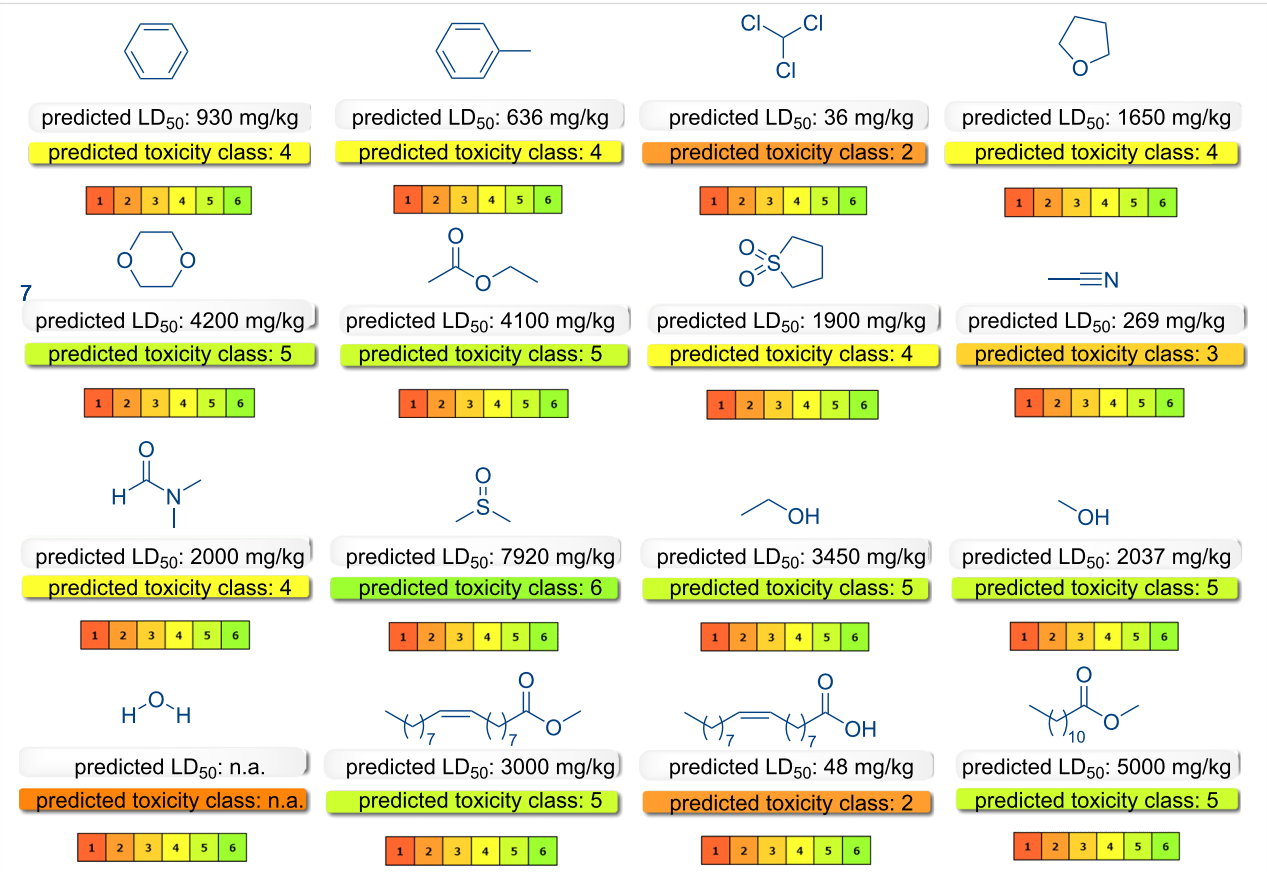


Figure 3: The oral toxicity values of all the solvents utilized in the present study obtained with *ProTox 3.0*.

not possess mutagenic, tumorigenic, irritant, or reproductive properties (Table 2). According to the toxicity risk assessments for solvents in this table, determined using the *OSIRIS PropertyExplorer* software, sulfolane appears to be a safe solvent and its use is recommended for certain purposes in some studies [89]. However, the toxicity of sulfolane has been mentioned in some other studies [90,91]. Moreover, as illustrated in the Table 2, only methyl oleate and methyl laurate, in conjunction with sulfolane, were categorized as entirely risk-free based on the four pertinent toxicity parameters. In the context of cycloadditions, the conventional solvents that are typically employed as reaction media encompass a range of options, including tetrahydrofuran (THF) (a problematic solvent, *p*), dioxane (considered hazardous, *h*), benzene (designated as highly hazardous, *hh*), toluene (*p*), chloroform (*hh*), acetonitrile (*p*), sulfolane (*h*), and DMSO (*p*) according to the guidelines outlined in the CHEM21 solvent selection guide [92].

A series of risk assessments was conducted, including ecological and environmental risk assessments, as well as pesticide similarity and biodegradability assessments of methyl laurate in comparison with toluene and chloroform, respectively (Figure 4, Figure 5, and Figure 6). These assessments were performed using the *ChemFREE* web platform [86].

According to the ecological risk assessments for some species based on the data shown in these figures, methyl laurate does not pose a risk to 4 species, while chloroform and toluene do not pose a risk to 3 species (please see the green colored icons). In terms of environmental risk factors, the persistence of methyl laurate in soil, sediment and water, with the exception of air, is significantly lower than that of the other two solvents (values are calculated in days). In addition, it can be seen that out of these three solvents, only methyl laurate is readily biodegradable on the basis of environmental risk factors (in the OECD 301C modified MITI (I) test, a substance can be considered ready biodegradable if 60% of the substance is mineralized in 28 days (in terms of ThOD)). On the other hand, pesticide-likeness radar, "According to Hao's pesticide-likeness rule“ [93], the radar plot gives an integrated measure of six properties of chemicals, which performs more comprehensive qualitative analysis to exclude chemicals with properties most probably incompatible with an acceptable bioavailable profile. As the molecules of methyl laurate contain more rotatable bonds than the molecules of the other two solvents, this value was slightly higher in the pesticide-likeness radar. Moreover, molecular complexities, pesticide-likeness scores, RDL, GAU, QEX scores are quantitative assessment methods, which rely on some of the physicochemical properties are relevant, accessible, and

Table 2: Toxicity risk assessments of the solvents (with *OSIRIS PropertyExplorer*).

Solvent	Mutagenic	Tumorigenic	Irritant	Reproductive effective
benzene	🔴	🔴	🔴	🔴
toluene	🔴	🔴	🔴	🔴
chloroform	🔴	🔴	🔴	🔴
THF	🔴	🔴	🟢	🔴
dioxane	🔴	🔴	🔴	🔴
EtOAc	🔴	🟢	🔴	🟢
sulfolane	🟢	🟢	🟢	🟢
MeCN	🔴	🔴	🔴	🔴
DMF	🟢	🔴	🟢	🟢
DMSO	🔴	🔴	🔴	🔴
EtOH	🔴	🔴	🔴	🔴
MeOH	🔴	🟢	🔴	🔴
water	🔴	🔴	🟢	🔴
methyl oleate	🟢	🟢	🟢	🟢
oleic acid	🔴	🔴	🔴	🟢
methyl laurate	🟢	🟢	🟢	🟢

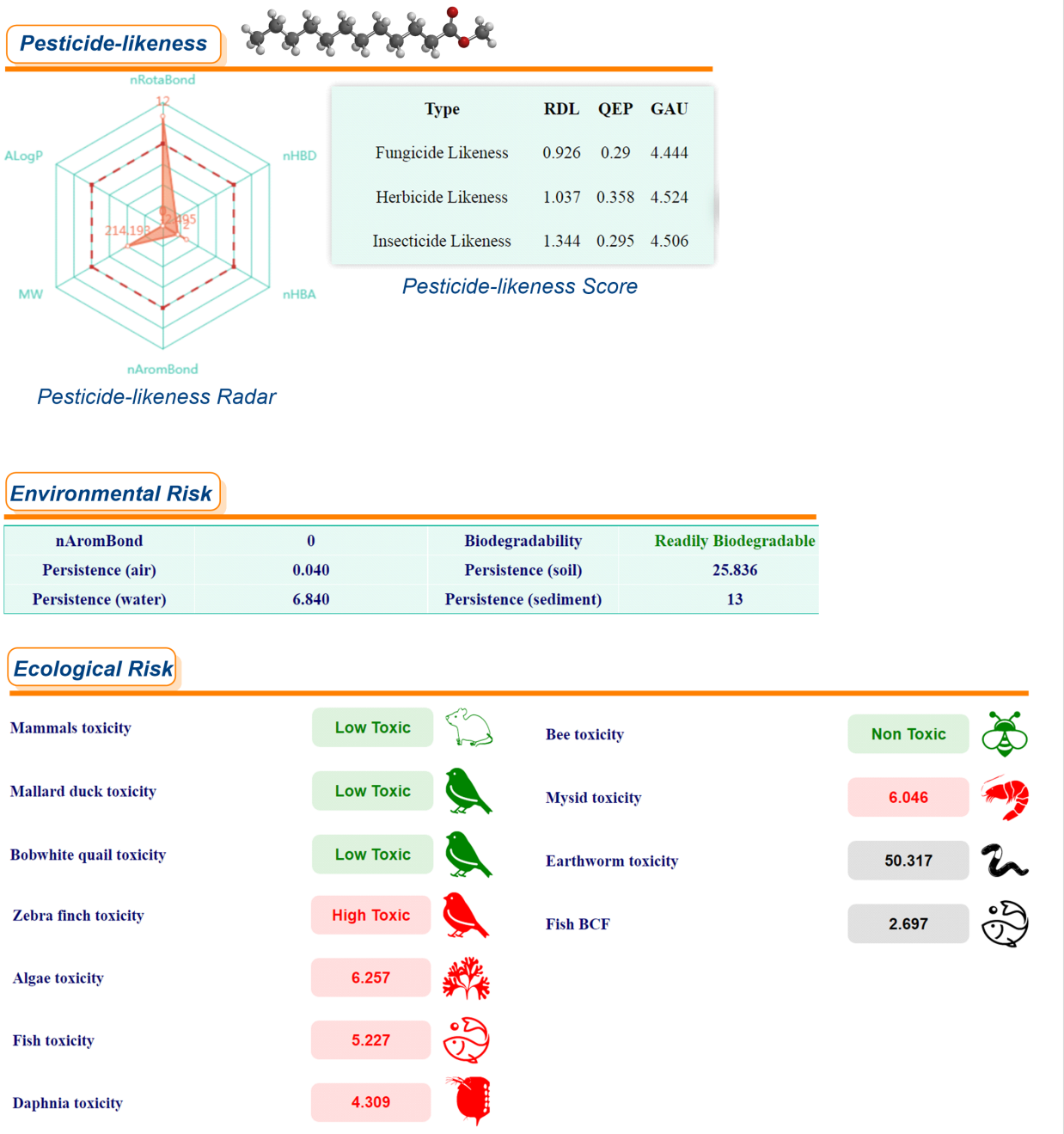


Figure 4: Ecological, environmental risk assessments, pesticide similarity and biodegradability assessments of methyl laurate.

easy to compute. A high score indicates a higher potential for chemicals to become new pesticides (the data obtained with *ChemFREE* for the other 13 solvents used in the study are given in Supporting Information File 1, Figure S1). In addition to the calculations already outlined, a series of toxicity properties of methyl laurate were calculated using *ADMETLab 3.0* in comparison with common organic solvents and some green solvents. The obtained results were visualized with a cylinder chart in Figure 7. Indeed, a significant proportion of the experimentally measured *Green Chemistry* parameters for methyl laurate are consistent with the predictions of various software or web platforms, and in some cases, even demonstrate that certain toxicity parameters of methyl laurate are more environmentally friendly. As demonstrated in the relevant literature, methyl laurate has been shown to be non-toxic to the acute oral route and to not induce mutagenic effects in the *S. typhimurium* reversion assay [94]. In the course of the experiments conducted with methyl laurate, no irritant effects on the skin of human subjects

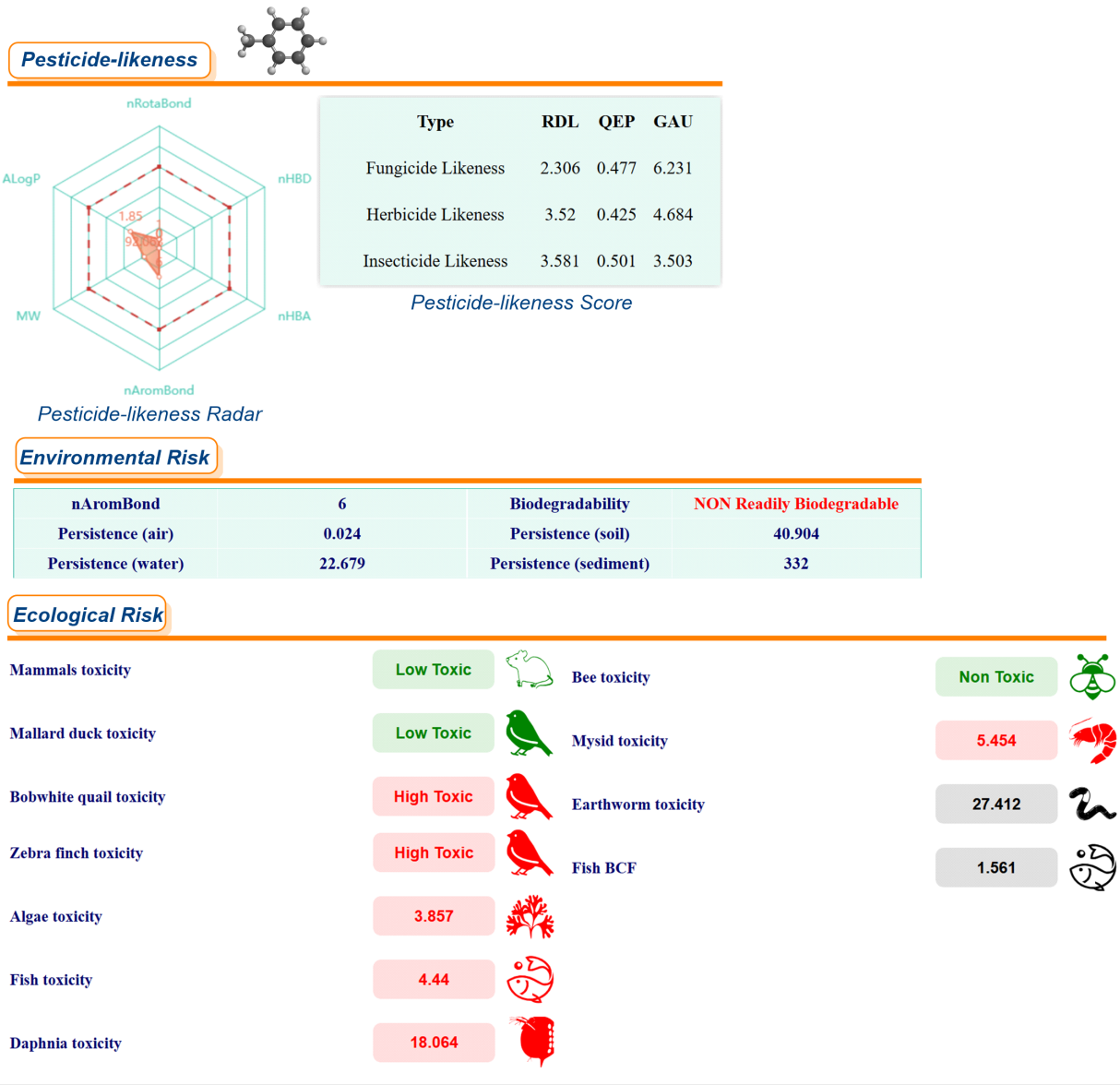


Figure 5: Ecological, environmental risk assessments, pesticide similarity and biodegradability assessments of toluene.

were detected. However, evidence of ocular irritation at very low levels was obtained. Furthermore, it has been determined that 100–69% of methyl laurate is readily biodegraded aerobically following a 30-day period. The utilization of certain fatty acid methyl esters, including but not limited to methyl laurate, has found application in a variety of direct and indirect food additive applications [94].

The Hansen solubility parameter is a numerical expression that quantifies a molecule's cohesive energy density from non-polar, polar, and hydrogen-bonding interactions. It is a widely utilized tool in the field of molecular science for predicting the miscibility of solutes with solvents, as well as the miscibility of solutes within themselves, based on the fundamental principle of "*like dissolves like*" [95]. The location of the selected common organic solvents in the 3D Hansen space is shown in Figure 8a. The distribution of these selected solvents with other organic solvents in the 3D Hansen solubility space is determined by three Hansen solubility parameters (HSPs): dispersion (δ_D), polarity (δ_P), and hydrogen bonding (δ_H). As is well established, information about their similarity in solubility properties can be obtained from the distance between solvents. The identification of problematic and non-problematic solvents is facilitated by the size and color of the specific sphere representing a particular solvent. As demonstrated by the figure, the position of methyl laurate (with values of δ_D = 16, δ_P = 2.1 and δ_H = 5.3) can be found in the middle of the model spheres belonging to nonpolar and polar protic or polar aprotic solvents,

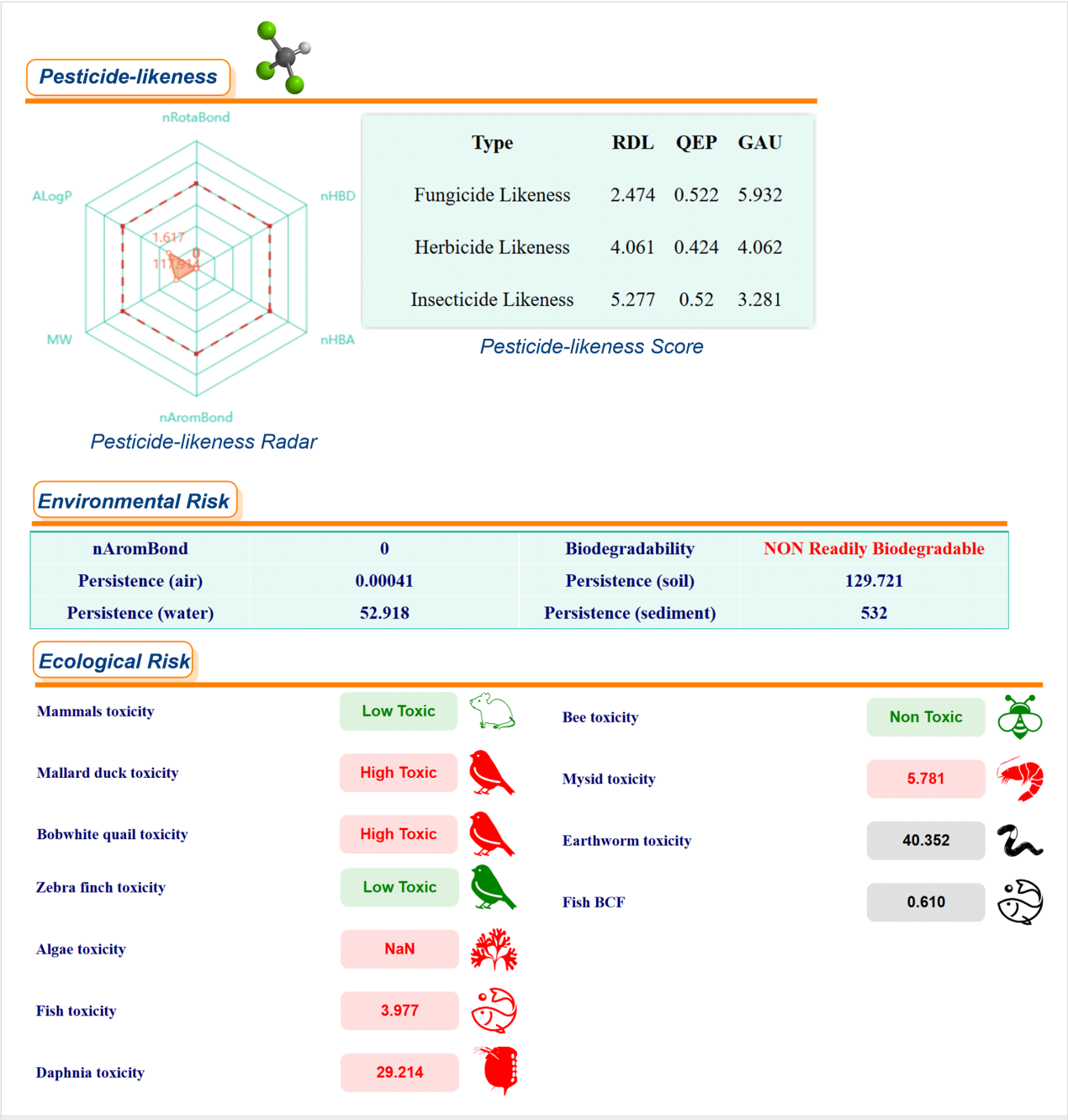


Figure 6: Ecological, environmental risk assessments, pesticide similarity and biodegradability assessments of chloroform.

which had previously been widely favored in cycloaddition reactions. These values reveal the similarity in solubility properties of the solvents. Furthermore, the evidence suggests that the majority of these solvents is hazardous and their utilization is to be avoided. As demonstrated in Figure 8a, the color of the spheres of the customary proportional solvents employed in [3 + 2] cycloadditions is red or yellow, thereby substantiating the potential hazard associated with their utilization as a solvent in the aforementioned reactions. For the solute component *C*,*N*-diphenylnitrone, the dispersion, polarity, and hydrogen bonding values for nitrone were determined as δ_D = 16.6, δ_P = 7.6 and δ_H = 8.7. Figure 8b clearly shows the position of the solute in the Hansen space. The "Green Solvent Selection Tool" was utilized to ascertain these three parameters [95]. For the purpose of this study, a series of solvents in which *C*,*N*-diphenylnitrone dissolves was determined through experimental means (at 22 °C) in our laboratory (Figure 8c). An experiment was conducted in which a series of organic solvents and water were subjected to solubility tests. For the purposes of this experiment, approximately 15 mg of nitrone was mixed with

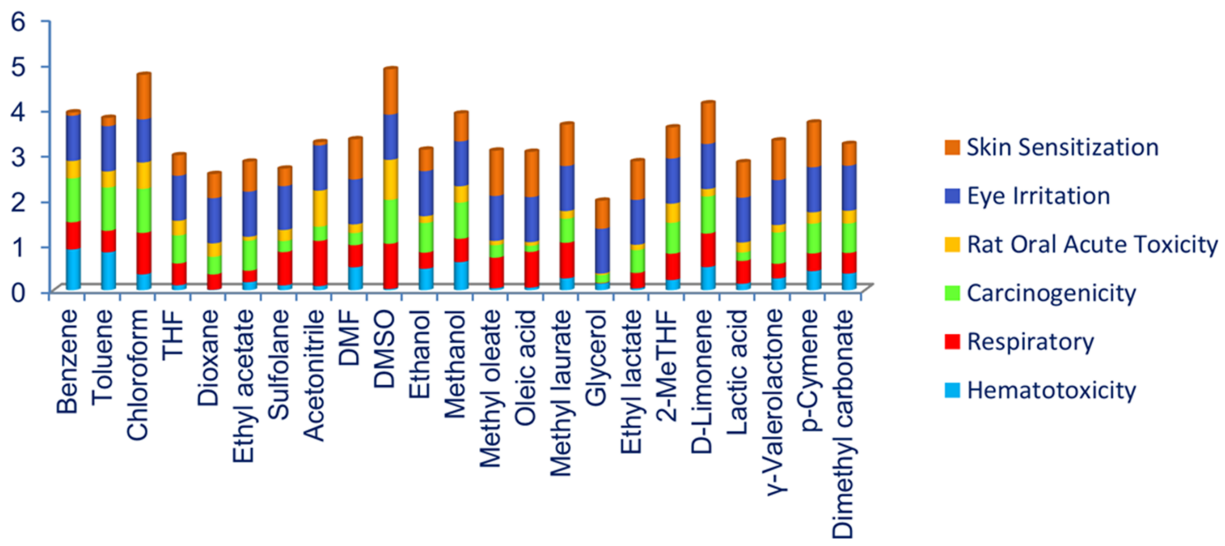
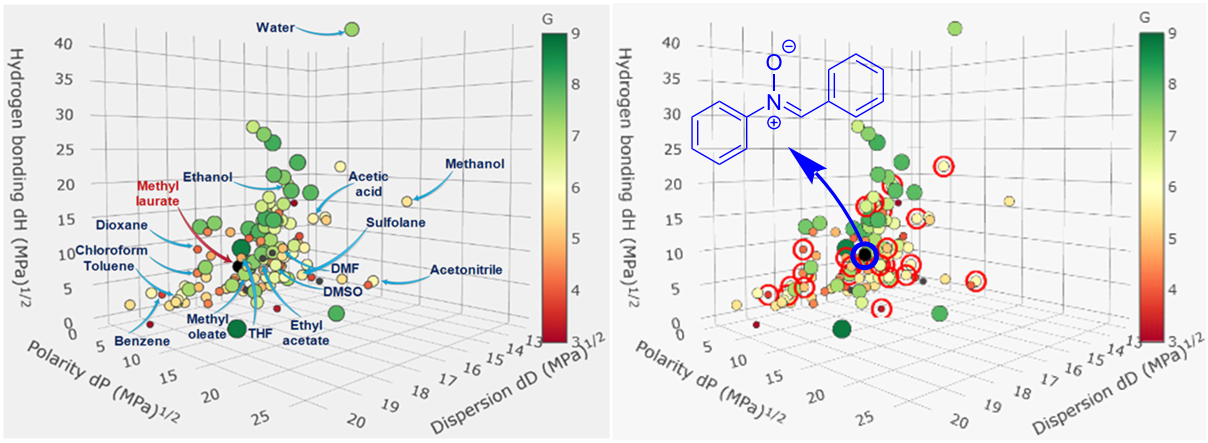


Figure 7: Various toxicity parameters of methyl laurate and a series of other solvents calculated by *ADMETLab 3.0*.



a b

1,2-dimethoxyethane	dimethyl formamide
1,4-dioxane	dimethyl sulfoxide
1-butanol	ethanol
2-propanol	ethyl acetate
acetic acid	methanol
acetone	methyl oleate
acetonitrile	methylethyl ketone
benzene	*p*-xylene
carbon tetrachloride	pyridine
chloroform	sulfolane
dichloromethane	*t*-butanol
diglyme	tetrahydrofuran
	toluene

c

Figure 8: a) Visualization of the localization of conventional organic and bio-based solvents in the Hansen space. b) Position of the nitrone in the Hansen space. c) Organic solvents that can dissolve *C*,*N*-diphenylnitrone (experimentally determined).

1 mL of solvent in a 10 mL test tube at room temperature (22 °C). As demonstrated in Figure 8c, the solvents under consideration are all effective in facilitating the dissolution of nitrone. However, under identical conditions, the nitrone was not fully soluble in solvents such as water, diethyl ether, petroleum ether, triethylene glycol, diethanolamine, and glycerol. Then, these solvents were selected with the known functional solvent(s) of our solute icon in this tool and following the update, the parameter values given above for the relevant nitrone were readily obtained. As can be seen from the figure, methyl laurate is a good alternative to competing toxic organic solvents that are good solvents for this compound.

As well-known the Hildebrand solubility parameter (HSP, δ_T) has been defined as a measure of the cohesive energy density of a material, thus facilitating prediction of the solubility of a solute in a solvent [96].

$$\delta_T = \sqrt{\delta_D^2 + \delta_P^2 + \delta_H^2} \quad (1)$$

Methyl laurate has been found to have HSPs that are in close proximity to those that have been predicted for nitrone, with a δ_T (the Hildebrand solubility parameter or the total Hildebrand parameter) of approximately 17. This finding indicates that methyl laurate is a suitable solvent for nitrone, which has a δ_T of around 20. On the other hand, the radius of interaction (R_a) is a critical factor in the assessment of solute solubility in a solvent, particularly in the context of HSPs [97,98]. It facilitates estimation of the extent of interaction between a solute and solvent, as determined by their respective solubility parameters. Consequently, the difference between the HSPs values can be utilized to calculate the R_a value between the nitrone and methyl laurate. In order to calculate the R_a value between the nitrone and methyl laurate, it is recommended to employ the following equation (n = nitrone, ml = methyl laurate):

$$R_a = \sqrt{4 \cdot \left(\delta_D^n - \delta_D^{ml}\right)^2 + \left(\delta_P^n - \delta_P^{ml}\right)^2 + \left(\delta_H^n - \delta_H^{ml}\right)^2} \quad (2)$$

According to Equation 2, R_a was calculated to be approximately ≈ 6.57 $MPa^{1/2}$. The radius of interaction (R_o) for a typical small organic molecule, such as the nitrone, is estimated to be approximately 7.5 $MPa^{1/2}$ which value is usually determined for solute molecules [97,99]. The relationship between R_a and R_o is denoted by the term relative energy difference (RED).

$$\mathrm{RED} = \frac{R_a}{R_o} \quad (3)$$

In the absence of any energy difference, the RED number is equivalent to 0. RED numbers that are less than 1 indicate high affinity, whilst RED numbers that are equal to or close to 1 represent a boundary circumstance. RED numbers that are progressively higher demonstrate increasingly lower affinities. Accordingly, when the values are substituted,

$$\mathrm{RED} = \frac{6.57}{7.5} \approx 0.876 \quad (4)$$

It is evident that, given the RED value of approximately 0.876, which is less than 1, the nitrone is likely to dissolve in a methyl laurate solvent. Methyl laurate is a medium-sized molecule that exhibits a combination of polar and non-polar characteristics, arising from the ester group and the non-polar hydrocarbon chain, respectively. The nitrone contains a polar functional group (N–O) and two aromatic rings, which serve to generate both polar and dispersion forces. Consequently, these findings indicate that fatty acid methyl esters may possess considerable promise as environmentally friendly solvents for cycloaddition reactions. Moreover, as pointed out by Gil et al., the δ_P and δ_H values for methyl esters of saturated fatty acids decrease with increasing chain length [100]. Consequently, the capacity of methyl laurate molecules to direct electric charge and hydrogen bonding is greater than that of methyl esters with longer chains.

Despite the proposal of a number of laborious green production processes for certain of the organic solvents selected for consideration in this study, they are still commercially produced using fossil reserves through conventional processes [101,102]. It is imperative to ascertain not only the cost-effective production processes of green solvents but also their static permeability, polarizability, solubility, viscosity, diffusivity, thermal behaviour and volumetric, surface or critical physicochemical properties that determine their interaction with other molecules in their environment [103]. It is evident that the dipole moment, a physical parameter which is macroscopic in nature, can be evaluated in order to characterize solvent polarity. The value calculated for methyl laurate is shown in Table S1 in Supporting Informaiton File 1 and is in good agreement with the values of other organic solvents commonly used in cycloaddition reactions. It may thus be considered an ideal solvent for nitrones and *N*-substituted maleimides, which possess varying degrees of polarity. The observation that methyl laurate exhibits no propensity for hydrogen bonding between its own molecules, yet functions as an H-bonding acceptor for other molecules, has the potential to facilitate free volume in the cycloaddition reaction medium for suitable substrates. This may, in turn, result in a favourable enhancement of the reaction rate. As demonstrated in Supporting Information File 1, Table S1, entries 14–16, the polarizability of fatty acid derivatives is greater than that of

other solvents, resulting in their enhanced dispersing power. Consequently, the attraction to dissolved molecules is also stronger.

Gu and Jérôme proposed a set of 12 criteria (*availability*, *price*, *recyclability*, *grade*, *synthesis*, *toxicity*, *biodegradability*, *performance*, *stability*, *flammability*, *storage*, *renewability*) with a view to defining the concept of green solvents [71]. Methyl laurate, predicted as the main potential green solvent in this study, fulfils almost all of the above criteria. For example, it can be synthesized easily and with high efficiency through the biodiesel production process, it can be reused, it is stable under storage conditions, it can be obtained from renewable resources, it is biodegradable, non-flammable etc. It is widely acknowledged that conventional organic solvents present significant challenges, primarily due to the fact that many of these solvents are volatile organic compounds, due to their high vapour pressures. Consequently, the examination of the vapour pressures of the solvents to be selected for utilization in organic reactions provides significant insights into their volatility. As demonstrated in Figure 9, the vapour pressures of fatty acids and their derivatives are comparatively low when compared to other solvents. Table 3 presents a summary of the physicochemical parameters, biodegradabilities, and percentage yields of compound **3a** in each of the solvents that were considered in the current study. Furthermore, as indicated in Table 3, the vapour pressures of the solvents at a reaction temperature of 80 °C suggest their suitability to be used in cycloaddition processes, superseding the utilization of other volatile solvents. A subsequent examination of the yields obtained for the cycloaddition product **3a** in Table 3 demonstrates that, in accordance with the expectations, the reaction rate is slower in polar solvents. It is hypothesized that the slightly higher yields in water are probably due to hydrophobic effects [61]. Conversely, while the yields of cycloaddition reactions conducted in toluene and chloroform are satisfactory (Table 3), both solvents are classified as highly toxic. The European regulation regarding the 'Registration, Evaluation, Authorization and Restriction of Chemicals' (REACH) has led to limitations on the use of chlorinated solvents, toluene, DMF etc., with the implementation of particular prerequisites [89]. The double bond present in oleic acid and methyl oleate may be disadvantageous for these solvents in comparison to methyl laurate. The potential isomerization and reactivity of this double bond can pose significant challenges, particularly in cycloadditions or other organic transformations that necessitate extended cycloaddition processes and elevated temperatures.

With a boiling point in excess of 260 °C, methyl laurate has the potential to function as a green solvent in a wide range of organic reactions that necessitate elevated temperatures. Furthermore, the oxidative stability index of methyl laurate at temperatures of 80 °C and 110 °C is greater than 40 (h), and the oxidation onset temperature is 198.5 °C which is better than those of methyl oleate [105]. In the case of castor oil, although all of the starting material was converted into the respective cycloadduct, the yield of the product was found to be lower than that observed in other solvents (Table 1, entry 6). This was primarily attributable to the utilization of a hexane/diethyl ether mixture in the isolation of the cycloadduct through precipitation, given that castor oil is insoluble in hexane. The solvent dissolves the product together with castor oil, causing it to pass to the filtrate phase and thereby reducing the amount present. In order to remain faithful to the principles of *Green Chemistry*, this study did not employ column chromatography for the isolation and purification of the products of interest from the reaction mixture. Otherwise, the yield of the reaction conducted in a castor oil medium would be similar to that of the other reactions. Furthermore, the rapid realization of the cycloaddition reaction in a non-polar solvent, such as methyl laurate, indicates that it proceeds via a non-polar mechanism. The lower polarity of the activated complex in comparison to the starting compounds supports the higher reaction rate in an non-polar solvent such as methyl laurate [61,106]. The 28:72 *exo/endo* (*cis/trans*) isomer ratio (Table 1, entry 9), obtained in this cycloaddition reaction indicates that the *endo* transition state is more stable, and that the thermodynamically more stable *trans* isomer is the major product in the reaction proceeding diastereoselectively through this transition state (Scheme 2). Meanwhile, the diastereomeric ratio of interest can be determined by integrating the ^{1}H NMR spectra, in particular by selecting the appropriate signal pairs (one from each diastereomer) belonging to the respective cycloaddition product. An example of these selected protons (*trans*-H6a and *cis*-H6a) is shown in Figure 10 for the compound **3a**.

Conversely, when these two reagents were heated in toluene, the ratio of *cis/trans* diastereoisomers was observed to be 1:1 [107], indicating that a remarkable diastereoselectivity can be achieved when methyl laurate is used as a solvent. The predominance of the *trans* isomer can be attributed to the stabilizing of secondary orbital interactions in the *endo* transition state, which results in the formation of this product, in contrast to the *exo* transition state [53,108]. In this case, the most significant factor is the π–π interaction (π–π stacking) between the phenyl rings substituted on the nitrogen atoms of both maleimide and nitrone [109]. The most significant evidence confirming the interactions that determine the diastereoselectivity observed here is that the *cis* diastereomer is the major addition product in the dipolar cycloaddition reaction using *N*-methyl,*C*-phenylnitrone and *N*-methylmaleimide [110]. Furthermore, although mono- and bifunctional *N*-methylnitrones exhibit higher cycloaddition

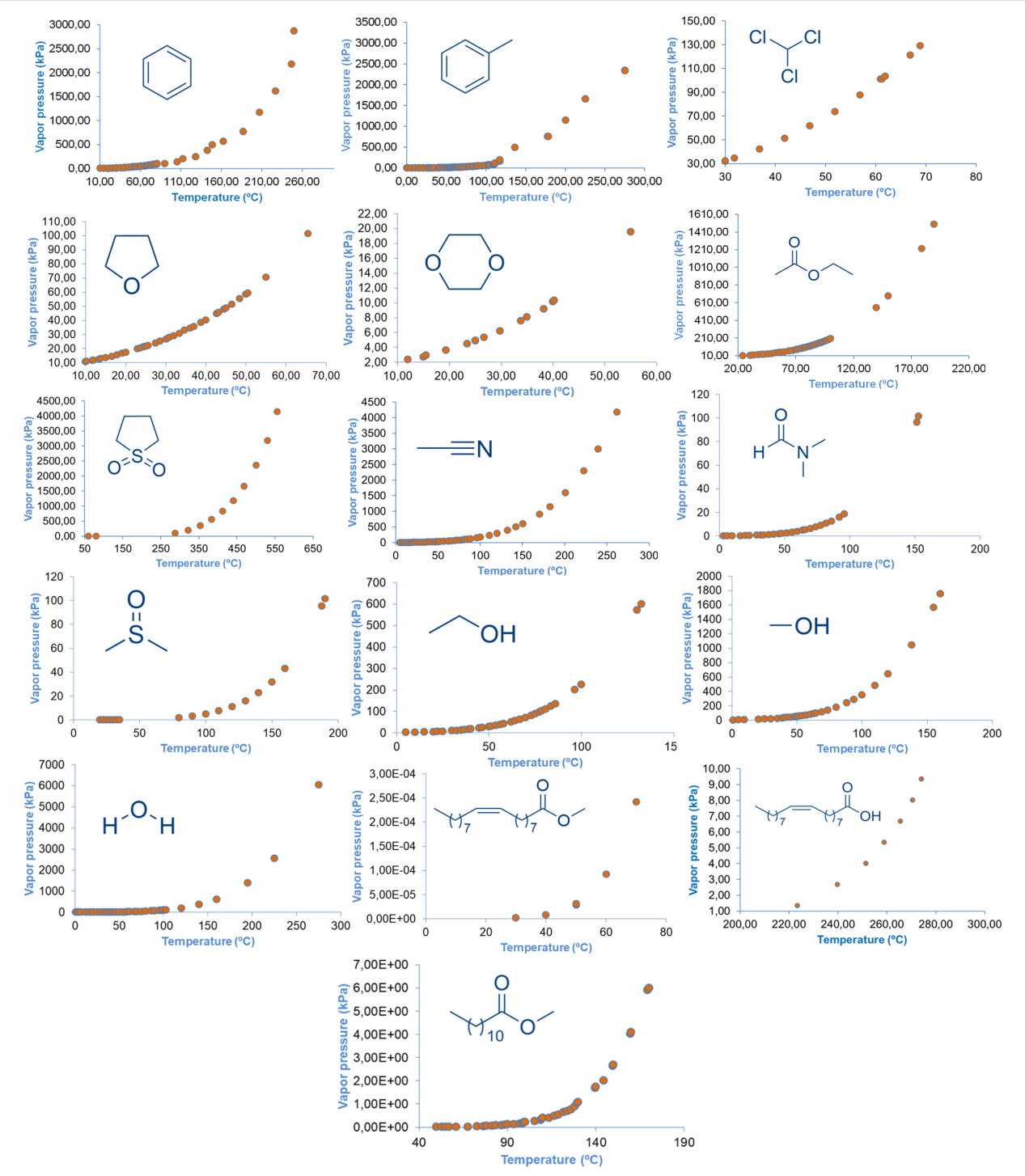


Figure 9: Vapour pressures of the solvents used (values retrieved from the *Chemeo* molecular database).

reaction rates than their *N*-phenyl analogues, their impact on selectivity is diminished [111]. It is well established that nitrones prepared from aromatic aldehydes exhibit a *Z*-configuration [112,113] and it appears that *endo*-coupling of the *Z*-configured *C*,*N*-diphenylnitrone with maleimide is more favorable. Indeed, the distribution of the *cis*/*trans* product is also found to be significantly influenced by the nature of the substituents present in the 1,3-dipole and/or dipolarophile and therefore, in some cases, *cis*-diastereoselectivity arises [85,114-117]. For instance, in the [3 + 2] cycloaddition reactions examined in earlier studies, intramolecular H-bonding, facilitated by the amide or alcohol functionality

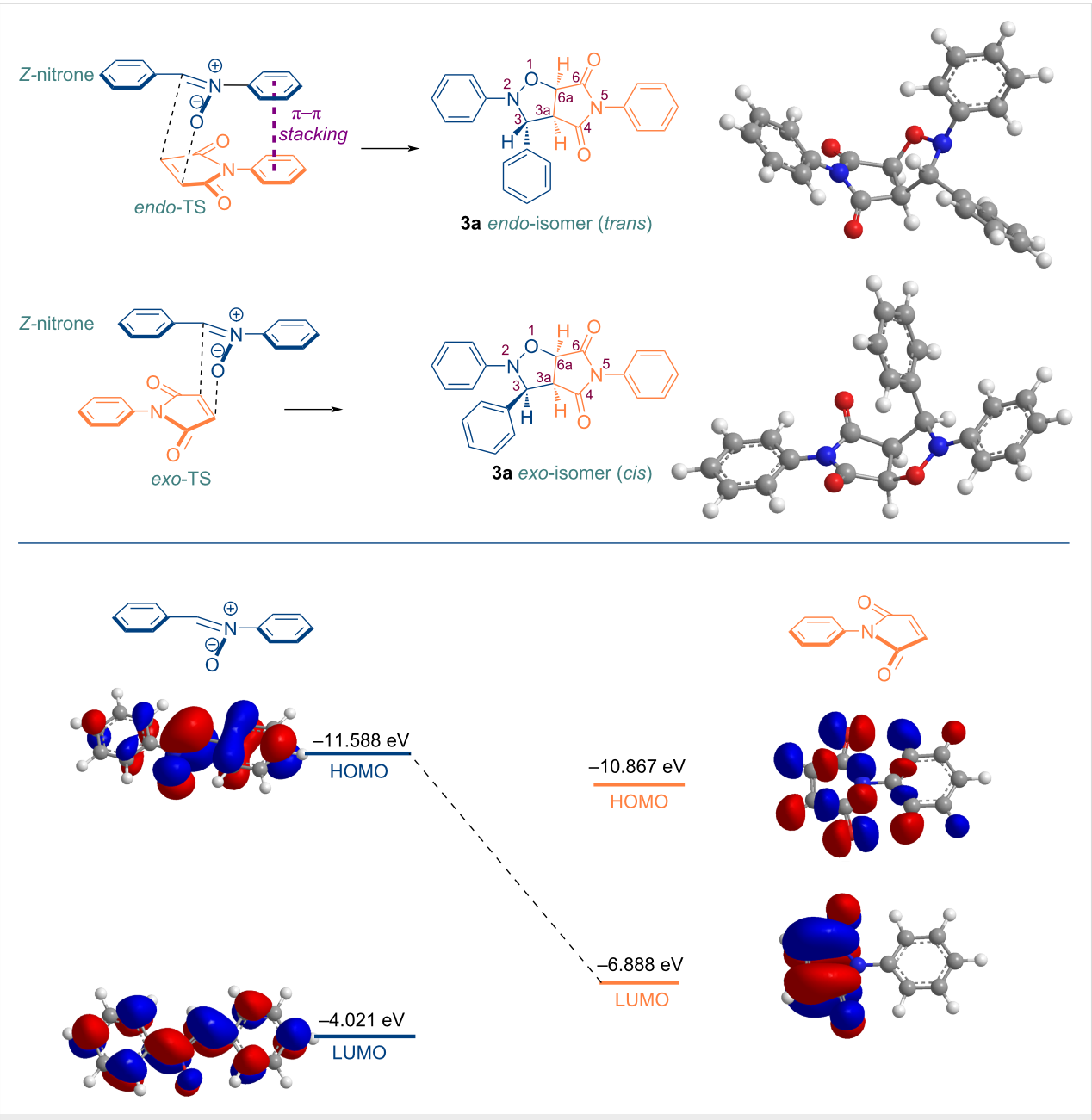
Table 3: The physicochemical parameters, toxicities, and yields of **3a** obtained in the used solvents.

Solvent	Vapour pressure (kPa)[a]	Boiling point (°C)[a]	Flash point (°C)[a]	Hazard statement	Dipol moment (D)[b]	Atom economy (ref. [104]) (%)[c]	Biodegradability[d]	Yield of **3a** (%)[e]
benzene	101.33	80	–12	highly flammable	0.00	–	non readily	54
toluene	38.87	111	4.4	highly flammable	0.27	–	non readily	84
chloroform	190.00	61	9.7	non flammable	1.35	–	non readily	74
THF	134.90	65	–21	highly flammable	1.71	80	readily	21
dioxane	64.54	101	12	highly flammable	0.45	–	readily	16
EtOAc	111.76	77	–4	highly flammable	1.89	96	readily	26
sulfolane	0.04	287	176	non flammable	4.50	–	readily	37
MeCN	96.34	82	5.56	highly flammable	3.22	–	readily	42
DMF	9.90	153	58	flammable	3.57	–	non readily	14
DMSO	2.00	189	87	non flammable	4.22	72	readily	34
EtOH	108.42	78	12	highly flammable	1.59	51	non readily	68
MeOH	182.61	64	12	highly flammable	1.54	100	non readily	34
water	47.37	100	–	non flammable	1.77	–	non readily	51
methyl oleate	0.0005	351	180	non flammable	1.74	–	readily	88
oleic acid	0.08	360	189	non flammable	1.69	–	readily	87
methyl laurate	0.06	262	134	non flammable	1.64	88	readily	100

[a]Values retrieved from the *Chemeo* molecular database (vapour pressure at 80 °C). [b]Values calculated with Gaussian. [c]Calculated value for the production of solvent. [d]The relevant results were obtained with *ChemFREE* web platform. [e]Yield obtained at the end of 10 minutes reaction time.

present in the nitrone structure, results in elevated *cis* or *trans* diastereoselectivity [85,111]. Furthermore, the [3 + 2] cycloaddition reactions of nitrones with electron-poor dipolarophiles, such as *N*-phenylmaleimide, is controlled by the HOMO FMO of the nitrone. Consequently, it can be deduced that $HOMO_{nitrone}$–$LUMO_{N\text{-phenylmaleimide}}$ interactions will be more pronounced in a non-polar methyl laurate environment (Scheme 2) [118].

In contrast, a limited number of studies have documented the occurrence of analogous cycloaddition reactions in water [62,108,113-121]. However, it should be noted that the isolation procedures employed in these studies to obtain the product from the aqueous reaction medium are time-consuming and inefficient. In this study, when water was used as a solvent, a similar problem was encountered to the one mentioned below, and the yield of the product was significantly reduced. The compounds employed in these studies are typically devoid of elongated hydrocarbon chains and in certain instances, bis-nitrone compounds have been employed as 1,3-dipoles. Furthermore, the reactions are known to be completed within approximately 3–4 or 20–32 hours at ambient temperature. Argyropoulou et al., obtained the cycloadduct products in relatively low yields (69%) from the reaction of hydrophobic nitrones with methyl acrylate over a 24-hour period in an aqueous suspension medium, in which hydrophobic effects are also involved [122]. In a further study conducted within an aqueous environment, it was possible to obtain the associated products resulting from the cycloaddition reactions of non-hydrophobic nitrones with ethyl cinnamate derivatives. These products were achieved with a yield of 78–85% within 12 hours, operating at 100 °C under conditions catalyzed by γ-cyclodextrin [123]. An attempt was



Scheme 2: *Endo* and *exo* stereoisomeric approaches of nitrone **1a** and maleimide **2a** in [3 + 2] cycloaddition reaction.

made to synthesize compound **3a** in water under the reaction conditions specified in Table 1, entry 10. TLC analysis after 10 minutes revealed the presence of the starting nitrone in the reaction medium. The isolation of the product was achieved through extraction with EtOAc, followed by drying over anhydrous Na_2SO_4. The solvent was then evaporated, and the residue was triturated with hexane to precipitate the targeted product. However, at this stage, the product became excessively adhesive to the walls of the reaction vessel, thereby making it difficult to precipitate. Following the completion of these steps, the desired addition product was obtained in a yield of 51%. In the event of water being utilized as the solvent, the primary factor contributing to the low reaction yield over the specified timeframe is the low solubility of both reactants in water. Furthermore, it is acknowledged that the well-documented hydrogen bonding and hydrophobic effects do not exert a favorable influence on the reaction. This result suggests that methyl laurate may be a superior green solvent candidate for such reactions compared to water. Furthermore, it is evident that the initial compounds with a high degree of hydrophobic character may result in significant solubility issues within an aqueous environment.

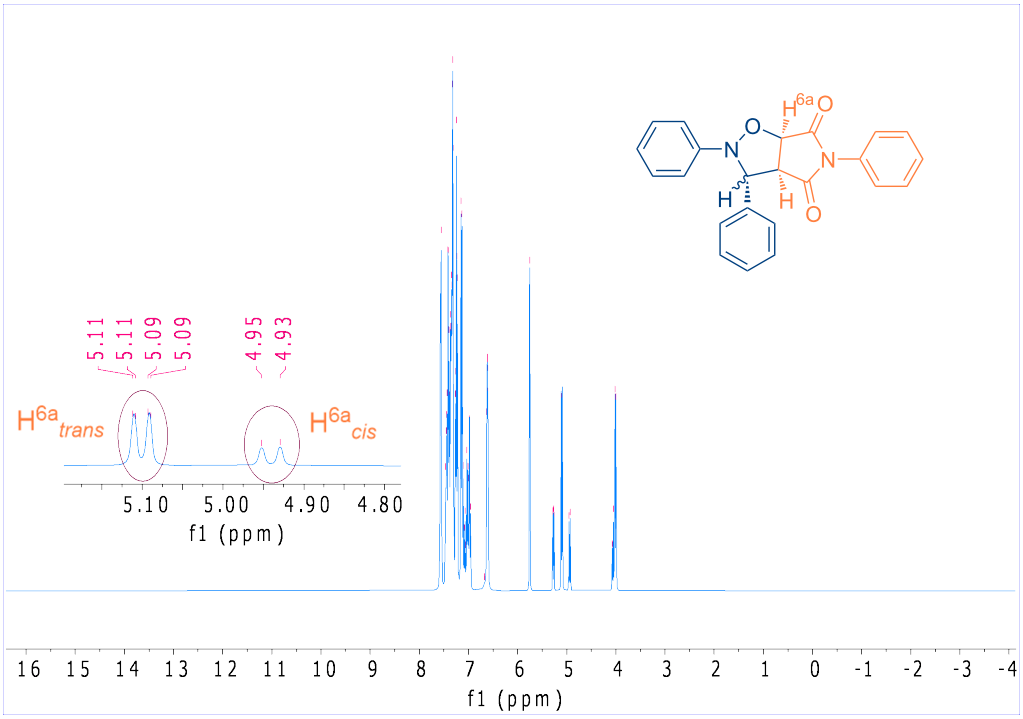


Figure 10: Signals of protons used in the calculation of the diastereomeric ratios (*cis*/*trans*) of cycloaddition products **3a–u**.

A series of studies were conducted with the objective of recovering and reusing the solvents utilized in the reaction and product isolation (Figure 11). To this end, a specific volume of hexane was introduced into the medium at the conclusion of the reaction, after which the product was precipitated and filtered under vacuum. The residue was then subjected to a subsequent wash with a volume of hexane, and the filtrate was transferred into a flask and concentrated at 45 °C using a rotary evaporator. The experimental conditions were such that 55% of the hexane was recovered, along with 99% of the methyl laurate. The methyl laurate that was recovered was then used as the reaction medium on four more occasions. The following report summa-

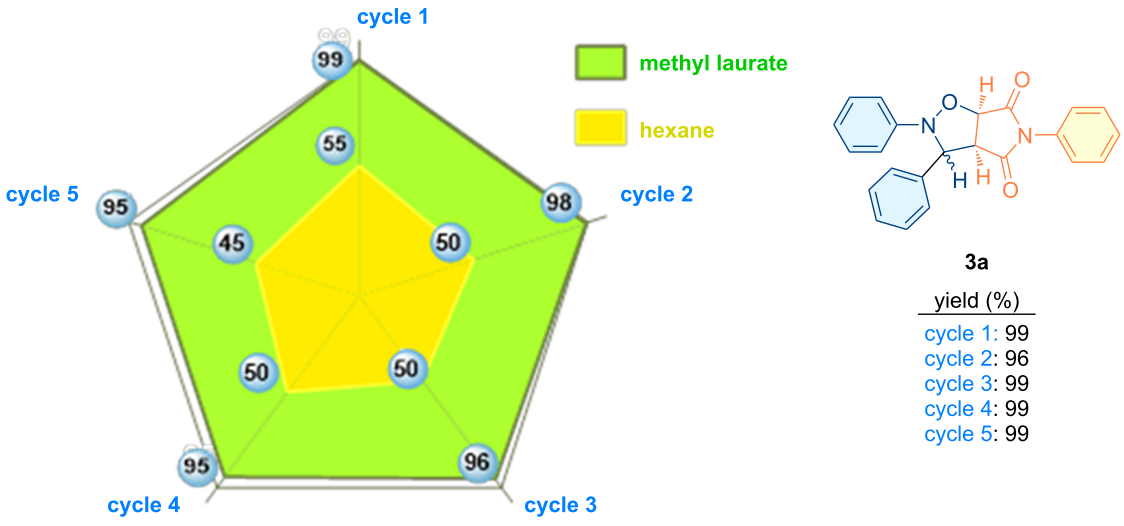


Figure 11: Results of studies on the recovery of solvents used in the reaction.

rizes the findings of studies conducted on the recovery of solvents utilized in the aforementioned reaction (Figure 11). In addition, the completion of the cycloaddition reaction can be readily monitored through the utilization of Fourier-transform infrared (FTIR) spectroscopy and/or thin-layer chromatography (TLC) analysis (Figure 12). In order to verify the purity of the recovered methyl laurate at the conclusion of the reaction, a number of chromatographic (TLC), spectroscopic (FTIR) and GC–MS analyses were performed (Figures S2, S3, and S4 in Supporting Information File 1). Although a trace amount of impurity was observed on the TLC plate, the FTIR spectrum of the methyl laurate recovered after the reaction revealed that it had almost the same purity level as the methyl laurate before the reaction. This degree of purity is also clearly confirmed by the GC–MS spectrum of the recovered methyl laurate. However, if desired, the methyl laurate can be readily purified by vacuum distillation at the end of the reaction and safely reused.

The synthesis of the corresponding cycloaddition products **3a**–**u** was achieved by heating equimolar amounts of nitrone and maleimide in methyl laurate at 80 °C for the times indicated in Table 4. The corresponding products were readily isolated as a mixture of diastereoisomers by precipitation from the reaction medium with the addition of solvents such as hexane, octane or a diethyl ether/hexane mixture. As Welton asserts, the environmental friendliness of a chemical process is contingent upon the properties of the solvent, which must facilitate practical isolation of the product at the end of the process [124].

As previously stated, the process of following the cycloaddition reactions within the scope of this study by means of FTIR spectroscopy is a relatively simple and practical task. The data obtained from the FTIR monitoring of the cycloaddition reaction between *C*,*N*-diphenylnitrone (**1a**) and *N*-phenylmaleimide (**2a**) carried out as a model reaction are given in Figure 13. As illustrated in Figure 13a, the superimposed spectra of *C*,*N*-diphenylnitrone and *N*-phenylmaleimide are presented. Figure 13b shows the spectrum of methyl laurate, which was utilized as a solvent. Figure 13c presents the spectrum of the reaction mixture, collected from the reaction medium after one hour had elapsed since the beginning of the reaction. Figure 13d shows the spectrum of the initial reaction mixture and the mixture collected from the reaction medium after five minutes. Figure 13e presents the spectrum of the isolated product **3a**. As demonstrated in Figure 13c and 13d, the signal attributed to the C=N stretching of starting nitrone **1a**, observed at 1548 cm^{-1}, disappears. This finding suggests that the nitrone is fully consumed by the end of the five-minute reaction period.

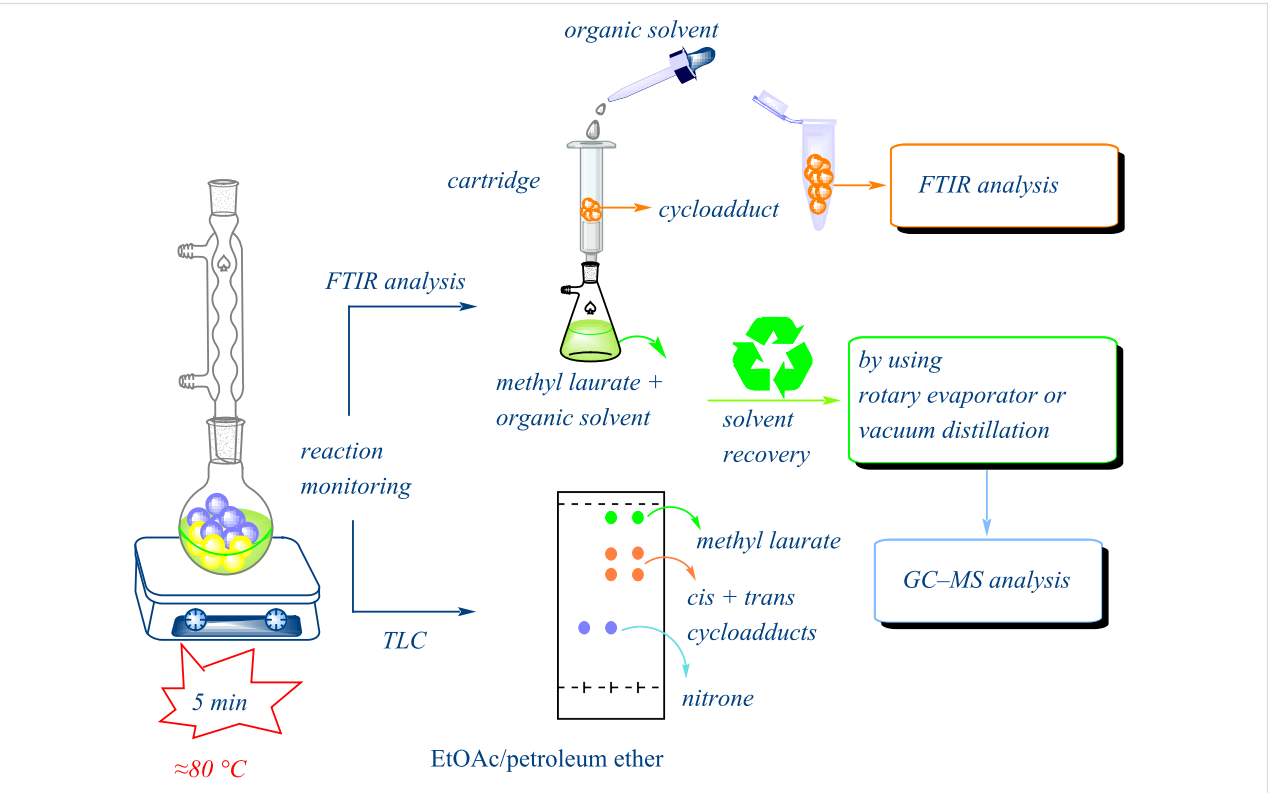


Figure 12: Simplified scheme describing the reaction monitoring and solvent recovery.

Table 4: Synthesized pyrrolo[3,4-*d*]isoxazolidines **3a–u** (*cis* + *trans* isomers).

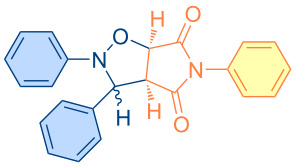
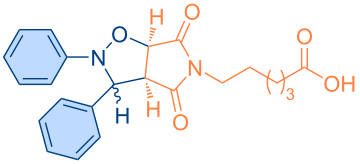
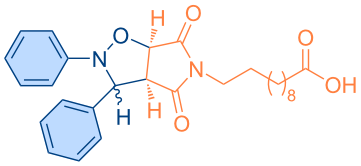
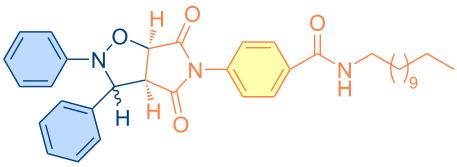
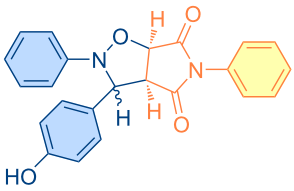
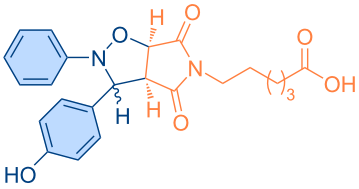
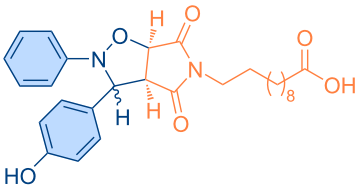
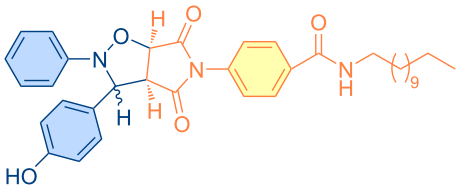
Compound	Structure	Time (min)	*cis*/*trans* ratio	Yield (%)[a]
3a		5	28:72	100
3b		10	29:71	100
3c		10	29:71	100
3d		10	29:71	100
3e		60	47:53	90
3f		60	9:91	86
3g		60	37:63	100
3h		40	33:67	89

Table 4: Synthesized pyrrolo[3,4-*d*]isoxazolidines **3a–u** (*cis* + *trans* isomers). (continued)

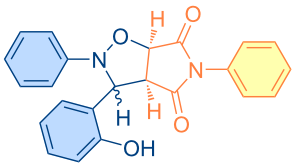
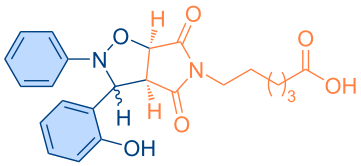
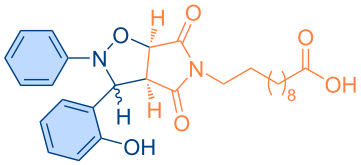
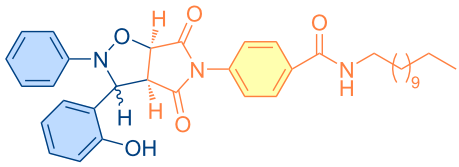
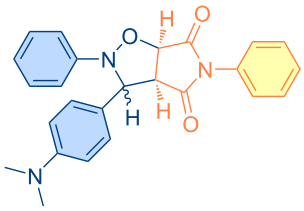
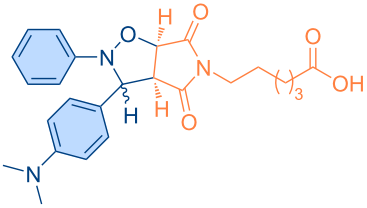
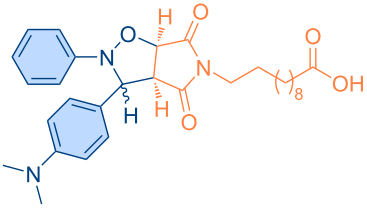
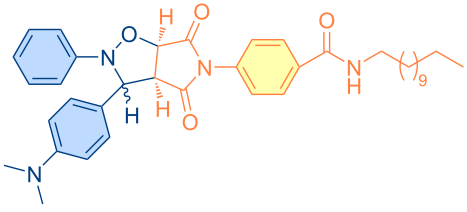
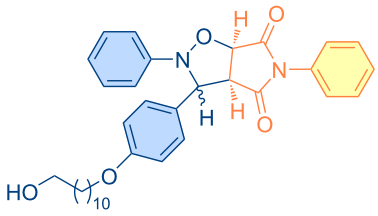
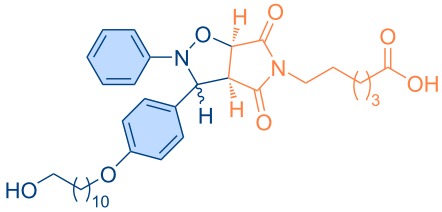
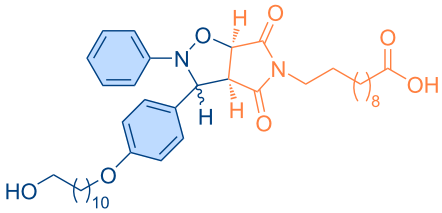
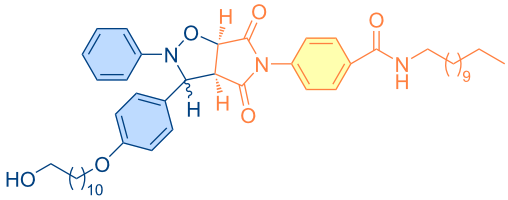
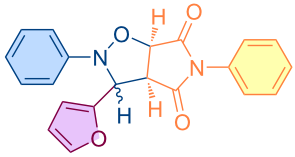
3i		60	34:66	83
3j		80	16:84	86
3k		80	20:80	89
3l		80	33:67	92
3m		20	40:60	94
3n		30	43:57	100
3o		10	31:69	88
3p		30	29:71	89

Table 4: Synthesized pyrrolo[3,4-*d*]isoxazolidines **3a–u** (*cis* + *trans* isomers). (continued)

3q		20	40:60	96
3r		10	42:58	96
3s		10	37:63	100
3t		10	44:56	97
3u		60	33:67	99

[a]Isolated yields.

In academic and industrial communities alike, there is a high level of interest in catalytic methods of *Green Chemistry* that allow stereoselective transformations [125-128]. It is imperative to develop stereoselective synthetic methods for cycloaddition reactions. In this study, a series of natural organic compounds from diverse classes and an acetonide [129] derivative were selected for investigation, with a focus on their potential catalytic effects in relation to the alteration of *cis/trans* product distribution under optimized [3 + 2] cycloaddition conditions. The primary strategy for the selection of these compounds as catalysts is predicated on their capacity to function as H-bond acceptors and/or H-bond donors. As has been documented in previous research, imine-based templates or [2]rotaxane that possess an amide functionality have been observed to exhibit notable *trans* diastereoselectivity in the context of cycloaddition reactions [130-135]. For this purpose, equivalent amounts of nitrone **1a** and maleimide **2a** were reacted with 5 mol % catalyst (Table 5) under the cycloaddition conditions determined in Table 1, entry 9. As illustrated in Table 5, the product yields obtained from the reactions are presented alongside the observed *cis/trans* diastereoisomer ratios in the presence of the respective catalysts. However, upon examination of the ^{1}H NMR spectra of compound **3a** synthesized in the presence of the relevant catalysts, it was found that these catalyst molecules had no significant effect on the *cis/trans* diastereoisomer distribution.

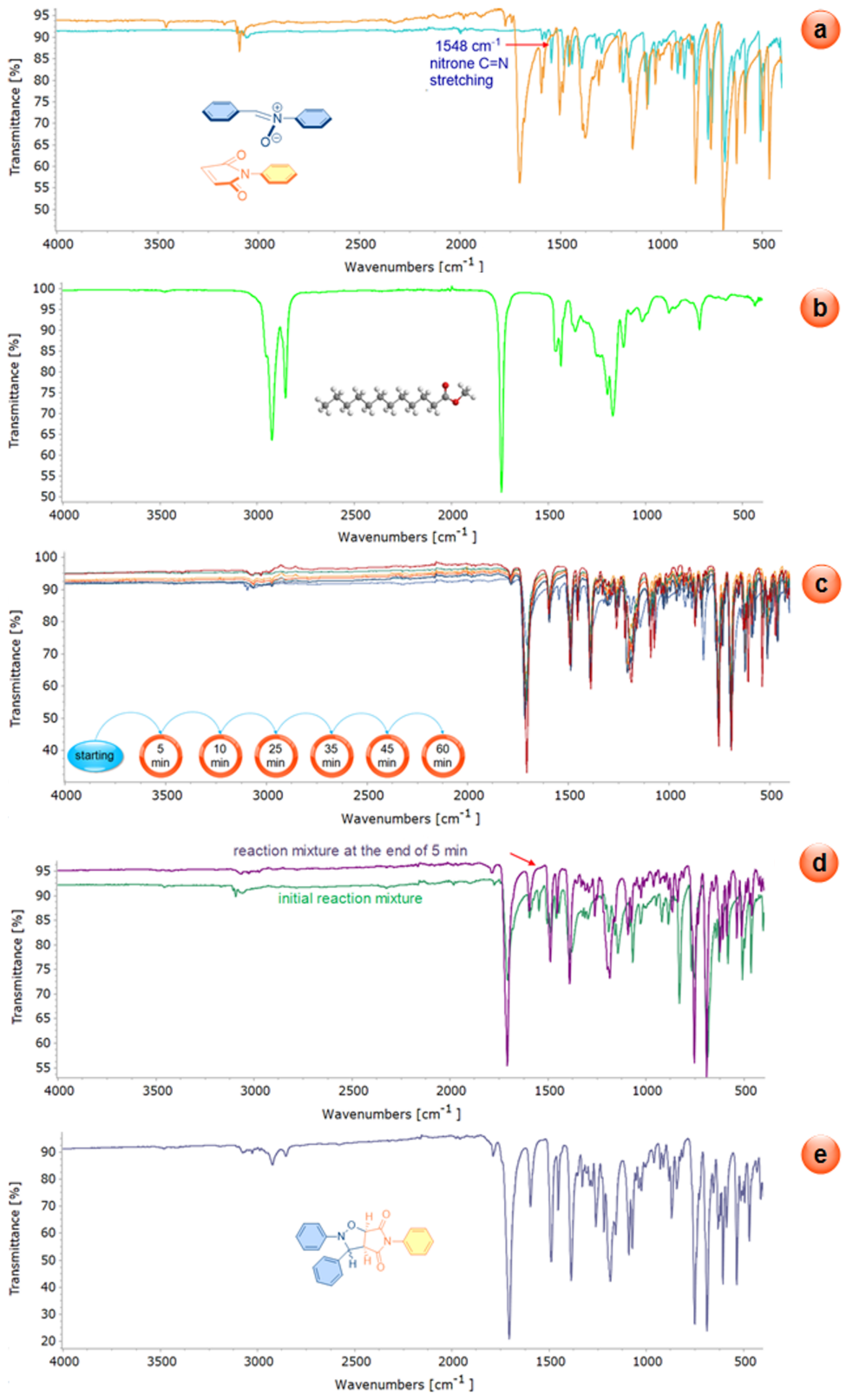
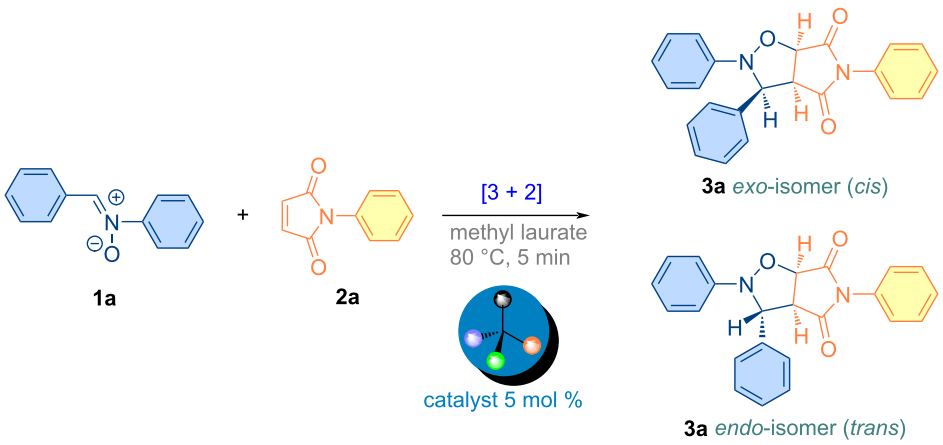


Figure 13: a) The superimposed spectra of *C*,*N*-diphenylnitrone and *N*-phenylmaleimide. b) The spectrum of methyl laurate. c) The spectrum of the reaction mixture, collected from the reaction medium after one hour had elapsed since the beginning of the reaction. d) The spectrum of the initial reaction mixture and the mixture collected from the reaction medium after five minutes. e) The spectrum of the isolated product **3a**.

Table 5: Catalyst survey for the synthesis of **3a** (*cis* + *trans* isomers).



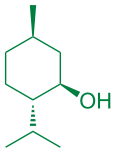
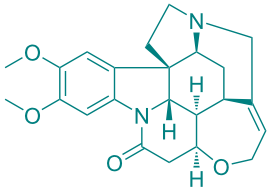
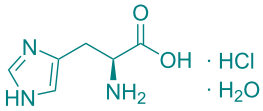
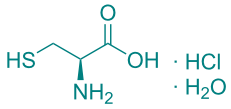
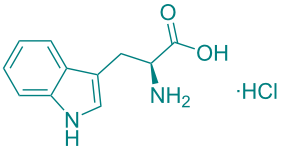
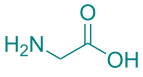
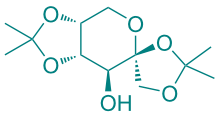
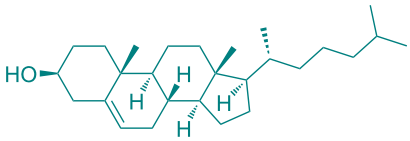
Entry	Catalyst (5 mol %)	*cis*/*trans* ratio	Yield (%)[a]
1	*without catalyst*	28:72	100
2	 DL-menthol	29:71	96
3	 brucine	28:72	92
4	 L-histidine hydrochloride monohydrate	30:70	94
5	 L-cysteine hydrochloride monohydrate	29:71	96
6	 L-tryptophan methyl ester hydrochloride	25:75	93
7	 glycine	31:69	94

Table 5: Catalyst survey for the synthesis of **3a** (*cis* + *trans* isomers). (continued)

8	 DL-camphor	31:69	99
9	 1,2;4,5-di-*O*-isopropylidene-β-D-fructopyranose	31:69	92
10	 cholesterol	31:69	92

[a]Isolated yields.

Conclusion

In conclusion, the present study reveals that methyl laurate is an excellent biocompatible solvent candidate for [3 + 2] cycloaddition reactions between nitrones and *N*-aryl-substituted maleimides. Methyl laurate meets most of the criteria for a readily available green solvent compared to the other 15 potential solvents compared. It is demonstrated that the toxicity prediction tools employed in the present study also indicate that methyl laurate is a more appropriate and eco-friendly solvent. Furthermore, a multitude of alternative vegetable oils could also be considered as green reaction media for such reactions. The pyrrolo-isoxazolidines targeted for synthesis in this *Green Chemistry* methodology were obtained as *cis/trans* diastereoisomer pairs in short reaction times and in very good yields. Despite the acknowledged fact that cycloaddition reactions remain unaffected by the solvent, this study demonstrates that the solvent can exert a substantial influence on the diastereomeric product distribution in such organic transformations. A series of studies were conducted on natural compounds selected for use as catalysts within the scope of this work. These studies revealed that there was no significant alteration to the ratio of diastereoisomers when the respective catalysts were utilized. In summary, methyl laurate is a solvent that has attracted attention as a potential alternative to conventional organic solvents on account of its environmentally friendly properties. The material is biodegradable, non-toxic and derived from renewable resources, thus making it a sustainable choice for a variety of applications. The primary benefit of this solvent lies in its reduced volatility and toxicity, characteristics that surpass many of the organic solvents evaluated in this study. Consequently, it presents itself as a promising reaction medium for [3 + 2] cycloaddition reactions, a process that conventional solvents may hinder due to their potential environmental or health implications.

Experimental

All reagents and solvents were purchased from Merck (Merck, Darmstadt, Germany), Sigma-Aldrich (St. Louis, MO), or Acros Organics (Thermo Fisher Scientific, Geel, Belgium) and used without further purification. Thin-layer chromatography was performed using silica gel (60 F_{254}, Merck, Darmstadt, Germany) plates. Melting points were recorded using a Büchi melting point B-540 apparatus (Büchi Labortechnik AG in Flawil, Switzerland). The IR spectra were measured by Spectrum Two FT-IR spectrometer (PerkinElmer, Massachusetts, USA). The NMR spectra were measured using Bruker ultrashield plus biospin 400 MHz NMR spectrometer and chloroform-*d* ($CDCl_3$) or hexadeuterodimethyl sulfoxide (DMSO-d_6) as a solvent. Chemical shifts (δ) are reported in ppm and *J* values in hertz. The elemental analyses were performed using a Leco CHNS-932 elemental analyzer (Saint Joseph, MI, USA). An Agilent 7890A gas chromatograph coupled with a 5975C mass spectrometer was used to analyze recovered methyl laurate. Chromatographic analysis of the methyl laurate dissolved in MeOH was performed in an HP-5MS fused silica capillary column (0.25 µm, 0.25 mm × 30 m). Helium

(99.999%) was used as carrier gas with a constant flow rate of 1.0 mL min^{-1}.

Representative procedure for cycloaddition reactions

To a 50 mL single-necked flask, (0.1 g, 0.51 mmol) of *C*,*N*-diphenylnitrone, (0.09 g, 0.52 mmol) of *N*-phenylmaleimide and 1 mL of methyl laurate were added. The flask was attached to a reflux cooler and heated in an oil bath with stirring for a period of five minutes, until the internal temperature reached 80 °C. The reaction mixture rapidly precipitates to form a white solid product. The results of the FTIR and TLC analysis indicate that the starting compounds have been completely consumed. Subsequently, the reaction mixture was cooled to room temperature and hexane was added with rapid stirring, allowing the cycloaddition product to precipitate as a mixture of *cis* and *trans* diastereoisomers in the form of a white solid. The precipitate was then washed with a small quantity of hexane and dried in open air. The resulting mixture of isomers was subjected to direct NMR analysis, without any additional purification or separation steps.

Supporting Information

Supporting Information File 1

Characterization data, copies of NMR spectra, additional Table and Figures.
[https://www.beilstein-journals.org/bjoc/content/supplementary/1860-5397-21-184-S1.pdf]

Funding

We gratefully acknowledge the Bursa Uludağ University Scientific Research Projects Unit for the financial support provided under project number (FHIZ-2024-2009).

Author Contributions

Ayhan Yıldırım: conceptualization; formal analysis; investigation; methodology; resources; supervision; validation; visualization; writing – original draft; writing – review & editing. Mustafa Göker: formal analysis; investigation.

ORCID® iDs

Ayhan Yıldırım - https://orcid.org/0000-0002-2328-9754
Mustafa Göker - https://orcid.org/0000-0003-4667-1670

Data Availability Statement

All data that supports the findings of this study is available in the published article and/or the supporting information of this article.

References

1. Ikeda, M. *Toxicol. Lett.* **1992,** *64–65,* 191–201. doi:10.1016/0378-4274(92)90189-q
2. Mckee, R. H.; Adenuga, M. D.; Carrillo, J.-C. *Crit. Rev. Toxicol.* **2015,** *45,* 273–365. doi:10.3109/10408444.2015.1016216
3. Cvjetko Bubalo, M.; Vidović, S.; Radojčić Redovniković, I.; Jokić, S. *J. Chem. Technol. Biotechnol.* **2015,** *90,* 1631–1639. doi:10.1002/jctb.4668
4. de Jesus, S. S.; Filho, R. M. *Renewable Sustainable Energy Rev.* **2020,** *133,* 110289. doi:10.1016/j.rser.2020.110289
5. Calvo-Flores, F. G.; Monteagudo-Arrebola, M. J.; Dobado, J. A.; Isac-García, J. *Top. Curr. Chem.* **2018,** *376,* 18. doi:10.1007/s41061-018-0191-6
6. Choi, Y. H.; Verpoorte, R. *Curr. Opin. Food Sci.* **2019,** *26,* 87–93. doi:10.1016/j.cofs.2019.04.003
7. Kumar, S. P. J.; Prasad, S. R.; Banerjee, R.; Agarwal, D. K.; Kulkarni, K. S.; Ramesh, K. V. *Chem. Cent. J.* **2017,** *11,* 9. doi:10.1186/s13065-017-0238-8
8. Janicka, P.; Płotka-Wasylka, J.; Jatkowska, N.; Chabowska, A.; Fares, M. Y.; Andruch, V.; Kaykhaii, M.; Gębicki, J. *Curr. Opin. Green Sustainable Chem.* **2022,** *37,* 100670. doi:10.1016/j.cogsc.2022.100670
9. Tzanova, M. T.; Yaneva, Z.; Ivanova, D.; Toneva, M.; Grozeva, N.; Memdueva, N. *Foods* **2024,** *13,* 605. doi:10.3390/foods13040605
10. Almohasin, J. A.; Balag, J.; Miral, V. G.; Moreno, R. V.; Tongco, L. J.; Lopez, E. C. R. *Eng. Proc.* **2023,** *56,* 174. doi:10.3390/asec2023-16278
11. Alahmad, W.; Kaya, S. I.; Cetinkaya, A.; Varanusupakul, P.; Ozkan, S. A. *Adv. Sample Prep.* **2023,** *5,* 100053. doi:10.1016/j.sampre.2023.100053
12. Cannavacciuolo, C.; Pagliari, S.; Frigerio, J.; Giustra, C. M.; Labra, M.; Campone, L. *Foods* **2023,** *12,* 56. doi:10.3390/foods12010056
13. Kar, S.; Sanderson, H.; Roy, K.; Benfenati, E.; Leszczynski, J. *Chem. Rev.* **2022,** *122,* 3637–3710. doi:10.1021/acs.chemrev.1c00631
14. Huang, C.; Chen, X.; Wei, C.; Wang, H.; Gao, H. *Front. Pharmacol.* **2021,** *12,* 794939. doi:10.3389/fphar.2021.794939
15. Huang, W.; Wu, X.; Qi, J.; Zhu, Q.; Wu, W.; Lu, Y.; Chen, Z. *Drug Discovery Today* **2020,** *25,* 901–908. doi:10.1016/j.drudis.2019.09.018
16. Sheldon, R. A. *Green Chem.* **2005,** *7,* 267–278. doi:10.1039/b418069k
17. Sheldon, R. A. *Curr. Opin. Green Sustainable Chem.* **2019,** *18,* 13–19. doi:10.1016/j.cogsc.2018.11.006
18. Clarke, C. J.; Tu, W.-C.; Levers, O.; Bröhl, A.; Hallett, J. P. *Chem. Rev.* **2018,** *118,* 747–800. doi:10.1021/acs.chemrev.7b00571
19. Yıldırım, A. *Beilstein J. Org. Chem.* **2024,** *20,* 1308–1319. doi:10.3762/bjoc.20.114
20. Škulcová, A.; Majová, V.; Dubaj, T.; Jablonský, M. *J. Mol. Liq.* **2019,** *287,* 110991. doi:10.1016/j.molliq.2019.110991
21. Zhou, J.; Sui, H.; Jia, Z.; Yang, Z.; He, L.; Li, X. *RSC Adv.* **2018,** *8,* 32832–32864. doi:10.1039/c8ra06384b
22. Mai, N. L.; Ahn, K.; Koo, Y.-M. *Process Biochem. (Oxford, U. K.)* **2014,** *49,* 872–881. doi:10.1016/j.procbio.2014.01.016
23. Vidal, C.; García-Álvarez, J. *Green Chem.* **2014,** *16,* 3515–3521. doi:10.1039/c4gc00451e
24. Smith, L. I. *Chem. Rev.* **1938,** *23,* 193–285. doi:10.1021/cr60075a001
25. Huisgen, R. *Angew. Chem., Int. Ed. Engl.* **1963,** *2,* 565–598. doi:10.1002/anie.196305651

26. Kaur, A.; Singh, B.; Jaggi, A. S. *Bioorg. Med. Chem. Lett.* **2013,** *23,* 797–801. doi:10.1016/j.bmcl.2012.11.080
27. Chatterjee, A.; Hota, S. K.; Banerjee, M.; Bhattacharya, P. K. *Tetrahedron Lett.* **2010,** *51,* 6700–6703. doi:10.1016/j.tetlet.2010.09.111
28. Badru, R.; Anand, P.; Singh, B. *Eur. J. Med. Chem.* **2012,** *48,* 81–91. doi:10.1016/j.ejmech.2011.11.037
29. Ni, M.; Xu, S.; Liu, Z.; Xue, Y.; Xie, W.; Yang, S.; Liu, L.; Bao, X. *BioMed Res. Int.* **2021,** 8889247. doi:10.1155/2021/8889247
30. Chiacchio, M. A.; Giofrè, S. V.; Romeo, R.; Romeo, G.; Chiacchio, U. *Curr. Org. Synth.* **2016,** *13,* 726–749. doi:10.2174/1570179412666150914195807
31. Singh, G.; Kaur, A.; Sharma, V.; Suri, N.; Sharma, P. R.; Saxena, A. K.; Ishar, M. P. S. *Med. Chem. Commun.* **2013,** *4,* 972–978. doi:10.1039/c3md00055a
32. Ghannay, S.; Kadri, A.; Aouadi, K. *Monatsh. Chem.* **2020,** *151,* 267–280. doi:10.1007/s00706-020-02550-4
33. Adhreai, A. A. L.; ALSaeedy, M.; Farooqui, M.; Alrabie, A.; Al-Qadsy, I.; Al-Timari, U. *J. Mol. Struct.* **2022,** *1256,* 132481. doi:10.1016/j.molstruc.2022.132481
34. Mellaoui, M. D.; Zaki, K.; Abbiche, K.; Imjjad, A.; Boutiddar, R.; Sbai, A.; Jmiai, A.; El Issami, S.; Al Lamsabhi, M.; Zejli, H. *J. Mol. Struct.* **2024,** *1308,* 138330. doi:10.1016/j.molstruc.2024.138330
35. Ghannay, S.; Bakari, S.; Ghabi, A.; Kadri, A.; Msaddek, M.; Aouadi, K. *Bioorg. Med. Chem. Lett.* **2017,** *27,* 2302–2307. doi:10.1016/j.bmcl.2017.04.044
36. Thakur, S.; Das, A.; Das, T. *New J. Chem.* **2021,** *45,* 11420–11456. doi:10.1039/d1nj02023d
37. Carruthers, W.; Coggins, P.; Weston, J. B. *J. Chem. Soc., Perkin Trans. 1* **1991,** 611–616. doi:10.1039/p19910000611
38. Sheng, C. C.; Nian, L. Z.; Yan, S. J.; Tao, L.; Yan, Z. B. *Chin. J. Org. Chem.* **2005,** *25,* 1392–1397.
39. Tufariello, J. J.; Asrof Ali, S. *J. Am. Chem. Soc.* **1979,** *101,* 7114–7116. doi:10.1021/ja00517a078
40. Werner, K. M.; de los Santos, J. M.; Weinreb, S. M.; Shang, M. *J. Org. Chem.* **1999,** *64,* 4865–4873. doi:10.1021/jo990266s
41. Lin, S.-T.; Wang, C.-H.; Chen, A.-L.; Wang, T.-S. A. *Chem. – Eur. J.* **2025,** *31,* e202403184. doi:10.1002/chem.202403184
42. Dondoni, A.; Franco, S.; Junquera, F.; Merchán, F. L.; Merino, P.; Tejero, T. *J. Org. Chem.* **1997,** *62,* 5497–5507. doi:10.1021/jo9702913
43. Merino, P.; Franco, S.; Merchan, F. L.; Tejero, T. *Tetrahedron Lett.* **1998,** *39,* 6411–6414. doi:10.1016/s0040-4039(98)01323-9
44. Merino, P.; Franco, S.; Merchan, F. L.; Tejero, T. *J. Org. Chem.* **2000,** *65,* 5575–5589. doi:10.1021/jo0002689
45. Kametani, T.; Nagahara, T.; Honda, T. *J. Org. Chem.* **1985,** *50,* 2327–2331. doi:10.1021/jo00213a025
46. Kametani, T.; Chu, S.-D.; Honda, T. *J. Chem. Soc., Perkin Trans. 1* **1988,** 1593–1597. doi:10.1039/p19880001593
47. Kasahara, K.; Iida, H.; Kibayashi, C. *J. Org. Chem.* **1989,** *54,* 2225–2233. doi:10.1021/jo00270a037
48. DeShong, P.; Dicken, C. M.; Leginus, J. M.; Whittle, R. R. *J. Am. Chem. Soc.* **1984,** *106,* 5598–5602. doi:10.1021/ja00331a033
49. Hoogenboom, J.; Zuilhof, H.; Wennekes, T. *Org. Lett.* **2015,** *17,* 5550–5553. doi:10.1021/acs.orglett.5b02662
50. Brandi, A.; Cardona, F.; Cicchi, S.; Cordero, F. M.; Goti, A. *Chem. – Eur. J.* **2009,** *15,* 7808–7821. doi:10.1002/chem.200900707
51. Zhong, J.; He, H.; Gao, S. *Org. Chem. Front.* **2019,** *6,* 3781–3785. doi:10.1039/c9qo01111k
52. Berthet, M.; Cheviet, T.; Dujardin, G.; Parrot, I.; Martinez, J. *Chem. Rev.* **2016,** *116,* 15235–15283. doi:10.1021/acs.chemrev.6b00543
53. Said, A. I.; El-Emary, T. I. *RSC Adv.* **2020,** *10,* 845–850. doi:10.1039/c9ra10039c
54. Vretik, L.; Ritter, H. *Macromolecules* **2003,** *36,* 6340–6345. doi:10.1021/ma0215565
55. Yusuf, M.; Singh, B. *Asian J. Chem.* **2019,** *31,* 220–228. doi:10.14233/ajchem.2019.21726
56. Guo, S.; Zhang, Z.; Wei, Z.; Zhu, Y.; Fan, X. *J. Org. Chem.* **2023,** *88,* 3845–3858. doi:10.1021/acs.joc.3c00117
57. Badru, R.; Shah, S.; Singh, B. *J. Heterocycl. Chem.* **2012,** *49,* 336–341. doi:10.1002/jhet.794
58. Anand, P.; Singh, B. *Bioorg. Med. Chem.* **2012,** *20,* 521–530. doi:10.1016/j.bmc.2011.05.027
59. Shah, S.; Badru, R.; Singh, B. *Synth. Commun.* **2013,** *43,* 1073–1082. doi:10.1080/00397911.2011.622063
60. Black, D. S. C.; Crozier, R. F.; Davis, V. C. *Synthesis* **1975,** 205–221. doi:10.1055/s-1975-23713
61. Gholami, M. R.; Yangjeh, A. H. *J. Chem. Res., Synop.* **1999,** 226–227. doi:10.1039/a809251f
62. Chakraborty, B.; Sharma, P. K. *Rasayan J. Chem.* **2010,** *3,* 454–460.
63. Molchanov, A. P.; Lukina, V. M.; Efremova, M. M.; Muryleva, A. A.; Slita, A. V.; Zarubaev, V. V. *Synth. Commun.* **2020,** *50,* 1367–1374. doi:10.1080/00397911.2020.1738494
64. Zhang, Y.; Wang, Q.; Long, Z.; Zuo, Y.; Liu, L.; Yan, L. *J. Org. Chem.* **2024,** *89,* 10327–10332. doi:10.1021/acs.joc.4c00744
65. Qiu, S.; Cao, T.; Zhu, S. *Org. Biomol. Chem.* **2021,** *19,* 3139–3143. doi:10.1039/d1ob00421b
66. Purkait, A.; Pal, S. V. S.; Soni, K.; Bhattacharyya, K.; Jana, C. K. *Chem. Commun.* **2024,** *60,* 8541–8544. doi:10.1039/d4cc02117g
67. Chakraborty, B. *J. Heterocycl. Chem.* **2020,** *57,* 477–485. doi:10.1002/jhet.3804
68. Chakraborty, B. *J. Heterocycl. Chem.* **2019,** *56,* 3414–3422. doi:10.1002/jhet.3736
69. Martina, K.; Tagliapietra, S.; Veselov, V. V.; Cravotto, G. *Front. Chem. (Lausanne, Switz.)* **2019,** *7,* 95. doi:10.3389/fchem.2019.00095
70. Basavanna, V.; Puttappa, S.; Chandramouli, M.; Ningaiah, S. *Polycyclic Aromat. Compd.* **2023,** *43,* 9377–9398. doi:10.1080/10406638.2022.2162933
71. Gu, Y.; Jérôme, F. *Chem. Soc. Rev.* **2013,** *42,* 9550–9570. doi:10.1039/c3cs60241a
72. Dandia, A.; Jain, A. K.; Laxkar, A. K. *Tetrahedron Lett.* **2013,** *54,* 3929–3932. doi:10.1016/j.tetlet.2013.05.035
73. Kong, D.; Dolzhenko, A. V. *Sustainable Chem. Pharm.* **2022,** *25,* 100591. doi:10.1016/j.scp.2021.100591
74. Abd-Elmonem, M.; Mekheimer, R. A.; Hayallah, A. M.; Elsoud, F. A. A.; Sadek, K. U. *Curr. Org. Chem.* **2019,** *23,* 3226–3246. doi:10.2174/1385272823666191025150646
75. Diacon, A.; Călinescu, I.; Vinatoru, M.; Chipurici, P.; Vlaicu, A.; Boscornea, A. C.; Mason, T. J. *Molecules* **2021,** *26,* 4388. doi:10.3390/molecules26144388
76. Clark, J. H.; Farmer, T. J.; Hunt, A. J.; Sherwood, J. *Int. J. Mol. Sci.* **2015,** *16,* 17101–17159. doi:10.3390/ijms160817101
77. Cue, B. W.; Zhang, J. *Green Chem. Lett. Rev.* **2009,** *2,* 193–211. doi:10.1080/17518250903258150

78. Zaki, M.; Oukhrib, A.; Akssira, M.; Berteina-Raboin, S. *RSC Adv.* **2017,** *7,* 6523–6529. doi:10.1039/c6ra25869g
79. Kaur, M.; Singh, B.; Singh, B. *World J. Pharm. Pharm. Sci.* **2014,** *3,* 1299–1316.
80. Zhong, M.; Sun, S.; Cheng, J.; Shao, Y. *J. Org. Chem.* **2016,** *81,* 10825–10831. doi:10.1021/acs.joc.6b01910
81. Liard, A.; Nguyen, T.-H.; Djelloul Smir, A. I.; Vaultier, M.; Derdour, A.; Mortier, J. *Chem. – Eur. J.* **2003,** *9,* 1000–1007. doi:10.1002/chem.200390102
82. Nour El-Din, A. M. *Bull. Chem. Soc. Jpn.* **1986,** *59,* 1239–1243. doi:10.1246/bcsj.59.1239
83. Parisotto, S.; Boggio, P.; Prandi, C.; Venturello, P.; Deagostino, A. *Tetrahedron Lett.* **2015,** *56,* 5791–5794. doi:10.1016/j.tetlet.2015.08.087
84. Maiuolo, L.; De Nino, A.; Merino, P.; Russo, B.; Stabile, G.; Nardi, M.; D'Agostino, N.; Bernardi, T. *Arabian J. Chem.* **2016,** *9,* 25–31. doi:10.1016/j.arabjc.2015.01.015
85. Yıldırım, A.; Kaya, Y. *J. Phys. Org. Chem.* **2017,** *30,* e3629. doi:10.1002/poc.3629
86. Chen, D.; Liu, Y.; Liu, Y.; Zhao, K.; Zhang, T.; Gao, Y.; Wang, Q.; Song, B.; Hao, G. *Nucleic Acids Res.* **2024,** *52,* W450–W460. doi:10.1093/nar/gkae446
87. Fu, L.; Shi, S.; Yi, J.; Wang, N.; He, Y.; Wu, Z.; Peng, J.; Deng, Y.; Wang, W.; Wu, C.; Lyu, A.; Zeng, X.; Zhao, W.; Hou, T.; Cao, D. *Nucleic Acids Res.* **2024,** *52,* W422–W431. doi:10.1093/nar/gkae236
88. Banerjee, P.; Kemmler, E.; Dunkel, M.; Preissner, R. *Nucleic Acids Res.* **2024,** *52,* W513–W520. doi:10.1093/nar/gkae303
89. Byrne, F. P.; Jin, S.; Paggiola, G.; Petchey, T. H. M.; Clark, J. H.; Farmer, T. J.; Hunt, A. J.; McElroy, C. R.; Sherwood, J. *Sustainable Chem. Processes* **2016,** *4,* 7. doi:10.1186/s40508-016-0051-z
90. Khan, M. F.; Yu, L.; Achari, G. *Environ. Rev. (Ottawa, ON, Can.)* **2022,** *30,* 217–227. doi:10.1139/er-2021-0071
91. Tilstam, U. *Org. Process Res. Dev.* **2012,** *16,* 1273–1278. doi:10.1021/op300108w
92. Prat, D.; Wells, A.; Hayler, J.; Sneddon, H.; McElroy, C. R.; Abou-Shehada, S.; Dunn, P. J. *Green Chem.* **2016,** *18,* 288–296. doi:10.1039/c5gc01008j
93. Avram, S.; Funar-Timofei, S.; Borota, A.; Chennamaneni, S. R.; Manchala, A. K.; Muresan, S. *J. Cheminf.* **2014,** *6,* 42. doi:10.1186/s13321-014-0042-6
94. USDA, Agricultural Marketing Service. https://www.ams.usda.gov/sites/default/files/media/Methyl%20laurate.pdf (accessed April 20, 2025).
95. Larsen, C.; Lundberg, P.; Tang, S.; Ràfols-Ribé, J.; Sandström, A.; Lindh, E. M.; Wang, J.; Edman, L. *Nat. Commun.* **2021,** *12,* 4510. doi:10.1038/s41467-021-24761-x
96. Tinjacá, D. A.; Martinez, F.; Peña, M. A.; Jouyban, A.; Acree, W. E., Jr. *Liquids (Basel, Switz.)* **2023,** *3,* 469–480. doi:10.3390/liquids3040030
97. Hansen, C. *Hansen Solubility Parameters: A user's handbook,* 2nd ed.; CRC Press: Boca Raton, FL, USA, 2007.
98. Wojeicchowski, J. P.; Ferreira, A. M.; Okura, T.; Pinheiro Rolemberg, M.; Mafra, M. R.; Coutinho, J. A. P. *Ind. Eng. Chem. Res.* **2022,** *61,* 15631–15638. doi:10.1021/acs.iecr.2c01592
99. Ruwoldt, J.; Tanase-Opedal, M.; Syverud, K. *ACS Omega* **2022,** *7,* 46371–46383. doi:10.1021/acsomega.2c04982
100. De La Peña-Gil, A.; Toro-Vazquez, J. F.; Rogers, M. A. *Food Biophys.* **2016,** *11,* 283–291. doi:10.1007/s11483-016-9440-9
101. Nightingale, P. D.; Malin, G.; Liss, P. S. *Limnol. Oceanogr.* **1995,** *40,* 680–689. doi:10.4319/lo.1995.40.4.0680
102. Wijaya, Y. P.; Kristianto, I.; Lee, H.; Jae, J. *Fuel* **2016,** *182,* 588–596. doi:10.1016/j.fuel.2016.06.010
103. Lomba, L.; Giner, B.; Bandrés, I.; Lafuente, C.; Pino, M. R. *Green Chem.* **2011,** *13,* 2062–2070. doi:10.1039/c0gc00853b
104. Clark, J. H.; Hunt, A. J.; Topi, C.; Paggiola, G.; Sherwood, J. An Appendix of Solvent Data Sheets. *Sustainable Solvents Perspectives from Research, Business and International Policy;* Green Chemistry Series; Royal Society of Chemistry: Cambridge, UK, 2017; pp 235–347. doi:10.1039/9781782624035-00235
105. Gopinath, A.; Sairam, K.; Velraj, R.; Kumaresan, G. *Proc. Inst. Mech. Eng., Part D* **2015,** *229,* 357–390. doi:10.1177/0954407014541103
106. Kuznetsov, M. L. *Russ. Chem. Rev.* **2006,** *75,* 935–960. doi:10.1070/rc2006v075n11abeh001195
107. Hisano, T.; Harano, K.; Matsuoka, T.; Watanabe, S.; Matsuzaki, T. *Chem. Pharm. Bull.* **1989,** *37,* 907–911. doi:10.1248/cpb.37.907
108. Majhool, A. A.; Khalaf, A. A.; Hasan, I. S.; Kumar, R.; Kaushal, S.; Badru, R. *RSC Sustainability* **2024,** *2,* 546–557. doi:10.1039/d3su00396e
109. Kaur, A.; Singh, B. *J. Heterocycl. Chem.* **2014,** *51,* 1421–1429. doi:10.1002/jhet.1838
110. Özkan, H.; Yildirir, Y. *J. Heterocycl. Chem.* **2010,** *47,* 954–959. doi:10.1002/jhet.395
111. Heaney, F.; Rooney, O.; Cunningham, D.; McArdle, P. *J. Chem. Soc., Perkin Trans. 2* **2001,** 373–378. doi:10.1039/b007164l
112. Jarošková, L.; Konopíková, M.; Fišera, Ľ. *Chem. Pap.* **1994,** *48,* 35–39.
113. Folting, K.; Lipscomb, W. N.; Jerslev, B.; Hatanaka, A.; Munch-Petersen, J. *Acta Chem. Scand.* **1963,** *17,* 2138–2139. doi:10.3891/acta.chem.scand.17-2138
114. Yıldırım, A. *Chem. Heterocycl. Compd. (N. Y., NY, U. S.)* **2020,** *56,* 365–370. doi:10.1007/s10593-020-02668-7
115. Umar, A. R.; Tia, R.; Adei, E. *Comput. Theor. Chem.* **2021,** *1195,* 113099. doi:10.1016/j.comptc.2020.113099
116. Blanáriková, I.; Dugovic, B.; Fišera, L.; Hametner, C.; Prónayová, N. *ARKIVOC* **2001,** No. ii, 109–121. doi:10.3998/ark.5550190.0002.213
117. Agirbas, H.; Guner, S.; Budak, F.; Keceli, S.; Kandemirli, F.; Shvets, N.; Kovalishyn, V.; Dimoglo, A. *Bioorg. Med. Chem.* **2007,** *15,* 2322–2333. doi:10.1016/j.bmc.2007.01.029
118. Molteni, G. *Heterocycles* **2016,** *92,* 2115. doi:10.3987/rev-16-848
119. Chatterjee, A.; Maiti, D. K.; Bhattacharya, P. K. *Org. Lett.* **2003,** *5,* 3967–3969. doi:10.1021/ol035535m
120. Chakraborty, B.; Chhetri, M. S.; Kafley, S.; Samanta, A. *Indian J. Chem., Sect. B: Org. Chem. Incl. Med. Chem.* **2010,** *49B,* 209–215.
121. Hota, S. K.; Chatterjee, A.; Bhattacharya, P. K.; Chattopadhyay, P. *Green Chem.* **2009,** *11,* 169–176. doi:10.1039/b812290c
122. Coutouli-Argyropoulou, E.; Sarridis, P.; Gkizis, P. *Green Chem.* **2009,** *11,* 1906–1914. doi:10.1039/b916765j
123. Floresta, G.; Talotta, C.; Gaeta, C.; De Rosa, M.; Chiacchio, U.; Neri, P.; Rescifina, A. *J. Org. Chem.* **2017,** *82,* 4631–4639. doi:10.1021/acs.joc.7b00227
124. Welton, T. *Proc. R. Soc. A* **2015,** *471,* 20150502. doi:10.1098/rspa.2015.0502
125. Hu, P.; Wu, X.; Zhang, Y.; Liu, M.; Tao, Y.; Huang, Z.; Chen, F. *Green Chem.* **2024,** *26,* 2124–2134. doi:10.1039/d3gc04344d

126. Yamamoto, D.; Hirano, I.; Narushima, Y.; Soga, M.; Ansai, H.; Makino, K. *Green Chem.* **2022,** *24,* 7162–7170. doi:10.1039/d2gc02205b
127. Mortko, C. J.; Garcia-Garibay, M. A. *J. Am. Chem. Soc.* **2005,** *127,* 7994–7995. doi:10.1021/ja0508166
128. Mohan, M.; Eldhose, S. P.; Sudheendranath, A.; G., J. E.; Deepthi, A. *Synthesis* **2023,** *55,* 2526–2536. doi:10.1055/a-2053-2811
129. Yıldırım, A. *Catal. Lett.* **2020,** *150,* 2566–2571. doi:10.1007/s10562-020-03175-2
130. Robertson, C. C.; Mackenzie, H. W.; Kosikova, T.; Philp, D. *J. Am. Chem. Soc.* **2018,** *140,* 6832–6841. doi:10.1021/jacs.7b13576
131. Kosikova, T.; Mackenzie, H.; Philp, D. *Chem. – Eur. J.* **2016,** *22,* 1831–1839. doi:10.1002/chem.201503740
132. Kosikova, T.; Hassan, N. I.; Cordes, D. B.; Slawin, A. M. Z.; Philp, D. *J. Am. Chem. Soc.* **2015,** *137,* 16074–16083. doi:10.1021/jacs.5b09738
133. Robertson, C. C.; Kosikova, T.; Philp, D. *J. Am. Chem. Soc.* **2020,** *142,* 11139–11152. doi:10.1021/jacs.0c03527
134. Kosikova, T.; Philp, D. *J. Am. Chem. Soc.* **2019,** *141,* 3059–3072. doi:10.1021/jacs.8b12077
135. Vidonne, A.; Kosikova, T.; Philp, D. *Chem. Sci.* **2016,** *7,* 2592–2603. doi:10.1039/c5sc04805b

License and Terms

This is an open access article licensed under the terms of the Beilstein-Institut Open Access License Agreement (https://www.beilstein-journals.org/bjoc/terms), which is identical to the Creative Commons Attribution 4.0 International License (https://creativecommons.org/licenses/by/4.0). The reuse of material under this license requires that the author(s), source and license are credited. Third-party material in this article could be subject to other licenses (typically indicated in the credit line), and in this case, users are required to obtain permission from the license holder to reuse the material.

The definitive version of this article is the electronic one which can be found at:
https://doi.org/10.3762/bjoc.21.184

BEILSTEIN JOURNAL OF ORGANIC CHEMISTRY

Continuous-flow carbonyl hydrogenation under subatmospheric to atmospheric hydrogen pressure enabled by robust heterogeneous Pt–Fe catalysts

Hiroyuki Miyamura[*1], Ryosuke Kajiyama[2], Shun-ya Onozawa[1], Yoshihiro Kon[1] and Shū Kobayashi[*1,3]

Full Research Paper

Open Access

Address:
[1]Catalytic Chemistry Research Institute, National Institute of Advanced Industrial Science and Technology (AIST), 1-1-1 Higashi, Tsukuba, Ibaraki 305-8565, Japan, [2]Interdisciplinary Research Center for Catalytic Chemistry, National Institute of Advanced Industrial Science and Technology (AIST), 1-1-1 Higashi, Tsukuba, Ibaraki 305-8565, Japan and [3]Department of Chemistry, School of Science, The University of Tokyo, 7-3-1 Hongo, Bunkyo-ku, Tokyo 113-0033, Japan

Email:
Hiroyuki Miyamura[*] - h.miyamura@aist.go.jp; Shū Kobayashi[*] - Shu_kobayashi@chem.s.u-tokyo.ac.jp

* Corresponding author

Keywords:
bimetallic nanostructure; carbonyl reduction; continuous-flow reaction; heterogeneous catalyst; subatmospheric hydrogen

Beilstein J. Org. Chem. **2026,** *22,* 575–582.
https://doi.org/10.3762/bjoc.22.43

Received: 08 January 2026
Accepted: 26 March 2026
Published: 10 April 2026

This article is part of the thematic issue "Green chemistry III: Technologies shaping future directions in synthesis".

Associate Editor: L. Vaccaro



© 2026 Miyamura et al.; licensee Beilstein-Institut.
License and terms: see end of document.

Abstract

The reduction of carbonyl compounds, including ketones and aldehydes, to alcohols is a fundamental and important reaction in organic synthesis. One of the most ideal methods is catalytic hydrogenation, however, the hydrogenation of ketones generally requires harsh reaction conditions, such as high temperature and high pressure. We developed a bimetallic Pt–Fe nanoparticle catalyst immobilized on a composite support of dimethylpolysilane and alumina. Both ketones and aldehydes, including highly bulky and sterically hindered substrates, were smoothly hydrogenated using the newly developed catalysts under continuous-flow conditions at room temperature and under subatmospheric to atmospheric hydrogen pressure. High durability of the heterogeneous catalysts was confirmed by a long-term continuous-flow operation. Interestingly, both the combination of metal species and the metal ratio strongly influenced the catalytic performance.

Introduction

The reduction of carbonyl compounds, ketones and aldehydes to alcohols is a fundamental and important reaction in organic synthesis that can provide valuable chemicals such as functional materials and pharmaceuticals [1-4]. While stoichiometric reagents and catalytic methods are widely developed for this transformation, one of the most ideal methods is heterogen-

eous catalysis using molecular hydrogen as a reductant, which realizes 100% atom economy [5-12]. In this context, advanced technologies represented by the precise control of the bimetallic structure of a heterogeneous catalyst, mechanochemical hydrogenation, and continuous-flow methods using packed-bed reactors greatly contributed to advancing this transformation [9,11-13].

Recently, continuous-flow organic synthesis has attracted much attention from both academia and industry, because it offers numerous advantages, such as not only a high productivity with limited space but also realizing green sustainable syntheses minimizing required energy and resources. When heterogeneous catalysts are used in a continuous-flow system, the catalyst included in a column allows semi-permanent use without recovery and reuse operations that are usually needed in a batch system. The integration of multiple column reactors also enables multistep continuous production. In addition, an enhanced catalytic performance could be achieved in case of continuous-flow hydrogenation reactions using a gas–liquid–solid catalyst-packed column reactor, in which both a liquid substrate and hydrogen gas can directly interact with the catalytically active sites of the heterogeneous catalyst at an optimal gas/flow ratio [14-29].

Although the hydrogenation of aldehydes is relatively easy to achieve, the hydrogenation of ketones is still challenging, due to their higher steric hindrance and lower electrophilicity. The hydrogenation of ketones often suffers from insufficient reactivity and conversion, even under harsh reaction conditions, such as high temperature and pressurized hydrogen, or when employing advanced technologies [8,9,11,12]. The selective hydrogenation of carbonyl moieties often needs to overcome the problem of overreduction of other functionalities like aromatic systems, and requires additives to suppress this unwanted side-reaction [6,10].

We have developed heterogeneous bimetallic nanoparticle catalysts for the selective hydrogenation of quinizarin to leucoquinizarin under continuous-flow conditions [30]. During our mechanistic study, we unexpectedly discovered that Pt–Fe bimetallic nanoparticles immobilized on a composite support of dimethylpolysilane (DMPSi) and alumina (Pt–Fe/DMPSi–Al_2O_3) exhibited extraordinary catalytic performance for the selective hydrogenation of ketones under continuous-flow and atmospheric pressure hydrogen conditions. In this article, we report the development of a continuous-flow carbonyl reduction system that achieves high performance and a wide substrate scope under atmospheric or subatmospheric hydrogen pressure and ambient temperature using Pt–Fe bimetallic heterogeneous catalysts.

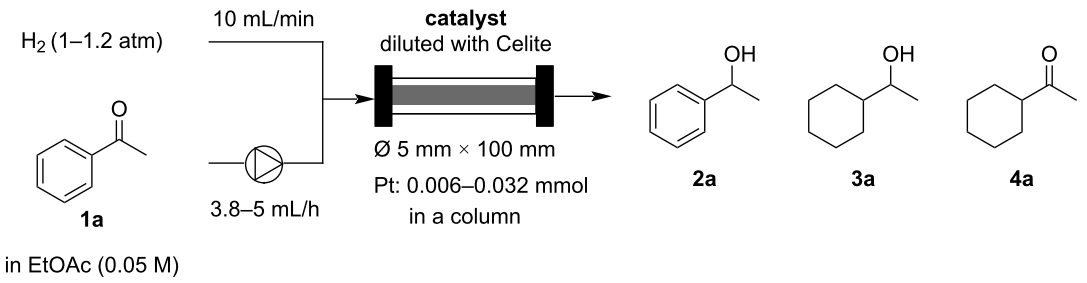
Results and Discussion

Catalyst preparation

First, we prepared Pt–Fe/DMPSi–Al_2O_3 with different Fe/Pt ratios by the simultaneous reduction of Pt and Fe salts in a solution containing dissolved sodium borohydride ($NaBH_4$) and suspended DMPSi [15,30-32]. After DMPSi stabilized the resulting bimetallic nanoparticles, Al_2O_3 was added to the mixture, followed by methanol. The resulting solid catalyst was collected by filtration, washed with solvents, and heated twice. Si–Si bonds in DMPSi were partially oxidized to form Si–O–Si bonds during the preparation process, and they became cross-linked to Al_2O_3 to form a stabilized composite support [32]. A plausible scenario for the formation of the bimetallic structure of Pt–Fe nanoparticles during the catalyst preparation would be the same as that for the formation of Pt–Ni bimetallic structures, and it involves the following steps [33]. $Na_2PtCl_6{\cdot}6H_2O$ might be reduced by $NaBH_4$ faster than $FeCl_2$ in the solution phase, and the generated Pt(0) nanoparticles are stabilized by DMPSi surface. The reduction of $FeCl_2$, which is usually more difficult to achieve can be catalyzed on the surface of Pt(0) nanoparticles and the formed Fe species are deposited and grown from the existing Pt nanoparticles. Therefore, a bimetallic structure of Pt and Fe is generated, and both elements are observed with similar distributions by STEM–EDS mapping analysis (Figure S1, Supporting Information File 1). The Pt nanoparticles are isolated by the surrounding Fe species, which prevents aggregation and preserves their small size (2–5 nm). The valence of the Pt and Fe species was found to be Pt(0) and Fe(II) in the catalyst by XPS analysis [30]. The valence of Fe species may have been 0 during the reduction step of the catalyst preparation procedure. However, the Fe species can easily oxidize to Fe(II) during the filtration and heating processes, resulting in the formation of a bimetallic structure comprising Pt(0) and Fe(II). Pt–Au, Pt–Co, and Pt–Ni bimetallic catalysts immobilized on DMPSi–Al_2O_3 were also prepared by the same procedure.

Comparison of the catalysts in the continuous-flow hydrogenation of a ketone

We compared the catalytic performance of the newly prepared bimetallic catalysts to that of commercially available heterogeneous Pt catalysts in the continuous-flow hydrogenation of acetophenone (**1a**) at room temperature. The heterogeneous catalysts were packed into a column with Celite, with the molar amount of Pt adjusted to 0.006 mmol within the column. Both the solution of acetophenone (**1a**) in ethyl acetate (EtOAc) and hydrogen gas were simultaneously passed through the catalyst-packed column without backpressure control at room temperature (Scheme 1). The powder-like catalysts were packed in a glass column equipped with glass wool filters at both ends of the column. The hydrogen gas and liquid substrate were introduced through a double-layered column head, in which the substrate



Scheme 1: Hydrogenation of a ketone under continuous-flow conditions.

solution is directly injected to the glass wool filter of the column by a PTFE tube and the hydrogen gas is supplied by an outer layer surrounding the PTFE tube (Figure S2, Supporting Information File 1). Thus, the hydrogen gas and liquid substrate can be mixed at the glass wool filter which is located at the top of the catalyst column, and the well mixed gas–liquid is supplied to the catalyst region in the column. No backpressure controller is installed, and the outlet of the column is directly released to atmosphere. When the flow rates of hydrogen gas and substrate solution were 10 mL/min and 3.8–5 mL/h, respectively, the pressure at the inlet of the column was almost 1.2 atm in this case (0.2 atm pressure loss). The yields of 1-phenetylalcohol (**2a**) and by-products **3a** and **4a** under these reaction conditions for each catalyst are summarized in Table 1. The commercially available catalysts (Pt/C, Pt/SiO_2, Pt/Al_2O_3) and $Pt/DMPSi–Al_2O_3$ showed poor to moderate reactivity, and the hydrogenation of the aromatic moiety proceeded as well to give by-products **3a** and **4a** (Table 1, entries 1–4). Pt–Au and Pt–Ni bimetallic catalysts immobilized on $DMPSi–Al_2O_3$ also showed moderate reactivity, accompanied by the formation of by-products (Table 1, entries 5 and 6). Interestingly, Pt–Co and Pt–Fe bimetallic catalysts immobilized on $DMPSi–Al_2O_3$ showed high activity with minimal by-product formation (Table 1, entries 7–11). Especially, $Pt–Fe/DMPSi–Al_2O_3$ (Fe/Pt = 0.62–2.3) demonstrated excellent catalytic performance under the continuous-flow conditions giving the desired product with 95% to >99% yield and almost no by-product formation (Table 1, entries 8–10). However, the reactivity of the $Pt–Fe/DMPSi–Al_2O_3$ catalyst decreased when the Fe/Pt ratio was excessively high (Table 1, entry 11). We also prepared a $Pt–Fe/Al_2O_3$ catalyst without the use of DMPSi during catalyst synthesis. However, $Pt–Fe/Al_2O_3$ catalyst showed very low catalytic activity compared to $Pt–Fe/DMPSi–Al_2O_3$ (Table 1, entry 12). This suggested that both the bimetallic structure of Pt–Fe and DMPSi in the support are required for the high catalytic performance. We also compared the catalytic performance in detail by varying the flow rate of the substrate solution in the flow system, and the catalytic turnover frequency (TOF) values

Table 1: Comparison of catalyst performance in the hydrogenation of a ketone under continuous-flow conditions.

Entry	Catalyst	Fe/Pt ratio	Yield (%)[a]			
			2a	**3a**	**4a**	**1a**
1	Pt/C	–	16	2	10	72
2	Pt/SiO_2	–	2	0	3	95
3	Pt/Al_2O_3	–	36	5	13	47
4	$Pt/DMPSi–Al_2O_3$	–	9	1	7	84
5	$Pt-Au/DMPSi–Al_2O_3$	–	38	3	12	47
6	$Pt-Ni/DMPSi–Al_2O_3$	–	32	2	0	66
7	$Pt-Co/DMPSi–Al_2O_3$	–	81	2	0	17
8	$Pt–Fe/DMPSi–Al_2O_3$	0.62	95	5	0	0
9	$Pt–Fe/DMPSi–Al_2O_3$	1.4	97	2	0	1
10	$Pt–Fe/DMPSi–Al_2O_3$	2.3	>99	0	0	0
11	$Pt–Fe/DMPSi–Al_2O_3$	4.4	74	0	0	26
12	$Pt-Fe/Al_2O_3$	0.73	11	trace	1	88

[a]Yield was determined by GC analysis using decane as an internal standard.

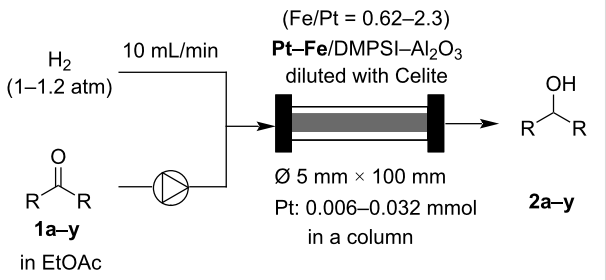
of all catalysts tested at each flow rate are summarized in Supporting Information File 1 (Tables S1–11 and Figures S3 and S4). The Pt–Fe/DMPSi–Al_2O_3 (Fe/Pt = 0.62) catalyst showed the highest TOF of >50 h^{-1} in this investigation, although overreduction occurred to some extent with this catalyst (Table 1, entry 8). Both the combination of metal species in bimetallic catalysts and the ratio of metals were important to optimize the catalytic performance with respect to activity and selectivity.

The binding energies of Pt 4d in Pt–Fe/DMPSi–Al_2O_3 (332, 315 eV) are lower than those of Pt/DMPSi–Al_2O_3 (333, 316 eV) and Pt–Ni/DMPSi–Al_2O_3 (334, 317 eV) [30]. Thus, the Pt species in Pt–Fe/DMPSi–Al_2O_3 is the most electronically negative among the catalysts, which leads to a stronger reducing ability after adsorption of hydrogen on the surface of the catalyst. Therefore, the more demanding carbonyl hydrogenation is enabled by the stronger reducing ability of the Pt-Fe/DMPSi–Al_2O_3 catalyst. We also investigated the effect of solvent and ethyl acetate (EtOAc) was found to be the best among the solvents tested (EtOAc, toluene, methylcyclohexane, tetrahydrofuran, and methanol) (see Supporting Information File 1, Figure S5). The hydroxy moiety has a stronger interaction with catalytically active sites at the surface of the heterogeneous catalyst, and smooth desorption of the alcohol product is key for a high catalytic turnover. The polar solvent, EtOAc, facilitates the desorption of the formed alcohol by stabilizing it in the solution phase, leading to the smooth product desorption and following substrate adsorption. Although methanol and THF are also polar solvents, they can be strongly adsorbed on the catalytically active sites of the catalyst leading to a poisoning effect by these solvents and disturbing the catalytic turnover.

Substrate scope

We also investigated the substrate scope under continuous-flow conditions using the best catalyst, Pt–Fe/DMPSi–Al_2O_3 (Fe/Pt = 0.62–2.3) (Scheme 2, Figure 1, and Table 2). 4'-Methoxyacetophenone (**1b**) and 4'-methylacetophenone (**1c**) were quantitatively hydrogenated to the corresponding alcohols **2b** and **2c** under continuous-flow conditions at room temperature (Table 2, entries 1 and 2). The bulky substrate 2-acetylnaphthalene (**1d**) was converted to the corresponding alcohol **2d** in 89% yield under continuous-flow conditions at room temperature (Table 2, entry 3). The desired product **2d** was obtained quantitatively at 50 °C (Table 2, entry 4). It is noteworthy that an analytically pure compound (confirmed by ^1H and ^{13}C NMR) was isolated by simple evaporation of the solvent (Table 2, entry 4).

Tetralone (**1e**) was also hydrogenated smoothly to afford the corresponding alcohol **2e** in 88% yield at room temperature



Scheme 2: Continuous-flow hydrogenation of carbonyl compounds.

Table 2: Substrate scope under the continuous-flow hydrogenation of carbonyl compounds.

Entry	Substrate	Temperature	Yield (%)
1	**1b**	rt	>99[a]
2	**1c**	rt	>99[a]
3	**1d**	rt	89[a]
4	**1d**	50 °C	>99[b]
5	**1e**	rt	88[a]
6	**1f**	rt	>99[b]
7	**1g**	rt	95[a]
8	**1h**	rt	>99[a]
9	**1i**	rt	98[a]
10	**1j**	50 °C	>99[a]
11	**1k**	80 °C	74[a,c]
12	**1l**	50 °C	>99[b,d]
13	**1m**	rt	>99[a]
14	**1n**	rt	>99[a]
15	**1o**	rt	>99[a]
16	**1p**	rt	>99[a]
17	**1q**	rt	>99[a]
18	**1r**	rt	98[a]
19	**1s**	rt	>99[a], >99[b]
20	**1t**	rt	>99[a], >99[b]
21	**1u**	rt	91[a]
22	**1v**	50 °C	61[a]
23	**1w**	rt	99[a]
24	**1x**	rt	>99[b]
25	**1y**	30 °C	95[a]

[a]Yield was determined by GC analysis using decane as an internal standard. [b]Analytically pure isolated compound was obtained after removal of the solvent from the eluted solution from the continuous-flow reactor. [c]The ratio of **2k**:**2k'** was 66:34. [d]A mixture of diastereomers was isolated, and the ratio of **2l**:**2l'** was determined to be 74:26 by ^1H NMR analysis. rt = room temperature.

(Table 2, entry 5). Ethyl benzoylacetate (**1f**) was converted to the corresponding alcohol **2f** quantitatively while retaining the ester moiety, and the product was isolated by simple evaporation of the solvent from the collected fraction eluted from the flow reactor (Table 2, entry 6). Cyclic ketones **1g**, **1h**, and **1i** and an aliphatic ketone **1j** were also hydrogenated in excellent

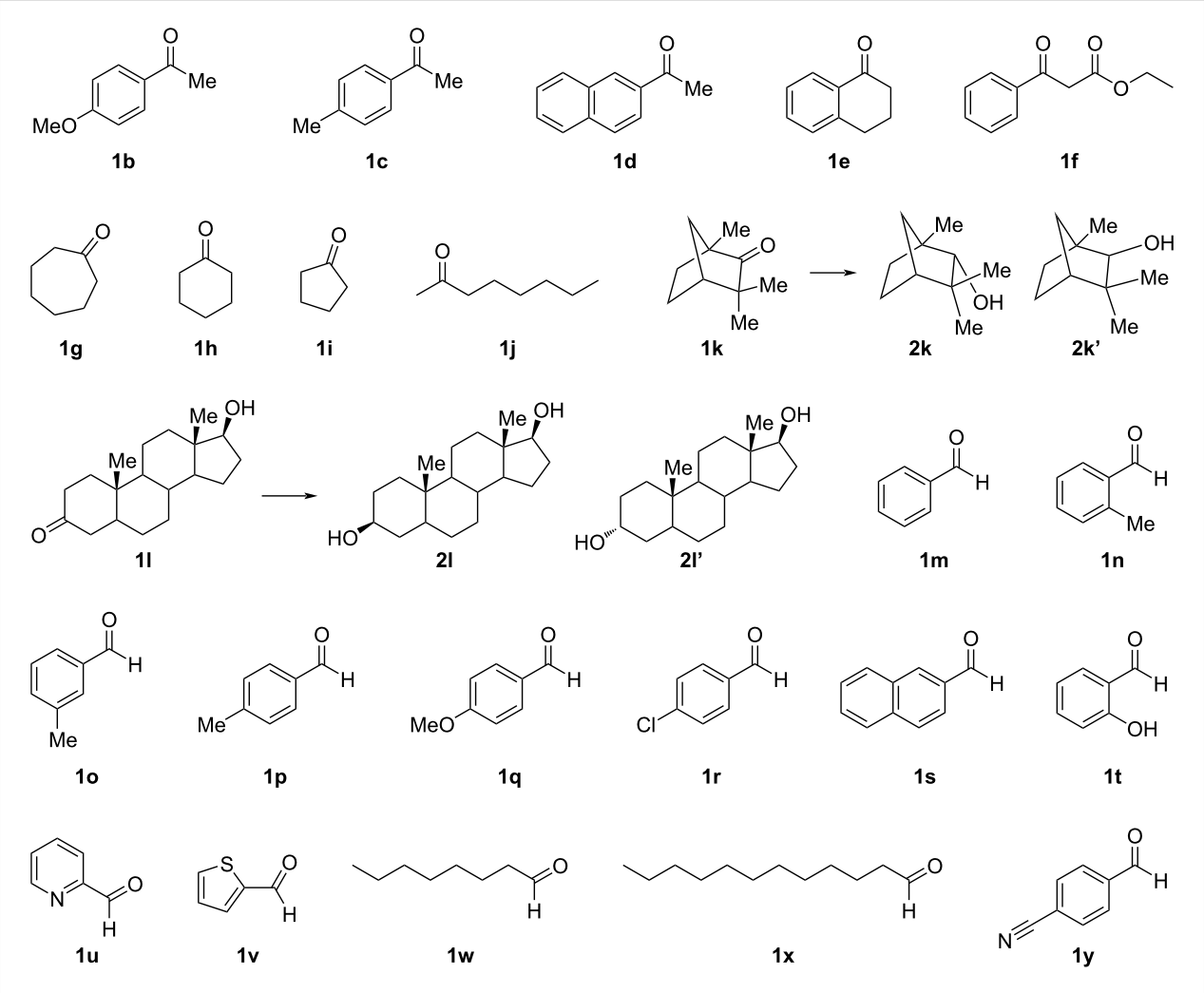


Figure 1: List of substrates.

yields at room temperature (Table 2, entries 7–10). Fenchone (**1k**) has a fused bicyclic skeleton with a carbonyl moiety positioned between two quaternary carbons. Therefore, its carbonyl moiety is sterically shielded and its hydrogenation is highly challenging. A mixture of two diastereomers **2k** and **2k'** was obtained in 74% yield (**2k**:**2k'** = 66:34) at 80 °C under the continuous-flow conditions (Table 2, entry 11). The high catalytic performance of Pt–Fe/DMPSi–Al_2O_3 enabled the hydrogenation of substrate **1k** even under almost atmospheric pressure hydrogen conditions. Stanolone (**1l**) is also a bulky ketone compound with a steroid skeleton, and its hydrogenation is challenging. The continuous-flow hydrogenation of **1l** proceeded quantitatively to afford two diastereomers in a 74:26 ratio even at room temperature (Table 2, entry 12).

Next, we investigated the hydrogenation of aldehydes. Benzaldehyde, 2-, 3-, and 4-methylbenzaldehyde **1m**, **1n**, **1o**, and **1p** were quantitatively hydrogenated to the corresponding alcohols without over-reduction (Table 2, entries 13–16). 4-Methoxybenzaldehyde (**1q**) was also hydrogenated quantitatively under the continuous-flow conditions (Table 2, entry 17). 4-Chlorobenzaldehyde (**1r**) was converted to 4-chlorobenzylalcohol quantitatively while retaining the chloride moiety (Table 2, entry 18). The catalytic turnover frequencies (TOFs) of these aldehydes under continuous-flow conditions reached 180 h^{-1} (**1m**: 180 h^{-1}, **1n**: 104 h^{-1}, **1o**: 144 h^{-1}, **1p**: 130 h^{-1}, **1q**: 88 h^{-1}, **1r**: 127 h^{-1}; see Supporting Information File 1 for details). 2-Naphthaldehyde (**1s**) and salicylaldehyde (**1t**) were hydrogenated quantitatively, and analytically pure products were isolated by simple evaporation of the collected fraction eluted from the flow reactor (Table 2, entries 19 and 20). Heterocyclic aldehydes **1u** and **1v** were also applicable, while the conversion of **1v** was moderate, probably because of the poisoning effect of the sulfur atom in the compound (Table 2, entries 21 and 22). Aliphatic aldehydes **1w** and **1x** were also hydrogenated quantitatively under atmospheric hydrogen and

room temperature conditions (Table 2, entries 23 and 24), and an analytically pure alcohol was isolated by simple evaporation of the collected fraction eluted from the flow reactor (Table 2, entry 24). Remarkably, when 4-cyanobenzaldehyde (**1y**) was used as the substrate, selective hydrogenation of the carbonyl moiety proceeded to afford 4-cyanobenzylalcohol (**2y**) in 95% yield, preserving the nitrile moiety which is typically hydrogenated under similar conditions (Table 2, entry 25).

Durability of the catalyst under the continuous-flow conditions

We investigated the durability of Pt–Fe/DMPSi–Al_2O_3 under continuous-flow hydrogenation conditions at steady state during a long-period run (Figure 2). Quantitative conversion of cyclohexanone (**1h**) was maintained over the initial 50 h; however, a small amount of **1h** remained after 54 h of continuous running. Then, the supply of substrate and hydrogen was stopped, and the catalyst column was heated at 100 °C for 3 h to reactivate the catalyst. The continuous-flow hydrogenation was restarted after the column had cooled to ambient temperature. Catalytic activity was successfully restored, and quantitative conversion was maintained for a further 24 h. A small amount of **1h** remained again, and the catalyst regeneration process was repeated. Finally, the catalytic activity was revived again, and quantitative conversion was observed over 90 h of total running. Water as contaminant in EtOAc or organic compounds strongly adsorbed on the catalyst's surface may have led to its deactivation; however, they could be removed by simple heating. We demonstrated the robustness of Pt–Fe/DMPSi–Al_2O_3 under continuous-flow hydrogenation conditions and showed that a simple heat treatment process for regenerating the catalytic activity is adaptable for practical use of this continuous-flow system.

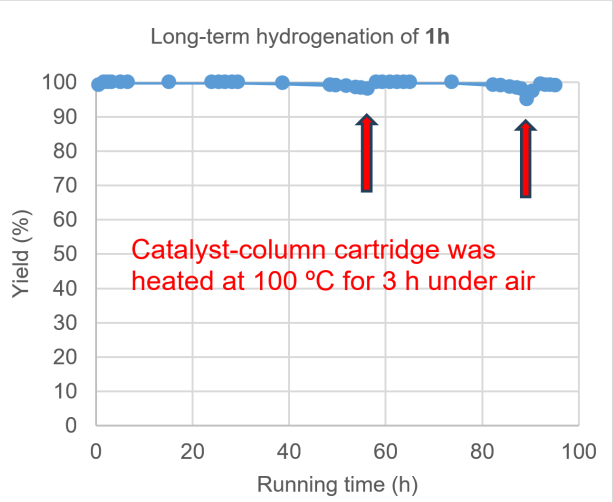
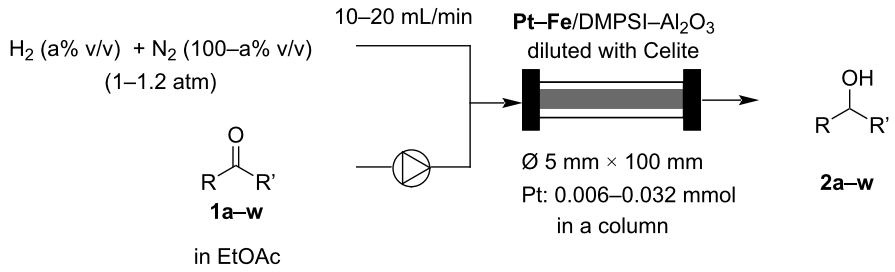


Figure 2: Continuous-flow hydrogenation of cyclohexanone **1h**. Conditions: solution of **1h** in EtOAc (0.06 M) with decane as an internal standard; substrate flow rate, 7.2 mL h^{-1}; hydrogen flow rate, 10 mL min^{-1}; amount of Pt in the column, 0.006 mmol; reaction temperature, 30 °C.

Continuous-flow hydrogenation of carbonyl compounds under subatmospheric pressure of hydrogen

Next, we investigated whether continuous-flow hydrogenation could proceed under subatmospheric partial pressure of hydrogen gas. The use of subatmospheric partial pressure of hydrogen gas is highly desired from the viewpoint of safety, as well as for utilizing green hydrogen produced by sustainable energy, because purifying and pressurizing hydrogen gas consumes large amounts of energy comparable to the energy required to generate green hydrogen [34]. We set up a continuous-flow system in which a mixture of H_2 and N_2 was introduced by two individually regulated mass-flow controllers (Scheme 3). First, the continuous-flow hydrogenation of benzaldehyde (**1m**) was investigated by varying the H_2/N_2 v/v ratio. Yields of **2m** and **1m** at the steady state of continuous-flow hydrogenation with different H_2/N_2 v/v ratios are plotted in Figure 3. Quantitative conversion of **1m** was observed with 50% and 30% v/v of hydrogen and product **2m** was obtained in 93% yield even at 20% v/v of hydrogen; the partial pressure of hydrogen in the catalyst column was 0.2–0.24 atm (Table 3, entry 4). A 69% yield of **2m** was obtained with just 10% v/v of hydrogen. Acetophenone (**1a**) was successfully hydrogenated with 20% v/v hydrogen to afford the desired product quantitatively



Scheme 3: Continuous-flow hydrogenation of carbonyl compounds under subatmospheric partial pressure of hydrogen.

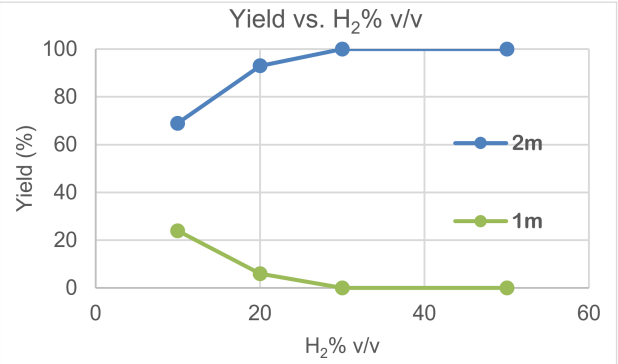


Figure 3: Continuous-flow hydrogenation of benzaldehyde **1m** by varying the H_2/N_2 v/v ratio. Conditions: solution of **1m** in EtOAc (0.06 M) with decane as an internal standard; substrate flow rate, 10 mL h^{-1}; H_2 + N_2 mixed-gas flow rate, 20 mL min^{-1}; amount of Pt in the column, 0.032 mmol; reaction temperature, room temperature.

(Table 3, entry 1). A cyclic ketone **1i** was converted to **2i** in 84% yield with 10% v/v hydrogen and in 97% yield with 20% v/v hydrogen (Table 3, entries 2 and 3). An aliphatic aldehyde **1w** was also hydrogenated to give the product in 97% yield with 20% v/v hydrogen (Table 3, entry 5). These results were compared with other representative catalytic systems for the hydrogenation of carbonyl compounds (see Supporting Information File 1, Table S12), and the high catalytic performance of Pt–Fe/DMPSi–Al_2O_3 even under subatmospheric partial pressure of hydrogen was highlighted [8-12].

Table 3: Substrate scope using subatmospheric partial pressure of hydrogen.

Entry	Substrate	H_2% v/v	Total gas flow rate (H_2 + N_2) (mL min^{-1})	Yield (%)[a]
1	**1a**	20	20	>99
2	**1i**	10	20	84
3	**1i**	20	20	97
4	**1m**	20	20	93
5	**1w**	20	10	97

[a]Yield was determined by GC analysis using decane as an internal standard.

Conclusion

In summary, we developed bimetallic Pt–Fe/DMPSi–Al_2O_3 as a powerful heterogeneous catalyst for the hydrogenation of carbonyl compounds under continuous-flow and ambient conditions. Both ketones and aldehydes, including highly bulky and sterically hindered substrates, were smoothly hydrogenated at room temperature under subatmospheric to atmospheric hydrogen pressure with a wide substrate scope. The high durability of the heterogeneous catalyst was confirmed by a long-term continuous-flow reaction, and the catalytic activity was revived by a simple operation even if the catalyst became slightly deactivated. Interestingly, both the combination of metal species in the catalysts and the ratio of metals had a great impact on catalytic performance. The newly developed continuous-flow hydrogenation reaction under mild conditions is adaptable to sustainable chemical synthesis, minimizing energy consumption and enabling the use of green hydrogen. In addition, the newly obtained insights regarding the relationships among the Fe/Pt ratios in the catalysts, the bimetallic structure, and the resulting catalytic performance for selective hydrogenation will guide the future development of heterogeneous catalysts.

Supporting Information

Supporting Information File 1

Additional experimental details, materials, and methods including photographs of reactor systems, STEM-EDS images and XPS spectra of heterogeneous catalysts, and copies of ^1H and ^{13}C NMR spectra for isolated compounds.
[https://www.beilstein-journals.org/bjoc/content/supplementary/1860-5397-22-43-S1.pdf]

Acknowledgements

H. M. also thanks the Joint Usage/Research Center for Catalysis (Proposal #23CY0303, #24AY0568).

Funding

Grant-in-Aid for Scientific Research from JSPS/MEXT (Transformative Research Areas (A), KAKENHI Grant Number JP24H01104), New Energy and Industrial Technology Development Organization (NEDO) of Japan (Project Number JPNP19004).

Author Contributions

Hiroyuki Miyamura: conceptualization; data curation; formal analysis; funding acquisition; investigation; methodology; project administration; supervision; validation; visualization; writing – original draft. Ryosuke Kajiyama: data curation; formal analysis. Shun-ya Onozawa: funding acquisition; writing – review & editing. Yoshihiro Kon: data curation; formal analysis; writing – review & editing. Shū Kobayashi: funding acquisition; validation; writing – review & editing.

ORCID® iDs

Hiroyuki Miyamura - https://orcid.org/0000-0002-0028-773X

Data Availability Statement

All data that supports the findings of this study is available in the published article and/or the supporting information of this article.

References

1. Hudlicky, M. *Reductions in Organic Chemistry;* Ellis Harwood Limited: Chichester, 1984.
2. Reduction. In *Comprehensive Organic Synthesis;* Trost, B. M.; Fleming, I., Eds.; Pergamon Press: Oxford, 1991; Vol. 8.
3. Nishimura, S. *Handbook of Heterogeneous Catalytic Hydrogenation for Organic Synthesis;* John Wiley & Sons, Inc.: New York, 2001.
4. de Vries, J. G.; Elsevier, C. J., Eds. *The Handbook of Homogeneous Hydrogenation;* Wiley-VCH Verlag GmbH & Co. KGaA: Weinheim, 2007.
5. Mäki-Arvela, P.; Hájek, J.; Salmi, T.; Murzin, D. Y. *Appl. Catal., A* **2005,** *292,* 1–49. doi:10.1016/j.apcata.2005.05.045
6. Fujiwara, Y.; Iwasaki, Y.; Maegawa, T.; Monguchi, Y.; Sajiki, H. *ChemCatChem* **2011,** *3,* 1624–1628. doi:10.1002/cctc.201100151
7. Cano, I.; Chapman, A. M.; Urakawa, A.; van Leeuwen, P. W. N. M. *J. Am. Chem. Soc.* **2014,** *136,* 2520–2528. doi:10.1021/ja411202h
8. Tan, J.; Cui, J.; Cui, X.; Deng, T.; Li, X.; Zhu, Y.; Li, Y. *ACS Catal.* **2015,** *5,* 7379–7384. doi:10.1021/acscatal.5b02170
9. Osako, T.; Torii, K.; Hirata, S.; Uozumi, Y. *ACS Catal.* **2017,** *7,* 7371–7377. doi:10.1021/acscatal.7b02604
10. Duraczyńska, D.; Serwicka, E. M.; Drelinkiewicz, A.; Socha, R. P.; Zimowska, M.; Lityńska-Dobrzyńska, L.; Bukowska, A. *Mol. Catal.* **2019,** *470,* 145–151. doi:10.1016/j.mcat.2019.04.003
11. Matsuda, S.; Masuda, S.; Takano, S.; Ichikuni, N.; Tsukuda, T. *ACS Catal.* **2021,** *11,* 10502–10507. doi:10.1021/acscatal.1c02703
12. Mayer, M.; Wohlgemuth, M.; Salomé Straub, A.; Grätz, S.; Borchardt, L. *Angew. Chem., Int. Ed.* **2025,** *64,* e202424139. doi:10.1002/anie.202424139
13. Zanette, T.; García-Zaragoza, A.; Mazarío, J.; Santiago Martinez, J.; Chaudret, B.; Cerezo-Navarrete, C.; Oña-Burgos, P. *Green Chem.* **2025,** *27,* 11438–11454. doi:10.1039/d5gc03853g
14. Irfan, M.; Glasnov, T. N.; Kappe, C. O. *ChemSusChem* **2011,** *4,* 300–316. doi:10.1002/cssc.201000354
15. Miyamura, H.; Suzuki, A.; Yasukawa, T.; Kobayashi, S. *J. Am. Chem. Soc.* **2018,** *140,* 11325–11334. doi:10.1021/jacs.8b06015
16. Cai, B.; Cheo, H. W.; Liu, T.; Wu, J. *Angew. Chem., Int. Ed.* **2021,** *60,* 18950–18980. doi:10.1002/anie.202010710
17. Asano, S.; Miyamura, H.; Matsushita, M.; Kudo, S.; Kobayashi, S.; Hayashi, J.-i. *J. Flow Chem.* **2024,** *14,* 329–335. doi:10.1007/s41981-023-00295-9
18. Laporte, A. A. H.; Masson, T. M.; Zondag, S. D. A.; Noël, T. *Angew. Chem., Int. Ed.* **2024,** *63,* e202316108. doi:10.1002/anie.202316108
19. Yoshida, J.-i.; Saito, K.; Nokami, T.; Nagaki, A. *Synlett* **2011,** 1189–1194. doi:10.1055/s-0030-1259946
20. Hessel, V.; Kralisch, D.; Kockmann, N.; Noël, T.; Wang, Q. *ChemSusChem* **2013,** *6,* 746–789. doi:10.1002/cssc.201200766
21. Wiles, C.; Watts, P. *Green Chem.* **2014,** *16,* 55–62. doi:10.1039/c3gc41797b
22. Gutmann, B.; Cantillo, D.; Kappe, C. O. *Angew. Chem., Int. Ed.* **2015,** *54,* 6688–6728. doi:10.1002/anie.201409318
23. Ley, S. V.; Fitzpatrick, D. E.; Myers, R. M.; Battilocchio, C.; Ingham, R. J. *Angew. Chem., Int. Ed.* **2015,** *54,* 10122–10136. doi:10.1002/anie.201501618
24. Kobayashi, S. *Chem. – Asian J.* **2016,** *11,* 425–436. doi:10.1002/asia.201500916
25. Plutschack, M. B.; Pieber, B.; Gilmore, K.; Seeberger, P. H. *Chem. Rev.* **2017,** *117,* 11796–11893. doi:10.1021/acs.chemrev.7b00183
26. Rogers, L.; Jensen, K. F. *Green Chem.* **2019,** *21,* 3481–3498. doi:10.1039/c9gc00773c
27. Weeranoppanant, N. *React. Chem. Eng.* **2019,** *4,* 235–243. doi:10.1039/c8re00230d
28. Ferlin, F.; Lanari, D.; Vaccaro, L. *Green Chem.* **2020,** *22,* 5937–5955. doi:10.1039/d0gc02404j
29. Capaldo, L.; Wen, Z.; Noël, T. *Chem. Sci.* **2023,** *14,* 4230–4247. doi:10.1039/d3sc00992k
30. Miyamura, H.; Sharma, A.; Takata, M.; Kajiyama, R.; Kobayashi, S.; Kon, Y. *ACS Catal.* **2024,** *14,* 10317–10323. doi:10.1021/acscatal.4c02955
31. Miyamura, H.; Tobita, F.; Suzuki, A.; Kobayashi, S. *Angew. Chem., Int. Ed.* **2019,** *58,* 9220–9224. doi:10.1002/anie.201904159
32. Kobayashi, S.; Okumura, M.; Akatsuka, Y.; Miyamura, H.; Ueno, M.; Oyamada, H. *ChemCatChem* **2015,** *7,* 4025–4029. doi:10.1002/cctc.201500973
33. Miyamura, H.; Kajiyama, R.; Kon, Y. *Top. Catal.* **2025,** in press. doi:10.1007/s11244-025-02232-7
34. Segovia-Hernández, J. G.; Hernández, S.; Cossío-Vargas, E.; Juarez-García, M.; Sánchez-Ramírez, E. *RSC Sustainability* **2025,** *3,* 134–157. doi:10.1039/d4su00630e

License and Terms

This is an open access article licensed under the terms of the Beilstein-Institut Open Access License Agreement (https://www.beilstein-journals.org/bjoc/terms), which is identical to the Creative Commons Attribution 4.0 International License (https://creativecommons.org/licenses/by/4.0). The reuse of material under this license requires that the author(s), source and license are credited. Third-party material in this article could be subject to other licenses (typically indicated in the credit line), and in this case, users are required to obtain permission from the license holder to reuse the material.

The definitive version of this article is the electronic one which can be found at:
https://doi.org/10.3762/bjoc.22.43

BEILSTEIN JOURNAL OF ORGANIC CHEMISTRY

Synthetic study of *vic*-bromination of diarylacetylenes, easy purification and separation

Akane Togo[1], Hiyono Suzuki[1], Yuto Akai[2], Makoto Matsumoto[2], Yoshinori Suzuma[2], Hidehiko Kodama[2] and Kouichi Matsumoto[*1]

Full Research Paper

Open Access

Address:
[1]Department of Chemistry, School of Science and Engineering, Kindai University, 3-4-1 Kowakae, Higashi-osaka, Osaka 577-8502, Japan and [2]Nippon Pharmaceutical Chemicals Co., Ltd., 2-8-18 Chodo, Higashi-osaka, Osaka 577-0056, Japan

Email:
Kouichi Matsumoto[*] - kmatsumo@chem.kindai.ac.jp

* Corresponding author

Keywords:
bromination; diarylacetylenes; green chemistry; purification and separation; stereoselective reaction

Beilstein J. Org. Chem. **2026,** *22,* 795–802.
https://doi.org/10.3762/bjoc.22.61

Received: 05 December 2025
Accepted: 20 January 2026
Published: 22 May 2026

This article is part of the thematic issue "Green chemistry III: Technologies shaping future directions in synthesis".

Associate Editor: L. Vaccaro

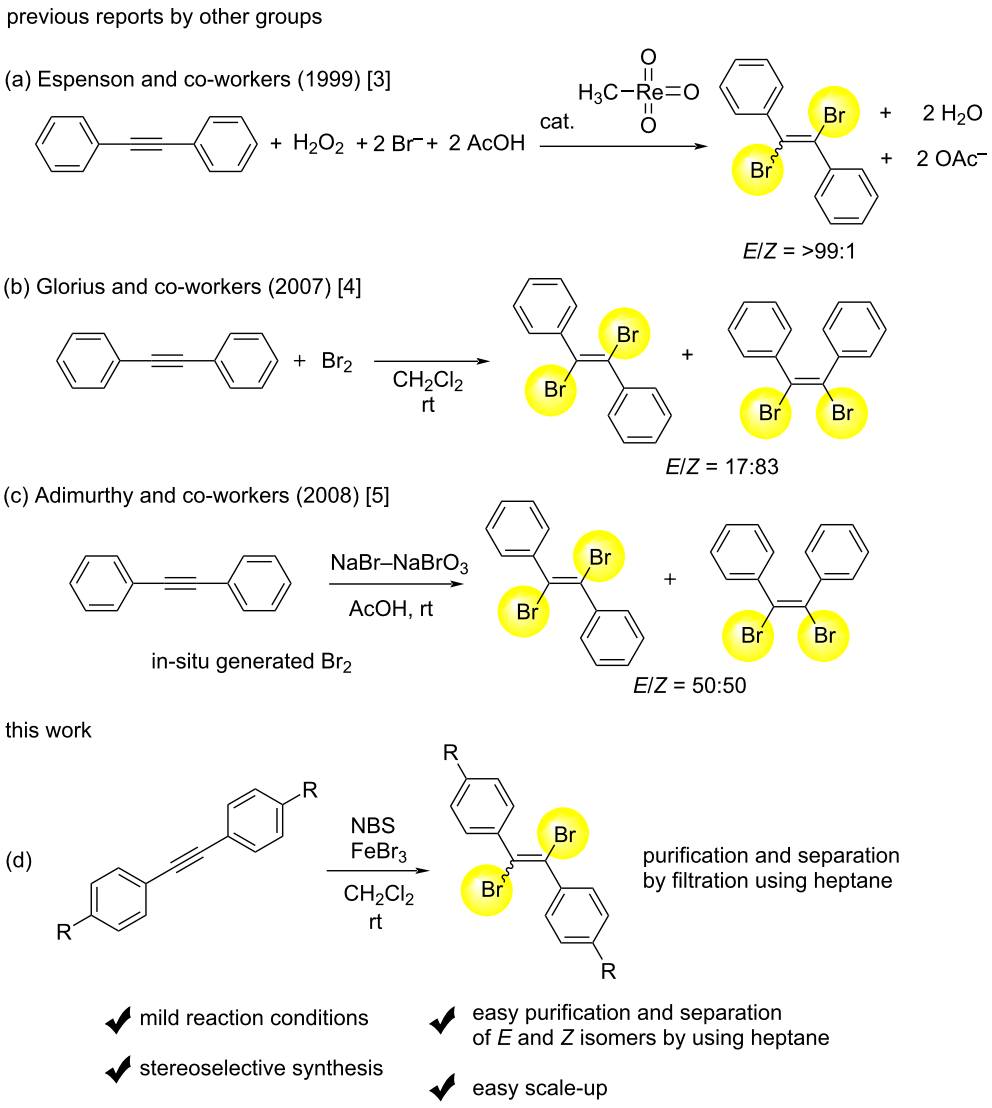
© 2026 Togo et al.; licensee Beilstein-Institut.
License and terms: see end of document.

Abstract

E-Selective bromination for diphenylacetylene was established by using the combination of NBS and $FeBr_3$ in CH_2Cl_2. In addition, easy purification and separation from the crude product were found. When the crude product was treated with heptane, the *E* isomer could be recovered as a solid material by utilizing the difference in solubility. On the other hand, the *Z* isomer could be removed by filtration while remaining in solution.

Introduction

The addition reaction of bromine to diphenylacetylene is one of basic reactions and is recognized as important, because resulting 1,2-dibromo-1,2-diphenylethylene can serve as a precursor for various molecular transformations in organic synthesis [1,2]. This reaction seems to be simple, but some reported studies suggest that it is surprisingly difficult to obtain the *E* isomer selectively (Scheme 1). For selected examples, Espenson and co-workers reported in 1999 that *E*-selective bromination of diphenylacetylene took place by using H_2O_2, NaBr, and AcOH in the presence of MTO (methyltrioxorhenium(VII)) to give (*E*)-1,2-dibromo-1,2-diphenylethylene, selectively (Scheme 1a) [3]. However, MTO is an expensive reagent and a more versatile synthetic method is highly needed. As a simple method, the reaction of diphenylacetylene and Br_2 in CH_2Cl_2 was reported by Glorius in 2007 [4], but the selectivity was reported for the *Z* isomer (Scheme 1b). As another example in 2008, Adimurthy and co-workers proposed the combination of NaBr-$NaBrO_3$ in AcOH in order to prepare in-situ generated Br_2, which was reacted with diphenylacetylene to give no selectivity between *E* and *Z* isomers of 1,2-dibromo-1,2-diphenylethylenes (Scheme 1c) [5]. Previous studies reported the selective synthesis of (*E*)-1,2-dibromo-1,2-diphenylethylene and related compounds, but Br_2 or expensive reagent, which was difficult to handle, was often used [6-15].



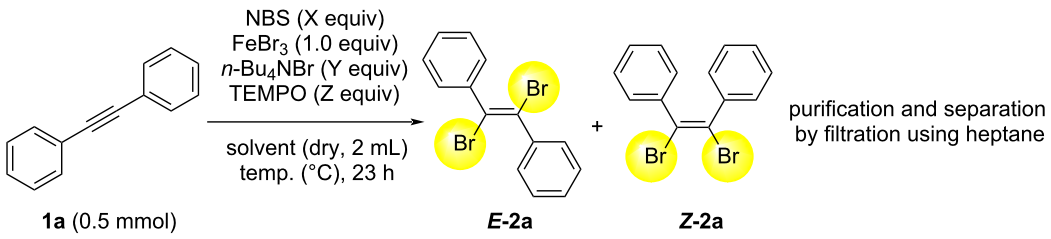
Scheme 1: Selected and previous reports for bromination of diphenylacetylenes (a–c), and this work (d).

Based on these research backgrounds, we have also been interested in the selective synthesis of the *E* isomer of 1,2-dibromo-1,2-diphenylethylene, together with simple purification and separation toward process chemistry, because the compound is an attractive synthetic intermediate for further transformations. During the course of our studies, we have found that the combination of NBS (*N*-bromosuccinimide) and $FeBr_3$ in CH_2Cl_2 was good for the reaction with diphenylacetylene [16-19] to give 1,2-dibromo-1,2-diphenylethylene with high *E*-selectivity. The present method has some advantages. First, is mild reaction conditions, and second is stereoselective synthesis. In addition, we have found an easy purification and separation method of *E* and *Z* isomers of the crude product by using heptane. The method utilizes the difference in solubility of *E* and *Z* isomers. Because of this technique, the purification, separation, and scale-up were easy to perform. In this paper, we wish to report the details of the results.

Results and Discussion

In order to obtain the *E* isomer of 1,2-dibromo-1,2-diphenylethylene, we have examined the reaction regarding optimized conditions (Table 1). The typical procedure is as follows: the reaction of diphenylacetylene (**1a**, 0.5 mmol) with NBS (*N*-bromosuccinimide, X equiv), $FeBr_3$ (1.0 equiv), *n*-Bu_4NBr (Y equiv), and TEMPO (2,2,6,6-tetramethylpiperidine 1-oxyl free radical, Z equiv) in solvent (2 mL) at the desired temperature was conducted for 23 h or 2 h. After the reaction, the typical work-up procedure was carried out and the crude prod-

Table 1: Reaction optimization of bromination reaction of diphenylacetylene (**1a**).



Entry	NBS (X equiv)	*n*-Bu_4NBr (Y equiv)	TEMPO (Z equiv)	Temp. (°C)	Solvent	Ratio of ***E*-2a**/***Z*-2a**/**1a**[a]	Yield (%) of ***E*-2a**[b]
1[c]	2.2	0	0	rt	CH_2Cl_2	86:14:0	78
2[c,d]	**2.2**	**0**	**0**	**rt**	**CH_2Cl_2**	**87:13:0**	**78**
3[d]	1.2	0	0	rt	CH_2Cl_2	88:12:0	79
4	2.2	0	1.0	rt	CH_2Cl_2	91:8:1	77
5[d]	2.2	0.5	1.0	rt	CH_2Cl_2	80:2:18	73
6[d]	2.2	1.0	1.0	rt	CH_2Cl_2	55:0:45	47
7	2.2	1.0	0.2	rt	CH_2Cl_2	88:12:0	79
8	2.2	1.0	0.5	rt	CH_2Cl_2	78:2:20	68
9[e]	2.2	1.0	0	rt	CH_2Cl_2	82:18:0	72
10	2.2	1.0	0.5	40	CH_2Cl_2	85:3:12	70
11	2.2	1.0	0.5	60	$C_2H_8Cl_2$	72:3:25	63
12	2.2	0	0	rt	$C_2H_8Cl_2$	58:42:0	54

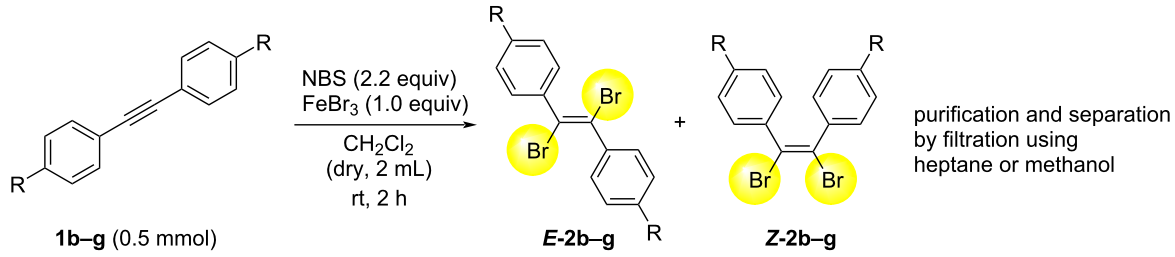
[a]Calculated from the ratio of HPLC area for the crude product. [b]Isolated yield of ***E*-2a** by filtration with heptane from the crude product. The yield of ***E*-2a** was obtained from the solids recovered after the filtration. [c]Reaction time was 2 hours. [d]Calculated from the ratio of GC area for the crude product. [e]Reaction time was 5 hours. $C_2H_8Cl_2$ = 1,2-dichloroethane.

uct was analyzed for the ratio of *E* and *Z* isomers and starting material **1a**, by using HPLC. Purification and separation from the crude product was conducted by the filtration using heptane (Table 1). At first, we have recognized that ***E*-2a** is solid and ***Z*-2a** is liquid in heptane. After various considerations, we found that ***E*-2a** could be isolated by only filtration, utilizing the difference in solubility of ***E*-2a** and ***Z*-2a** in heptane from the crude product.

In Table 1, entry 1, the combination of NBS (2.2 equiv) and $FeBr_3$ (1.0 equiv) for 2 h gave the ratio of ***E*-2a**/***Z*-2a**/**1a** such as 86:14:0 by HPLC, in which ***E*-2a** was obtained in 78% yield. Similarly, to examine the reproducibility of the chemical yield and the ratio of ***E*-2a**/***Z*-2a**/**1a** by GC analysis, Table 1, entry 2 was shown. The reaction time of 2 h gave the same ratio of ***E*-2a**/***Z*-2a**/**1a** by GC analysis, and ***E*-2*a*** was obtained in 78% yield (Table 1, entry 2). The use of a smaller amount of NBS (1.2 equiv) did not result in a decrease of yield, indicating that $FeBr_3$ is thought to be one of the sources of bromine (Table 1, entry 3). To increase the chemical yield and ratio of ***E*-2a**/***Z*-2a**/**1a**, various parameters such as NBS, *n*-Bu_4NBr, TEMPO, temperature, and solvent were examined (Table 1, entries 3–12). Because there was a possibility that a bromine radical was involved, TEMPO was used for the purpose of the ratio-control of *E* and *Z* isomers. TEMPO was found to have a tendency to suppress the generation of ***Z*-2a** in CH_2Cl_2 (Table 1, entries 6 and 8) [20]. Among Table 1, entries 5–11, the addition of *n*-Bu_4NBr did not seem to have any effect. Instead of CH_2Cl_2, $C_2H_8Cl_2$ (1,2-dichloroethane) was used as the solvent, but the yield of ***E*-2a** was decreased (Table 1, entries 11 and 12). Generally, decomposition of the product or over reaction was not observed by GC and/or GC–MS analysis, in the case of the longer reaction time of 23 h. We have examined other Lewis acids such as $ZnBr_2$, LiBr, and $FeBr_2$ instead of the use of $FeBr_3$ under similar reaction conditions. The use of $ZnBr_2$ for reaction time of 4 h showed a ratio of ***E*-2a**/***Z*-2a**/**1a** = 86:14:0 by HPLC analysis and 68% yield of ***E*-2a**. In the case of LiBr, the desired reaction progressed only slightly, even after two days, and the ratio of ***E*-2a**/***Z*-2a**/**1a** = 17:3:80 was indicated by GC analysis. In addition, the use of $FeBr_2$ for a reaction time of 3 h gave an ***E*-2a**/***Z*-2a**/**1a** ratio of 67:13:20 by GC analysis and 57% yield of ***E*-2a**. Based on these investigations, we have adopted the conditions of Table 1, entry 2, because better chemical yield of ***E*-2a** as well as a higher ratio of ***E*-2a**/***Z*-2a**/**1a** with short reaction time were attractive for chemical synthesis in the laboratory [21].

Next, we have investigated the scope and limitations by using various diarylacetylenes bearing the substituents on the benzene ring at *para*-position. The results were summarized in Table 2. Depending on the product's characteristics, either heptane or methanol was used for purification and separation. The reaction of 1,2-di-*p*-tolylethyne (**1b**) under the optimized conditions gave the corresponding product with a ratio of 68:32 of *E* and *Z* isomers. The isolated yield of ***E*-2b** was <54% yield (Table 2, entry 1). Likewise, 1,2-bis(4-(*tert*-butyl)phenyl)ethyne (**1c**) showed the similar tendency to give ***E*-2c** in 45% yield

Table 2: Scope and limitations for bromination of various diarylacetylenes **1**.



1b–g (0.5 mmol) ***E*-2b–g** ***Z*-2b–g**

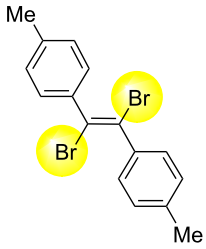
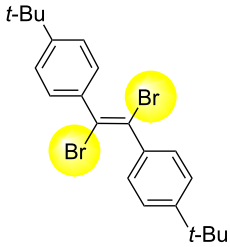
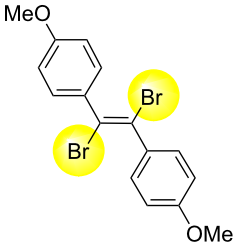
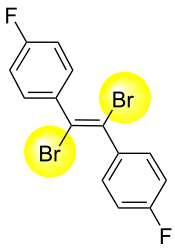
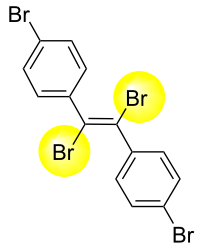
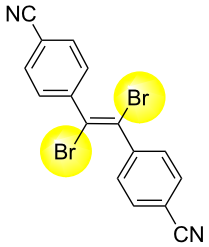
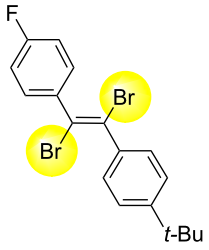
Entry	Product	Ratio of ***E*-2**/***Z*-2**[a]	Yield (%) of ***E*-2**
1[b]	 ***E*-2b**	68:32	<54[c]
2[b]	 ***E*-2c**	57:43	45
3[b]	 ***E*-2d**	82:18	75
4[b]	 ***E*-2e**	89:11	56

Table 2: Scope and limitations for bromination of various diarylacetylenes **1**. (continued)

5[d]	 ***E*-2f**	89:11	78
6[b]	 ***E*-2g**	82:18[e]	70
7[b]	 ***E*-2h**	78:22	41

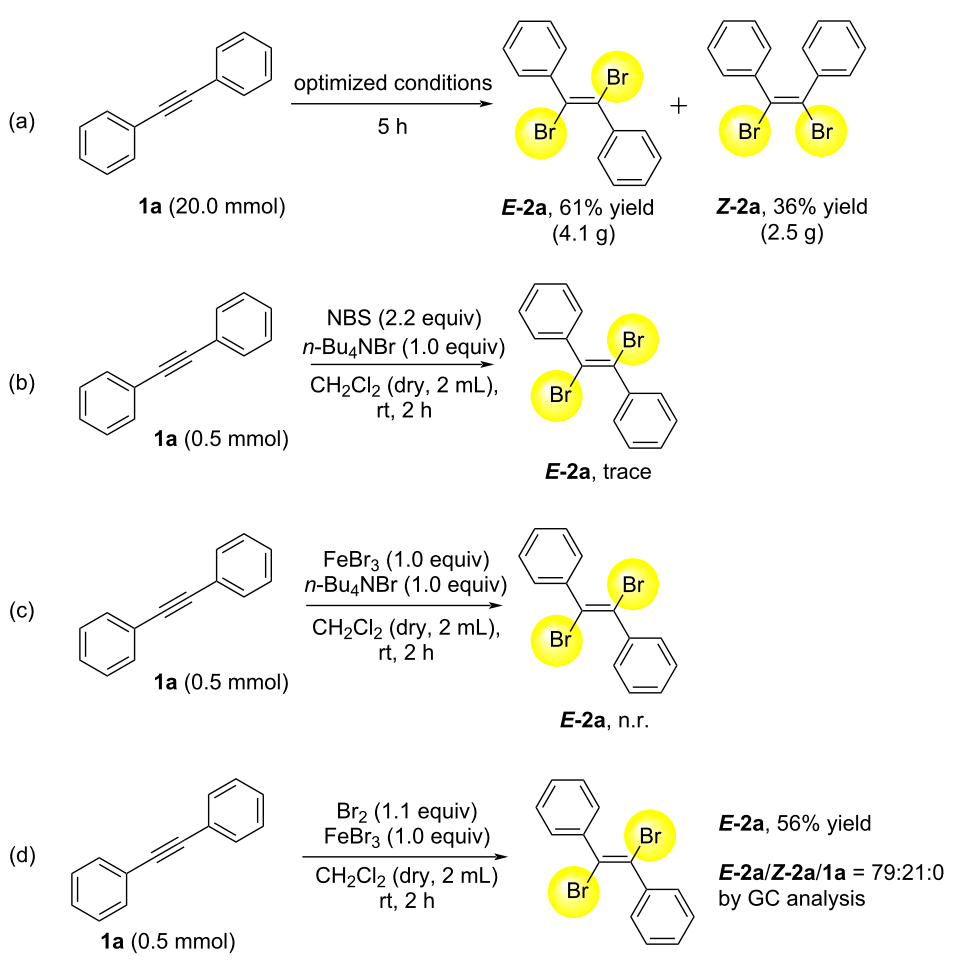
[a]Calculated from the ratio of GC area for crude product. [b]Isolated yield of *E*-isomer by filtration with methanol. [c]Because a small amount of impurity after the isolation was confirmed, the chemical yield was expressed as "<54% yield". See NMR spectra in Supporting Information File 1. [d]Isolated yield of *E*-isomer by filtration with heptane. [e]Calculated from the ratio of ^{1}H NMR for crude product.

(Table 2, entry 2). Poor selectivity as shown in entries 1 and 2 might be due to the stability of the intermediate. In the cases of Table 2, entries 3–6 residues such as MeO, F, Br and CN as the substituent at *para* position of the benzene ring in **1d**–**g**, the selectivity of *E* and *Z* and the isolated yield of the *E* isomer seemed to be good. In the case of unsymmetrical diarylacetylene, 1-(*tert*-butyl)-4-((4-fluorophenyl)ethynyl)benzene (**1h**) was tested and the corresponding ***E*-2h** was isolated and purified with MeOH. ***E*-2h** was obtained in 41% yield (Table 2, entry 7).

A gram-scale synthesis of ***E*-2a** and ***Z*-2a** from **1a** was performed (Scheme 2a). **1a** (20.0 mmol) was allowed to react under optimized conditions for 5 hours. The purification and separation by using heptane from the crude product afforded ***E*-2a** (4.1 g, 12.2 mmol, 61% yield) and ***Z*-2a** (2.5 g, 7.2 mmol, 36% yield), indicating that purification and separation by heptane make scale-up very easy. The *E*-selectivity was dropped in gram-scale synthesis, although the reason is unclear at present.

For the understanding of the reaction mechanism, some control experiments were carried out. The reaction of **1a** with NBS and n-Bu_4NBr without $FeBr_3$ gave trace amount of ***E*-2a** (Scheme 2b). In addition, the reaction of **1a** with $FeBr_3$ and n-Bu_4NBr without NBS showed no reaction (Scheme 2c). Instead of NBS, Br_2 (1.1 equiv) was reacted with **1a** and $FeBr_3$ (1.0 equiv) to give ***E*-2a** in 56% yield, with a ratio of ***E*-2a**/***Z*-2a**/**1a** = 79:21:0. These results indicate that the combination of NBS and $FeBr_3$ might be important and in situ Br_2 might be generated and formed. $FeBr_3$ might react with Br_2 to form $[FeBr_4]^-$ and "Br^+", which can react with **1a**.

As for the reaction mechanism, the plausible pathway might be the following (Scheme 3). The reaction of NBS and $FeBr_3$ might generate Br_2 or "Br^+", which can react with **1a** to form intermediate **A**. **A** reacts with Br^- to give ***E*-2a**. Another possibility is the reaction of NBS and $FeBr_3$ gives coordinated intermediate **B**, which can react with **1a** to give **A**, leading to the formation of ***E*-2a** [21,22]. Both pathways may be mixed together. One reason why *E* and *Z* isomers are formed together



Scheme 2: Gram-scale synthesis of (a), and control experiments of (b), (c) and (d). n.r. = no reaction.

might be due to the equilibrium between **A** and **C**, although there are many unknown points.

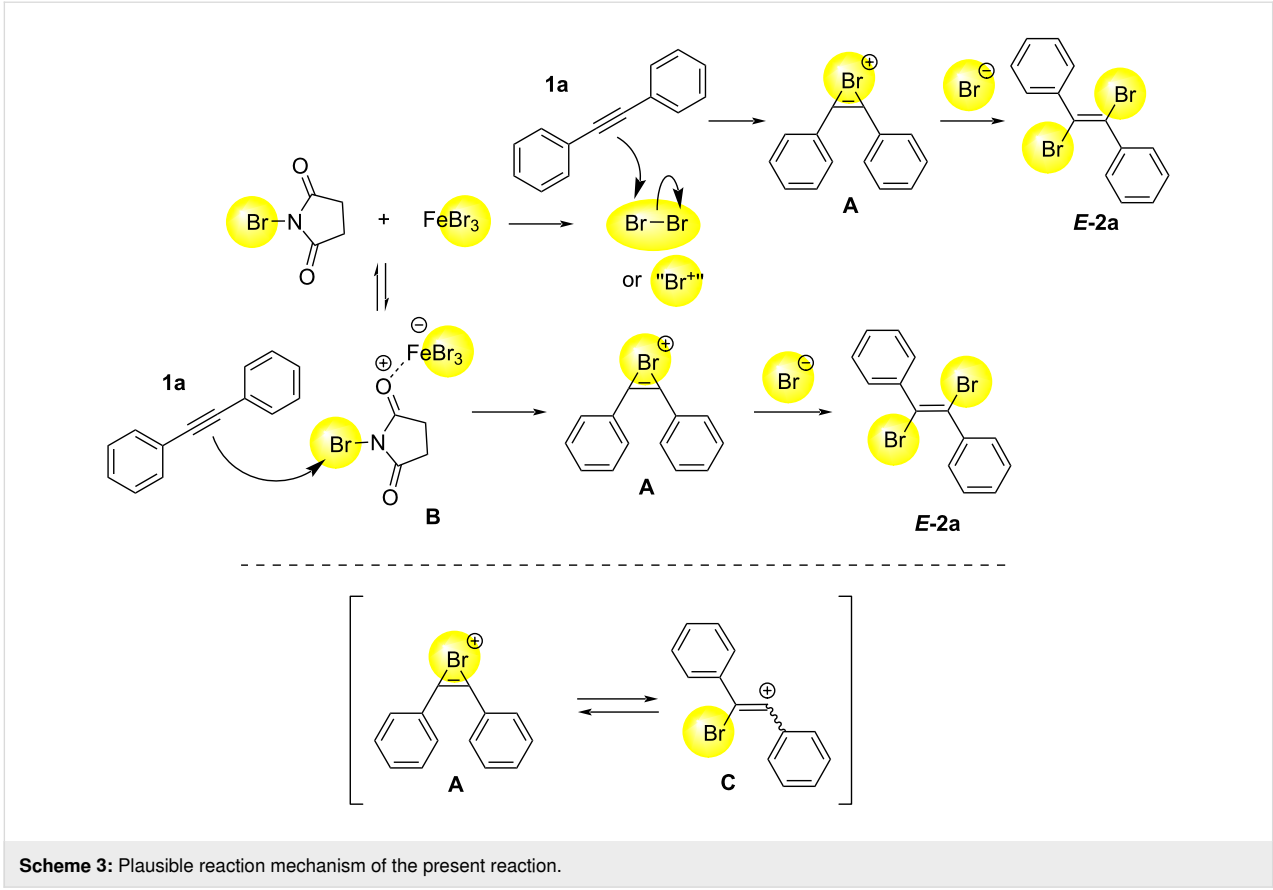
Conclusion

In summary, we have developed a simple and selective procedure of the synthesis of (*E*)-1,2-dibromo-1,2-diphenylethylene from diphenylacetylene by using NBS and $FeBr_3$ in CH_2Cl_2. In addition, heptane played an important and critical role for purification and separation of the crude product. Scope and limitations for bromination of various diarylacetylenes together with the gram-scale synthesis and control experiments were also investigated. These results and findings can contribute to process chemistry for the synthesis of (*E*)-1,2-dibromo-1,2-diphenylethylene and their derivatives. Further synthetic investigations are currently underway in our laboratory.

Experimental

The experimental procedures and characterization data (Table 1, entry 1). The glass flask was dried and heated by a heating gun. After cooled to room temperature, the flask was filled with N_2. $FeBr_3$ (154.2 mg, 0.52 mmol) and NBS (*N*-bromosuccinimide, 196.0 mg, 1.10 mmol) were added to the glass flask. Then, CH_2Cl_2 (dry, 2.0 mL) and 1,2-diphenylacetylene (**1a**, 89.4 mg, 0.502 mmol) were added and the mixture was stirred at room temperature for 2 hours. A 10% aqueous solution of $Na_2S_2O_3$ (20 mL) was added to stop the reaction. The mixture was extracted with CH_2Cl_2 (20 mL × 1), and separated. The aqueous phase was extracted with CH_2Cl_2 (20 mL × 2). The combined organic phase was washed with H_2O (20 mL) and brine (20 mL), and dried over Na_2SO_4. After this, filtration and concentration were performed; the organic phase was passed through a short column of silica gel using CH_2Cl_2 (100 mL) to remove inorganic materials and others; then it was concentrated under reduced pressure to give the crude product. This crude product was purified three times with heptane to obtain (*E*)-1,2-dibromo-1,2-diphenylethylene (***E*-2a**, 132.6 mg, 0.392 mmol, 78% yield) of high-purity.

(*E*)-1,2-Dibromo-1,2-diphenylethylene (*E*-2a) [4]: White solid. ^{1}H NMR (400 MHz, $CDCl_3$) δ 7.34–7.46 (m, 6H),



Scheme 3: Plausible reaction mechanism of the present reaction.

7.50–7.57 (m, 4H) ppm; ^{13}C NMR (100 MHz $CDCl_3$) δ 118.0, 128.4, 128.9, 129.1, 140.7 ppm; HRMS (ESI) *m/z*: $[M + Na]^+$ calcd for $C_{14}H_{10}Br_2Na$, 358.9041; found, 358.9028.

(*Z*)-1,2-Dibromo-1,2-diphenylethylene (*Z*-2a) [7]: Yellow solid. ^{1}H NMR (300 MHz, $CDCl_3$) δ 7.10–7.22 (m, 10H) ppm; ^{13}C NMR (75 MHz, $CDCl_3$) δ 125.7, 128.0, 128.3, 129.8, 139.4 ppm; HRMS (ESI) *m/z*: $[M + Na]^+$ calcd for $C_{14}H_{11}Br_2$, 336.9222; found, 336.9215.

Supporting Information

Supporting Information File 1

General remarks, preparation of substrates, experimental procedure, characterization data of compounds, and copies of ^{1}H and ^{13}C NMR spectra.
[https://www.beilstein-journals.org/bjoc/content/supplementary/1860-5397-22-61-S1.pdf]

Acknowledgements

We appreciate Kazuki Miyamoto, Junya Kikuzawa and Ryoichi Tomiyama at Kindai University for useful advice and the cooperation related to this paper. We also thank Akiko Kuwabara and Dr. Masafumi Kobayashi at Kanto Denka Kogyo Co., Ltd. for various supports in this work. Finally, we wish to express our acknowledgments for Kindai University Joint Research Center for use of facilities.

Funding

This work was financially supported in part by JSPS KAKENHI (JP24K08506) (Grant-in-Aid for Scientific Research [C]) and 2025 Kindai University Research Enhancement Grant (KD2501).

Author Contributions

Akane Togo: conceptualization; data curation; formal analysis; investigation; methodology; writing – original draft. Hiyono Suzuki: conceptualization; formal analysis; investigation; methodology. Yuto Akai: formal analysis; methodology; supervision; validation. Makoto Matsumoto: formal analysis; methodology; supervision; validation. Yoshinori Suzuma: methodology; project administration; supervision. Hidehiko Kodama: funding acquisition; methodology; project administration; supervision. Kouichi Matsumoto: conceptualization; funding acquisition; methodology; project administration; supervision; validation; visualization; writing – original draft.

ORCID® iDs

Kouichi Matsumoto - https://orcid.org/0000-0003-2592-7403

Data Availability Statement

All data that supports the findings of this paper is available in the published article and/or the supporting information to this article.

References

1. Saikia, I.; Borah, A. J.; Phukan, P. *Chem. Rev.* **2016,** *116,* 6837–7042. doi:10.1021/acs.chemrev.5b00400
   See for a review of bromination to carbon–carbon multiple bonds.
2. Gombos, L. G.; Waldvogel, S. R. *Sustainable Chem.* **2022,** *3,* 430–454. doi:10.3390/suschem3040027
   See for a review of bromination to carbon–carbon multiple bonds.
3. Espenson, J. H.; Zhu, Z.; Zauche, T. H. *J. Org. Chem.* **1999,** *64,* 1191–1196. doi:10.1021/jo9817164
4. Schuh, K.; Glorius, F. *Synthesis* **2007,** 2297–2306. doi:10.1055/s-2007-983782
5. Adimurthy, S.; Ghosh, S.; Patoliya, P. U.; Ramachandraiah, G.; Agrawal, M.; Gandhi, M. R.; Upadhyay, S. C.; Ghosh, P. K.; Ranu, B. C. *Green Chem.* **2008,** *10,* 232–237. doi:10.1039/b713829f
6. Ma, K.; Li, S.; Weiss, R. G. *Org. Lett.* **2008,** *10,* 4155–4158. doi:10.1021/ol801327n
   See for other examples of bromination for diphenylacetylene.
7. Yao, M.-L.; Kabalka, G. W.; Blevins, D. W.; Reddy, M. S.; Yong, L. *Tetrahedron* **2012,** *68,* 3738–3743. doi:10.1016/j.tet.2012.03.016
   See for other examples of bromination for diphenylacetylene.
8. Sohmiya, H.; Kimura, T.; Fujita, M.; Ando, T. *Tetrahedron* **1998,** *54,* 13737–13750. doi:10.1016/s0040-4020(98)00844-8
   See for other examples of bromination for diphenylacetylene.
9. Windmon, N.; Dragojlovic, V. *Tetrahedron Lett.* **2008,** *49,* 6543–6546. doi:10.1016/j.tetlet.2008.09.007
   See for other examples of bromination for diphenylacetylene.
10. Cristiano, R.; Ma, K.; Pottanat, G.; Weiss, R. G. *J. Org. Chem.* **2009,** *74,* 9027–9033. doi:10.1021/jo901735h
    See for other examples of bromination for diphenylacetylene.
11. Dağalan, Z.; Koçak, R.; Daştan, A.; Nişancı, B. *Org. Lett.* **2022,** *24,* 8261–8264. doi:10.1021/acs.orglett.2c02627
    See for other examples of bromination for diphenylacetylene.
12. Podgoršek, A.; Eissen, M.; Fleckenstein, J.; Stavber, S.; Zupan, M.; Iskra, J. *Green Chem.* **2009,** *11,* 120–126. doi:10.1039/b814989e
    See for other examples of bromination for diphenylacetylene.
13. Okumura, H.; Prakoso, N. I.; Morozumi, T.; Umezawa, T. *Org. Lett.* **2024,** *26,* 9817–9821. doi:10.1021/acs.orglett.4c03483
    See for other examples of bromination for diphenylacetylene.
14. Muathen, H. A. *Synth. Commun.* **2004,** *34,* 3545–3552. doi:10.1081/scc-200031007
    See for other examples of bromination for diphenylacetylene.
15. Cho, E.; Jayaraman, A.; Lee, J.; Ko, K. C.; Lee, S. *Adv. Synth. Catal.* **2019,** *361,* 1846–1858. doi:10.1002/adsc.201801535
    See for other examples of bromination for diphenylacetylene.
16. Hamasaki, K.; Tomiyama, R.; Yoneyama, S.; Xu, P.; Matsumoto, K. *Electrochemistry* **2024,** *92,* 107002. doi:10.5796/electrochemistry.24-00079
    See for selected examples of the development of synthetic procedures of diphenylacetylene or diarylacetylenes by our group.
17. Suzuki, H.; Togo, A.; Kikuzawa, J.; Miyamoto, K.; Marumoto, S.; Kuwabara, A.; Kobayashi, M.; Matsumoto, K. *Chem. Lett.* **2024,** *53,* upae079. doi:10.1093/chemle/upae079
    See for selected examples of the development of synthetic procedures of diphenylacetylene or diarylacetylenes by our group.
18. Fujiki, Y.; Suzuki, H.; Kikuzawa, J.; Nishiwaki, K.; Kawashita, N.; Matsuoka, J.; Nakamura, A.; Maegawa, T.; Kuwabara, A.; Kobayashi, M.; Matsumoto, K. *Chem. Lett.* **2024,** *53,* upae043. doi:10.1093/chemle/upae043
    See for selected examples of the development of synthetic procedures of diphenylacetylene or diarylacetylenes by our group.
19. Miyamoto, K.; Kikuzawa, J.; Togo, A.; Fujiki, Y.; Kawashita, N.; Matsumoto, K. *Bull. Chem. Soc. Jpn.* **2025,** *98,* uoaf025. doi:10.1093/bulcsj/uoaf025
    See for selected examples of the development of synthetic procedures of diphenylacetylene or diarylacetylenes by our group.
20. Kong, Y.; Cao, T.; Zhu, S. *Chin. J. Chem.* **2021,** *39,* 3004–3010. doi:10.1002/cjoc.202100472
21. Zheng, Y. F.; Yu, J.; Yan, G. B.; Li, X.; Luo, S. *Chin. Chem. Lett.* **2011,** *22,* 1195–1198. doi:10.1016/j.cclet.2011.05.005
22. Catano, B.; Lee, J.; Kim, C.; Farrell, D.; Petersen, J. L.; Xing, Y. *Tetrahedron Lett.* **2015,** *56,* 4124–4127. doi:10.1016/j.tetlet.2015.05.039

License and Terms

This is an open access article licensed under the terms of the Beilstein-Institut Open Access License Agreement (https://www.beilstein-journals.org/bjoc/terms), which is identical to the Creative Commons Attribution 4.0 International License (https://creativecommons.org/licenses/by/4.0). The reuse of material under this license requires that the author(s), source and license are credited. Third-party material in this article could be subject to other licenses (typically indicated in the credit line), and in this case, users are required to obtain permission from the license holder to reuse the material.

The definitive version of this article is the electronic one which can be found at:
https://doi.org/10.3762/bjoc.22.61

BEILSTEIN JOURNAL OF ORGANIC CHEMISTRY

Beyond a solvent: HFIP as a game-changing medium in heterocyclic ring construction

Laxman M. Alakonda[1], Ravi Varala[*2,3,4], Vittal Seema[5] and Mohammed Mujahid Alam[6]

Review

Open Access

Address:
[1]School of Pharmacy, College of Health Sciences, University of Wyoming, Laramie, WY 82071, USA, [2]Scrips Pharma, Mallapur, Hyderabad 500076, Telangana, India, [3]Research Fellow in Health Sciences, INTI International University, 71800 Nilai, Malaysia, [4]Research Fellow, Shinawatra University, Pathum Thani 12160, Thailand, [5]Department of Chemistry, Rajiv Gandhi University of Knowledge Technologies (RGUKT), Basar, Nirmal-504107, Telangana, India and [6]Department of Chemistry, College of Science, King Khalid University, Abha, 61421, Saudi Arabia

Email:
Ravi Varala[*] - ravivarala@gmail.com

* Corresponding author

Keywords:
additive; catalyst; heterocycles; HFIP (hexafluoroisopropanol); reaction medium

Beilstein J. Org. Chem. **2026,** *22,* 1425–1468.
https://doi.org/10.3762/bjoc.22.116

Received: 30 May 2026
Accepted: 30 September 2026
Published: 14 October 2026

This article is part of the thematic issue "Green chemistry III: Technologies shaping future directions in synthesis".

Associate Editor: L. Vaccaro



© 2026 Alakonda et al.; licensee Beilstein-Institut.
License and terms: see end of document.

Abstract

1,1,1,3,3,3-Hexafluoroisopropanol (HFIP) has emerged as one of the most powerful and versatile solvents in modern organic synthesis owing to its exceptional hydrogen-bond-donating ability, low nucleophilicity, high ionizing power, and remarkable capacity to stabilize ionic and radical intermediates. These unique physicochemical properties enable HFIP to facilitate proton transfer, activate otherwise unreactive bonds, and promote a wide range of intermolecular interactions, making it highly valuable in heterocycle synthesis. Over the past decade, the application of HFIP has expanded significantly, particularly in C–H functionalization and heterocyclic ring construction, where it frequently acts not only as a solvent but also as a promoter, cocatalyst, and reaction-directing medium. In this review, we comprehensively and critically summarize the latest representative advances in HFIP-enabled heterocyclic ring formation reported from 2022 to 2025. Particular emphasis is placed on mechanistic understanding, synthetic efficiency, substrate scope, and the multifunctional role of HFIP in controlling chemo-, regio-, and stereoselectivity. HFIP-mediated transformations often proceed under mild, metal-free, oxidant-free, or redox-neutral conditions and enable challenging cyclizations, annulations, dearomatizations, rearrangements, and cross-dehydrogenative coupling reactions that are difficult to achieve using conventional solvents. Mechanistic discussions throughout the review highlight the ability of HFIP to stabilize cationic, radical, and transition-state intermediates through extensive hydrogen-bonding networks and cooperative interactions with catalysts or reagents. For clarity, the review is organized according to the structural classes of the target heterocycles and the nature of the synthetic strategies employed. The review focuses on the construction of simple five-membered heterocycles; fused heterocyclic systems, including five–six- and six–six-fused frameworks and polycyclic fused architectures; spiro heterocycles, including five–five- and

five–six-spiro systems generated through radical, ionic, electrochemical, and dearomative cascade processes; and saturated and non-aromatic heterocycles, encompassing three-, five-, six-, seven-, and nine-membered rings, mixed five-/six-membered frameworks, and polyfused saturated systems. Overall, this review demonstrates that HFIP has evolved far beyond a conventional fluorinated solvent and now serves as a powerful reaction-enabling platform in modern heterocyclic chemistry. By critically comparing recent methodologies and mechanistic paradigms, this review aims to provide a unified perspective on the expanding role of HFIP and inspire future developments in sustainable heterocycle synthesis.

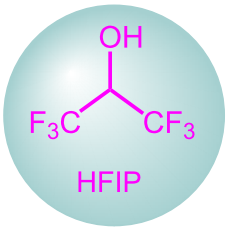
Introduction

Fluorinated solvents have attracted increasing attention in recent years as specialized reaction media and co-solvents [1]. Among them, fluorinated alcohols exhibit distinctive physicochemical properties, including strong hydrogen-bond-donating ability, high polarity, and, depending on their molecular structure, varying degrees of water miscibility and volatility [2-4]. In particular, 1,1,1,3,3,3-hexafluoro-2-propanol (HFIP) is widely used in organic synthesis and allows facile product isolation [5]. Its high polarity and strong hydrogen-bond-donating ability promote the formation and stabilization of cationic intermediates, facilitating their reaction with nucleophiles [6]. The electron-withdrawing $-CF_3$ groups also increase the acidity of the hydroxy proton, while fluorinated alcohols are weak nucleophiles and poor hydrogen-bond acceptors. Consequently, they exhibit reduced self-association compared with conventional alcohols [7].

Figure 1 summarizes the key physicochemical properties and diverse applications of HFIP. HFIP ($C_3H_2F_6O$; MW 168.038 $g{\cdot}mol^{-1}$) is a colorless, highly volatile liquid (density 1.596 $g{\cdot}mL^{-1}$; bp 58.2 °C) with strong hydrogen-bond-donating ability, high polarity, and moderate acidity ($pK_a \approx 9.3$). These properties make HFIP a useful specialty solvent and reaction-promoting medium in organic synthesis, as well as in biochemistry, analytical chemistry, and electrochemistry. It can also stabilize reactive intermediates and enhance reaction efficiency in various transformations.

A key advantage of HFIP and related fluorinated alcohols is their ability to promote reactions that would otherwise require catalysts or Lewis acids [8]. HFIP is a strong hydrogen-bond donor, as demonstrated by calorimetric and spectroscopic studies, as well as by the formation of stable complexes with various nucleophiles. With a boiling point of 58 °C, HFIP combines strong hydrogen-bond-donating ability, high ionizing power, moderate acidity ($pK_a \approx 9.3$), and relatively low nucleophilicity [9]. Its strong hydrogen bonding with carbonyl groups can activate C=O bonds and enhance their electrophilic character. These properties arise from its high hydrogen-bond donor strength (α = 1.96), polarity (Ps = 11.08), and ionizing ability (YOTs = 3.79).

Owing to its unique combination of physicochemical properties, HFIP is often described as a “magic solvent” and has been widely applied across organic synthesis [10-21], photochemistry [22], electrochemistry [23], etc. Its use in organic synthesis has increased rapidly in recent years and continues to grow. HFIP exhibits several distinctive features, including strong



IUPAC name: 1,1,1,3,3,3-hexafluoropropan-2-ol
MF: $C_3H_2F_6O$
MW: 168.038 g/mol
appearence: colorless liquid
density: 1.596 g/mL
boiling point: 58.2 °C

Chemical properties:
Preparation: $(CF_3)_2CO + H_2 \rightarrow (CF_3)_2CHOH$
Applications:
Organic synthesis: HFIP is widely used as a specialty solvent for reactions involving oxidations and strong electrophiles, enhancing reactivity in transformations such as Baeyer–Villiger oxidation and Lewis acid-catalyzed epoxide ring opening.
Reaction promotion: Its strong hydrogen-bonding ability, high polarity, and acidity ($pK_a \approx 9.3$) help stabilize intermediates and increase reaction efficiency.
Biochemistry: Used to solubilize and disrupt β-sheet protein aggregates, enabling studies of protein structure and aggregation
Analytical chemistry: Serves as a volatile acidic component in ion-pair HPLC-MS for the analysis of nucleic acids
Electrochemistry: Investigated as a solvent for electrolysis due to its unique physicochemical properties

Figure 1: Structural features, preparation, and applications of HFIP.

hydrogen-bond donating ability, high polarity with low nucleophilicity, significant Brønsted acidity, excellent ion (particularly carbocation) stabilizing capability, strong solvation power, redox stability, and ease of recovery and recyclability. Collectively, these properties enable efficient synthetic transformations, often under catalyst-free and mild reaction conditions.

Environmental, toxicological, and safety considerations of HFIP

Despite its useful properties, HFIP should not be considered inherently a green solvent. Its highly fluorinated nature raises environmental concerns related to solvent production, persistence, waste management, and disposal. HFIP is also volatile and requires appropriate handling to minimize exposure, including the use of a fume hood and suitable personal protective equipment. Fluorinated solvent waste should be collected and disposed of according to applicable institutional and regulatory requirements.

Therefore, the sustainability of HFIP-based processes should be evaluated beyond reaction efficiency, considering solvent quantity, recovery and recycling, energy use, and waste generation. While HFIP can offer significant advantages in reactivity and selectivity, these benefits should be balanced against its environmental and safety considerations.

The growing significance of HFIP has also been reflected in several comprehensive reviews. Solyev summarized HFIP-mediated C–H functionalization strategies [24], while Aubé and co-workers provided an extensive overview of its applications in organic synthesis [25]. More recently, Gao and co-workers updated the progress in homogeneous catalytic reactions involving HFIP [26].

Review

The role of HFIP in the heterocyclic ring formations

Five-membered heterocyclic rings

Synthesis of 3-acyl-1,4-diaryl/alkylpyrroles: A catalyst-free, microwave-assisted multicomponent strategy has been developed by Siddaiah and co-workers for the synthesis of 1,3,4-trisubstituted pyrroles **4** from 3-(dimethylamino)propenones **2**, amines **1**, and α-bromoketones **3** using recyclable HFIP [27] (Scheme 1). This protocol provides a simple and efficient approach, affording the desired products in 1 h with yields ranging from 52% to 99%. A key advantage of this methodology is the use of HFIP as a reusable reaction medium under microwave irradiation, enabling a catalyst-free multicomponent transformation for the efficient synthesis of 3-acyl-1,4-di(hetero)aryl/(cyclo)alkylpyrroles.

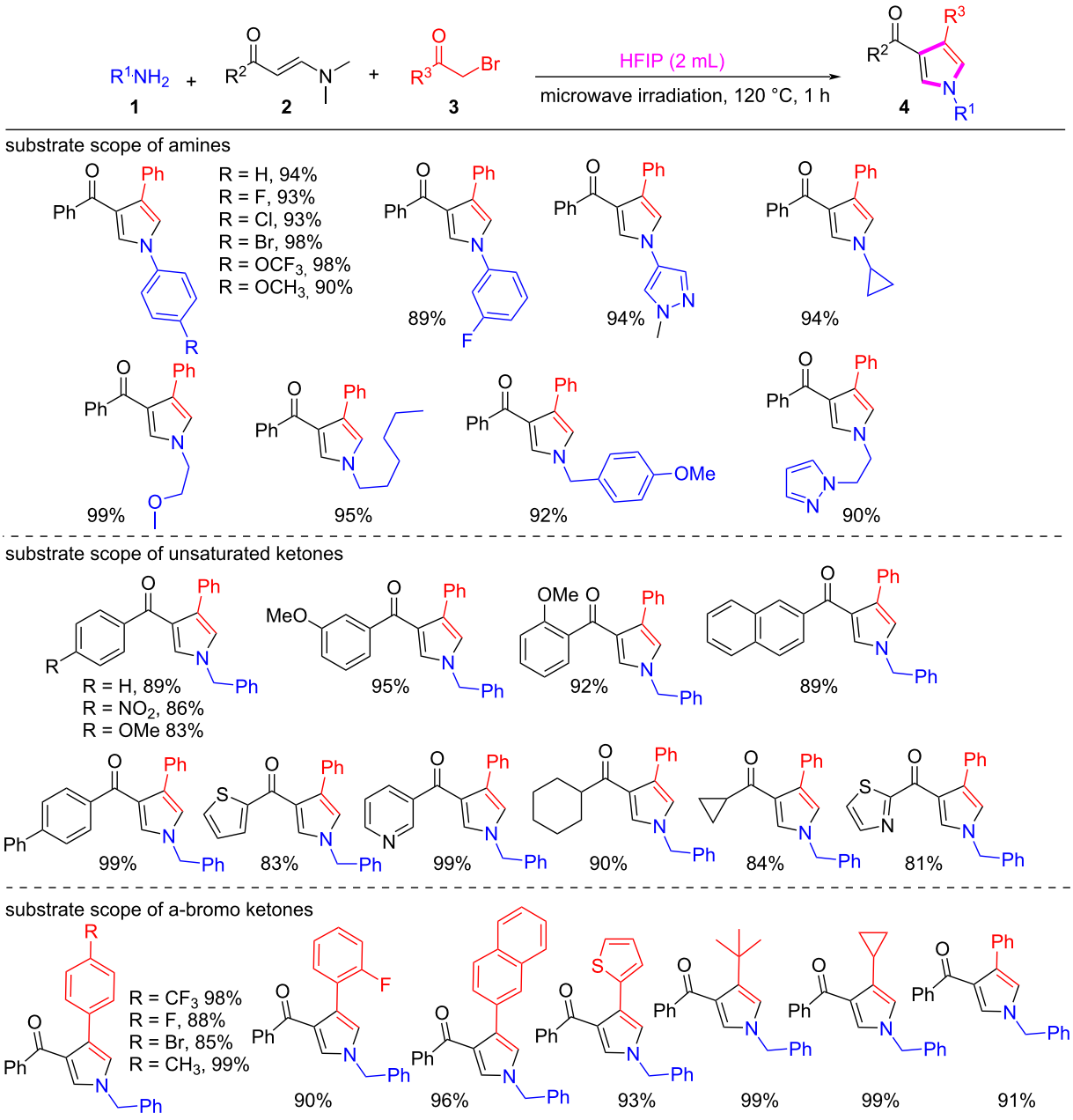
The substrate scope demonstrates broad functional-group tolerance across all three reaction components (Scheme 1). Aromatic amines bearing either electron-withdrawing or electron-donating substituents generally afforded good to excellent yields, although *ortho*-substituted fluoroaniline showed diminished reactivity, likely due to steric effects. In contrast, heteroaryl, cycloalkyl, and aliphatic amines consistently produced pyrroles in high yields, underscoring the versatility of the protocol. Similarly, diverse 3-(dimethylamino)propenones and α-bromoketones containing electron-rich, electron-deficient, heteroaryl, alkyl, and cycloalkyl substituents were well tolerated, furnishing polysubstituted pyrroles in excellent yields, often approaching quantitative conversion. Notably, substituent position on the aromatic ring exerted minimal influence on the reaction outcome, further supporting the robustness of the method.

Synthesis of furan derivatives: A mild metal-free protocol employing *p*-TSA (*para*-toluenesulfonic acid) in HFIP has been developed by Nguyen and Pu for the cyclization of ynones **5** into 2-aryl-3-carboxylate ester furans and 2,3-diarylfurans **6** (Scheme 2a) [28]. This methodology proceeds under relatively mild conditions and affords the desired products in good to excellent yields (up to 94%). The operational simplicity of the protocol is notable, as reactions generally produced clean mixtures with minimal byproducts and required no extensive workup prior to purification.

Substrate scope studies revealed broad tolerance toward structurally diverse ynones, although substrate electronics strongly influenced reaction efficiency. The substrate scope revealed a dependence of the reaction yield on the electronic nature of the substituents; however, no consistent correlation between electron-rich or electron-deficient substrates and higher yields was observed. In particular, α-carboxyloxy ynones initially exhibited lower conversions under room-temperature conditions, but increasing either the reaction time or temperature substantially improved yields, demonstrating the adaptability of the method. In contrast, electron-rich 2,3-diarylfurans could be synthesized efficiently even under ambient conditions (Scheme 2a).

Mechanistically, HFIP appears to play a dual role as a highly ionizing, hydrogen-bond-donating solvent and as an activator of *p*-TSA, effectively enhancing its Brønsted acidity. The reaction is proposed to proceed through protonation of the enolized ynone, followed by formation of a carbocation intermediate **I** and subsequent 5-*exo*-*dig* cyclization **II** to furnish the furan core after aromatization (Scheme 2b).

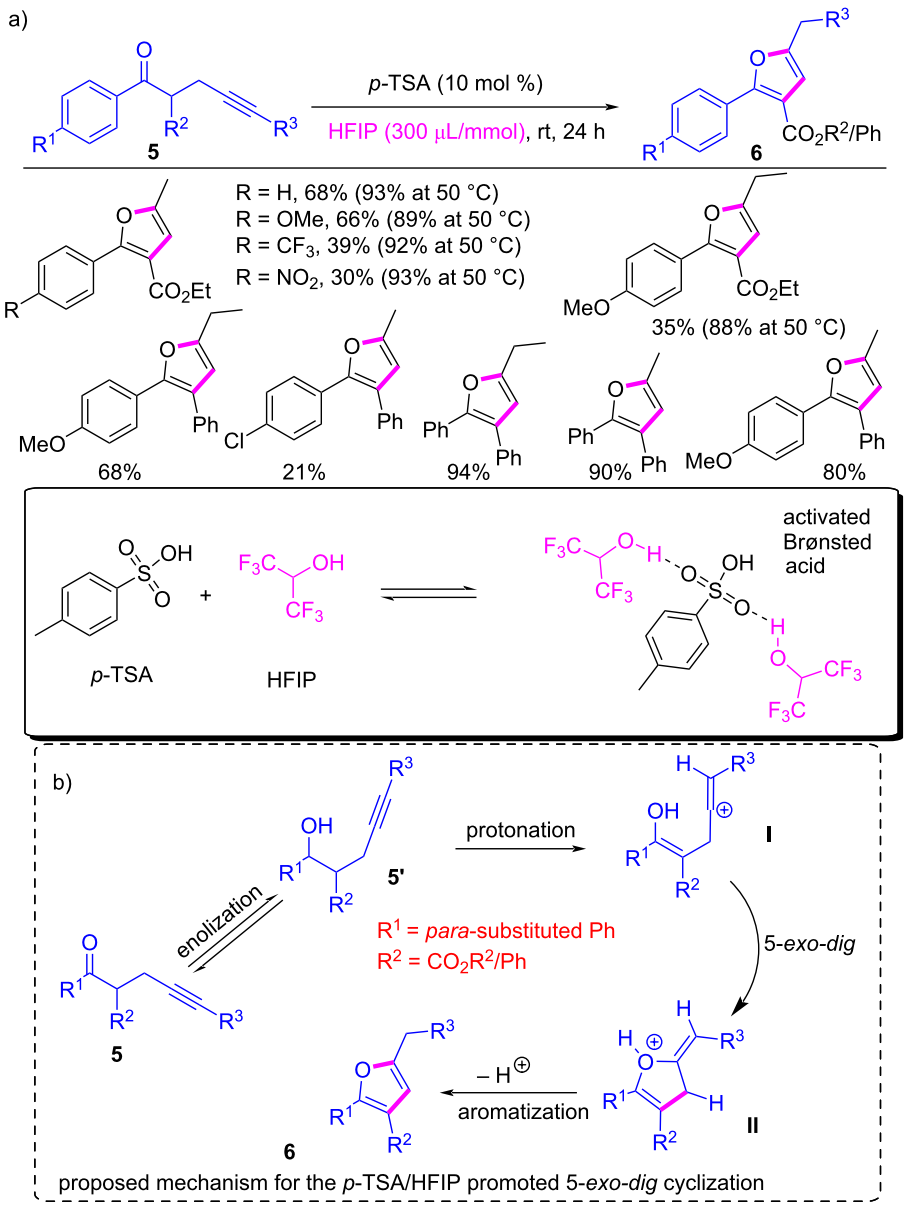
Synthesis of 3,4-fused fully substituted furan derivatives: Nitrones are versatile synthetic intermediates widely employed in the rapid assembly of structurally complex molecules rele-



Scheme 1: Synthesis of 3-acyl-1,4-diaryl/alkyl pyrroles **4**.

vant to pharmaceutical and materials chemistry [29]. In this context, a Rh(I)-catalyzed and HFIP-assisted cascade annulation of 1,*n*-diynyl nitrones **7** has been developed by Rao and co-workers for the synthesis of fully substituted furans **8** fused to diverse 5–8 membered carbocycles, heterocycles, and spirocycles (Scheme 3a) [30].

The transformation proceeds through a complex cascade sequence involving Rh(I)-mediated oxycyclization, N–O bond cleavage, and generation of an α-oxo rhodium carbene intermediate, followed by carbene-assisted migration (CAM), heterocyclization, and hydrolysis. Mechanistic studies suggest that HFIP plays a crucial role through hydrogen-bonding interactions with organorhodium intermediates, suppressing competing azomethine ylide pathways and instead promoting an unprecedented CAM/heterocyclization sequence leading to fused furan frameworks. This highlights the unique ability of HFIP to modulate organometallic reactivity beyond its conventional solvent role. This cascade annulation offers a highly modular and structurally diverse route to fused and spirocyclic furan archi-

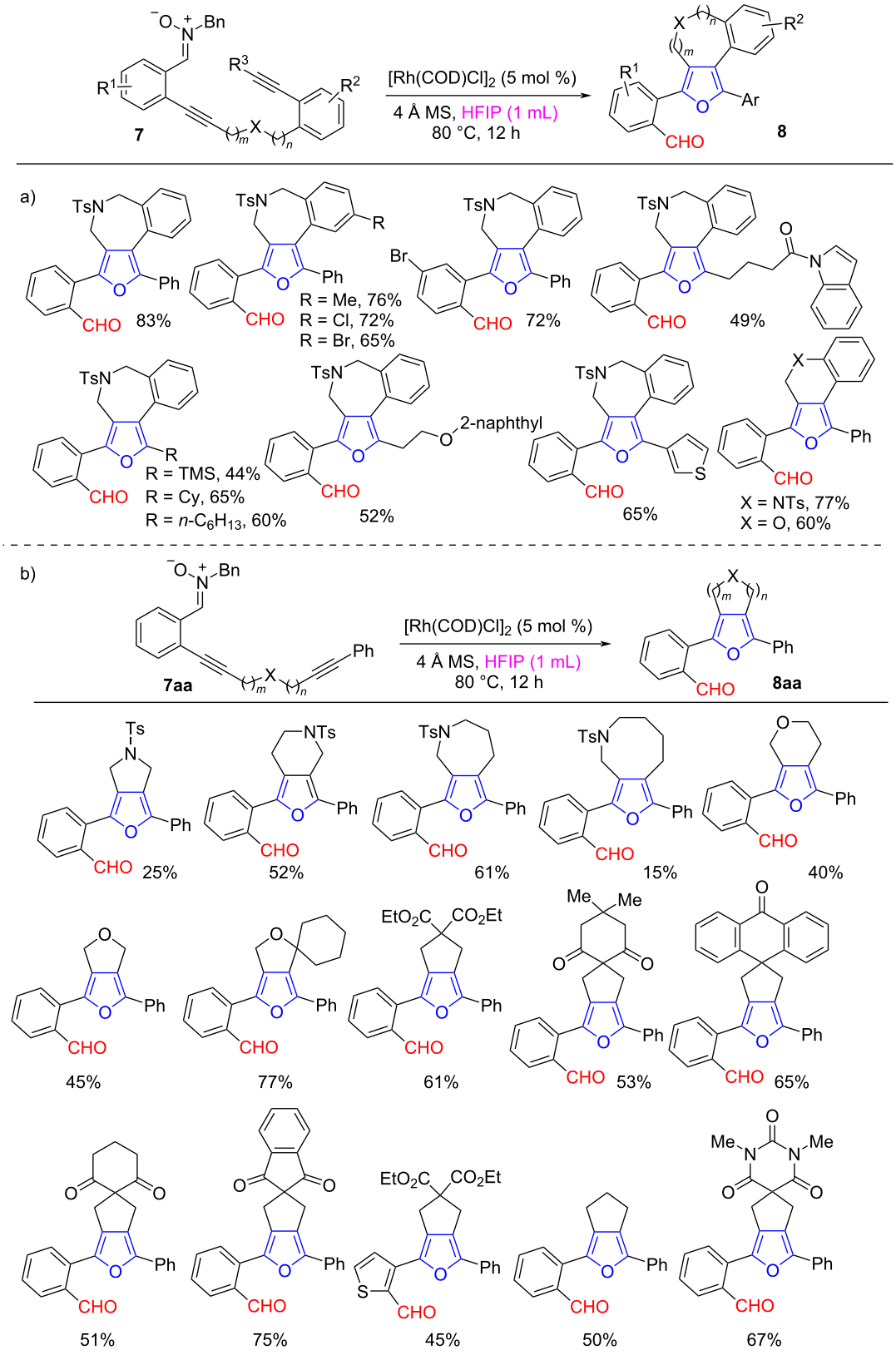


Scheme 2: Substrate scope for the synthesis of furan derivatives and proposed mechanism.

tectures in a single operation. The combination of Rh(I) catalysis and HFIP-assisted pathway control enables access to reactivity patterns that are otherwise difficult to achieve, while the scalability and downstream functionalization of the products further underscore the synthetic utility of the methodology.

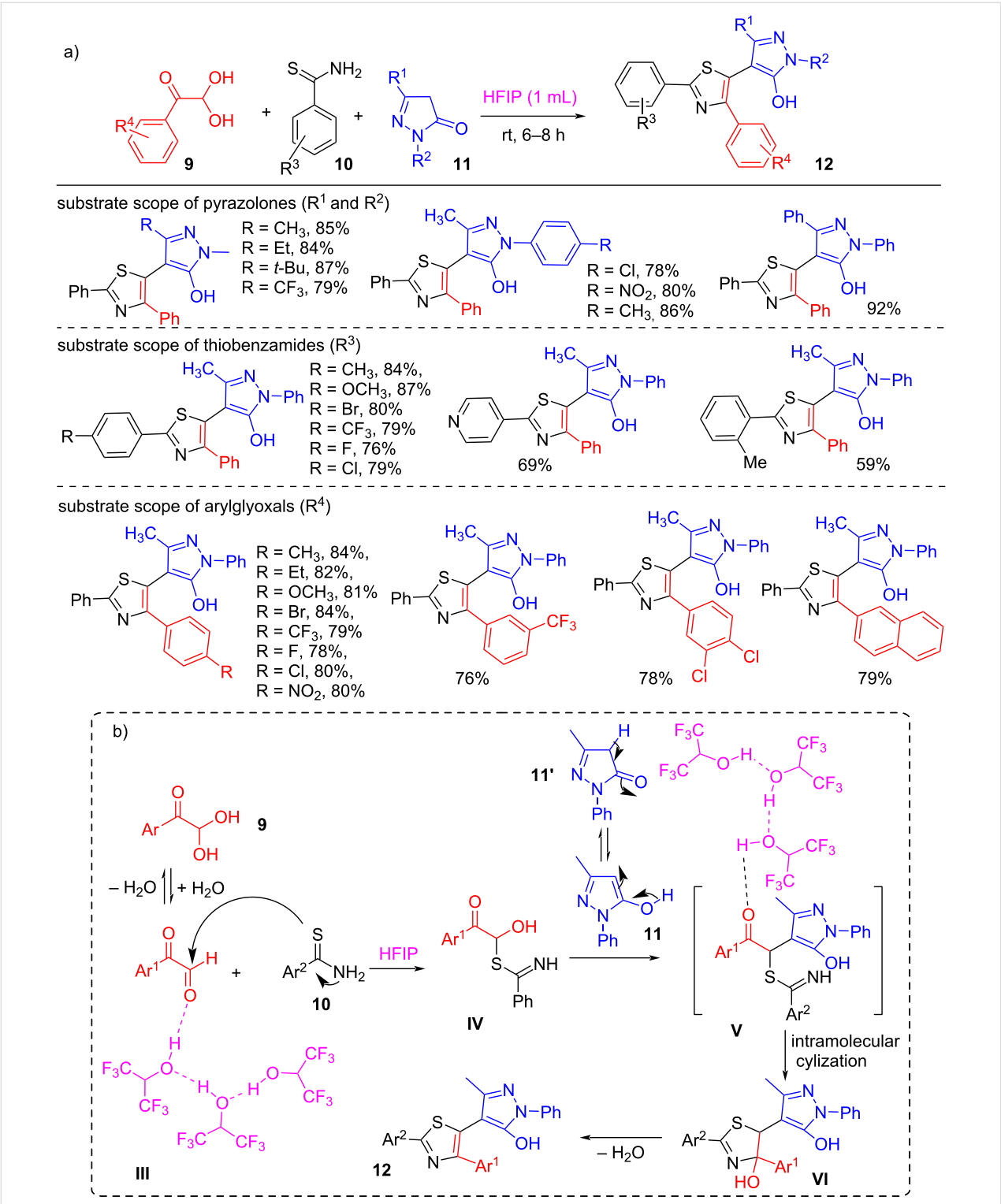
The methodology demonstrates a broad substrate scope and accommodates a wide range of tether architectures and functional groups (Scheme 3b). N- and O-tethered diynyl nitrones **7aa** efficiently furnish fused furans **8aa** containing zepine, chromene, pyridine, pyran, tetrahydrofuran, cyclopentene, and spirocyclic motifs in moderate to good yields. Substrates bearing alkyl, cycloalkyl, heteroaryl, sulfone, sulfonamide, ester, hydroxy, and ferrocenyl substituents are all well tolerated. In contrast, terminal alkynes and larger ring-forming substrates such as certain 1,9-diynyl systems provide diminished yields, likely due to unfavorable entropic and transannular effects during cyclization. The protocol is also applicable to late-stage functionalization, as demonstrated by annulation of estrone-derived substrates to generate structurally complex furanyl derivatives.

Synthesis of pyrazole-linked thiazole derivatives: Thiazoles are important sulfur- and nitrogen-containing heterocycles



Scheme 3: a) Rhodium(I)-catalyzed cascade annulation of benzene-tethered 1,*n*-diynyl nitrones. b) Rhodium(I)-catalyzed cascade annulation of alkyl-tethered 1,*n*-diynyl nitrones.

widely encountered in natural products, pharmaceuticals, and functional materials [31]. In this context, a green multicomponent protocol has been developed by Choudhury and co-workers for the synthesis of pyrazole-linked thiazoles **12** using arylglyoxals **9**, aryl thioamides **10**, and pyrazolones **11** in HFIP under room temperature and additive-free conditions (Scheme 4a) [32]. Compared with conventional thiazole syntheses that often require elevated temperatures, catalysts, or multi-



Scheme 4: a) Substrate scope of pyrazolones. b) Proposed mechanism for the products **12**.

step procedures, this methodology proceeds under remarkably mild conditions while efficiently constructing multiple C–C, C–N, and C–S bonds in a single operation. The protocol also demonstrates broad applicability, furnishing structurally diverse thiazole-linked pyrazoles **12** in good to excellent yields, and can be extended to the synthesis of thiazole-linked barbiturates and imidazole-linked pyrazoles **12**. The present approach offers several advantages from a green chemistry perspective, including room temperature operation, metal- and additive-free conditions, high atom economy, water as the sole byproduct, solvent recyclability, and operational simplicity. The absence of chromatographic purification further enhances its practicality and scalability.

Substrate scope investigations revealed good tolerance toward electronically diverse pyrazolones, aryl thioamides, and arylglyoxals. Both electron-donating and electron-withdrawing substituents on thioamides and arylglyoxals generally afforded the desired products in high yields, indicating the robustness of the transformation. However, pyridyl and *ortho*-substituted thioamides showed comparatively lower reactivity, likely due to electronic and steric effects, respectively, whereas aliphatic thioamides were ineffective under the optimized conditions. In contrast, substituent variation on arylglyoxals had minimal influence on product yields, and even aliphatic glyoxals were compatible, further highlighting the versatility of the protocol (Scheme 4a).

Mechanistically, HFIP is proposed to play a crucial role by activating the glyoxal substrate through hydrogen bonding **III** and facilitating formation of key intermediates prior to intramolecular cyclization **V** and dehydration **VI** to yield the product **12** (Scheme 4b).

Synthesis of 4-aryl-*NH*-1,2,3-triazoles and 1,5-disubstituted 1,2,3-triazolyl glycoconjugates: 1,2,3-Triazoles constitute an important class of nitrogen-containing heterocycles widely employed in medicinal chemistry, materials science, and chemical biology because of their remarkable stability and diverse biological activities [33]. Consequently, the development of efficient, metal-free, and regioselective methods for triazole synthesis remains an active area of research. In this regard, an HFIP-promoted multicomponent strategy has been developed by Tiwari and co-workers for the synthesis of *N*-unsubstituted **16** and *N*-substituted 1,2,3-triazoles **18** from aldehydes **13**, nitromethane (**14**), and sodium azide (**15**) or glycosyl azides **17** (Scheme 5) [34]. This methodology enables sequential formation of one C–C and two C–N bonds in a single operation under metal-free conditions. The protocol proceeds with high regioselectivity, gram-scale applicability, operational simplicity, and broad functional-group tolerance while providing the desired triazoles in generally good to excellent yields. Herein, HFIP provides the required mildly acidic environment to achieve optimal triazole formation, serving as a safer alternative to hazardous hydrazoic acid while enabling high product yields under the optimized conditions.

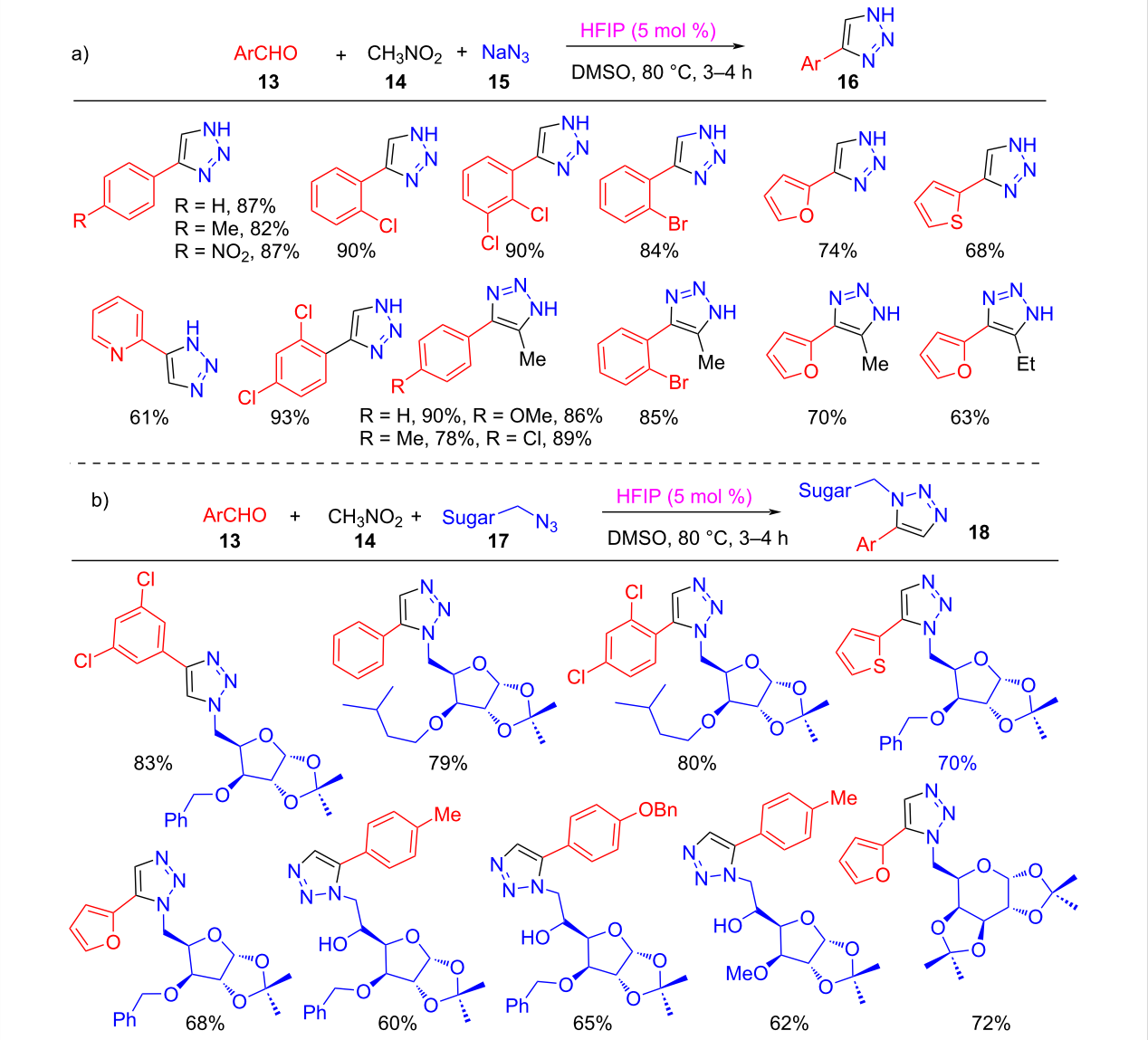
Substrate scope studies demonstrated that aromatic aldehydes bearing electron-donating, electron-neutral, and electron-withdrawing substituents were all compatible with the reaction conditions (Scheme 5a). Halogen- and nitro-substituted substrates afforded products in particularly high yields, while *ortho*-substituted aldehydes were also well tolerated, indicating minimal steric sensitivity. Heteroaromatic aldehydes containing furan, thiophene, and pyridine motifs underwent smooth conversion to the corresponding triazoles, although aliphatic aldehydes proved unreactive under the optimized conditions. Extension of the methodology to nitroethane enabled efficient access to 4,5-disubstituted *NH*-1,2,3-triazoles **16**, with electronic variations on the aldehyde component exerting little influence on product yields.

Importantly, the strategy was further expanded to the regioselective synthesis of 1,5-disubstituted triazolyl glycoconjugates **18** using glycosyl azides **17** and aldehydes **13**, nitromethane (**14**) (Scheme 5b). Both substituted aromatic and heteroaromatic aldehydes were well tolerated, providing glycoconjugates in moderate to good yields. This extension highlights the synthetic utility of the protocol for accessing biologically relevant triazole-linked architectures.

Five-six fused heterocycles

Synthesis of coumarin-linked naphthoquinone-fused pyrrole derivatives: Coumarin-, pyrrole-, and naphthoquinone-based scaffolds are well known for their broad spectrum of biological and pharmacological activities, making hybrid molecules containing these motifs highly attractive targets in medicinal chemistry [35]. In this context, Chaurasia and Parvin reported a simple one-pot protocol for the synthesis of coumarin-linked pyrrole–naphthoquinone hybrids **21** via the reaction of arylglyoxals **9**, 4-hydroxycoumarins **19**, and 2-amino-1,4-naphthoquinones **20** in HFIP under reflux conditions (Scheme 6a) [36].

This method provides a catalyst-free, operationally straightforward, and efficient alternative for assembling structurally complex heterocycles. Notably, the reaction enables the formation of two C–C bonds and one C–N bond in a single operation, delivering the desired products in good yields within relatively short reaction times. Here, HFIP acts as an effective reaction medium, promoting efficient multicomponent coupling under reflux conditions and facilitating clean bond-forming events without the need for external catalysts. A key practical advan-



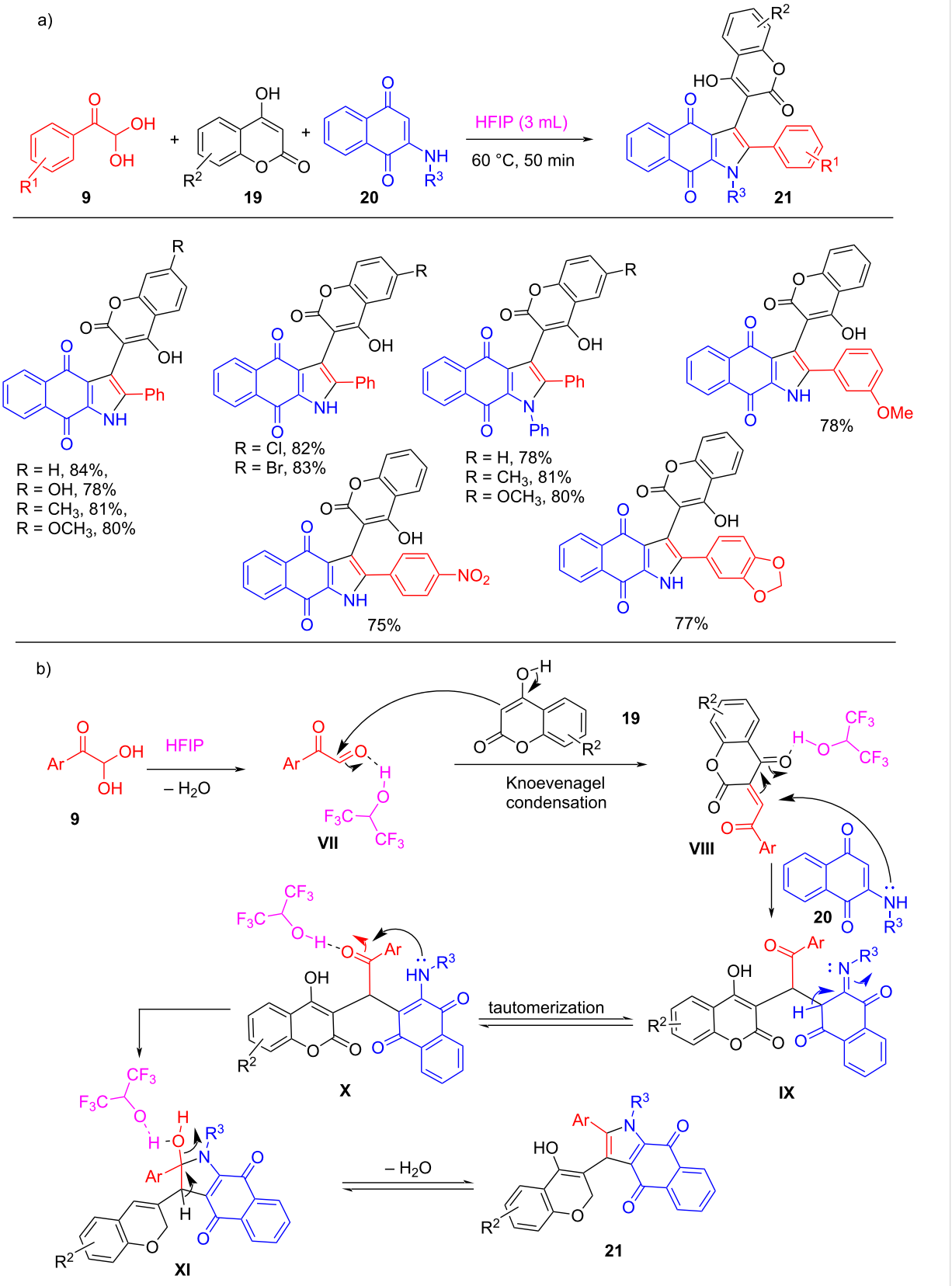
Scheme 5: Substrate scope of the a) synthesis of *N*-unsubstituted **16** and b) *N*-substituted 1,2,3-triazoles **18**.

tage of this protocol is its simple work-up, as the products can be purified by recrystallization rather than column chromatography, thereby enhancing both scalability and synthetic convenience.

Substrate scope studies demonstrated broad tolerance toward structurally diverse coupling partners. Various substituted 4-hydroxycoumarins bearing halogen, hydroxy, methyl, and methoxy groups underwent smooth conversion to the corresponding products in good yields. Similarly, aryl glyoxals containing either electron-donating or electron-withdrawing substituents were compatible with the reaction conditions, indicating minimal electronic sensitivity. The methodology also tolerated different *N*-substituted amino-naphthoquinones, further supporting the generality of the transformation (Scheme 6a).

Mechanistically, HFIP is proposed to activate the carbonyl functionality of arylglyoxals **9** through strong hydrogen-bonding interactions (**VII**), facilitating nucleophilic addition of 4-hydroxycoumarin **19** followed by Michael-type addition (**VIII**) of amino-naphthoquinone **20**. Subsequent tautomerization (**IX**), cyclization (**X**), and dehydration (**XI**) steps furnish the fused pyrrole products **21** (Scheme 6b).

Construction of nitrogen-containing heterocycles: Nitrogen-containing heterocycles are among the most important structural motifs in pharmaceuticals and functional materials, with a substantial proportion of FDA (Food and Drug Administration)-approved drugs incorporating at least one nitrogen heterocycle [37]. In particular, isoindolin-1-imines and related isoquinolinium salts have attracted increasing attention because of their

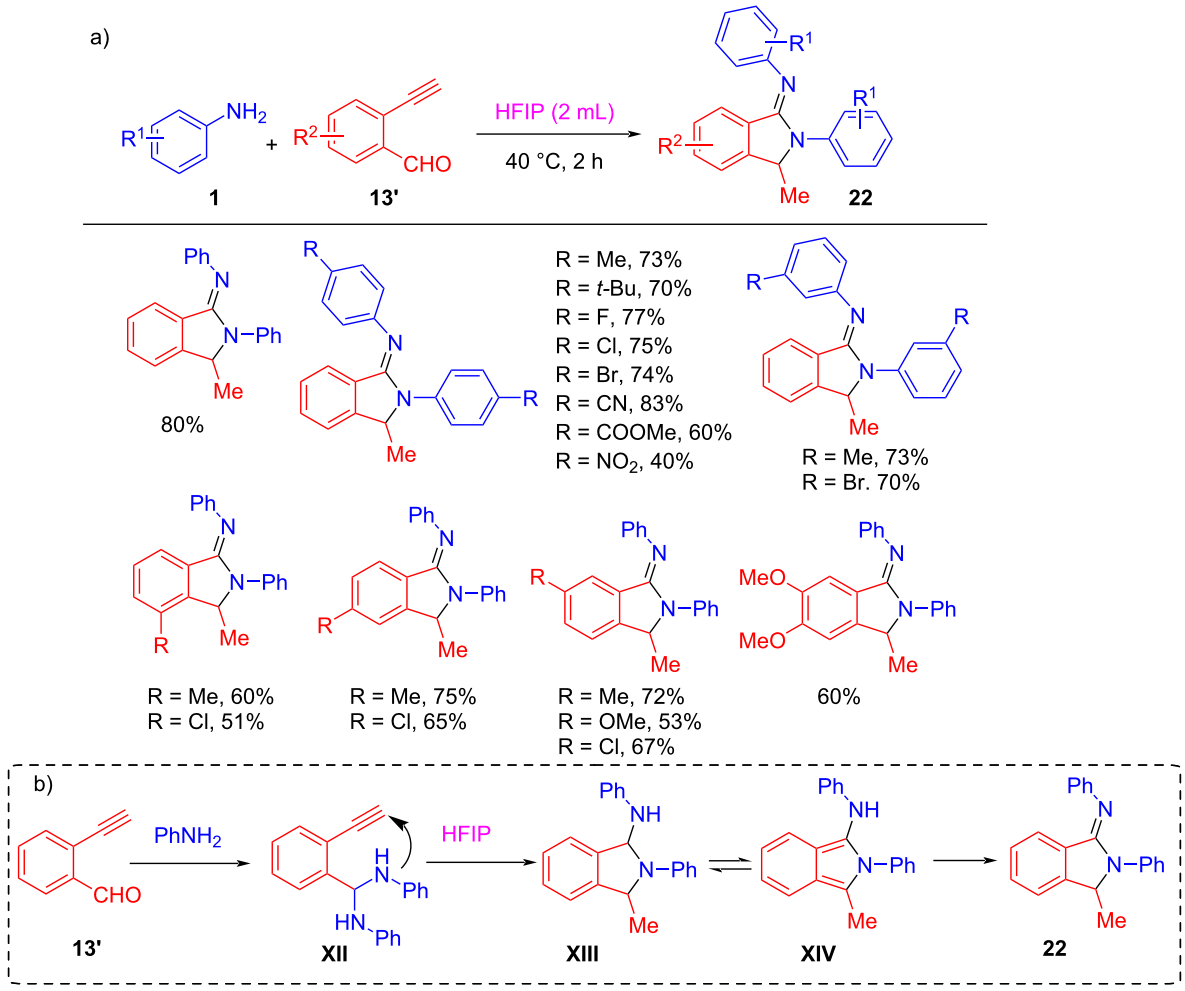


Scheme 6: a) Substrate scope for synthesizing naphthoquinone-fused pyrrole derivatives **21**. b) Proposed mechanism.

diverse biological and synthetic utility [38]. To access these frameworks, a mild and transition-metal-free strategy has been developed by Ji and co-workers using *ortho*-ethynylbenzaldehydes **13'** and anilines **1** in HFIP (Scheme 7) [39]. This methodology offers a simpler and more sustainable route to isoindolin-1-imines **22** and isoquinolinium salts under relatively mild conditions.

The protocol demonstrated a broad substrate scope and good functional-group tolerance (Scheme 7a). Anilines bearing electron-donating substituents generally afforded the desired isoindolin-1-imines in good yields, while halogen substituents were also well tolerated, providing synthetically useful products suitable for further derivatization. Electron-withdrawing groups such as cyano substituents remained compatible, although ester- and nitro-substituted anilines exhibited reduced reactivity, likely due to decreased nucleophilicity. Meta-substituted anilines and a variety of substituted *ortho*-ethynylbenzaldehydes also participated effectively, highlighting the versatility of the transformation. Notably, steric hindrance exerted only a limited effect on reaction efficiency. However, amides, aliphatic amines, and hydroxylamine hydrochloride were ineffective under the optimized conditions, indicating certain substrate limitations.

Mechanistically, HFIP plays a central role by promoting nucleophilic addition and facilitating subsequent cyclization through its strong proton-donating and hydrogen-bonding properties. The proposed pathway involves initial aminal formation (**XII**) followed by intramolecular annulation (**XIV**) to generate the isoindolin-1-imine framework **22**. In the presence of ammonium iodide, the reaction pathway diverges toward isoquinolinium salt formation via hydroiodination and cyclization processes. Density functional theory (DFT) calculations supported the proposed mechanism and provided insight into the energetics of the key transition states (Scheme 7b).

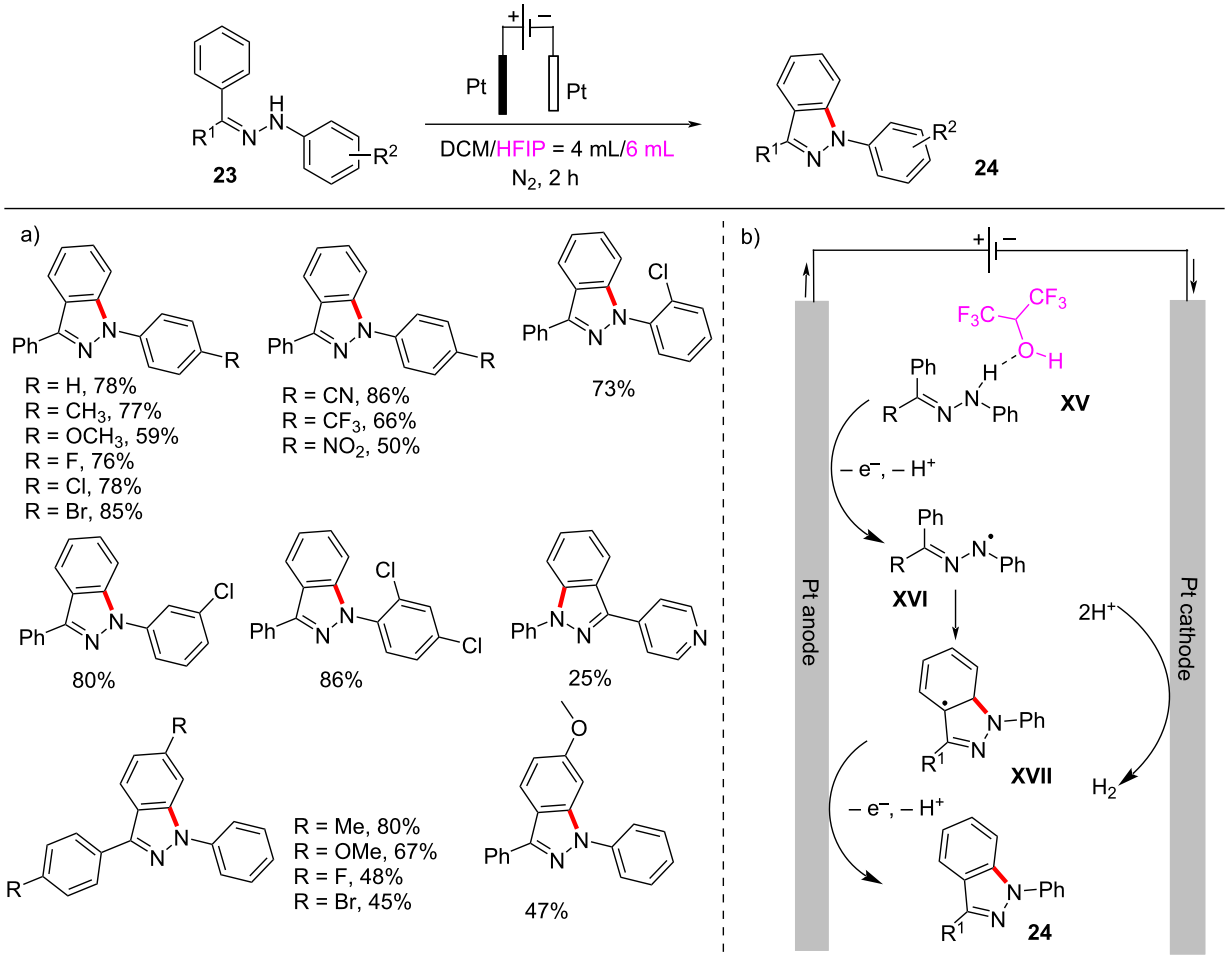


Scheme 7: a) Substrate scope for the synthesis of **22**. b) Proposed mechanism.

Synthesis of 1*H*-indazoles by an electrochemical radical C(sp^2)–H/N–H cyclization: An electrochemical oxidative C(sp^2)–H/N–H cyclization strategy has been developed by Lei and co-workers for the synthesis of 1*H*-indazoles through anodic oxidation of arylhydrazones under metal- and chemical oxidant-free conditions (Scheme 8) [40]. HFIP played a dual role as solvent/proton donor and promoter of N-centered radical formation via hydrogen-bond-assisted activation. This protocol offers operational simplicity, low-cost electrode compatibility, and sustainable reaction conditions while avoiding external oxidants. The methodology exhibited broad functional-group tolerance, affording 1*H*-indazole derivatives **24** in moderate to good yields. This electrochemical protocol provides a greener and mechanistically distinct alternative, although regioselectivity issues and reduced efficiency with heterocyclic or protected substrates remain notable limitations.

Both electron-donating and electron-withdrawing substituents on the N-phenyl ring were compatible with the reaction conditions (Scheme 8a), with several electron-withdrawing substituents providing good to high yields. Halogenated substrates, including mono- and disubstituted analogues, also reacted efficiently, demonstrating the broad substrate tolerance of the protocol and the synthetic utility of halide-containing products for further derivatization.

Substituent effects on the hydrazone aryl ring significantly influenced the reaction outcome. Electron-rich disubstituted substrates delivered comparatively higher yields, whereas electron-deficient analogs afforded only moderate yields, indicating differing electronic effects depending on the substitution pattern. Monosubstituted methyl and methoxy derivatives generated regioisomeric mixtures. The detailed regioisomeric substrate scope and product distributions are not shown in Scheme 8a; readers are referred to the original report for further details. In contrast, N-protected substrates failed to undergo cyclization, highlighting the necessity of a free N–H bond for radical generation. Heterocycle-containing substrates were



Scheme 8: a) Substrate scope of arylhydrazones. b) Proposed mechanism for **24**.

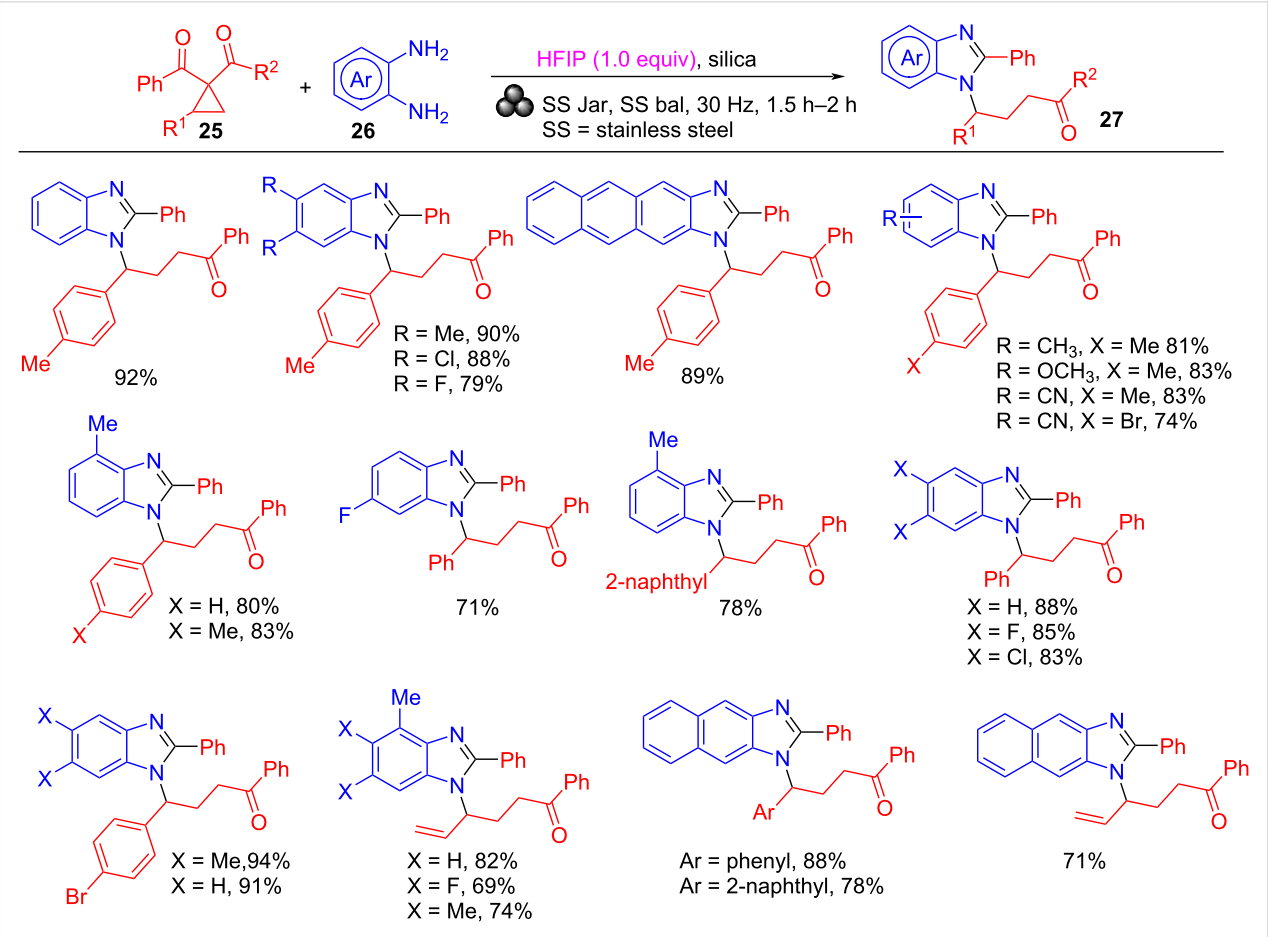
tolerated only in low yields, and alkene- or alkyne-substituted substrates converged to the same product. Certain substrates predominantly decomposed under the reaction conditions, reflecting limitations in substrate stability and substrate scope.

Mechanistic studies suggested that HFIP-assisted activation of arylhydrazones **23** facilitates proton-coupled electron transfer (PCET) at the anode to generate an N-centered radical intermediate **XVI**. Subsequent intramolecular radical addition (**XVII**) to the arene ring, followed by anodic oxidation and deprotonative aromatization, furnished the indazole products **24**, while cathodic proton reduction released H_2 (Scheme 8b). Cyclic voltammetry studies further confirmed the critical role of the DCM/HFIP system in promoting N-centered radical formation.

Direct synthesis of 1,2-disubstituted benzimidazoles: Benzimidazoles are important dinitrogen-containing bicyclic heterocycles widely found in pharmaceuticals, agrochemicals, and biologically active molecules [41]. A solvent-free and metal-free mechanochemical strategy has been developed by Yaragorla and co-workers for the synthesis of 1,2-disubstituted benzimidazoles **27** from donor–acceptor cyclopropyl ketones **25** and *o*-phenylenediamines **26** using stoichiometric HFIP under ambient conditions (Scheme 9) [42]. This mechanochemical approach significantly reduced reaction times while maintaining high efficiency, highlighting the advantages of mechanochemistry in sustainable heterocycle synthesis.

The protocol demonstrated a broad substrate scope with both symmetrical and unsymmetrical *o*-phenylenediamines **26**, generally affording the desired benzimidazoles **27** in good to excellent yields (Scheme 9). Symmetrical diamines generally underwent clean cyclization, whereas unsymmetrical substrates afforded regioisomeric mixtures, with the regioselectivity influenced by the electronic nature of the substituents. The detailed substrate scope, including the regioisomeric distributions, is not shown in Scheme 9; readers are referred to the original report for comprehensive details on the observed regioselectivity and product distributions.

In several cyano-substituted cases, the major regioisomers were separable and isolated in high yields. The methodology also



Scheme 9: Generality of the reaction for the synthesis of compound **27**.

tolerated a wide range of donor-acceptor cyclopropanes, including aryl-, vinyl-, diketone-, and keto ester-substituted systems. Notably, unsymmetrical cyclopropanes bearing both methyl ketone and aryl ketone functionalities displayed marked chemoselectivity, preferentially forming 2-methylbenzimidazoles over the corresponding 2-aryl analogues. Mechanistic studies suggested a tandem sequence involving cyclopropane ring opening, cyclization, and retro-Mannich fragmentation. Herein, HFIP acts both as the reaction solvent and as a crucial promoter of the mechanochemical transformation, as no reaction occurred in its absence, highlighting its key role in enhancing reaction efficiency.

Substrate-dependent selective synthesis of diversely functionalized indazole derivatives: Diversity-oriented synthesis (DOS) has emerged as a powerful strategy in drug discovery for rapidly accessing structurally diverse molecular libraries from simple building blocks [43]. In parallel, direct C–H functionalization has transformed modern synthesis by enabling step- and atom-economical construction of complex molecules, including pharmaceuticals and functional materials [44]. Within this context, a substrate-dependent divergent cascade approach has been developed by Fan and co-workers for the selective synthesis of functionalized indazole derivatives **30** and **31** from N-nitrosoanilines **28** and diazo compounds **29** and **29'** (Scheme 10) [45]. This strategy demonstrates how cascade C–H activation combined with substrate-dependent divergence can efficiently generate structurally distinct indazole scaffolds under mild conditions. This approach offers enhanced molecular diversity, high chemoselectivity, and operational simplicity, making it particularly valuable for diversity-oriented synthesis and early-stage drug discovery.

Notably, product divergence is controlled by the nature of the diazo coupling partner (Scheme 10): *N*-alkyl diazo homophthalimides **29** furnish benzoyl carbamate-substituted indazoles **30**, whereas *N*-phenyl analogues **29'** lead to benzoate-functionalized indazoles **31** via an additional O-nucleophilic addition and subsequent fragmentation. This switchable reactivity highlights a key advantage of substrate-controlled selectivity in building molecular diversity from a common intermediate (Scheme 10). Herein, HFIP functions not only as the solvent but also as a key reaction participant, promoting product formation through O-nucleophilic addition to reactive intermediates. Its involvement facilitates the proposed ketal collapse, oxidative dehydrogenation, and subsequent C–C and/or C–N bond cleavage pathways, thereby contributing to the formation of the distinct products. The detailed mechanistic pathway, including the ketal collapse step, is not shown in Scheme 10; readers are referred to the original article for further mechanistic details.

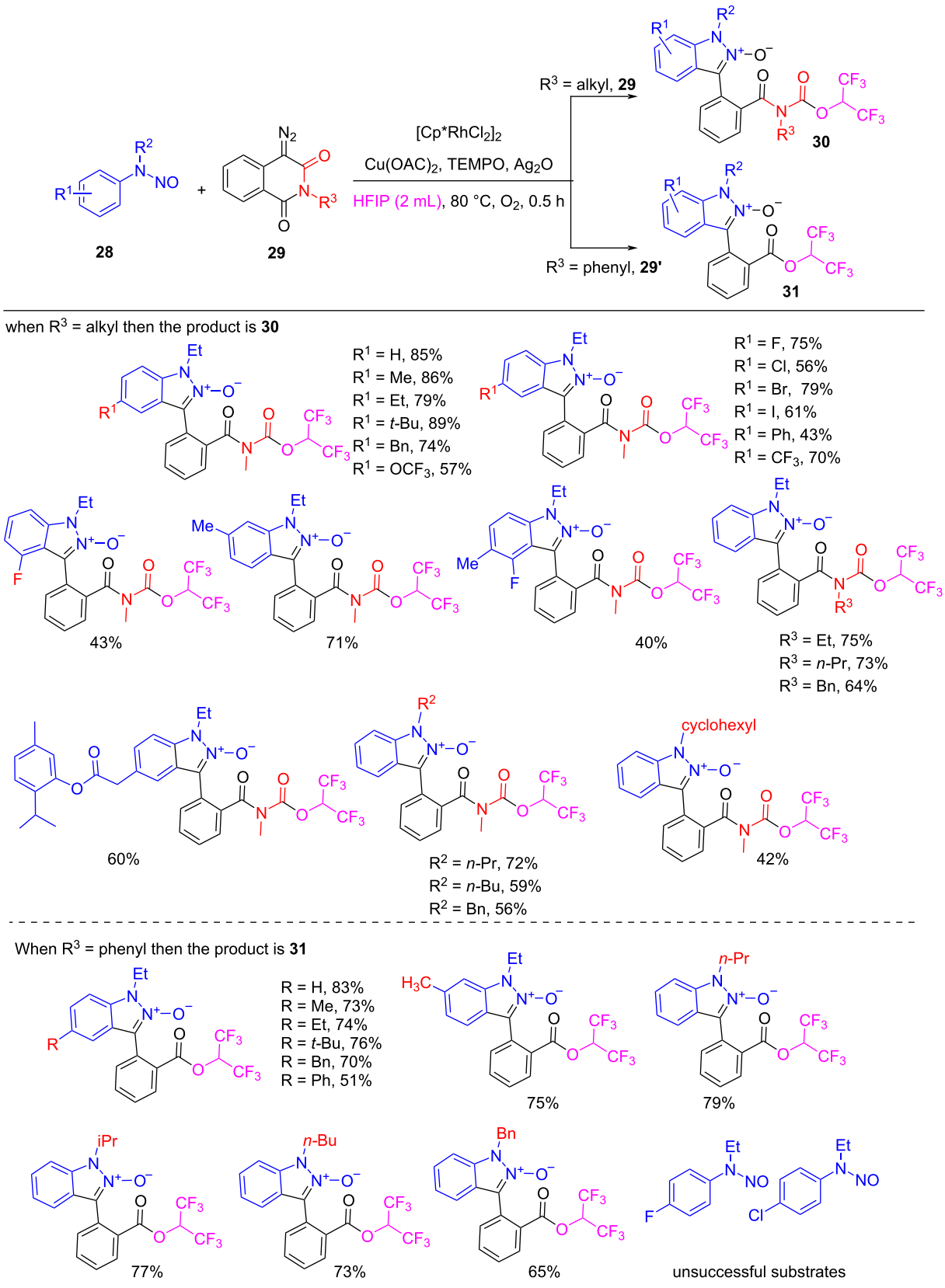
A range of *N*-nitrosoanilines bearing electron-donating and electron-withdrawing groups at the *para*-position undergo smooth conversion to give products in moderate to excellent yields, while *meta*-substituted systems exhibit predictable regioselectivity governed by electronic and steric effects. Likewise, variation in alkyl substituents is well tolerated, reflecting the robustness of the cascade process. Diazo component variation is also feasible, further expanding structural diversity and enabling late-stage functionalization, including derivatization of bio-relevant motifs such as thymol.

The transformation proceeds through a cascade sequence involving nitroso-directed C–H alkylation followed by intramolecular and intermolecular nucleophilic additions, C–C or C–N bond cleavage, and dehydrogenation.

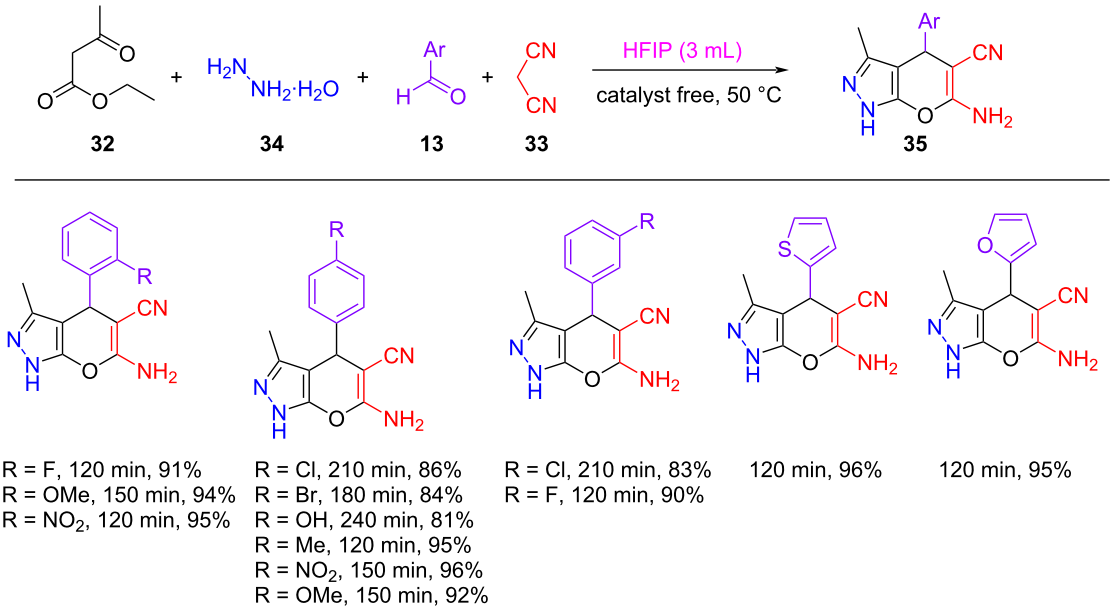
Synthesis of dihydropyrano[2,3-c]pyrazole scaffolds: Dihydropyrano[2,3-*c*]pyrazoles are important heterocyclic scaffolds that exhibit a wide range of biological activities, including anticancer, antimicrobial, analgesic, molluscicidal, and kinase inhibitory properties [46]. A catalyst-free protocol has been developed by Mohamadpour for the synthesis of dihydropyrano[2,3-*c*]pyrazoles **35** using HFIP as a reusable promoting medium (Scheme 11) [47]. The transformation proceeds through a tandem Knoevenagel–Michael cyclocondensation sequence under mild conditions, enabling rapid one-pot construction of the heterocyclic framework in excellent yields. This strategy employs polyfluorinated alcohol as both solvent and promoter, highlighting the unique activating ability of HFIP in facilitating multicomponent cyclizations and provides a greener and more sustainable alternative by eliminating external catalysts, minimizing waste generation, and avoiding hazardous reagents.

The methodology demonstrates a broad substrate tolerance, with a variety of aldehyde derivatives **13** reacting efficiently irrespective of their electronic nature (Scheme 11). Product isolation is operationally straightforward, involving simple filtration and recrystallization without extensive purification procedures.

Synthesis of 2-aminobenzoxazole and 2-aminobenzothiazole derivatives: Azole derivatives such as benzoxazoles **39** and benzothiazoles **40** are important pharmacophores widely encountered in biologically active molecules and therapeutic agents, making their efficient synthesis a central objective in heterocyclic chemistry. In this context [48], a straightforward HFIP-promoted cyclodesulfurization strategy has been developed by Malakar and co-workers for the synthesis of pharmaceutically relevant 2-aminobenzoxazoles **39** and 2-aminobenzothiazoles **40** from 2-aminophenols **36**, 2-aminothiophenols **37**, and functionalized phenyl isothiocyanates **38** (Scheme 12a).



Scheme 10: Substrate scope for the synthesis of products **30** and **31**.



Scheme 11: Synthesis of dihydropyrano[2,3-*c*]pyrazoles **35**.

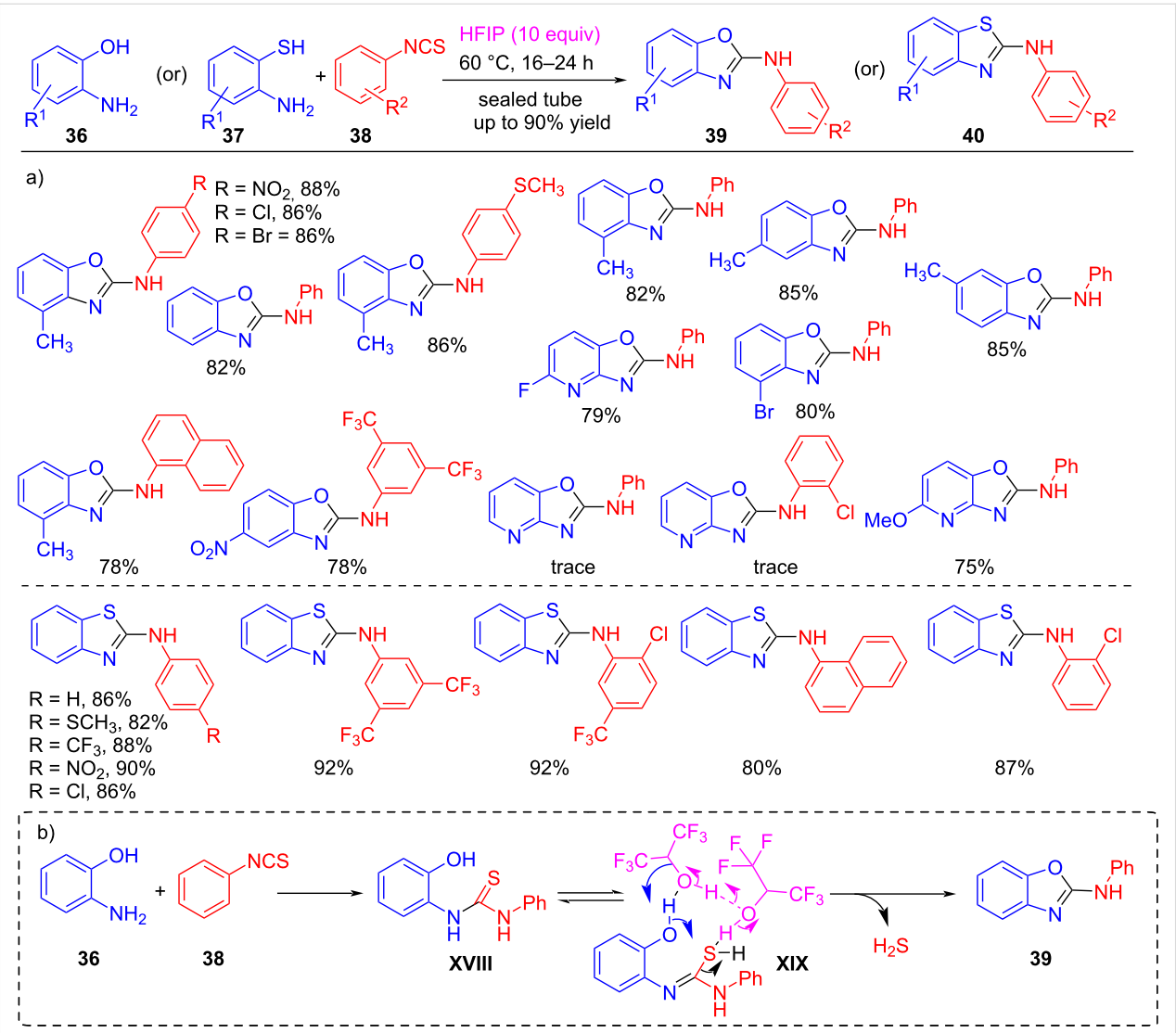
The methodology exhibits a broad substrate scope and tolerates a wide range of electron-donating and electron-withdrawing substituents on both aminophenol and isothiocyanate partners (Scheme 12a). In general, electron-rich aminophenols afforded slightly higher yields than electron-deficient analogues, whereas electron-poor isothiocyanates performed better due to enhanced electrophilicity of the isothiocyanate carbon center, which facilitates thiourea formation and subsequent cyclization. Notably, benzothiazole **40** formation generally proceeded more efficiently than benzoxazole synthesis, likely reflecting the greater nucleophilicity of sulfur relative to oxygen. However, heteroaryl substrates such as 2-amino-3-hydroxypyridine were reported to be incompatible with the reaction conditions. This example is not shown in the scheme; readers are referred to the original article for further details. The incompatibility was attributed to the decreased nucleophilicity of the amino group due to the electron-withdrawing effect of the ring nitrogen, which may hinder intermediate formation (Scheme 12a).

The transformation proceeds under metal-, base-, and oxidant-free conditions at moderate temperature, with HFIP serving as both solvent and promoter. Mechanistically, the process involves initial thiourea formation (**XVIII**) followed by HFIP-assisted cyclodesulfurization of interemediate **XIX** through hydrogen-bond activation of hydroxy or thiol groups, ultimately leading to heterocycle formation **39** with concomitant release of H_2S (Scheme 12b). The dual role of HFIP as a proton donor and activating medium is crucial for facilitating bond cleavage and cyclization under mild conditions.

Construction of six-six fused heterocycles

Synthesis of 2-aminoquinazoline derivatives: Quinazoline derivatives are important nitrogen-containing heteroaromatic scaffolds widely recognized for their diverse biological and pharmaceutical activities [49]. Among them, 2-aminoquinazolines constitute a prominent class of bioactive molecules and medicinally relevant intermediates. In this context, an efficient hydrochloric acid-mediated [4 + 2] annulation strategy has been developed by Wu and co-workers for the synthesis of 2-aminoquinazolines **44** from *N*-benzyl cyanamides **41** and 2-aminoaryl ketones **42** (Scheme 13) [50]. This acid-mediated annulation provides a concise and operationally simple route to two distinct classes of quinazoline derivatives. The broad substrate tolerance, high efficiency, and divergent product formation underscore the practicality and synthetic utility of this methodology for the preparation of pharmaceutically relevant quinazoline frameworks. Replacing the ketone substrates with 2-aminobenzonitriles **43** enabled direct access to 2-amino-4-iminoquinazolines **45**, thereby expanding the synthetic versatility of the protocol. Herein, HFIP functions as the reaction solvent, while MsOH was identified as an effective acid additive during the optimization studies. Under the reported reaction conditions, HCl was used as the acid to facilitate the overall transformation.

The methodology demonstrates a broad substrate scope and excellent functional-group tolerance (Scheme 13). *N*-Benzyl cyanamides **41** bearing electron-donating, electron-withdrawing, halogen, and heteroaromatic substituents undergo



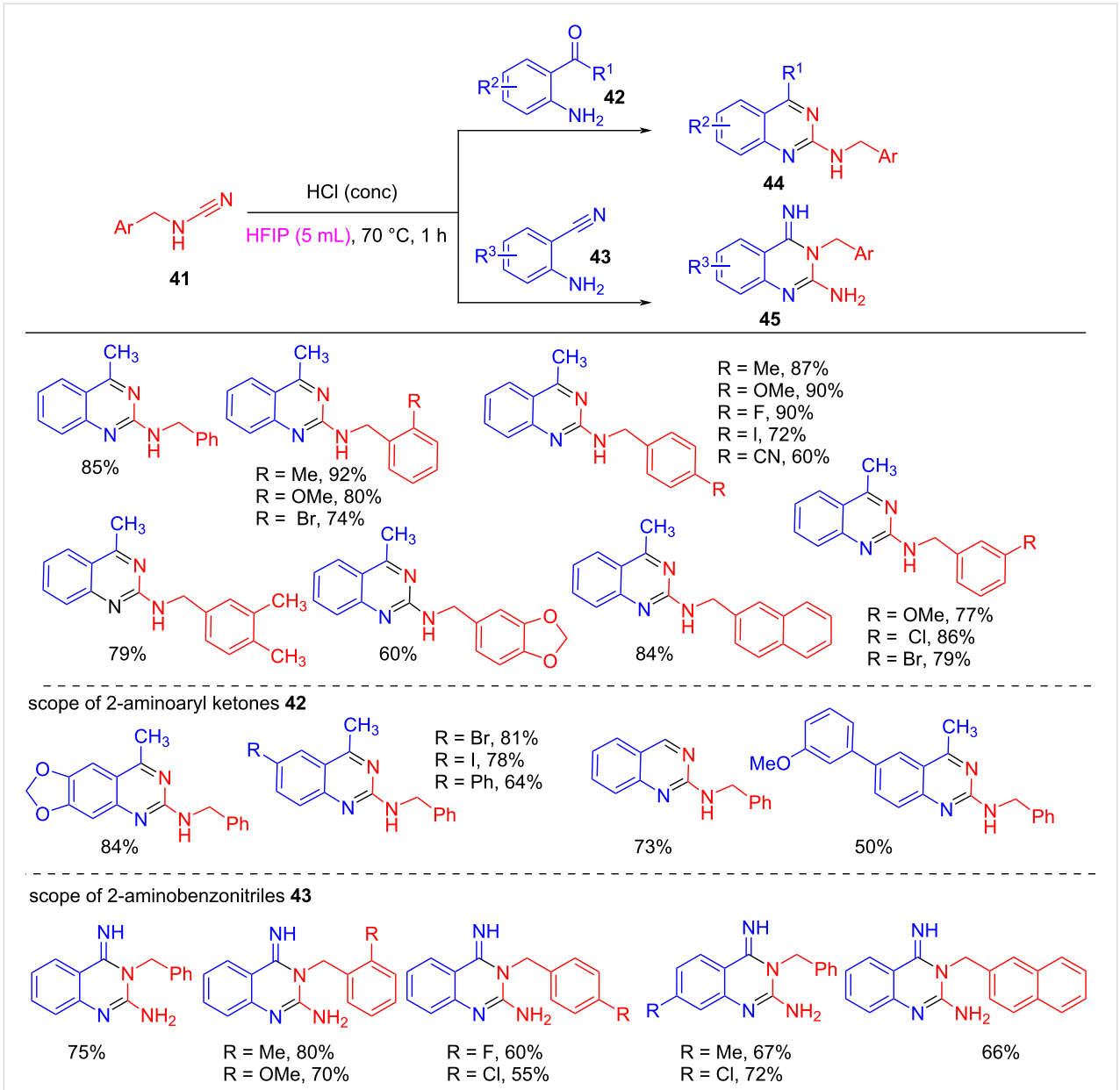
Scheme 12: a) Substrate scope for the synthesis of **39** and **40**. b) Proposed mechanism.

smooth annulation to furnish the desired quinazoline products in generally good to excellent yields. Notably, sterically demanding substrates such as 2-naphthyl derivatives remain compatible, indicating the robustness of the transformation. Similarly, various substituted 2-aminoaryl ketones **42**, including electron-rich, electron-poor, and halogenated systems, participate effectively in the cyclization process. Aldehyde- and diaryl ketone-derived substrates are also well tolerated, further highlighting the flexibility of the reaction design. An interesting divergence in reactivity was observed when 2-aminobenzonitriles **43** were employed instead of 2-aminoaryl ketones **42**, leading selectively to 2-amino-4-iminoquinazolines **45**. This alternative pathway also accommodates a diverse range of cyanamide and aminobenzonitrile substrates, including electronically varied and sterically hindered derivatives, generally affording moderate to high yields.

Construction of polycyclic fused heterocycles

Divergent synthesis of 1-trifluoromethylated cyclopenta[*b*]indoles: Cyclopenta[*b*]indole frameworks are prominent structural motifs widely encountered in biologically active natural products and pharmaceutical compounds, where their rigid fused-ring architecture contributes to diverse biological activities [51]. In particular, trifluoromethyl-substituted cyclopenta[*b*]indoles **47** are attractive targets in medicinal chemistry because incorporation of the CF_3 group can significantly modulate metabolic stability and bioactivity [52].

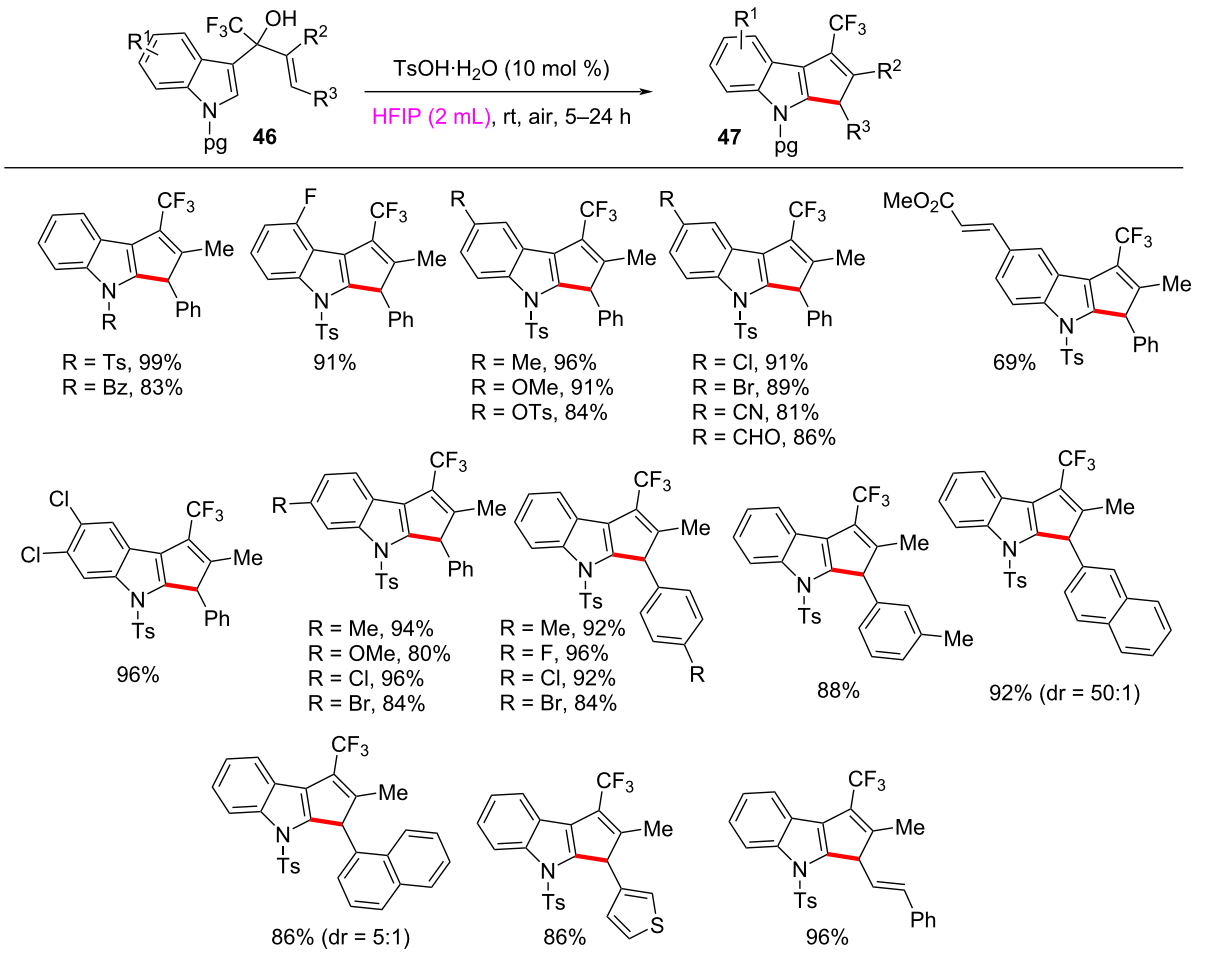
An efficient Brønsted acid-catalyzed dehydrative Nazarov-type cyclization has been developed by Rao and co-workers for the divergent synthesis of 1-trifluoromethylated cyclopenta[*b*]indoles **47** from CF_3-substituted 3-indolylallyl alcohols **46** (Scheme 14) [53]. Remarkably, product selectivity is



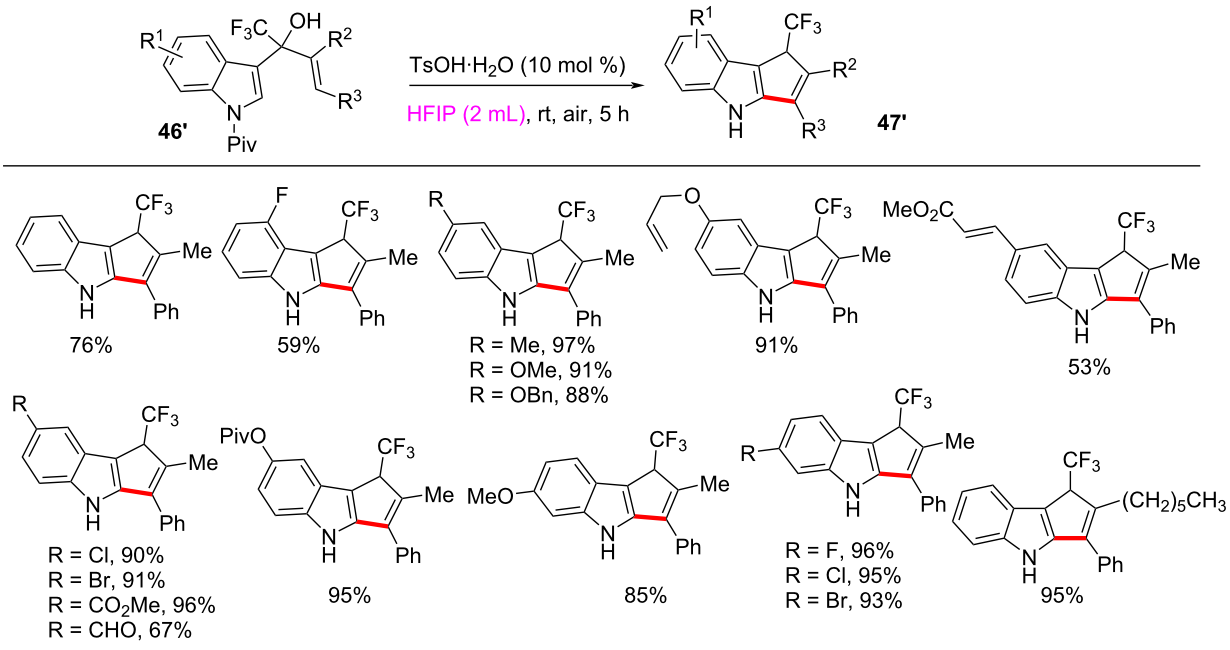
Scheme 13: Synthesis of 2-aminoquinazoline derivatives **44** and **45**.

governed by the nature of the indole NH-protecting group. Arylsulfonyl-protected substrates selectively furnish protected cyclopenta[*b*]indoles, whereas pivaloyl-protected analogues undergo further deacylative rearrangement to generate NH-free cyclopenta[*b*]indoles with altered alkene geometry. This tunable chemoselectivity highlights the versatility of the methodology and enables access to two distinct classes of valuable fluorinated scaffolds from common precursors. This strategy offers operational simplicity, scalable synthesis, mild reaction conditions, and controllable product divergence, providing a practical route to structurally diverse trifluoromethylated cyclopenta[*b*]indoles. Wherein, HFIP acts not only as a solvent but also as a key promoter in the reaction, where its combination with TsOH is proposed to generate the highly active catalytic species $TsOH(H_2O)_m(HFIP)_n$, thereby enhancing the overall catalytic efficiency of the transformation.

The reaction proceeds under mild metal-free conditions and demonstrates excellent functional-group compatibility. A broad range of substrates bearing electron-donating and electron-withdrawing substituents on the indole core are efficiently transformed into the corresponding cyclopenta[*b*]indoles in generally good to excellent yields (Scheme 14). Sensitive functionalities such as formyl, α,β-unsaturated ester, halogen, cyano, and



substarte scope of *N*-pivaloyl-protected trifluoroalkylated 3-indolylallyl alcohols



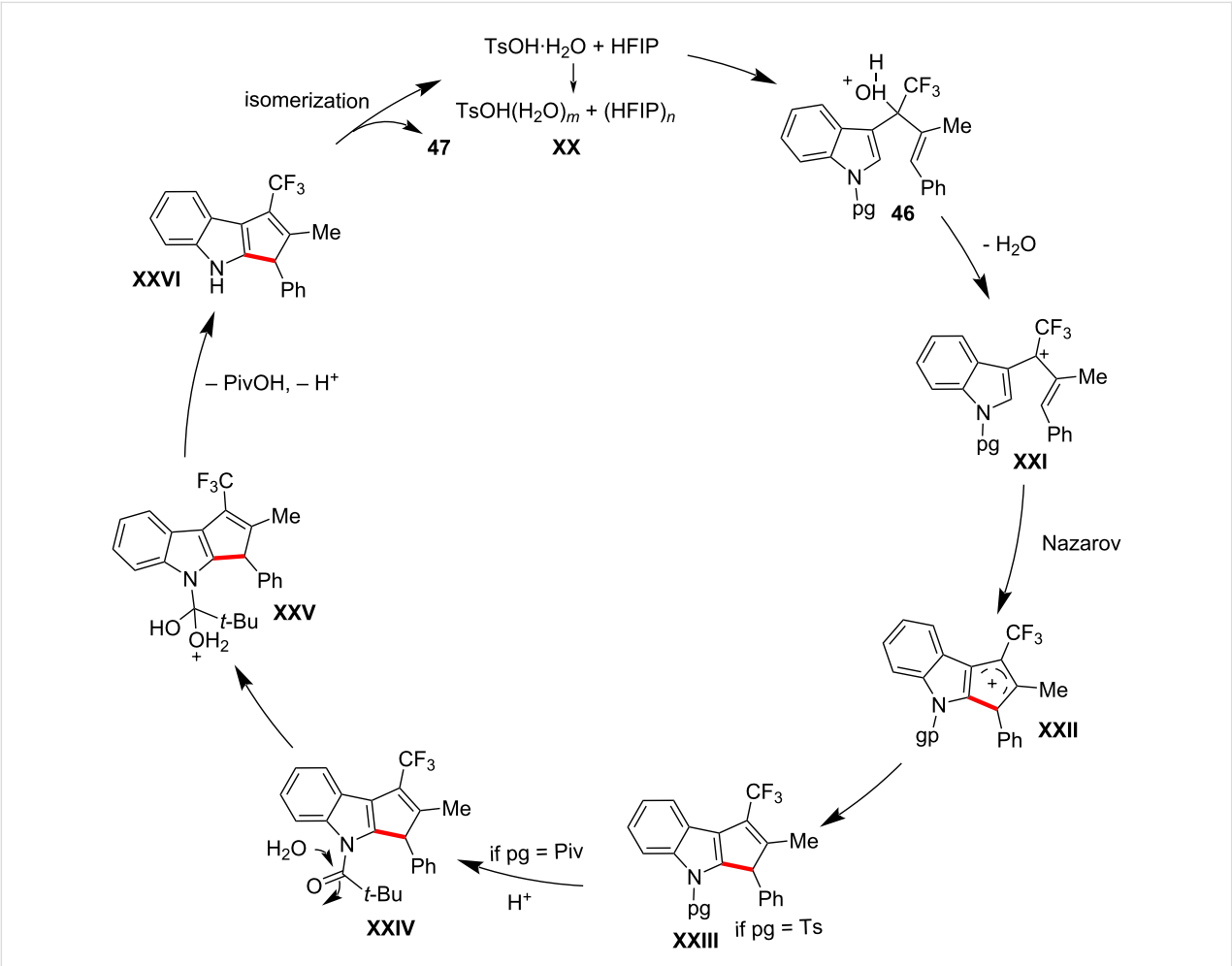
Scheme 14: Substrate scope for the synthesis of 1-trifluoromethylated cyclopenta[*b*]indoles **47**.

alkene groups are well tolerated, underscoring the mildness of the conditions. Variations in alkyl substituents and aryl groups on the alkenyl fragment are also accommodated, although sterically demanding naphthyl and heteroaryl substrates can lead to regio- or diastereomeric mixtures. In contrast, less substituted or unactivated allylic alcohols prove unsuitable for the transformation.

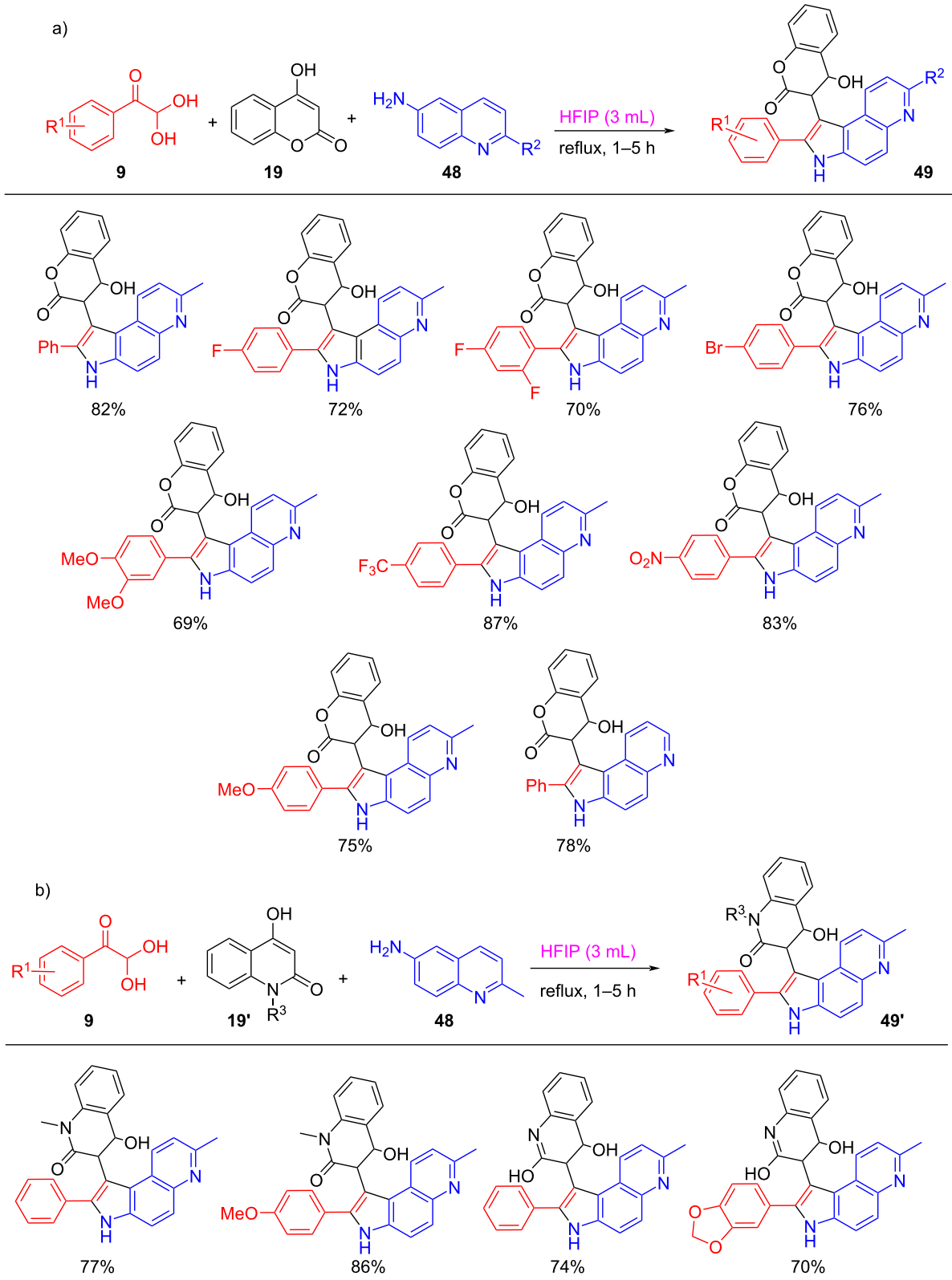
Mechanistically, the reaction involves formation of a highly active TsOH/HFIP catalytic species **XX** that promotes dehydration of the allylic alcohol **46** to generate a carbocation intermediate **XXI** (Scheme 15), followed by Nazarov-type 4π electrocyclization (**XXII**). In the case of pivaloyl-protected substrates, subsequent hydrolysis of **XXIV** and alkene isomerization of **XXVI** lead to NH-free products **47**.

Synthesis of fluorescent quinoline-fused pyrroles: Quinolines and pyrroles are among the most important nitrogen-containing heterocycles in medicinal chemistry, and hybrid structures incorporating both motifs frequently display significant biological and photophysical properties [54]. In particular, quinoline-fused pyrroles are present in numerous natural products and synthetic bioactive molecules, motivating the development of efficient and sustainable approaches for their synthesis [55].

A metal-free multicomponent strategy has been developed by Choudhury and co-workers for the regioselective synthesis of quinoline- and isoquinoline-fused pyrroles **49** using arylglyoxals **9**, cyclic 1,3-dicarbonyl compounds **19**, and aminoquinolines **48** in HFIP under reflux conditions (Scheme 16) [56]. In this transformation, HFIP acts simultaneously as solvent and promoter, facilitating rapid assembly of the fused heterocyclic framework without the need for external catalysts. The protocol combines operational simplicity with straightforward product isolation and provides direct access to structurally complex fused pyrroles containing multiple biologically relevant motifs. The combination of broad substrate compatibility, short reaction times, easy purification, and incorporation of multiple phar-



Scheme 15: Proposed mechanism for the synthesis of trifluoroalkylated 3-indolylallyl alcohols.



Scheme 16: a) Substrate scope for the synthesis of coumarin containing quinoline-fused pyrroles **49**. b) Substrate scope for the synthesis of 4-hydroxy-1-methylquinolone/quinoline-2,4-diol **49'**.

macologically important heterocyclic units underscores the utility of this HFIP-mediated methodology for the synthesis of complex fused N-heterocycles.

The methodology exhibits broad substrate scope and good functional-group tolerance (Scheme 16a). Arylglyoxals bearing both electron-donating and electron-withdrawing substituents participate efficiently, although electron-deficient substrates generally afford higher yields than electron-rich analogues, likely due to enhanced electrophilicity of the glyoxal component. Halogenated, trifluoromethyl-, nitro-, methoxy-, and naphthyl-substituted glyoxals are all compatible with the reaction conditions. Variation of the aminoquinoline and cyclic 1,3-dicarbonyl partners further expands structural diversity, enabling the synthesis of a range of quinoline- and isoquinoline-fused pyrroles in moderate to very good yields (Scheme 16b).

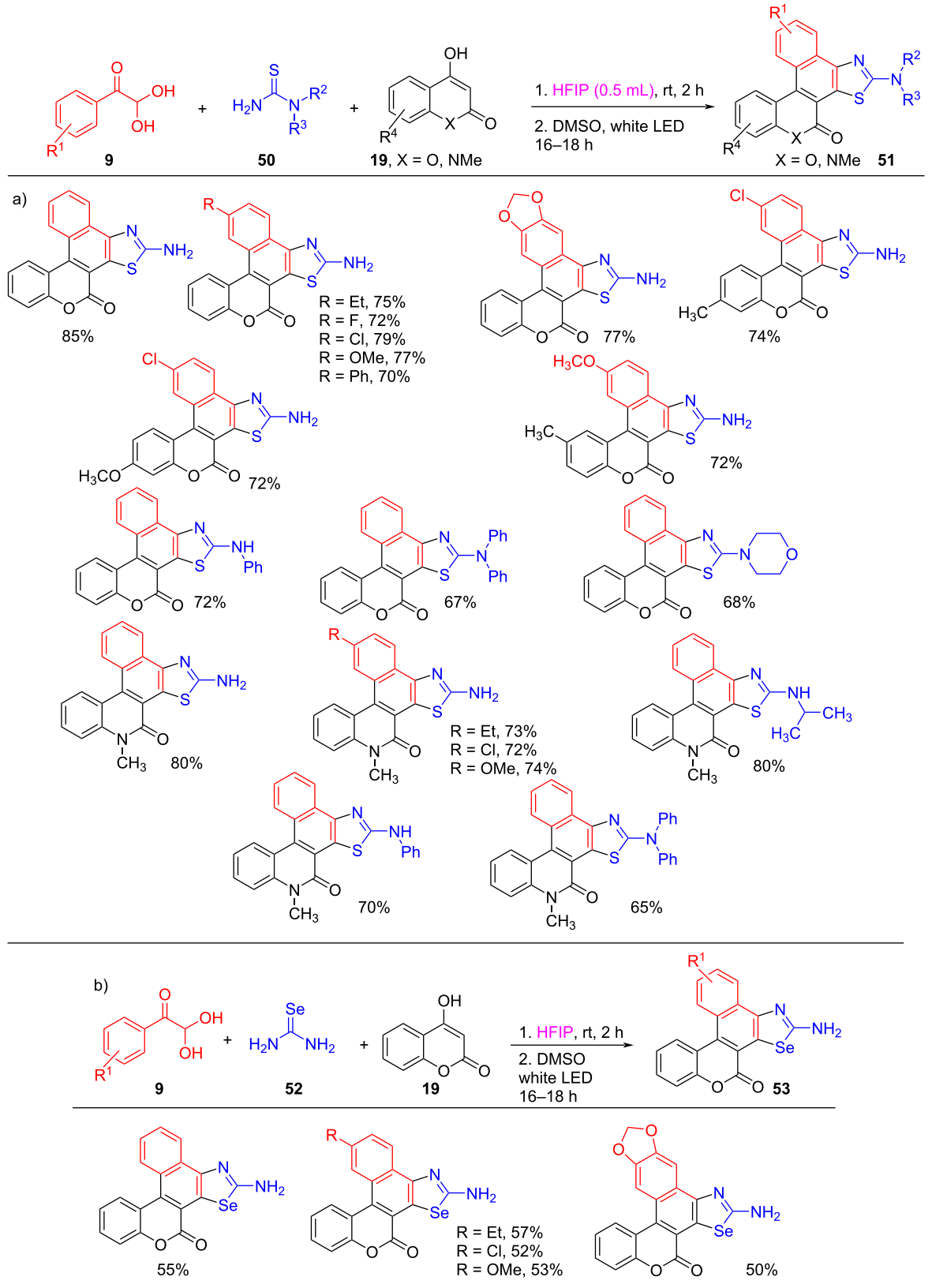
Synthesis of polycyclic-fused aminothiazoles and aminoselenazoles: The development of fused aminothiazole and aminoselenazole scaffolds through multicomponent reactions (MCRs) has emerged as an efficient strategy for accessing structurally complex and biologically relevant heterocycles [57]. In this context, a visible-light-assisted, HFIP-mediated one-pot protocol was reported by Choudhury and co-workers for the synthesis of pentacyclic-fused aminothiazoles **51** and aminoselenazoles **53** from arylglyoxals **9**, thioureas/selenoureas **50/52**, and 4-hydroxycoumarin or 4-hydroxy-1-methyl-2-quinolone derivatives (Scheme 17) [22]. The significant enhancement in reaction efficiency highlights the distinctive role of HFIP in promoting the transformation, which can likely be attributed to its strong hydrogen-bond-donating ability and high polarity. The methodology combines an initial MCR cyclization with subsequent photocyclization under white LED irradiation, enabling rapid construction of multiple C–C, C–N, and C–S/Se bonds under mild and metal-free conditions. This strategy offers improved atom economy, operational simplicity, and the use of visible light as a sustainable energy source. Critically, the protocol demonstrates several advantages over traditional transition-metal-catalyzed annulation approaches, including avoidance of metal contaminants, ambient reaction conditions, and minimal waste generation, with water as the only benign byproduct. However, the reduced efficiency observed for selenourea substrates and sterically hindered thioureas indicates certain limitations in substrate compatibility.

A broad substrate scope was demonstrated, with both electron-donating and electron-withdrawing substituents on arylglyoxals providing the desired fused aminothiazoles in generally good to excellent yields (Scheme 17a). Thiourea derivatives bearing mono-substitution showed higher efficiency, whereas *N,N*-disubstituted thioureas resulted in comparatively diminished yields, likely due to steric and electronic effects. Similarly, coumarin-based substrates consistently outperformed 4-hydroxy-1-methyl-2-quinolone analogues, which furnished slightly lower yields under identical conditions. Notably, replacement of thiourea with selenourea successfully extended the methodology to aminoselenazole synthesis, although these reactions afforded only moderate yields, highlighting the comparatively lower reactivity and stability of selenium-containing intermediates (Scheme 17b).

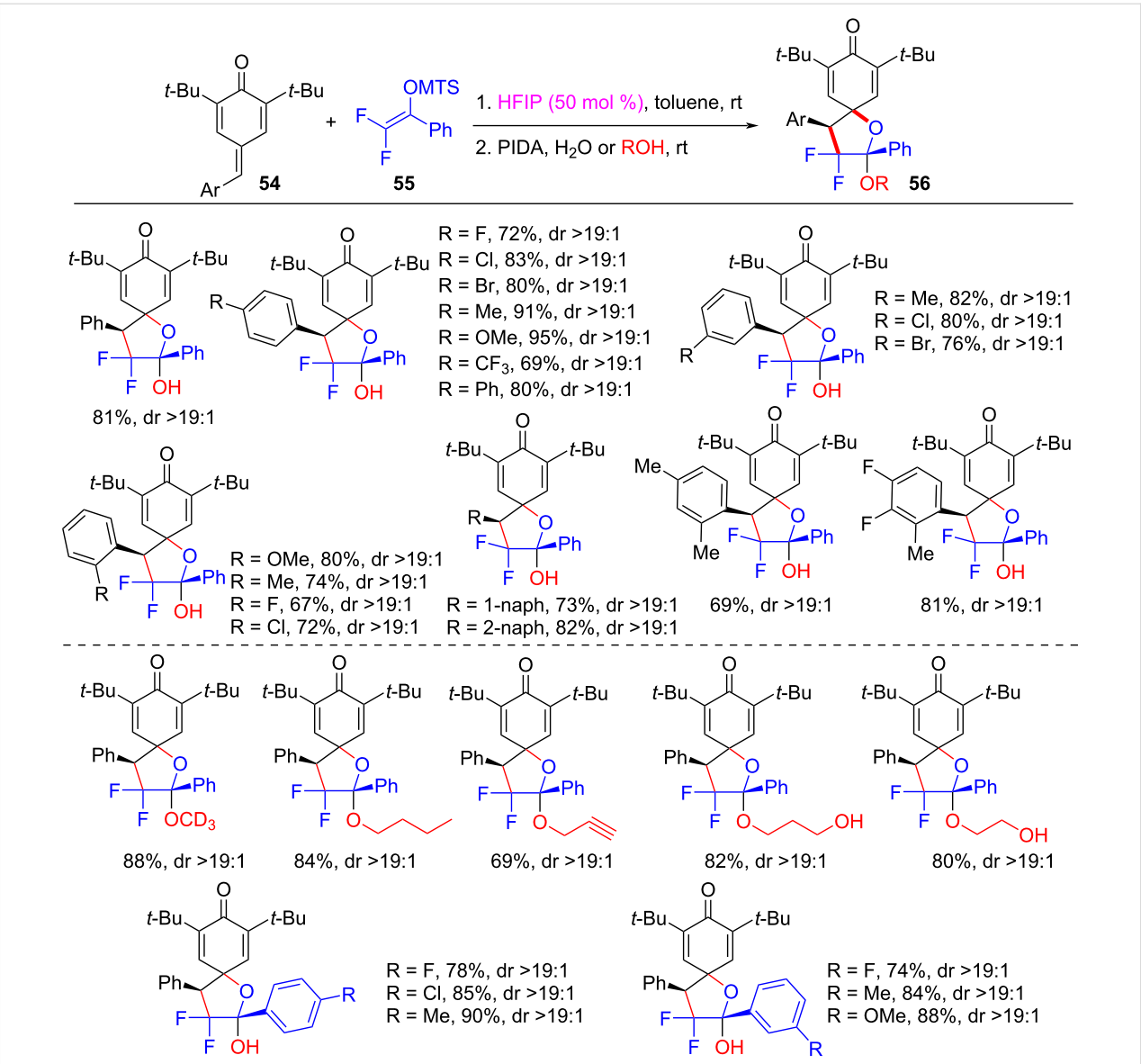
Spiro heterocyclic rings

Construstion of five-six membered spiro heterocyclic rings: *Synthesis of fluorine-containing multisubstituted oxaspiro[4,5]cyclohexadienones: para*-quinone methides (*p*-QMs) are highly reactive intermediates widely encountered in natural products and bioactive systems [58], and they serve as versatile synthons in modern organic synthesis due to their ability to participate in diverse bond-forming processes [59]. In this context, a one-pot sequential cascade strategy has been developed by Wang and co-workers for the construction of fluorinated multisubstituted oxaspiro[4,5]cyclohexadienones **56** using *p*-QMs **54** and difluoroenoxysilanes **55** under HFIP catalysis, followed by oxidative dearomatization (Scheme 18) [60]. Mechanistically, the reaction proceeds through an HFIP-promoted 1,6-conjugate addition of difluoroenoxysilanes to *p*-QMs **54**, followed by intramolecular hemiacetalization and oxidative dearomatization using $PhI(OAc)_2$, delivering the spirocyclic framework with high diastereoselectivity. In contrast to conventional solvent roles, HFIP functions as a mild Brønsted acid catalyst, enabling efficient cascade reactivity under relatively mild conditions and highlighting the emerging catalytic potential of fluorinated alcohols in complex molecule construction. This work offers superior atom economy, operational simplicity, and rapid access to fluorine-rich spirocyclic architectures that are of significant interest in medicinal chemistry and drug discovery.

The methodology exhibits a broad substrate scope (Scheme 18). A variety of *p*-QMs bearing electron-donating, electron-withdrawing, and neutral substituents participate effectively, generally affording moderate to good yields, although electron-deficient systems show slightly reduced efficiency. Sterically demanding naphthyl-derived substrates are also compatible, while disubstituted and heterocyclic *p*-QMs, although not shown in Scheme 18, further expands the reported structural diversity. In parallel, difluoroenoxysilanes with varied electronic and steric profiles are well tolerated, enabling access to a wide range of fluorinated spirocyclic products. Additionally, diverse alcohol nucleophiles, including deuterated methanol and diols, participate successfully, whereas amines and thiols are unreactive under the oxidative conditions.



Scheme 17: a) Substrate scope for the synthesis of polycyclic-fused aminothiazoles **51**. b) Substrate scope for the synthesis of polycyclic aromatic aminoselenazoles **53**.

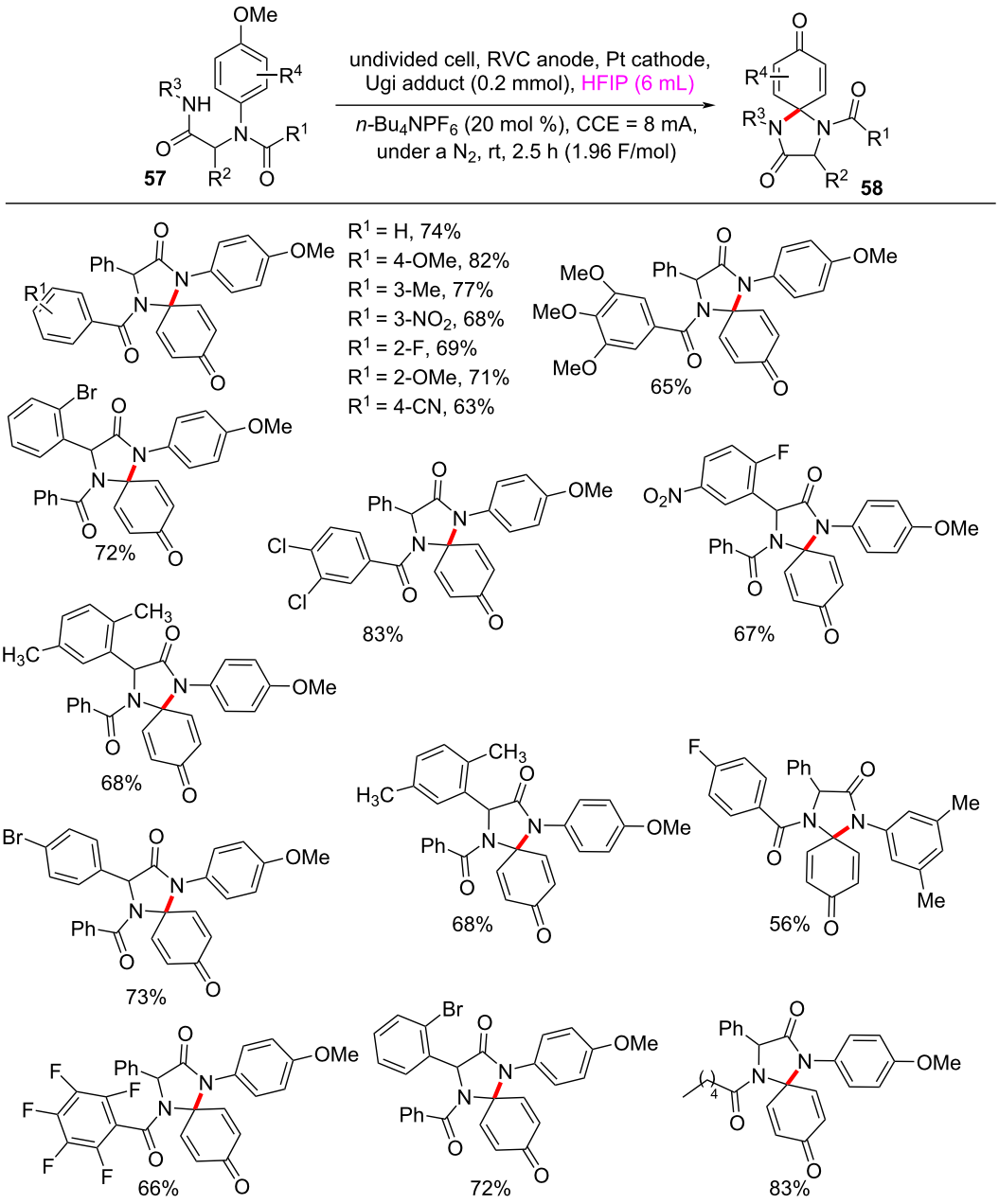


Scheme 18: Substrate scope for the synthesis of spiro[4.5]cyclohexadienones **56**.

Synthesis of 4-imidazolidinones via electrochemical and post-Ugi cyclization method: Organic electrosynthesis has emerged as a sustainable and powerful strategy for generating reactive radical intermediates under mild conditions [61], enabling efficient construction of structurally complex molecules without the need for stoichiometric oxidants or metal catalysts. In this context, an electrochemical approach has been developed by Sharma and co-workers for the synthesis of spirocyclic 4-imidazolidinones **58** through post-Ugi cyclization of bis-amide intermediates via N-centered radical-mediated intramolecular *ipso* cyclization (Scheme 19) [62].

The transformation demonstrates a broad substrate scope and notable functional-group tolerance (Scheme 19). Aromatic substrates bearing electron-donating and electron-withdrawing substituents at various positions react efficiently, while electrochemically sensitive groups such as bromo, nitro, cyano, methoxy, and alkenyl functionalities remain intact. Both aromatic and aliphatic carboxylic acid-derived Ugi adducts participate successfully, and structurally diverse aldehydes and isocyanides further expand the accessible spirocyclic library. In contrast, phenyl and aliphatic isocyanide-derived substrates proved ineffective, likely due to insufficient stability of the intermediate amidyl radicals.

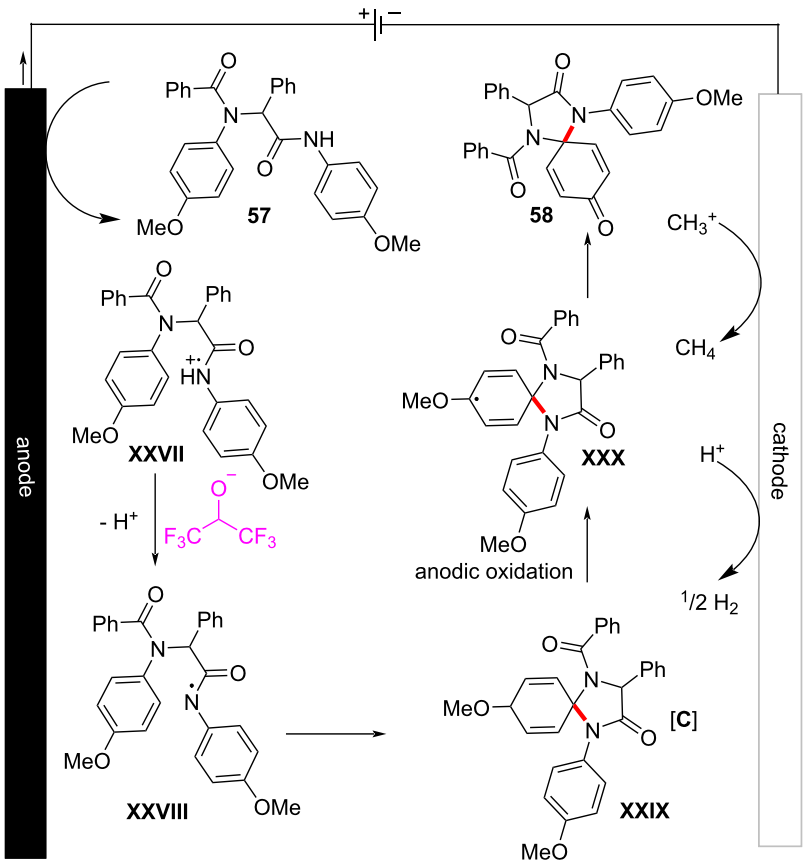
The method employs constant-current electrolysis in an undivided carbon-platinum cell to generate amidyl radicals directly from Ugi adducts. Mechanistically, anodic oxidation produces



Scheme 19: Substrate scope for synthesis of diverse 4-imidazolidinones **58**.

an N-centered radical **XXVIII** that undergoes intramolecular cyclization (**XXIX**) and subsequent oxidation (**XXX**) to furnish the spirocyclic scaffold **58** following demethylation. HFIP plays a dual role of facilitating deprotonation and stabilizing reactive intermediates, while its recyclability further enhances the sustainability of the protocol (Scheme 20). Compared with traditional oxidative dearomatization methods, this electrochemical strategy avoids external catalysts, oxidants, and additives, broad functional-group tolerance, scalability, and efficient access to structurally diverse N-heterocycles, highlighting the growing utility of electro-organic synthesis in heterocyclic chemistry and late-stage functionalization.

Synthesis of highly functionalized spirolactams: Spirocyclic compounds are prominent structural motifs in natural products, pharmaceuticals, and functional materials due to their rigid three-dimensional architectures and unique biological properties [63]. Among them, spiro[4.5]trienones have attracted considerable attention as versatile intermediates for the construction of complex molecular frameworks [64]. In this regard, the



Scheme 20: Proposed mechanism for the synthesis of diverse 4-imidazolidinones **58**.

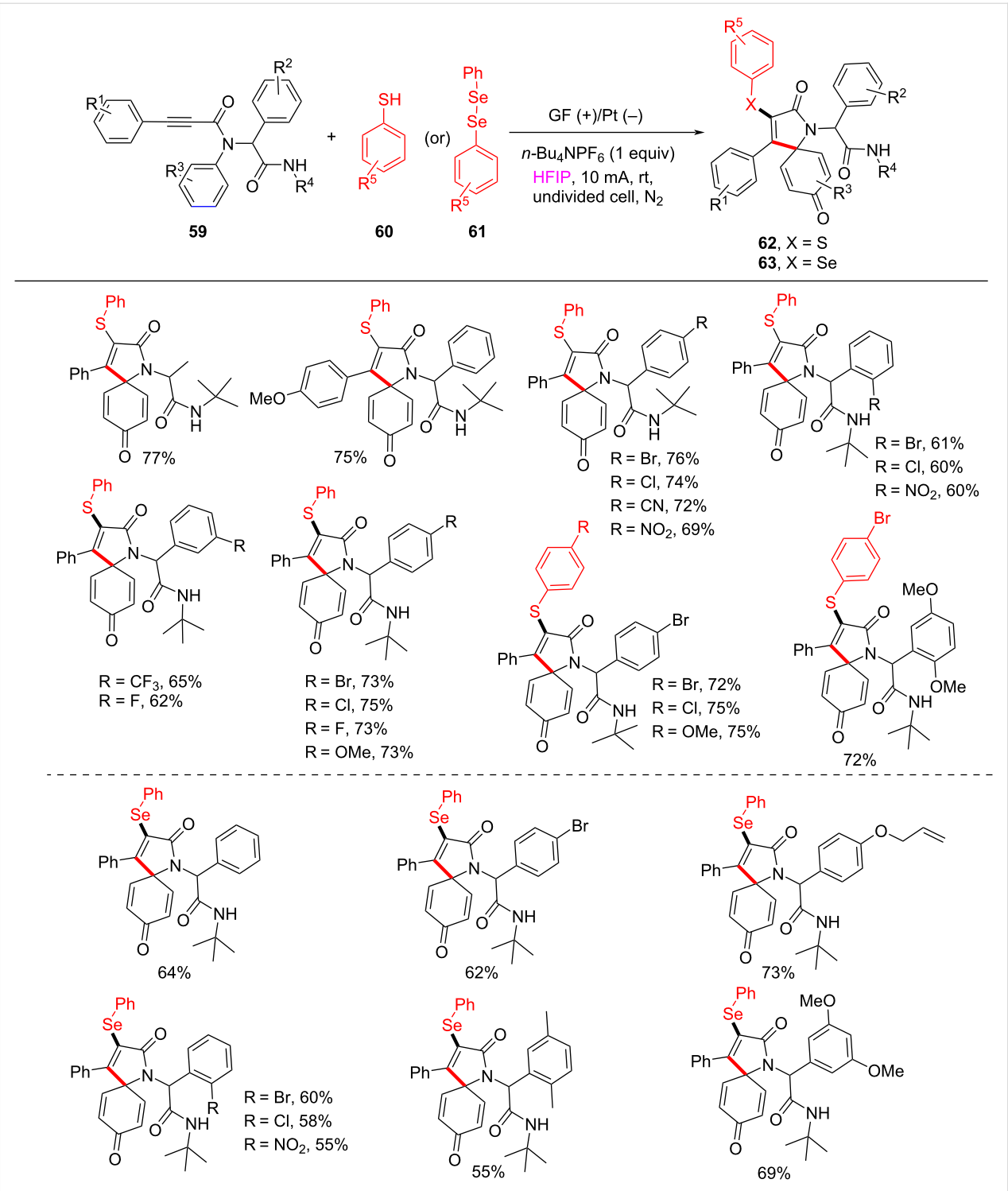
merger of multicomponent Ugi chemistry with electro-organic synthesis has provided an efficient platform for the rapid assembly of structurally diverse azaspirocyclic systems.

A catalyst- and metal-free electrochemical strategy has been developed by Sharma and co-workers for the synthesis of C–S, C–Se, and C–C=O functionalized spirolactams from Ugi-derived bisamides through oxidative dearomatizing spirocyclization [65]. The transformation proceeds under mild electrochemical conditions via a radical-mediated cascade cyclization, enabling the formation of azaspiro-fused bicyclic scaffolds **62** and **63** (Scheme 21). The detailed regioisomeric and diastereomeric substrate scope is not shown in Scheme 21; readers are referred to the original report for further details. This electrochemical method offers a cleaner and more sustainable alternative by avoiding external oxidants, catalysts, and metals. The successful application of a micro-electro-flow reactor for gram-scale synthesis further demonstrates the practicality and scalability of the protocol.

The protocol exhibits a broad substrate scope and excellent functional-group tolerance (Scheme 21). Ugi adducts derived from various acids, aldehydes, amines, and isocyanides undergo smooth electrochemical cyclization irrespective of the electronic nature of aromatic substituents. Both electron-rich and electron-deficient aldehydes are well tolerated, while substituted anilines and diverse isocyanides further expand structural diversity. In addition, a wide range of thiols and diselenides bearing halogen, methoxy, and naphthyl substituents participate effectively, affording sulfur- and selenium-containing azaspirocycles in moderate to excellent yields. The methodology also accommodates aliphatic isocyanide-derived substrates and enables further transformation of the spirocyclic products into fully fused tricyclic systems.

Mechanistic investigations suggest that anodic oxidation simultaneously generates radical intermediates (**XXXI** and **XXXII**) from both the Ugi adduct and thiol/diselenide coupling partners, followed by radical addition to give **XXXIII**, cyclization, and demethylation of **XXXIV** to furnish the final spirocyclic products **62** and/or **63** (Scheme 22).

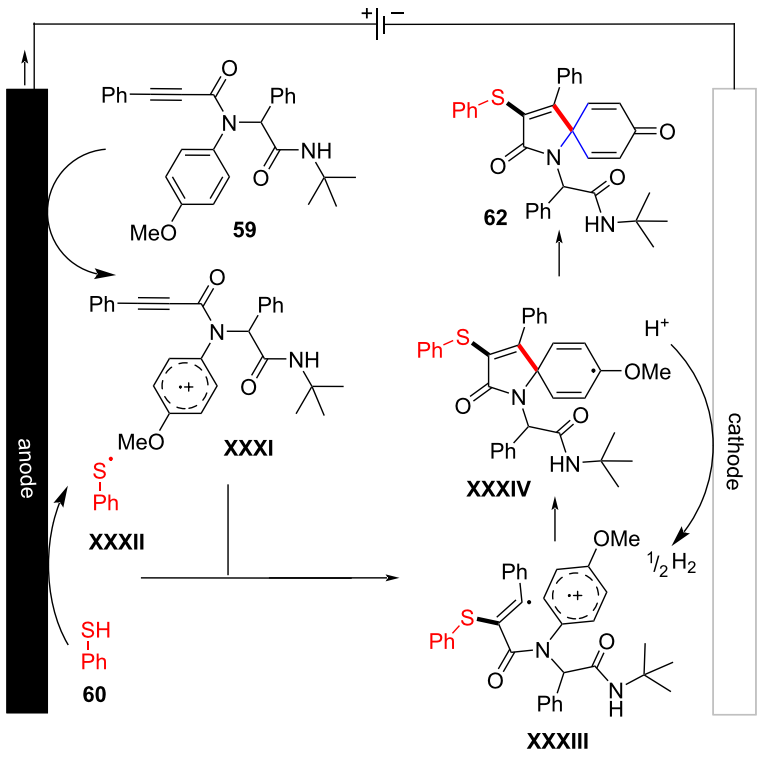
Five-five spiro-fused heterocyclic frameworks: *Synthesis of spirooxindole-γ-lactones:* Among spirocyclic frameworks,



Scheme 21: Substrate scope of electrochemical spirocyclization and selinidation conversions.

spirooxindoles constitute an especially important class owing to their broad biological activities and frequent occurrence in natural products and bioactive molecules [66]. In particular, spirooxindole-γ-lactones **66** and bis-spirooxindole **67**, in which the oxindole core is connected through the C3 position to an oxygen-containing five-membered ring, have emerged as attractive synthetic targets (Scheme 23a).

An efficient HFIP-mediated strategy has been developed by Saha and co-workers for the synthesis of spirooxindole-γ-



Scheme 22: Proposed mechanism for electrochemical spirocyclization conversions.

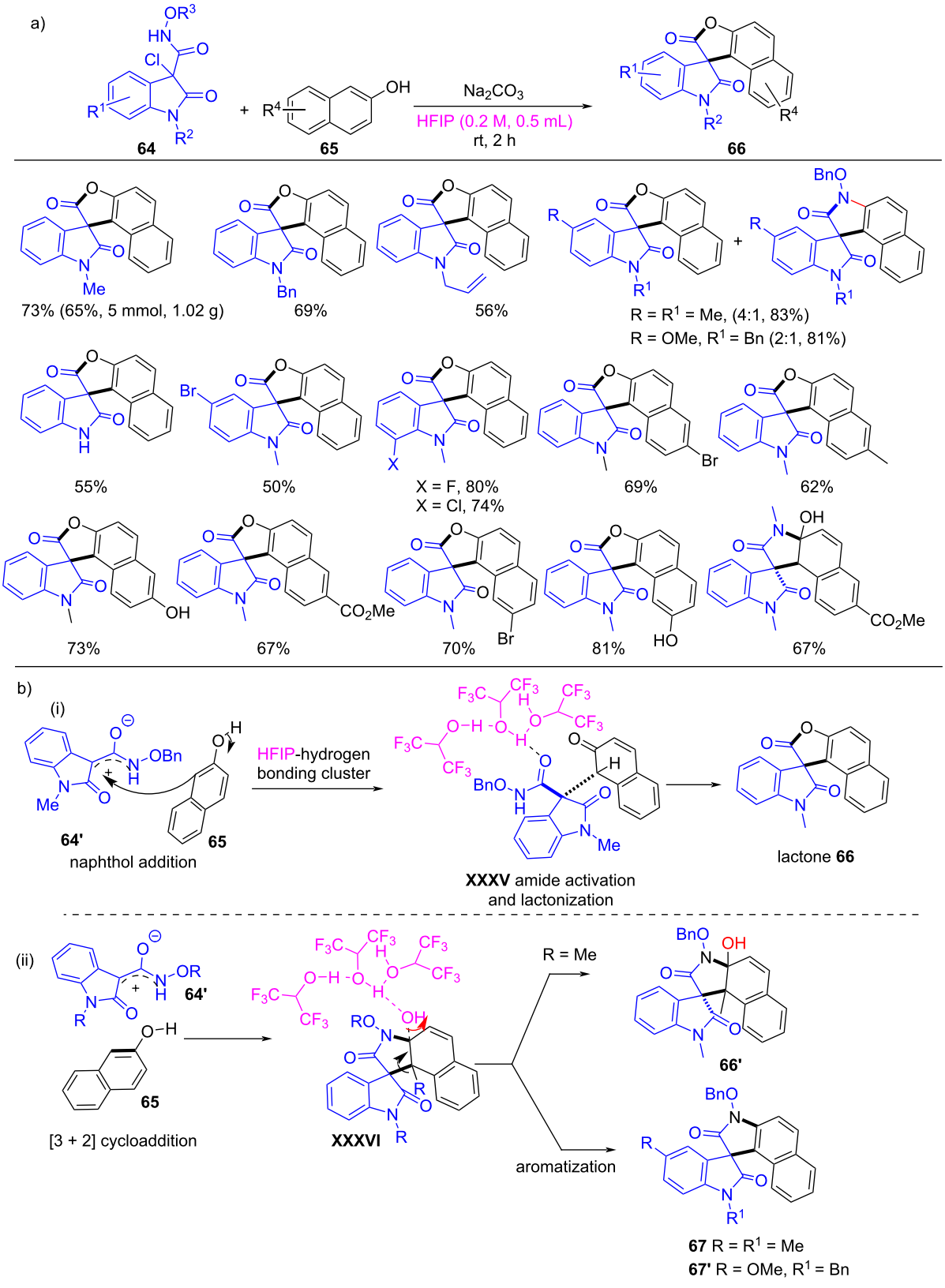
lactones **66** through the reaction of transient oxindolyl azaoxyallyl **64** cations with β-naphthols **65** [67]. In this transformation, HFIP acts not only as the sole activator for generating the azaoxyallyl cation but also facilitates the key lactonization step through hydrogen-bond-assisted activation.

The methodology demonstrates a broad substrate compatibility. Oxindoles bearing various N-substituents, including free NH derivatives, undergo smooth annulation, while substitutions at different positions of the oxindole ring significantly influence product distribution. Electron-rich C5-substituted oxindoles partially favor competing bis-spirooxindole formation, whereas halogen substitution, particularly at the C7 position, improves reaction efficiency and selectivity toward lactones. A variety of substituted β-naphthols containing electron-donating, electron-withdrawing, and halogen substituents are also well tolerated, generally affording moderate to good yields. Interestingly, sterically modified naphthol substrates can alter the reaction pathway, leading exclusively to dearomative [3 + 2] cycloaddition products (Scheme 23a). Overall, this HFIP-enabled strategy provides a versatile and selective route to biologically relevant spirooxindole-γ-lactones and related fused oxygen heterocycles, while also expanding the synthetic utility of azaoxyallyl cation intermediates in complex spirocycle synthesis.

Mechanistically, nucleophilic addition of β-naphthol **65** to the azaoxyallyl intermediate **64'** is followed by rapid intramolecular cyclization (**XXXV**) to furnish the spiro-lactone scaffold **66**. In contrast to competing [3 + 2] cycloaddition pathways that generate bis-spirooxindole products **67**, lactonization predominates in most cases, highlighting the high chemoselectivity of the protocol (Scheme 23b).

Five-six spiro-fused heterocyclic frameworks: *PIDA-Promoted/HFIP-controlled dearomative spirocyclization of phenolic ketones:* Spirocyclohexadienones are important structural motifs found in numerous biologically active natural products and pharmaceutical compounds [68], and they also serve as versatile intermediates for the synthesis of architecturally complex molecules. Dearomative spirocyclization has emerged as a powerful strategy for constructing these highly functionalized three-dimensional frameworks from simple aromatic precursors [69].

In this context, a PIDA (phenyliodine(III) diacetate)-promoted and HFIP-controlled dearomative spirocyclization of phenolic ketones **68** has been developed by Peng and co-workers [70], enabling the efficient synthesis of spirocyclohexadienonic ketals **70** and their acetoxylated analogues under mild condi-



Scheme 23: a) Substrate scope for various oxindolyl α-halohydroxamate **64** and 2-naphthols **65.** b) Proposed mechanism for lactonization vs [3 + 2] cycloaddition–aromatization sequence.

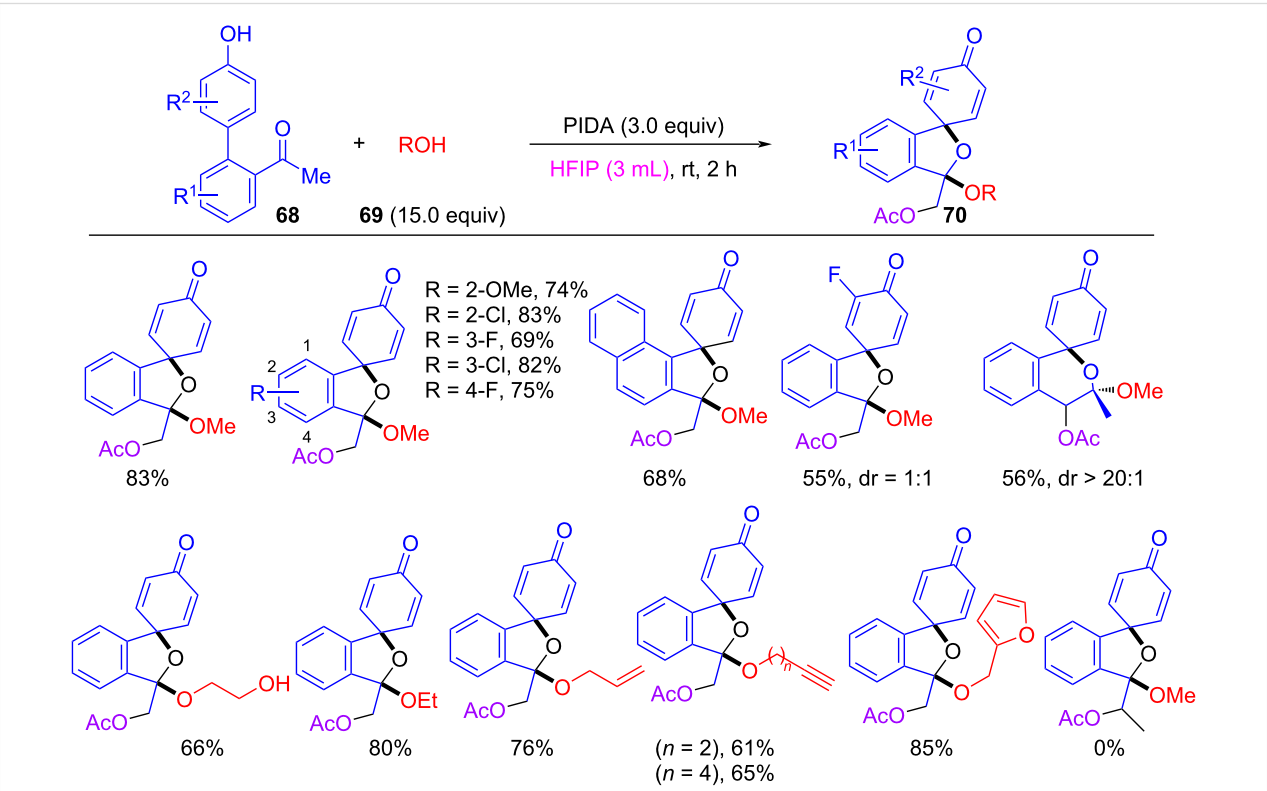
tions (Scheme 24). The combined use of alcohols **69** as the nucleophile and HFIP as the solvent proved crucial for controlling the cascade process, highlighting the distinctive role of HFIP in stabilizing cationic intermediates and promoting selective dearomatization.

The methodology exhibits good substrate generality, with a variety of substituted phenolic ketones and functionalized alcohols participating effectively to afford the desired products in moderate to excellent yields under mild oxidative conditions (Scheme 24). Both electronic and steric variations on the aromatic framework are well tolerated, and the process provides good regio- and diastereoselectivity in selected cases. However, deviations in substitution patterns, particularly at specific alkyl substituents, negatively influence reactivity, indicating some substrate limitations. Mechanistic studies suggest that the transformation proceeds through the generation of a spirocyclohexadienone oxocarbenium intermediate, which undergoes nucleophilic trapping to furnish the final spirocyclic products. In situ-generated hypervalent iodine catalytic version is observed in this phenomenon.

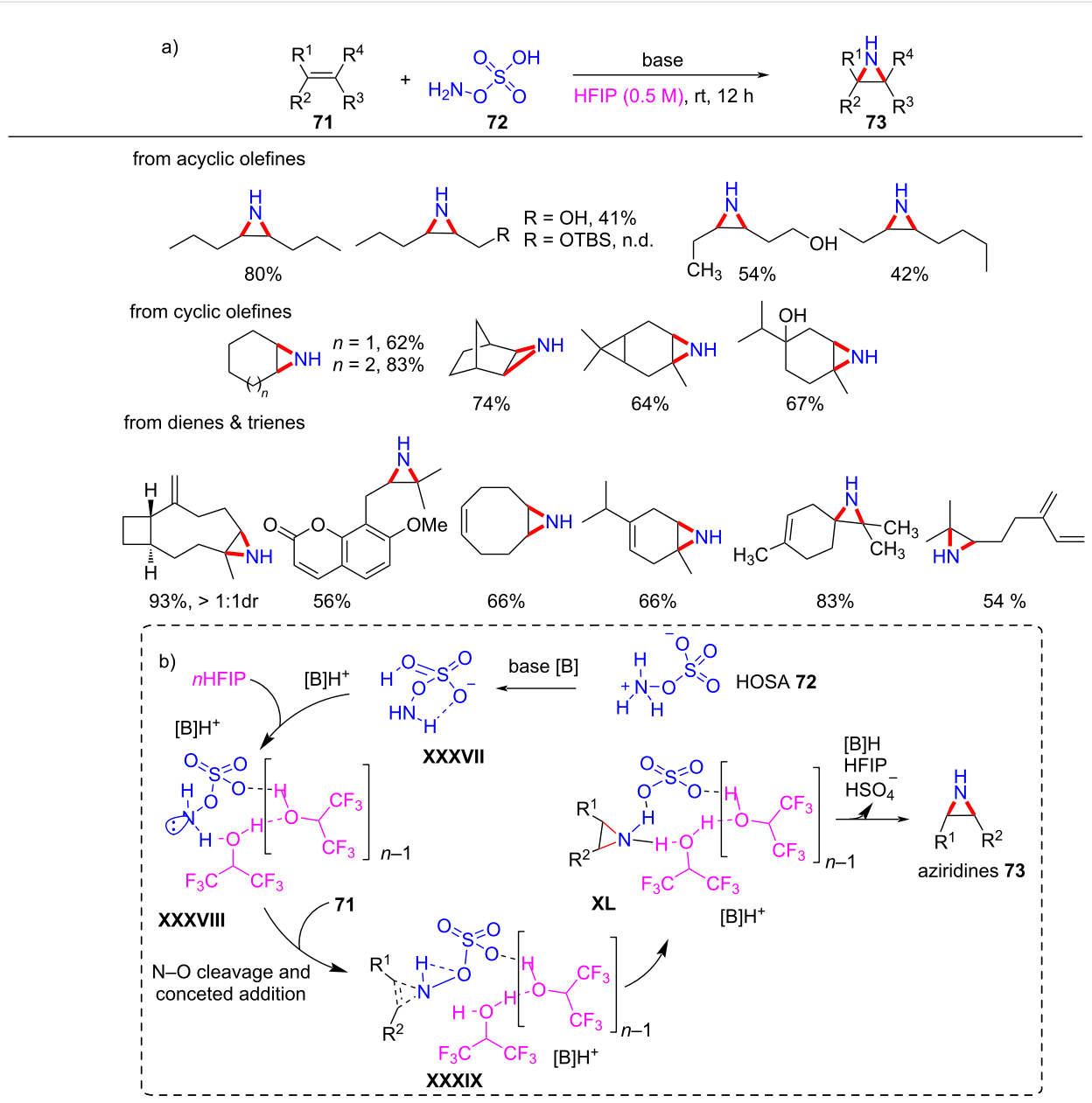
Saturated and non-aromatic heterocyclic rings

Three-membered saturated heterocycle construction: *Synthesis of N–H aziridines from unactivated olefins:* Aziridines, the smallest nitrogen-containing heterocycles, are important privileged scaffolds frequently encountered in natural products and biologically active molecules, including antitumor and antimicrobial agents [71]. A practical and efficient intermolecular aziridination protocol has been developed by Wang and co-workers using hydroxylamine-*O*-sulfonic acid (HOSA, **72**) as the aminating reagent in an HFIP-based solvent system with pyridine or piperidine as base additives (Scheme 25) [72]. The method enables direct conversion of a broad range of alkenes **71** into free N–H aziridines **73** under mild and operationally simple conditions. This HFIP-enabled protocol offers a simple, scalable, and metal-free alternative for accessing free N–H aziridines directly from unactivated alkenes. The combination of mild conditions, broad alkene scope, high regioselectivity, and gram-scale applicability underscores its potential utility for synthetic and medicinal chemistry applications.

The protocol exhibits broad substrate scope and particularly high efficiency with nonactivated alkenes (Scheme 25a). Mono-, di-, tri-, and tetrasubstituted alkenes all participate effectively, generally affording moderate to excellent yields. Electron-rich alkenes display enhanced reactivity, while terminal olefins are comparatively less reactive (not shown in the Scheme 25a). Cyclic and bridged cycloalkenes are well tolerated and often provide products with high stereoselectivity. The



Scheme 24: Scope of substrates for the synthesis of products **70**.



Scheme 25: a) Functional group compatibility for the products **73**. b) Proposed mechanism.

methodology also demonstrates remarkable regioselectivity in polyunsaturated systems, where aziridination selectively occurs at the more electron-rich double bond, even in the presence of multiple olefinic sites. Importantly, dienes and trienes undergo exclusive monoaziridination despite excess aminating reagent, highlighting the chemoselective nature of the process. Functional group compatibility is generally good, although free hydroxy groups can alter reactivity or lead to competing intramolecular ring-opening processes. In some substrates, protecting groups or changes in base were necessary to achieve optimal outcomes. Particularly noteworthy is the observation of cascade aziridination/ring-opening sequences in allylic alcohol substrates, illustrating the synthetic versatility of the generated aziridines.

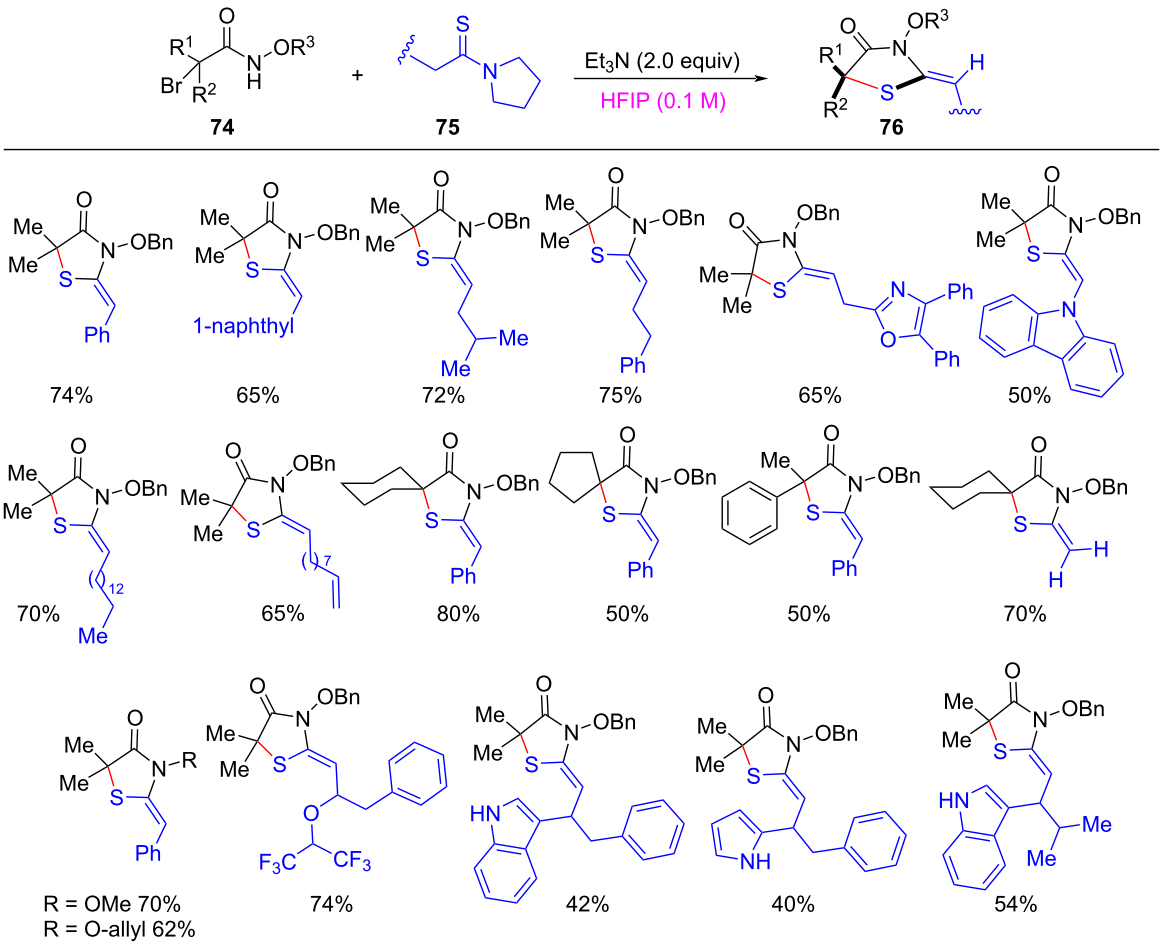
Mechanistically, the transformation is proposed to proceed through base-assisted activation of HOSA (**72**) followed by formation of a hydrogen-bonded HFIP cluster **XXXVIII** that facilitates N–O bond cleavage to generate a highly electrophilic aminating species **XXXIX**. Subsequent concerted addition (**XXXIX**) across the alkenes **71** furnish aziridine products **73**. The critical role of HFIP appears to arise from its ability to

stabilize reactive intermediates through extensive hydrogen-bonding interactions, thereby promoting efficient aziridination under metal-free conditions (Scheme 25b).

Five-membered saturated heterocycle construction: *Synthesis of structurally diverse alkylidene-4-thiazolidinones/selenazolidinones:* Thiazolidine-4-ones are an important class of S,N-heterocycles widely associated with diverse biological activities, including antimicrobial, antiviral, anticancer, and anti-inflammatory properties [73]. A mild and efficient HFIP-promoted one-pot strategy has been developed by Saha and co-workers for the synthesis of structurally diverse alkylidene-4-thiazolidinones **76** through cycloaddition of α-bromohydroxamates **74** with thioamides **75** (Scheme 26) [74], followed by spontaneous E_1-type elimination of the C2 amino group from the intermediate cycloadduct. Notably, the transformation proceeds under metal- and acid-free conditions without the need for amine quaternization, while enabling stereoselective formation of the exocyclic olefin.

This protocol offers a concise, modular, and operationally simple alternative for accessing highly functionalized alkylidene-4-thiazolidinones **76** and related heterocycles. The combination of broad substrate compatibility, stereoselective olefin formation, scalability, and extension to spirocyclic and selenium-containing systems underscores the versatility and synthetic value of the methodology.

The methodology displays a broad substrate scope and excellent functional-group tolerance (Scheme 26). A variety of aryl, naphthyl, and alkyl-substituted thioamides participate efficiently, including substrates containing terminal or internal alkenes that remain chemoselectively untouched despite the potential for competing cycloaddition reactions. The protocol also accommodates heteroatom-containing side chains, conjugated systems, and drug-derived thioamides, illustrating its applicability for late-stage diversification. Particularly noteworthy is the compatibility of β-hydroxy thioamides, which enables access to conjugated α,β-unsaturated thiazolidinones



Scheme 26: Substrate scope for the synthesis of alkylidene-4-thiazolidinone **76**.

after oxidation, providing motifs commonly encountered in biologically active molecules [74].

The scope further extends to diverse α-halohydroxamates bearing cycloalkyl, aryl, allyl, *tert*-butyl, and propargyl substituents (not shown in the Scheme 26), while oxindole-derived precursors enable direct synthesis of spirooxindolyl thiazolidinones with medicinally relevant architectures. In addition, the methodology was successfully adapted to the synthesis of selenazolidinones from selenomides, significantly broadening the heterocyclic diversity accessible through this platform. Several downstream transformations, including sulfur oxidation and N–O bond cleavage, further demonstrate the synthetic utility of the products.

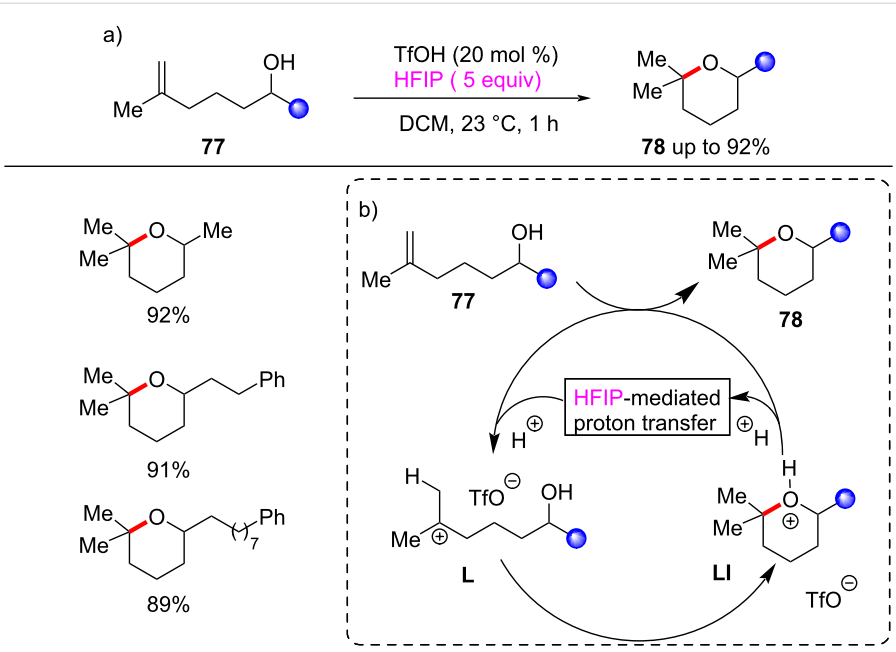
Mechanistically, the reaction involves in situ generation of an azaoxyallyl cation that undergoes annulation with thioamides to form aminothiazolidinone intermediates. HFIP plays a central role throughout the process by facilitating azaoxyallyl cation formation, stabilizing carbocationic intermediates, and promoting stereoselective α-deprotonation to furnish predominantly *Z*-configured alkylidene products. The study highlights the multifaceted influence of HFIP in controlling both reactivity and selectivity.

Six-membered saturated heterocycle construction: *Synthesis tetrahydropyran derivatives:* Tetrahydropyrans (THPs) and tetrahydrofurans (THFs) are important oxygen-containing heterocycles frequently encountered in natural products, pharmaceuticals, fragrances, and flavoring agents [75]. A mild Brønsted acid-catalyzed intramolecular hydroalkoxylation strategy has been developed by Maulide and co-workers for the regioselective synthesis of trisubstituted tetrahydropyran derivatives **78** using catalytic triflic acid in the presence of HFIP (Scheme 27a) [76].

This approach provides a straightforward and operationally simple route to cyclic ethers with high efficiency and minimal purification requirements. The combination of catalytic Brønsted acid activation and HFIP-mediated proton transfer offers an effective strategy for constructing structurally diverse THP and THF scaffolds under mild conditions.

The methodology exhibits good substrate generality and tolerates both aromatic and aliphatic side chains without significant loss in efficiency (Scheme 27a), affording the desired tetrahydropyrans **78** in consistently high yields. In addition to six-membered ring formation, the protocol also enables access to bridged bicyclic tetrahydrofuran derivatives when dictated by conformational or ring-strain preferences. In one notable case, cyclization selectively produced a THF rather than the corresponding THP, likely due to the unfavorable conformational requirements associated with the alternative six-membered ring system. This observation highlights the influence of substrate geometry and ring stability on regioselectivity.

Mechanistic observations suggest that HFIP plays a crucial role in facilitating proton-transfer processes and stabilizing reactive



Scheme 27: a) Scope of TfOH-catalyzed reaction. b) Proposed mechanism for products **78**.

cationic intermediates, thereby enabling efficient cyclization under catalytic acid conditions and relatively mild reaction parameters (Scheme 27b). The transformation proceeds through protonation of the alkene to generate a tertiary carbocation intermediate **L**, followed by intramolecular nucleophilic attack of the hydroxy group and subsequent deprotonation of **LI** to furnish the cyclic ether product **78**.

Mixed five-/six-membered heterocycle construction: *Leveraging the domino skeletal expansion of thia-/selenazolidinones:* Functionalization and skeletal editing of heterocycles remain central strategies in modern organic synthesis and medicinal chemistry [77]. In this context, a highly regioselective domino skeletal-expansion protocol has been developed by Saha and co-workers for the conversion of 2-aminothiazolidinones **79** into six-membered S,N-heterocycles **81** using TMS-azide (**80**) in HFIP at ambient temperature and under metal-free conditions (Scheme 28) [78]. The transformation exploits the latent nucleofugal reactivity of the C2 tertiary amine in thiazolidinones, enabling relay substitution with azide followed by ring expansion through an intermolecular nitrogen-atom transfer process. The mild reaction conditions, broad substrate compatibility, scalability, and applicability to late-stage modification make the methodology particularly attractive for medicinal chemistry and heterocyclic scaffold diversification.

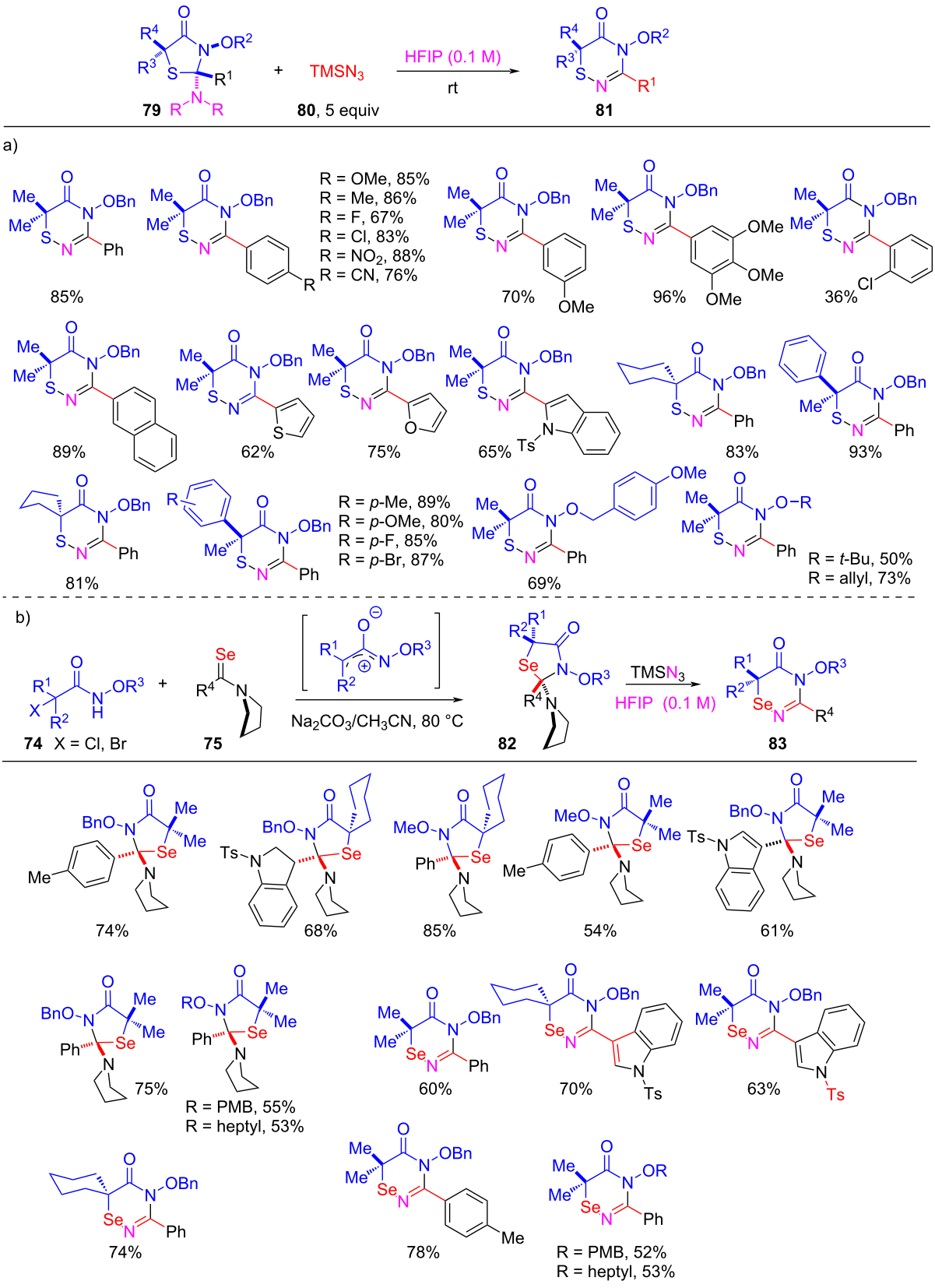
The methodology exhibits a broad substrate scope and tolerates a wide range of substituents on the thiazolidinone framework (Scheme 28a). Electron-donating and electron-withdrawing aryl groups at the C2 position are well accommodated, generally providing the expanded heterocycles in good to excellent yields. Extended π-systems and heteroaryl substituents, including naphthyl, furyl, thienyl, and protected indolyl motifs, are also compatible. In contrast, *ortho*-substituted substrates display diminished efficiency due to steric effects, while free indole NH groups inhibit the transformation. The practicality of the protocol is further demonstrated through gram-scale synthesis and late-stage functionalization of the drug deferasirox.

Variation at the C5 position and N–OR substituent further highlights the versatility of the strategy. Spirocyclic and *gem*-disubstituted substrates undergo efficient ring expansion, whereas monosubstituted analogues fail to initiate the key solvolysis step required for rearrangement. Diverse alkyl, allyl, propargyl, and carbohydrate-derived substituents at the N–OR site are all tolerated, enabling access to structurally diverse heterocyclic architectures (Scheme 28b). Importantly, the methodology could be extended to previously unexplored 4-selenazolidinone substrates, providing access to six-membered Se,N-heterocycles under analogous conditions. This extension significantly broadens the heteroatom diversity accessible through the strategy and further demonstrates the generality of the underlying ring-expansion concept.

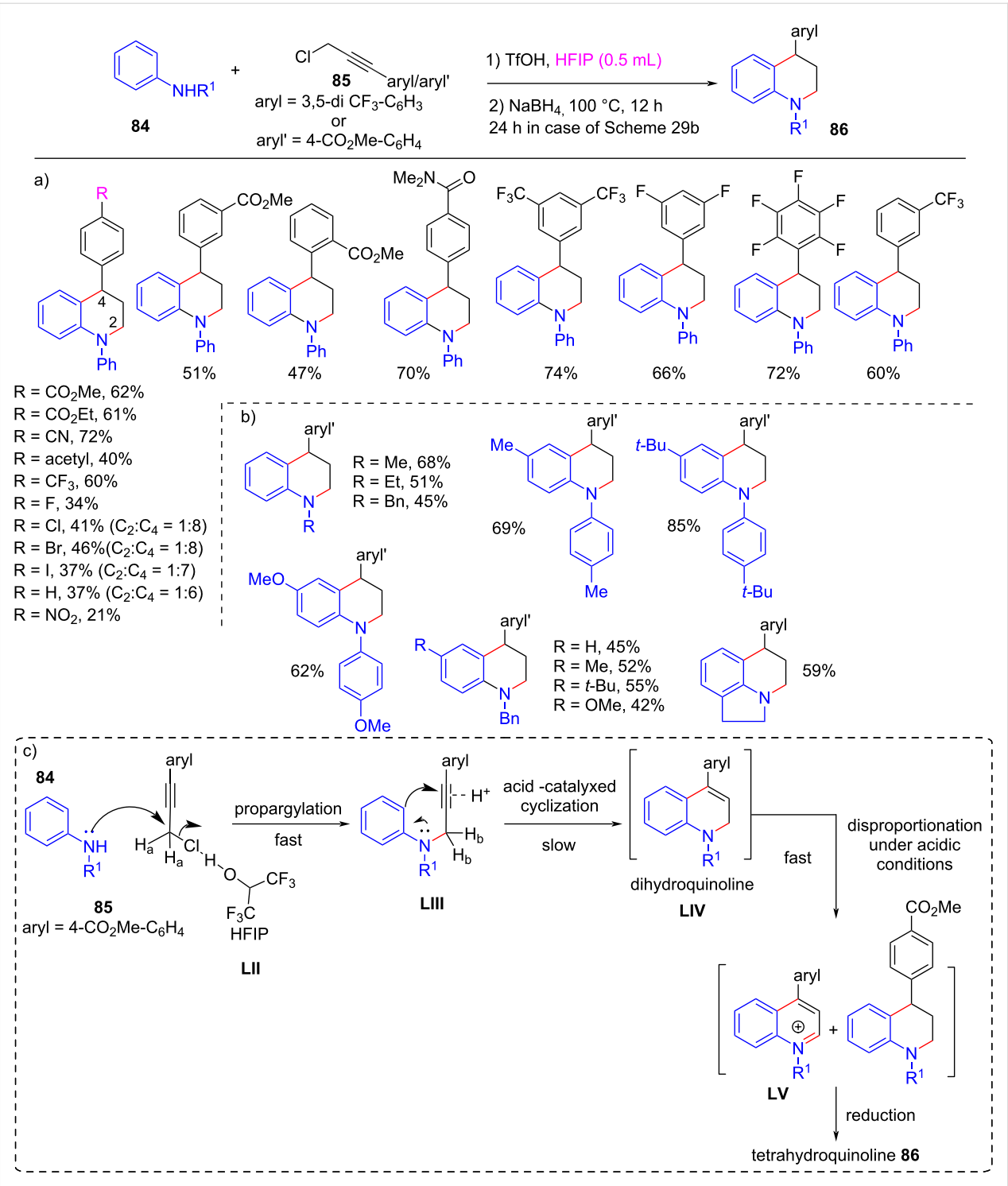
Mechanistic investigations, supported by control experiments and DFT calculations, indicate that HFIP plays a multifaceted role in promoting C–N bond cleavage, stabilizing reactive intermediates, and facilitating nitrogen transfer and ring expansion. The process proceeds under exceptionally mild conditions without the need for metals, acids, or additional additives, emphasizing the unique activating ability of HFIP in skeletal rearrangement chemistry.

Six-membered fused saturated heterocycle construction: *Synthesis of C4-aryl-substituted tetrahydroquinolines:* In particular, HFIP-assisted activation of C–H and C-heteroatom bonds has enabled the development of efficient transition-metal-free heterocycle syntheses under mild reaction conditions [79]. A notable example is the one-pot synthesis of C4-aryl-substituted tetrahydroquinolines **86** from simple anilines **84** and propargylic chlorides **85** under transition-metal-free conditions and this protocol was developed by Chi and Lee (Scheme 29) [80]. In this transformation, HFIP plays a decisive role in activating the C–Cl bond of propargylic chlorides, thereby enabling propargylation of anilines even in acidic media. Subsequent acid-promoted cyclization and reductive rearomatization furnished tetrahydroquinoline products **86** efficiently through a sequential propargylation–cyclization pathway. This strategy offers operational simplicity, avoidance of metal catalysts, and broad substrate compatibility. This HFIP-enabled strategy highlights the broader synthetic potential of fluorinated alcohols in heterocycle construction. Compared with traditional metal-catalyzed tetrahydroquinoline syntheses, the protocol provides a more sustainable and operationally straightforward alternative while maintaining broad functional-group tolerance and scalability. At the same time, the dependence on substrate electronics and the moderate efficiency observed for certain electron-deficient systems illustrate the continuing challenges associated with fully general HFIP-mediated activation processes.

The methodology demonstrated substantial tolerance toward electronically diverse propargylic chlorides, including ester, amide, nitrile, ketone, trifluoromethyl, trifluoromethoxy, triflate, and halogen-substituted systems, generally affording moderate to good yields (Scheme 29a). Electron-deficient fluorinated substrates often provided improved reactivity, suggesting beneficial interactions between substrate electronics and HFIP-mediated activation. In contrast, strongly electron-withdrawing nitro substituents significantly reduced efficiency, likely because of competing hydrogen-bond interactions that interfere with effective substrate activation. Halogenated substrates, including chloro, bromo, and iodo derivatives, were also



Scheme 28: Substrate scope for six-membered (a) S,N-heterocycles **81** and (b) Se,N-heterocycles **83**.



Scheme 29: a) Reaction scope of propargylic chlorides. b) Scope of aniline moieties. c) Proposed mechanism.

compatible, although regioisomeric mixtures were occasionally observed.

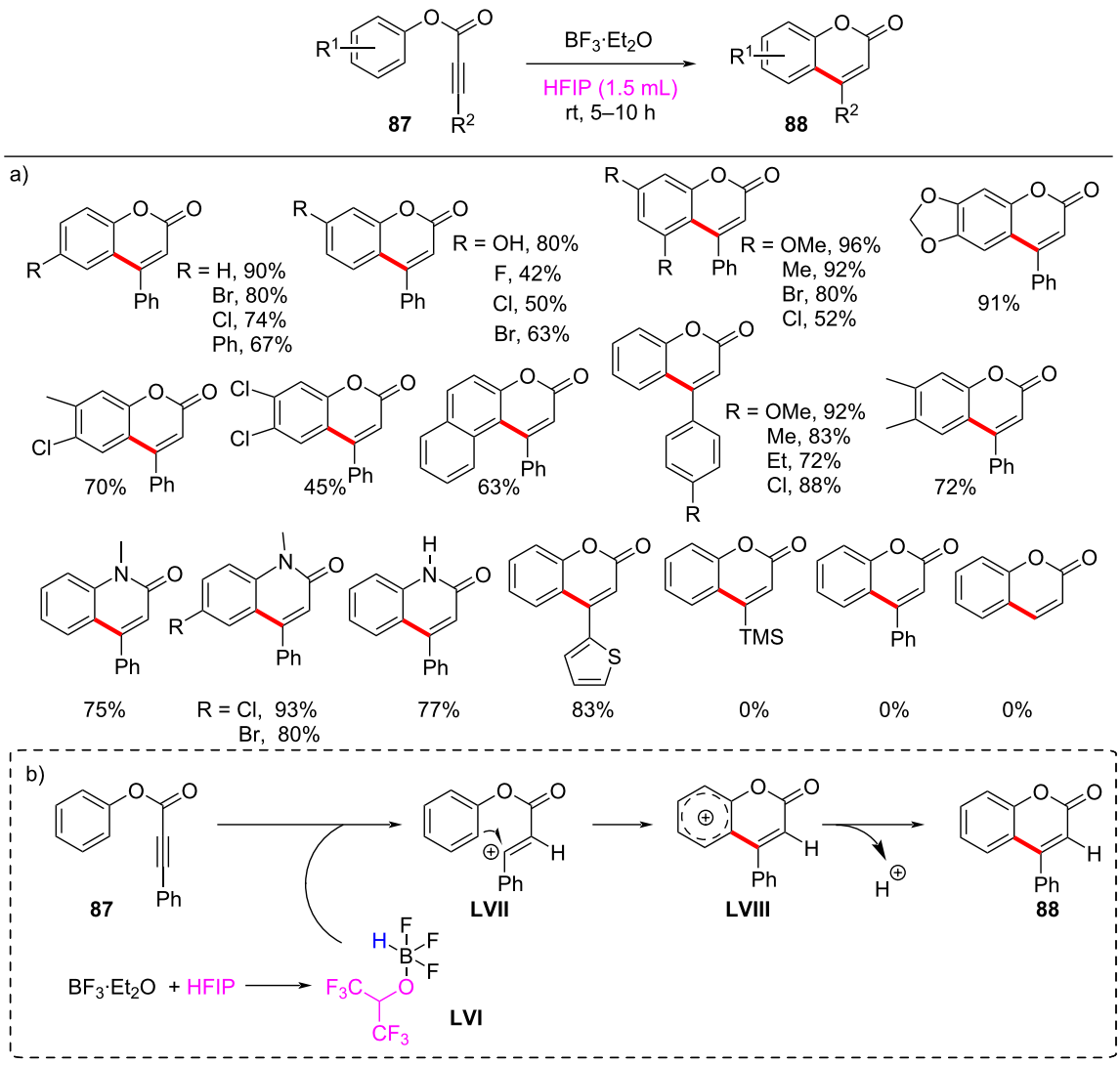
Variation of the aniline component further highlighted the scope and limitations of the protocol. Alkyl-, alkoxy-, and sterically substituted diarylamines underwent smooth cyclization to provide functionalized tetrahydroquinolines in moderate to excellent yields, whereas highly electron-deficient diarylamines proved less effective. The methodology also accommodated benzyl-protected anilines and heterocyclic substrates such as

indoline, demonstrating applicability toward biologically relevant tetrahydroquinoline frameworks and late-stage scaffold diversification (Scheme 29b).

Mechanistic studies supported a pathway involving HFIP-assisted activation of the propargylic chloride **85**, followed by rapid formation of propargylic amine intermediates **LII** and **LIII** (Scheme 29c). Acid-catalyzed intramolecular cyclization generated dihydroquinoline intermediates **LIV**, which subsequently underwent disproportionation and reductive conversion of **LV** to the final tetrahydroquinolines **86**. Importantly, HFIP was proposed not only to activate the C–Cl bond but also to modulate the reactivity of sodium borohydride through hydrogen-bonded ionic complexes, thereby enabling compatibility with sensitive carbonyl-containing substrates under otherwise strongly reducing conditions.

Intramolecular alkyne cyclization to coumarins: Coumarins represent an important class of naturally occurring heterocycles with broad pharmacological relevance, including antioxidant, anticancer, antimicrobial, and neuroprotective activities [81]. In this context, HFIP-based catalytic systems have recently enabled efficient and sustainable approaches to coumarin construction, particularly through intramolecular alkyne cyclization strategies that proceed under metal-free and mild conditions [82]. Among these, a cooperative HFIP/$BF_3{\cdot}Et_2O$ system has emerged as a particularly effective platform, illustrating how solvent-catalyst synergy can be exploited to access complex oxygen heterocycles and this was reported by Wu and co-workers (Scheme 30) [82].

In this methodology, electron-rich and moderately substituted phenyl propiolates **87** undergo smooth cyclization to furnish



Scheme 30: a) Substrate scope coumarin synthesis. b) Proposed mechanism.

4-aryl- and heteroarylcoumarins **88** in generally high yields, whereas electron-withdrawing substituents tend to decrease reactivity, consistent with an electrophilic addition–cyclization mechanism (Scheme 30a). This contrasts with more electronically tolerant HFIP-only or radical-based systems, highlighting the greater charge-dependence of BF_3-assisted pathways. Nevertheless, the protocol shows broad functional-group compatibility overall, including cyclic, heteroaromatic, and amide-derived substrates, with the latter significantly expanding access to nitrogen-containing analogues. This strategy avoids metal residues while maintaining operational simplicity, though it can require elevated temperatures for less reactive substrates.

Mechanistically, the reaction is proposed to proceed through in situ formation of a strongly acidic species **LVI** arising from interaction between HFIP and $BF_3{\cdot}Et_2O$. This activated complex promotes carbocation formation **LVII** from the alkyne precursor **87**, followed by intramolecular cyclization (**LVIII**) to construct the coumarin framework **88**. HFIP plays a dual and non-trivial role: beyond serving as a polar, hydrogen-bonding medium, it stabilizes key cationic intermediates through an extended hydrogen-bond network and facilitates smooth progression of the electrophilic cascade (Scheme 30b). Compared with electrochemical or radical HFIP-enabled systems, this approach is more ionically driven, relying on carbocation stabilization rather than radical generation or redox processes.

This strategy is distinct in its reliance on electrophilic activation of alkynes rather than radical or oxidative pathways. Despite some limitations in substrate scope for deactivated systems, the methodology provides a valuable, scalable, and metal-free route to biologically relevant coumarin frameworks and further underscores the multifunctional role of HFIP as both solvent and catalytic partner in modern heterocycle synthesis.

Seven-membered fused saturated heterocycle construction: *Direct synthesis of benzo[b]azepines:* Benzo[*b*]azepines **90** are structurally important seven-membered nitrogen heterocycles frequently found in bioactive molecules and drug candidates [83]. In this context, a metal-free I_2-mediated [6 + 1] annulation using protonated aminating reagent ($MsONH_3OTf$) and alkynes **89** has been developed by Yan and co-workers as an efficient route to this scaffold under mild conditions, highlighting the growing utility of radical and Brønsted acid cooperative systems in medium-ring heterocycle construction (Scheme 31) [84].

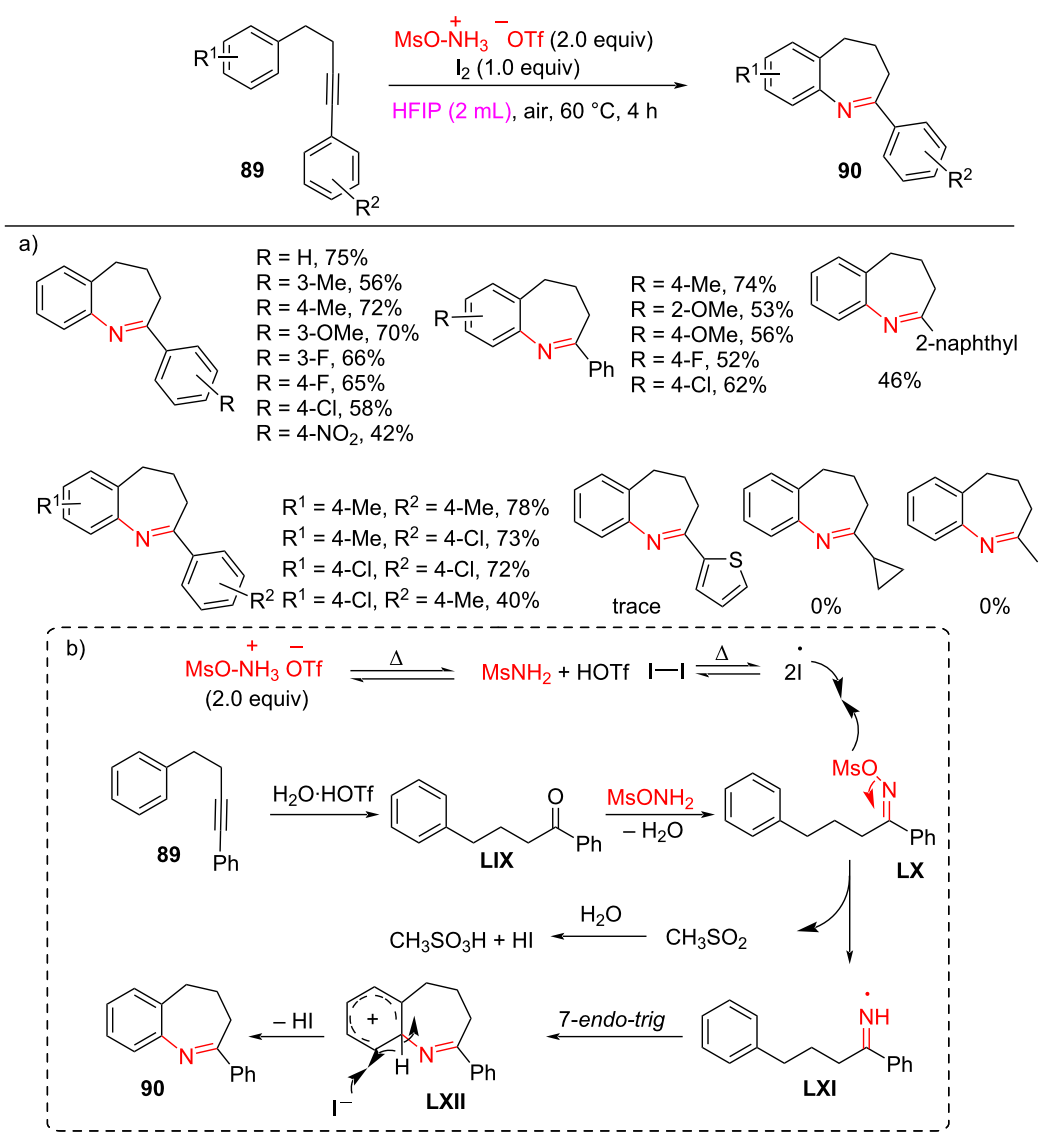
The method shows broad tolerance toward both electron-donating and electron-withdrawing substituents on the aromatic ring (Scheme 31a), with generally moderate to good yields across *para*-, *meta*-, and *ortho*-substituted substrates. The transformation displays relatively low sensitivity to electronic effects and steric variation, indicating a robust reaction manifold. However, limitations are observed with certain alkynes bearing heteroaryl (e.g., thienyl), strained alkyl (cyclopropyl), or simple alkyl substituents, which fail to deliver the desired products, suggesting constraints in radical stabilization and intermediate reactivity.

Mechanistically, the reaction is proposed to proceed through in situ generation of HOTf, which catalyzes alkyne hydration to yield **LIX** followed by condensation with $MsONH_2$ to form an oxime intermediate **LX**. This is then activated by iodine to generate an N-centered radical **LXI** via N–O bond homolysis, followed by radical cyclization (**LXII**) to construct the seven-membered ring **90** (Scheme 31b). Compared with HFIP-stabilized ionic pathways or electrochemical radical systems, this transformation relies on a hybrid acid-radical sequence where iodine serves as the key redox mediator rather than an external oxidant or electrode. The absence of transition metals and the in situ generation of reactive species make the protocol operationally simple, although dependence on radical propagation and substrate compatibility limits its universality compared to more general HFIP-enabled cyclizations.

Overall, this benzo[*b*]azepine **90** synthesis complements other modern heterocycle-forming strategies by occupying a mechanistic space between ionic HFIP as a solvent mediated cyclizations and electrochemical radical processes. While HFIP-based systems excel in stabilizing cationic intermediates and electrochemical methods offer controlled redox activation, this iodine-mediated approach provides a practical alternative for accessing medium-sized N-heterocycles **90** through radical annulation under mild, metal-free conditions.

Nine-membered fused saturated heterocycle construction: *Synthesis of nine-membered heterocyclic derivatives:* Medium-sized ring systems, particularly nine-membered frameworks, are prevalent in complex natural products and bioactive molecules, yet their synthesis remains challenging due to unfavorable entropic constraints and transannular strain effects [85]. In response, a metal-free, redox-neutral hydride-transfer (HT)-triggered cross-dehydrogenative coupling (CDC) strategy has been developed by Xiao and co-workers for the construction of quinoline-fused nine-membered rings **92**, offering a step- and atom-economical alternative to traditional prefunctionalized approaches (Scheme 32) [86].

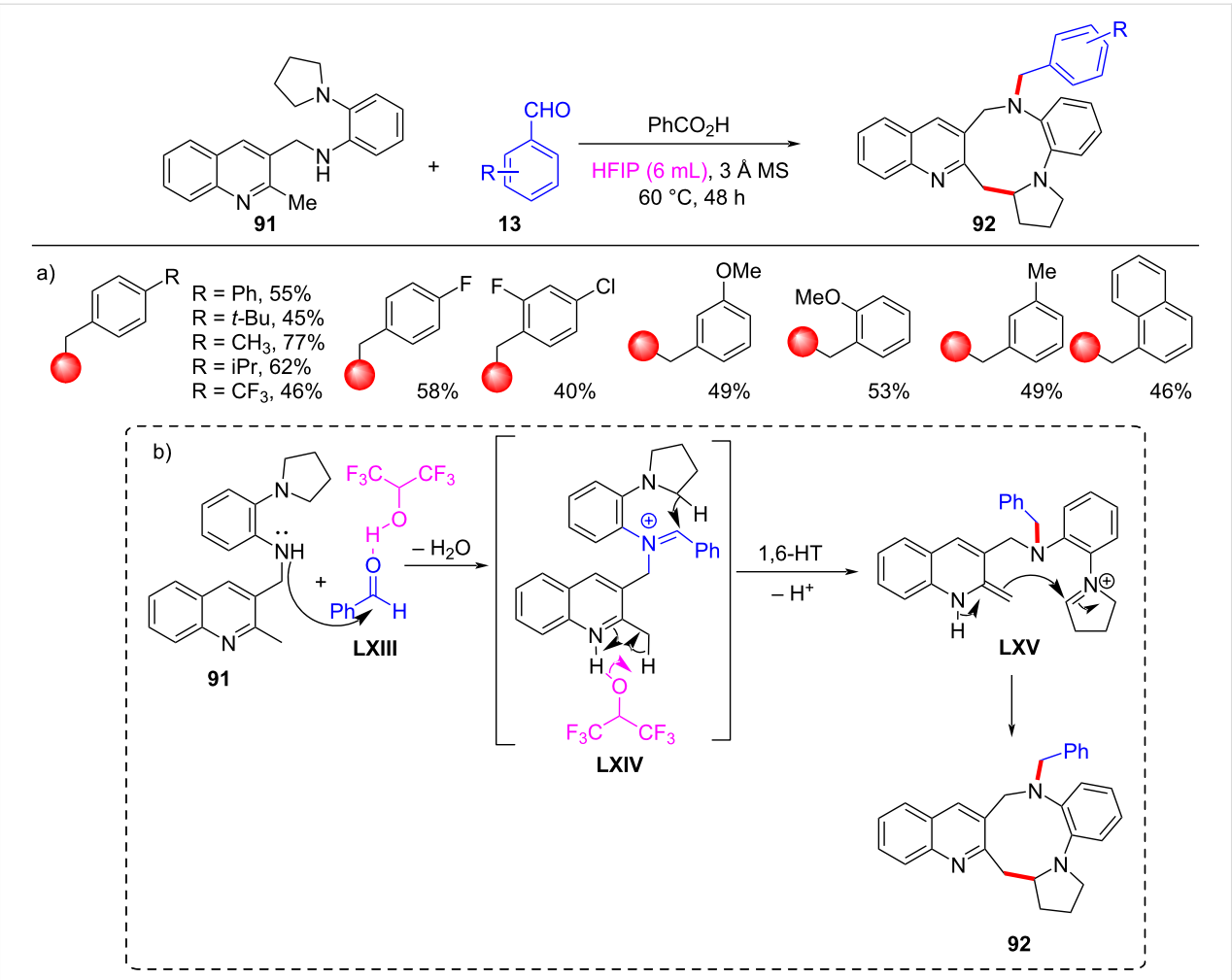
This transformation proceeds efficiently across a broad range of aromatic aldehydes and diamines, demonstrating generally good functional-group tolerance (Scheme 32a). Electron-rich aldehydes tend to give higher yields, whereas electron-withdrawing



Scheme 31: a) Scope of 1,4-diarylalkynes for the synthesis of **90**. b) Proposed mechanism.

substituents lead to reduced efficiency, reflecting the key role of iminium ion stability in governing reactivity. Steric effects are also significant, with *meta*-substitution resulting in diminished yields, while heteroaromatic systems such as naphthaldehydes remain competent substrates. This CDC process is more strongly governed by iminium ion formation and hydride-transfer dynamics, making it particularly sensitive to electronic effects. While highly efficient and environmentally favorable, its strong dependence on iminium stability and electronic effects contrasts with the broader functional tolerance often observed in HFIP-stabilized radical or electrochemical systems. Nevertheless, it represents a valuable complement within modern CDC and medium-ring synthetic methodologies, particularly for accessing complex quinoline-fused architectures in a single-step, green fashion.

Mechanistically, HFIP plays a central dual role: it facilitates aldimine formation to generate iminium ion intermediates and stabilizes charged transition states through an extended hydrogen-bonding network (Scheme 32b). The reaction is initiated by HFIP-assisted iminium formation (**LXIII**), followed by an intramolecular hydride transfer that activates a C(sp^3)–H bond and generates a second iminium species **LXIV**. Subsequent nucleophilic capture by an enamine intermediate **LXV** delivers the cyclized product **92**. The addition of benzoic acid further enhances acidity through a "combined acid" effect, reinforcing the catalytic environment. Compared with electrochemical or radical CDC methodologies, this approach is distinctive in its purely redox-neutral nature, avoiding external oxidants or catalysts while relying instead on internal hydride transfer and acid-assisted activation.

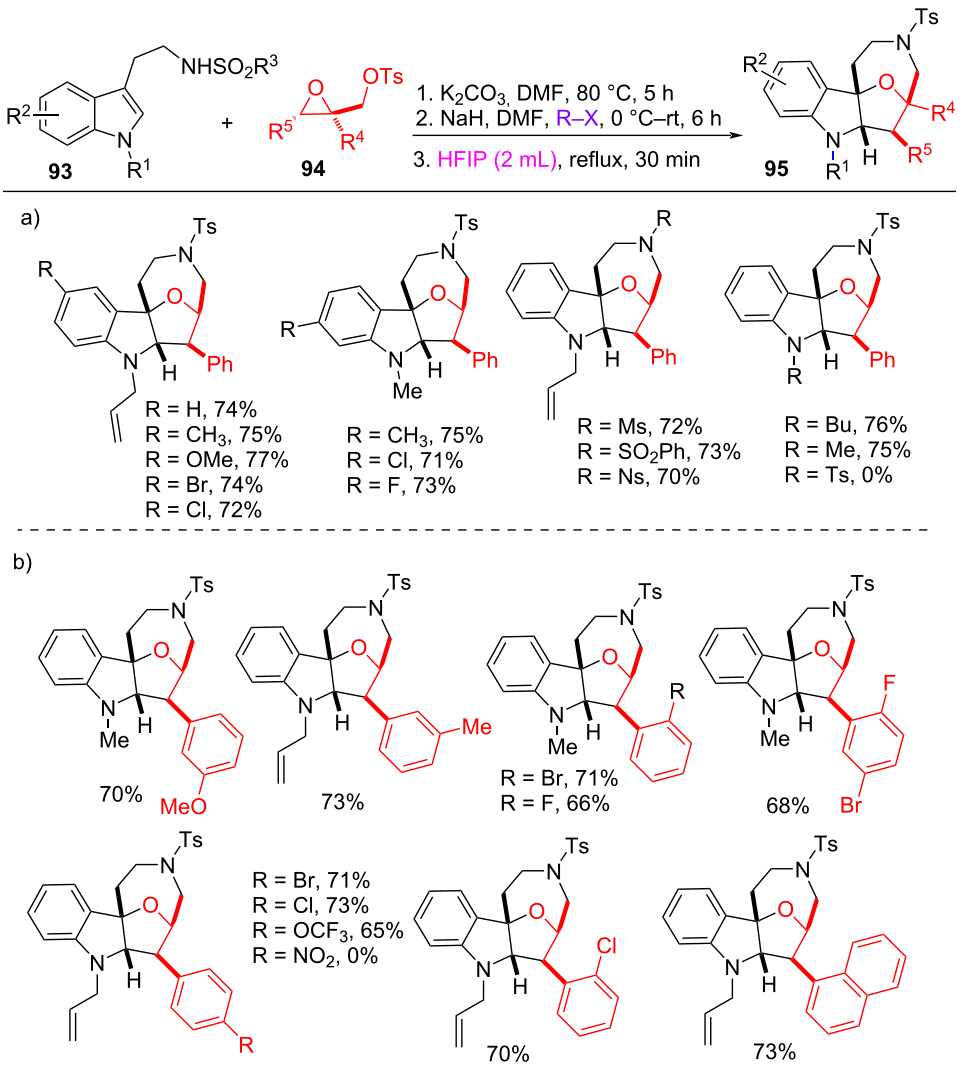


Scheme 32: a) Substrate scope for the synthesis of nine-membered rings. b) Proposed mechanism.

Polyfused saturated heterocycle construction: *Formal umpolung reactivity of indole derivatives:* Indole functionalization, particularly at the C2 and C3 positions, has long been dominated by its inherent nucleophilicity toward electrophiles [87,88]. In this context, an HFIP as a solvent promoted cascade process developed by Das and Chouhan involving epoxide-tethered indoles provides an unusual and conceptually important deviation from conventional indole reactivity, enabling a formal C3 umpolung through a dearomative cyclization–rearrangement sequence [89]. This strategy delivers highly complex fused-bridged indoline architectures **95** in a single operation with excellent regio- and diastereocontrol, significantly expanding the synthetic landscape of indole chemistry (Scheme 33).

The transformation exhibits a broad substrate scope across tryptamine derivatives **93** bearing diverse electronic and steric substitution patterns on the aromatic ring, including electron-donating and moderately electron-withdrawing groups, which generally furnish products **95** in high yields (Scheme 33). Variations in *N*-protection and *N*-alkyl substituents are also well tolerated, indicating that the reaction is relatively insensitive to modification of the indole side chain. However, clear limitations emerge when the intrinsic nucleophilicity of the indole C3 position is reduced, particularly under strongly electron-withdrawing *N*-substitution, or when the epoxide framework lacks sufficient π-activation, leading to unreactive or decomposed substrates. Compared with HFIP-stabilized ionic cyclizations or electrochemical radical processes, this system is more sensitive to subtle electronic tuning of the indole core and the epoxide electrophile.

Mechanistically, HFIP plays a decisive role in enabling the initial dearomative epoxide-indole cyclization by stabilizing developing cationic character through extensive hydrogen-bonding interactions. This activation triggers nucleophilic attack of the indole onto the epoxide, followed by an interrupted Plancher-type rearrangement that reorganizes the inter-



Scheme 33: Substarte scope of (a) tryptamine and (b) epoxy tosylates derivatives.

mediate into a fused-bridged indoline framework. The process effectively reverses the conventional polarity of indole reactivity at C_3, achieving a formal umpolung through substrate activation and rearrangement rather than prefunctionalization or external redox control. Compared with electrochemical or radical indole functionalizations, this approach uniquely combines dearomatization and skeletal rearrangement in a single cascade, relying primarily on HFIP-mediated ion stabilization rather than radical generation or metal catalysis.

Overall, this HFIP-enabled cascade represents a powerful example of complexity-building indole chemistry, converting simple indole-epoxide precursors into highly strained bridged frameworks with excellent selectivity. While its efficiency and stereocontrol are notable, its dependence on epoxide activation and indole electronic properties defines a narrower reactivity window compared to more general HFIP-assisted cyclizations. Nevertheless, it provides a distinct and valuable strategy for accessing architecturally complex indoline scaffolds and demonstrates how HFIP can unlock non-intuitive reactivity patterns in heteroaromatic systems.

Conclusion and Outlook

In conclusion, HFIP has evolved from a specialized fluorinated solvent into a powerful reaction-enabling medium that plays a central role in modern heterocyclic chemistry. Its unique combination of strong hydrogen-bond-donating ability, high ionizing power, low nucleophilicity, and exceptional capacity to stabilize ionic and radical intermediates has enabled numerous synthetic transformations that are often difficult to achieve under conventional conditions. As highlighted throughout this review, HFIP not only serves as a solvent but frequently acts as a

promoter, cocatalyst, proton-transfer mediator, and reaction-directing component, significantly influencing reaction pathways, selectivity, and overall efficiency.

The recent advances summarized from 2022 to 2025 clearly demonstrate the versatility of HFIP across a broad spectrum of heterocyclic ring constructions, including simple heterocycles, fused and polycyclic systems, spirocyclic frameworks, and saturated or non-aromatic heterocycles. HFIP-enabled methodologies have facilitated diverse transformations such as cyclizations, annulations, dearomatizations, rearrangements, electrochemical reactions, and cross-dehydrogenative coupling processes under mild, metal-free, oxidant-free, or redox-neutral conditions. In many cases, these strategies exhibit broad substrate scope, high chemo-, regio-, and stereoselectivity, operational simplicity, and improved sustainability compared with traditional protocols.

Mechanistically, the ability of HFIP to stabilize reactive intermediates through extensive hydrogen-bonding networks and cooperative interactions with catalysts or reagents has emerged as a recurring theme across many transformations. The solvent has proven particularly valuable in promoting cationic, radical, and cascade processes, thereby enabling rapid molecular complexity generation and access to structurally diverse heterocyclic scaffolds with significant pharmaceutical and synthetic relevance. At the same time, the reviewed studies also reveal certain limitations, including substrate-dependent reactivity, solvent cost, and challenges associated with solvent recovery and large-scale applications.

Nevertheless, the rapidly growing number of HFIP-mediated methodologies underscores its continuing impact on synthetic design and reaction development. Future progress in recyclable fluorinated solvent systems, asymmetric variants, electrochemical processes, photocatalytic transformations, and sustainable catalytic protocols is expected to further expand the utility of HFIP in heterocyclic synthesis. The authors have anticipated that the mechanistic insights and synthetic strategies discussed in this review will provide valuable guidance for the development of next-generation HFIP-enabled transformations and inspire further innovation in sustainable heterocyclic chemistry.

Emerging Alternatives to HFIP

Although HFIP remains a valuable solvent in heterocyclic synthesis, its environmental, toxicological, and economic concerns have encouraged the search for more sustainable alternatives. Emerging approaches include alternative fluorinated alcohols, HFIP–water or mixed-solvent systems, and non-fluorinated hydrogen-bond-donating solvents, ionic liquids, and deep eutectic solvents. Solvent-free and low-solvent approaches, including mechanochemistry, electrochemistry, and photochemistry, also offer promising directions. Rather than seeking a single replacement for HFIP, future studies may focus on identifying reaction media that reproduce its specific beneficial properties while reducing its environmental impact. Comparative studies and solvent-recycling strategies will be important in assessing the practical potential of these alternatives.

Acknowledgements

Dr. RV is grateful to Dr. Ch. V. Rajasekhar for kind support and encouragement. Dr. MMA is grateful to the Deanship of Scientific Research and Graduate Studies at King Khalid University, Saudi Arabia, through the Small Research Group Project under the grant number (R. G. P. 2/743/1446).

Funding

This research is financially supported by Deanship of Scientific Research and Graduate Studies at King Khalid University, Saudi Arabia, through the Large Research Group Project under the grant number (R. G. P. 2/743/1446).

Conflict of Interest

The author declares that we have no known competing financial interests or personal relationships that could have appeared to influence the work reported in this paper.

Author Contributions

Laxman M. Alakonda: writing – review & editing. Ravi Varala: conceptualization; investigation; supervision. Vittal Seema: resources; software. Mohammed Mujahid Alam: formal analysis; funding acquisition; supervision.

ORCID® iDs

Laxman M. Alakonda - https://orcid.org/0009-0000-6749-0479
Ravi Varala - https://orcid.org/0000-0002-6466-9454

Data Availability Statement

Data sharing is not applicable as no new data was generated or analyzed in this study.

References

1. Gladysz, J. A.; Emnet, C. Fluorous Solvents and Related Media. In *Handbook of Fluorous Chemistry;* Gladysz, J. A.; Curran, D. P.; Horváth, I. T., Eds.; Wiley-VCH: Weinheim, Germany, 2004; pp 11–23. doi:10.1002/3527603905.ch3
2. Khaksar, S. *J. Fluorine Chem.* **2015,** *172,* 51–61. doi:10.1016/j.jfluchem.2015.01.008
3. Siegemund, G.; Schwertfeger, W.; Feiring, A.; Smart, B.; Behr, F.; Vogel, H.; McKusick, B. *Fluorine Compounds, Organic; Ullmann's Encyclopedia of Industrial Chemistry*; Wiley-VCH: Weinheim, Germany, 2000. doi:10.1002/14356007.a11_349

4. Khandelia, T.; Panigrahi, P.; Ghosh, S.; Mandal, R.; Doley, B.; Patel, B. K. *Chem. – Asian J.* **2024,** *19,* e202400603. doi:10.1002/asia.202400603
5. Luo, G.; Su, W. *Pharm. Fronts* **2024,** *06,* e1–e8. doi:10.1055/s-0044-1779594
6. Colomer, I.; Chamberlain, A. E. R.; Haughey, M. B.; Donohoe, T. J. *Nat. Rev. Chem.* **2017,** *1,* 0088. doi:10.1038/s41570-017-0088
7. Ammer, J.; Mayr, H. *J. Phys. Org. Chem.* **2013,** *26,* 59–63. doi:10.1002/poc.3064
8. Pozhydaiev, V.; Power, M.; Gandon, V.; Moran, J.; Lebœuf, D. *Chem. Commun.* **2020,** *56,* 11548–11564. doi:10.1039/d0cc05194b
9. Laurence, C.; Gal, J.-F. *Lewis Basicity and Affinity Scales: Data and Measurement;* John Wiley & Sons: Chichester, UK, 2009; pp 50–51. doi:10.1002/9780470681909
10. Lee, S. H.; Hong, S. W.; Chi, H. M. *J. Org. Chem.* **2026,** *91,* 7513–7518. doi:10.1021/acs.joc.6c00591
11. Yang, E. X.; Pecora, A.; Fisher, E. L.; am Ende, C. W.; Humphrey, J. M. *J. Org. Chem.* **2026,** *91,* 7126–7133. doi:10.1021/acs.joc.5c02406
12. Liu, X.-L.; Liu, N.-X.; Li, Y.-N.; Li, Y.-R.; Zheng, X.-B.; Wei, B.-G. *J. Org. Chem.* **2026,** *91,* 6134–6143. doi:10.1021/acs.joc.6c00597
13. Aniyan, A.; Kandasamy, J. *J. Org. Chem.* **2026,** *91,* 5070–5084. doi:10.1021/acs.joc.5c03288
14. Lv, S.; Zhong, J.; Xing, Y.; Song, X.; Fu, W.; Guo, Y.; Zhu, T.; Wang, Z. *J. Org. Chem.* **2026,** *91,* 1737–1744. doi:10.1021/acs.joc.5c02849
15. Taskesenligil, Y.; Aslan, M.; Saracoglu, N. *J. Org. Chem.* **2026,** *91,* 1405–1411. doi:10.1021/acs.joc.5c02643
16. Zhao, Y.; Ma, X.; Wang, J.; Voloshkin, V. A.; Nolan, S. P. *Chem. Commun.* **2026,** *62,* 2664–2667. doi:10.1039/d5cc07022h
17. Yu, Y.; Ji, X.; Wu, X.; Liu, L. *Org. Lett.* **2026,** *28,* 3712–3717. doi:10.1021/acs.orglett.6c00343
18. Huang, J.; Zeng, Z.; Zhou, Z.; Yi, W.; Wang, S. *Org. Lett.* **2026,** *28,* 3463–3467. doi:10.1021/acs.orglett.6c00340
19. Huang, W.-C.; Lin, Y.-J.; Hsu, S.-J.; Reddy, J. S.; Lin, S.-Y. *Adv. Synth. Catal.* **2026,** *368,* e70304. doi:10.1002/adsc.70304
20. Nie, J.-J.; Wang, Z.-X. *Org. Chem. Front.* **2025,** *12,* 629–635. doi:10.1039/d4qo01719f
21. Pan, X.-F.; Ji, P.; Qi, X.; Wu, X.-F. *J. Catal.* **2024,** *438,* 115730. doi:10.1016/j.jcat.2024.115730
22. Mondal, N.; Raj, S.; Choudhury, L. H. *J. Org. Chem.* **2025,** *90,* 14565–14578. doi:10.1021/acs.joc.5c01525
23. Ramos-Villaseñor, J. M.; Rodríguez-Cárdenas, E.; Barrera Díaz, C. E.; Frontana-Uribe, B. A. *J. Electrochem. Soc.* **2020,** *167,* 155509. doi:10.1149/1945-7111/abb83c
24. Solyev, P. N. HFIP-Mediated C-H functionalization. *Handbook of CH Functionalization;* Wiley-VCH: Weinheim, Germany, 2022; pp 1–25. doi:10.1002/9783527834242.chf0214
25. Motiwala, H. F.; Armaly, A. M.; Cacioppo, J. G.; Coombs, T. C.; Koehn, K. R. K.; Norwood, V. M., IV; Aubé, J. *Chem. Rev.* **2022,** *122,* 12544–12747. doi:10.1021/acs.chemrev.1c00749
26. Xu, H.; Luo, H.; Wang, Y.; Gao, H. *Tetrahedron Green Chem* **2025,** *5,* 100071. doi:10.1016/j.tgchem.2025.100071
27. Guravaiah, M.; Sampurnamma, G.; Sruthi, T.; Jadhav, V. D.; Ramakrishna, B.; Doddipalla, R.; Krishna Seemakurti, S. R.; Siddaiah, V.; Venkateswarlu, K. *Tetrahedron* **2025,** *185,* 134815. doi:10.1016/j.tet.2025.134815
28. Pu, B.; Nguyen, T. V. *Aust. J. Chem.* **2023,** *76,* 58–62. doi:10.1071/ch22212
29. Santos, R. A. L. S.; Silva, A. M. S.; Pinto, D. C. G. A. *Molecules* **2026,** *31,* 13. doi:10.3390/molecules31010013
30. Yu, X.; Ji, X.; Shang, D.; Yu, L.; Chan, P. W. H.; Rao, W. *Org. Lett.* **2024,** *26,* 6631–6636. doi:10.1021/acs.orglett.4c02287
31. Thorat, D. N.; Sonar, K. S.; Kale, S. R.; Singh, A.; Patil, S. D.; Awasthi, P. *Discover Chem.* **2026,** *3,* 88. doi:10.1007/s44371-026-00550-7
32. Banerjee, R.; Ali, D.; Mondal, N.; Choudhury, L. H. *J. Org. Chem.* **2024,** *89,* 4423–4437. doi:10.1021/acs.joc.3c02567
33. Varala, R.; Bollikolla, H. B.; Kurmarayuni, C. M. *Curr. Org. Synth.* **2021,** *18,* 101–124. doi:10.2174/1570179417666200914142229
34. Jaiswal, M. K.; Yadav, M. S.; Maurya, S.; Ansari, D.; Tiwari, V. K. *J. Org. Chem.* **2024,** *89,* 17213–17227. doi:10.1021/acs.joc.4c01700
35. Mansour, Y. E.; Mohamed, M. S.; Fatahala, S. S.; Riad, J. Y. *Chem. Pap.* **2026,** in press. doi:10.1007/s11696-026-05373-5
36. Chaurasia, U.; Parvin, T. *J. Chem. Sci.* **2023,** *135,* 60. doi:10.1007/s12039-023-02185-y
37. Amin, A.; Qadir, T.; Sharma, P. K.; Jeelani, I.; Abe, H. *Open Med. Chem. J.* **2022,** *16,* e187410452209010. doi:10.2174/18741045-v16-e2209010
38. Madaan, K.; Singh, R. *ChemMedChem* **2025,** *20,* e202500420. doi:10.1002/cmdc.202500420
39. Zhao, J.; Qian, H.-M.; Zi, Y.; Ji, S.-J.; Xu, X.-P. *Org. Biomol. Chem.* **2025,** *23,* 6938–6942. doi:10.1039/d5ob00634a
40. Wan, H.; Li, D.; Xia, H.; Yang, L.; Alhumade, H.; Yi, H.; Lei, A. *Chem. Commun.* **2022,** *58,* 665–668. doi:10.1039/d1cc04656j
41. Mahurkar, N. D.; Gawhale, N. D.; Lokhande, M. N.; Uke, S. J.; Kodape, M. M. *Results Chem.* **2023,** *6,* 101139. doi:10.1016/j.rechem.2023.101139
42. Yaragorla, S.; Tiwari, D.; Lone, M. S. *J. Org. Chem.* **2024,** *89,* 9427–9439. doi:10.1021/acs.joc.4c00716
43. Pavlinov, I.; Gerlach, E. M.; Aldrich, L. N. *Org. Biomol. Chem.* **2019,** *17,* 1608–1623. doi:10.1039/c8ob02327a
44. Ashraf, B.; Kanwal, A.; Ahmad, M.; Rasool, N.; Malik, A.; Arshad, M.; Suleman, M. *ChemistrySelect* **2025,** *10,* e03379. doi:10.1002/slct.202503379
45. Xu, H.; Sun, Y.; Zhang, X.; Fan, X. *J. Org. Chem.* **2025,** *90,* 9236–9248. doi:10.1021/acs.joc.5c01234
46. Das, D.; Banerjee, R.; Mitra, A. *J. Chem. Pharm. Res.* **2014,** *6,* 108–116.
47. Mohamadpour, F. *Results Chem.* **2024,** *9,* 101629. doi:10.1016/j.rechem.2024.101629
48. Kant, K.; Patel, C. K.; Banerjee, S.; Naik, P.; Padhi, A.; Sharma, V.; Singh, V.; Almeer, R.; Keremane, K. S.; Atta, A. K.; Malakar, C. C. *Asian J. Org. Chem.* **2024,** *13,* e202400223. doi:10.1002/ajoc.202400223
49. Varala, R.; Kamsali, M. M. A.; Hussein, M.; Alam, M. M. *J. Heterocycl. Chem.* **2025,** *62,* 848–879. doi:10.1002/jhet.70013
50. Qin, Z.-Y.; Sun, C.-X.; Zhang, W.-W.; Li, J.-R.; Gong, Y.-X.; Shu, W.-M.; Wu, A.-X. *Catalysts* **2023,** *13,* 1447. doi:10.3390/catal13111447
51. Vivekanand, T.; Satpathi, B.; Bankar, S. K.; Ramasastry, S. S. V. *RSC Adv.* **2018,** *8,* 18576–18588. doi:10.1039/c8ra03480j
52. Zhu, W.; Wang, J.; Wang, S.; Gu, Z.; Aceña, J. L.; Izawa, K.; Liu, H.; Soloshonok, V. A. *J. Fluorine Chem.* **2014,** *167,* 37–54. doi:10.1016/j.jfluchem.2014.06.026
53. Teng, Y.; Yu, X.; Shang, D.; Wang, Z.; Rao, W. *J. Org. Chem.* **2024,** *89,* 1147–1159. doi:10.1021/acs.joc.3c02331
54. Varala, R.; Seema, V.; Kamsali, M. M. A.; Kousar, N.; Hussein, M.; Alam, M. M. *Tetrahedron Lett.* **2026,** *175,* 155922. doi:10.1016/j.tetlet.2025.155922

55. Dias do Espírito Santo, R.; Capitão, R. M.; Santos Barbosa, P.; Simão dos Santos, E. F.; Roque Duarte Correia, C. *Asian J. Org. Chem.* **2021,** *10,* 1938–1957. doi:10.1002/ajoc.202100223
56. Kumar, R.; Acharya, S. S.; Bhaumick, P.; Parvin, T.; Choudhury, L. H. *Tetrahedron* **2023,** *132,* 133250. doi:10.1016/j.tet.2023.133250
57. Das, D.; Sikdar, P.; Bairagi, M. *Eur. J. Med. Chem.* **2016,** *109,* 89–98. doi:10.1016/j.ejmech.2015.12.022
58. Liu, X.; Ren, Y.; Zhu, L.; Li, T.; Xu, W.; Liu, Y.; Tang, K.-W.; Xiong, B. *Tetrahedron* **2023,** *148,* 133655. doi:10.1016/j.tet.2023.133655
59. Singh, G.; Pandey, R.; Pankhade, Y. A.; Fatma, S.; Anand, R. V. *Chem. Rec.* **2021,** *21,* 4150–4173. doi:10.1002/tcr.202100137
60. Zhang, J.; Sun, M.; Gao, K.; Wu, H.; Li, J.; Wang, Z.; Yang, J. *J. Org. Chem.* **2024,** *89,* 2847–2857. doi:10.1021/acs.joc.3c02105
61. Leech, M. C.; Garcia, A. D.; Petti, A.; Dobbs, A. P.; Lam, K. *React. Chem. Eng.* **2020,** *5,* 977–990. doi:10.1039/d0re00064g
62. Suwalka, D.; Malviya, B. K.; Verma, V. P.; Jassal, A. K.; Sharma, S. *J. Org. Chem.* **2023,** *88,* 9199–9212. doi:10.1021/acs.joc.3c00772
63. Varela, M. T.; Dias, G. G.; de Oliveira, L. F. N.; de Oliveira, R. G.; Aguiar, F. D.; Nogueira, J. P.; Cruz, L. R.; Dias, L. C. *Eur. J. Med. Chem.* **2025,** *287,* 117368. doi:10.1016/j.ejmech.2025.117368
64. Hua, J.; Fang, Z.; Bian, M.; Ma, T.; Yang, M.; Xu, J.; Liu, C.; He, W.; Zhu, N.; Yang, Z.; Guo, K. *ChemSusChem* **2020,** *13,* 2053–2059. doi:10.1002/cssc.202000098
65. Nagar, R.; Suwalka, D.; Malviya, B. K.; Verma, V. P.; Jassal, A. K.; Sharma, S. *J. Org. Chem.* **2023,** *88,* 13977–13994. doi:10.1021/acs.joc.3c01532
66. Liandi, A. R.; Cahyana, A. H.; Alfariza, D. N.; Nuraini, R.; Sari, R. W.; Wendari, T. P. *Green Synth. Catal.* **2024,** *5,* 1–13. doi:10.1016/j.gresc.2023.08.001
67. Mondal, S.; Bera, T.; Hazra, S.; Hajra, S.; De, S.; Saha, J. *J. Org. Chem.* **2025,** *90,* 16478–16487. doi:10.1021/acs.joc.5c02023
68. Zhu, Y.; Zhao, Y.; Yao, L.; Pu, E.; Yang, S.; Zhang, Y.; Zhang, H.; Chen, J. *JACS Au* **2026,** *6,* 1988–1997. doi:10.1021/jacsau.6c00074
69. Chen, X.; Zhu, C.; Ji, L.; Liu, C.; Zhang, Y.; Rao, Y.; Yuan, Z. *Catalysts* **2025,** *15,* 673. doi:10.3390/catal15070673
70. Peng, S.; He, J.; Yang, L.; Zhang, H.; Li, H.; Lang, M.; Chen, C.; Wang, J. *J. Org. Chem.* **2022,** *87,* 6247–6262. doi:10.1021/acs.joc.2c00482
71. Dequina, H. J.; Jones, C. L.; Schomaker, J. M. *Chem* **2023,** *9,* 1658–1701. doi:10.1016/j.chempr.2023.04.010
72. Huang, Y.; Zhu, S.-Y.; He, G.; Chen, G.; Wang, H. *J. Org. Chem.* **2024,** *89,* 6263–6273. doi:10.1021/acs.joc.4c00253
73. Mech, D.; Kurowska, A.; Trotsko, N. *Int. J. Mol. Sci.* **2021,** *22,* 11533. doi:10.3390/ijms222111533
74. Mondal, S.; Patel, M.; Biswas, A.; Hazra, S.; Saha, J. *Org. Lett.* **2025,** *27,* 2715–2720. doi:10.1021/acs.orglett.5c00488
75. Boivin, T. L. B. *Tetrahedron* **1987,** *43,* 3309–3362. doi:10.1016/s0040-4020(01)81626-4
76. Brutiu, B. R.; Tang, L.; Kaiser, D.; Maulide, N. *Monatsh. Chem.* **2024,** *155,* 709–713. doi:10.1007/s00706-024-03214-3
77. Sharma, R.; Arisawa, M.; Takizawa, S.; Salem, M. S. H. *Org. Chem. Front.* **2025,** *12,* 1633–1670. doi:10.1039/d4qo02157f
78. Jaiswal, V.; Godara, M.; Das, D.; Gandon, V.; Saha, J. *J. Org. Chem.* **2022,** *87,* 613–627. doi:10.1021/acs.joc.1c02621
79. Xie, J.; Zhang, J.; Kasemthaveechok, S.; López-Resano, S.; Cots, E.; Maseras, F.; Pérez-Temprano, M. H. *Nat. Synth.* **2024,** *3,* 1021–1030. doi:10.1038/s44160-024-00566-w
80. Lee, S. H.; Chi, H. M. *Org. Lett.* **2023,** *25,* 1083–1087. doi:10.1021/acs.orglett.2c04299
81. Abdel-Aziem, A.; Elsharabasy, S. A.; Sayed, M. T. *J. Heterocycl. Chem.* **2026,** *63,* 169–194. doi:10.1002/jhet.70127
82. Zhao, Y.; Cheng, Y.; Liu, Q.; Li, M.; Li, W.; Wu, D. *J. Org. Chem.* **2025,** *90,* 14304–14311. doi:10.1021/acs.joc.5c01199
83. Adarve-Cardona, L.; Garay-Talero, A.; Gamba-Sánchez, D. Synthesis of naturally occurring seven-membered nitrogen heterocycles and related bioactive compounds. In *Studies in Natural Products Chemistry;* Rahman, A., Ed.; Elsevier: Amsterdam, Netherlands, 2023; Vol. 78, pp 189–235. doi:10.1016/b978-0-323-91253-2.00016-9
84. Zhuang, D.; Jiang, S.; Wang, Y.; Wang, X.; Shen, S.; Yan, R. *Org. Lett.* **2023,** *25,* 3007–3012. doi:10.1021/acs.orglett.3c00790
85. Zhou, H.; O'Brien, P.; Unsworth, W. P. *J. Org. Chem.* **2025,** *90,* 5070–5074. doi:10.1021/acs.joc.5c00202
86. An, X.-D.; Shao, D.-Y.; Qiu, B.; Xiao, J. *Org. Lett.* **2023,** *25,* 2432–2437. doi:10.1021/acs.orglett.3c00193
87. Deka, B.; Deb, M. L.; Baruah, P. K. *Top. Curr. Chem.* **2020,** *378,* 22. doi:10.1007/s41061-020-0287-7
88. Arockiaraj, M.; Nayak, R.; Rajeshkumar, V. *Org. Biomol. Chem.* **2026,** *24,* 4782–4815. doi:10.1039/d6ob00635c
89. Chouhan, R.; Das, S. K. *Org. Lett.* **2024,** *26,* 11156–11161. doi:10.1021/acs.orglett.4c04215

License and Terms

This is an open access article licensed under the terms of the Beilstein-Institut Open Access License Agreement (https://www.beilstein-journals.org/bjoc/terms), which is identical to the Creative Commons Attribution 4.0 International License (https://creativecommons.org/licenses/by/4.0). The reuse of material under this license requires that the author(s), source and license are credited. Third-party material in this article could be subject to other licenses (typically indicated in the credit line), and in this case, users are required to obtain permission from the license holder to reuse the material.

The definitive version of this article is the electronic one which can be found at:
https://doi.org/10.3762/bjoc.22.116